plants

Special Issue Reprint

Recent Advances in Plant Genetics and Genomics

Edited by
Longbiao Guo and Qian-Hao Zhu

mdpi.com/journal/plants

MDPI

Recent Advances in Plant Genetics and Genomics

Recent Advances in Plant Genetics and Genomics

Guest Editors

Longbiao Guo
Qian-Hao Zhu

MDPI

Basel • Beijing • Wuhan • Barcelona • Belgrade • Novi Sad • Cluj • Manchester

Guest Editors

Longbiao Guo
State Key Laboratory of Rice Biology and Breeding
Chinese Academy of Agricultural Sciences
Hangzhou
China

Qian-Hao Zhu
Commonwealth Scientific and Industrial Research Organization, Agriculture and Food
Canberra
Australia

Editorial Office

MDPI AG
Grosspeteranlage 5
4052 Basel, Switzerland

This is a reprint of the Special Issue, published open access by the journal *Plants* (ISSN 2223-7747), freely accessible at: https://www.mdpi.com/journal/plants/special_issues/MXH474H4Y5.

For citation purposes, cite each article independently as indicated on the article page online and as indicated below:

Lastname, A.A.; Lastname, B.B. Article Title. *Journal Name* **Year**, *Volume Number*, Page Range.

ISBN 978-3-7258-8693-7 (Hbk)
ISBN 978-3-7258-8694-4 (PDF)
https://doi.org/10.3390/books978-3-7258-8694-4

© 2026 by the authors. Articles in this reprint are Open Access and distributed under the Creative Commons Attribution (CC BY) license. The reprint as a whole is distributed by MDPI under the terms and conditions of the Creative Commons Attribution-NonCommercial-NoDerivs (CC BY-NC-ND) license (https://creativecommons.org/licenses/by-nc-nd/4.0/).

Contents

About the Editors . . . . . **vii**

Salma Kelany, Qianhao Zhu and Longbiao Guo
Recent Advances in Plant Genetics and Genomics
Reprinted from: *Plants* **2026**, *15*, 1947, https://doi.org/10.3390/plants15131947 . . . . . **1**

Alexander A. Arkhipov, Nadezhda L. Bolsheva, Elena N. Pushkova, Vladislav V. Babenko, Yury A. Zubarev, Valentina A. Krasnova, et al.
Nanopore Data-Driven Near-T2T Genome Assembly of *Hippophae rhamnoides* ssp. *mongolica* Rousi and Its Complex Annotation
Reprinted from: *Plants* **2026**, *15*, 1726, https://doi.org/10.3390/plants15111726 . . . . . **7**

Jariya Roddee, Kamolchanok Umnajkitikorn, Napatson Chansawang, Jirapong Jairin and Jureemart Wangkeeree
Screening and Evaluation of Rice to Assess Antibiosis and Antixenosis Resistance to White-Backed Planthopper (*Sogatella furcifera*)
Reprinted from: *Plants* **2026**, *15*, 811, https://doi.org/10.3390/plants15050811 . . . . . **28**

Yueying Wang, Faming Yu, Sirinthorn Kongpraphrut, Congcong Liu, Muhammad Asad Ullah Asad, Salma Kelany, et al.
Genomic Variation and GWAS Analysis for Salt Tolerance Discovered in Egyptian Rice Germplasm
Reprinted from: *Plants* **2026**, *15*, 128, https://doi.org/10.3390/plants15010128 . . . . . **52**

Xuemei Liang, Qi Liu, Li Qin, Peng Jia, Jianfeng Wang, Changjiang Zhang, et al.
Transcriptomic Analysis of Rice (Jijing129) Reveals Growth and Gene Expression Responses to Different Red-Blue Laser Light Treatments
Reprinted from: *Plants* **2025**, *14*, 3712, https://doi.org/10.3390/plants14243712 . . . . . **65**

Huan Wang, Robert D. Slocum, Xingbo Cai, Greg Clark and Stanley J. Roux
Chromatin-Associated Pea Apyrase psNTP9 Function as a DNA-Binding Regulatory Protein in Yeast and Arabidopsis
Reprinted from: *Plants* **2025**, *14*, 3514, https://doi.org/10.3390/plants14223514 . . . . . **86**

Yu-Jia Leng, Shi-Yu Qiang, Wen-Yu Zhou, Shuai Lu, Tao Tao, Hao-Cheng Zhang, et al.
Rolling Leaf 2 Controls Leaf Rolling by Regulating Adaxial-Side Bulliform Cell Number and Size in Rice
Reprinted from: *Plants* **2025**, *14*, 3373, https://doi.org/10.3390/plants14213373 . . . . . **108**

Yirong Jin, Guiju Chen, Xiaodong Qiu, Fuyan Wang, Hui Jin, Liang Zhang, et al.
Genome-Wide Linkage Mapping of Root System Architecture-Related Traits Under Drought Stress in Common Wheat (*Triticum aestivum* L.)
Reprinted from: *Plants* **2025**, *14*, 3023, https://doi.org/10.3390/plants14193023 . . . . . **124**

Yining Kong, Changlai Liu, Tianshuai Li, Ji Fang and Guohua Liu
Identification and Expression Characteristics of the Cryptochrome Gene Family in *Chimonobambusa sichuanensis*
Reprinted from: *Plants* **2025**, *14*, 1637, https://doi.org/10.3390/plants14111637 . . . . . **145**

Khwanruedee Thepphomwong, Makawan Srichan, Artitaya Deeroum, Kularb Laosatit and Prakit Somta
QTL-Seq and Fine-Mapping Analyses Identify QTL and Candidate Genes Controlling Snake-like Pod Surface Trait in Vegetable Cowpea Yardlong Bean
Reprinted from: *Plants* **2025**, *14*, 1447, https://doi.org/10.3390/plants14101447 . . . . . **162**

Gengmi Li, Baohua Feng, Qian-Hao Zhu, Kaifeng Jiang and Tao Zhang
Protein Post-Translational Modifications in Plant Abiotic Stress Responses
Reprinted from: *Plants* **2025**, *15*, 52, https://doi.org/10.3390/plants15010052 . . . . . **177**

Biaobiao Cheng, Beibei Lv, Qiangbing Xuan, Yunfang Li, Jing Li, Weihong Liang and Junjie Wang
Research Progress on Rice-Blast-Resistance-Related Genes
Reprinted from: *Plants* **2025**, *14*, 2698, https://doi.org/10.3390/plants14172698 . . . . . **208**

Alexander A. Lezzhov, Anastasia K. Atabekova, Denis A. Chergintsev, Andrey G. Solovyev and Sergey Y. Morozov
Expression of the *Nicotiana benthamiana* Retrozyme 1 (NbRZ1) Genomic Locus
Reprinted from: *Plants* **2025**, *14*, 1205, https://doi.org/10.3390/plants14081205 . . . . . **236**

About the Editors

Longbiao Guo

Longbiao Guo is engaged in long-term research on rice genetic materials creation, molecular mechanism dissection of important agronomy traits, and molecular application in CNRRI since 1986. Achieved significant progress in the utilization of superior germplasm, the breeding of new varieties, and the genetic mapping of important traits. Discovered and developed crucial genetic resources in rice, creating and screening over 100 new superior germplasms; constructed six RILs and CSSLs populations using varieties such as Nipponbare, 9311, and wild rice. Positionally cloned more than 20 functional genes, including LTS1, OsSLA4, WGL2, and GHD10. Established a genotype-phenotype (GP) yield database and molecular breeding platforms. Published over 60 papers in journals such as "Nature Communications," "Trends in Plant Science," and "Plant Physiology", and etc.

Qian-Hao Zhu

Qian-Hao Zhu is a plant geneticist and molecular biologist. He has been working on rice and Arabidopsis functional genomics, and cotton molecular breeding. His current research concentrates on molecular strategies for breeding cotton varieties with improved disease/pest resilience, fibre yield and quality by integrating genomics, functional genomics, gene editing, and genomic prediction. His work has led to the successful development and commercial release of cotton varieties resistant to two-spotted spider mites.

plants

MDPI

Editorial

Recent Advances in Plant Genetics and Genomics

Salma Kelany [1], Qianhao Zhu [2,*] and Longbiao Guo [1,*]

[1] State Key Laboratory of Rice Biology and Breeding, China National Rice Research Institute, Hangzhou 310006, China; salmakelany93@gmail.com
[2] Commonwealth Scientific and Industrial Research Organization, Agriculture and Food, GPO Box 1700, Canberra, ACT 2601, Australia
* Correspondence: qianhao.zhu@csiro.au (Q.Z.); guolongbiao@caas.cn (L.G.)

1. Introduction

Publication of the genome sequences of *Arabidopsis thaliana* in 2000 and of *Oryza sativa* in 2002 marked the beginning of an exciting era in which advances in molecular technology and methodology uncovered the genetic blueprints of hundreds of plant species [1]. The rapid development of high-throughput sequencing technology, particularly third-generation sequencing technology, enables not only affordable resequencing of a large number of plant genomes, but also generates gapless telomere-to-telomere genomes of plant species, most importantly of crops pivotal to humanity. These fundamental genomic resources, together with multi-omics data, greatly facilitate exploration of the genetic diversity of plants, the discovery of genes underlying important agronomic traits of crops, and elucidation of the molecular mechanisms of the genes. The resources and knowledge accumulated are now being translated into real-world impact through the breeding of climate-smart new crop varieties, thereby benefiting global food security [2–4].

Building on this foundation, this Special Issue, "Recent Advances in Plant Genetics and Genomics", continues to report the recent advancements in this field. It compiles nine research articles and two review papers covering diverse research topics on major staple crops and other plants, including the screening of germplasm that is tolerant to biotic or abiotic stress, the characterization of a plant's response to environmental variables, genome-wide identification of the gene family, genome-wide association studies (GWAS), quantitative trait locus (QTL) mapping, and gene cloning. Next, we briefly summarize these studies with the following aims: (i) understanding transcriptional and post-translational gene regulation, (ii) mining QTLs and genes associated with agronomic traits, and (iii) examining the responses of plant growth and development to environment variables.

2. Understanding Transcriptional and Post-Translational Gene Regulation

Both the expression and function of genes are regulated at multiple levels, including transcriptional, post-transcriptional, translational, and epigenetic. Three papers included in this Special Issue exemplified transcriptional gene expression and reviewed protein post-translational modifications in response to abiotic stresses.

Apyrases (NTPDases) hydrolyze NTP and NDP, removing their terminal phosphates and producing NMP. The regulation of extracellular ATP [eATP] by "ecto-apyrase" activities is important for phosphate uptake and diverse growth, along with other developmental processes of plants. Wang et al. [5] generated transgenic Arabidopsis lines, overexpressing either a pea apyrase PS (psNTP9) or a modified PS. DM was designated due to double

mutations in a potential calmodulin (CaM)-binding site that overlapped a predicted nuclear localization signal site. Using the transgenics, the authors investigated the binding differences in the two proteins in the promoters of Arabidopsis genes using ChIP-seq. This revealed that mutations in the CaM-binding site of PS changed the interacting sites of PS in the promoters of Arabidopsis genes, and, consequently, the expression profiles of the PS target genes. The PS-specific binding sites in promoters of Arabidopsis genes were verified by electrophoretic mobility shift assays (EMSA); DM showed minimal binding to the PS-specific binding sites [5]. These findings demonstrate the role of PS in regulating gene expression on top of its known enzymatic function.

Retrozymes are a class of non-autonomous plant retrotransposons that contain long terminal repeats (LTRs). These LTRs contain hammerhead ribozymes (HHRs) that facilitate the circularization of the retrozyme RNA to form circular RNA. In order to uncover the transcription start site of *Nicotiana benthamiana retrozyme 1* (*NbRZ1*) and its function, Lezzhov et al. [6] compared transcription of the *GUS* reporter gene driven by the 35S promoter, wild-type *NbRZ1* LTR, or a mutated LTR, in which a point mutation (G to A substitution) was introduced in the *NbRZ1* LTR to prevent the retrozyme from self-cleavage. The *GUS* transcript was detected for all three constructs, but the GUS protein was detected only for the *GUS* driven by the 35S promoter and mutated LTR. These results indicated the promoter activity of *NbRZ1* LTR and untranslatability of the LTR-GUS transcript, likely due to the self-cleavage activity of the wild-type ribozyme. The transcription start site of *NbRZ1* was further mapped to an adenosine residue at position 116 of the *NbRZ1* LTR via 5′-RACE. In addition, *NbRZ1* was shown to encode a protein targeted for proteasomal degradation in plant cells; overexpression of this protein in plants is known to causes severe necrosis [6]. These findings imply a potential mechanism involved in regulating the expression of proteins encoded by *NbRZ1* at transcriptional and post-transcriptional levels.

Protein post-translational modifications (PTMs) can regulate the chemical decoration, structures, and functions of translated proteins. Li et al. [7] summarized the molecular mechanisms of major types of PTMs, including phosphorylation, ubiquitination, SUMOylation, glycosylation, methylation, and acetylation, with a focus on their regulatory roles in plant responses to abiotic stresses. Phosphorylation can activate SUMOylation-HSFA1/HSFA2 to regulate the heat stress signaling pathway. Phosphorylation, ubiquitination, and S-acylation collectively regulate the expression of cold-tolerance-related genes. SnRK2s-phosphorylation regulates drought stress response. Upon exposure to salt stress, the coupling of phosphorylation of SOS pathway-related proteins, ubiquitination, and phospholipid metabolism maintains ion homeostasis, conferring salt tolerance. Additionally, PTMs play a key role in ABA-mediated abiotic stress responses via signal transduction involving PYR/PYL/RCAR receptors, PP2Cs, and SnRK2s. The authors also proposed strategies for how PTMs can be manipulated to breed abiotic-stress-resilient crops [7].

Looking ahead, to fully understand gene function and its contribution to phenotype, it is important to investigate the regulatory mechanisms simultaneously at multiple levels, which has been enabled by rapid progress in multi-omics technologies.

3. Mining QTLs and Genes Associated with Agronomic Traits

Six studies within this Special Issue reported results on genetic mapping of quantitative trait loci (QTLs) and genes associated with agronomic traits in different plants.

Yardlong bean (*Vigna unguiculata* ssp. *unguiculata* cv.gr. *sesquipedalis*) is a vegetable variety of cowpea, and is an economic crop of several Southeast Asia countries and China. Pod traits determine appearance and are related to eating and cooking qualities. Thua Ngu is a local yardlong bean cultivar in southern Thailand which has a unique snake-like pod appearance and crispiness. In order to determine the genetic basis of the snake-like pod

https://doi.org/10.3390/plants15131947

(SLP) trait, Thepphomwong et al. [8] constructed an F2 segregation population by crossing Thua Ngu with Raya, and sequenced the genomes of the two parents and two bulked DNA samples pooled from progeny with extreme traits (SLP and normal pod). QTL-seq analysis using Δ(SNP-index) identified a major QTL, *qSlp4.1*, for the SLP trait on chromosome 4. Further fine-mapping delimited *qSlp4.1* to a 152.88 Kbp region containing nine genes, and potential candidate genes for the SLP trait were shortlisted based on gene annotation, paving the foundation for revealing the genetic basis underlying the trait [8].

Leaf rolling affects plant architecture and photosynthesis. Leng et al. [9] generated a *rolling leaf2* (*rll2*) mutant from *japonica* variety Wuyunjing27 (WYJ27) via ethylmethanesulfonate (EMS) mutagenesis, and identified the underlying gene *RLL2* based on map-based cloning using an F2 population derived from *rll2* x IR36. *RLL2* encoding a plant-specific calpain-like cysteine proteinase was cloned. *RLL2* is mainly expressed in young shoots, roots, panicles, and spikelets. *RLL2* seems to control leaf rolling by regulating bulliform cells; the size and number of bulliform cells were significantly increased in *rll2* compared to those of the wild type [9]. Manipulating the expression of *RLL2* specifically in leaves may allow us to breed rice cultivars with an ideal plant architecture.

To explore the genetic basis of salt tolerance (ST) in Egyptian rice germplasm, Wang et al. [10] re-sequenced 56 Egyptian rice accessions, subjected them to salt stress to evaluate their salt tolerance using the Standard Evaluation System (SES) scale, and performed genome-wide associations (GWAS) in combination with another 258 rice accessions. The investigation identified a total of 19 ST QTLs, with 17 of them being newly identified. The QTLs included three previously reported salt-tolerance-related genes, including *OsIPK1*, *OsRPH1/STG5*, and *ONAC063*. Comparative RNA-Seq analysis was carried out using Giza 176 (salt-tolerant) and 9311 (salt-susceptible). Interestingly, *ONAC063* was one of the differentially expressed genes, implying a potential role of the gene in the salt response of Giza 176. The role of *ONAC063* in salt tolerance was further confirmed by the finding of a favorable haplotype (Hap3) in the 258 rice accessions [10]. The results showed the power of an integrated approach in accelerating the discovery of functional genes.

The experiment conducted by Jin et al. [11] aimed to identify root system architecture traits related to drought tolerance in wheat. To this end, the authors developed 262 recombinant inbred lines (RILs) derived from Zhoumai16 × DK171 (drought-tolerant, DT). Based on the high-density SNP genetic map, five QTLs accounting for 6.1% to 18.9% of the phenotypic variances were identified based on root weight, length, area, and number of root tips; two overlapped with previously reported QTLs, and three were novel ones. Markers were developed for each QTL, enabling marker-assisted incorporation of the DT loci in the new wheat cultivars [11].

The white-backed planthopper (WBPH) severely impacts rice production. Roddee et al. [12] conducted a set of experiments aiming to establish effective methods for identifying WBPH-resistant rice varieties. The authors first quantified the feeding intensity of WBPH on ten rice varieties based on honeydew excretion and salivary sheath formation after a 24 h feeding. The authors further evaluated the tolerance of the rice varieties to WBPH feeding using the electrical penetration graph technique, the growth/survival rate of WBPH, and the impact of the morphological (trichome) trait. In addition, changes in hormones and secondary metabolites, as well as the expression of resistance-related genes, in rice following WBPH feeding were investigated. The results led the authors to conclude that the method based on the growth/survival rate of WBPH was the most suitable for screening WBPH-resistant rice varieties [12].

Blast is one of the major biotic threats to rice growth and development. Controlling the occurrence of rice blast will ensure sustainable rice production. On the basis of presenting the impact of rice blast on rice production, food security, and global economy, Cheng

https://doi.org/10.3390/plants15131947

et al. [13] reviewed the reported rice genes associated with blast resistance or susceptibility along with the immune mechanisms underlying rice blast resistance. The authors also discussed how the findings can be applied in breeding blast-resistant rice varieties [13]. Overall, this article provides an overview of the research progress on rice blast and breeding of rice varieties resistant to blast.

4. Responses of Plant Growth and Development to Environment Variables

Light is one of the most important environmental factors determining plant growth and development, affecting both photosynthesis and photomorphogenesis. Two studies included in this Special Issue exemplified how light quality affects plant growth and development in rice and *Chimonobambusa sichuanensis* (an ornamental shrubby bamboo).

Liang et al. [14] investigated the effects of different red-to-blue light ratios on rice seedlings of Jijing129 under an LGI-660/450 dual-wavelength semiconductor laser system. Rice seedlings treated with three red-to-blue light ratios (50:50, 60:40 or 75:25) were compared to those grown under natural light. It was found that all three treatments significantly increased the root weight and nitrogen content of rice seedlings, and even final grain yield, particularly the 60:40 (R:B) ratio. Compared to the seedlings under natural light, those treated with different R:B laser lights showed altered gene expression, with 101, 1645, and 2247 DEGs identified in the 50:50, 60:40, and 75:25 treatments, respectively. DEGs were found to be mainly involved in pathways related to metabolic processes, nitrogen metabolism, and protein amino acid phosphorylation [14]. While the findings are intriguing, it is of interest how the findings can be implemented in commercial rice production.

In the study by Kong et al. [15], the authors first identified four cryptochrome genes (*CRY*) in *Chimonobambusa sichuanensis* using the *Phyllostachys edulis* CRY genes as queries. The newly found genes were designated as *CsCRY1a*, *CsCRY1b*, *CsCRY2*, and *CsCRY3*. The proteins encoded by the four genes together with 55 CRYs proteins of 10 other species were used in a phylogenetic analysis. These CRYs were divided into three subfamilies, with CsCRY1a and CsCRY1b clustered in subfamily I, CsCRY2 in subfamily II, and CsCRY3 in subfamily III. To understand the response of the four genes to different light qualities and temperatures, their expression levels were compared in *C. sichuanensis* seedlings treated with different light qualities (red, blue, and a mixture of red and blue) or temperatures (−5 °C to 20 °C). It was found that the four genes responded differently to light quality; moreover, *CsCRY2* seemed to have a higher expression level than other three genes, particularly under low temperatures [15].

5. Conclusions and Perspectives

This Special Issue, entitled "Recent Advances in Plant Genetics and Genomics", compiles nine research articles and two review papers. The studies display the scope of the research areas, from the characterization of germplasm in response to abiotic and biotic stress to the identification of potential genes underlying important agronomic traits. The studies also showcase the application of a wide range of tools and methodologies in plant genetics and genomics research. The practical approaches suggested by the review papers not only provide tools for further advancement in the areas of the review papers' focus, but are also widely applicable to other related areas.

Agriculture—specifically, crop production—is currently facing a series of challenges, such as high temperatures, drought, soil salinization, and biotic stresses, which can lead to crop yields dropping by more than 30%. Combating these challenges necessitates enhancing studies on plant genetics, genomics, and functional genomics. Crop germplasms that

https://doi.org/10.3390/plants15131947

have undergone long-term adaptation to extreme environments are invaluable resources and provide a critical foundation for future breakthroughs in crop improvement. Their allelic variation should be systematic explored through the integration of multi-omics approaches, so as to identify and elucidate the complex genetic architectures and regulatory pathways underlying key agronomic traits and stress tolerances. With that, advanced breeding strategies, including marker-assisted selection, CRISPR/Cas9-mediated genome editing, and breeding by design, can then be implemented in breeding crop varieties that combine high yield potential, superior quality, and resilience to diverse environmental stresses [16]. Ultimately, future research on plant genetics, genomics, and functional genomics should follow the conceptual framework of 'mining elite genes—dissecting genetic mechanisms—developing novel germplasm—implementing in crop breeding'.

Author Contributions: S.K. drafted the editorial; Q.Z. and L.G. edited the editorial. All authors have read and agreed to the published version of the manuscript.

Funding: This project was funded by the National Natural Science Foundation of China (32261143470) and the Agricultural Science and Technology Innovation Program (ASTIP).

Data Availability Statement: No new data were created or analyzed in this study. Data sharing is not applicable to this article.

Conflicts of Interest: The authors declare no conflicts of interest.

References

1. Sun, Y.Q.; Shang, L.G.; Zhu, Q.H.; Fan, L.J.; Guo, L.B. Twenty years of plant genome sequencing: Achievements and challenges. *Trends Plant Sci.* **2022**, *27*, 391–401. [CrossRef] [PubMed]
2. Huang, X.Y.; Chao, D.Y.; Gao, J.P.; Zhu, M.Z.; Shi, M.; Lin, H.X. A previously unknown zinc finger protein, DST, regulates drought and salt tolerance in rice via stomatal aperture control. *Genes Dev.* **2009**, *23*, 1805–1817. [CrossRef] [PubMed]
3. Ren, Z.H.; Gao, J.P.; Li, L.G.; Cai, X.L.; Huang, W.; Chao, D.Y.; Zhu, M.Z.; Wang, Z.Y.; Luan, S.; Lin, H.X. A rice quantitative trait locus for salt tolerance encodes a sodium transporter. *Nat. Genet.* **2005**, *37*, 1141–1146. [CrossRef] [PubMed]
4. Wei, H.; Wang, X.; Zhang, Z.; Yang, L.; Zhang, Q.; Li, Y.; He, H.; Chen, D.; Zhang, B.; Zheng, C.; et al. Uncovering key salttolerant regulators through a combined eQTL and GWAS analysis using the super pan-genome in rice. *Natl. Sci. Rev.* **2024**, *11*, nwae043. [PubMed]
5. Wang, H.; Slocum, R.D.; Cai, X.B.; Clark, G.; Roux, S.J. Chromatin-associated pea apyrase psNTP9 function as a DNA-binding regulatory protein in yeast and arabidopsis. *Plants* **2025**, *14*, 3514. [CrossRef] [PubMed]
6. Lezzhov, A.; Atabekova, A.K.; Chergintsev, D.A.; Solovyev, A.G.; Morozov, S.Y. Expression of the *Nicotiana benthamiana* Retrozyme 1 (NbRZ1) genomic locus. *Plants* **2025**, *14*, 1205. [CrossRef] [PubMed]
7. Li, G.M.; Feng, B.H.; Zhu, Q.H.; Jiang, K.F.; Zhang, T. Protein post-translational modifications in plant abiotic stress responses. *Plants* **2026**, *15*, 52. [CrossRef] [PubMed]
8. Thepphomwong, K.; Srichan, M.; Deeroum, A.; Laosatit, K.; Somta, P. QTL-seq and fine-mapping analyses identify QTL and candidate genes controlling snake-like pod surface trait in vegetable cowpea Yardlong bean. *Plants* **2025**, *14*, 1447. [CrossRef] [PubMed]
9. Leng, Y.J.; Qiang, S.Y.; Zhou, W.Y.; Lu, S.A.; Tao, T.; Zhang, H.C.; Cui, W.X.; Zheng, Y.F.; Liu, H.B.; Yang, Q.Q.; et al. Rolling Leaf 2 controls leaf rolling by regulating adaxial-side bulliform cell number and size in rice. *Plants* **2025**, *14*, 3373. [CrossRef] [PubMed]
10. Wang, Y.Y.; Yu, F.M.; Kongpraphrut, S.; Liu, C.C.; Asad, M.; Kelany, S.; Sun, M.R.; Wang, Y.X.; Lv, Y.; Anis, G.; et al. Genomic variation and GWAS analysis for salt tolerance discovered in Egyptian rice germplasm. *Plants* **2026**, *15*, 128. [CrossRef] [PubMed]
11. Jin, Y.R.; Chen, G.J.; Qiu, X.D.; Wang, F.Y.; Jin, H.; Zhang, L.; Liu, C.; Liu, J.J.; Li, W.J.; Liu, P. Genome-wide linkage mapping of root system architecture-related traits under drought stress in common wheat (*Triticum aestivum* L.). *Plants* **2025**, *14*, 3023. [CrossRef] [PubMed]
12. Roddee, J.; Umnajkitikorn, K.; Chansawang, N.; Jairin, J.; Wangkeeree, J. Screening and evaluation of rice to assess antibiosis and antixenosis resistance to White-Backed Planthopper (*Sogatella furcifera*). *Plants* **2026**, *15*, 811. [CrossRef] [PubMed]
13. Cheng, B.B.; Lv, B.B.; Xuan, Q.B.; Li, Y.F.; Li, J.; Liang, W.H.; Wang, J.J. Research progress on rice-blast-resistance-related genes. *Plants* **2025**, *14*, 2698. [CrossRef] [PubMed]

14. Liang, X.M.; Liu, Q.; Qin, L.; Jia, P.; Wang, J.F.; Zhang, C.J.; Dai, X.T.; Yu, W.B.; Lei, X.Y.; Wang, N.N.; et al. Transcriptomic analysis of rice (Jijing129) reveals growth and gene expression responses to different red-blue laser light treatments. *Plants* **2025**, *14*, 3712. [CrossRef] [PubMed]
15. Kong, Y.N.; Liu, C.L.; Li, T.S.; Fang, J.; Liu, G.H. Identification and expression characteristics of the cryptochrome gene family in *Chimonobambusa sichuanensis*. *Plants* **2025**, *14*, 1637. [CrossRef] [PubMed]
16. Qian, Q.; Guo, L.B.; Steven, S.M.; Li, J.Y. Breeding high-yield superior quality hybrid super rice by rational design. *Natl. Sci. Rev.* **2016**, *3*, 283–294. [CrossRef]

Disclaimer/Publisher's Note: The statements, opinions and data contained in all publications are solely those of the individual author(s) and contributor(s) and not of MDPI and/or the editor(s). MDPI and/or the editor(s) disclaim responsibility for any injury to people or property resulting from any ideas, methods, instructions or products referred to in the content.

plants

MDPI

Article

Nanopore Data-Driven Near-T2T Genome Assembly of *Hippophae rhamnoides* ssp. *mongolica* Rousi and Its Complex Annotation

Alexander A. Arkhipov [1,†], Nadezhda L. Bolsheva [1,†], Elena N. Pushkova [1,†], Vladislav V. Babenko [2], Yury A. Zubarev [3], Valentina A. Krasnova [1], Vera L. Kovalenko [1,4], Fedor D. Kostromskoy [1], Elizaveta A. Ivankina [1,4], Ekaterina M. Dvorianinova [1], Nikolai M. Barsukov [1], Daiana A. Krupskaya [1], Elena V. Borkhert [1], Ksenia M. Klimina [2], Alexey A. Dmitriev [1,4] and Nataliya V. Melnikova [1,*]

[1] Engelhardt Institute of Molecular Biology, Russian Academy of Sciences, 119991 Moscow, Russia; arkhipov.aleksandr2.0@gmail.com (A.A.A.); nlbolsheva@mail.ru (N.L.B.); pushkova18@gmail.com (E.N.P.); lakunina.va@gmail.com (V.A.K.); verakovalenko96@gmail.com (V.L.K.); fkostr@gmail.com (F.D.K.); sigova1567@gmail.com (E.A.I.); eugenevarenyuk@gmail.com (E.M.D.); keepter@yandex.ru (N.M.B.); zhernova.d@ya.ru (D.A.K.); sashai@inbox.ru (E.V.B.); alex_245@mail.ru (A.A.D.)
[2] Lopukhin Federal Research and Clinical Center of Physical-Chemical Medicine of Federal Medical Biological Agency, 119435 Moscow, Russia; daniorerio34@gmail.com (V.V.B.); ppp843@yandex.ru (K.M.K.)
[3] Federal Altai Scientific Center of Agrobiotechnologies, 656910 Barnaul, Russia; niilisavenko@yandex.ru
[4] Moscow Center for Advanced Studies, 123592 Moscow, Russia
* Correspondence: mnv-4529264@yandex.ru
† These authors contributed equally to this work.

Abstract

Sea buckthorn (*Hippophae rhamnoides* L.) is a valuable plant whose fruits are rich in biologically active compounds. We sequenced the genome of variety Triumf of *H. rhamnoides* ssp. *mongolica* Rousi on the Oxford Nanopore Technologies (ONT) platform. With the Hifiasm algorithm optimized for ONT data, we assembled the 1.17-Gb genome into eleven complete chromosomes and one chromosome consisting of two contigs, which were scaffolded (Chr3). Eleven of twelve chromosomes had pronounced telomeric repeats at both ends and were assembled as telomere-to-telomere (T2T), and one chromosome (Chr12) had telomeric repeats only at one end. We also sequenced transcriptomes of thirteen Triumf organs/tissues and performed genome annotation using these and previously obtained RNA-Seq data for this variety. As a result, we predicted 25,915 genes and 30,527 transcripts. Repetitive elements comprised 66.9% of the genome size. The obtained near-T2T annotated genome assembly of *H. rhamnoides* ssp. *mongolica* variety Triumf enabled the identification of correct composition and sequences of important gene families in sea buckthorn. We demonstrated this with the *FAT*, *SAD*, and *FAD* gene families involved in fatty acid synthesis. Expression analysis revealed which *FAT*, *SAD*, and *FAD* genes are essential for specific organs/tissues. Thus, the Triumf genome assembly is a crucial tool for basic and applied studies of *H. rhamnoides*.

Keywords: sea buckthorn; *Hippophae rhamnoides*; nanopore sequencing; T2T genome; genome annotation; FAT; SAD; FAD

1. Introduction

Sea buckthorn (*Hippophae rhamnoides* L.) is a dicotyledonous woody oil plant belonging to the Elaeagnaceae family. It grows in the wild across much of Eurasia, from the

Himalayas and Central Asia to Russia and most of Europe [1]. It is cultivated in China, Russia, Romania, Mongolia, and several other countries [1]. Its fruits and leaves contain various biologically active compounds, including essential fatty acids, carotenoids, flavonoids, tocopherols, and vitamins [2,3]. Sea buckthorn extracts exhibit antioxidant, anti-inflammatory, and immunomodulatory properties, as well as protective effects on the nervous and cardiovascular systems [4–7]. Additionally, sea buckthorn is highly adaptive to adverse environmental conditions, such as saline soils and low temperatures, which makes it a promising candidate for protecting against soil erosion, stabilizing sand dunes, and reclaiming land [1,8,9].

Despite the great potential for using of sea buckthorn fruits in food and pharmaceuticals, modern breeding approaches, such as marker-assisted and genomic selection, are not widely used [1]. This issue is likely due to the insufficient genetic research on this plant. Only a few DNA markers have been proposed for the *Hippophae* species. These markers are predominantly associated with the sex of plants (male or female) and frequently work only on specific populations [10–16].

Complete and accurate genome assemblies are essential for many plant studies, including transcriptomic analyses, gene family identification, repetitive element representation estimation, valuable trait DNA marker development, genome editing, and pangenome analysis [17–20]. In recent years, tremendous advances have occurred in third-generation sequencing technologies, providing tools for obtaining continuous chromosome-level plant genome assemblies [21–24]. These advances have enabled high-quality genome assemblies of *H. rhamnoides* and other *Hippophae* species, predominantly obtained using the Pacific Biosciences (PacBio) platform, with the size from 716 to 1453 Mb [25–31]. These assemblies are necessary for the molecular genetic studies of sea buckthorn and for using genetic tools to breed this valuable oil crop. However, the progress of the Oxford Nanopore Technologies (ONT) platform in recent years enabled the assembly of telomere-to-telomere (T2T) genomes [32–35], suggesting that ONT data can be effectively used for genome assembly of sea buckthorn. In addition to genome assembly, most studies require high-quality genome annotation. However, annotation is either unavailable or contains errors for most assembled *H. rhamnoides* genomes [25–27]. For example, errors were found in five genes from the *FAT* (acyl-acyl carrier protein (ACP) thioesterase), *SAD* (Stearoyl-ACP Carrier Protein Desaturase), and *FAD* (Fatty Acid Desaturase) families in the *H. rhamnoides* genome assembly under the ID CNA0022752 in the CNGB database (https://db.cngb.org/, Project ID CNP0001846, accessed on 25 November 2025) [36]. Furthermore, *H. rhamnoides* is characterized by high genetic diversity, and the subspecies *H. rhamnoides* ssp. *mongolica* Rousi and *H. rhamnoides* ssp. *sinensis* Rousi, differ greatly [1]. The present study aimed to obtain the T2T genome assembly of *H. rhamnoides* ssp. *mongolica,* the breeding of which focused on developing high-yielding varieties with large high-oil fruits, and to generate high-quality annotation of this assembly.

2. Results

2.1. De Novo Genome Assembly

DNA sequencing of the variety Triumf of *H. rhamnoides* ssp. *mongolica* on the ONT platform produced 155 Gb of raw reads with an N50 of 31.4 kb. Reads of at least 10 kb with Q10 or higher score (126 Gb in total) were then used for genome assembly with Hifiasm.

The obtained Triumf genome assembly was 1171.9 Mb in length and consisted of 13 contigs. The chromosome number of *H. rhamnoides* is known to be 2n = 24 [37,38]. Therefore, the genome was assembled into eleven complete chromosomes and one chromosome (Chr3) consisting of two contigs. GC content of the Triumf genome assembly was 29.05%.

The assembly had a high BUSCO completeness score of 96.8%, with 85.3% of the BUSCOs being complete and single-copy and 11.5% being complete and duplicated.

An initial genome assembly quality assessment based on the available Illumina whole-genome sequencing (WGS) data for Triumf (25.0 Gb, ~10× coverage for a diploid genome; NCBI SRA PRJNA1177110, SRR32309890) showed a QV score of 28.6 and a high estimated completeness of 99.1%, according to Merqury, with a high Illumina alignment rate of 99.3%. However, the low genome coverage likely limited the reliability of the consensus accuracy estimates (QV score). To further evaluate the assembly's accuracy, we incorporated additional Illumina WGS data from closely related *Hippophae* specimens (SRR32309891 and SRR32309892). Inclusion of the additional data increased the estimated QV score to 45.9, demonstrating the high accuracy of the assembled Triumf genomic sequences. The alignment rates of these data to the Triumf assembly were 99.0% and 98.9%, respectively, indicating minor genomic divergence between the specimens.

2.2. Comparison of Hippophae Genome Assemblies

We compared the obtained genome assembly of *H. rhamnoides* ssp. *mongolica* with the available assemblies of the genus *Hippophae*. The Triumf assembly was longer than genome assemblies of most other *Hippophae* species [25–27,29–31] but shorter than the *H. tibetana* assembly from the study by Wang et al. [28] (Table 1). It is quite possible that there are differences in genome size among different *Hippophae* species. According to the contig N50 parameter, the Triumf assembly was the best among the available genome assemblies of *Hippophae* species (as of 25 November 2025). A comparison of the available sea buckthorn genome assemblies was previously conducted across a wide range of parameters in the study by Chen et al. [31]. However, it is preferable to standardize the methodological approaches used in such an analysis rather than relying on data from individual articles, since the methods for evaluating specific parameters may vary across different articles. For this reason, our study focused on a few significant parameters.

Table 1. Statistics of genome assemblies of the variety Triumf and other *Hippophae* genotypes.

Species, Reference, Assembly Project	Method	Length, Mb	Contig N50, Mb
H. rhamnoides ssp. *mongolica* (variety Triumf), present study	ONT, Hi-C	1171.9	83.7
H. rhamnoides, Ref. [26], CNGB CNP0001846	PacBio, Hi-C	730.5	3.5
H. rhamnoides ssp. *mongolica* × *H. rhamnoides* ssp. *sinensis*, Ref. [27], NCBI PRJNA1003561	ONT, Hi-C	918.6 (752.1) [1]	14.8
H. rhamnoides ssp. *mongolica*, Ref. [25] [2]	PacBio, Hi-C	849.0	2.2
H. tibetana, Ref. [29], NCBI PRJNA1070417	PacBio, Hi-C	957.2	36.4
H. tibetana, Ref. [28], NCBI PRJNA796061, CNGB CNP0003543	PacBio, Hi-C	1452.8	74.3
H. gyantsensis, Ref. [30], NCBI PRJNA997223	ONT, Hi-C	716.3	23.2
H. neurocarpa, Ref. [31]	PacBio, Hi-C	1002.5	24.4

[1] based on the article data [27] and, in brackets, on the NCBI genome assembly GCA_033030585.1 (obtained in the study [27]); [2] the genome assembly is unavailable (http://hipp.shengxin.ren/, accessed on 25 November 2025).

We compared the variety Triumf genome assembly (*H. rhamnoides* ssp. *mongolica*) with the genome assemblies of *H. rhamnoides* ssp. *mongolica* × *H. rhamnoides* ssp. *sinensis* [27] (NCBI, GCA_033030585.1, Figure 1) and *H. rhamnoides* [26] (CNGB, CNA0022752, Figure 2). The *H. rhamnoides* ssp. *mongolica* genome [25] was unavailable for download (http://hipp.shengxin.ren/, accessed on 25 November 2025). The alignment proved that 11 of 12 assembled contigs represented whole chromosomes, and the remaining two contigs were scaffolded in Chr3. The regions of the Triumf genome assembly that made it longer than the other two available *H. rhamnoides* assemblies were predominantly located in the likely centromeric and pericentric regions of chromosomes, where repeated sequences are usually

found. The greatest differences in length were characteristic of Chr1, Chr2, Chr3, Chr4, and Chr8.

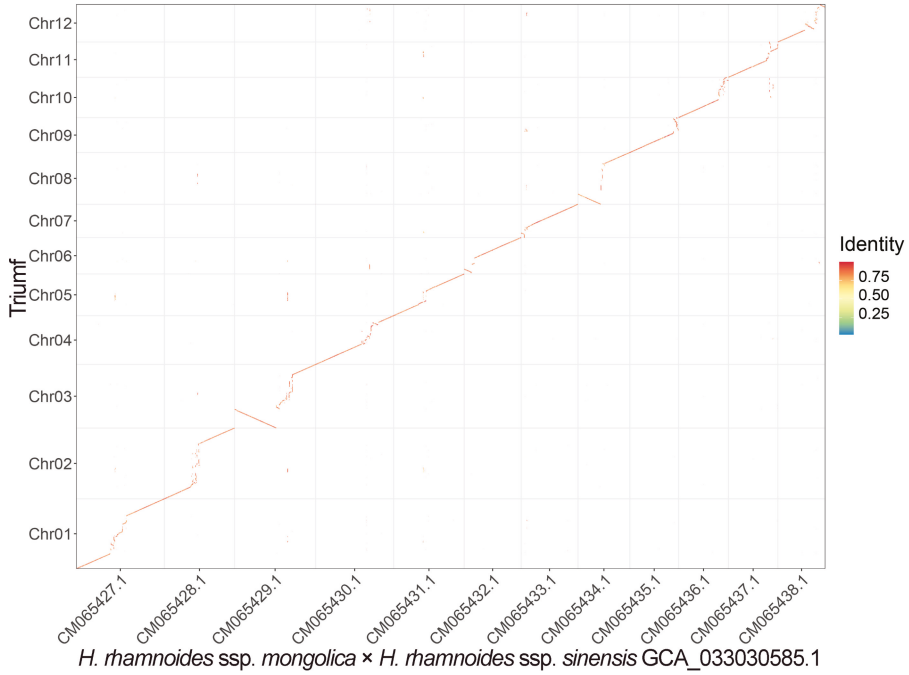

Figure 1. Global alignment of the genome assemblies of *H. rhamnoides* variety Triumf (Y axis) and *H. rhamnoides* ssp. *mongolica* × *H. rhamnoides* ssp. *sinensis* genotype [27], NCBI, GCA_033030585.1 (X axis).

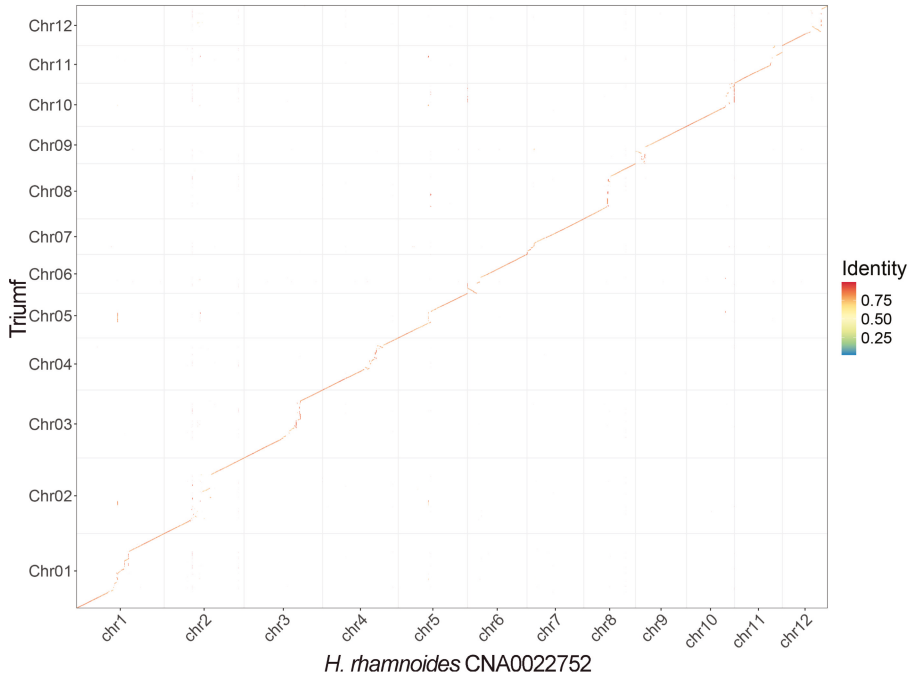

Figure 2. Global alignment of the genome assemblies of *H. rhamnoides* variety Triumf (Y axis) and another *H. rhamnoides* genotype [26], CNGB, CNA0022752 (X axis).

We also compared the genome assembly of Triumf with those of *H. tibetana* [29] (NCBI, GCA_037013495.1) and *H. gyantsensis* [30] (NCBI, GCA_030763125.1) (Supplementary Figure S1). Similar to the comparison with *H. rhamnoides* genome assemblies, the main differences were present in the likely centromeric and pericentric regions of chromosomes.

https://doi.org/10.3390/plants15111726

However, we also observed more noise—mapping of small fragments to other parts of the assemblies. This is likely because of the significant genetic differences between the species being compared.

In the Triumf genome assembly, eleven chromosomes had pronounced telomeric repeats at both ends and were assembled as T2T; one chromosome (Chr12) had telomeres only at one end (Figure 3). This result supported the high quality of the Triumf genome assembly. We also analyzed the presence of telomeric repeats in other available sea buckthorn genome assemblies (Supplementary Figure S2). The absence of telomeric repeats at the ends of chromosomes or their mislocation were very common. This may indicate incomplete or erroneous assemblies.

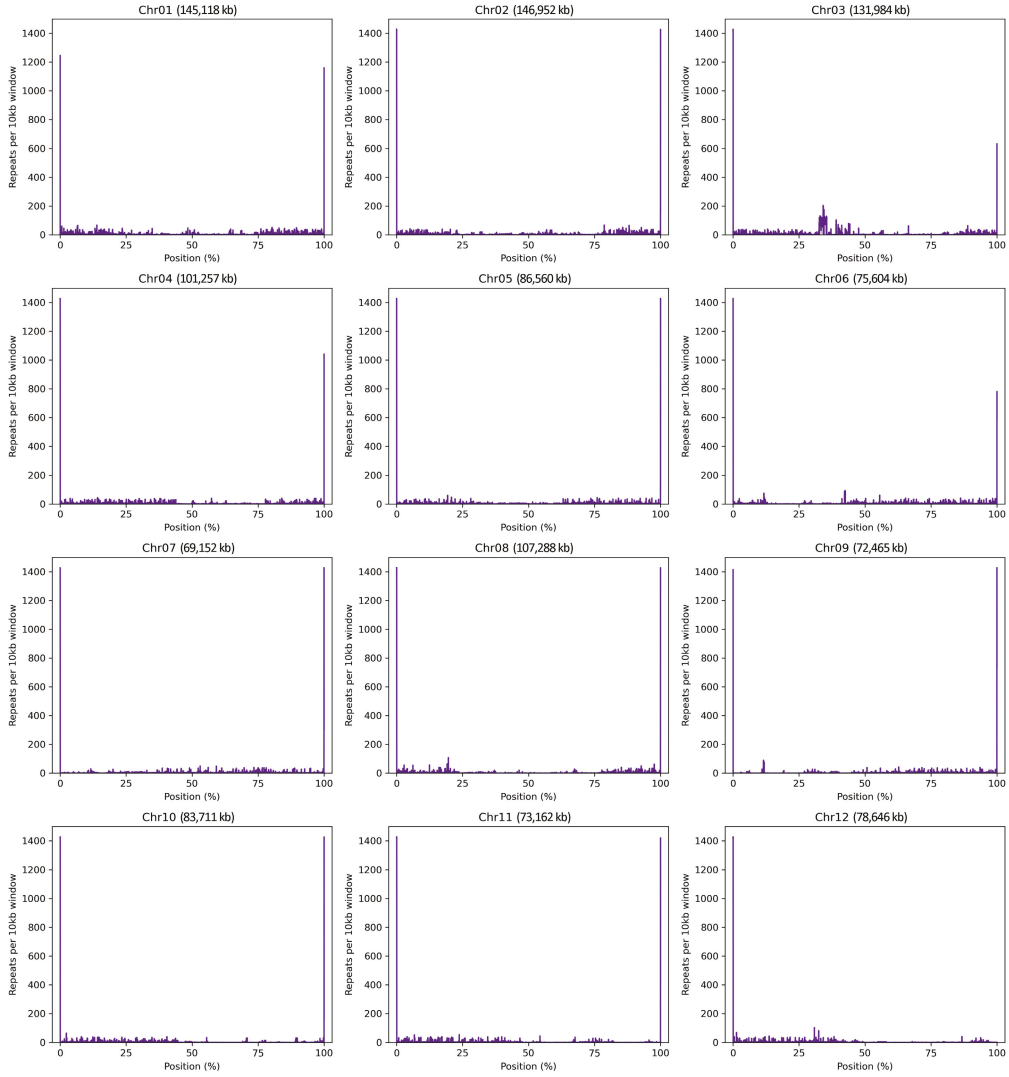

Figure 3. Density of telomeric repeats in the variety Triumf genome assembly. High peaks at both ends of eleven chromosomes and at one end of Chr12 can be seen. Chromosome size is indicated for each chromosome in brackets.

We also generated 110.9 Gb of Hi-C genomic data (95× genome coverage) for the variety Triumf and constructed a Hi-C interaction heatmap (Figure 4). The interaction heatmap revealed no significant contacts outside the main diagonal, confirming the accuracy of the obtained genome assembly. Regions with low coverage were associated with low presence of restriction site for the DpnII enzyme (GATC; Supplementary Figure S3), which was used to prepare the Hi-C library.

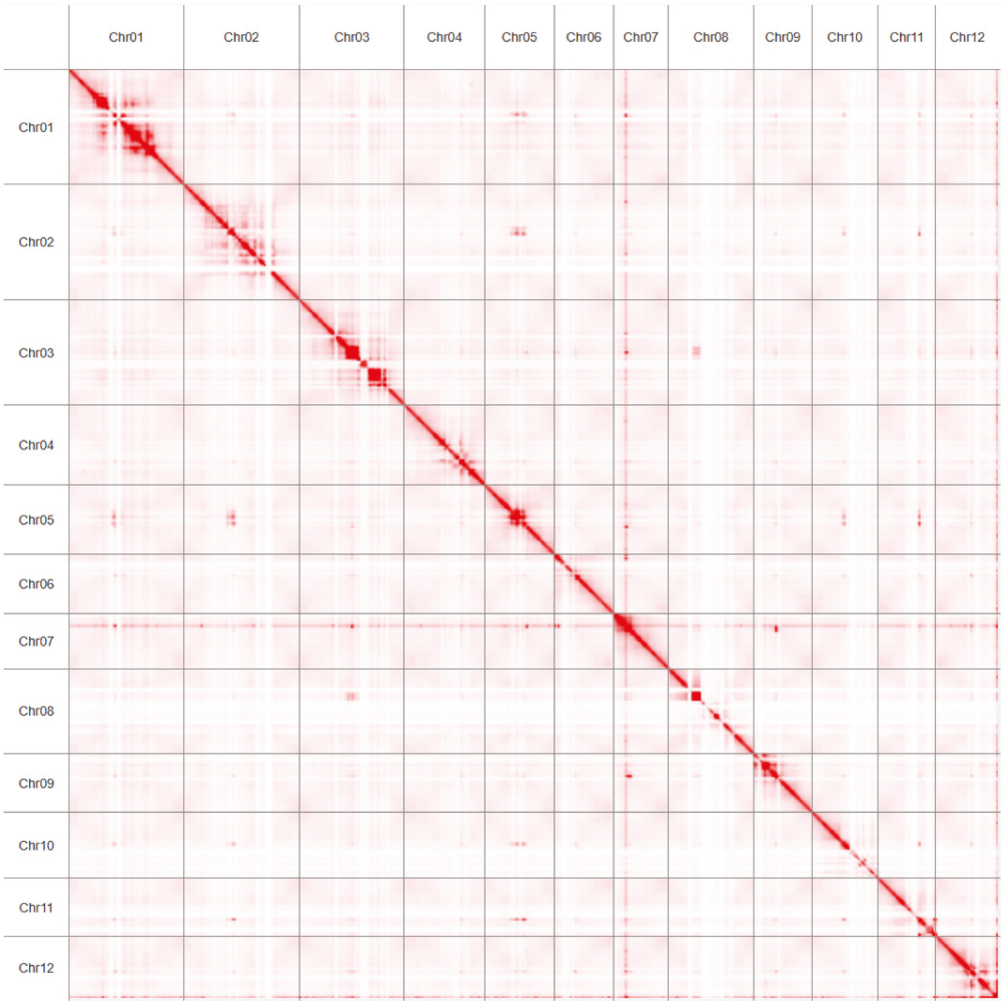

Figure 4. Hi-C interaction heatmap for the variety Triumf genome assembly. The frequencies of Hi-C contacts on chromosomes are presented by colors, varied from white (low) to red (high). All multiple alignments of Hi-C reads were preserved.

2.3. Annotation of the Variety Triumf Genome Assembly

A total of 2,259,619 repetitive elements were annotated, with a combined length of about 793.5 Mb, accounting for 66.9% of the assembly length. Retrotransposons comprised 41.5% of the length, DNA transposons accounted for 1.6%, and 21.8% of the assembly consisted of unclassified repetitive elements.

Among transposable elements, long terminal repeat elements presented 40.1% of the assembly length, with the Copia and Gypsy repeat families comprising 15.4% and 14.4%, respectively.

We predicted 25,915 genes and 30,527 transcripts in the obtained genome assembly using transcriptomic data generated in the present study for 13 different organs/tissues of the variety Triumf in two-fold replication (on average, 2.6 million reads per sample): roots, wood, bark, bud scales, early buds, middle buds, late buds, whole leaves, leaf bases, leaf apices, leaf margins, leaf midribs, and pistils. We also used transcriptomic data previously obtained by us for fruit seeds and pulp at four development stages of the same variety (NCBI SRA, PRJNA1163394, SRR35247990–SRR35247993, SRR35247995–SRR35247998) [39]. A Circos plot was drawn based on the GC content, gene and repeat density of the Triumf genome assembly, as well as chromosome synteny (Figure 5).

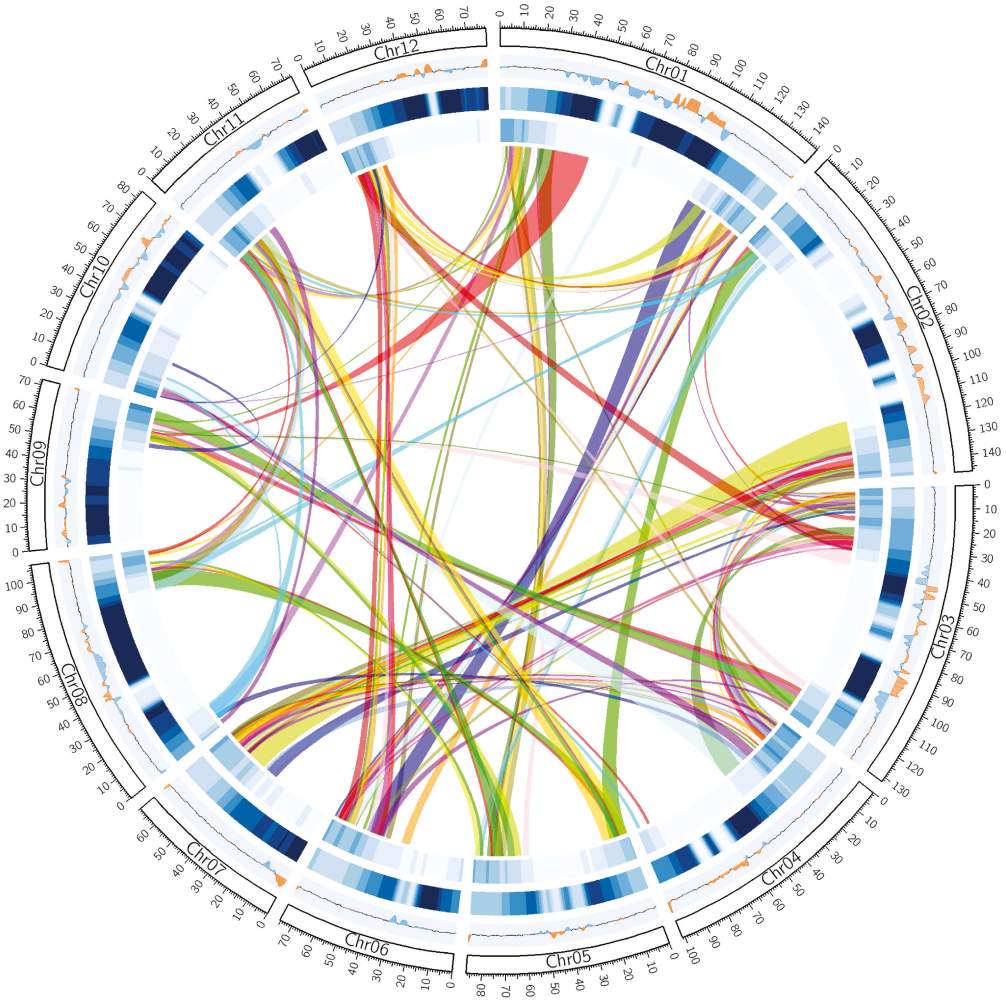

Figure 5. Features of the Triumf genome assembly, shown from the outside inward: chromosome assembly, GC content, repeat density, gene density, and intragenomic synteny (colored lines).

2.4. Identification and Characterization of the FAT Genes of H. rhamnoides

In our previous study, we demonstrated that *FATB* (*Hiprha1gene28610*), *SAD* (*Hiprha1gene18766*), *FAD2* (*Hiprha1gene21624*), *FAD2* (*Hiprha1gene12459*), and *FAD3* (*Hiprha1gene24146*) genes identified using the *H. rhamnoides* CNA0022752 annotated genome assembly (CNGB, Project ID CNP0001846) contained errors [36]. Therefore, we identified genes of the *FAT*, *SAD*, and *FAD* families in the Triumf genome assembly and compared them with genes of these families identified in the CNA0022752 genome assembly.

The AtFATA1 (AT3G25110.1), AtFATA2 (AT4G13050.1), and AtFATB (AT1G08510.1) proteins were initially identified using the TAIR database (https://www.arabidopsis.org/, TAIR, accessed on 25 November 2025) by searching with the "FATA", "FATB", "AtFATA", and "AtFATB" keywords. A further BLASTP search was performed against representative *Arabidopsis thaliana* protein models to identify potential close homologs. A BLASTP search was then performed against the annotated genome assemblies of variety Triumf and genotype CNA0022752. The candidates found were filtered based on minimum identity (30%) to the reference sequences, as well as a set of conserved domains and gene exon-intron structure.

Two *FATA* genes and five *FATB* genes (named *Triumf.gene.xxx*) were identified in the Triumf genome assembly. Two *FATA* genes and six *FATB* genes (named *Hiprha.gene.xxx*) were identified in the CNA0022752 genome assembly. Phylogenetic analysis (Figure 6a) revealed the correspondence of the following genes in the *H. rhamnoides* genome assemblies:

FATA:

1. *Triumf.gene.5781—Hiprha.gene.14109*
2. *Triumf.gene.20369—Hiprha.gene.14745*

FATB:

1. *Triumf.gene.11138—Hiprha.gene.17924*
2. *Triumf.gene.18341—Hiprha.gene.07959 and Hiprha.gene.24276*
3. *Triumf.gene.22547—Hiprha.gene.28610*
4. *Triumf.gene.816—Hiprha.gene.18201*
5. *Triumf.gene.12395—Hiprha.gene.03360*

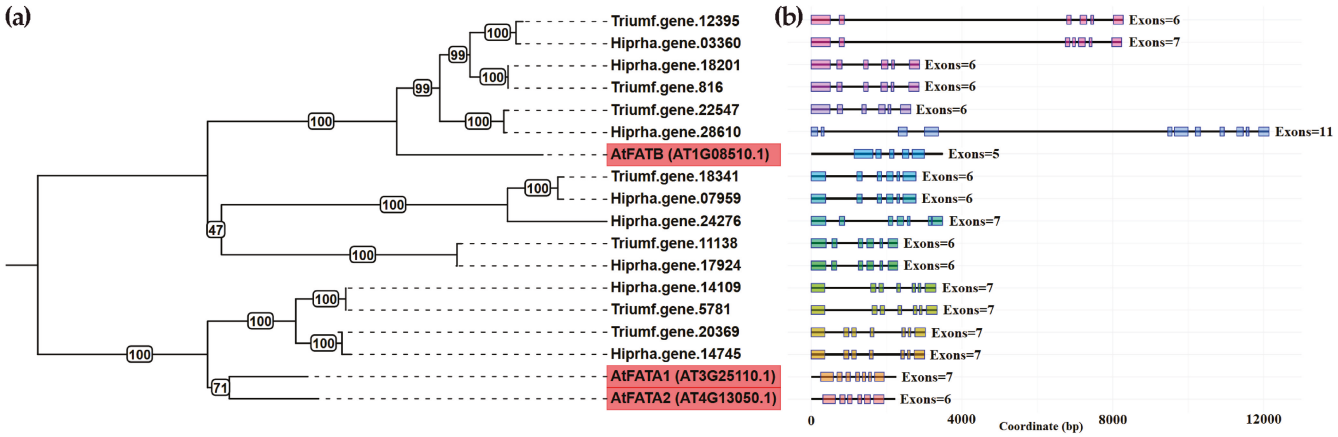

Figure 6. Analysis of the *FATA* and *FATB* genes of *H. rhamnoides*. (**a**) Dendrogram of the FATA and FATB proteins. Constructed using the Neighbor-Joining (NJ) method with a bootstrap value of 1000 and rerooted at midpoint. The proteins of the reference species *A. thaliana* (At…, highlighted in red) and their homologs identified in two annotated genome assemblies of *H. rhamnoides* are shown: Hiprha.gene.xxx—the CNA0022752 genome assembly (CNGB), Triumf.gene.xxx—the Triumf genome assembly obtained in the present study. (**b**) Exon-intron structures of the *FATA* and *FATB* genes. UTRs were not predicted for genes from the *H. rhamnoides* genome assemblies. The *Hiprha.gene.03360*, *Hiprha.gene.28610*, and *Hiprha.gene.24276* genes likely contain errors.

Several differences were identified in the *FAT* genes between the two sea buckthorn genome assemblies. For example, the *Hiprha.gene.28610* gene (the CNA0022752 assembly) had 11 exons, though the expected number was 5–6 (Figure 6b). This discrepancy suggested an error in the assembly and subsequent annotation. The corresponding gene in the Triumf genome assembly (*Triumf.gene.22547*) had six exons. Additionally, *Hiprha.gene.03360* (the CNA0022752 assembly) contained seven exons instead of the expected six (Figure 6b). Upon analyzing the conserved domain structure characteristic of this gene family, we discovered that the Acyl-ACP_TE domain was truncated in the region corresponding to the additional exons (Supplementary Figure S4). This suggested a local assembly and annotation error in the CNA0022752 genome assembly. In contrast, the corresponding gene in the Triumf assembly (*Triumf.gene.12395*) contained six exons and a complete set of the expected conserved domains. Furthermore, *Hiprha.gene.24276* (the CNA0022752 assembly) contained seven exons instead of the expected six (Figure 6b). It is likely that a large exon region was split into two separate fragments. Further analysis of this gene domain structure revealed a significantly shortened Acyl-ACP_TE_C domain (Supplementary Figure S4), suggesting an assembly and annotation error. This gene has no complete analog in the Triumf genome assembly; its origin is unclear. It may be a chimera resulting from an assembly error in the CNA0022752 genome. Thus, the Triumf genome assembly enabled correction of the *FAT* gene family sequences.

2.5. Identification and Characterization of the SAD Genes of H. rhamnoides

AtSAD1 (AT5G16240.1), AtSAD2 (AT3G02610.2), AtSAD3 (AT5G16230.1), AtSAD4 (AT3G02620.2), AtSAD5 (AT3G02630.1), AtSAD6 (AT1G43800.1), and AtFAB2 (AT2G43710.1) were initially identified using the TAIR database (https://www.arabidopsis.org/, TAIR, accessed on 25 November 2025) using the "stearoyl-ACP desaturase" keyword and a BLASTP search against the representative *A. thaliana* protein models to identify potential closely related genes.

After filtration, eight *SAD* genes were identified in both the Triumf and CNA0022752 genome assemblies. Phylogenic analysis of the SAD family (Figure 7a) revealed the correspondence of the following genes in the *H. rhamnoides* assemblies:

1. *Triumf.gene.18878—Hiprha.gene.23875*
2. *Triumf.gene.23889—Hiprha.gene.18830*
3. *Triumf.gene.23278—Hiprha.gene.26748*
4. *Triumf.gene.12901—Hiprha.gene.07832*
5. *Triumf.gene.55—Hiprha.gene.28095*
6. *Triumf.gene.23887—Triumf.gene.23888—Triumf.gene.23886—Hiprha.gene.18803—Hiprha.gene.21192—Hiprha.gene.18766*

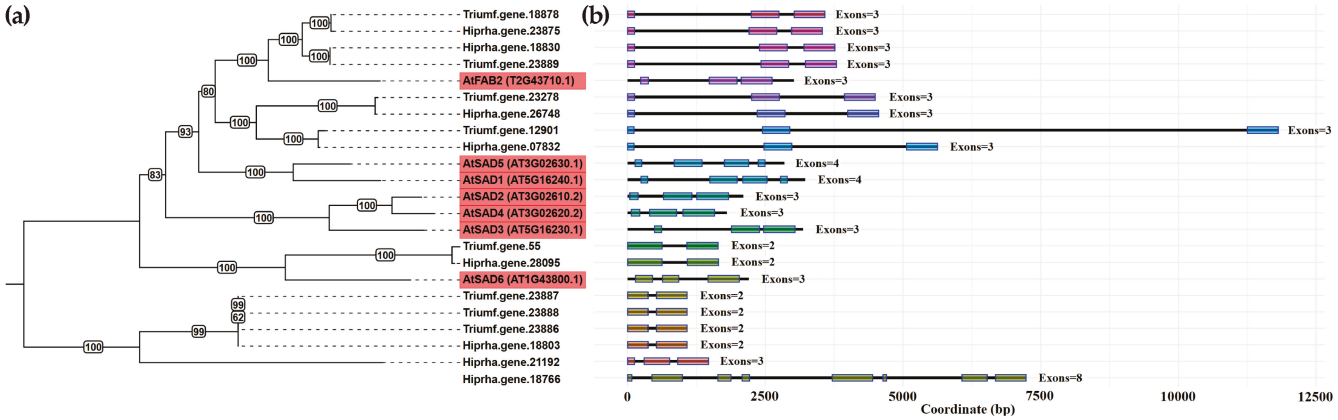

Figure 7. Analysis of the *SAD* genes. (**a**) Dendrogram of the SAD proteins. Constructed using the Neighbor-Joining (NJ) method with a bootstrap value of 1000 and rerooted at midpoint. The proteins of the reference species *A. thaliana* (At. . ., highlighted in red) and their homologs identified in two annotated genome assemblies of *H. rhamnoides* are shown: Hiprha.gene.xxx—the CNA0022752 genome assembly (CNGB), Triumf.gene.xxx—the Triumf genome assembly obtained in the present study. The chimeric protein Hiprha.gene.18766 was excluded from the dendrogram, as it negatively impacted genomic distance calculations. (**b**) Exon-intron structures of the *SAD* genes. UTRs were not predicted for genes from the *H. rhamnoides* genome assemblies. The *Hiprha.gene.18766* gene likely contains errors.

A number of differences between the *SAD* genes of the annotated *H. rhamnoides* genome assemblies were identified. *Hiprha.gene.18766* contained excessive exons (Figure 7b) and atypical conserved domains (Supplementary Figure S4), resulting from the erroneous merging of two gene models in the CNA0022752 assembly annotation, which led to a chimeric sequence.

2.6. Identification and Characterization of the FAD Genes of H. rhamnoides

The AtFAD2 (AT3G12120.1), AtFAD3 (AT2G29980.1), AtFAD4 (AT4G27030.1), AtFAD5 (AT3G15850.1), AtFAD6 (AT4G30950.1), AtFAD7 (AT3G11170.1), and AtFAD8 (AT5G05580.1) were initially identified using the TAIR database (https://www.arabidopsis.org/, TAIR, accessed on 25 November 2025) by searching with the "FAD", "AtFAD", and "fatty acid

desaturase" keywords. A further BLASTP search was performed against representative *A. thaliana* protein models to identify potential close homologs of these genes.

After filtration, thirteen *FAD* genes were identified in the Triumf genome assembly and fifteen *FAD* genes in the CNA0022752 genome assembly. Phylogenic analysis of the FAD family (Figure 8a) revealed the correspondence of the following genes in the *H. rhamnoides* assemblies:

FAD2:

1. *Triumf.gene.2346—Hiprha.gene.21624*
2. *Triumf.gene.9854—Hiprha.gene.12459*
3. *Triumf.gene.21232—Hiprha.gene.27005*

FAD3:

1. *Triumf.gene.13247—Hiprha.gene.07426*
2. *Triumf.gene.5224—Hiprha.gene.24879*
3. *Triumf.gene.18644—Hiprha.gene.05528*
4. *Hiprha.gene.10700* and *Hiprha.gene.24146* did not have equivalents in the Triumf genome assembly

FAD4:

1. *Triumf.gene.16794—Hiprha.gene.21782*

FAD5:

1. *Triumf.gene.14976—Hiprha.gene.00542*
2. *Triumf.gene.1641—Hiprha.gene.18847*

FAD6:

1. *Triumf.gene.7715—Hiprha.gene.25786*

FAD7/8:

1. *Triumf.gene.24628—Hiprha.gene.02511*
2. *Triumf.gene.15893—Hiprha.gene.07747*
3. *Triumf.gene.8761—Hiprha.gene.17598*

A number of differences in the *FAD* family genes between the annotated *H. rhamnoides* genome assemblies were also identified. In the Triumf assembly, only three *FAD3* genes were identified, compared to five in the CNA0022752 genome assembly. The additional genes, *Hiprha.gene.10700* and *Hiprha.gene.24146*, contained truncated conserved domain structures (Supplementary Figure S4). Furthermore, *Hiprha.gene.24146* contained an atypically long intron sequence (Figure 8b), which may have resulted from either an assembly or annotation error.

Hiprha.gene.07747 contained only seven exons instead of the expected eight (Figure 8b). Further inspection of the alignments of obtained RNA-Seq reads determined this to be an annotation error in the CNA0022752 genome assembly (Supplementary Figure S5). Both seven-exon and eight-exon variants of the corresponding *Triumf.gene.15893* gene are present in the Triumf annotation.

A single exon of *Hiprha.gene.12459* was incorrectly split into two parts, while *Hiprha.gene.21624* contained a short additional exon sequence (Figure 8b). These exon-intron structures were not supported by the RNA-Seq read alignment analysis and therefore attributed to annotation errors (Supplementary Figures S6 and S7).

The location of *FAT*, *SAD*, and *FAD* genes on twelve chromosomes of the Triumf genome assembly is presented in Supplementary Figure S8.

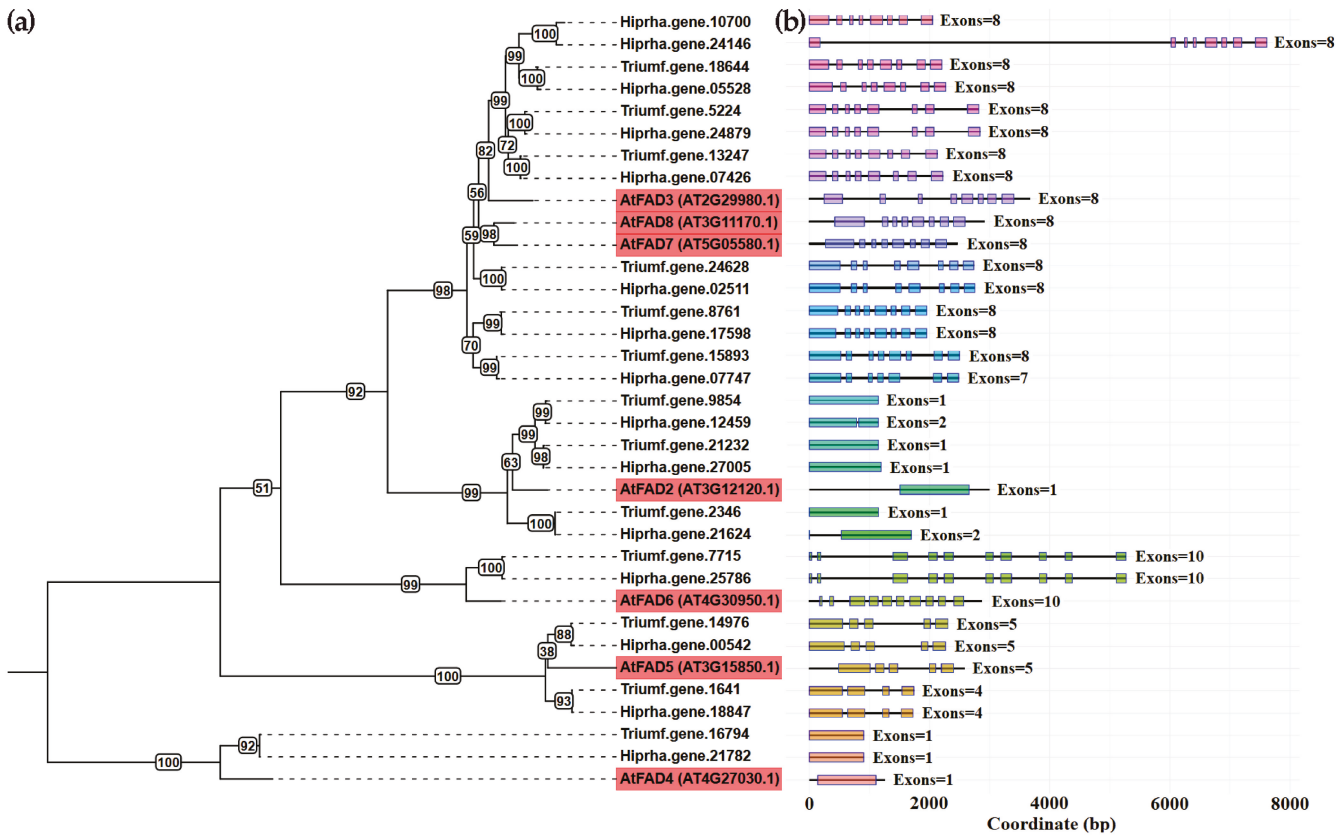

Figure 8. Analysis of the *FAD* genes. (**a**) Dendrogram of the FAD proteins. Constructed using the Neighbor-Joining (NJ) method with a bootstrap value of 1000 and rerooted at midpoint. The proteins of the reference species *A. thaliana* (At. . ., highlighted in red) and their homologs identified in two annotated genome assemblies of *H. rhamnoides* are shown: Hiprha.gene.xxx—the CNA0022752 genome assembly (CNGB), Triumf.gene.xxx—the Triumf genome assembly obtained in the present study. (**b**) Exon-intron structures of the *FAD* genes. UTRs were not predicted for genes from the *H. rhamnoides* genome assemblies. The *Hiprha.gene.10700*, *Hiprha.gene.24146*, *Hiprha.gene.07747*, *Hiprha.gene.12459*, and *Hiprha.gene.21624* likely contain errors.

2.7. Expression Analysis of FAT, SAD, and FAD Genes

We also analyzed expression levels of the identified *FAT*, *SAD*, and *FAD* family genes in 34 samples of sea buckthorn variety Triumf as read counts per million reads (CPM), calculated based on the transcriptomic data obtained in this study for 13 different organs/tissues (roots, wood, bark, buds, bud scales, leaves, and pistils), as well as our previously obtained transcriptomic data from the NCBI database (PRJNA1163394) for fruit seeds and pulp (Supplementary Table S1). Certain genes exhibited the highest levels of expression in specific organs/tissues at particular stages of development. For instance, *FATA* (*Triumf.gene.5781* and *Triumf.gene.20369*), *SAD* (*Triumf.gene.18878*, *Triumf.gene.23889*, *Triumf.gene.23278*, *Triumf.gene.12901*, and *Triumf.gene.55*), and *FAD2* (*Triumf.gene.2346*) had high expression levels in seeds and pulp of sea buckthorn fruits. These genes are likely involved in the synthesis of fatty acids in the fruits. Some genes, including *FATB* (*Triumf.gene.12395*), exhibited moderate expression in all of the studied organs/tissues. These genes are likely to be involved in processes occurring in most sea buckthorn plant cells. We also identified genes that were virtually unexpressed in the studied samples, including *FATB* (*Triumf.gene.18341*) and *SAD* (*Triumf.gene.23888*, *Triumf.gene.23887*, and *Triumf.gene.23886*). These genes may only function under specific conditions, such as stress. Alternatively, they may not be expressed at all in sea buckthorn plants. This issue requires further study.

3. Discussion

We obtained a near-T2T genome assembly of the variety Triumf of *H. rhamnoides* ssp. *mongolica* using ONT sequencing and the Hifiasm genome assembler optimized for ONT data. The assembly consisted of 13 contigs—eleven complete chromosomes and one chromosome in two parts, which were then scaffolded.

The Triumf genome assembly was longer than previous *H. rhamnoides* assemblies [25–27]: 1171.9 Mb versus 730.5, 752.1, and 849.0 Mb. Comparison of the genome assembly of Triumf with those of other available *Hippophae* species revealed that the main differences were associated with the centromeric and pericentric regions of chromosomes. The PacBio reads, predominantly used to assemble the *Hippophae* genomes [25,26,28], were shorter than the ONT reads [40]. The shorter read length could result in problems when assembling extended genomic regions rich in repetitive sequences [41]. Therefore, the centromeric and pericentric regions, which contain repeats [42,43], may be underrepresented in *Hippophae* genomes initially assembled using only PacBio reads and then scaffolded with Hi-C data. To assemble the *Hippophae* genomes from ONT reads, NextPolish [30] and NextDenovo [27] algorithms were used. However, as of 25 August 2025, ONT recommends using the Hifiasm (ONT) algorithm to obtain near-T2T genome assemblies from standard ONT Simplex reads based on a recent study [32] (https://nanoporetech.com/news/breakthrough-algorithm-enables-partially-phased-near-telomere-to-telomere-assembly-using-standard-oxford-nanopore-simplex-reads, accessed on 25 November 2025). For the variety Triumf genome assembly, we used Hifiasm (ONT) and obtained excellent results. Furthermore, we generated ONT reads with a high N50 parameter (31.4 kb), and a significant proportion of reads exceeded 50 kb. This could positively impact the quality of the obtained assembly. Therefore, the variety Triumf assembly may contain repeated regions of the genome that were not assembled in previous *H. rhamnoides* studies, surpassing previous assemblies in completeness. We also obtained Hi-C reads, and the contact map confirmed the accuracy of the Triumf genome assembly.

The analysis of telomeric repeats, which are located at the ends of chromosomes, also supported the high quality of the variety Triumf genome assembly. Eleven of the twelve chromosomes had telomeres at both ends, and one chromosome had a telomere at one end. In contrast, analysis of other *Hippophae* genome assemblies revealed errors in the location of telomeric repeats (i.e., within the chromosomes rather than at their ends) or their near absence. This discrepancy may be because of the initial incompleteness of the genome assemblies followed by merging contigs into scaffolds using Hi-C data.

Analyzing the *FAT*, *SAD*, and *FAD* gene families in the annotated Triumf genome assembly allowed us to obtain the correct sequences of genes of these families, which had errors in the annotated CNA0022752 genome assembly, the only available annotated genome assembly of *H. rhamnoides* as of 25 November 2025 (CNGB, Project ID CNP0001846). The *FAT* family analysis suggested that the *Hiprha.gene.24276* gene in the CNA0022752 assembly is potentially a chimera gene that is actually absent. Among the *SAD* genes, *Hiprha.gene.18766* in the CNA0022752 assembly had an atypical structure that probably resulted from the erroneous merging of two gene models. This problem was not presented in the Triumf genome assembly. A significant number of errors were revealed in the *FAD* genes of the CNA0022752 assembly. There were wrong additional *FAD* genes with truncated conserved domains. Additionally, lack of exons, incorrect additional exons, and erroneous split of one exon into two parts were revealed for *FAD* genes in the CNA0022752 annotation compared to the Triumf annotation and confirmed by the analysis of transcriptomic data. To annotate the Triumf genome assembly, we used a representative set of transcriptomic data, including data obtained for fruits in which fatty acid synthesis actively occurred. To annotate the CNA0022752 assembly, fewer transcriptomic samples were used, and no fruits were analyzed that could decrease the annotation results for the *FAT*, *SAD*, and

FAD genes. Additionally, other tools were used to annotate the CNA0022752 assembly in comparison with the Triumf assembly. This may have also contributed to the differences in the annotations. *FAT* genes play an essential role in fatty acid biosynthesis by hydrolyzing acyl-ACP complexes to release free fatty acids in plastids [44]. *SAD* genes are essential for converting of saturated fatty acids into monounsaturated ones [45], while *FAD* genes play a key role in the synthesis of polyunsaturated fatty acids [46,47]. To comprehend the process of fatty acid biosynthesis in sea buckthorn fruits during ripening, it is essential to determine the precise sequences of the *FAT*, *SAD*, and *FAD* genes.

T2T genomes are becoming the new standard for genome assemblies, not only for model organisms but also for a wide range of plant species. T2T genomes provide insights into genome organization and function, distribution of repetitive elements, polyploid features and evolution, genetic diversity, and host–pathogen interactions [18,48–55].

We obtained a near-T2T genome of *H. rhamnoides* ssp. *mongolica* variety Triumf using only ONT sequencing data. It became possible due to significant advancements in ONT technology and genome assembly tools. As of 20 April 2026, the Triumf assembly is a reference for *H. rhamnoides* in the NCBI Genome database (GCA_056149425.1). The variety Triumf was created as a part of the Russian breeding program and differs from the *H. rhamnoides* genotypes used in previous genome assembly studies. The Triumf genome can be useful for identifying differences between genetically distant genotypes at the whole-genome level. Furthermore, Triumf is a high-quality fruit variety, and its genome can be valuable for identifying gene variants that determine important characteristics of sea buckthorn fruits for food and pharmaceutical applications. The variety Triumf genome also provides a solid foundation for studying particular gene families, including their representation and structure. It is an essential tool for various basic and applied studies, as well as genome editing of *H. rhamnoides*.

4. Materials and Methods

4.1. DNA Extraction and ONT Sequencing

The variety Triumf was selected for the study. It is characterized by high yields and large, cylindrical, red fruits with dense flesh, firm skin, and high carotenoid content.

Nuclei isolation was performed using the LN2 plant tissue protocol (https://www.pacb.com/wp-content/uploads/Procedure-checklist-Isolating-nuclei-from-plant-tissue-using-LN2-disruption.pdf, accessed on 25 November 2025) with some modifications. Young sea buckthorn leaves weighing 0.5 g were frozen in liquid nitrogen and ground in a mortar for 20 min. The resulting powder was transferred to 25 mL of ice-cold NIB buffer consisting of 1× HB buffer (10 mM Tris pH 9.4 (Diaem, Moscow, Russia), 80 mM KCl (Helicon, Moscow, Russia), and 10 mM EDTA (Diaem)), supplemented with 0.5 M sucrose (Merck, Rahway, NJ, USA), 1% Triton X-100 (Diaem), 1% β-mercaptoethanol (NeoFroxx, Einhausen, Germany), 2% PVP K30 (CDH, New Delhi, India), and 100 mM spermine and spermidine (Sigma-Aldrich, St. Louis, MO, USA). The suspension was placed on ice and stirred on a rocker at 100 rpm for 15–20 min. Then, it was centrifuged at 3000× *g* and 4 °C for 20 min. The supernatant was carefully removed, and the precipitate was resuspended in 4 mL of a 36% iodixanol solution (Sigma-Aldrich) in 1× HB buffer. The solution was then centrifuged for 30 min at 5000× *g* and 4 °C. The upper phase was transferred to a new tube and resuspended in 12.5 mL of NIB buffer. The tube was then centrifuged for 10 min at 3000× *g* and 4 °C. The supernatant was then removed. Washing in NIB buffer was repeated one more time. The resulting precipitate was washed with 1 mL of HB buffer and centrifuged for 10 min at 3000× *g* and 4 °C.

To lyse the nuclei, the precipitate was transferred to 1 mL of Carlson buffer prewarmed to 65 °C containing 100 mM Tris-HCl, pH 9.5 (Diaem), 2% CTAB (Helicon), 1.4 M NaCl (Diaem), 1% PEG-8000 (PanReac AppliChem, Darmstadt, Germany), 20 mM EDTA (Diaem),

3 µL β-mercaptoethanol (NeoFroxx), 1% PVP K30 (CDH), and 4 µL RNase A (100 mg/mL; 7000 units/mL; Qiagen, Chatsworth, MD, USA). The mixture was incubated at 65 °C for one hour then cooled to room temperature. Then, an equal volume of chloroform (Diaem) was added to the homogenate. The tube was gently inverted ten times until a homogeneous emulsion formed. The mixture was then centrifuged for 5 min at 3000× *g* and 4 °C. The aqueous phase was carefully transferred to a new tube, and the chloroform extraction procedure was repeated.

DNA was precipitated from the aqueous phase with 0.7 volumes of isopropanol (VWR Chemicals, Radnor, PA, USA). The tube was then centrifuged for 5 min at 3000× *g* and 4 °C. The supernatant was subsequently removed. The DNA was air-dried for 2 min, dissolved in 2 mL of G-buffer (Blood & Cell Culture DNA Mini Kit, Qiagen), and 25 µL of proteinase K (>600 mU/mL; Qiagen) was added. The mixture was incubated at 56 °C overnight. Then, the DNA was purified using Blood & Cell Culture DNA Mini Kit columns (Qiagen) according to the manufacturer's protocol.

The quality and concentration of the DNA were assessed using a NanoDrop 2000C spectrophotometer (Thermo Fisher Scientific, Waltham, MA, USA) and a Qubit 4.0 fluorometer (Thermo Fisher Scientific). Similarity of the DNA concentration values obtained by the two methods served as an additional criterion for sample purity. The sizes of the isolated DNA fragments were evaluated by electrophoresis in a 0.8% agarose gel.

The SQK-LSK114 kit (Oxford Nanopore Technologies, Oxford, UK) was used to prepare the DNA library for ONT sequencing. Genome sequencing was performed using a PromethION (Oxford Nanopore Technologies) with two R10.4.1 flow cells (Oxford Nanopore Technologies).

4.2. Construction and Sequencing of Hi-C Library

Vacuum infiltration with formaldehyde was used to fix the chromatin. Next, nuclei were isolated from the fixed leaves as described above. At the final stage, the resulting precipitate was washed with PBS. According to the optimized protocol [56], the following steps were performed: restriction with DpnII (New England Biolabs, Ipswich, MA, USA); biotin labeling with Biotin-15-dCTP (Biosan, Novosibirsk, Russia); and subsequent ligation of DNA fragments with T4 DNA ligase (New England Biolabs). The DNA was then isolated using phenol-chloroform extraction. Additionally, DNA purification was performed using MagicPure DNA beads (TransGen, Beijing, China). Biotin was then removed from the unligated ends of the DNA fragments. The Hi-C library was prepared using the Qiaseq FX DNA kit (Qiagen) up to the amplification step. Next, Streptavidin Magnetic Beads (New England Biolabs) were used to enrich the biotinylated fragments. Finally, the obtained Hi-C library was amplified. The quality of the library was assessed using a 2100 Bioanalyzer (Agilent Technologies, Santa Clara, CA, USA), and the concentration was measured with a Qubit 4.0 fluorometer (Thermo Fisher Scientific). Sequencing was performed on a NovaSeq X Plus instrument (Illumina, San Diego, CA, USA) with 150 + 150 nucleotide reads.

4.3. Transcriptome Sequencing

For the transcriptomic analysis, plant material was collected for the sea buckthorn variety Triumf. The cuttings, which were collected at the Federal Altai Scientific Center of Agrobiotechnologies (Barnaul, Russia), were cut into pieces that were 13–15 cm long and placed in containers with an indolebutyric acid solution. After 24 h, the cuttings were transferred to containers with water. The water was changed daily, and samples were taken at necessary points as the plants grew. The samples included roots, wood, bark, bud scales (from dormant buds), early buds (beginning of swelling), middle buds (swollen/unfolding buds), and late buds (fully opened buds), leaves (whole and separated into bases, apices,

margins, and midribs), and pistils. The plant material was collected in 1.5 mL tubes (at least three samples for each organ/tissue), immediately frozen in liquid nitrogen, and stored in a freezer at −70 °C until RNA extraction. Thirteen pools of samples were subjected to further transcriptomic studies in twofold replicates.

Before RNA extraction, the samples were ground in 1.5 mL tubes in liquid nitrogen using disposable homogenization pestles attached to a DCD701D2 cordless drill/driver (DEWALT, Towson, MD, USA) to a fine powder to prevent thawing. RNA extraction was performed based on a modified CTAB buffer protocol [57]. Total RNA was then purified using a CleanRNA kit (Evrogen, Moscow, Russia), following the manufacturer's protocol and including a DNase I treatment step. RNA quality and concentration were assessed using horizontal agarose gel electrophoresis and a Qubit 4.0 fluorometer (Thermo Fisher Scientific). To prepare the cDNA libraries, we used the MagicPure mRNA Kit (TransGen), TransNGS Fast RNA-Seq Library Prep Kit for Illumina (TransGen), and MagicPure Size Selection DNA Beads (TransGen) in accordance with the manufacturer's protocols. We assessed the quality of the resulting cDNA libraries using the Qsep1-Plus capillary electrophoresis system (BiOptic, New Taipei City, Taiwan) and horizontal electrophoresis in a 2% agarose gel. The concentration of the libraries was determined using a Qubit 4.0 fluorometer (Thermo Fisher Scientific). The cDNA libraries were sequenced on NextSeq2000 (Illumina) with 100 + 100 nucleotide reads.

4.4. Genome Assembly and Evaluation

Basecalling of ONT data was performed using the Dorado software package (dorado basecaller v.1.0.2, https://github.com/nanoporetech/dorado, accessed on 25 November 2025) with a minimum average read quality of Q10 (--min-qscore 10). The most accurate model, dna_r10.4.1_e8.2_400bps_sup@v5.2.0 (sup), was used for this purpose. The length and quality of the resulting ONT reads were assessed via NanoPlot (v.1.44.1) [58].

The genome assembly was performed using the Hifiasm algorithm (v.0.25.0) [32] with a parameter set optimized for ONT reads (--ont). The ONT reads were filtered to a minimum length of 10 kb. The following assembly parameters were used: --telo-m CCCTAAA.

Basic assembly parameters, such as length, number of contigs, etc., were obtained and visualized using QUAST (v.5.3.0) [59]. BUSCO (v.5.8.3) [60] was used to evaluate the completeness of the genome assembly using the eudicots_odb10 database of universal single-copy orthologs. BUSCO was used in the eukaryotic genomic data analysis mode (--genome).

Global alignment of the genome assemblies was performed using LAST (v.1639) [61]. Only contigs 10 Mb or longer were considered for alignment. The --uRY128 option, which was designed for whole-genome comparisons, was used for alignment; initial matches between query and reference sequences were searched at ~1/128 of positions in each sequence. Global alignment of the genome assemblies was also performed using minimap2 (v2.3.1) (https://github.com/lh3/minimap2, accessed on 20 April 2026). Only contigs 10 Mb or longer were considered for alignment. The asm10 alignment preset was used. The alignments were visualized with paf2dotplot (https://github.com/moold/paf2dotplot, accessed on 20 April 2026).

The TIDK software package (v.0.2.64) [62] was used to detect telomeric sequences in the assemblies. The CCCTAAA telomeric motif, characteristic of sea buckthorn, was searched in 10 kb windows. Telomere repeat density per 10 kb windows was visualized with matplotlib (v3.10.8) [63].

Hi-C reads were aligned to the obtained Triumf genome assembly using HiC-Pro v3.1.0 [64]. The mapping quality filter was disabled, and all multi-mapped reads were kept.

The contact map was generated with Juicer Tools (v.1.22.01) and visualized with Juicebox (v.1.11.08) [65].

DpnII restriction site (GATC) density across the Triumf assembly was computed in 50 kb windows, normalized to sites per kilobase, smoothed using a centered rolling mean (5 bins), and visualized with matplotlib (v3.10.8) [63].

Both the genomic and transcriptomic Illumina reads were trimmed and filtered with fastp (v.1.0.1) using default parameters [66].

Illumina genome sequencing data (NCBI SRA, PRJNA1177110, obtained for varieties Triumf (SRR32309890), 681-09-01 (SRR32309891), and Zarnitsa (SRR32309892)) were used to validate the assembly quality with the following approaches: read mapping using bowtie2 (v2.5.5) [67] and k-mer distribution analysis with Jellyfish (v.2.3.1) [68] with k set to 20. For the k-mer analysis, the high count of the histogram was set at 1,000,000 as recommended for highly repetitive genomes. Genome size and duplication rate estimation was performed with GenomeScope2 (v.2.0.1) [69].

QV score and completeness estimation was calculated using Meryl (v1.4.1) and Merqury (v1.3) [70] with k set to 20.

4.5. Genome Annotation

Repetitive genomic region annotation and genome masking were performed with RepeatModeler 2.0.7 and RepeatMasker 4.2.1 [71]. RepeatModeler 2.0.7 was used with the -LTRStruct option enabling the LTR structural discovery pipeline and databases dfam 3.9 [72] and Repbase 2018 [73]. Structural annotation of the assembly was performed with the BRAKER3 (v.3.0.8) [74] using the Viridiplantae protein database [75] and Illumina transcriptome sequencing data obtained for variety Triumf at the present study and previously (NCBI SRA, PRJNA1163394).

GC content, intragenomic synteny, and genome coverage of gene and repeat annotations were calculated per 250 kb windows and visualized with Circos (v0.69.0) [76].

Intragenomic synteny was calculated with MCScanX (v1.0.0) [77], based on BLASTP (v2.17.0) self-alignment of protein sequences derived from primary transcripts. Only the top five best hits for each query were kept. For collinearity detection, the minimum number of genes required to call a collinear block was set to 15, with gap penalty of -5 and max gaps of 10.

4.6. Gene Identification

Representative FAT, SAD, and FAD protein models were retrieved from The Arabidopsis Information Resource (TAIR; https://www.arabidopsis.org/, accessed on 25 November 2025) and used as queries for a local BLASTP (v2.17.0) search against *H. rhamnoides* genome assemblies of variety Triumf and genotype CNA0022752 (https://db.cngb.org/, Project ID CNP0001846, accessed on 25 November 2025) [26]. Candidate *H. rhamnoides* protein sequences with less than 30% sequence identity to the reference proteins were discarded.

Protein sequences from *A. thaliana* and *H. rhamnoides* were further analyzed using a local HMMER 3.0 (http://hmmer.org/, accessed on 25 November 2025) search against the Pfam conserved domain database [78]. *H. rhamnoides* sequences lacking the characteristic conserved domains of FAT, SAD, and FAD families were excluded.

Exon-intron structures of the candidate genes were visualized using the ggplot2 v.4.0.1 R package [79] and manually inspected. The retained protein sequences were aligned using MAFFT v7.525. Phylogenetic trees were constructed using RapidNJ v2.3.2 with 1000 bootstrap replicates and visualized with iTOL v7.3 [80]. Gene locations on the chromosome assembly were visualized with Circos (v0.69.0) [76].

https://doi.org/10.3390/plants15111726

To further assess the differences between the relevant gene models, the transcriptomic Illumina reads obtained in the present study and earlier (NCBI SRA, PRJNA1163394) were aligned to the annotated *H. rhamnoides* genome assemblies using PPline [81]. The resulting alignments were visualized with IGV (v2.19.2) [82]. Gene expression analysis was performed using PPline.

Supplementary Materials: The following supporting information can be downloaded at: https://www.mdpi.com/article/10.3390/plants15111726/s1, Figure S1: Global alignment of the genome assemblies of *H. rhamnoides* variety Triumf and other *Hippophae* species; Figure S2: Density of telomeric repeats in the analyzed genome assemblies of *Hippophae* species; Figure S3: Density of restriction site for the DpnII enzyme (GATC) in the *H. rhamnoides* variety Triumf genome assembly; Figure S4: Conserved domain structure of the FAT, SAD, and FAD proteins identified in the *H. rhamnoides* genome assemblies of variety Triumf and genotype CNA0022752; Figure S5: Mapping of RNA-Seq reads to the *H. rhamnoides* Triumf and CNA0022752 (CNGB, Project ID CNP0001846) genome assemblies for the *FAD7/8* gene region: (a) *Triumf.gene.15893* in the Triumf assembly and (b) *Hiprha.gene.07747* in the CNA0022752 assembly; Figure S6: Mapping of RNA-Seq reads to the *H. rhamnoides* Triumf and CNA0022752 (CNGB, Project ID CNP0001846) genome assemblies for the *FAD2* gene region: (a) *Triumf.gene.9854* in the Triumf assembly and (b) *Hiprha.gene.12459* in the CNA0022752 assembly; Figure S7: Mapping of RNA-Seq reads to the *H. rhamnoides* Triumf and CNA0022752 (CNGB, Project ID CNP0001846) genome assemblies for the *FAD2* gene region: (a) *Triumf.gene.2346* in the Triumf assembly and (b) *Hiprha.gene.21624* in the CNA0022752 assembly; Figure S8: Location of identified in the present study *FAT*, *SAD*, and *FAD* genes on twelve chromosomes of the sea buckthorn variety Triumf genome assembly; Table S1. Expression levels of *FAT*, *SAD*, and *FAD* genes in 34 sea buckthorn Triumf samples calculated as CPM (counts per million reads) based on transcriptomic data obtained in the present study for 13 different organs/tissues (roots, wood, bark, buds, bud scales, leaves, and pistils) and from the NCBI BioProject PRJNA1163394 (fruit seeds and pulp).

Author Contributions: Conceptualization, A.A.D. and N.V.M.; performing experiments, N.L.B., E.N.P., V.V.B., V.L.K., N.M.B., D.A.K. and E.V.B.; data analysis, A.A.A., Y.A.Z., V.A.K., F.D.K., E.A.I., E.M.D., K.M.K., A.A.D. and N.V.M.; writing, A.A.A., E.N.P., A.A.D. and N.V.M. All authors have read and agreed to the published version of the manuscript.

Funding: This work was financially supported by the Russian Science Foundation, grant 23-46-00026, https://rscf.ru/project/23-46-00026/, accessed on 25 November 2025.

Data Availability Statement: The data generated in this study are available at NCBI under the BioProject accession numbers PRJNA1177110 (genomic data, linked to BioSample SAMN46736376) and PRJNA1163394 (transcriptomic data, linked to BioSamples SAMN60524364–SAMN60524389). Triumf genome assembly annotation is available at Zenodo (https://zenodo.org/records/19655687, accessed on 20 April 2026).

Acknowledgments: This work was performed using the equipment of the EIMB RAS "Genome" center (http://www.eimb.ru/ru1/ckp/ccu_genome_ce.php, accessed on 25 November 2025). ONT sequencing was performed using the core facilities of the Lopukhin FRCC PCM "Genomics, proteomics, metabolomics" (http://rcpcm.org/?p=2806, accessed on 25 November 2025).

Conflicts of Interest: The authors declare no conflicts of interest.

References

1. Nybom, H.; Ruan, C.; Rumpunen, K. The Systematics, Reproductive biology, biochemistry, and breeding of sea buckthorn-A review. *Genes* **2023**, *14*, 2120. [CrossRef] [PubMed]
2. Ciesarova, Z.; Murkovic, M.; Cejpek, K.; Kreps, F.; Tobolkova, B.; Koplik, R.; Belajova, E.; Kukurova, K.; Dasko, L.; Panovska, Z.; et al. Why is sea buckthorn (*Hippophae rhamnoides* L.) so exceptional? A review. *Food Res. Int.* **2020**, *133*, 109170. [CrossRef]
3. Jasniewska, A.; Diowksz, A. Wide spectrum of active compounds in sea buckthorn (*Hippophae rhamnoides*) for disease prevention and food production. *Antioxidants* **2021**, *10*, 1279. [CrossRef]

4. Du, W.; Ding, J.; Lu, S.; Wen, X.; Hu, J.; Ruan, C. Identification of the key flavonoid and lipid synthesis proteins in the pulp of two sea buckthorn cultivars at different developmental stages. *BMC Plant Biol.* **2022**, *22*, 299. [CrossRef]
5. Wang, Z.; Zhao, F.; Wei, P.; Chai, X.; Hou, G.; Meng, Q. Phytochemistry, health benefits, and food applications of sea buckthorn (*Hippophae rhamnoides* L.): A comprehensive review. *Front. Nutr.* **2022**, *9*, 1036295. [CrossRef] [PubMed]
6. Chen, Y.; He, W.; Cao, H.; Wang, Z.; Liu, J.; Wang, B.; Wang, C. Research progress of sea buckthorn (*Hippophae rhamnoides* L.) in prevention and treatment of cardiovascular disease. *Front. Cardiovasc. Med.* **2024**, *11*, 1477636. [CrossRef]
7. Gatlan, A.M.; Gutt, G. Sea buckthorn in plant based diets. An analytical approach of sea buckthorn fruits composition: Nutritional value, applications, and health benefits. *Int. J. Environ. Res. Public Health* **2021**, *18*, 8986. [CrossRef]
8. Stobdan, T.; Dolkar, P.; Chaurasia, O.; Kumar, B. Seabuckthorn (*Hippophae rhamnoides* L.) in trans-Himalayan Ladakh, India. *Def. Life Sci. J.* **2017**, *2*, 46–53. [CrossRef]
9. Ma, Q.G.; He, N.X.; Huang, H.L.; Fu, X.M.; Zhang, Z.L.; Shu, J.C.; Wang, Q.Y.; Chen, J.; Wu, G.; Zhu, M.N.; et al. *Hippophae rhamnoides* L.: A comprehensive review on the botany, traditional uses, phytonutrients, health benefits, quality markers, and applications. *J. Agric. Food Chem.* **2023**, *71*, 4769–4788. [CrossRef] [PubMed]
10. Zeng, Z.; Wang, J.; Tian, Z.; Norbu, N.; Chen, Y.; Chen, J.; Zhang, W.; Qiong, L. Development of sex-specific molecular markers for early sex identification in *Hippophae gyantsensis* based on whole-genome resequencing. *BMC Plant Biol.* **2024**, *24*, 1187. [CrossRef]
11. Zeng, Z.; Wang, R.; Wang, J.; Chen, Y.; Wang, Y.; Song, Z.; Zhang, W.; Qiong, L. Development and validation of sex-linked molecular markers for rapid and accurate identification of male and female *Hippophae tibetana* plants. *Sci. Rep.* **2024**, *14*, 19243. [CrossRef] [PubMed]
12. Ding, J.; Ruan, C.J.; Guan, Y.; Shan, J.Y.; Li, H.; Bao, Y.H. Characterization and identification of ISSR markers associated with oil content in sea buckthorn berries. *Genet. Mol. Res. GMR* **2016**, *15*, 1–10. [CrossRef]
13. Korekar, G.; Sharma, R.K.; Kumar, R.; Meenu; Bisht, N.C.; Srivastava, R.B.; Ahuja, P.S.; Stobdan, T. Identification and validation of sex-linked SCAR markers in dioecious *Hippophae rhamnoides* L. (Elaeagnaceae). *Biotechnol. Lett.* **2012**, *34*, 973–978. [CrossRef]
14. Zeng, Z.; Zhang, S.; Tan, X.; Tso, N.; Shang, Z.; Zhang, J.; Li, W.; Wang, J.; Zhang, W.; Qiong, L. Development and application of sex-specific indel markers for *Hippophae salicifolia* based on third-generation sequencing. *BMC Plant Biol.* **2025**, *25*, 692. [CrossRef]
15. Zhou, W.; Wang, Y.; Zhang, G.; Luan, G.; Chen, S.; Meng, J.; Wang, H.; Hu, N.; Suo, Y. Molecular sex identification in dioecious *Hippophae rhamnoides* L. via RAPD and SCAR markers. *Molecules* **2018**, *23*, 1048. [CrossRef]
16. Li, H.; Ruan, C.J.; Teixeira da Silva, J.A.; Liu, B.Q. Associations of SRAP markers with dried-shrink disease resistance in a germplasm collection of sea buckthorn (*Hippophae* L.). *Genome* **2010**, *53*, 447–457. [CrossRef] [PubMed]
17. Bernal-Gallardo, J.J.; de Folter, S. Plant genome information facilitates plant functional genomics. *Planta* **2024**, *259*, 117. [CrossRef]
18. Garg, V.; Bohra, A.; Mascher, M.; Spannagl, M.; Xu, X.; Bevan, M.W.; Bennetzen, J.L.; Varshney, R.K. Unlocking plant genetics with telomere-to-telomere genome assemblies. *Nat. Genet.* **2024**, *56*, 1788–1799. [CrossRef] [PubMed]
19. Gladman, N.; Goodwin, S.; Chougule, K.; Richard McCombie, W.; Ware, D. Era of gapless plant genomes: Innovations in sequencing and mapping technologies revolutionize genomics and breeding. *Curr. Opin. Biotechnol.* **2023**, *79*, 102886. [CrossRef]
20. Jayakodi, M.; Shim, H.; Mascher, M. What are we learning from plant pangenomes? *Annu. Rev. Plant Biol.* **2025**, *76*, 663–686. [CrossRef]
21. Medhi, U.; Chaliha, C.; Singh, A.; Nath, B.K.; Kalita, E. Third generation sequencing transforming plant genome research: Current trends and challenges. *Gene* **2025**, *940*, 149187. [CrossRef]
22. Pucker, B.; Irisarri, I.; de Vries, J.; Xu, B. Plant genome sequence assembly in the era of long reads: Progress, challenges and future directions. *Quant. Plant Biol.* **2022**, *3*, e5. [CrossRef]
23. Sun, Y.; Shang, L.; Zhu, Q.H.; Fan, L.; Guo, L. Twenty years of plant genome sequencing: Achievements and challenges. *Trends Plant Sci.* **2022**, *27*, 391–401. [CrossRef]
24. Dmitriev, A.A.; Pushkova, E.N.; Melnikova, N.V. Plant genome sequencing: Modern technologies and novel opportunities for breeding. *Mol. Biol.* **2022**, *56*, 495–507. [CrossRef]
25. Yu, L.; Diao, S.; Zhang, G.; Yu, J.; Zhang, T.; Luo, H.; Duan, A.; Wang, J.; He, C.; Zhang, J. Genome sequence and population genomics provide insights into chromosomal evolution and phytochemical innovation of *Hippophae rhamnoides*. *Plant Biotechnol. J.* **2022**, *20*, 1257–1273. [CrossRef] [PubMed]
26. Wu, Z.; Chen, H.; Pan, Y.; Feng, H.; Fang, D.; Yang, J.; Wang, Y.; Yang, J.; Sahu, S.K.; Liu, J.; et al. Genome of *Hippophae rhamnoides* provides insights into a conserved molecular mechanism in actinorhizal and rhizobial symbioses. *New Phytol.* **2022**, *235*, 276–291. [CrossRef]
27. Yang, X.; Luo, S.; Yang, S.; Duoji, C.; Wang, Q.; Chen, Z.; Yang, D.; Yang, T.; Wan, X.; Yang, Y.; et al. Chromosome-level genome assembly of *Hippophae rhamnoides* variety. *Sci. Data* **2024**, *11*, 776. [CrossRef] [PubMed]
28. Wang, R.; Wu, B.; Jian, J.; Tang, Y.; Zhang, T.; Song, Z.; Zhang, W.; Qiong, L. How to survive in the world's third poplar: Insights from the genome of the highest altitude woody plant, *Hippophae tibetana* (Elaeagnaceae). *Front. Plant Sci.* **2022**, *13*, 1051587. [CrossRef] [PubMed]

29. Zhang, G.; Song, Y.; Chen, N.; Wei, J.; Zhang, J.; He, C. Chromosome-level genome assembly of *Hippophae tibetana* provides insights into high-altitude adaptation and flavonoid biosynthesis. *BMC Biol.* **2024**, *22*, 82. [CrossRef]
30. Chen, M.; Yang, D.; Yang, S.; Yang, X.; Chen, Z.; Yang, T.; Yang, Y.; Yang, Y. Chromosome-level genome assembly of *Hippophae gyantsensis*. *Sci. Data* **2024**, *11*, 126. [CrossRef]
31. Chen, N.; Zhang, G.Y.; Song, Y.T.; Yang, Y.; Zhang, J.G.; He, C.Y. A chromosome-scale genome of *Hippophae neurocarpa* provides new insights into serotonin biosynthesis and chlorophyll-derived brown fruit coloration. *Plant J. Cell Mol. Biol.* **2025**, *121*, e70031. [CrossRef] [PubMed]
32. Cheng, H.; Qu, H.; McKenzie, S.; Lawrence, K.R.; Windsor, R.; Vella, M.; Park, P.J.; Li, H. Efficient near telomere-to-telomere assembly of Nanopore Simplex reads. *bioRxiv* **2025**, 2025.04.14.648685. [CrossRef]
33. Lu, D.; Liu, C.; Ji, W.; Xia, R.; Li, S.; Liu, Y.; Liu, N.; Liu, Y.; Deng, X.W.; Li, B. Nanopore ultra-long sequencing and adaptive sampling spur plant complete telomere-to-telomere genome assembly. *Mol. Plant* **2024**, *17*, 1773–1786. [CrossRef]
34. Zhang, T.; Li, H.; Jiang, M.; Hou, H.; Gao, Y.; Li, Y.; Wang, F.; Wang, J.; Peng, K.; Liu, Y.X. Nanopore sequencing: Flourishing in its teenage years. *J. Genet. Genom.* **2024**, *51*, 1361–1374. [CrossRef]
35. Sigova, E.A.; Dvorianinova, E.M.; Arkhipov, A.A.; Rozhmina, T.A.; Kudryavtseva, L.P.; Kaplun, A.M.; Bodrov, Y.V.; Pavlova, V.A.; Borkhert, E.V.; Zhernova, D.A.; et al. Nanopore data-driven T2T genome assemblies of *Colletotrichum lini* strains. *J. Fungi* **2024**, *10*, 874. [CrossRef]
36. Arkhipov, A.A.; Dvorianinova, E.M.; Turba, A.A.; Novakovskiy, R.O.; Zubarev, Y.A.; Predushchenko, P.A.; Sigova, E.A.; Zhernova, D.A.; Borkhert, E.V.; Pushkova, E.N.; et al. Identification and analysis of *KAS II*, *FAT*, *SAD*, and *FAD* gene families in *Hippophae rhamnoides*. *Plants* **2024**, *13*, 3486. [CrossRef] [PubMed]
37. Shchapov, N.S. Caryology of *Hippophae rhamnoides* L. *Cytol. Genet.* **1979**, *13*, 45–47.
38. Rousi, A.; Arohonka, T. C-bands and ploidy level of *Hippophaë rhamnoides*. *Hereditas* **1980**, *92*, 327–330. [CrossRef]
39. Melnikova, N.V.; Arkhipov, A.A.; Zubarev, Y.A.; Novakovskiy, R.O.; Turba, A.A.; Pushkova, E.N.; Zhernova, D.A.; Mazina, A.S.; Dvorianinova, E.M.; Sigova, E.A.; et al. Genetic diversity of *Hippophae rhamnoides* varieties with different fruit characteristics based on whole-genome sequencing. *Front. Plant Sci.* **2025**, *16*, 1542552. [CrossRef] [PubMed]
40. Scarano, C.; Veneruso, I.; De Simone, R.R.; Di Bonito, G.; Secondino, A.; D'Argenio, V. The third-generation sequencing challenge: Novel insights for the omic sciences. *Biomolecules* **2024**, *14*, 568. [CrossRef]
41. Chaushevska, M.; Alapont-Celaya, K.; Schack, A.K.; Krych, L.; Garrido Navas, M.C.; Krithara, A.; Madjarov, G. Get ready for short tandem repeats analysis using long reads-the challenges and the state of the art. *Front. Genet.* **2025**, *16*, 1610026. [CrossRef]
42. Xu, R.; Pan, Z.; Nakagawa, T. Gross chromosomal rearrangement at centromeres. *Biomolecules* **2023**, *14*, 28. [CrossRef]
43. Naish, M. Bridging the gap: Unravelling plant centromeres in the telomere-to-telomere era. *New Phytol.* **2024**, *244*, 2143–2149. [CrossRef]
44. Jones, A.; Davies, H.M.; Voelker, T.A. Palmitoyl-acyl carrier protein (ACP) thioesterase and the evolutionary origin of plant acyl-ACP thioesterases. *Plant Cell* **1995**, *7*, 359–371. [CrossRef] [PubMed]
45. Shanklin, J.; Somerville, C. Stearoyl-acyl-carrier-protein desaturase from higher plants is structurally unrelated to the animal and fungal homologs. *Proc. Natl. Acad. Sci. USA* **1991**, *88*, 2510–2514. [CrossRef]
46. Okuley, J.; Lightner, J.; Feldmann, K.; Yadav, N.; Lark, E.; Browse, J. Arabidopsis *FAD2* gene encodes the enzyme that is essential for polyunsaturated lipid synthesis. *Plant Cell* **1994**, *6*, 147–158. [CrossRef] [PubMed]
47. Arondel, V.; Lemieux, B.; Hwang, I.; Gibson, S.; Goodman, H.M.; Somerville, C.R. Map-based cloning of a gene controlling omega-3 fatty acid desaturation in *Arabidopsis*. *Science* **1992**, *258*, 1353–1355. [CrossRef]
48. Li, H.; Durbin, R. Genome assembly in the telomere-to-telomere era. *Nat. Rev. Genet.* **2024**, *25*, 658–670. [CrossRef]
49. Chen, J.; Wang, Z.; Tan, K.; Huang, W.; Shi, J.; Li, T.; Hu, J.; Wang, K.; Wang, C.; Xin, B.; et al. A complete telomere-to-telomere assembly of the maize genome. *Nat. Genet.* **2023**, *55*, 1221–1231. [CrossRef] [PubMed]
50. Chen, W.; Wang, X.; Sun, J.; Wang, X.; Zhu, Z.; Ayhan, D.H.; Yi, S.; Yan, M.; Zhang, L.; Meng, T.; et al. Two telomere-to-telomere gapless genomes reveal insights into *Capsicum* evolution and capsaicinoid biosynthesis. *Nat. Commun.* **2024**, *15*, 4295. [CrossRef]
51. Liu, W.; Xu, S.; Ou, C.; Liu, X.; Zhuang, F.; Deng, X.W. T2T genomes of carrot and *Alternaria dauci* and their utility for understanding host-pathogen interactions during carrot leaf blight disease. *Plant J. Cell Mol. Biol.* **2024**, *120*, 1643–1661. [CrossRef]
52. Zhang, Y.; Zhao, M.; Tan, J.; Huang, M.; Chu, X.; Li, Y.; Han, X.; Fang, T.; Tian, Y.; Jarret, R.; et al. Telomere-to-telomere *Citrullus* super-pangenome provides direction for watermelon breeding. *Nat. Genet.* **2024**, *56*, 1750–1761. [CrossRef]
53. Zhang, C.; Xie, L.; Yu, H.; Wang, J.; Chen, Q.; Wang, H. The T2T genome assembly of soybean cultivar ZH13 and its epigenetic landscapes. *Mol. Plant* **2023**, *16*, 1715–1718. [CrossRef]
54. Li, M.; Chen, C.; Wang, H.; Qin, H.; Hou, S.; Yang, X.; Jian, J.; Gao, P.; Liu, M.; Mu, Z. Telomere-to-telomere genome assembly of sorghum. *Sci. Data* **2024**, *11*, 835. [CrossRef] [PubMed]
55. Yan, H.; Han, J.; Jin, S.; Han, Z.; Si, Z.; Yan, S.; Xuan, L.; Yu, G.; Guan, X.; Fang, L.; et al. Post-polyploidization centromere evolution in cotton. *Nat. Genet.* **2025**, *57*, 1021–1030. [CrossRef] [PubMed]

56. Zelenka, T.; Spilianakis, C. HiChIP and Hi-C protocol optimized for primary murine T cells. *Methods Protoc.* **2021**, *4*, 49. [CrossRef] [PubMed]
57. Pushkova, E.N.; Povkhova, L.V.; Dvorianinova, E.M.; Novakovskiy, R.O.; Rozhmina, T.A.; Gryzunov, A.A.; Sigova, E.A.; Zhernova, D.A.; Borkhert, E.V.; Turba, A.A. Expression of *FAD* and *SAD* genes in developing seeds of flax varieties under different growth conditions. *Plants* **2024**, *13*, 956. [CrossRef]
58. De Coster, W.; Rademakers, R. NanoPack2: Population-scale evaluation of long-read sequencing data. *Bioinformatics* **2023**, *39*, btad311. [CrossRef]
59. Gurevich, A.; Saveliev, V.; Vyahhi, N.; Tesler, G. QUAST: Quality assessment tool for genome assemblies. *Bioinformatics* **2013**, *29*, 1072–1075. [CrossRef]
60. Manni, M.; Berkeley, M.R.; Seppey, M.; Simao, F.A.; Zdobnov, E.M. BUSCO update: Novel and streamlined workflows along with broader and deeper phylogenetic coverage for scoring of eukaryotic, prokaryotic, and viral genomes. *Mol. Biol. Evol.* **2021**, *38*, 4647–4654. [CrossRef]
61. Kielbasa, S.M.; Wan, R.; Sato, K.; Horton, P.; Frith, M.C. Adaptive seeds tame genomic sequence comparison. *Genome Res.* **2011**, *21*, 487–493. [CrossRef]
62. Brown, M.R.; Manuel Gonzalez de La Rosa, P.; Blaxter, M. tidk: A toolkit to rapidly identify telomeric repeats from genomic datasets. *Bioinformatics* **2025**, *41*, btaf049. [CrossRef]
63. The Matplotlib Development Team. Matplotlib: Visualization with Python. Zenodo. 2025. Available online: https://zenodo.org/records/20149089 (accessed on 13 May 2026). [CrossRef]
64. Servant, N.; Varoquaux, N.; Lajoie, B.R.; Viara, E.; Chen, C.J.; Vert, J.P.; Heard, E.; Dekker, J.; Barillot, E. HiC-Pro: An optimized and flexible pipeline for Hi-C data processing. *Genome Biol.* **2015**, *16*, 259. [CrossRef]
65. Durand, N.C.; Shamim, M.S.; Machol, I.; Rao, S.S.; Huntley, M.H.; Lander, E.S.; Aiden, E.L. Juicer provides a one-click system for analyzing loop-resolution Hi-C experiments. *Cell Syst.* **2016**, *3*, 95–98. [CrossRef]
66. Chen, S.; Zhou, Y.; Chen, Y.; Gu, J. fastp: An ultra-fast all-in-one FASTQ preprocessor. *Bioinformatics* **2018**, *34*, i884–i890. [CrossRef]
67. Langmead, B.; Salzberg, S.L. Fast gapped-read alignment with Bowtie 2. *Nat. Methods* **2012**, *9*, 357–359. [CrossRef] [PubMed]
68. Marcais, G.; Kingsford, C. A fast, lock-free approach for efficient parallel counting of occurrences of k-mers. *Bioinformatics* **2011**, *27*, 764–770. [CrossRef]
69. Ranallo-Benavidez, T.R.; Jaron, K.S.; Schatz, M.C. GenomeScope 2.0 and Smudgeplot for reference-free profiling of polyploid genomes. *Nat. Commun.* **2020**, *11*, 1432. [CrossRef]
70. Rhie, A.; Walenz, B.P.; Koren, S.; Phillippy, A.M. Merqury: Reference-free quality, completeness, and phasing assessment for genome assemblies. *Genome Biol.* **2020**, *21*, 245. [CrossRef] [PubMed]
71. Flynn, J.M.; Hubley, R.; Goubert, C.; Rosen, J.; Clark, A.G.; Feschotte, C.; Smit, A.F. RepeatModeler2 for automated genomic discovery of transposable element families. *Proc. Natl. Acad. Sci. USA* **2020**, *117*, 9451–9457. [CrossRef] [PubMed]
72. Storer, J.; Hubley, R.; Rosen, J.; Wheeler, T.J.; Smit, A.F. The Dfam community resource of transposable element families, sequence models, and genome annotations. *Mob. DNA* **2021**, *12*, 2. [CrossRef]
73. Bao, W.; Kojima, K.K.; Kohany, O. Repbase Update, a database of repetitive elements in eukaryotic genomes. *Mob. DNA* **2015**, *6*, 11. [CrossRef]
74. Gabriel, L.; Bruna, T.; Hoff, K.J.; Ebel, M.; Lomsadze, A.; Borodovsky, M.; Stanke, M. BRAKER3: Fully automated genome annotation using RNA-seq and protein evidence with GeneMark-ETP, AUGUSTUS, and TSEBRA. *Genome Res.* **2024**, *34*, 769–777. [CrossRef]
75. Kuznetsov, D.; Tegenfeldt, F.; Manni, M.; Seppey, M.; Berkeley, M.; Kriventseva, E.V.; Zdobnov, E.M. OrthoDB v11: Annotation of orthologs in the widest sampling of organismal diversity. *Nucleic Acids Res.* **2023**, *51*, D445–D451. [CrossRef]
76. Krzywinski, M.; Schein, J.; Birol, I.; Connors, J.; Gascoyne, R.; Horsman, D.; Jones, S.J.; Marra, M.A. Circos: An information aesthetic for comparative genomics. *Genome Res.* **2009**, *19*, 1639–1645. [CrossRef] [PubMed]
77. Wang, Y.; Tang, H.; Debarry, J.D.; Tan, X.; Li, J.; Wang, X.; Lee, T.H.; Jin, H.; Marler, B.; Guo, H.; et al. MCScanX: A toolkit for detection and evolutionary analysis of gene synteny and collinearity. *Nucleic Acids Res.* **2012**, *40*, e49. [CrossRef]
78. Mistry, J.; Chuguransky, S.; Williams, L.; Qureshi, M.; Salazar, G.A.; Sonnhammer, E.L.L.; Tosatto, S.C.E.; Paladin, L.; Raj, S.; Richardson, L.J.; et al. Pfam: The protein families database in 2021. *Nucleic Acids Res.* **2021**, *49*, D412–D419. [CrossRef]
79. Wickham, H. *ggplot2: Elegant Graphics for Data Analysis*; Springer International Publishing: Cham, Switzerland, 2016.
80. Letunic, I.; Bork, P. Interactive Tree of Life (iTOL) v6: Recent updates to the phylogenetic tree display and annotation tool. *Nucleic Acids Res.* **2024**, *52*, W78–W82. [CrossRef]

81. Krasnov, G.S.; Dmitriev, A.A.; Kudryavtseva, A.V.; Shargunov, A.V.; Karpov, D.S.; Uroshlev, L.A.; Melnikova, N.V.; Blinov, V.M.; Poverennaya, E.V.; Archakov, A.I.; et al. PPLine: An automated pipeline for SNP, SAP, and splice variant detection in the context of proteogenomics. *J. Proteome Res.* **2015**, *14*, 3729–3737. [CrossRef] [PubMed]
82. Robinson, J.T.; Thorvaldsdottir, H.; Winckler, W.; Guttman, M.; Lander, E.S.; Getz, G.; Mesirov, J.P. Integrative genomics viewer. *Nat. Biotechnol.* **2011**, *29*, 24–26. [CrossRef] [PubMed]

Disclaimer/Publisher's Note: The statements, opinions and data contained in all publications are solely those of the individual author(s) and contributor(s) and not of MDPI and/or the editor(s). MDPI and/or the editor(s) disclaim responsibility for any injury to people or property resulting from any ideas, methods, instructions or products referred to in the content.

plants

MDPI

Article

Screening and Evaluation of Rice to Assess Antibiosis and Antixenosis Resistance to White-Backed Planthopper (*Sogatella furcifera*)

Jariya Roddee [1,*,†], Kamolchanok Umnajkitikorn [1,†], Napatson Chansawang [1], Jirapong Jairin [2] and Jureemart Wangkeeree [3]

[1] School of Crop Production Technology, Institute of Agricultural Technology, Suranaree University of Technology, Nakhon Ratchasima 30000, Thailand; k.umnajkitikorn@g.sut.ac.th (K.U.); 123tiptib@gmail.com (N.C.)
[2] Ubon Ratchathani Rice Research Center, Muang, Ubon Ratchathani 34000, Thailand; jjairin@gmail.com
[3] Department of Agricultural Technology, Faculty of Science and Technology, Thammasat University Rangsit Centre, Pathum Thani 10200, Thailand; jureemart@yahoo.com
* Correspondence: jariyaroddee@g.sut.ac.th
† These authors contributed equally to this work.

Abstract

The white-backed planthopper, *Sogatella furcifera*, and the brown planthopper, *Nilaparvata lugens*, severely impact rice production, necessitating effective selection methods for resistant cultivars. *S. furcifera* poses a significant threat to rice cultivation, particularly in Asia. Through this study, we aimed to establish an effective approach to identifying resistant rice varieties based on feeding behavior, physiological and chemical responses, and genetic analysis. Three key activities were involved: (1) evaluation of planthopper feeding behavior utilizing the honeydew drop method, the electrical penetration graph technique, and growth rate analysis; (2) investigation into the physiological and chemical traits of rice; and (3) analysis of resistance-related gene expression. The results indicated larger honeydew drop areas, fewer and shorter probing events, and structural defenses such as increased trichome density in resistant rice genotypes, likely hindering insect attachment and feeding. We confirmed the suitability of the growth rate method for resistance screening. Gene expression analysis identified *PR10a* upregulation in resistant rice, suggesting a molecular basis for resistance. This study enables the selection of rice varieties resistant to planthoppers, supporting sustainable pest management and breeding programs. The findings support sustainable pest management by enabling the targeted selection of resistant varieties, ultimately aiding in the development of rice genotypes with enhanced resistance across growth stages.

Keywords: *Sogatella furcifera*; feeding behavior; physiological responses; gene expression

1. Introduction

Rice (*Oryza sativa* L.) underpins global food security; however, recurrent outbreaks of planthoppers—principally the brown planthopper (*Nilaparvata lugens* Stål; BPH) and the white-backed planthopper (*Sogatella furcifera* Horváth; WBPH)—continue to impact yield stability across South, Southeast, and East Asia. Beyond direct phloem-feeding injuries (hopperburns), these vectors transmit rice ragged stunt virus (RRSV) and rice grassy stunt virus (RGSV), intensifying the risks to production systems already under stress from climate variability and intensive cultivation (e.g., high-nitrogen monocultures) [1]. Rice

production is persistently impacted by sap-sucking insect pests, particularly planthoppers (Hemiptera: Delphacidae). Among these, the WBPH is one of the most destructive pests, causing severe yield losses through direct phloem ingestion and disruption of plant physiological processes [2,3]. Frequent WBPH outbreaks have been reported across South and Southeast Asia, often associated with shifting cultivation systems and mismanagement of insecticides [4].

Chemical insecticides remain the primary strategy for WBPH control. However, their intensive and repeated use has led to the development of resistance, pest resurgence, and adverse effects on non-target organisms and the environment [5,6]. Consequently, host plant resistance is widely recognized as a sustainable and environmentally sound approach to long-term planthopper management [7]. In rice, planthopper resistance is typically categorized into three mechanisms: antibiosis, antixenosis, and tolerance [8]. Among these, antibiosis and antixenosis play central roles in limiting planthopper feeding success, development, and host selection behavior and are therefore the primary focus of resistance breeding programs. Antibiosis resistance directly affects the insect's biology by reducing survival, growth, or reproduction after feeding on resistant plants [8,9]. In rice–planthopper interactions, antibiosis is often associated with impaired phloem sap ingestion, reduced feeding efficiency, and delayed insect development [10]. These effects can be quantified using feeding-related parameters, such as honeydew excretion [11], insect growth rate, and detailed analysis of feeding behavior. A choice test is utilized to select plant varieties resistant to insect pests. This practical method for observing the non-preference behavior of insect pests toward host plants involves many factors, such as signals and information content, volatile compounds specific to individual host plants, and sensory aspects, enabling insects to receive signals from the host [12]. In contrast, antixenosis resistance influences insect behavior through deterring host acceptance, settling, or sustained feeding [8,13]. Morphological traits, including trichome density and leaf sheath surface characteristics, may create physical barriers that impede insect attachment and probing, thereby discouraging feeding initiation [14].

Advances in plant–insect interaction research have highlighted the importance of comprehensive screening approaches that combine behavioral, physiological, biochemical, and molecular analyses. The honeydew excretion assay is a rapid and effective method for estimating phloem ingestion efficiency in planthoppers [15]. The electrical penetration graph (EPG) technique provides detailed insights into stylet penetration, probing frequency, and phloem sap ingestion, allowing discrimination between resistant and susceptible host plants at a fine behavioral scale [16–23]. In addition, insect growth rate assays offer a robust indicator of antibiosis, directly reflecting host plant effects on insect development and fitness [10,17]. At the plant level, resistance to planthoppers is frequently associated with structural defenses, altered phytohormone signaling, and the activation of defense-related genes [24]. Pathogenesis-related (PR) proteins, particularly *PR10*, have been associated with rice defense responses against sap-sucking insects and may contribute to antibiosis by impairing insect feeding and development [25–27]. The integration of phenotypic resistance traits with molecular markers such as *PR10a* expression can therefore enhance resistance screening and facilitate breeding for durable resistance.

Despite the economic importance of WBPH in Thailand, comprehensive screening frameworks that integrate feeding behavior, plant physiological traits, and molecular resistance indicators remain limited. Previous studies have primarily focused on BPH resistance or relied on single evaluation methods, which often fail to capture the complex WBPH–rice interactions [7,8]. Therefore, in this study, we aimed to establish an integrated approach to identifying WBPH-resistant rice genotypes by combining feeding-behavior analysis (honeydew excretion, EPG, and insect growth rate), evaluation of plant morphological and

chemical traits, and expression analysis of resistance-related genes. By linking antibiosis and antixenosis mechanisms with multi-level phenotypic and molecular indicators, this work provides a robust framework for WBPH resistance screening, supporting sustainable rice breeding and pest management programs.

2. Results

2.1. Honeydew Excretion and Salivary Sheath Formation Assay

The feeding intensity of the WBPH on 10 rice genotypes/lines was quantified using honeydew excretion and salivary sheath formation after a 24 h feeding (Figure 1). Differences in honeydew excretion were significant among the rice genotypes (Figure 1A) ($F_{9194} = 1.03$, $p = 0.041$). The PTB33 showed the largest honeydew area (mean 1.4 cm^2), significantly exceeding other genotypes. Honeydew excretion was intermediate on Babawee and KDML105, whereas TN1, UBN03078-80-354-7, UBN03078-101-342-4-148, and ASD7 demonstrated relatively low honeydew areas. Honeydew excretion was lowest in Rathu Heenati and Mudgo, indicating reduced WBPH feeding activity in these genotypes (Figure S1).

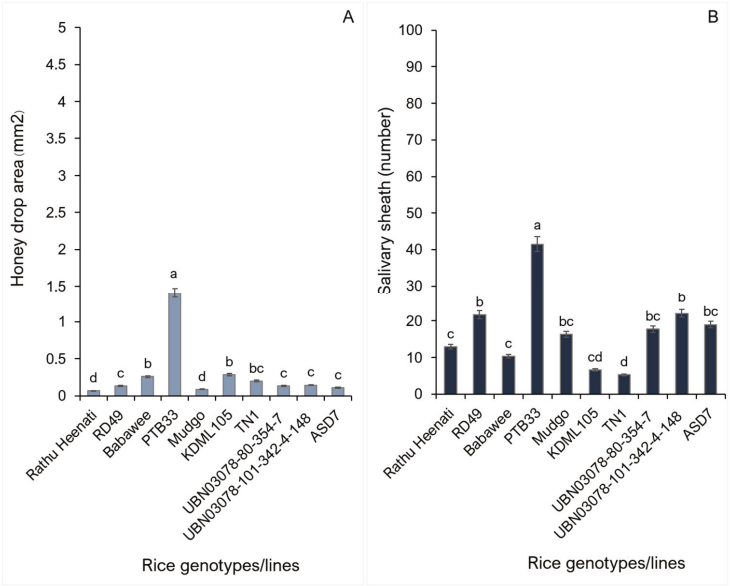

Figure 1. Feeding activity of the white-backed planthopper on 10 rice genotypes: (**A**) honeydew area excreted after 24 h and (**B**) number of salivary sheaths. Bars indicate mean ± SE ($n = 20$). Different letters indicate significant differences among genotypes (one-way ANOVA, Tukey's HSD, $p < 0.05$).

The salivary sheath numbers are shown in Figure 1B. WBPH feeding on PTB33 resulted in the highest frequency of salivary sheaths (>40), significantly exceeding the remaining genotypes ($F_{9197} = 9.23$, $p < 0.001$). In contrast, Rathu Heenati, Babawee, and TN1 supported significantly fewer salivary sheaths, reflecting limited probing and feeding behavior. Genotypes characterized by low honeydew excretion generally corresponded to lower salivary sheath numbers.

2.2. Electrical Penetration Graph Study

2.2.1. Feeding Behavior of White-Backed Planthopper (WBPH) on Different Rice Genotypes

EPG analysis revealed seven distinct waveform patterns associated with WBPH probing and feeding behavior, as illustrated. These waveforms were classified as Np, N1-N2, N3, N4-a, N4-b, and N5, and their characteristics were consistent with previously described feeding activities [19,20,28].

2.2.2. Number of Waveform Events per Insect (NEWI)

The NEWI differed significantly among rice genotypes across all EPG waveform categories (Figure 2), indicating genotype-dependent effects on the insect's probing and feeding behavior. Non-probing (Np) events were generally low across genotypes, with TN1 and Rathu demonstrating significantly higher frequencies than PTB33 and Babawee ($F_{9292} = 1.49$, $p = 0.016$). The frequency of pathway-phase waveforms (N1–N2) varied markedly among genotypes, with PTB33 and Mudgo indicating significantly higher NEWI values than Rathu Heenati, RD49, and Babawee ($F_{9420} = 2.16$, $p = 0.034$).

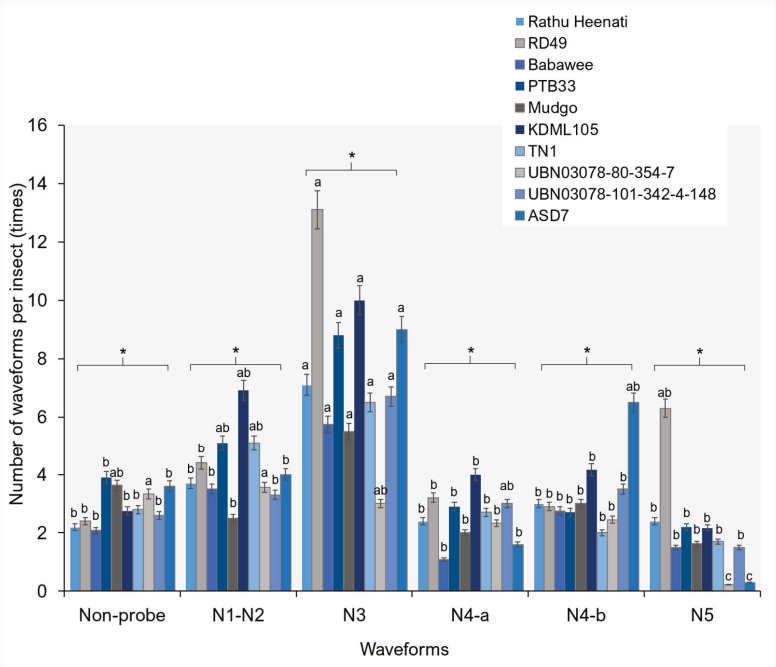

Figure 2. Number of waveform events per insect in the white-backed planthopper on different rice genotypes. Bars (mean ± SEM) with the same letter at the top within a waveform category are not significantly different at $p = 0.05$ (Tukey's test). Np = non-probe; N1, N2 = Pathway phase; N3 = pathway in epidermis/mesophyll; N4-a = phloem salivation or sieve-element salivation; N4-b = sustained phloem sap ingestion or phloem ingestion; and N5 = xylem ingestion. An asterisk (*) in a figure indicates a statistically significant difference between groups, where the p-value < 0.05.

Significant differences were also observed during the phloem contact phase (N3). The genotype RD49 demonstrated the highest frequency of N3 events, followed by KDML105 and PTB33, whereas genotypes such as Mudgo indicated significantly fewer N3 events ($F_{9754} = 1.90$, $p = 0.0041$). For phloem sap ingestion waveforms, both N4-a and N4-b phases demonstrated clear genotype-specific patterns. In particular, KDML105 and ASD7 indicated significantly higher N4-a ($F_{9252} = 3.73$, $p = 0.005$) and N4-b ($F_{9329} = 3.17$, $p = 0.002$), respectively. Xylem ingestion events (N5) occurred at low frequencies across all genotypes; however, RD49 varieties demonstrated significantly higher NEWI values than other genotypes/lines ($F_{9199} = 5.01$, $p < 0.001$) (Figure 2).

2.2.3. Waveform Duration per Event per Insect (WDEI)

WDEI differed significantly among rice genotypes across all EPG waveform categories (Figure 3). In the NP phase, genotypes, particularly RD49, PTB33, TN1, and Rathu, showed significantly longer waveform durations than Babawee and Mudgo ($F_{9292} = 2.17$, $p = 0.041$), suggesting prolonged searching or resting behavior before stylet insertion. During the pathway phase (N1–N2), significant genotype-dependent variation was detected ($F_{9420} = 3.57$, $p = 0.048$). UBN03078-80-354-7 and ASD7 genotypes demonstrated prolonged

https://doi.org/10.3390/plants15050811

event durations compared to other genotypes, indicating increased difficulty in stylet penetration through plant tissues. Significant differences were also observed in the N3 waveform duration ($F_{9754} = 4.65$, $p = 0.037$). In particular, Babawee and UBN03078-80-354-7 PTB33 demonstrated significantly longer N3 durations than KDML105 genotypes. For phloem-related feeding, the durations of the N4-a and N4-b waveforms differed significantly among genotypes. UBN03078-80-354-7 genotypes demonstrated significantly longer N4-a ($F_{9252} = 1.94$, $p = 0.042$) and N4-b ($F_{9329} = 2.47$, $p = 0.041$), indicating sustained phloem sap ingestion. In contrast, resistant genotypes demonstrated markedly reduced phloem-feeding durations, indicating impaired feeding efficiency. Xylem ingestion events (N5) also showed significant variation among genotypes ($F_{9199} = 7.24$, $p = 0.021$), with the Mudgo and UBN03078-80-354-7 genotypes exhibiting prolonged N5 durations compared to other lines (Figure 3).

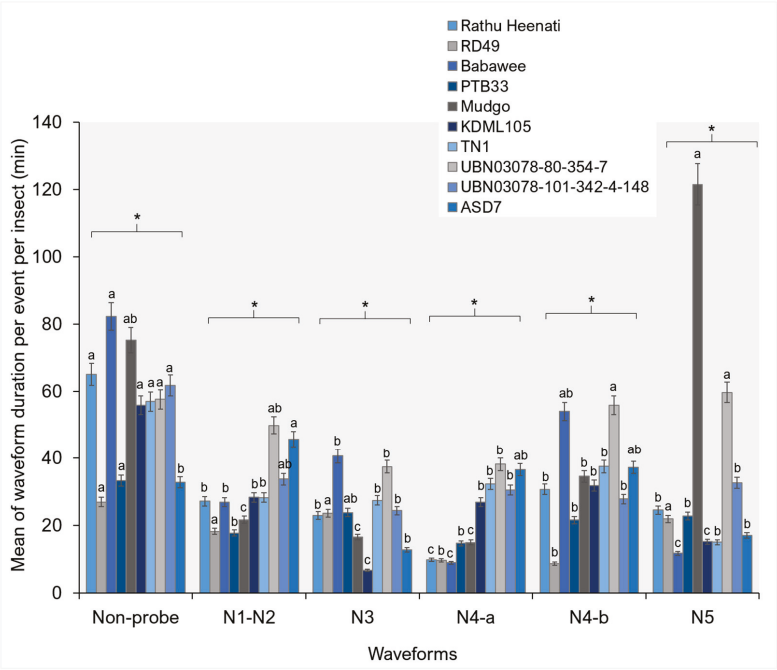

Figure 3. The waveform duration per event per insect in the white-backed planthopper on different rice genotypes. Bars (mean ± SEM) with the same letter at the top within a waveform category are not significantly different at $p = 0.05$ (Tukey's test). Np = non-probe; N1, N2 = pathway phase; N3 = pathway in epidermis/mesophyll; N4-a = phloem salivation or sieve-element salivation; N4-b = sustained phloem sap ingestion or phloem ingestion; and N5 = xylem ingestion. An asterisk (*) in a figure indicates a statistically significant difference between groups, where the p-value < 0.05.

2.2.4. Waveform Duration per Insect (WDI)

WDI differed significantly among rice genotypes for all EPG waveform categories (Figure 4). The Np phase indicated that the RD49 and PTB33 genotypes had significantly shorter cumulative durations than the other genotypes ($F_{9292} = 0.64$, $p = 0.047$). In particular, Mudgo and Babawee demonstrated the longest NP durations. During the pathway phase (N1–N2), significant genotype-dependent variation in WDI was observed ($F_{9420} = 1.57$, $p = 0.041$). ASD7 and UBN03078-80-354-7 genotypes exhibited longer pathway durations than RD49 and PTB33 genotypes. Significant differences were also detected in the N3 waveform duration, with KDML105 and Mudgo indicating shorter durations ($F_{9754} = 1.53$, $p = 0.014$). For phloem-related feeding phases, both N4-a waveform durations differed significantly among rice genotypes ($F_{9252} = 4.57$, $p < 0.001$). TN1, UBN03078-80-354-7, UBN03078-101-342-4-148, and ASD4 genotypes demonstrated significantly extended cumulative durations of phloem ingestion. Similarly, N4-b waveform durations in UBN03078-

80-354-7 genotypes were prolonged, indicating impaired sustained phloem sap ingestion (F_{9329} = 1.84, p = 0.043). Xylem ingestion (N5) durations also varied significantly among genotypes (F_{9199} = 8.40, p = 0.005), with Mudgo genotypes demonstrating prolonged N5 durations compared to other genotypes.

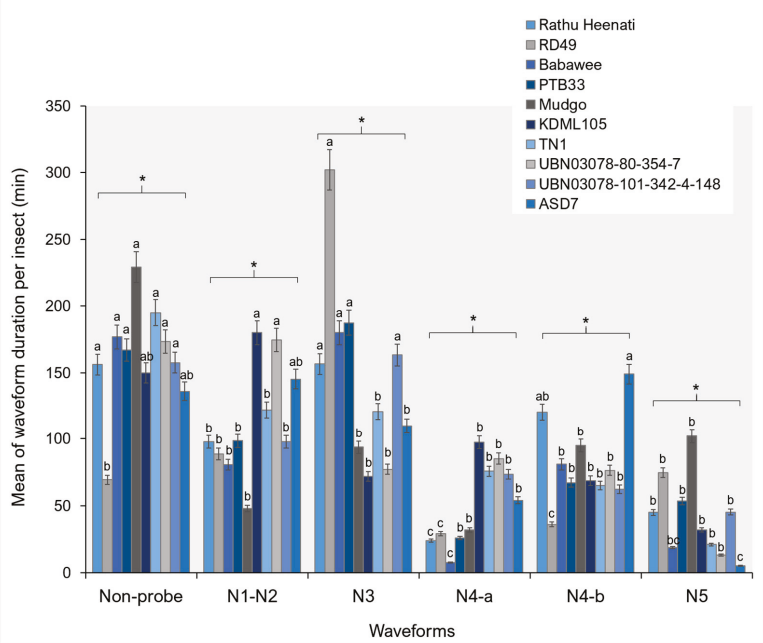

Figure 4. The WDI of the white-backed planthopper on different rice genotypes. Bars (mean ± SEM) with the same letter at the top within a waveform category are not significantly different at p = 0.05 (Tukey's test). Np = non-probe; N1, N2 = pathway phase; N3 = pathway in epidermis/mesophyll; N4-a = phloem salivation or sieve-element salivation; N4-b = sustained phloem sap ingestion or phloem ingestion; and N5 = xylem ingestion. An asterisk (*) in a figure indicates a statistically significant difference between groups, where the p-value < 0.05.

2.3. WBPH Survival and Development Bioassays on Different Rice Genotypes

The nymphal development and survival of the WBPH differed markedly among the 10 rice genotypes evaluated at the seedling stage (Figure 5). Survival remained at 100% during the egg stage and the first- and second-instar stages across all genotypes, indicating no early-stage mortality. From the third instar onward, genotype-dependent divergence was evident in survival trajectories. Kaplan–Meier survival analysis demonstrated significant differences in cumulative survival probabilities among rice genotypes (χ^2 = 5.42, df = 9, N = 199, p < 0.001). The ASD7, Babawee, and Rathu Heenati genotypes exhibited a rapid decline in survival from the third-to-fourth-instar stage onward. Survival on TN1 decreased to approximately 50% at adult emergence (15.26 days). In contrast, the TN1 and KDML105 genotypes demonstrated significantly higher survival probabilities throughout nymphal development. Kaplan–Meier curves for these genotypes indicated minimal mortality during mid- and late-nymphal stages, with survival exceeding 80–90% at adult emergence. Intermediate survival patterns were observed in the Babawee and UBN03078-80-354-7 lines, which demonstrated gradual declines in survival, primarily during the fourth- and fifth-instar stages (24.43 and 17.14 days), resulting in adult emergence rates of approximately 70–75%. RD49 lines demonstrated low survival in the fifth-instar stage and failed to develop to the adult stage. In contrast, the RD49 line showed markedly reduced survival at the fifth instar, and no individuals survived to the adult stage.

https://doi.org/10.3390/plants15050811

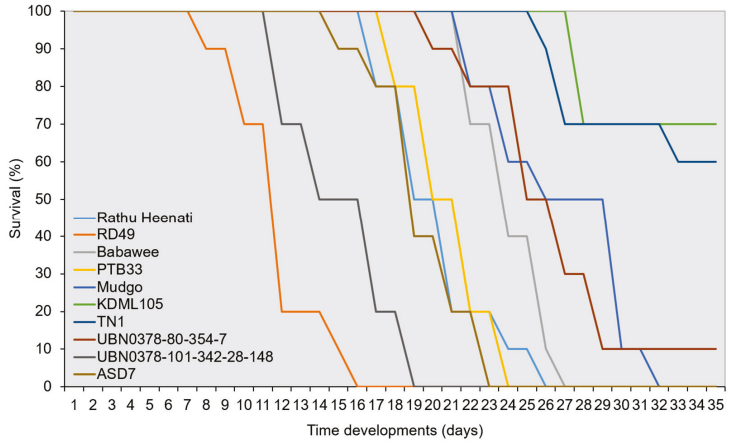

Figure 5. Survival dynamics of the white-backed planthopper (*Sogatella furcifera*) across developmental stages on 10 rice genotypes.

The developmental duration of WBPH varied significantly among the 10 rice genotypes evaluated (Table 1). Significant genotype effects were detected at the first-instar, third-instar, and adult stages ($p \leq 0.05$), whereas no significant differences were observed during the second-, fourth-, and fifth-instar stages. In the first-instar stage, nymphs reared on Babawee and UBN03078-80-354-7 demonstrated extended developmental durations compared to those reared on KDML105, TN1, UBN03078-101-342-4-148, and Rathu Heenati, which demonstrated significantly shorter durations (1 ± 0.0 days, $p \leq 0.05$). During the third instar, development was significantly prolonged on PTB33 (mean 3.30 ± 1.38 days) and Rathu Heenati (mean 3.25 ± 1.47 days). Nymphs on UBN03078-80-354-7 and Mudgo completed this stage more rapidly (1.60 ± 0.83 and 1.05 ± 0.59, $p \leq 0.05$, respectively). Adult longevity also differed significantly among rice genotypes, with a mean of 12.83 ± 4.29 days. The longest adult duration was observed on Mudgo (12.83 ± 4.29 days), followed by Babawee (9.24 ± 0.83 days) and KDML105 (8.86 ± 2.71 days), whereas substantially shorter adult durations were observed on RD49 and UBN03078-101-342-148.

Table 1. Growth and developmental parameters of the white-backed planthopper (*Sogatella furcifera*) reared on 10 rice genotypes/lines: Rathu Heenati, RD49, Babawee, PTB33, Mudgo, ASD7, Khao Dawk Mali 105 (KDML105), TN1, UBN03078-80-354-7, and UBN03078-101-342-4-148.

Rice Varieties	Mean ± SEM (Days)						Sex Ratio (Male/Female)
	First-Instar Nymph	Second-Instar Nymph	Third-Instar Nymph	Fourth-Instar Nymph	Fifth-Instar Nymph	Adult	
KDML105	1.20 ± 0.36 d	1.19 ± 0.51	2.19 ± 1.12 bc	2.33 ± 0.47	6.43 ± 4.87	8.86 ± 2.71 ab	2:1
TN1	1.50 ± 0.49 d	1.20 ± 0.41	1.60 ± 0.83 c	2.13 ± 2.13	3.93 ± 3.90	7.4 ± 1.06 ab	2:1
UBN03078-80-354-7	2.24 ± 0.54 a	1.57 ± 0.51	1.05 ± 0.59 dc	2.86 ± 1.39	4.71 ± 3.78	4.71 ± 5.19 b	1:0.3
UBN03078-101-342-148	1.20 ± 0.41 d	1.24 ± 0.54	2.9 ± 2.55 ab	2.48 ± 2.27	3.67 ± 4.02	1.29 ± 0.04 c	1:1
PTB33	1.85 ± 0.59 b	1.65 ± 0.81	3.30 ± 1.38 a	3.60 ± 3.23	5.55 ± 4.60	2.15 ± 1.29 bc	1:1
RD49	1.40 ± 0.52 c	1.50 ± 0.53	2.20 ± 0.79 bc	1.2 ± 1.04	1.60 ± 1.73	NA	NA
Babawee	2.29 ± 0.46 a	1.95 ± 0.28	2.52 ± 0.81 ab	2.19 ± 1.20	6.24 ± 3.26	9.24 ± 0.83 ab	1:1.35
ASD7	1.50 ± 0.51 c	1.55 ± 0.86	2.55 ± 1.32 ab	2.18 ± 1.56	3.77 ± 1.68	4.64 ± 0.29 b	1:1.42
Mudgo	2.08 ± 0.28 ab	1.90 ± 0.20	1.46 ± 0.66 c	2.88 ± 1.08	4.54 ± 1.47	12.83 ± 4.29 a	1.1:1
Rathu Heenati	1.23 ± 0.31 d	1.83 ± 0.37	3.25 ± 1.47 a	2.50 ± 1.15	3.38 ± 1.35	5.54 ± 4.12 b	1:1.24
p-value	**	NS	**	NS	NS	**	

Values followed by different letters indicate significant differences at $p \leq 0.05$ according to Duncan's multiple range test (DMRT). ** indicates a statistically significant difference at $p \leq 0.05$ according to Duncan's multiple range test. NS in a table indicates a statistically significant difference between groups, where the *p*-value < 0.05.

https://doi.org/10.3390/plants15050811

2.4. Trichome Density

Scanning electron microscopy (SEM) revealed significant variation in trichome density on the abaxial surface of leaves among the ten genotypes investigated (Figure 6). All plant trichomes were found in this non-granular trichome type. The TN1 demonstrated the highest macrotrichome and total trichome densities, significantly greater than those of all other genotypes ($F_{989} = 1.84$, $p < 0.050$) (Figure 7). Similarly, PTB33 showed high total trichome density. In contrast, the ASD7, Mudgo, KDML105, RD49, Babawee, and Rathu Heenati genotypes showed significantly lower macrotrichome and total trichome densities, with no significant differences among them ($p > 0.05$).

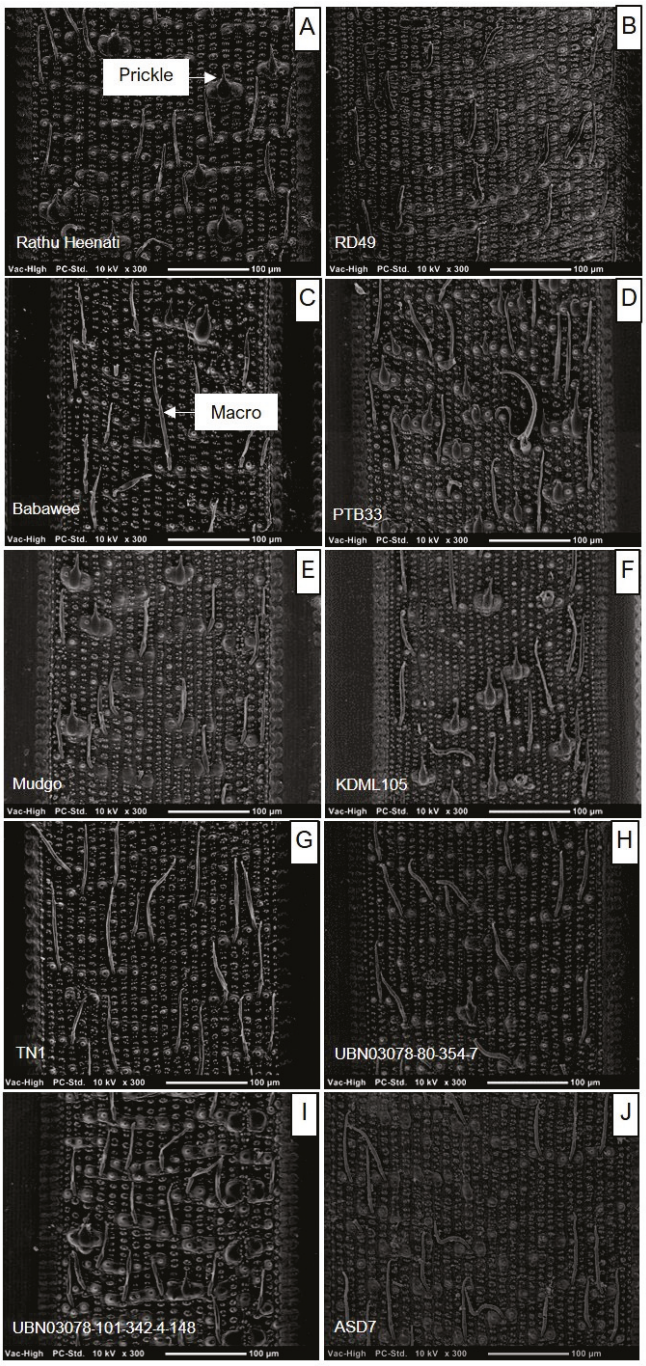

Figure 6. Trichome of abaxial leaf surface for 10 rice genotypes using scanning electron micrography: (**A**) Rathu Heenati, (**B**) RD49, (**C**) Babawee, (**D**) PTB33, (**E**) Mudgo, (**F**) KDML105, (**G**) TN1, (**H**) UBN03078-80-354-7, (**I**) UBN03078-101-342-148, (**J**) ASD7. SEM of abaxial leaf surface at 0.3 mm^2.

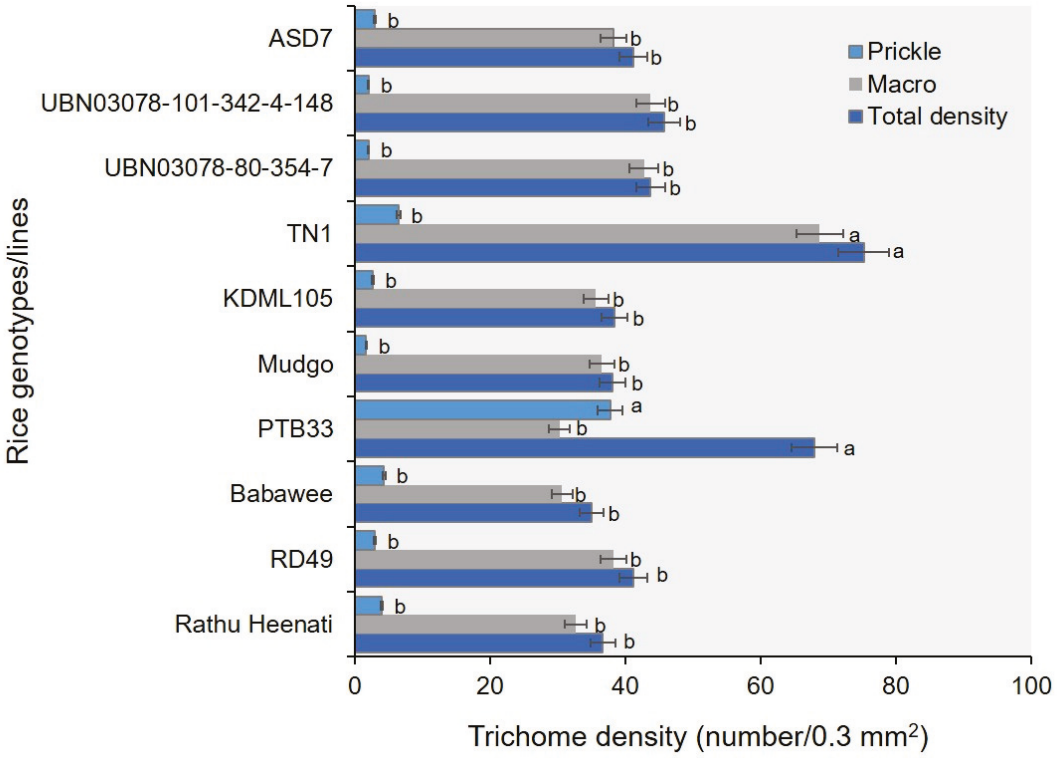

Figure 7. Comparison of trichome density on the abaxial leaf surface among rice genotypes. Bars (mean ± SEM) with the same letter at the top within a waveform category are not significantly different according to Tukey's honestly significant difference (HSD) test ($p = 0.05$).

2.5. Correlation and Principal Component Analysis Between the Parameters

The correlation analysis conducted in this study was designed to explore the relationships among honeydew excretion, salivary sheath, EPG analysis for WBPH feeding behavior, development and survival rate, and trichome factors (Figure 8). Conversely, the mean honeydew value was positively correlated with WDI N4 ($r = 0.93$ *) and WDEI N5 ($r = 0.91$ *) and with NWI N3, WDEI N3, salivary sheath, and WDI N1N2 ($r = 0.78$ *, $r = 0.75$ *, $r = 0.74$, and $r = 0.73$, respectively). Additionally, negative correlations were observed between mean honeydew and specific EPG waveform parameters, such as NWI NP ($r = -0.79$ *). Additionally, the salivary sheath was positively correlated with NWI N3 ($r = 0.75$ *) but negatively correlated with NEI NP ($r = -0.79$ *).

Principal component analysis (PCA) demonstrated that the first two PCs together accounted for 79.05% of the total variance, with PC1 contributing 60.76% and PC2 contributing 18.29%. Using PCA, the rice genotypes were grouped into four distinct clusters (Figure 9). The first group comprised the ASD7, Rathu Heenati, and PTB33 genotypes/lines, suggesting similarities in their characteristics concerning honeydew excretion, salivary sheaths, EPG analysis for WBPH feeding behavior, development, and survival rate, and trichome factors. The second group comprised the RD49 and UBN03078-101-342-148 genotypes/lines. The third group consisted of the TN1 and KDML105 genotypes, and the last group included the Mudgo, Babawee, and UBN03078-80-354-7 genotypes/lines. The results demonstrated that the distances between (resistant) ASD7 genotypes/lines were greater than those between UBN03078-80-354-7 genotypes/lines (susceptible). Thus, two varieties were used in the plant hormone and secondary metabolite profiling analysis.

https://doi.org/10.3390/plants15050811

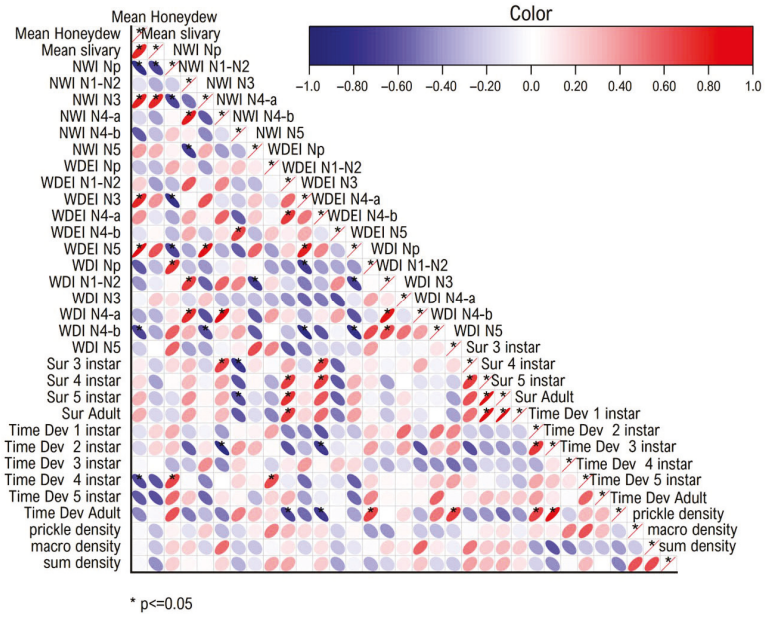

Figure 8. Correlation coefficients (Pearson correlation) and significance levels of honeydew excretion, salivary sheath, EPG analysis for white-backed planthopper's (*Sogatella Furcifera*) feeding behavior, development, and survival rate, and trichome factors. Red circles indicate positive correlations, whereas blue circles indicate negative correlations. The shape and narrowness of the ellipses reflect the strength of the correlation, with narrower ellipses representing stronger correlations approaching ± 1 and more circular shapes indicating weaker relationships. The color intensity corresponds to the magnitude of the correlation coefficient, ranging from -1 (strong negative correlation) to +1 (strong positive correlation). Asterisks (*) denote statistically significant correlations at $p \leq 0.05$.

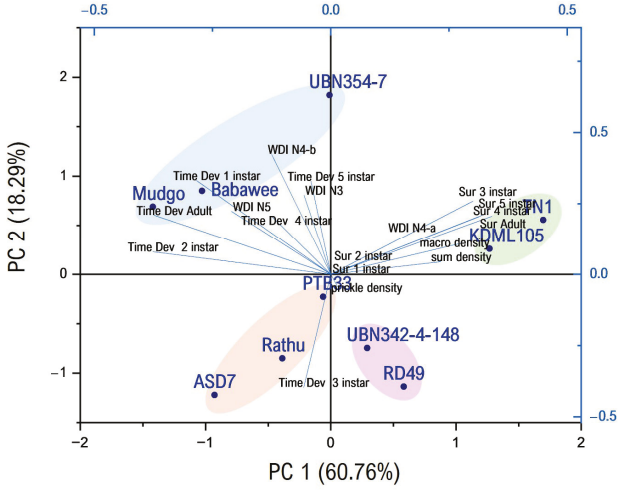

Figure 9. Principal component analysis (PC1 and PC2) of 10 rice genotypes based on honeydew excretion, salivary sheath, EPG analysis for WBPH's (*Sogatella Furcifera)* feeding behavior, development, and survival rate, and trichome factors.

2.6. Profiling of Plant Hormones and Secondary Metabolites

2.6.1. Quantitative Changes in Phytohormone-Related Metabolites Following WBPH Infestation

Quantitative analysis indicated significant changes in the concentrations of gibberellin A3 (GA_3), abscisic acid (ABA), and dihydrojasmonic acid (DHJA) in rice leaf samples following WBPH infestation, with distinct responses between the resistant genotype ASD7 and the susceptible genotype UBN03078-80-354-7 (Table 2). In the resistant genotype ASD7, GA_3 content increased significantly following WBPH infestation, increasing from

14.00 ng mg^{-1} in control plants to 28.78 ng mg^{-1} in infested plants ($p \leq 0.01$). A similar trend was observed in the susceptible genotype, where GA_3 concentration increased significantly from 4.08 to 8.39 ng mg^{-1} following infestation ($p \leq 0.01$), although the absolute levels remained substantially lower than those detected in ASD7. In contrast, the ABA content in ASD7 decreased significantly following WBPH infestation, declining from 0.310 to 0.107 ng mg^{-1} ($p \leq 0.01$). Conversely, the susceptible genotype demonstrated a pronounced and significant increase in ABA concentration upon WBPH infestation, from 0.310 to 0.107 ng mg^{-1} ($p \leq 0.01$), indicating a genotype-specific hormonal response to insect feeding. No significant changes in DHJA concentration were observed following WBPH infestation in either genotype.

Table 2. Quantitative analysis of the metabolites gibberellin A3 (GA_3), abscisic acid (ABA), and dihydrojasmonic acid in rice leaf samples from all three treatments.

Metabolites and Treatments		Hormone Content (ng/mg^{-1})	
		ASD7	UBN03078-80-354-7(s)
Gibberellin A3 (GA3)	Control	13.997 ± 0.007	4.082 ± 0.002
	WBPH	28.780 ± 0.026 **	8.394 ± 0.008 **
Abscisic Acid (ABA)	Control	0.310 ± 0.003	0.313 ± 0.001
	WBPH	0.107 ± 0.002 **	0.907 ± 0.001 **
Dihydrojasmonic Acid	Control	0.0433 ± 0.003	0.009 ± 0.001
	WBPH	0.0432 ± 0.004	0.011 ± 0.000

SEM denotes standard error of the mean, and hormone content represents the calculated amount derived from the standard curve. $n = 3$. ** a statistically significant difference compared with the control ($p \leq 0.01$), ** a highly significant statistical difference compared with the control ($p \leq 0.01$), as determined using the *t*-test.

2.6.2. Changes in Secondary Metabolite Profiles in Rice Leaves Following WBPH Infestation

The accumulation of secondary metabolites in rice leaves differed markedly between the resistant genotype ASD7 and the susceptible genotype UBN03078-80-354-7 following infestation by the WBPH (Table 3). Genotype-dependent differences were observed in both the diversity and the magnitude of metabolite induction, as measured based on the ratio of WBPH-infested plants to uninfested controls. In the resistant genotype ASD7, WBPH infestation resulted in a pronounced and significant increase in multiple secondary metabolites. Notably, Imidazo [1,2-a]pyrazin-1-ium demonstrated the highest induction level, with a more than 10-fold increase compared with the control ($p \leq 0.01$). Several fatty acid-related compounds, including octadec-9-enoic acid, γ-linolenic acid ethyl ester, palmitic acid, and palmitoleic acid, were also significantly elevated (ratios ranging from 1.84 to 2.32; $p \leq 0.01$). In addition, defense-associated compounds such as ouabain, 2-hydroxybenzothiazole, and 3-nitro-1H-1,2,4-triazole-1,5-diamine were upregulated considerably in ASD7 following WBPH infestation ($p \leq 0.01$). The phenylpropanoid-related compound trans-cinnamaldehyde was significantly, though moderately, induced ($p \leq 0.05$). In contrast, the susceptible genotype UBN03078-80-354-7 exhibited minimal or negligible changes in secondary metabolite accumulation following WBPH infestation. Most compounds detected in ASD7 were absent or present at extremely low levels in the susceptible genotype, with WBPH/control ratios close to zero. Only trace induction was observed for γ-linolenic acid ethyl ester, 4-[3,5-di(tert-butyl)-1H-pyrazol-1-yl] benzoic acid, palmitoleic acid, ouabain, and 2-hydroxybenzothiazole. However, these changes were substantially lower than those observed in ASD7 and were not of strong statistical significance.

Table 3. Analysis of secondary metabolites in leaf samples of the resistant rice genotype ASD7 and the susceptible genotype UBN03078-80-354-7.

Compound	ASD7	UBN03078-80-354-7(s)
	(WBPH)/(Control) Ratio	(WBPH)/(Control) Ratio
Imidazo [1,2-a]pyrazin-1-ium	10.924 **	N/A
Octadec-9-enoic acid	2.167 **	N/A
γ-Linolenic acid ethyl ester	2.322 **	0.002
Palmitic acid	2.277 **	N/A
4-[3,5-di(tert-butyl)-1H-pyrazol-1-yl] benzoic acid	1.657 **	0.652
Palmitoleic acid	1.84 **	0.008
Ouabain	1.76 **	0.005
3-Nitro-1H-1,2,4-triazole-1,5-diamine	1.055 **	N/A
2-Hydroxybenzothiazole	1.264 **	0.006
Trans-Cinnamaldehyde	1.15 *	0.003

* A statistically significant difference compared with the control ($p \leq 0.05$); ** a highly statistically significant difference compared with the control ($p \leq 0.01$), as determined using the *t*-test.

2.7. Gene Expression Analysis of SA/JA-Responsive Pathways Following WBPH Infestation

The expression patterns of salicylic acid (SA)- and jasmonic acid (JA)-responsive genes differed markedly between the tolerant genotype ASD7 and the susceptible genotype UBN03078-80-354-7 following infestation by the WBPH (Figure 10). In ASD7, WBPH infestation induced a significant upregulation of multiple defense-related genes compared with the uninfested control. Transcript levels of JAMyb and *PR1a* were significantly increased ($p \leq 0.05$), whereas *PR10a* demonstrated a robust induction, reaching more than threefold higher expression relative to the control ($p \leq 0.01$). Moderate but consistent increases were also observed for *JAR1*, *PAL1*, and *chitinase*, indicating coordinated activation of both JA- and SA-associated defense pathways in the tolerant genotype.

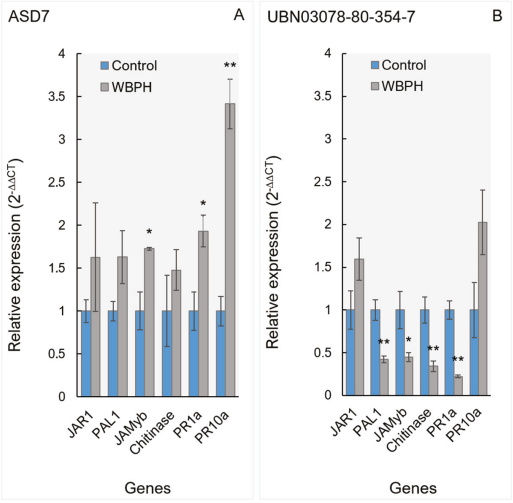

Figure 10. Relative expression of salicylic acid (SA)- and jasmonic acid (JA)-responsive genes in rice genotypes following infestation by the white-backed planthopper (*Sogatella furcifera*). (**A**) ASD7 (tolerant) and (**B**) UBN03078-80-354-7 (susceptible). Transcript levels of JAR1, PAL1, JAMyb, chitinase, PR1a, and *PR10a* were quantified via qRT-PCR in the youngest fully expanded leaves 14 days after WBPH infestation. Gene expression was normalized to OsActin and expressed relative to the uninfested control of the same genotype using the $2^{-\Delta\Delta CT}$ method. Bars represent mean ± SE of three biological replicates ($n = 3$), each with three technical replicates. Asterisks indicate significant differences between infested and control plants within the same genotype (* $p \leq 0.05$; ** $p \leq 0.01$; Student's *t*-test).

https://doi.org/10.3390/plants15050811

In contrast, the susceptible genotype UBN03078-80-354-7 demonstrated a markedly different transcriptional response to WBPH infestation. Expression levels of *PAL1*, *JAMyb*, chitinase, and *PR1a* were significantly downregulated in infested plants compared with their respective controls ($p \leq 0.05$ or $p \leq 0.01$). Although *PR10a* indicated a slight increase in expression following infestation, this induction was substantially lower than that observed in ASD7. No significant induction of *JAR1* was detected in the susceptible genotype.

3. Discussion

3.1. Honeydew Excretion and Salivary Sheath Formation

Honeydew excretion and salivary sheath formation are established indirect indicators of feeding intensity in sap-sucking insects. In this study, rice genotypes differed significantly in both parameters, indicating variation in host suitability to WBPH. PTB33 supported greater honeydew excretion and salivary sheath numbers, indicating efficient probing and sustained phloem ingestion. These observations align with the role of honeydew as a proxy for phloem acceptance and salivary sheaths as markers of successful stylet pathway construction [7,29,30]. In contrast, Rathu Heenati and Mudgo exhibited reduced honeydew output and fewer salivary sheaths, suggesting impaired probing and restricted phloem ingestion. Such reductions are commonly associated with physical and biochemical resistance traits that limit stylet penetration or reduce phloem suitability [31,32]. The positive correspondence between honeydew excretion and salivary sheath formation across genotypes further indicates that phloem ingestion success is contingent upon early probing events. Similar patterns have been reported in resistant rice challenged by WBPH and BPH, where reduced feeding correlates with impaired insect performance [33,34].

Honeydew excretion and salivary sheath formation assays revealed clear genotype-dependent differences in the feeding behavior of *Sogatella furcifera*, reflecting variation in host suitability among rice varieties (Figure 1A,B). Honeydew area is commonly used as an indirect indicator of sap ingestion, whereas the number of salivary sheaths reflects probing frequency and stylet pathway activities during host penetration [35]. However, these parameters primarily capture short-term insect responses during the host establishment phase rather than sustained feeding success.

PTB33 exhibited the largest honeydew drop area (Figure 1A), which might superficially suggest high susceptibility. In contrast, the same variety induced the highest number of salivary sheaths (Figure 1B), indicating frequent probing and repeated stylet insertions. Such feeding behavior is typically associated with difficulty in locating or maintaining access to phloem tissues, rather than effective phloem feeding [3]. Moreover, honeydew excretion does not exclusively represent phloem sap ingestion, as xylem-derived excretions may increase under conditions of feeding disruption or osmotic stress [35]. Therefore, the large honeydew area observed for PTB33 likely reflects compensatory non-phloem feeding rather than true host susceptibility.

3.2. Feeding Behavior by Electrical Penetration Graph

In the present study, apparent genotype-dependent differences in waveform occurrence and duration demonstrate that rice genotypes modulate WBPH feeding behavior at multiple stages, from stylet insertion and pathway activities to phloem and xylem ingestion. The identification of six distinct waveform patterns (Np, N1–N2, N3, N4-a, N4-b, and N5) aligns with previous characterizations of planthopper feeding behavior and confirms the reliability of waveform interpretation in this system. Variation in Np events among genotypes suggests differences in host acceptance and in surface-level cues that influence initial feeding decisions. Prolonged Np durations in specific genotypes indicate prolonged searching or hesitation before stylet insertion, typically associated with

https://doi.org/10.3390/plants15050811

antixenosis-based resistance mediated by surface wax composition, trichome density, or deterrent metabolites [7,29,36,37].

Significant differences in the frequency and duration of pathway-phase waveforms (N1–N2 and N3) highlight genotype-specific effects on stylet penetration through epidermal and mesophyll tissues. Genotypes showing higher frequencies or extended durations of these waveforms likely impose greater mechanical or biochemical constraints on stylet progression. Such constraints have been linked to reinforced cell walls, increased silica deposition, and altered lignin or phenolic profiles in resistant rice genotypes, which collectively impede stylet movement and increase the metabolic costs for planthoppers [27,31]. Prolonged N3 durations in some genotypes further suggest repeated stylet adjustments or unsuccessful attempts to locate vascular tissues, a hallmark of pre-phloem resistance. Phloem-related waveforms (N4-a and N4-b) provided critical insights into post-phloem resistance mechanisms. Genotype-dependent variation in both the frequency and duration indicates differential phloem acceptance and sap ingestion efficiency. Prolonged N4-a durations are generally associated with increased salivation into sieve elements, often reflecting insect attempts to overcome phloem-based defenses such as callose deposition or phloem occlusion. In contrast, reduced frequency or duration of N4-b events in resistant genotypes suggests impaired sustained phloem sap ingestion, consistent with antibiosis mechanisms that restrict nutrient acquisition and reduce insect fitness [36–39]. These findings align with recent reports demonstrating that resistance genes and quantitative resistance loci in rice frequently target phloem-level interactions rather than causing the immediate cessation of feeding.

Collectively, the combined analysis of waveform number (NEWI), duration per event (WDEI), and cumulative duration per insect (WDI) reveals that resistance to WBPH is expressed through multiple interacting mechanisms operating across distinct feeding stages. Resistant genotypes often disrupt feeding early by prolonging NP and pathway phases and further restrict insect performance by reducing sustained phloem sap ingestion [36,37]. Such multi-layered resistance is highly advantageous for durable pest management, as it exerts continuous but moderate pressure on insect populations and may reduce the likelihood of rapid resistance breakdown.

3.3. Survival and Development Bioassays in WBPH

Survival and developmental traits provide integrative measures of host suitability for sap-feeders. In this study, WBPH survival and development differed significantly among rice genotypes, indicating genotype-dependent antibiosis. Early instars demonstrated negligible mortality across all genotypes, consistent with reports that initial nymphal stages rely on maternal reserves and exhibit limited feeding activity [7,38]. Divergent survival trajectories from the third instar onward suggest that resistance factors become effective as feeding intensity increases.

Pronounced reductions in survival on ASD7, Babawee, and Rathu Heenati support antibiosis-based resistance, a pattern frequently associated with phloem-mediated defensive traits that restrict nutrient acquisition [27,39]. In contrast, high survival and rapid development on TN1 and KDML105 indicate high host suitability and the absence of antibiosis [30]. Several genotypes, including RD49 and UBN03078-80-354-7, exhibited intermediate survival, suggesting partial resistance, underscoring their value in breeding programs [40]. Prolonged nymphal development and reduced adult longevity on resistant genotypes indicate nutritional stress or chronic exposure to plant defenses, highlighting trans-stadial effects of antibiosis [7,31]. Overall, the survival and developmental assays demonstrate mid- to late-instar antibiosis as a key resistance mechanism, complemented by feeding-based metrics from honeydew and EPG analyses.

3.4. The Biological Rice Genotypes Factor

Scanning electron microscopy revealed substantial variation in trichome density among rice genotypes, particularly on the adaxial leaf sheath, which is the primary feeding site of WBPH. Genotypes such as TN1 and PTB33 exhibited significantly higher macrotrichome and total trichome densities, whereas resistant genotypes, including ASD7, Mudgo, and Rathu Heenati, showed consistently lower trichome densities. These findings suggest that trichomes alone do not confer direct resistance to WBPH; rather, they modulate insect settling and probing behavior in a genotype-dependent manner. Trichomes are considered to represent a first line of defense by acting as physical barriers that interfere with insect attachment, movement, and stylet insertion, thereby contributing to antixenosis [41,42]. However, high trichome density does not necessarily confer resistance. In some host–herbivore systems, dense trichomes may even facilitate insect settling by providing shelter or anchorage points, particularly for small-bodied sap-feeders [42]. This dual role aligns with the observed susceptibility of TN1 despite its high trichome density, indicating that physical defenses must operate in conjunction with chemical and physiological traits to effectively restrict WBPH feeding.

3.5. The Correlation and Principal Component Analysis Between Factors

Correlations underscore the importance of integrating physical and behavioral metrics when evaluating resistance. Previous studies have demonstrated that surface traits, including trichome density and cuticular composition, can modulate the frequency and duration of EPG waveforms associated with pathway and phloem phases, thereby influencing overall feeding success [36–39]. Nevertheless, the present results suggest that trichomes alone are insufficient to prevent sustained phloem ingestion, reinforcing the need for post-penetration defenses. The honeydew excretion and salivary sheath assays provided rapid and synergistic insights into WBPH feeding performance and host plant suitability. These methods effectively differentiated resistant, moderately resistant, and susceptible genotypes, supporting their utility as reliable phenotyping tools in rice resistance breeding programs. When integrated with advanced techniques such as EPG analysis and biochemical profiling, these assays contribute to a robust, multi-level framework for elucidating resistance mechanisms against WBPH and improving sustainable rice pest management strategies.

3.6. Plant Hormone and Secondary Metabolite Profiling

Quantitative phytohormone analysis revealed contrasting hormonal responses between the resistant genotype ASD7 and the susceptible genotype UBN03078-80-354-7 following WBPH infestation. The significant increase in GA_3 in both genotypes indicates that WBPH feeding modulates growth-related signaling pathways. However, the substantially higher GA_3 levels in ASD7 may reflect a compensatory growth response that offsets feeding damage, contributing to tolerance rather than direct resistance [43]. In contrast, ABA exhibited opposing trends between genotypes. The reduction in ABA in ASD7 following infestation aligns with enhanced defense activation, as ABA antagonizes JA and SA-mediated defense pathways. Conversely, the pronounced ABA accumulation in the susceptible genotype suggests the suppression of effective defense signaling, thereby facilitating WBPH feeding and performance. Such antagonistic interactions between the ABA and JA/SA signaling pathways are well established in plant–insect interactions and are considered a key determinant of resistance outcomes [44,45].

Secondary metabolite profiling further revealed pronounced genotype-dependent differences in chemical defenses. While WBPH infestation triggered substantial accumulation of multiple defense-associated metabolites in ASD7, the susceptible genotype indicated

minimal or negligible induction. The robust upregulation of fatty acid-related compounds, phenylpropanoids, and heterocyclic defense molecules in ASD7 suggests the activation of multiple biosynthetic pathways that collectively contribute to antibiosis by reducing insect survival, delaying development, and restricting feeding efficiency.

Fatty acid derivatives and phenylpropanoid-related compounds are implicated in direct toxicity, feeding deterrence, and reinforcement of cell wall defenses against herbivores [31,46]. The dramatic induction of certain compounds, such as imidazo [1,2-a]pyrazin-1-ium and ouabain-like molecules, further supports the presence of potent chemical defenses in *ASD7*. In contrast, the minimal metabolic response in the susceptible genotype suggests a failure to mount effective inducible defenses upon WBPH attack.

3.7. Gene Expression Profiling of SA/JA Signaling Pathways

Gene expression analysis corroborated the metabolomic and hormonal findings by demonstrating the coordinated activation of SA- and JA-responsive pathways in *ASD7*. The robust induction of *PR10a*, along with the upregulation of *JAMyb*, *PR1a*, *JAR1*, *PAL1*, and *chitinase*, indicates a broad-spectrum defense response that integrates both SA- and JA-mediated signaling. Such coordinated activation is a hallmark of durable resistance against piercing–sucking insects, which often evade or suppress single-pathway defenses [47,48]. In contrast, the downregulation of key defense genes in the susceptible genotype suggests active suppression or a failure of defense signaling, consistent with elevated ABA accumulation and insufficient induction of secondary metabolites. The nominal induction of *PR10a* alone appears insufficient to confer effective resistance, highlighting the importance of network-level defense activation rather than isolated gene responses.

4. Materials and Methods

The experiment was conducted in a laboratory and in a field at Suranaree University of Technology (14°58′14.38″ N 102°06′7.06″ E), Nakorn Ratchasima, Thailand.

4.1. Plant Materials and Insect Colony

Ten rice genotypes/lines were utilized for feeding and growth assays. Seeds of Rathu Heenati, RD49, Babawee, PTB33, Mudgo, ASD7, KDML105, TN1, UBN03078-80-354-7, and UBN03078-101-342-4-148 were obtained from the Ubon Ratchathani Rice Research Center and the Pathum Thani Rice Research Center in Thailand. A panel of rice genotypes was assembled, comprising the resistant donors (e.g., PTB33, Rathu Heenati) and breeding lines under evaluation, along with a susceptible check (e.g., TN1). Seeds were surface-sterilized with 1% sodium hypochlorite for 2 min, rinsed 3×, and germinated on moist paper for 48 h. Seedlings were subsequently transplanted into 10 cm pots (two plants per pot) filled with sterilized loam/peat/sand (2:1:1, $v/v/v$) and grown in a controlled greenhouse at 28 ± 2 °C, 60 ± 10% relative humidity (RH) and a 14:10 L:D photoperiod, with non-limiting nutrients provided weekly using half-strength Hoagland solution. Unless stated otherwise, plants were used at the tillering stage (25–30 days after sowing); panicle-stage assays were repeated at heading to test tissue/stage specificity.

White-backed planthoppers were obtained from the Ubon Ratchathani Rice Research Center. Colonies were maintained and multiplied on seedlings (≤14-day-old) of the susceptible genotypes TN1 and Khao Dawk Mali 105 (KDML105) under controlled conditions (28 °C, 60–70% RH, 14:10 light/dark photoperiod) in insect-proof cages. For bioassays, first-instar nymphs were used for growth and development tests, and fourth-instar nymphs were used for feeding rate and honeydew excretion assays. Unless stated otherwise, cohorts were synchronized via daily collections of newly molted nymphs.

https://doi.org/10.3390/plants15050811

4.2. Honeydew Excretion Assays

To quantify feeding intensity, honeydew excretion by WBPH was measured across 10 rice genotypes in a controlled experiment. A completely randomized design (CRD) was employed. Twenty biological replicates were prepared (one nymph per replicate). All assays were conducted at the Scientific and Technological Equipment Center, Suranaree University of Technology, at 28 °C and 60–70% RH. Fourth-instar nymphs were gently transferred to the leaf sheath of a test plant and confined using a ventilated clip cage. The exposure lasted 24 h (tillering stage). Honeydew was collected on Whatman No. 1 filter paper placed beneath the confined insect. After 24 h, the papers were immersed in a 0.1% (*w*/*v*) ninhydrin solution (ethanol solvent), air-dried at room temperature until purple spots developed (indicating amino-acid reaction), and then digitized using a flatbed scanner with fixed resolution and lighting [49]. Quantification involved measuring the honeydew area (mm^2) from images using ImageJ version 1.54, National Institutes of Health, Bethesda, MD, USA. Calibration was performed with a stage micrometer, and the thresholding parameters were kept constant across samples. For each replicate, the total stained area per insect per 24 h was recorded as the response variable (Figure S2).

4.3. Leaf Staining Assay (Eosin) for Visualizing Feeding Punctures (Salivary Sheath Method)

To quantify planthopper stylet pathway traits and feeding success, salivary sheaths were enumerated in the leaf sheath tissue of the same genotype panel under controlled conditions. Plants at tillering (45 days after sowing) were used. Fourth-instar WBPH nymphs were starved for two hours (moistened air only) before assays to standardize motivation. A CRD was applied, with $n = 20$ biological replicates per genotype (one nymph per plant/leaf area). Assays were conducted at the Scientific and Technological Equipment Center, Suranaree University of Technology, at 28 °C and 60–70% RH. A ventilated clip cage (Ø 2.5–3.0 cm) was attached to the mid-leaf sheath (the primary feeding site). One fourth-instar nymph was confined for eight hours during the photophase. Following exposure, the insects were removed. Leaf sheath segments (≈2–3 cm) were excised and cleared in ethanol/acetic acid (3:1, *v*/*v*) for 30 min then rinsed twice in 70% ethanol and once in distilled water (1–2 min each). Leaves were immersed in 1% (*w*/*v*) eosin Y (in distilled water) for 10 min at room temperature, rinsed three times in distilled water (30 s each) to remove excess dye, and air-dried on lint-free paper (≈5 min). Pilot tests can be used to adjust staining to 8–12 min depending on cuticle thickness. Stained areas were examined under a stereomicroscope (e.g., 20–40×). Eosin-positive feeding punctures appeared as distinct red/crimson dots along the stylet pathway. For each replicate, we recorded the puncture count per field (fixed field of view), feeding puncture density (punctures cm^{-2}; using a 1 cm^2 graticule or calibrated image), and the proportion of fields with ≥1 puncture (host acceptance proxy). When needed, images were captured (with fixed illumination and magnification) and analyzed in ImageJ to confirm counts. Unstained leaves served as negative controls to verify the background. The response variable was feeding puncture density (cm^{-2}) per replicate [50].

4.4. Electrical Penetration Graph Recordings of Feeding Behavior

This experiment aimed to quantify and compare the feeding behavior of the 10 rice genotypes/lines using DC-EPG. Feeding-behavior experiments were conducted using a Giga-8 DC electropenetrography (EPG) system (EPG Systems, Wageningen, The Netherlands) with an input resistance of 109 Ω (1 GΩ) and an adjustable plant voltage. The cassava plant and the insect with the EPG probe were placed within a Faraday cage ($1.5 \times 2 \times 1.5\ m^3$) to block electrical noise. The system was installed in a temperature-controlled room at 28 ± 2 °C and 60 ± 5% RH. EPG signals were recorded using Stylet+d

software, with the signal range adjusted from −5 to +5 V, and displayed on a computer. Fourth-instar nymphs of WBPH were placed in a glass vial and immobilized on ice for 5–10 s before being connected to a gold wire electrode (2.5 cm long, 12 µm diameter) (EPG Systems, Wageningen, The Netherlands), with water-based silver glue (Wageningen University) applied to the insect's pronotum. The other end of the wire was attached to a copper electrode (1 mm diameter, 2.5 cm long) (Sigmund Cohn Corp, Mt Vernon, NY, USA), which was connected to the EPG probe. The WBPH was placed on the abaxial leaf surface and fixed with parafilm. Signal adjustments were made if needed, and data were recorded using Stylet+d software. Each WBPH was observed for three hours daily, with 20 WBPH tested per genotype in a completely randomized design. Annotated waveforms (NP, stylet pathway, phloem salivation, phloem ingestion, intracellular puncture, and xylem ingestion) were analyzed using EPG Systems software and a modified Ebert 3.0 program in SAS Enterprise Guide 7.1, SAS 9.4 statistical software.

EPG data recorded using EPG Systems Stylet+d were manually annotated utilizing EPG Systems Stylet+a software. The annotated waveforms included Np, pathway in epidermis/mesophyll (N1, N2), phloem salivation or sieve-element salivation (N4-a), sustained phloem sap ingestion or phloem ingestion (N4-b), and xylem ingestion (N5). The waveform patterns were categorized based on amplitude, relative voltage level, R/emf origin, frequency, and waveform context, as described in previous EPG studies on brown planthoppers, planthoppers, the whitefly *B. tabaci*, and leafhoppers [37–39,41–45]. Annotation files were then directly transferred to a modified version of the Ebert 3.0 program in SAS Enterprise Guide 7.1, SAS 9.4 statistical software (SAS Institute, Cary, NC, USA), for further analysis, producing the same parameters as the popular Sarria Excel workbook [51,52].

4.5. Development and Survival Bioassays (First Instar to Adult)

This assay was designed to compare the nymphal development and survival of WBPH across 10 rice genotypes/lines. Each seedling was grown individually in a 7–10 cm pot (sterilized substrate), watered daily, and kept free of pesticides. Newly hatched first-instar (N1) nymphs of WBPH (≤24 h old) were utilized. Assays were conducted in a controlled-environment room at 28 °C and 75% RH, with a 12:12 light/dark photoperiod. A completely randomized design (CRD) was employed, with n = 20 biological replicates per genotype (one nymph per seedling = one replicate). A single N1 nymph was gently transferred with a camel-hair brush to the leaf sheath/collar of a seedling and confined using a ventilated clip cage (Ø 2.5–3.0 cm) or a mesh sleeve that allowed free movement on that plant only. Plants were spaced to prevent cage contact. Each replicate was inspected at the same time every 24 h. For each nymph, we recorded the instar transitions (N1→N2→N3→N4→N5→adult) based on exuviae and morphology; instar duration (days); cumulative development time to adult (days); stage-specific mortality (cause noted if evident: desiccation, escape, handling); adult emergence (%); and sex ratio [53,54]. Plants were replaced with fresh seedlings every 3–4 days or immediately if wilting occurred. Escaped or physically injured nymphs were recorded and excluded (censored) a priori (Figure S3).

4.6. Biophysical Factors

The morphology of the abaxial surface of the ten rice leaves—RD49, Babawee, Rathu Heenati, PTB33, Mudgo, ASD7 (putative resistant), TN1, KDML105, UBN03078-80-354-7 (susceptible), and UBN03078-101-342-4-148 (susceptible)—was analyzed for trichome density. Samples from the leaf sheath at the stem of 45-day-old plants were fixed in 37% formaldehyde overnight, washed in phosphate-buffered saline, and dehydrated in an ethanol series (70%, 80%, 95%, and 100%). Samples were critical-point-dried and coated with a gold–palladium alloy. The fixed surfaces of the leaves were then observed under a

cutting-edge scanning electron microscope (SEM) (SEM™, FEI, Quanta450, Netherlands). Trichome density was assessed manually at 0.3 mm^2 intervals, with 10 biological replications and five images per leaf [50].

4.7. Pearson Correlation and Principal Component Analysis Between the Parameters

A correlation analysis (Pearson correlation) was conducted on the mean values for honeydew excretion, salivary sheath formation, EPG analysis for WBPH feeding behavior, development and survival rate, and trichome factors to identify the relationships among these parameters in this study. Differences were considered significant at the 5% level. PCA was used to evaluate the relationships among the 10 rice genotypes. Principal component analysis and cluster analysis were utilized as multivariate statistical methods to discern patterns among the investigated rice genotypes based on multiple parameters, including honeydew excretion, salivary sheath formation, EPG analysis for WBPH feeding behavior, development and survival rate, and trichome factors. Pearson correlation analysis, PCA, and cluster analysis were performed using OriginPro 2024 (OriginLab Corporation, Northampton, MA, USA).

Based on the results of correlation, PCA, and hierarchical cluster analyses, two rice genotypes exhibiting contrasting resistance phenotypes (resistant and susceptible) were selected for further studies. These selected genotypes were used to compare plant hormone and secondary metabolite profiles and analyze gene expression in SA- and JA-responsive pathways.

4.8. Plant Hormone and Secondary Metabolite Analysis

Leaves from the resistant rice genotypes ASD7 and the susceptible line UBN03078-80-354-7 were collected from each experimental set (n = 3 biological replicates per genotype). Samples were immediately frozen in liquid nitrogen, ground to a fine powder, and freeze-dried to a constant weight. Freeze-dried leaf powder (35 mg) was used for hormone extraction. Leaf powder was extracted with 3.5 mL methanol containing 0.01% (v/v) formic acid, vortexed for 30 s, and incubated at −20 °C for 48 h. Extracts were centrifuged at 14,000× g for 60 min at 4 °C, and supernatants were collected. To reduce matrix effects, extracts were diluted with acetonitrile and ultrapure water and subsequently purified using solid-phase extraction (SPE) cartridges pre-conditioned with methanol and water. Analytes were eluted with acetonitrile, evaporated to dryness under vacuum, reconstituted in methanol, diluted (1:1, v/v) with 0.2% formic acid in water, and filtered (0.22 μm PTFE) before analysis.

UHPLC–Orbitrap MS was used for phytohormone analysis, with a UHPLC system coupled to a Q-Exactive Orbitrap mass spectrometer (Thermo Fisher Scientific, Waltham, MA, USA) equipped with a C18 column (2.1 mm × 100 mm, 1.9 μm particle size). Mobile phases consisted of water (A) and acetonitrile (B), both containing 0.1% formic acid. A gradient elution was applied from 10% to 100% B at a flow rate of 0.3 mL min^{-1}. The column temperature was maintained at 40 °C, the injection volume was 5 μL, and the autosampler temperature was set to 10 °C. The ion polarity was in positive mode, the capillary temperature was 350 °C, and the spray voltage was 3.8 kV. Data were acquired in Full-MS and targeted PRM modes as described in [55].

Calibration and quantification involved preparing stock solutions (1 mg mL^{-1}) of GA, ABA, and DHJA in methanol and diluting them in series to generate external calibration standards (0.25–40 mg mL^{-1}). Quantification was conducted using PRM with the following precursor ions: GA (m/z 347.14891), ABA (m/z 265.14344), and DHJA (m/z 213.14852). Analytes were quantified based on extracted ion chromatograms (±5 ppm) using linear

regression, and concentrations were expressed as mg g^{-1} dry weight. Procedural blanks and spiked samples were included for quality control.

4.9. Gene Expression Analysis of SA/JA-Responsive Pathways

The youngest fully expanded leaves of ASD7 (resistant) and UBN03078-80-354-7 (susceptible) were collected 14 days after insect infestation (WBPH), alongside uninfested controls. Leaves were flash-frozen and stored at −80 °C. RNA was extracted using the Plant Total RNA Mini Kit (Favorgen Biotech Corp., Ping Tung, Taiwan) following the manufacturer's protocol, including on-column DNase treatment. RNA quality was verified ($A_{260}/_{280} \approx 2.0$; intact rRNA bands), and 500 ng total RNA was reverse-transcribed with iScript Reverse Transcriptase Supermix (Bio-Rad Laboratories, Hercules, CA, USA) to synthesize cDNA (20 µL reaction). SA/JA pathway markers were as follows: JAR1 (conjugates JA→JA-Ile), PAL1 (phenylpropanoid entry enzyme), JAMyb (JA/SA-responsive TF), chitinase (defense enzyme), *PR1a*, and *PR10a* (pathogenesis-related) (Table S1). OsActin served as the reference gene [56]. These genes were selected to represent a functional continuum from the essential activation of bioactive JA-Ile (JAR1) and transcriptional regulation (JAMyb) to the structural reinforcement of cell walls via the phenylpropanoid pathway (PAL1) and, finally, the production of direct defensive effectors (Chitinase, *PR1a*, *PR10a*) that target the physiological integrity of the herbivore [57–65].

Reactions (10–20 µL) contained SYBR Green master mix, gene-specific primers (Table S1), and 2 µL diluted cDNA. Cycling was performed using a real-time PCR system: 95 °C 3 min; 40 cycles of 95 °C 10 s/58–60 °C 20–30 s/72 °C 20–30 s. Melt-curve analysis was employed to verify specificity. No-RT and no-template controls were included. There were three biological replicates per genotype × infestation ($n = 3$). CT values were processed after baseline/threshold inspection; outliers due to melt-curve anomalies were excluded a priori. Relative expression was calculated as $2^{-\Delta\Delta CT}$, normalized to OsActin and then to the uninfested control of the same genotype.

4.10. Statistical Analysis

For all experiments, the honeydew area, salivary sheath, mean development time (days) from N1 to adult, stage-specific mortality (%) per instar, adult emergence (%), and trichome density were analyzed utilizing one-way ANOVA with genotype as the factor (CRD). When significant, means were separated using Tukey's honestly significant difference (HSD) test ($p = 0.05$) in SAS. If required, data were checked for normality and homoscedasticity; the Cox transformation was applied when assumptions were violated.

EPG waveforms were characterized based on feeding-behavior events as follows: Np, pathway in epidermis/mesophyll (N1, N2), phloem salivation or sieve-element salivation (N4-a), sustained phloem sap ingestion or phloem ingestion (N4-b), and xylem ingestion (N5). The variables of total probing duration (TPD), total waveform duration (TWD), frequency of waveform events per insect (NWEI), WDEI, and waveform duration per insect (WDI) were also calculated (mean ± standard error), as described in previous studies [66]. The variables were compared using the Tukey–Kramer test at $p < 0.05$. All analyses were performed using SAS V9.4. Pearson correlation analysis was conducted for the mean values of honeydew area, salivary sheath method, mean development time (days) from N1 to adult, stage-specific mortality (%) per instar, adult emergence (%), and trichome density using OriginPro 2024 software, with significance set at $p < 0.05$ [67].

5. Conclusions

This study demonstrates that rice resistance to *S. furcifera* is governed by the integrated action of physical and chemical defense mechanisms. Leaf surface traits contributed to

antixenosis by modulating insect settling and probing behavior. In contrast, inducible hormonal signaling, secondary metabolite accumulation, and defense-related gene activation played a primary role in antibiosis by restricting feeding efficiency, survival, and development. Behavioral assays (honeydew excretion, salivary sheath formation, and EPG) aligned with life-history outcomes, validating their utility for resistance screening. Notably, gene expression analysis revealed robust upregulation of *PR10a* in resistant rice, highlighting its potential role as a molecular marker of WBPH resistance. Rice genotypes that exhibit coordinated antixenosis and antibiosis responses, such as *ASD7*, represent valuable sources of durable resistance. Overall, multi-trait phenotyping provides a robust framework for screening and deploying rice genotypes with sustainable resistance to WBPH.

Supplementary Materials: The following supporting information can be downloaded at: https://www.mdpi.com/article/10.3390/plants15050811/s1, Figure S1. The size of the honeydew area and the intensity of the honeydew color correspond to the white-backed planthopper (Sogatella furcifera) feeding activity. Figure S2. (A) Collection of white-backed planthopper (Sogatella furcifera) honeydew on Whatman filter paper that was placed at the bottom of insect cages, and (B) representative staining of honeydew spots on filter paper with 0.1% ninhydrin. Figure S3. The Rice phenology used for development and survival bioassays. Each seedling was grown individually in a 7–10 cm pot (sterilized substrate), watered daily, and kept free of pesticides. Table S1. Sequencing primer and the function of the genes.

Author Contributions: Conceptualization, J.R., K.U., J.J. and J.W.; methodology, J.R., K.U. and N.C.; software, J.R., K.U. and N.C.; validation, J.R. and K.U.; formal analysis, J.R., K.U. and N.C.; investigation, J.R.; resources, J.R., K.U., N.C. and J.J.; data curation, N.C.; writing—original draft preparation, J.R. and K.U.; writing—review and editing, J.R., K.U., J.J. and J.W.; visualization, J.R., K.U., J.J. and J.W.; supervision, J.R. and J.W.; project administration, J.R., K.U. and J.J.; funding acquisition, J.R., K.U. and J.J. All authors have read and agreed to the published version of the manuscript.

Funding: Agricultural Research Development Agency (Public Organization) (Grant no. 99766) and the Suranaree University of Technology (Grant no. PRP6405030060).

Data Availability Statement: The original contributions presented in this study are included in the article/Supplementary Materials. Further inquiries can be directed to the corresponding author.

Acknowledgments: The authors would like to thank Thitinan Rianthong and Putsayanat Chonpho for the resources, sampling, and methodology. Thanks to Tatpong Tulyananda and Sucheewin Krobthong for their kind assistance with secondary metabolite extraction and analysis. We would like to thank the Center for Scientific and Technological Equipment at Suranaree University of Technology for providing the equipment for this research.

Conflicts of Interest: The authors declare no conflicts of interest.

Abbreviations

The following abbreviations are used in this manuscript:

CRD	Completely Randomized Design
EPG	Electrical Penetration Graph
IRRI	International Rice Research Institution
JA	Jasmonic acid
RGSV	Rice grassy stunt virus
SEM	Scanning Electron Microscope
SA	Salicylic acid
SAS	Statistical Analysis System
v/v	Volume/volume percentage

References

1. Ye, Y.; Xiong, S.; Guan, X.; Tang, T.; Zhu, Z.; Zhu, X.; Hu, J.; Wu, J.; Zhang, S. Insight into rice resistance to the brown planthopper: Gene cloning, functional analysis, and breeding applications. *Int. J. Mol. Sci.* **2024**, *25*, 13397. [CrossRef] [PubMed]
2. Heong, K.L.; Hardy, B. *Planthoppers: New Threats to the Sustainability of Intensive Rice Production Systems in Asia*; IRRI: Los Baños, Philippines, 2009.
3. Sogawa, K. The rice brown planthopper: Feeding physiology and host plant interactions. *Annu. Rev. Entomol.* **1982**, *27*, 49–73. [CrossRef]
4. Cheng, J.A. *Rice planthopper problems and relevant causes in China. Planthoppers: New Threats to the Sustainability of Intensive rice production systems in Asia*; IRRI: Los Baños, Philippine, 2009; pp. 157–178.
5. Matsumura, M.; Takeuchi, H.; Satoh, M.; Sanada-Morimura, S.; Otuka, A.; Watanabe, T.; Van Thanh, D. Current status of insecticide resistance in rice planthoppers in Asia. *Pest Manag. Sci.* **2009**, *65*, 113–120.
6. Bottrell, D.G.; Schoenly, K.G. Resurrecting the ghost of green revolutions past: The brown planthopper as a recurring threat to high-yielding rice production in tropical Asia. *J. Asia-Pac. Entomol.* **2012**, *15*, 122–140. [CrossRef]
7. Horgan, F.G.; Crisol, E. Hybrid rice and insect herbivores in Asia. *Entomol. Exp. Appl.* **2013**, *148*, 1–19. [CrossRef]
8. Painter, R.H. *Insect Resistance in Crop Plants*; University Press of Kansas: Lawrence, KS, USA, 1951.
9. Smith, C.M. *Plant Resistance to Arthropods: Molecular and Conventional Approaches*; Springer: Dordrecht, The Netherlands, 2005.
10. Velusamy, R.; Heinrichs, E.A.; Medrano, F.G. Greenhouse techniques to identify field resistance to brown planthopper. Nilaparvata lugens. *Crop Sci.* **1986**, *26*, 1024–1027.
11. Cao, T.T.; Lu, J.; Lou, Y.G.; Cheng, J.A. feeding-induced interactions between two rice planthoppers, *Nilaparvata lugens* and *Sogatella furcifera* (Hemiptera: Delphacidae): Effects on feeding and honeydew excretion. *Environ. Entomol.* **2013**, *42*, 1281–1291. [CrossRef]
12. Carrasco, D.; Larsson, M.C.; Anderson, P. Insect host plant selection in complex environments. *Curr. Opin. Insect Sci.* **2015**, *8*, 1–7. [CrossRef]
13. Panda, N.; Khush, G.S. *Host Plant Resistance to Insects*; CAB International: Wallingford, UK, 1995.
14. Yoshihara, T.; Sogawa, K.; Pathak, M.D.; Juliano, B.O. Soluble silicic acid as a sucking inhibitory substance in rice against the brown planthopper. *Entomol. Exp. Appl.* **1979**, *26*, 314–322. [CrossRef]
15. Pathak, P.K.; Saxena, R.C. Honeydew excretion by Nilaparvata lugens as an indicator of feeding activity. *Entomol. Exp. Appl.* **1981**, *30*, 119–123.
16. Mclean, D.; Kinsey, M. A Technique for electronically recording aphid feeding and salivation. *Nature* **1964**, *202*, 1358–1359. [CrossRef]
17. TjallingiI, W.F. Mechanoreceptors of the aphid labium. *Entomol. Exp. Appl.* **1978**, *24*, 731–737. [CrossRef]
18. Tjallingii, W.F. Electrical recording of stylet penetration activities. In *Aphids: Their Biology, Natural Enemies and Control*; Elsevier: Amsterdam, The Netherlands, 1988; pp. 95–108.
19. Seo, B.Y.; Kwon, Y.H.; Jung, J.K.; Kim, G.H. Feeding behavior of the brown planthopper on resistant and susceptible rice varieties. *Entomol. Exp. Appl.* **2009**, *130*, 287–295.
20. Seo, B.Y.; Jung, J.K.; Choi, B.R.; Park, H.M.; Lee, S.W.; Lee, B.H. Survival rate and stylet penetration behavior of current Korean populations of the brown planthopper, *Nilaparvata lugens*, on resistant rice varieties. *J. Asia Pac. Entomol.* **2010**, *13*, 1–7. [CrossRef]
21. Lei, W.; Li, P.; Han, Y.; Gong, S.; Yang, L.; Hou, M. EPG recordings reveal differential feeding behaviors in Sogatella furcifera in response to plant virus infection and transmission success. *Sci. Rep.* **2016**, *6*, 30240. [CrossRef] [PubMed]
22. Chandrasekar, K.; Suresh, S.; Soundararajan, R.P.; Boopathi, T. Feeding behavior of whitebacked planthopper, *Sogatella furcifera* (Horvath) on selected rice genotypes. *J. Entomol. Zool. Stud.* **2017**, *5*, 1655–1659.
23. Kang, Y.; Koo, H.N.; Kim, H.K.; Kim, G.H. Analysis of the feeding behavior and life table of *Nilaparvata lugens* and *Sogatella furcifera* (Hemiptera: Delphacidae) under sublethal concentrations of imidacloprid and sulfoxaflor. *Insects* **2022**, *13*, 1130. [CrossRef] [PubMed]
24. Heinrichs, E.A.; Medrano, F.G.; Rapusas, H.R. *Genetic Evaluation for Insect Resistance in Rice*; IRRI: Los Baños, Philippines, 1985.
25. War, A.R.; Paulraj, M.G.; Ahmad, T.; Buhroo, A.A.; Hussain, B.; Ignacimuthu, S.; Sharma, H.C. Mechanisms of plant defense against insect herbivores. *Plant Signal. Behav.* **2012**, *7*, 1306–1320. [CrossRef]
26. Mitsuhara, I.; Matsufuru, H.; Ohshima, M.; Kaku, H.; Nakajima, Y.; Murai, N.; Natori, S.; Ohashi, Y. Induced expression of PR10 genes in rice plants. *Plant Mol. Biol.* **2008**, *68*, 361–371.
27. Du, B.; Zhang, W.; Liu, B.; Hu, J.; Wei, Z.; Shi, Z.; He, R.; Zhu, L.; Chen, R.; Han, B.; et al. Identification and characterization of Bph14, a gene conferring resistance to brown planthopper in rice. *Proc. Natl. Acad. Sci. USA* **2009**, *106*, 22163–22168. [CrossRef]
28. He, Y.; Chen, L.; Chen, J.; Zhang, J.; Chen, L.; Shen, J.; Zhu, Y.C. Electrical penetration graph evidence thatpymetrozine toxicity to the rice brown planthopper is byinhibition of phloem feeding. *Pest Manag. Sci.* **2011**, *67*, 483–491. [CrossRef]
29. Backus, E.A.; Cline, A.R.; Ellerseick, M.R.; Serrano, M.S. Lygus hesperus feeding behavior: New EPG waveforms and expanded behavioral meanings. *Ann. Entomol. Soc. Am.* **2015**, *108*, 41–61.

30. Ning, S.; Yang, L.; Chen, Z.; Zhou, H.; Wang, X.; Li, Z. Integrating EPG and honeydew analysis reveals resistance mechanisms in rice against planthoppers. *J. Econ. Entomol.* **2022**, *115*, 1871–1881.
31. Li, R.; Weldegergis, B.T.; Li, J.; Jung, C.; Qu, J.; Sun, Y.; Qian, H.; Tee, C.; van Loon, J.J.A.; Dicke, M.; et al. Virulence factors of insect herbivores and plant defense responses. *New Phytol.* **2019**, *223*, 1383–1398.
32. Hu, L.; Ye, M.; Li, R.; Lou, Y. Plant-mediated interactions between herbivores and rice defense signaling. *Front. Plant Sci.* **2023**, *14*, 1187421.
33. Heinrichs, E.A. Perspectives and directions for the continued development of insect-resistant rice varieties. *Agric. Ecosyst. Environ.* **1986**, *18*, 9–36. [CrossRef]
34. Qiu, Y.; Guo, J.; Jing, S.; Tang, M.; He, G. Identification of antibiosis and antixenosis in rice varieties resistant to the brown planthopper. *J. Econ. Entomol.* **2011**, *104*, 738–746.
35. Heong, K.L.; Sogawa, K. Relationship between feeding activity and honeydew excretion of the brown planthopper *Nilaparvata lugens* (Stål) on rice plants. *Appl. Entomol. Zool.* **1989**, *24*, 449–455.
36. Roddee, J.; Wangkeeree, J.; Hanboonsong, Y. Identification and Evaluation of Sugarcane Cultivars for Antixenosis Resistance to the Leafhopper *Yamatotettix flavovittatus* Matsumura (Hemiptera: Cicadellidae). *Plants* **2024**, *13*, 2299. [CrossRef]
37. Pimkornburee, S.; Pombud, S.; Buensanteai, K.; Namanusart, W.; Aiamla-or, S.; Roddee, J. Impact of cassava cultivars on stylet penetration behavior and settling of *Bemisia tabaci* Gennadius (Hemiptera: Aleyrodidae). *Plants* **2024**, *13*, 3218. [CrossRef]
38. Wu, Y.; Zhang, Y.; Xu, J.; Li, Z.; Wang, X.; He, G. Behavioral and physiological mechanisms of brown planthopper resistance in rice. *Pest Manag. Sci.* **2021**, *77*, 3505–3516.
39. Zhang, C.; Luo, S.; Xu, J.; Lou, Y.; He, G. Advances in understanding rice resistance mechanisms to planthoppers. *Plants* **2023**, *12*, 2418.
40. Crowder, D.W.; Jabbour, R. Relationships between biodiversity and biological control in agroecosystems. *Curr. Opin. Insect Sci.* **2014**, *2*, 8–17.
41. Levin, D.A. The role of trichomes in plant defense. *Q. Rev. Biol.* **1973**, *48*, 3–15. [CrossRef]
42. Karabourniotis, G.; Liakopoulos, G.; Nikolopoulos, D.; Bresta, P. Protective and defensive roles of non-glandular trichomes against multiple stresses: Structure–function coordination. *J. Plant Physiol.* **2020**, *255*, 153–175. [CrossRef]
43. Huot, B.; Yao, J.; Montgomery, B.L.; He, S.Y. Growth–defense tradeoffs in plants: A balancing act to optimize fitness. *Mol. Plant* **2014**, *7*, 1267–1287. [CrossRef]
44. Robert-Seilaniantz, A.; Grant, M.; Jones, J.D.G. Hormone crosstalk in defense. *Annu. Rev. Phytopathol.* **2011**, *49*, 317–343. [CrossRef]
45. De Vleesschauwer, D.; Xu, J.; Höfte, M. Hormone-mediated defense networking in rice. *Front. Plant Sci.* **2014**, *5*, 611. [CrossRef]
46. Erb, M.; Reymond, P. Plant–insect molecular interactions. *Annu. Rev. Plant Biol.* **2019**, *70*, 527–557. [CrossRef]
47. Zhou, G.; Qi, J.; Ren, N.; Cheng, J.; Erb, M.; Mao, B.; Lou, Y. Silencing insect herbivore genes by plant-mediated RNAi: A new dimension of plant defense. *Plant Cell* **2019**, *31*, 2567–2585.
48. Fujita, D.; Kohli, A.; Horgan, F.G. Rice resistance to planthoppers and leafhoppers. *Crit. Rev. Plant Sci.* **2013**, *32*, 162–191. [CrossRef]
49. Xiao, C.; Hu, J.; Ao, Y.T.; Cheng, M.X.; Gao, G.J.; Zhang, Q.L.; He, G.C.; He, Y.Q. Development and evaluation of near-isogenic lines for brown planthopper resistance in rice cv. 9311. *Sci. Rep.* **2016**, *6*, 38159. [CrossRef]
50. Roddee, J.; Wangkeeree, J.; Backus, E.A.; Hanboonsong, Y. Probing behavior of the leafhopper analyzed through DC electropenetrography and microscopy. *J. Insect Physiol.* **2023**, *151*, 104584. [CrossRef]
51. Sarria, E.; Cid, M.; Garzo, E.; Fereres, A. Excel workbook for automatic parameter calculation of EPG data. *Comput. Electron. Agric.* **2009**, *67*, 35–42. [CrossRef]
52. Ebert, T.A.; Backus, E.A.; Cid, M.; Fereres, A.; Rogers, M.E. A new SAS program for behavioral analysis of electrical penetration graph data. *Comput. Electron. Agric.* **2015**, *116*, 80–87. [CrossRef]
53. Horgan, F.G.; Amin, I.; Cristóbal, M.S.; Carvalho, L.M.; Barrion, A.T. Resistance and tolerance to the brown planthopper Nilaparvata lugens (Hemiptera: Delphacidae) in rice: Estimating functional relationships among plant resistance traits. *Crop Prot.* **2018**, *107*, 1–10.
54. Zhang, J.-H.; Liu, Y.; Wang, L. Evaluation of rice lines with Bph resistance genes against Nilaparvata lugens: Effects on nymph survival and developmental duration. *Agriculture* **2020**, *10*, 109.
55. Yingchutrakul, Y.; Sittisaree, W.; Mahatnirunkul, T.; Chomtong, T.; Tulyananda, T.; Krobthong, S. Cosmeceutical potentials of *Grammatophyllum speciosum* extracts: Anti-inflammations and anti-collagenase activities with phytochemical profile analysis using an untargeted metabolomics approach. *Cosmetics* **2021**, *8*, 116. [CrossRef]
56. Li, C.; Ni, P.; Francki, M.; Hunter, A.; Zhang, Y.; Schibeci, D.; Li, H.; Tarr, A.; Wang, J.; Cakir, M.; et al. Genes controlling seed dormancy and pre-harvest sprouting in a rice-wheat-barley comparison. *Funct. Integr. Genom.* **2004**, *4*, 84–93. [CrossRef] [PubMed]

57. van Loon, L.C.; Rep, M.; Pieterse, C.M.J. Significance of inducible defense-related proteins in infected plants. *Annu. Rev. Phytopathol.* **2006**, *44*, 135–162. [CrossRef]
58. Fu, Z.Q.; Dong, X. Systemic acquired resistance: Turning local infection into global defense. *Annu. Rev. Plant Biol.* **2013**, *64*, 839–863. [CrossRef]
59. Xie, Y.; Chen, Z.; Brown, R.L.; Bhatnagar, D. Expression and functional analysis of rice PR10 genes in defense responses. *Plant Mol. Biol.* **2014**, *85*, 73–88.
60. Wang, Y.; Li, J.; Li, Y.; Zhu, S.; Zhang, Y. PR10 proteins in plant defense: Structure, function and regulation. *Plants* **2020**, *9*, 115.
61. Wasternack, C.; Song, S. Jasmonates. Biosynthesis, metabolism, and signaling by proteins activating and repressing transcription. *J. Exp. Bot.* **2017**, *68*, 1303–1321. [PubMed]
62. Niu, Y.; Figueroa, P.; Browse, J. Characterization of JAZ-Interacting MYC transcription factors in jasmonate signaling. *Plant Cell* **2011**, *23*, 287–303.
63. Li, C.; Wang, Y.; Liu, L.; Hu, Y.; Zhang, F.; Mergen, S.; Wang, G. The OsMYB transcription factor family in rice: Functional roles in hormone signaling and stress responses. *Plants* **2021**, *10*, 1380.
64. Sharma, H.C.; Sujana, G.; Rao, D.M. Morphological and biochemical components of resistance to insect pests in plants. *Agric. Res.* **2018**, *7*, 235–250.
65. Grover, A. Plant chitinases: Genetic diversity and physiological roles. *Crit. Rev. Plant Sci.* **2012**, *31*, 57–73. [CrossRef]
66. Backus, E.A.; Cline, A.R.; Ellerseick, M.R.; Serrano, M.S. Lygus hesperus (Hemiptera: Miridae) feeding on cotton: New methods and parameters for analysis of nonsequential electrical penetration graph data. *Ann. Entomol. Soc. Am.* **2007**, *100*, 296–310. [CrossRef]
67. Moberly, J.G.; Bernards, M.T.; Waynant, K.V. Key features and updates for Origin 2018. *J. Cheminform.* **2018**, *10*, 5. [CrossRef]

Disclaimer/Publisher's Note: The statements, opinions and data contained in all publications are solely those of the individual author(s) and contributor(s) and not of MDPI and/or the editor(s). MDPI and/or the editor(s) disclaim responsibility for any injury to people or property resulting from any ideas, methods, instructions or products referred to in the content.

plants

MDPI

Article

Genomic Variation and GWAS Analysis for Salt Tolerance Discovered in Egyptian Rice Germplasm

Yueying Wang [1,†], Faming Yu [2,†], Sirinthorn Kongpraphrut [1,3,†], Congcong Liu [1], Muhammad Asad Ullah Asad [2], Salma Kelany [1], Mengrui Sun [1], Yuxuan Wang [1], Yang Lv [2], Galal Anis [4], Mohamed Hazman [5], Qian Qian [1], Yuexing Wang [1,*] and Longbiao Guo [1,*]

[1] State Key Laboratory of Rice Biology and Breeding, China National Rice Research Institute, Hangzhou 310006, China; wyywangyueying@163.com (Y.W.); sirinthorn.k@rice.mail.go.th (S.K.); lcc43932@163.com (C.L.); salmakelany93@gmail.com (S.K.); 15864914259@163.com (M.S.); yuxuan_wang21@163.com (Y.W.); qianqian188@hotmail.com (Q.Q.)
[2] Institute of Crop and Nuclear Technology Utilization, Zhejiang Academy of Agricultural Sciences, Hangzhou 310021, China; yfm4679@163.com (F.Y.); asad.gu@hotmail.com (M.A.U.A.); lvyang0725@163.com (Y.L.)
[3] Krabi Rice Research Center, Rice Department, Krabi 81130, Thailand
[4] Rice Research and Training Centre, Field Crops Research Institute, Agriculture Research Center, Kafrelsheikh 33717, Egypt; galalanis@arc.sci.eg
[5] Agricultural Genetic Engineering Research Institute, Agricultural Research Center, Giza 12619, Egypt; yousof.hazman@outlook.com
* Correspondence: wangyuexing@caas.cn (Y.W.); guolongbiao@caas.cn (L.G.); Tel.: +86-0571-63530527 (Y.W.); +86-0571-63370136 (L.G.)
† These authors contributed equally to this work.

Abstract

Egyptian rice landraces represent a unique genetic reservoir shaped by arid environments, yet their genomic and transcriptional response to salt stress remains largely unexplored. Here, we integrated genomic, transcriptomic, and population genetic analyses to systematically unravel the mechanisms of salt tolerance in this vital germplasm. Resequencing 56 Egyptian accessions uncovered a treasure trove of genetic variation, including 18,204 novel SNPs. An expanded GWAS on 258 accessions discovered 17 novel loci for salt tolerance. Parallel RNA-Seq analysis of a salt-tolerant-susceptible pair (Giza 176 vs. 9311) under stress delineated a defense network centered on phenylpropanoid and lipid metabolic pathways in the tolerant genotype. The power of our integrated approach was exemplified by the convergent identification of *ONAC063*, where GWAS loci, transcriptional responsiveness, and haplotype-phenotype association collectively validated its role. Furthermore, selection sweep analysis highlighted 62 candidate genes under divergent selection. Our study not only positions Egyptian rice as a key resource for allele mining but also establishes a robust multi-omics pipeline for bridging genetic diversity with complex traits, accelerating the discovery of functional genes for breeding climate-resilient crops.

Keywords: salt tolerance; Egyptian rice; genomic divergence; GWAS; haplotype

1. Introduction

Rice (*Oryza sativa* L.) is a staple food for nearly half of the world's population, making the stability of its production crucial for global food security [1]. Soil salinization represents a major constraint on sustainable rice cultivation, whose exacerbation is closely linked to irrational human agricultural practices and natural elements [2]. Rice is a crop that is relatively sensitive to salt stress. There are significant differences in salt tolerance among

different rice varieties and across various growth stages, with the early seedling and reproductive stages being the most sensitive [3,4]. Rice grown in saline soil often exhibits physiological metabolic disorders, which in turn lead to reduced biomass and severe yield losses [5]. Excessive soluble salts in soil impair photosynthesis, induce ionic toxicity and oxidative stress in rice, resulting in a substantial reduction in panicle number, grain number, and thousand-grain weight [6]. The rice germplasm resources exhibit abundant genetic variation in salt tolerance, providing a basis for breeding improvements. Enhancing the salt tolerance of rice to boost yields in saline-alkali fields is a key strategy to tackle the global soil salinization challenge and ensure food security [7].

The plant salt stress response involves a complex set of physiological and biochemical processes [8]. Stress sensor is the first response of plants to abiotic stress, and it is an effective adaptation strategy of plants to the external environment. Under salt stress conditions, osmotic and ionic stress are sensed by membrane-bound cytosolic sensors that ultimately trigger early salt stress signaling pathways [9]. Stress signals are regulated by rapid and long-distance signaling processes, including phospholipid-based signaling, mitogen-activated protein kinases (MAPK), reactive oxygen species (ROS) and abscisic acid (ABA), calcium signaling, and long-range electrical signaling [10,11]. Under osmotic stress, activated sensory factors promote the production of tocopherols and related metabolites. This response serves to lower water potential, which in turn minimizes the loss of intracellular water. In addition, a variety of ion transporters and channel proteins, including High-affinity K^+ Transporters (HKT), Na^+/H^+ Exchangers (NHX), and High-affinity K^+ transporters (HAK), are involved in rebuilding ion balance in plants and regulating tolerance to high salts [12,13]. However, when the salt concentration transcends the plant's tolerance threshold, the plant fails to sustain K^+/Na^+ homeostasis within cells, giving rise to ion toxicity.

Rice salt tolerance, a quintessential quantitative trait with an intricate polygenic inheritance, has been the focus of extensive genetic mapping efforts [14]. To date, more than a thousand genes/QTLs associated with various salt tolerance-related traits (e.g., survival days, ion homeostasis, stomatal aperture) across different developmental stages have been identified [15]. The shift towards genome-wide association studies (GWAS), leveraging high-density SNP chips and linkage disequilibrium, has marked a significant advancement, offering superior resolution and power in allele detection for complex traits [16,17]. This methodology has been successfully applied to dissect rice salt tolerance, yielding numerous associated loci from studies involving hundreds of diverse accessions [18,19]. The resulting QTLs have catalyzed the functional validation of key genes, including *DST* [20], *OsHKT1;5* [21], and *RST1* [22]. Concurrently, breakthroughs in sequencing technology have facilitated gene cloning via transcriptomic analyses in structured populations, exemplified by the discovery of *STG5* [23]. Ultimately, deciphering the distinct genetic mechanisms underpinning salt tolerance across varied rice germplasm is crucial for developing resilient cultivars.

Egyptian rice germplasm, evolved under a tropical desert climate, is a potential source of unique alleles for salt tolerance, yet the genetic basis of this trait is poorly characterized. To systematically decipher the adaptive mechanisms, we implemented an integrated genomic and transcriptomic approach. This study combines GWAS on a diverse panel of 56 Egyptian and 202 Asian rice accessions with comparative RNA-Seq analysis of tolerant and sensitive cultivars under salt stress. This strategy enables us to not only map genomic loci associated with tolerance but also to validate and prioritize candidates within functional transcriptional networks, thereby identifying novel genes for the molecular breeding of resilient rice.

https://doi.org/10.3390/plants15010128

2. Results

2.1. Population Structure Analysis

To elucidate the population structure of 56 Egyptian rice accessions, we integrated their genomic data with 202 publicly available Asian cultivated rice genomes. A Neighbor-Joining phylogenetic tree constructed from this combined dataset of 258 accessions revealed two primary clades corresponding to the *indica* (*Osi*) and *japonica* (*Osj*) subspecies. The Egyptian accessions were equally distributed between these two lineages, with 28 accessions clustering within the *indica* branch and the remaining 28 within the *japonica* branch, indicating their distinct genetic affiliations with these major subgroups (Figure 1A).

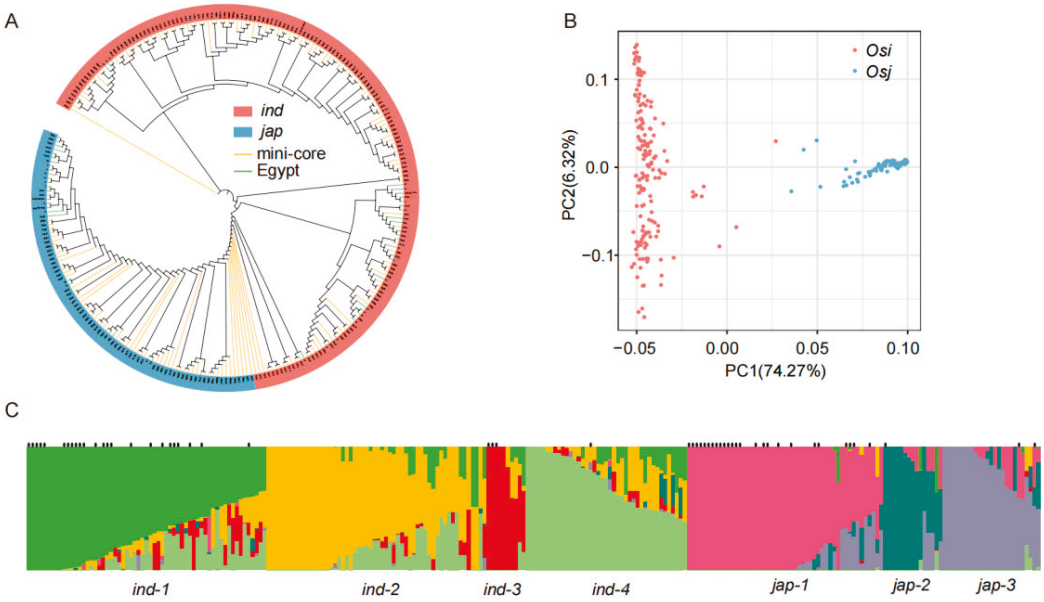

Figure 1. Population structure analysis. (**A**) Principal component analysis; (**B**) phylogenetic tree; (**C**) population structure distribution.

Principal component analysis (PCA) was performed on the SNP and Indel sets of the 258 rice samples based on all obtained SNPs, and the first 10 principal components (PCs) were calculated (Figure 1B). The first two principal components accounted for over 80% of the variation, with PC1 (74.27%) and PC2 (6.32%). According to the distribution pattern of genetic background, there was a clear population differentiation, and all samples could essentially be divided into two subgroups, *Osi* and *Osj*. Among them, 28 Egyptian rice samples were assigned to *Osi*, and another 28 to *Osj*, consistent with the results of the phylogenetic tree. Additionally, we used the admixture software to assess the ancestral components of the 258 accessions (Figure 1C). The analysis indicated that the optimal classification was at K = 7, and the visualization of the population structure clearly displayed the ancestral components of each sample, showing distinct population affiliations: 24 newly sequenced materials were distributed in the ind-1 group, and 26 newly sequenced materials were distributed in the jap1 group.

2.2. Genomic Variation

Whole-genome resequencing of the 56 Egyptian rice accessions yielded 614.22 million clean reads, totaling 89.5 Gb of data. An average of 95.02% of the reads were successfully aligned to the reference genome (MSUv7). Our analysis identified a total of 4,410,690 high-quality SNPs and 689,718 indels (Figure 2). Chromosome 1 harbored the highest density of variants (396,001 sites). Functional annotation revealed that 21.71% of variants resided in intergenic regions, 62.9% were located within 2 kb of gene promoters/terminators,

and 15.39% were within gene bodies (Figure 2A). Within coding sequences, we observed 487,283 nonsynonymous SNPs and 34,715 frameshift indels. Notably, these variants introduced 21,352 premature stop codons (SNPs) and 1030 (indels), and disrupted the native stop codon in 2010 and 408 cases, respectively (Figure 2B). A comparative analysis with a mini-core collection of 202 Asian cultivated rice accessions identified 18,204 novel SNPs and 2405 novel indels, underscoring the value of this Egyptian germplasm as a unique resource for rice genetics and breeding.

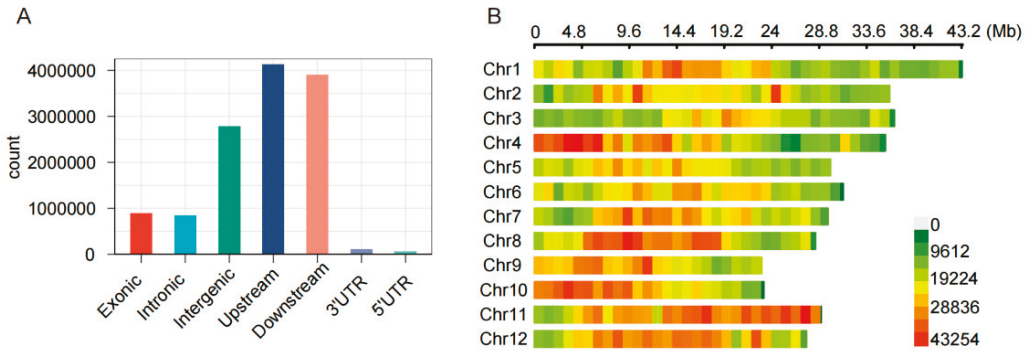

Figure 2. Genome-wide SNP variation statistics. (**A**) Distribution of SNPs across different functional genomic regions; (**B**) SNP density distribution across different chromosomes.

2.3. Salinity Tolerance Evaluation

The newly sequenced 56 Egyptian rice varieties provide a valuable resource for discovering novel candidate genes and key genetic variants associated with salt tolerance. In a previous study [24], we performed the GWAS analysis on 202 Asian cultivated rice accessions under salt stress, identifying several candidate genes for this trait. Here, under consistent experimental conditions, we evaluated the salt tolerance of the 56 Egyptian germplasms using the same standardized scoring system (Figure 3A, Table S1). Forty-one of these accessions displayed salt tolerance scores of 5 or higher (Figure 3B), demonstrating a notable level of salt tolerance and underscoring their potential for subsequent genetic analysis.

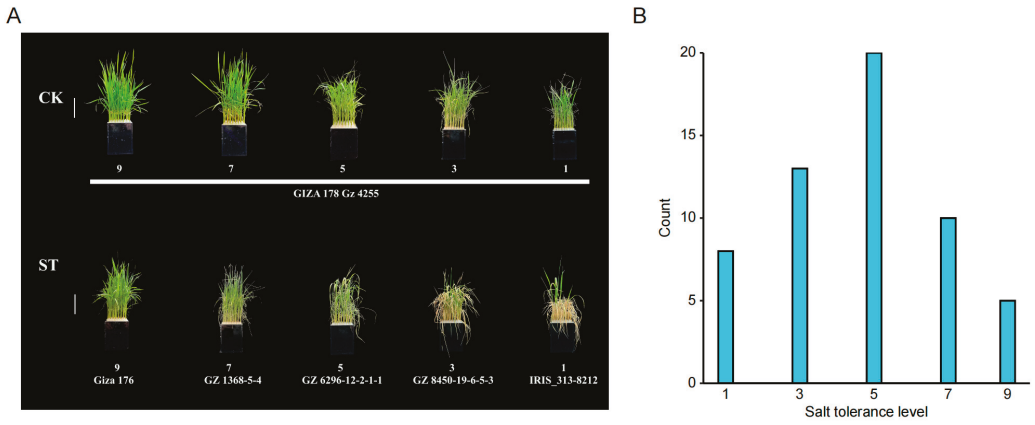

Figure 3. Salt tolerance scores of 56 Egyptian rice accessions. (**A**) Frequency distribution of salt tolerance scores; (**B**) phenotypic characteristics of plants with different salt tolerance scores.

2.4. RNA-Seq and DEGs Analysis

To investigate the transcriptional response mechanism of Egyptian rice to salt stress, we performed RNA-Seq analysis on the salt-tolerant Egyptian landrace Giza 176 and the salt-sensitive model indica rice variety 9311. Giza 176 represents a local salt-tolerant germplasm resource, while 9311 was selected as an ideal control due to its well-defined

salt-sensitive phenotype and comprehensive genome annotation. At the seedling stage, plants were treated with the NaCl solution. Samples from both treated and control groups were collected for RNA extraction, library construction, and sequencing. Based on gene expression (FPKM) analysis under salt stress, comparing 9311 with Giza 176 (9311 vs. Giza1), we identified 6504 significantly differentially expressed genes (DEGs), of which 2149 were up-regulated and 4355 were down-regulated (Figure 4A). Compared to normal growth conditions, salt stress induced a more extensive and pronounced transcriptional reprogramming, indicating a significant activation of gene expression reconfiguration.

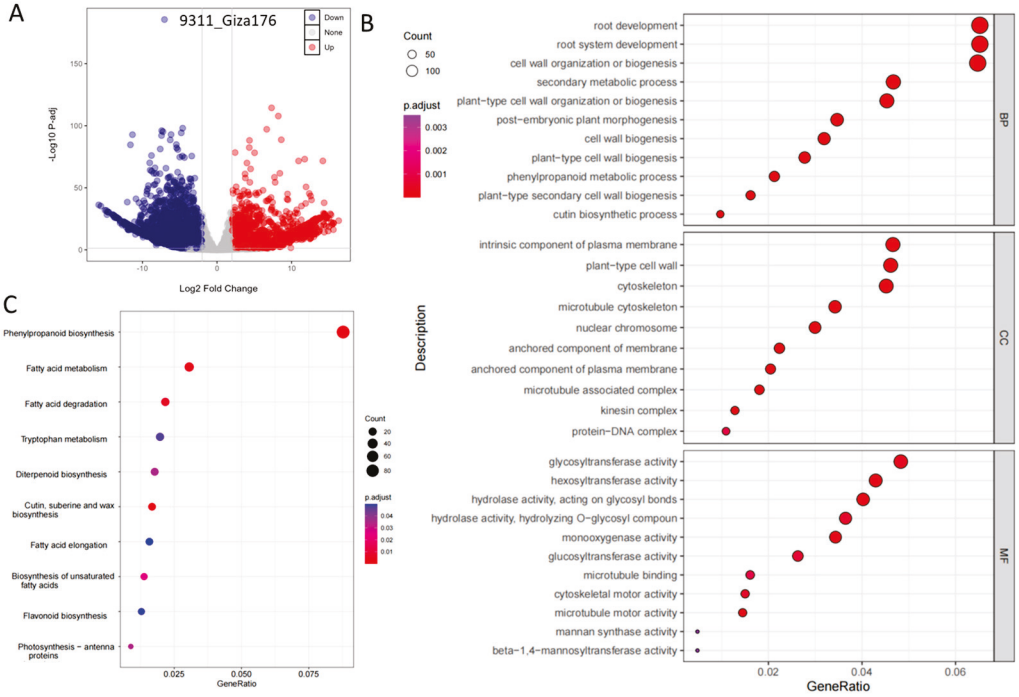

Figure 4. Transcriptome analysis of salt tolerance in Giza 176 and 9311 cultivars. (**A**) DEG analysis of Giza 176 and 9311; (**B**) GO classification and (**C**) KEGG classification of Giza 176 and 9311.

To further decipher the biological functions of the DEGs under salt stress, we conducted Gene Ontology (GO) enrichment analysis and KEGG pathway annotation on the set of genes specifically expressed in Giza 176. GO analysis revealed that the significantly up-regulated genes in this cultivar were primarily enriched in biological processes closely associated with salt tolerance, including phenylpropanoid biosynthesis, and cutin, suberin, and wax biosynthesis, as well as fatty acid metabolism (Figure 4B). KEGG pathway analysis further indicated significant enrichment of these genes in phenylpropanoid biosynthesis, cutin, suberin and wax biosynthesis, fatty acid metabolism, and fatty acid degradation pathways (Figure 4C). Notably, in Giza 176, multiple pathway genes related to lipid metabolism and secondary metabolite synthesis exhibited more pronounced up-regulation compared to their homologs in 9311. These results demonstrate that Giza 176 establishes its unique salt adaptation mechanism by activating multiple pathways, including phenylpropanoid synthesis, lipid metabolism, and plant hormone signal transduction. The dissection of this regulatory network not only provides new insights into the physiological mechanism of salt tolerance in Egyptian rice landraces but also offers a valuable basis for screening key candidate genes in molecular breeding for salt-tolerant rice.

2.5. GWAS and Haplotype Analysis of Candidate Genes

The GWAS analysis was conducted using the FARMCUP software (v1.02). The GWAS analysis integrated the salt tolerance phenotypes of 202 Asian cultivated rice materials

and 56 Egyptian germplasms, enabling us to mine new candidate loci for salt tolerance (Figure 5). The GWAS results showed that the salt tolerance scores of 258 materials identified a total of 19 significant loci, of which 17 were newly identified significant loci (Supplementary Table S2). This suggests that more candidate genes for salt tolerance can be identified.

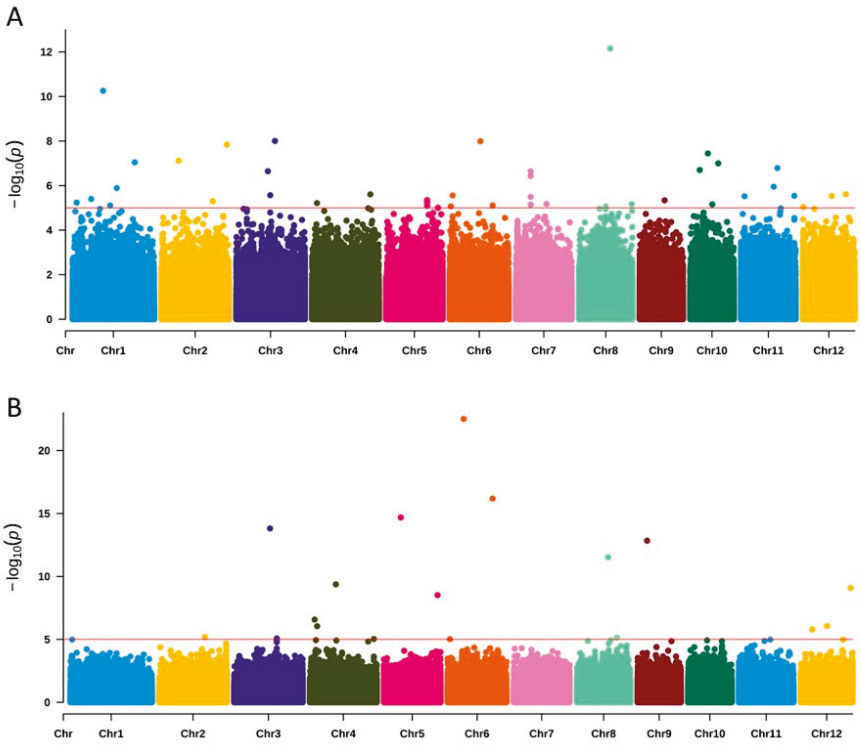

Figure 5. GWAS for salt tolerance identifies novel loci. Manhattan plot of GWAS in (**A**) 202 rice accessions and (**B**) 258 rice accessions. Threshold line is 5.

The GWAS analysis provided a novel dataset of candidate genes for salt tolerance, defining 19 candidate QTL intervals. These intervals encompass three previously cloned salt tolerance-related genes: *OsIPK1* (*LOC_Os04g56580*, encoding inositol 1,3,4,5,6-pentakisphosphate 2-kinase) [25], *OsRPH1/STG5* (*LOC_Os05g49700*, encoding an AP2/ERF transcription factor) [23], and *ONAC063* (*LOC_Os08g33910*, encoding a NAC transcription factor) [26]. Furthermore, integrated transcriptomic analysis facilitated additional gene mining, revealing an overlap between the DEGs and candidate genes from GWAS. Specifically, the two datasets co-localized the *ONAC063* gene, which has previously been cloned as a salt-tolerance gene. To comprehensively assess genetic variation within *ONAC063*, we systematically examined all polymorphic sites across 258 rice accessions for potential impacts on the coding sequence. We identified that nucleotide variation within this gene resulted in missense mutations. Therefore, based on salt tolerance phenotypes (Figure 6A), haplotype analysis of *ONAC063*—defined by these missense variant site—across 258 rice accessions revealed multiple haplotypes, with Hap3 identified as a favorable haplotype associated with enhanced salt tolerance (Figure 6B).

A

	Physical position (bp)			
Hap/Pos	21,218,697	21,218,966	21,219,202	Num.
Hap.1	A	A	TTA	156
Hap.2	T	G	T	75
Hap.3	A	A	/	23

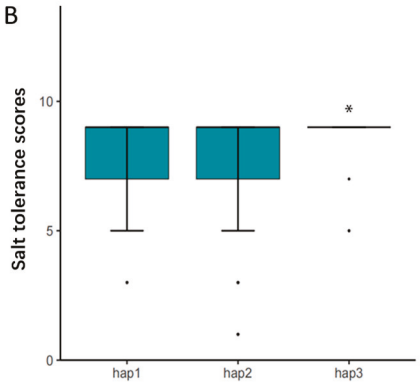

Figure 6. Haplotype analyses of *ONAC063*. Gene structure (**A**) and salt tolerance scores (**B**) of different haplotypes. *t*-test, * $p < 0.01$.

2.6. Genetic Selection Analysis

To elucidate the genetic basis of salt tolerance variation in Egyptian rice varieties, we performed a population differentiation analysis on 56 Egyptian rice accessions and 202 rice mini-core accessions, applying *Fst* analysis to measure allele frequency divergence between populations and detect genomic regions that may be under selection (Figure 7). Setting the top 5% of *Fst* values as the threshold revealed 17,679 significantly differentiated loci, including 62 annotated salt tolerance genes (Supplementary Table S3). Functional annotation implicated these genes in processes critical to salt tolerance, such as ion transport, osmotic regulation, and antioxidant responses. Several key genes (e.g., *OREB1* [27], *OsHKT1;1* [21], *OsSOS1* [28]) were prioritized. These results indicate that genes within divergent genomic regions have experienced differential selection and likely underpin salt tolerance adaptations, potentially driven by distinct breeding histories or environmental pressures.

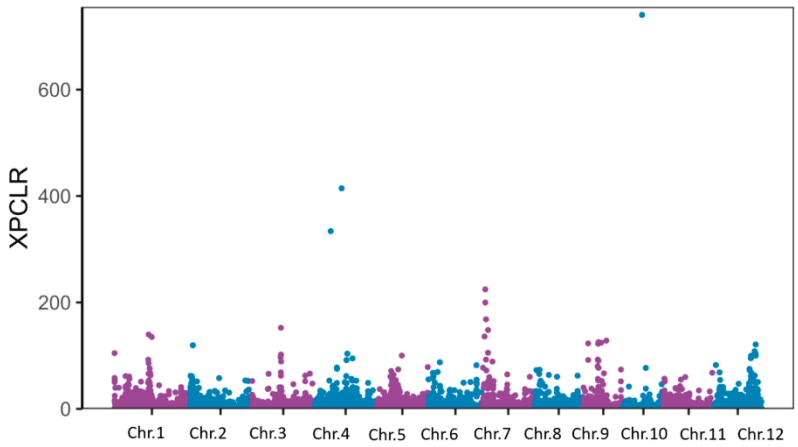

Figure 7. *Fst* analysis highlights genomic differentiation.

3. Discussion

Soil salinization poses a major threat to global food security by severely impacting rice, a salt-sensitive crop, thereby making the genetic enhancement of salt tolerance an urgent breeding priority [8,10]. This study provides a comprehensive genomic characterization of a unique panel of 56 Egyptian rice accessions and integrates it with a diverse Asian mini-core collection to elucidate the genetic architecture of salt tolerance. Our findings confirm that the Egyptian germplasm represents a valuable and distinct genetic reservoir, equally divided between the indica and japonica subspecies, and harbors substantial novel

genetic variation, including over 20,000 novel SNPs and indels not found in the Asian panel. This underscores the critical importance of exploring locally adapted, non-reference germplasms to fully capture the genetic diversity of cultivated rice.

Salt tolerance in rice is a complex quantitative trait governed by multiple genes, which has been extensively investigated through genetic mapping studies [14]. This study provides a comprehensive genomic characterization of a unique panel of 56 Egyptian rice accessions and integrates it with a diverse Asian mini-core collection to elucidate the genetic architecture of salt tolerance. Our findings confirm that the Egyptian germplasm represents a valuable and distinct genetic reservoir, equally divided between the indica and japonica subspecies, and harbors substantial novel genetic variation, including over 20,000 novel SNPs and indels not found in the Asian panel. This underscores the critical importance of exploring locally adapted, non-reference germplasms to fully capture the genetic diversity of cultivated rice.

The core of our strategy was a multi-faceted genomic analysis. The GWAS conducted on the expanded panel of 258 accessions proved highly effective, identifying 19 significant loci for salt tolerance, 17 of which are novel. This significant increase in discovery power highlights the advantage of incorporating genetically distinct populations like the Egyptian accessions into association studies, which helps to break down linkage disequilibrium and uncover new trait-associated loci. Critically, our integrated transcriptomic analysis provided functional context to these genomic findings. The comparative RNA-Seq of the salt-tolerant cultivar Giza 176 and the sensitive 9311 under stress revealed comprehensive transcriptional reprogramming, with 6504 DEGs identified. The significant enrichment of these DEGs in key pathways such as phenylpropanoid biosynthesis, cutin/suberin/wax deposition, and fatty acid metabolism in the tolerant genotype delineates a robust, multi-faceted defense strategy at the transcriptional level. The validation of our approach is reinforced by the fact that our candidate intervals encompassed known salt-tolerance genes such as *OsIPK1* [25], *STG5* [23], and *ONAC063* [26]. The convergence of GWAS and transcriptomic data was particularly powerful for *ONAC063*, which was not only located within a significant GWAS locus but also emerged as a salt-responsive DEG, providing strong multi-omics support for its central role. The haplotype analysis of *ONAC063* further confirmed its role, identifying a specific haplotype (Hap3) associated with enhanced tolerance, suggesting potential for marker-assisted selection.

Complementary to the GWAS, the population differentiation (*Fst*) and selection sweep (XP-CLR) analyses offered an evolutionary perspective on salt tolerance. The identification of 62 annotated salt-tolerance genes within the highly differentiated genomic regions suggests that the Egyptian germplasm has been subjected to selective pressures, potentially related to its adaptation to local environments, that have shaped its unique genetic makeup. Genes involved in ion homeostasis (e.g., *OsHKT1;1* [21], *OsSOS1* [28]) and osmotic stress response were prominently represented, aligning with the fundamental physiological mechanisms of salt tolerance in plants. Notably, several genes within these selected regions are implicated in similar biological processes (e.g., lipid metabolism and secondary cell wall formation) that were highlighted by our transcriptomic data, suggesting a potential concordance between evolutionary selection and stress-responsive regulation.

This study also has limitations. The phenotypic evaluation, while standardized, was conducted at the seedling stage in a controlled hydroponic system. The genetic mechanisms of tolerance at reproductive stages, which are equally critical for yield, may differ and require further investigation. Furthermore, the transcriptomic analysis, while revealing the defense network in Giza 176, was based on a single tolerant-susceptible pair; expanding this to a diverse set of accessions would capture a broader spectrum of transcriptional strategies. The candidate genes and loci identified here are predominantly based on statistical genetic

evidence. Functional validation through mutagenesis or transgenic approaches is an essential next step to confirm the biological role of these genes, particularly the novel loci.

In conclusion, our work demonstrates that Egyptian rice germplasm is a rich and underexplored source of allelic diversity for salt tolerance. By employing an integrated genomic approach, we have successfully delineated a set of high-confidence candidate genes and loci, bridging genomic polymorphisms with stress-responsive transcriptional networks. These findings not only advance our understanding of the polygenic nature of salt tolerance in rice but also provide a practical foundation for molecular breeding programs. The molecular markers and candidate genes identified here can be directly utilized to develop elite cultivars with improved resilience to salinity, contributing to the goal of securing rice production in saline-affected regions worldwide.

4. Materials and Methods

4.1. Materials and Phenotypic Variation

A total of 56 accessions of Egyptian rice germplasm, conserved at the germplasm bank of the China National Rice Research Institute (CNRRI), were evaluated for salt tolerance using a hydroponic system. The experiments were conducted in the greenhouses at CNRRI, following the previously described methodology. Strict controls were employed to ensure that all seeds were from a single harvest batch, treatment applications were synchronized, and all environmental and experimental conditions were kept uniform [24]. The grains were germinated in water at 37 °C in the dark for 3 days. Seeds were germinated for three days, and the resulting seedlings were grown in a nutrient solution for two weeks. We conducted pre-experiments to determine the appropriate salt stress level and observed that a 100 mM NaCl treatment resulted in the most diverse phenotypic distribution, effectively discriminating accessions with different tolerance levels. The seedlings were cultivated in Yoshida's culture solution, the composition of which was prepared as described by Jahan et al. [29]. The nutrient solution was renewed every two days. After a 14-day pre-culture period, uniformly growing seedlings from each accession were subjected to salt stress by introducing 100 mM NaCl into the nutrient solution for 14 days. A control group was maintained in the standard nutrient solution without NaCl. The whole experiment was conducted in a randomized complete block design with two independent biological replications for each accession. In each replicate, ten uniformly grown seedlings per accession were evaluated. The experiment was conducted twice for each accession, with ten seedlings evaluated per replicate. Following the salt treatment, the plants were assigned a salt tolerance score based on growth and development phenotypes, according to the Standard Evaluation System (SES) scale of 1, 3, 5, 7, and 9 established by Gregorio et al. [30]. The final result for each accession was calculated as the average across the three replicates. This scoring system effectively discriminated susceptible from tolerant and moderately tolerant genotypes, with lower scores correlating with more severe symptoms such as brown leaf tips, leaf yellowing, drying, and stunted growth.

4.2. Variant Calling

DNA from a single plant per accession was sequenced on the DNBSEQ-T7 platform (v0.23.2) (15×coverage) (Mgi Tech Co., Ltd., Shenzhen, China). The bioinformatic processing pipeline included: quality control with Fastp (v0.23.2) [31], alignment to the Nipponbare genome (MSU v7.0) using BWA (v0.7.17-r1188) (mem-M-R-K 10000000), and file handling with Samtools (v1.9) [32]. SNPs were called using the GATK4 HaplotypeCaller pipeline (GVCF mode), followed by joint genotyping [33]. The initial SNP set was filtered with GATK's VariantFiltration tool using standard quality metrics, and subsequently with

https://doi.org/10.3390/plants15010128

VCFtools (maf 0.05 [34], max missing 0.8 to apply a minor allele frequency (MAF) cutoff of 0.05 and remove sites with more than 20% missing data.

4.3. Genotype and Population Structure Analysis

The genomic data for this study were sourced from two sets of materials. One comprised 202 Asian cultivated rice accessions with publicly available genotypes [35], and the other consisted of 58 Egyptian accessions sequenced specifically for this project. The resequencing data for the Egyptian rice were processed through the SENTIEON DNAseq pipeline. Following functional annotation of all SNPs using SnpEff, we performed a suite of population genetic analyses [36]. This included PCA implemented in PLINK (v1.90b6.21), population structure assessment with ADMIXTURE [37] and phylogeny reconstruction using IQ-TREE [38]. The final tree was rendered for visualization in iTol (http://itol.embl.de/) (accessed on 2 November 2025).

4.4. Fst Analysis and Selected Signal Calculation Method

To identify genetic signatures of selection for salt tolerance in Egyptian rice, we conducted a genome-wide analysis using the cross-population composite likelihood ratio (XP-CLR) test [39]. The analysis was performed with a non-overlapping 10 kb sliding window across the genome. Key parameters included a step size of 100 kb, and a maximum of 500 SNPs per window. Genomic regions with elevated XP-CLR scores are indicative of potential selective sweeps. Consequently, we defined candidate selected regions based on the top 5% of the XP-CLR scores, and all genes located within these regions were considered candidate genes associated with salt tolerance.

4.5. Transcriptome Analysis

Transcriptome analysis was conducted on the salt-tolerant cultivar Giza 176 and salt-sensitive cultivar 9311. Seedlings were grown hydroponically and treated with 100 mM NaCl for 14 days. The samples from three experimental replicates were pooled to form three biological replicates per cultivar. Total RNA was extracted from shoot tissues using TRIzol reagent (Invitrogen). Raw reads were processed using fastp (v0.23.2) [23,24].

Clean reads were aligned to the Nipponbare reference genome (MSUv7.0) using HISAT2 (v2.2.1) [40]. Gene expression was quantified using featureCounts (v2.0.1) with parameters: -T 2 -p -t exon -g gene_id [41]. Differentially expression genes (DEGs) analysis was performed using edgeR (v3.40.2) with thresholds: CPM > 1, bcv = 0.2, p-value < 0.01, $|\log_2 FC| \geq 2$ [42]. Genes that were differentially expressed in both biological replicates were defined as core DEGs and subjected to functional annotation via GO and KEGG pathway analyses using TBtools (v2.370) [43].

4.6. Whole Genome Association Analysis

Using the FarmCPU model from the R package rMVP (v1.02) for whole genome association analysis. Filter out the high-quality SNPs (missing rate ≤ 0.2; minimum allele frequency MAF ≥ 0.05) [44]. The significance threshold for the association analysis is $-\lg P = 5$ [45,46], and genes within $\pm$ 200 kb upstream and downstream of the significant SNPs are selected as candidate genes [47].

4.7. Haplotype Analysis

When conducting haplotype analysis on target genes, variance analysis in the study employs t-tests and Wilcoxon tests using R version 4.3.0, and multiple comparisons are performed using the R package multcomp (version 1.4-25).

https://doi.org/10.3390/plants15010128

4.8. Statistical and Visualization

Data were subjected to one-way analysis of variance (ANOVA) to determine significant differences between treatments. Subsequent post hoc analysis was performed using Duncan's multiple range test. For data visualization, GraphPad Prism 10 was utilized to create bar graphs, while Cloud tools (www.igenebook.com) (accessed on 2 November 2025) were employed to generate Venn diagrams, scatter plots, and heat maps.

5. Conclusions

This study establishes Egyptian rice germplasm as a valuable genetic reservoir for salt tolerance breeding. Through an integrated genomic and transcriptomic approach, we identified 17 novel loci and high-confidence candidate genes. Comparative transcriptomics further revealed activated defense pathways in the tolerant genotype, and the convergence of GWAS with transcriptomic data strengthened evidence for key genes like *ONAC063*. These findings expand the genetic landscape of salt tolerance and provide a robust foundation for molecular breeding. Future work will focus on functional validation to develop resilient cultivars for saline-affected regions.

Supplementary Materials: The following supporting information can be downloaded at: https://www.mdpi.com/article/10.3390/plants15010128/s1, Table S1: List of evaluated salt tolerance scores for the 56 rice accessions. Table S2: Summary of significant loci associated with salt tolerance identified in the GWAS; Table S3: Identification of the salt tolerance genes among the Top 5% differentiated Loci.

Author Contributions: L.G., Y.W. (Yuexing Wang) and Q.Q.: conceived and designed the study. Y.L. and C.L.: performed GWAS, F.Y. and M.H.: provided advice for the experimental design. Y.W. (Yueying Wang), Y.W. (Yuxuan Wang), M.S. and M.A.U.A.: performed the phenotyping measurement. G.A. and S.K. (Salma Kelany): performed the data analysis. Y.W. (Yueying Wang) and S.K. (Sirinthorn Kongpraphrut): wrote the manuscript. All authors have read and agreed to the published version of the manuscript.

Funding: This work was funded by the China Postdoctoral Science Foundation (2024M763601), Major Science and Technology project of Zhejiang Province (2021C02063-4), Zhejiang Natural Science Foundation project (LQN25C130002), National Natural Science Foundation of China (W2433049), the National Key R&D Program of China (Grant No. 2022YFE0139400), the Egyptian-Chinese Research Fund, and Science, Technology & Innovation Funding Authority Egypt (Grant No. 46512), and the National Natural Science Foundation of China (Grant No. 32261143470).

Data Availability Statement: The original contributions presented in the study are included in the article/Supplementary Materials, further inquiries can be directed to the corresponding author.

Conflicts of Interest: The authors declare that they have no conflict of interest.

References

1. Chen, R.; Deng, Y.; Ding, Y.; Guo, J.; Qiu, J.; Wang, B.; Wang, C.; Xie, Y.; Zhang, Z.; Chen, J.; et al. Rice functional genomics: Decades' efforts and roads ahead. *Sci. China Life Sci.* **2022**, *65*, 33–92. [CrossRef] [PubMed]
2. Jahan, N.; Zhang, Y.; Lv, Y.; Song, M.; Zhao, C.; Hu, H.; Cui, Y.; Wang, Z.; Yang, S.; Zhang, A.; et al. QTL analysis for rice salinity tolerance and fine mapping of a candidate locus *qSL7* for shoot length under salt stress. *Plant Growth Regul.* **2019**, *90*, 307–319. [CrossRef]
3. Liu, M.; Pan, T.; Allakhverdiev, S.I.; Yu, M.; Shabala, S. Crop halophytism: An environmentally sustainable solution for global food security. *Trends Plant Sci.* **2020**, *25*, 630–634. [CrossRef] [PubMed]
4. Zhao, C.; Zhang, H.; Song, C.; Zhu, J.K.; Shabala, S. Mechanisms of plant responses and adaptation to soil salinity. *Innovation* **2020**, *1*, 100017. [CrossRef]
5. Bhatt, T.; Sharma, A.; Puri, S.; Minhas, A.P. Salt tolerance mechanisms and approaches: Future scope of halotolerant genes and rice landraces. *Rice Sci.* **2020**, *27*, 368–383. [CrossRef]

6. Ponce, K.S.; Meng, L.; Guo, L.; Leng, Y.; Ye, G. Advances in sensing, response and regulation mechanism of salt tolerance in rice. *Int. J. Mol. Sci.* **2021**, *22*, 2254. [CrossRef]
7. Morton, M.J.L.; Awlia, M.; Al-Tamimi, N.; Saade, S.; Pailles, Y.; Negrao, S.; Tester, M. Salt stress under the scalpel—Dissecting the genetics of salt tolerance. *Plant J.* **2019**, *97*, 148–163. [CrossRef]
8. Amanat, M.A.; Naeem, M.K.; Algwaiz, H.I.M.; Uzair, M.; Attia, K.A.; AlKathani, M.D.F.; Zaid, I.U.; Zafar, S.A.; Inam, S.; Fiaz, S.; et al. Evaluation of green super rice lines for agronomic and physiological traits under salinity stress. *Plants* **2022**, *11*, 1461. [CrossRef]
9. Miller, G.; Suzuki, N.; Ciftci-Yilmaz, S.; Mittler, R. Reactive oxygen species homeostasis and signalling during drought and salinity stresses. *Plant Cell Environ.* **2010**, *33*, 453–467. [CrossRef]
10. Mittler, R.; Vanderauwera, S.; Suzuki, N.; Miller, G.; Tognetti, V.B.; Vandepoele, K.; Gollery, M.; Shulaev, V.; Van Breusegem, F. ROS signaling: The new wave? *Trends Plant Sci.* **2011**, *16*, 300–309. [CrossRef]
11. Roy, S.J.; Negrao, S.; Tester, M. Salt resistant crop plants. *Curr. Opin. Biotechnol.* **2014**, *26*, 115–124. [CrossRef]
12. Fukuda, A.; Nakamura, A.; Tagiri, A.; Tanaka, H.; Miyao, A.; Hirochika, H.; Tanaka, Y. Function, intracellular localization and the importance in salt tolerance of a vacuolar $Na^{(+)}/H^{(+)}$ antiporter from rice. *Plant Cell Physiol.* **2004**, *45*, 146–159. [CrossRef]
13. El Mahi, H.; Perez-Hormaeche, J.; De Luca, A.; Villalta, I.; Espartero, J.; Gamez-Arjona, F.; Fernandez, J.L.; Bundo, M.; Mendoza, I.; Mieulet, D.; et al. A critical role of sodium flux via the plasma membrane $Na^{(+)}/H^{(+)}$ exchanger SOS1 in the salt tolerance of rice. *Plant Physiol.* **2019**, *180*, 1046–1065. [CrossRef] [PubMed]
14. Ganie, S.A.; Wani, S.H.; Henry, R.; Hensel, G. Improving rice salt tolerance by precision breeding in a new era. *Curr. Opin. Plant Biol.* **2021**, *60*, 101996. [CrossRef] [PubMed]
15. Fan, X.; Jiang, H.; Meng, L.; Chen, J. Gene mapping, cloning and association analysis for salt tolerance in rice. *Int. J. Mol. Sci.* **2021**, *22*, 11674. [CrossRef] [PubMed]
16. Huang, X.; Feng, Q.; Qian, Q.; Zhao, Q.; Wang, L.; Wang, A.; Guan, J.; Fan, D.; Weng, Q.; Huang, T.; et al. High-throughput genotyping by whole-genome resequencing. *Genome Res.* **2009**, *19*, 1068–1076. [CrossRef]
17. Huang, X.; Kurata, N.; Wei, X.; Wang, Z.X.; Wang, A.; Zhao, Q.; Zhao, Y.; Liu, K.; Lu, H.; Li, W.; et al. A map of rice genome variation reveals the origin of cultivated rice. *Nature* **2012**, *490*, 497–501. [CrossRef]
18. Huang, X.; Wei, X.; Sang, T.; Zhao, Q.; Feng, Q.; Zhao, Y.; Li, C.; Zhu, C.; Lu, T.; Zhang, Z.; et al. Genome-wide association studies of 14 agronomic traits in rice landraces. *Nat. Genet.* **2010**, *42*, 961–967. [CrossRef]
19. Yano, K.; Yamamoto, E.; Aya, K.; Takeuchi, H.; Lo, P.C.; Hu, L.; Yamasaki, M.; Yoshida, S.; Kitano, H.; Hirano, K.; et al. Genome-wide association study using whole-genome sequencing rapidly identifies new genes influencing agronomic traits in rice. *Nat. Genet.* **2016**, *48*, 927–934. [CrossRef]
20. Huang, X.Y.; Chao, D.Y.; Gao, J.P.; Zhu, M.Z.; Shi, M.; Lin, H.X. A previously unknown zinc finger protein, DST, regulates drought and salt tolerance in rice via stomatal aperture control. *Genes Dev.* **2009**, *23*, 1805–1817. [CrossRef]
21. Ren, Z.H.; Gao, J.P.; Li, L.G.; Cai, X.L.; Huang, W.; Chao, D.Y.; Zhu, M.Z.; Wang, Z.Y.; Luan, S.; Lin, H.X. A rice quantitative trait locus for salt tolerance encodes a sodium transporter. *Nat. Genet.* **2005**, *37*, 1141–1146. [CrossRef] [PubMed]
22. Deng, P.; Jing, W.; Cao, C.; Sun, M.; Chi, W.; Zhao, S.; Dai, J.; Shi, X.; Wu, Q.; Zhang, B.; et al. Transcriptional repressor RST1 controls salt tolerance and grain yield in rice by regulating gene expression of asparagine synthetase. *Proc. Natl. Acad. Sci. USA* **2022**, *119*, e2210338119. [CrossRef] [PubMed]
23. Wei, H.; Wang, X.; Zhang, Z.; Yang, L.; Zhang, Q.; Li, Y.; He, H.; Chen, D.; Zhang, B.; Zheng, C.; et al. Uncovering key salt-tolerant regulators through a combined eQTL and GWAS analysis using the super pan-genome in rice. *Natl. Sci. Rev.* **2024**, *11*, nwae043. [CrossRef] [PubMed]
24. Lv, Y.; Ma, J.; Wei, H.; Xiao, F.; Wang, Y.; Jahan, N.; Hazman, M.; Qian, Q.; Shang, L.; Guo, L. Combining GWAS, genome-wide domestication and a transcriptomic analysis reveals the loci and natural alleles of salt tolerance in rice (*Oryza sativa* L.). *Front. Plant Sci.* **2022**, *13*, 912637. [CrossRef]
25. Jiang, M.; Liu, Y.; Li, R.; Li, S.; Tan, Y.; Huang, J.; Shu, Q. An inositol 1,3,4,5,6-Pentakisphosphate 2-Kinase 1 mutant with a 33-nt deletion showed enhanced tolerance to salt and drought stress in rice. *Plants* **2020**, *10*, 23. [CrossRef]
26. Yokotani, N.; Ichikawa, T.; Kondou, Y.; Matsui, M.; Hirochika, H.; Iwabuchi, M.; Oda, K. Tolerance to various environmental stresses conferred by the salt-responsive rice gene *ONAC063* in transgenic Arabidopsis. *Planta* **2009**, *229*, 1065–1075. [CrossRef]
27. Li, Y.; Zhou, J.; Li, Z.; Qiao, J.; Quan, R.; Wang, J.; Huang, R.; Qin, H. SALT AND ABA RESPONSE ERF1 improves seed germination and salt tolerance by repressing ABA signaling in rice. *Plant Physiol.* **2022**, *189*, 1110–1127. [CrossRef]
28. Martinez-Atienza, J.; Jiang, X.; Garciadeblas, B.; Mendoza, I.; Zhu, J.K.; Pardo, J.M.; Quintero, F.J. Conservation of the salt overly sensitive pathway in rice. *Plant Physiol.* **2007**, *143*, 1001–1012. [CrossRef]
29. Jahan, N.; Lv, Y.; Song, M.; Zhang, Y.; Shang, L.; Lu, Y.; Ye, G.; Qian, Q.; Gao, Z.; Guo, L. Transcriptomic analysis of short-term salt-stress response in mega hybrid rice seedlings. *Agronomy* **2021**, *11*, 1328. [CrossRef]
30. Gregorio, G.B.; Senadhira, D.; Mendoza, R.D. *Screening Rice for Salinity Tolerance*; International Rice Research Institute: Los Baños, Philippines, 1997.

31. Chen, S. Ultrafast one-pass FASTQ data preprocessing, quality control, and deduplication using fastp. *Imeta* **2023**, *2*, e107. [CrossRef]
32. Li, H.; Handsaker, B.; Wysoker, A.; Fennell, T.; Ruan, J.; Homer, N.; Marth, G.; Abecasis, G.; Durbin, R.; Genome Project Data Processing, S. The sequence alignment/map format and SAMtools. *Bioinformatics* **2009**, *25*, 2078–2079. [CrossRef] [PubMed]
33. Heldenbrand, J.R.; Baheti, S.; Bockol, M.A.; Drucker, T.M.; Hart, S.N.; Hudson, M.E.; Iyer, R.K.; Kalmbach, M.T.; Kendig, K.I.; Klee, E.W.; et al. Recommendations for performance optimizations when using GATK3.8 and GATK4. *BMC Bioinform.* **2019**, *20*, 557. [CrossRef] [PubMed]
34. Danecek, P.; Auton, A.; Abecasis, G.; Albers, C.A.; Banks, E.; DePristo, M.A.; Handsaker, R.E.; Lunter, G.; Marth, G.T.; Sherry, S.T.; et al. The variant call format and VCFtools. *Bioinformatics* **2011**, *27*, 2156–2158. [CrossRef] [PubMed]
35. Shang, L.; Li, X.; He, H.; Yuan, Q.; Song, Y.; Wei, Z.; Lin, H.; Hu, M.; Zhao, F.; Zhang, C.; et al. A super pan-genomic landscape of rice. *Cell Res.* **2022**, *32*, 878–896. [CrossRef]
36. Kawahara, Y.; de la Bastide, M.; Hamilton, J.P.; Kanamori, H.; McCombie, W.R.; Ouyang, S.; Schwartz, D.C.; Tanaka, T.; Wu, J.; Zhou, S.; et al. Improvement of the Oryza sativa Nipponbare reference genome using next generation sequence and optical map data. *Rice* **2013**, *6*, 4. [CrossRef]
37. Alexander, D.H.; Lange, K. Enhancements to the ADMIXTURE algorithm for individual ancestry estimation. *BMC Bioinform.* **2011**, *12*, 246. [CrossRef]
38. Minh, B.Q.; Schmidt, H.A.; Chernomor, O.; Schrempf, D.; Woodhams, M.D.; von Haeseler, A.; Lanfear, R. IQ-TREE 2: New models and efficient methods for phylogenetic inference in the genomic era. *Mol. Biol. Evol.* **2020**, *37*, 1530–1534. [CrossRef]
39. Chen, H.; Patterson, N.; Reich, D. Population differentiation as a test for selective sweeps. *Genome Res.* **2010**, *20*, 393–402. [CrossRef]
40. Kim, D.; Langmead, B.; Salzberg, S.L. HISAT: A fast spliced aligner with low memory requirements. *Nat. Methods* **2015**, *12*, 357–360. [CrossRef]
41. Trapnell, C.; Roberts, A.; Goff, L.; Pertea, G.; Kim, D.; Kelley, D.R.; Pimentel, H.; Salzberg, S.L.; Rinn, J.L.; Pachter, L. Differential gene and transcript expression analysis of RNA-seq experiments with TopHat and Cufflinks. *Nat. Protoc.* **2012**, *7*, 562–578. [CrossRef]
42. Robinson, M.D.; McCarthy, D.J.; Smyth, G.K. edgeR: A Bioconductor package for differential expression analysis of digital gene expression data. *Bioinformatics* **2010**, *26*, 139–140. [CrossRef]
43. Chen, C.; Chen, H.; Zhang, Y.; Thomas, H.R.; Frank, M.H.; He, Y.; Xia, R. TBtools: An Integrative Toolkit Developed for Interactive Analyses of Big Biological Data. *Mol. Plant* **2020**, *13*, 1194–1202. [CrossRef]
44. Visscher, P.M.; Brown, M.A.; McCarthy, M.I.; Yang, J. Five years of GWAS discovery. *Am. J. Hum. Genet.* **2012**, *90*, 7–24. [CrossRef]
45. Gao, H.; Zhang, C.; He, H.; Liu, T.; Zhang, B.; Lin, H.; Li, X.; Wei, Z.; Yuan, Q.; Wang, Q.; et al. Loci and alleles for submergence responses revealed by GWAS and transcriptional analysis in rice. *Mol. Breed.* **2020**, *40*, 75. [CrossRef]
46. Lv, Y.; Ma, J.; Wang, Y.; Wang, Q.; Lu, X.; Hu, H.; Qian, Q.; Guo, L.; Shang, L. Loci and natural alleles for low-nitrogen-induced growth response revealed by the genome-wide association study analysis in rice (*Oryza sativa* L.). *Front. Plant Sci.* **2021**, *12*, 770736. [CrossRef]
47. Kang, H.M.; Sul, J.H.; Service, S.K.; Zaitlen, N.A.; Kong, S.Y.; Freimer, N.B.; Sabatti, C.; Eskin, E. Variance component model to account for sample structure in genome-wide association studies. *Nat. Genet.* **2010**, *42*, 348–354. [CrossRef]

Disclaimer/Publisher's Note: The statements, opinions and data contained in all publications are solely those of the individual author(s) and contributor(s) and not of MDPI and/or the editor(s). MDPI and/or the editor(s) disclaim responsibility for any injury to people or property resulting from any ideas, methods, instructions or products referred to in the content.

plants

MDPI

Article

Transcriptomic Analysis of Rice (Jijing129) Reveals Growth and Gene Expression Responses to Different Red-Blue Laser Light Treatments

Xuemei Liang [1,†], Qi Liu [1,†], Li Qin [2], Peng Jia [2], Jianfeng Wang [3], Changjiang Zhang [4], Xintong Dai [1], Wenbo Yu [1], Xiaoyu Lei [1], Ningning Wang [4,*] and Minglai Yang [1,*]

[1] College of Information and Technology, Jilin Agricultural University, Changchun 130118, China; xuemeil@jlau.edu.cn (X.L.); 20231617@mails.jlau.edu.cn (Q.L.); daixintong20@163.com (X.D.); 20221137@mails.jlau.edu.cn (W.Y.); 20231258@mails.jlau.edu.cn (X.L.)
[2] State Key Laboratory of Luminescence and Application, Changchun Institute of Optics, Fine Mechanics and Physics, Chinese Academy of Sciences, Changchun 130033, China; qinl@ciomp.ac.cn (L.Q.); jiapeng@ciomp.ac.cn (P.J.)
[3] Key Laboratory of Facility Vegetable of Jilin Province, Jilin Academy of Vegetable and Flower Sciences, Changchun 130119, China; hortwjf@163.com
[4] Faculty of Agronomy, Jilin Agricultural University, Changchun 130117, China; 17861922969@163.com
* Correspondence: ningningw@jlau.edu.cn (N.W.); yangminglai@163.com (M.Y.)
† These authors contributed equally to this work.

Abstract

Artificial supplemental lighting represents a crucial agricultural technique for enhancing plant growth and development, with researchers continuously investigating the effectiveness of various light sources in horticultural applications. Laser technology, characterized by its monochromatic nature, high coherence, and elevated energy density, presents a promising light source whose potential applications and underlying mechanisms in plant supplemental lighting remain to be thoroughly explored. To investigate the effects of different red-to-blue light ratios in laser supplemental lighting on rice (*Oryza sativa* L. cv. Jijing129) seedlings, we conducted a seedling-stage lighting experiment on the rice cultivar Jijing129 in a greenhouse using an LGI-660/450 dual-wavelength semiconductor laser system. The experimental design included a natural light control (AL) and three laser treatment groups, with red: blue (R:B) ratios and corresponding photon flux densities as follows: BL (50:50; 150:150 μmol m^{-2} s^{-1}), CL (60:40; 180:120 μmol m^{-2} s^{-1}), and DL (75:25; 225:75 μmol m^{-2} s^{-1}). We systematically analyzed short-term morphological, physiological, and gene expression changes to elucidate the potential mechanisms underlying yield enhancement under different laser spectra. The results indicated that, compared to AL, all laser treatments (BL, CL, and DL) significantly increased root fresh weight, dry weight, and nitrogen content in seedlings. Furthermore, the final yield was significantly improved in all laser-treated groups, with the CL treatment exhibiting the highest yield. Transcriptome sequencing identified 10,497, 10,441, 10,700, and 10,757 expressed genes in the AL, BL, CL, and DL groups, respectively. Comparative analysis revealed 101, 1645, and 2247 differentially expressed genes (DEGs) in the BL/AL, CL/AL, and DL/AL comparisons, respectively. Gene Ontology (GO) enrichment analysis showed that these DEGs were significantly enriched in pathways such as metabolic processes, nitrogen metabolism, and protein amino acid phosphorylation. Notably, genes involved in the regulation of nitrogen compound metabolism were significantly upregulated in the CL and DL treatments. Further analysis of nitrogen metabolism and photosynthesis pathways revealed that laser irradiation induced the upregulation of specific genes. Interestingly, although physiological assays showed no significant changes in CAT, SOD, and POD activities, the

expression of their corresponding genes was upregulated by laser treatment, suggesting these genes play a regulatory role during the supplemental lighting process. Therefore, our results indicated that laser supplemental lighting during the rice seedling stage increased the nitrogen content in plants and modulated the expression of related genes, and these changes might have been associated with the subsequent increase in rice yield. This study lays a foundation for understanding the molecular mechanisms of laser supplemental lighting and provides empirical support for the application of laser technology as an effective light source in agriculture.

Keywords: RNA-seq; light quality; red: blue ratio; differentially expressed genes (DEGs); nitrogen metabolism; photosynthesis

1. Introduction

Plant supplemental lighting technologies have been increasingly applied in agricultural production. Laser technology, characterized by its monochromaticity, coherence, and high energy density, represents a distinct approach to delivering light stimuli in plant science research [1,2]. While conventional artificial light sources—particularly light-emitting diodes (LEDs)—are widely adopted for their efficiency, uniformity, and cost-effectiveness in large-scale applications, they typically emit broader wavelength bands [3,4]. Consequently, lasers offer complementary advantages due to their exceptional spectral purity, making them ideal for investigating fundamental plant responses to specific narrow-band light [5,6].

The synergistic effects of red and blue light components are particularly critical for plant physiology [7]. Red light (650–670 nm) corresponds closely to the absorption peaks of chlorophyll, directly driving photosynthesis, while blue light (450–470 nm) regulates photomorphogenic responses through photoreceptors such as cryptochromes and phototropins [8,9]. In rice, modulating the red-to-blue ratio has been shown to influence key agronomic traits, including RuBisCO activation and the expression of genes involved in flavonoid synthesis [10,11]. At the molecular level, specific wavelengths can enhance the repair cycle of Photosystem II and affect the cyclic electron flow around Photosystem I, thereby influencing photosynthetic efficiency [12–14]. Concurrently, blue light mediates auxin distribution by regulating PIN protein localization, intricately linking light signaling with developmental patterning [15,16]. Although the phenotypic plasticity of plants in response to light quality is well-documented [17,18], the precise transcriptional mechanisms through which defined light signals, particularly from monochromatic sources like lasers, interface with the core regulatory networks in rice remain inadequately explored. This knowledge gap currently limits the rational design of precision light regimes for smart agriculture [19,20].

Lasers exhibit diverse regulatory effects across different plant species [5]. In soybeans, high-intensity blue light preferentially activates genes involved in nodule formation and biological nitrogen fixation, while concurrently suppressing the expression of flowering-related genes [21,22]. Conversely, red light promotes stem elongation through gibberellin-pathway genes but impairs nodule development [23,24]. Ultraviolet laser treatment has been shown to activate stress-resistance gene networks, thereby enhancing disease resistance in plants [1]. In tomato cultivation, dynamically optimized red–blue light combinations coordinately regulate photoreceptor and sink-strength–related genes, achieving a balance between light capture and fruit biomass accumulation [25,26]. Pulsed ultraviolet lasers specifically induce flavonoid biosynthetic genes, leading to targeted en-

hancement of fruit antioxidant capacity [27,28]. In lettuce, red-light–dominant conditions stimulate the expression of genes involved in biomass accumulation but simultaneously inhibit nitrate metabolism [29,30], whereas blue light supplementation activates nitrate reductase genes, thereby optimizing both growth performance and food safety [31,32]. Collectively, these studies demonstrate that laser-based light treatments can modulate plant growth and development by regulating gene expression. However, much of the current evidence comes from vegetables and other horticultural species. Due to constraints related to operational conditions, cultivation scale, and field management, research on supplemental laser lighting in major field crops remains relatively limited and requires further systematic investigation.

Although laser-based supplemental lighting has been shown to play an important role in regulating plant growth and development [5,33], it remains unclear whether different red-to-blue light ratios exert similar or distinct effects, and its impact on field crops is still largely unexplored. In this study, we used the LGI-660/450 dual-wavelength semiconductor laser system to conduct supplemental lighting experiments on the rice cultivar Jijing129 during the seedling stage, a critical phase for stand establishment. Three red–blue light ratio treatments were applied: BL (R:B = 50:50; 150:150 $\mu mol \cdot m^{-2} \cdot s^{-1}$), CL (R:B = 60:40; 180:120 $\mu mol \cdot m^{-2} \cdot s^{-1}$), and DL (R:B = 75:25; 225:75 $\mu mol \cdot m^{-2} \cdot s^{-1}$), with natural light (AL) serving as the control. By comparing the effects of laser supplementation and natural light on rice traits and yield, and by analyzing morphological, physiological, and gene expression changes in Jijing129 under different light ratios, this study provides a foundation for further in-depth research on the mechanisms of laser-based supplemental lighting.

2. Results

2.1. Effects of Short-Term Laser Irradiation on Root Morphology and Yield in Rice

We applied laser-based supplemental lighting to Jijing129 rice seedlings in a green house, using natural light as the control (AL). Three red-to-blue light ratios were tested: BL (RED: BLUE = 50:50; 150:150 $\mu mol \cdot m^{-2} \cdot s^{-1}$), CL (RED: BLUE = 60:40; 180:120 $\mu mol \cdot m^{-2} \cdot s^{-1}$), and DL (RED: BLUE = 75:25; 225:75 $\mu mol \cdot m^{-2} \cdot s^{-1}$). The results showed that, compared with AL, all laser treatments significantly increased root fresh weight and root dry weight ($p < 0.05$) (Figure 1a), and grain yield was also significantly improved ($p < 0.05$) (Figure 1b,c). Among the three laser regimes, DL led to the smallest improvements in both root biomass and yield relative to BL and CL. The significant increase in root dry weight across all laser treatments ($p < 0.05$) indicates that laser supplementation promotes dry matter accumulation in roots, possibly through enhanced dry-matter accumulation in root tissues.

Regarding yield, all treatment groups showed significant increases (Figure 1b), with the CL treatment exhibiting the most notable effect. This suggests that CL has a strong optimizing influence on rice yield formation than BL and DL (Table S1). The BL and DL groups also demonstrated significantly higher yields than the AL control, further confirming that laser irradiation positively influences yield development. In contrast, above-ground traits such as plant height, leaf fresh weight, and leaf dry weight showed no significant differences among treatments (Figure 1c). These results demonstrate that the application of laser supplemental lighting during the seedling phase significantly influences both root biomass and final yield in Jijing129.

2.2. Effect of Short-Term Laser Irradiation on the Small Organic Compounds Content in Rice

To investigate the alterations in small organic compounds content in rice plants subjected to short-term laser irradiation, we measured the contents of total nitrogen, zinc, and trace organic compounds in both the roots and leaves of Jiling129 rice under different

treatments. The results (Figure 2) showed that, across treatments (AL, BL, CL, DL), the total nitrogen (TN) content gradually increased. Notably, the TN levels in the BL, CL, and DL groups were significantly higher than in the AL control ($p < 0.05$), suggesting that different laser treatments may promote nitrogen accumulation in the plants.

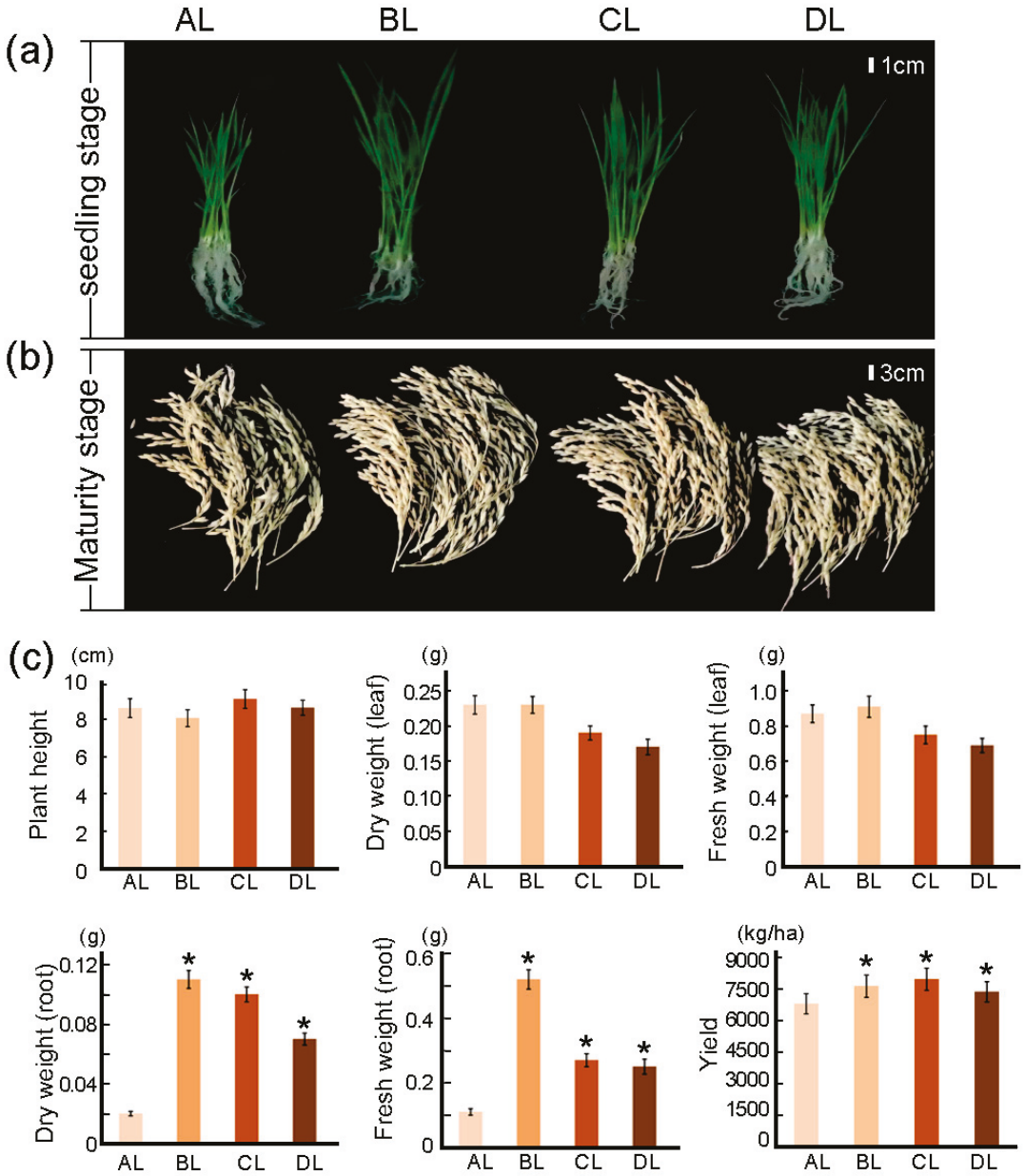

Figure 1. Results of rice phenotype and morphological index measurements under laser irradiation. (**a**) Jijing129 rice was irradiated with different light intensity ratios (AL, BL, CL, DL) for 28 days at both the seedling and maturity stages. (**b**) Root dry weight, root fresh weight, and actual yield of Jijing129 rice. (**c**) Morphological indices including plant height, leaf dry weight, leaf fresh weight, root dry weight, root fresh weight, and grain yield of Jijing129 rice under different treatments. The abbreviations BL, CL, and DL refer to the treatment groups BL (R50:B50; 150:150 μmol m^{-2} s^{-1}), CL (R60:B40; 180:120 μmol m^{-2} s^{-1}), and DL (R75:B25; 225:75 μmol m^{-2} s^{-1}), while AL represents the control under natural light conditions. * indicates a statistically significant difference compared with the control AL group (* indicates $p < 0.05$).

We also measured the contents of zinc and malondialdehyde (MDA), as well as the activities of catalase (CAT), superoxide dismutase (SOD), and peroxidase (POD). Although the measured values varied among treatments, no statistically significant differences were

detected among the AL, BL, CL, and DL groups. These physiological indicators showed no obvious changes, which indirectly indicates that the primary effect of laser supplemental lighting during the seedling stage is to significantly enhance nitrogen content in Jijing129 seedlings. Meanwhile, although Figure 2 suggests a trend of increasing TN from BL to CL to DL, statistical comparisons among the laser treatments did not reveal significant differences ($p > 0.05$), indicating that the nitrogen enhancement may be primarily attributable to laser irradiation per se rather than to the specific red–blue ratio.

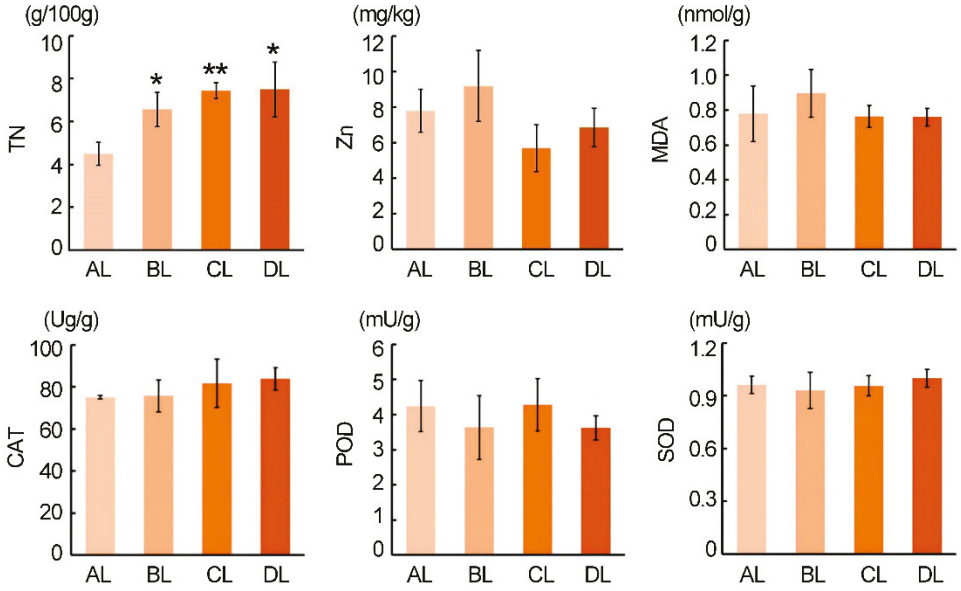

Figure 2. The variation in physical characteristics induced by laser irradiation. The abbreviations BL, CL, and DL refer to the treatment groups BL (R50:B50; 150:150 μmol m^{-2} s^{-1}), CL (R60:B40; 180:120 μmol m^{-2} s^{-1}), and DL (R75:B25; 225:75 μmol m^{-2} s^{-1}), while AL represents the control under natural light conditions. *, ** indicates $p < 0.05$ and $p < 0.01$, respectively.

2.3. Effects of Short-Term Laser Irradiation on Genome-Wide Gene Expression in Rice

In this study, we examined genome-wide gene expression changes in rice leaves after 28 days of laser irradiation using RNA-seq (Table S2). The results revealed (Figure 3a) that the AL, BL, CL, and DL samples expressed 10,401, 10,237, 10,480, and 10,497 genes, respectively. To identify common and unique gene expression patterns among the samples, Venn diagram analysis was conducted (Figure 3b). As shown, 9965 genes were co-expressed in all samples, while 121 genes were specifically expressed in AL, 59 genes in BL, 96 genes in CL, and 182 genes uniquely in AL, respectively. Furthermore, by analyzing the number of co-expressed and differentially expressed genes using Venn diagrams (Figure 3c), 10,283 genes were co-expressed in both the AL and CL groups. In comparison, 417 genes were specifically expressed in CL, and 214 genes were uniquely expressed in AL. The results observed genome-wide variations in both treatment-specific and treatment-specific gene expression responses following laser irradiation. These findings highlight the complexity of the transcriptional response to laser treatment across different rice genotypes.

2.4. Comparative Analysis of Differentially Expressed Genes in Rice Under Laser Irradiation

To further study the gene variation, we analyzed the differentially expressed genes (DEGs) under light conditions (BL, CL, and DL) and compared them with the control (AL). We quantified up- and down-regulated genes and characterized their functional enrichment. The results demonstrated that different light treatments significantly influenced gene expression patterns. Specifically, 101 DEGs were identified in the BL vs. AL comparison, consisting of 64 up-regulated and 37 down-regulated genes; 1645 DEGs were detected

in CL vs. AL, with 752 up-regulated and 893 down-regulated genes; and 2247 DEGs were identified in DL vs. AL, including 874 up-regulated and 1373 down-regulated genes (Figure 4a).

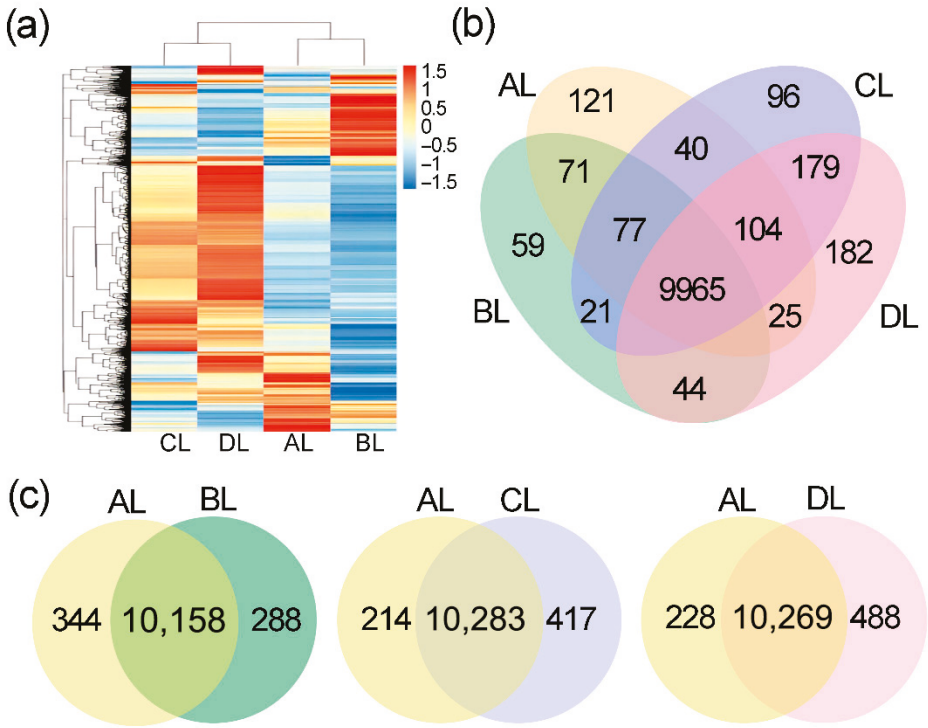

Figure 3. The variation in gene expression induced by laser irradiation. (**a**) Heatmap showing hierarchical clustering of gene expression profiles across AL, BL, CL, and DL samples. (**b**) Venn diagram displaying the number of co-expressed and specifically expressed genes among AL, BL, CL, and DL groups. (**c**) Pairwise Venn diagrams illustrating co-expressed genes between AL and each laser treatment group (BL, CL, and DL). The abbreviations BL, CL, and DL refer to the treatment groups BL (R50:B50; 150:150 μmol m^{-2} s^{-1}), CL (R60:B40; 180:120 μmol m^{-2} s^{-1}), and DL (R75:B25; 225:75 μmol m^{-2} s^{-1}), while AL represents the control under natural light conditions.

Venn diagram analysis was used to explore the overlapping and specific DEGs among the groups (Figure 4b,c). Among the up-regulated genes, seven were commonly up-regulated in both BL vs. AL and CL vs. AL, with 57 specific to BL vs. AL and 745 specific to CL vs. AL. Additionally, one gene was up-regulated in both BL vs. AL and DL vs. AL, with 63 genes specific to BL vs. AL and 873 specific to DL vs. AL. For the comparison between CL vs. AL and DL vs. AL, 382 genes were commonly up-regulated, with 370 specific to CL vs. AL and 492 specific to DL vs. AL.

Regarding down-regulated genes, four were common between BL vs. AL and CL vs. AL, with 33 specific to BL vs. AL and 889 specific to CL vs. AL. Between BL vs. AL and DL vs. AL, 6 shared down-regulated genes were identified, along with 31 specific to CL vs. AL and 1367 specific to DL vs. AL. For the comparison of CL vs. AL and DL vs. AL, 471 DEGs were commonly down-regulated, with 422 specific to CL vs. AL and 902 specific to DL vs. AL.

Overall, the most pronounced gene down-regulation was observed under BL treatment, whereas CL and DL induced a greater number of up-regulated genes. These findings suggest that different light conditions exert distinct regulatory effects on gene expression.

2.5. Comparative Analysis of GO and KEGG Enrichment in Rice Under Laser Irradiation

This study analyzed Gene Ontology (GO) enrichment in rice leaves subjected to various laser treatments. Analysis of up-regulated DEGs across different groups (Figure 5). In the comparison between AL and BL, the most enriched GO term in the biological process (BP) category was "metabolic process" (GO:0008152). In contrast, in the molecular function (MF) category, it was "oxidoreductase activity" (GO:0016491) (Figure 5a).

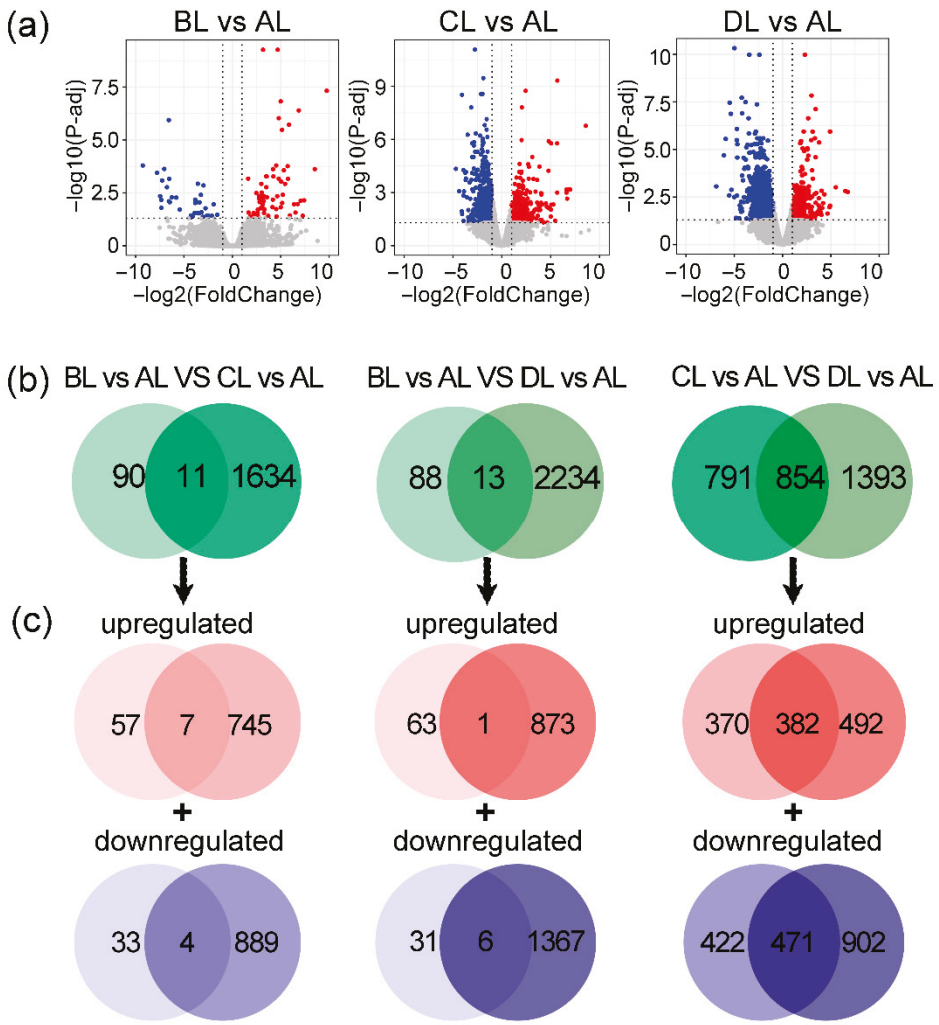

Figure 4. Changes in differentially expressed genes (DEGs) in the rice genome induced by different laser treatments. (**a**) Volcano plot displaying statistically significant up-regulated (red) and down-regulated (blue) DEGs. (**b**) Venn diagram illustrating overlapping and unique DEGs across three comparative groups (vs. control). (**c**) Shared and group-specific up-/down-regulated DEGs among the three comparisons. The abbreviations BL, CL, and DL refer to the treatment groups BL (R50:B50; 150:150 μmol m^{-2} s^{-1}), CL (R60:B40; 180:120 μmol m^{-2} s^{-1}), and DL (R75:B25; 225:75 μmol m^{-2} s^{-1}), while AL represents the control under natural light conditions.

In the AL vs. CL comparison, the most enriched BP GO term was "regulation of nitrogen compound metabolic process" (GO:0051171), followed by "regulation of biosynthesis" (GO:0009889), "regulation of macromolecular biosynthesis" (GO:0010556), and "regulation of cell biosynthesis" (GO:0031326). The most significantly enriched cellular component (CC) GO terms were "apoplast" (GO:0048046) and "nucleus" (GO:0005634), while in the MF category, "transcriptional regulation activity" (GO:0030528) was predominant (Figure 5a).

For the AL vs. DL comparison, the most enriched BP GO terms were "microtubule-based movement" (GO:0007018) and "protein amino acid phosphorylation" (GO:0006468).

The top CC GO terms included "components of the light membrane" (GO:0016021) and "membrane intrinsic" (GO:0031224), whereas in MF, "ATP binding" (GO:0005524) was most prominent. Additionally, highly enriched activities included "microtubule motor activity" (GO:0003777), "adenylate binding" (GO:0030554), and "purine nucleoside binding" (GO:0001883) (Figure 5a, Table S3).

To further elucidate the metabolic pathways involved, Kyoto Encyclopedia of Genes and Genomes (KEGG) enrichment analysis was conducted (Figure 5b, Table S4). In the AL vs. BL comparison, pathways related to diterpenoid biosynthesis and secondary metabolite biosynthesis were significantly enriched. In the AL vs. CL comparison, DNA replication and mismatch repair pathways were notably enriched. Meanwhile, in the AL vs. DL comparison, DNA replication and motor protein pathways demonstrated significant enrichment.

By integrating GO and KEGG analyses, we observed that up-regulated genes involved in nitrogen regulation were notably affected by laser irradiation. Specifically, the activity related to "regulation of nitrogen compound metabolic process" (GO:0051171) was significantly increased in the AL vs. CL comparison.

Down-regulated genes under BL condition exhibited distinct functional profiles. Similarly, we analyzed down-regulated genes in the differential expression groups, with results presented in Figure S1 (Tables S5 and S6) demonstrating significant enrichment of pathways, such as 'photosynthesis' (FDR < 0.05).

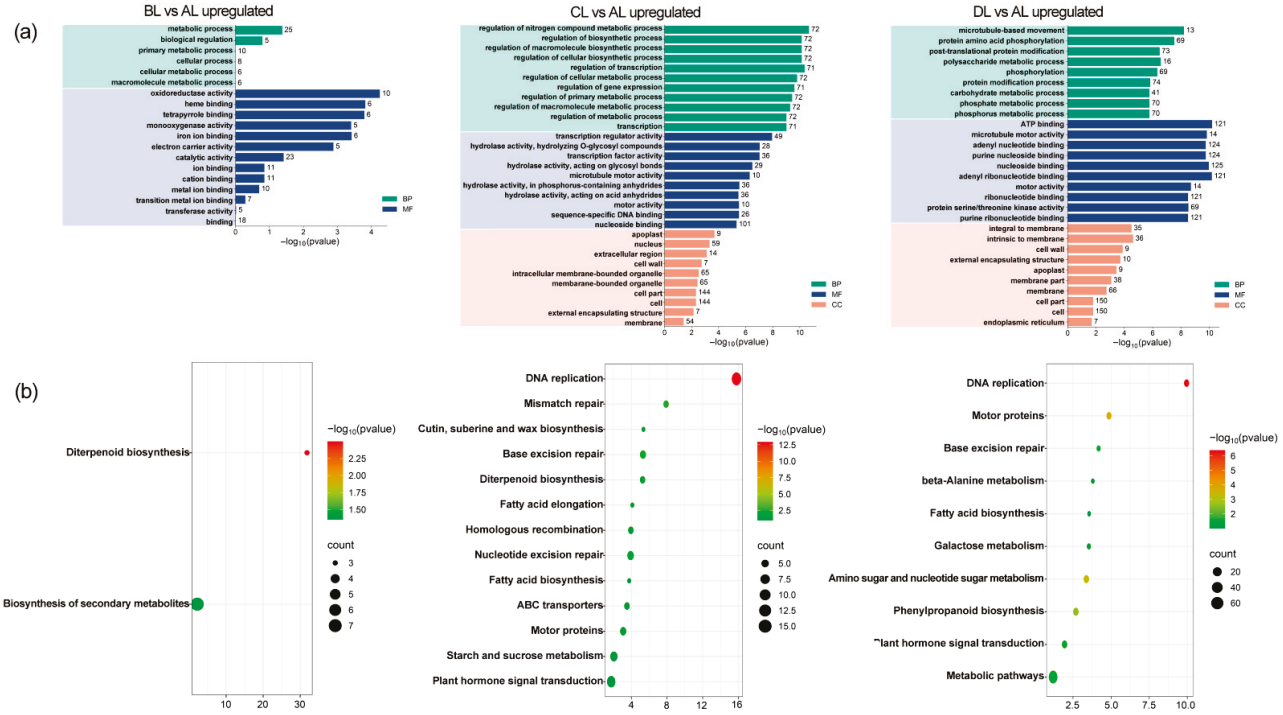

Figure 5. GO (**a**) and KEGG (**b**) enrichment analysis of rice up-regulated DEGs in response to laser irradiation. The abbreviations BL, CL, and DL refer to the treatment groups BL (R50:B50; 150:150 μmol m^{-2} s^{-1}), CL (R60:B40; 180:120 μmol m^{-2} s^{-1}), and DL (R75:B25; 225:75 μmol m^{-2} s^{-1}), while AL represents the control under natural light conditions.

2.6. Laser Irradiation Differentially Regulates Nitrogen-Related Genes

GO enrichment analysis revealed that genes upregulated by laser irradiation were significantly enriched in the "regulation of nitrogen compound metabolic process" pathway (GO term). Expression levels and fold changes for all genes in this pathway were visualized using a heatmap (Figure 6a, Table S7). The results demonstrated a widespread

and significant upregulation of these genes, particularly pronounced in the CL/AL and DL/AL comparison groups.

KEGG pathway enrichment analysis identified that genes downregulated by laser irradiation were significantly enriched in the "nitrogen metabolism" pathway (Figure S1, Figure 6b). Further analysis of the genes involved in this pathway revealed that down-regulated genes predominated between the three red–blue light ratios and the control. Interestingly, however, a subset of genes was significantly up-regulated: in particular, *OsNR1* and *OsNR2* were markedly up-regulated under the BL treatment; *OsGDH3* was significantly up-regulated under CL; and *OsGDH1* and *GLU* were significantly up-regulated under DL (Figure 6c).

These results indicate that the changes in nitrogen content in jijing129 seedlings following supplemental laser treatment are likely closely associated with a set of significantly differentially expressed genes, including both those directly involved in nitrogen metabolism and those regulating it. Furthermore, the roles and contributions of these genes may vary under different red–blue light ratios.

2.7. Laser Irradiation Differentially Regulates Photosynthesis-Related Gene Expression in Rice

Although we did not measure physiological parameters directly related to photosynthesis, GO and KEGG enrichment analyses revealed that photosynthesis-related pathways were significantly enriched (Figure S1). Consequently, we further analyzed genes within the photosynthesis pathway (Figure 7, Table S8). The results indicated that gene expression patterns exhibited distinct trends under different red–blue light ratios. Specifically, *OsPsbH1*, *OsPsbH3*, *OsPsbH4*, *OsAtpC*, and *OsAtpA2* were significantly upregulated under the BL treatment. In the CL treatment, *OsPsbA1*, *OsPsbA3*, and *OsPsbA4* were significantly upregulated, whereas *OsFd1.1* was significantly upregulated under the DL treatment.

PsbH is one of the major subunits of the Photosystem II (PSII) reaction center complex and is closely associated with the assembly, stability, and electron transport efficiency of PSII [34]. In contrast, AtpC and AtpA2 encode key subunits of chloroplast ATP synthase, which directly participate in ATP synthesis during the process of photophosphorylation [35]. The *PsbA* gene family encodes the D1 protein of the PSII reaction center, one of the core components responsible for primary charge separation and electron transfer [36]. *OsFd1.1* encodes ferredoxin, which is located at the acceptor side of Photosystem I (PSI) and serves as a key electron carrier linking the light reactions to multiple downstream metabolic pathways, such as carbon assimilation, nitrate reduction, and reactive oxygen species scavenging [37].

These results suggest that supplemental laser irradiation induces the expression of these genes during the rice seedling stage, thereby participating in the regulation of photosynthesis.

2.8. Laser Irradiation Differentially Regulates Rice Genes Associated with Physical Characteristics

Although no significant changes were detected in physiological indices such as CAT, SOD, and POD in this study, GO and KEGG enrichment analyses of the DEGs revealed that they were primarily enriched in pathways related to redox processes. Based on these findings, we further analyzed genes associated with lipoxygenase (LOX), glutathione (GSH), reactive oxygen species (ROS), and the activities of CAT, SOD, and POD (Figure 8, Table S9). The results indicated that under laser treatment, the expression of a subset of these genes was induced in rice seedlings, and their expression patterns differed significantly under different red–blue light ratios. Specifically, a considerable proportion of these genes were significantly upregulated or downregulated under laser treatment, suggesting that laser supplemental lighting can elicit molecular responses related to lipid peroxidation, the glutathione cycle, and ROS scavenging systems.

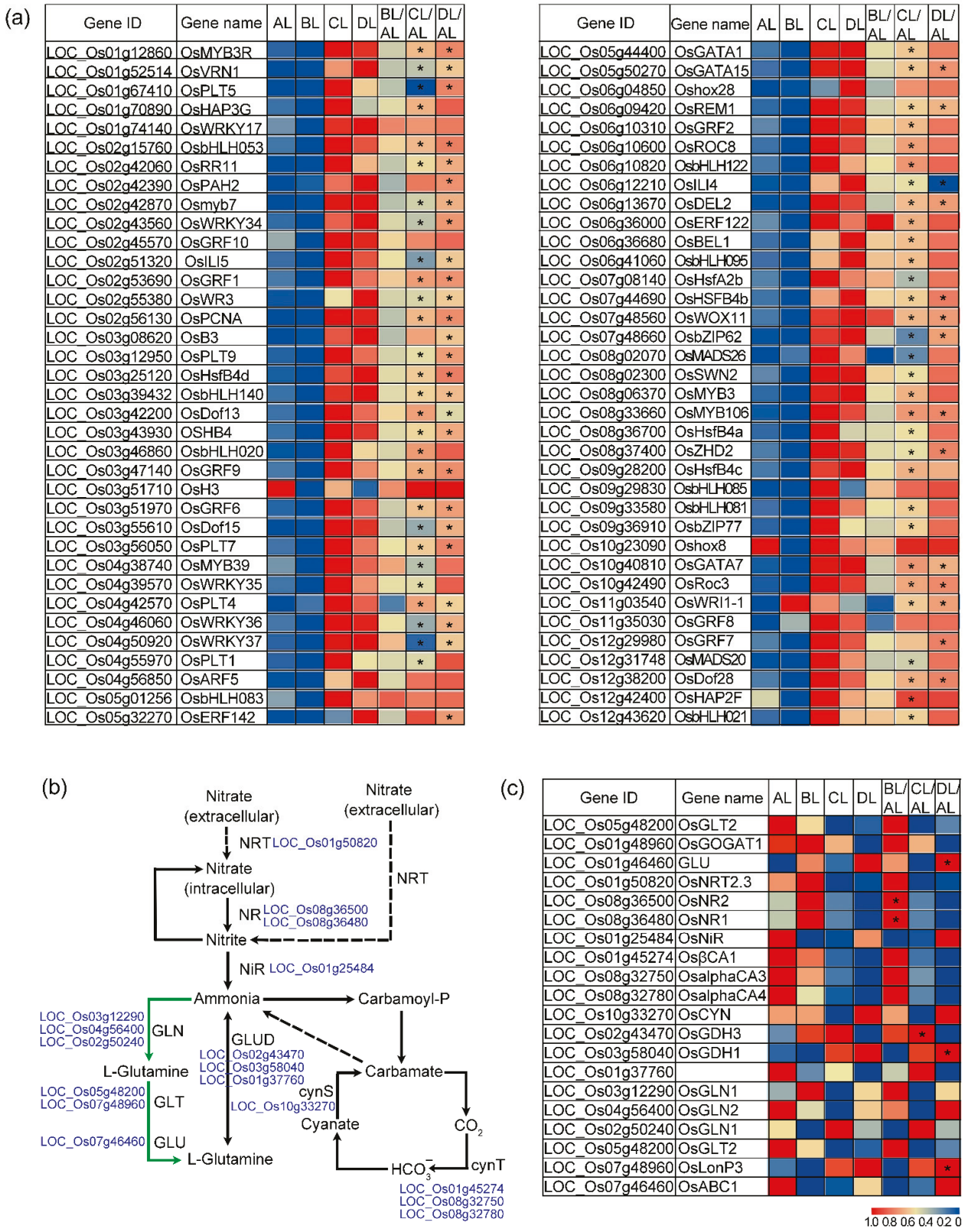

Figure 6. Differential response of nitrogen metabolism-related genes to short-term laser irradiation in rice. (**a**) Expression of genes involved in the regulation of the nitrogen compound metabolic process. (**b**) KEGG nitrogen metabolism pathway map. (**c**) Expression patterns of genes associated with the nitrogen metabolism pathway. The abbreviations BL, CL, and DL refer to the treatment groups BL (R50:B50; 150:150 μmol m^{-2} s^{-1}), CL (R60:B40; 180:120 μmol m^{-2} s^{-1}), and DL (R75:B25; 225:75 μmol m^{-2} s^{-1}), while AL represents the control under natural light conditions. * indicates a statistically significant difference compared with the AL control group (* indicates $p < 0.05$).

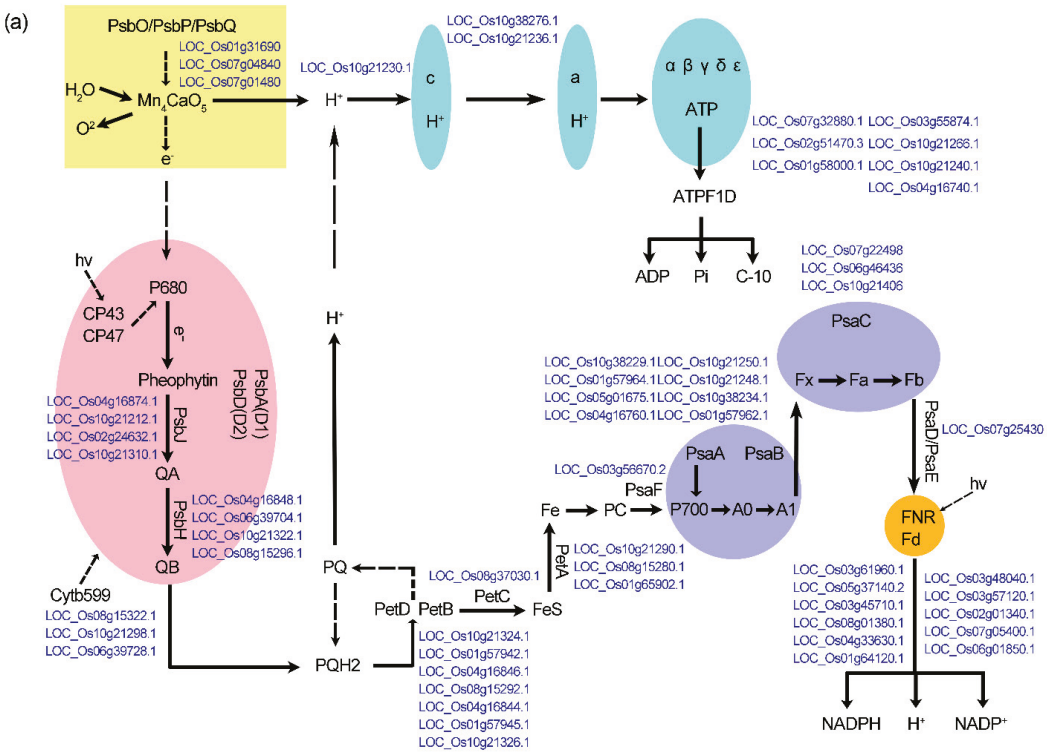

(b)

Gene ID	Gene name	AL	BL	CL	DL	BL/AL	CL/AL	DL/AL
LOC_Os01g31690	OsPSBO							
LOC_Os07g04840	OsPsbP							
LOC_Os07g01480	OSPsbQ							
LOC_Os04g16874.1	OsPsbC1							
LOC_Os10g21212.1	OsPsbC2							
LOC_Os02g24632.1	OsPsbC3							
LOC_Os10g21310.1	OsPsbB1							
LOC_Os10g21192	OsPsbA1						*	
LOC_Os10g39880	OsPsbA2							
LOC_Os08g35420	OsPsbA3						*	
LOC_Os04g16770.1	OsPsbA4						*	
LOC_Os10g41689	OsPsbD1							
LOC_Os04g16872.1	OsPsbD2							
LOC_Os02g24634.1	OsPsbD3							
LOC_Os04g16848.1	OsPsbH1					*		
LOC_Os06g39704.1	OsPsbH2							
LOC_Os10g21322.1	OsPsbH3					*		
LOC_Os08g15296.1	OsPsbH4					*		
LOC_Os08g15322.1	OsPsbE1							
LOC_Os10g21298.1	OsPsbE2							
LOC_Os06g39728.1	OsPsbE3							
LOC_Os10g21324.1	OsPetB1							
LOC_Os01g57942.1	OsPetB2							
LOC_Os04g16846.1	OsPetB3							
LOC_Os08g15292.1	OsPetD1							
LOC_Os04g16844.1	OsPetD2							
LOC_Os01g57945.1	OsPetD3							
LOC_Os10g21326.1	OsPetD4							
LOC_Os08g37030.1	OsPetC							
LOC_Os10g21290.1	OsPetA1							
LOC_Os08g15280.1	OsPetA2							
LOC_Os01g65902.1	OsPetA3							

1.0 0.8 0.6 0.4 0.2 0

Gene ID	Gene name	AL	BL	CL	DL	BL/AL	CL/AL	DL/AL
LOC_Os03g56670.2	OsPS1-F							
LOC_Os10g38229.1	OsPsaA1							
LOC_Os01g57964.1	OsPsaA2							
LOC_Os05g01675.1	OsPsaA3							
LOC_Os04g16760.1	OsPsaA4							
LOC_Os10g21250.1	OsPsaA5							
LOC_Os10g21248.1	OsPsaB1							
LOC_Os10g38234.1	OsPsaB2							
LOC_Os01g57962.1	OsPsaB3							
LOC_Os07g22498	OsPsaC1							
LOC_Os06g46436	OsPsaC2							
LOC_Os10g21406	OsPsaC3							
LOC_Os06g01210.1	OsPETE							
LOC_Os03g61960.1	OsFd3							
LOC_Os05g37140.2	OsFd4							
LOC_Os03g45710.1	OsFdC1							
LOC_Os08g01380.1	OsFd1							
LOC_Os04g33630.1	OsFd1.1							*
LOC_Os01g64120.1	OsFdR-b1							
LOC_Os03g48040.1	OsFdC2							
LOC_Os03g57120.1	OsFNR							
LOC_Os02g01340.1	OsLFNR1							
LOC_Os06g01850.1	OsLFNR2							
LOC_Os10g21230.1	OsAtpC					*		
LOC_Os10g38276.1	OsAtpA1							
LOC_Os10g21236.1	OsAtpA2					*		
LOC_Os03g55874.1	OsAtpB1							
LOC_Os10g21266.1	OsAtpB2							
LOC_Os10g21240.1	OsAtpα1							
LOC_Os04g16740.1	OsAtpα2							
LOC_Os07g32880.1	OsAtpγ							
LOC_Os02g51470.3	OsF-type							
LOC_Os01g58000.1	OsAtpE							

Figure 7. Differential regulation of rice photosynthetic pathway genes by laser irradiation. (**a**) KEGG photosynthesis pathway map. (**b**) The heatmap shows gene expression and fold change. Gene abbreviations: PSII (photosystem II), Pet (plastoquinone-electron transporter), PSI (photosystem I), ATPase (ATP synthase). The abbreviations BL, CL, and DL refer to the treatment groups BL (R50:B50; 150:150 μmol m^{-2} s^{-1}), CL (R60:B40; 180:120 μmol m^{-2} s^{-1}), and DL (R75:B25; 225:75 μmol m^{-2} s^{-1}), while AL represents the control under natural light conditions. * indicates a statistically significant difference compared with the AL control group (* indicates $p < 0.05$).

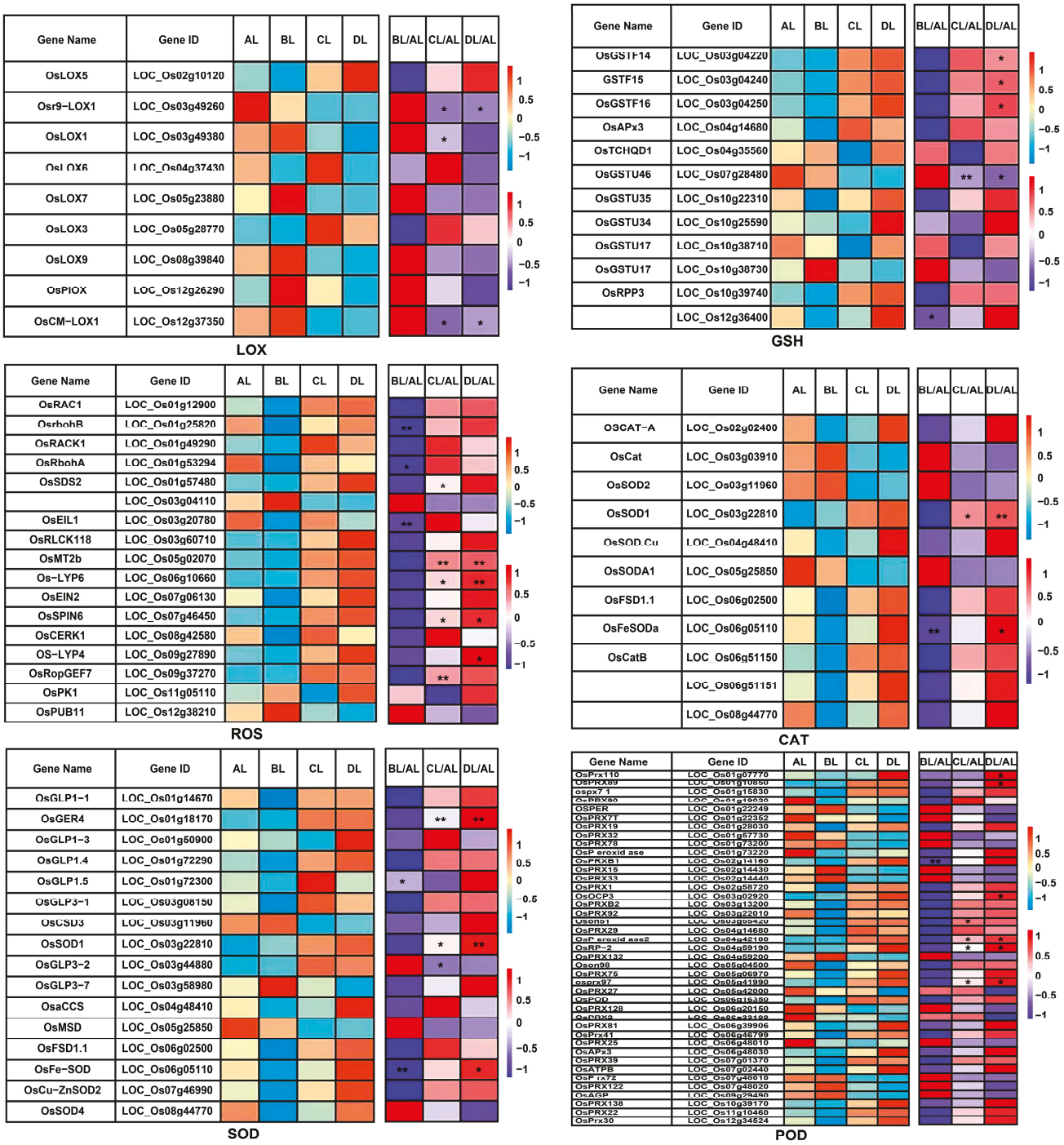

Figure 8. Heatmaps of gene expression related to antioxidant and signaling regulatory genes in rice under laser irradiation. The abbreviations BL, CL, and DL refer to the treatment groups BL (R50:B50; 150:150 μmol m^{-2} s^{-1}), CL (R60:B40; 180:120 μmol m^{-2} s^{-1}), and DL (R75:B25; 225:75 μmol m^{-2} s^{-1}), while AL represents the control under natural light conditions. * and ** indicate statistically significant differences compared with the AL control group at $p < 0.05$ and $p < 0.01$, respectively.

3. Discussion

In this study, we applied laser supplementary lighting with different red/blue ratios at the seedling stage of rice, and compared seedling morphology, physiological parameters, and gene expression under three light combinations (red: blue = 50:50, 60:40, and 75:25). Grain yield was further evaluated at maturity. The results showed that all three laser treatments increased root biomass in rice seedlings. The enhancement of root dry weight

may indicate that laser exposure promoted dry matter accumulation in roots, a phenomenon that has also been reported in wheat and other crops under optimized light conditions [38]. Consistently, the anise study [39] demonstrated that He–Ne laser irradiation significantly increased the biomass of both anise sprouts and mature plants, confirming its growth-promoting effect, which is in line with our expectations.

However, that anise study also showed that different developmental stages (fruits, sprouts, and mature plants) displayed stage-specific responses to laser treatment in terms of pigments, total nutrients, minerals, vitamins, essential oils, and phenolic compounds. In contrast, in our seedling-focused measurements, among all physiological parameters examined, only nitrogen content was significantly increased, whereas other indicators such as SOD, POD, CAT, and MDA showed no obvious changes. In flax, the study [40] reported that combined treatment with laser and 6-benzylaminopurine (BAP) enhanced nitrogen metabolism and increased the activities of key nitrogen assimilation enzymes (GS, GOGAT, and GDH). In agreement with this, we also observed an increase in nitrogen content in our rice plants, together with up-regulation of the *GDH gene* under the CL and DL laser treatments.

The discrepancy between transcript levels and the corresponding enzyme activities may reflect the multilayered nature of metabolic regulation. On the one hand, changes in mRNA abundance can be buffered at the protein level and therefore may not markedly affect enzyme activity; on the other hand, many key metabolic enzymes are subject to post-translational regulation, such as phosphorylation, redox modification, or allosteric control, which can amplify or attenuate the effects of transcriptional changes.

Moreover, laser supplementation improved the grain yield of the rice cultivar Jijing129, which is consistent with the findings of a previous study [1]. That study showed that, under pot conditions in the field, low-intensity laser treatment increased both the number of effective tillers and grain yield per plant, with a 16.8% increase in effective panicle number and a 9.01% increase in per-plant yield. Similarly, in our field trial, overall yield was enhanced, with the most pronounced improvement observed under the CL treatment (red: blue = 60:40). Notably, a 60:40 red/blue ratio can improve photosynthetic efficiency and yield without markedly altering vegetative growth, a result that has already been validated in sweet pepper [38].

It is noteworthy that the transcriptomic responses exhibited a substantial disparity in the number of DEGs among treatments: only 101 DEGs were detected in BL, compared with 1645 and 2247 in CL and DL, respectively, despite the relatively modest phenotypic differences. This pattern suggests that the specific red–blue ratios in CL and DL may trigger much broader photoreceptor-mediated transcriptional reprogramming, whereas BL may represent a relatively stable or balanced state that requires only limited transcriptional adjustment. Although minor variation among biological replicates cannot be completely excluded and may have contributed to the absolute DEG counts to some extent, the pronounced quantitative contrast among treatments is unlikely to be explained solely by experimental variation. Instead, it most likely reflects genuinely different regulatory strategies adopted by plants under the distinct laser light conditions.

The DEGs identified under CL/AL treatment were significantly enriched in the pathway of "regulation of nitrogen metabolic process." Further analysis revealed that laser irradiation under both CL and DL conditions markedly up-regulated the expression of a large number of genes, including several classes of transcription factors, such as members of the WRKY family (*OsWRKY17*, *OsWRKY34*, *OsWRKY35*, *OsWRKY36*, *OsWRKY37*), the bHLH family (*OsbHLH020*, *OsbHLH021*, *OsbHLH053*, *OsbHLH081*, *OsbHLH083*, *OsbHLH085*, *OsbHLH095*, *OsbHLH140*), and the MYB family (*OsMYB3*, *OsMYB3R*, *OsMYB7*, *OsMYB39*, *OsMYB106*). These transcription factors are likely to act together within tran-

scriptional regulatory networks that govern stress responses, hormone signaling, and plant growth and development. The functions of some of these genes have been relatively well characterized. For example, *OsMYB3* is a key R2R3-MYB gene that controls anthocyanin biosynthesis and accumulation in the pericarp of black rice [41]. In contrast, many members of the WRKY, bHLH, and MYB families identified here have not yet been subjected to systematic genetic and mechanistic studies. Their pronounced up-regulation under both CL and DL treatments suggests that they may be involved in the regulation of nitrogen metabolism, responses to light conditions, and adaptation to environmental stresses. Therefore, future functional studies are warranted to elucidate their roles and to explore their potential utility in improving nitrogen use efficiency and enhancing stress tolerance in rice.

The analysis showed that, under different red–blue light ratios, photosynthesis-related genes exhibited markedly distinct expression patterns, displaying a typical "light-quality-specific response" profile. Specifically, under the blue-light-dominant BL treatment, the expression of *OsPsbH1*, *OsPsbH3*, *OsPsbH4*, *OsAtpC*, and *OsAtpA2* was significantly upregulated. PsbH proteins are important subunits of the photosystem II (PSII) reaction center complex and are closely associated with PSII assembly, stability, and electron transport efficiency [34]. AtpC and AtpA2 encode key subunits of chloroplast ATP synthase and are directly involved in ATP production during photophosphorylation [35]. The coordinated upregulation of these genes suggests that, under BL conditions, plants may simultaneously enhance PSII reaction center function and energy conversion efficiency, thereby improving the capacity of rice seedlings to utilize light energy.

Under the CL treatment, *OsPsbA1*, *OsPsbA3*, and *OsPsbA4* were markedly upregulated. The *PsbA* gene family encodes the D1 protein of the PSII reaction center, which is a core component responsible for primary charge separation and electron transfer, and is also the protein most prone to damage and frequent turnover under photoinhibitory conditions [36]. The strong induction of multiple *PsbA* copies under CL conditions may be associated with accelerated D1 turnover, enhanced PSII repair capacity, and increased tolerance to photoinhibition, thereby helping to maintain stable operation of the photosynthetic apparatus under higher light input or specific light-quality environments.

In contrast, under the DL treatment with a higher proportion of red light, *OsFd1.1* was significantly upregulated. *OsFd1.1* encodes ferredoxin, located at the terminal acceptor side of PSI, which serves as a key electron carrier linking the light reactions to multiple downstream metabolic pathways, such as carbon assimilation, nitrate reduction, and reactive oxygen species scavenging [37]. Its induced expression under DL conditions may help increase the flow of electrons from PSI into various metabolic routes, optimize the distribution of reducing power within the cell, and thereby coordinate the balance between photosynthetic electron transport and metabolic processes.

Taken together, the differential regulation of genes encoding PSII structural proteins, ATP synthase subunits, and ferredoxin under distinct red–blue light ratios may represent an important molecular basis underlying the effects of laser light supplementation on photosynthetic performance and growth of rice seedlings. Under laser supplemental lighting during the seedling stage of jijing129, an in-depth elucidation of the regulatory mechanisms of nitrogen metabolism pathways and key genes such as *PsbA* and *OsGDH3* should be a primary focus of future research.

Although no significant changes in the activities of antioxidant enzymes such as CAT, SOD, and POD were detected at the physiological level in this study, GO and KEGG enrichment analyses of the transcriptome, together with the expression patterns of related genes, indicated that rice seedlings had already mounted a clear molecular response in redox and antioxidant pathways under laser supplemental lighting.

On the one hand, this phenomenon of "transcriptional responses preceding detectable physiological changes" may reflect a preventive regulatory strategy, whereby plants grown under different red–blue laser light ratios fine-tune the expression of genes associated with LOX, GSH metabolism, ROS scavenging, and antioxidant enzymes (CAT, SOD, POD) to mitigate potential oxidative stress in advance. Such regulation likely keeps ROS levels and the extent of lipid peroxidation within a range that is insufficient to cause marked changes in enzyme activities. On the other hand, the pronounced divergence in expression patterns of these genes under different red–blue light ratios suggests that laser light quality not only affects photosynthetic electron transport and energy metabolism but may also reshape the dynamic balance between ROS production and scavenging, thereby establishing light-quality-specific antioxidant regulatory schemes.

Taken together, although conventional physiological indices did not show significant differences, the transcriptomic data reveal an underlying molecular regulatory network activated by the combined effects of laser illumination and light quality, providing the clues for further elucidating how red–blue light ratios modulate cellular redox homeostasis and defense responses.

4. Materials and Methods

4.1. Plant Materials and Treatments

Jijing129 rice (*Oryza sativa L.* ssp. japonica) was used in this study. Seeds were surface-sterilized with 75% ethanol for 30 s followed by 2% sodium hypochlorite for 10 min, then germinated on moist filter paper at 28 °C in darkness for 3 days. Uniformly germinated seeds were transferred to a greenhouse for seedling cultivation. During the seedling stage, the temperature in the greenhouse was controlled at 28 ± 2 °C during the day and 20 ± 2 °C at night, with the relative humidity maintained at 60–70%. Laser supplemental lighting with different red-to-blue light ratios was applied during the seedling period. When the seedlings reached an appropriate height for transplanting, they were transplanted to experimental plots (total area 0.5 ha, with separate plots for each treatment) located in Zhenlai Township, Baicheng City, Jilin Province, where they were grown under conventional field management practices until maturity for yield determination.

The laser treatment system (Model LGI-660/450, Changchun Optical Instrument Co., Changchun, China) consisted of diode lasers emitting at 660 nm (red) and 450 nm (blue), with total photon flux density maintained at 300 μmol m^{-2} s^{-1} at plant canopy level. The supplemental laser light treatments were defined by both the red: blue (R:B) ratio and the corresponding photon flux densities as follows: R50:B50 (150:150 μmol m^{-2} s^{-1}), R60:B40 (180:120 μmol m^{-2} s^{-1}), and R75:B25 (225:75 μmol m^{-2} s^{-1}), with natural daylight (AL) serving as the control.

Both the laser-supplemented treatment and the control were cultivated in the same greenhouse under identical baseline environmental conditions (temperature, humidity, and natural photoperiod). The only difference between them was that the control received no laser supplemental lighting, whereas the treatment group received additional laser light on top of the natural daylight. The irradiation schedule (1:00–9:00 and 17:00–23:00) was designed to provide supplemental lighting during periods of natural light deficiency while avoiding overlap with peak sunlight hours, ensuring that the treatment groups received a consistent, specific light source at fixed intervals.

Samples were collected at the three-leaf stage of rice seedlings (about 28 days after sowing), and the harvested tissues included leaves and roots. A portion of the samples was immediately flash-frozen in liquid nitrogen after collection and stored at −80 °C for subsequent RNA extraction and gene expression analyses.

Measurements of seedling plant height and morphological traits of leaves and roots were conducted with 10 biological replicates per treatment. The mean values of each parameter were calculated, and differences among treatments were statistically analyzed. Physiological parameters were measured using 5 biological replicates, with three technical replicates per sample; the mean of the technical replicates was used for statistical analysis of treatment differences. RNA-seq was performed with three biological replicates. qRT-PCR was conducted with three biological replicates, each with three technical replicates.

At the end of the growth cycle, rice plants from each treatment plot were harvested and yield was determined. For yield determination, harvested rice grains were manually weighed, and dry weight yield data (after moisture removal) were recorded and standardized to ensure that the results accurately reflected actual field productivity.

4.2. Determination of Small Organic Compounds, Enzyme Activity, and SOD and POD Activity

All biochemical assays were performed with five biological replicates and three technical replicates. Fresh leaf tissue (500 mg) was homogenized in respective extraction buffers for each assay.

LOX activity was measured by spectrometry according to the method of Zhang et al. [42]. 0.5 g of fresh sample was homogenized in ice-cold 50 mM sodium phosphate buffer (pH 6.5), centrifuged (12,000× *g*, 15 min, 4 °C). The supernatant was incubated with linoleic acid as the substrate, and the absorbance change at 234 nm was measured. GSH content was determined according to the method of Griffith [43]. The tissue was homogenized in 5% perchloric acid, centrifuged, and the supernatant was reacted with 5,5′-dithiobis (2-nitrobenzoic acid) (DTNB). The absorbance was measured at 412 nm, and the reduced glutathione (GSH) content was calculated. ROS level was assessed by measuring H_2O_2 content according to the method of Velikova et al. [44]. Antioxidant enzyme activities were measured as follows: Superoxide dismutase (SOD) activity at 560 nm based on nitroblue tetrazolium photoreduction inhibition [45]; Peroxidase (POD) activity at 470 nm using guaiacol-H_2O_2 system [46]; Catalase (CAT) activity at 240 nm by monitoring H_2O_2 decomposition [47]. All spectrophotometric measurements were conducted using a SmartSpec™ Plus spectrophotometer (Bio-Rad, Hercules, CA, USA).

4.3. RNA Extraction and Sequencing

Total RNA was extracted from the collected Jijing 129 rice tissue samples using a plant total RNA extraction kit (Qiagen RNeasy Kit, Suzhou, China). To ensure the reliability of subsequent experiments, we used previously reported RNA extraction and cDNA library construction methods and analyzed RNA quality by agarose gel electrophoresis [48]. Three biological replicates were used for each sample. The RNA samples that passed quality control were sequenced on a high-throughput sequencing platform (Illumina HiSeq 2000, San Diego, CA, USA). After sequencing, we removed the adapter sequence, poly(A) tail, and low-quality reads, yielding more than 4 GB of clean data with a 150 bp read length per sample. The Q20 and Q30 values for the sequencing data were both greater than 92%, indicating high data quality and suitability for subsequent analysis (Table S2). To further analyze the sequencing data, we used HISAT2 (version 2.2.1) to align the quality-controlled reads to the reference genome and performed statistical analysis of the alignment results using RSeQC (version 5.0.1) [49]. It establishes a sequence index containing more than 90% of the introns of known genes for short-fragment splicing reads and uses hierarchical indexing and multiple alignment strategies to address alignment issues for these reads. It has high alignment accuracy and fast running speed.

4.4. Identification and Enrichment Analysis of Differentially Expressed Genes

In this study, we systematically conducted selection and enrichment analyses of DEGs. The R package DESeq2 (version 1.42.0) was used for differential expression analysis. The criteria for selecting differentially expressed genes (DEGs) were MAX normalized counts > 30 (one of which was sufficient), $|\log2(\text{FoldChange})| > 1$, and p-value < 0.05 (Table S10). In terms of enrichment analysis, we determined the main biological functions of differentially expressed genes through GO functional significance enrichment analysis, in which the selection condition for significantly enriched GO terms was the corrected FDR value < 0.05. Similarly, the hypergeometric test was applied to each pathway in the Kyoto Encyclopedia of Genes and Genomes for enrichment analysis, and a corrected FDR < 0.05 was used as the threshold to identify significantly enriched metabolic pathways among the differentially expressed genes. These analyses helped us determine the biological functions of differentially expressed genes and the metabolic pathways they mainly affected, providing a basis for subsequent functional studies. In addition, we used the microbial bioinformatics platform (https://www.bioinformatics.com.cn/, accessed on 2 May 2025), TBTools (version 2.056), and RStudio (version 2024.04.0) to generate heat maps from experimental data for visualization. GO enrichment was analyzed using the online agriGOv2 platform (http://systemsbiology.cau.edu.cn/agriGOv2/index.php, accessed on 10 May 2025), and KEGG graph drawing was performed on the KEGG catalog website (http://www.genome.ad.jp/kegg/kegg2.html, accessed on 10 May 2025).

4.5. qRT-PCR Validation

To verify the reliability of RNA sequencing data, six DEGs were randomly selected for qRT-PCR analysis. The total RNA extraction method was as described above, and about 2 μg of total RNA was used to synthesize first-strand cDNA using gene-specific primers. The primer design was based on our previous study and obtained from the qPCR primer database (https://biodb.swu.edu.cn/qprimerdb/, accessed on 12 May 2025). The total volume of the qRT-PCR reaction system was 20 μL, using the Top Green qPCR SuperMix kit (Beijing Quanshijin Biotechnology Co., Ltd., Beijing, China), which included 10 μL of 2× TransStart® Top Green qPCR SuperMix. Each sample was set up with three technical replicates and three biological replicates, and expression levels were normalized to the reference gene GADPH. The qRT-PCR results are shown in Figure S2. The primers are listed in Table S10. The results showed that qRT-PCR data were highly consistent with transcriptomic data, demonstrating the reliability of the latter.

4.6. Statistical Analysis

In this study, statistical data analysis and heat maps were generated based on correlation values or gene expression levels. Other physiological data were analyzed using one-way analysis of variance (ANOVA). Data are presented as the mean ± SE (standard error) of three, five or ten biological replicates. Data visualization was performed in GraphPad Prism version 9.0 (GraphPad Software, San Diego, CA, USA) or Microsoft Office Excel, with * $p < 0.05$ and ** $p < 0.01$ as significant.

5. Conclusions

This study investigated Jijing 129 rice by setting up three laser supplemental lighting treatments with different red-to-blue light ratios against a natural light control. It systematically compared the effects on morphological and physiological indicators, gene expression during the seedling stage, and yield at maturity, aiming to explore the potential mechanisms for yield enhancement.

The results demonstrated that, compared to natural light, the laser supplemental lighting treatments significantly promoted root growth, increased plant nitrogen content in seedlings, and ultimately led to an effective increase in yield at maturity. Notably, among all treatments, the CL (red-to-blue ratio 60:40) treatment exhibited the most significant yield-enhancing effect, indicating that different red-to-blue light ratios have a significant impact on the yield of jijing129 rice.

To further elucidate the underlying molecular mechanisms, we performed a differential gene expression analysis. The results revealed that laser treatment induced expression changes in several key genes involved in nitrogen metabolism, photosynthesis, and redox pathways (e.g., *OsNR1* and *OsNR2*). Importantly, the gene expression profiles induced by different red-to-blue light ratios were markedly different, suggesting that they may regulate rice growth and development through distinct molecular pathways.

The obtained data, together with the identified candidate genes and key pathways, provide an important theoretical basis and practical reference for further elucidating the molecular mechanisms of laser supplemental lighting and for carrying out precise light-environment regulation and variety improvement.

Supplementary Materials: The following supporting information can be downloaded at: https://www.mdpi.com/article/10.3390/plants14243712/s1, Figure S1: GO (a) and KEGG (b) enrichment analysis of rice down-regulated DEGs in response to laser irradiation. The abbreviations BL, CL, and DL refer to the treatment groups BL (R50:B50; 150:150 μmol m^{-2} s^{-1}), CL (R60:B40; 180:120 μmol m^{-2} s^{-1}), and DL (R75:B25; 225:75 μmol m^{-2} s^{-1}), while AL represents the control under natural light conditions; Figure S2: qRT-PCR validation of transcriptome reliability. Bars: qPCR data; Lines: Transcriptome data. The abbreviations BL, CL, and DL refer to the treatment groups BL (R50:B50; 150:150 μmol m^{-2} s^{-1}), CL (R60:B40; 180:120 μmol m^{-2} s^{-1}), and DL (R75:B25; 225:75 μmol m^{-2} s^{-1}), while AL represents the control under natural light conditions. Table S1: Yield assessment of rice cultivar Jijing129 under laser supplemental lighting with different red:blue ratios. Three red-to-blue light ratios were tested: BL (RED: BLUE = 50:50; 150:150 μmol·m^{-2}·s^{-1}), CL (RED: BLUE = 60:40; 180:120 μmol·m^{-2}·s^{-1}), and DL (RED: BLUE = 75:25; 225:75 μmol·m^{-2}·s^{-1}). Data are means ± SE ($n \geq 4$). Means with different letters are significantly different ($p < 0.05$) within the same treatments. Asterisks (*) indicate significant differences between control and treatments of the same genotype which were determined by Student's *t*-test (* $p < 0.05$); Table S2:The overview of RNA-seq data; Table S3: Upregulated results of GO analysis; Table S4: Upregulated results of KEGG analysis; Table S5: Downregulated results of GO analysis; Table S6: Downregulated results of KEGG analysis; Table S7: Expression analysis of nitrogen metabolism-related genes based on GO and KEGG; Table S8: Expression analysis of photosynthesis-related genes based on GO and KEGG; Table S9: Expression analysis of related genes LOX, GSH, ROS, CAT, SOD and POD; Table S10: DEGs data between different comparison groups; Table S11:List of primers used for qRT-PCR.

Author Contributions: Conceptualization, X.L. (Xuemei Liang) and Q.L.; methodology, Q.L., X.D. and X.L. (Xiaoyu Lei); software, J.W. and X.D.; visualization, C.Z.; validation, Q.L., X.D. and C.Z.; investigation, P.J. and W.Y.; formal analysis, Q.L. and M.Y.; resources, X.L. (Xuemei Liang), M.Y. and L.Q.; data curation, L.Q., W.Y. and X.D.; writing—original draft preparation, Q.L.; writing—review and editing, N.W., Q.L. and M.Y.; supervision, N.W. and X.L. (Xuemei Liang); project administration, P.J. and L.Q.; funding acquisition, M.Y. and X.D. All authors have read and agreed to the published version of the manuscript.

Funding: This study was funded by the Artificial Intelligence Light and Temperature Control Facility Fruit and Vegetable Yield Increase and Quality Technology (2025XT0808), Laser Light Supplementary Lamp Rice Seedling Cultivation Mechanism Research (20250601058RC), and Jilin Province Key Laboratory of Photoagriculture (YDZJ202502CXJD006).

Data Availability Statement: The datasets generated and analyzed in this study are available at PRJNA1297612 (http://www.ncbi.nlm.nih.gov/bioproject/1297612, accessed on 28 July 2025).

Conflicts of Interest: The authors declare no conflicts of interest.

References

1. Qi, Y.; Lei, Y.; Ahmed, T.; Cheng, F.; Lei, K.; Yang, H.; Ali, H.M.; Li, Z.; Qi, X. Low-intensity laser exposure enhances rice (*Oryza sativa* L.) growth through physio-biochemical regulation, transcriptional modulation, and microbiome alteration. *BMC Plant Biol.* **2025**, *25*, 698. [CrossRef]
2. Ooi, A.; Wong, A.; Ng, T.K.; Marondedze, C.; Gehring, C.; Ooi, B.S. Growth and development of *Arabidopsis thaliana* under single-wavelength red and blue laser light. *Sci. Rep.* **2016**, *6*, 33885. [CrossRef]
3. Demmig-Adams, B.; Polutchko, S.K.; Stewart, J.J.; Adams, W.W., III. History of excess-light exposure modulates the extent and kinetics of fast-acting non-photochemical energy dissipation. *Plant Physiol. Rep.* **2022**, *27*, 560–572. [CrossRef]
4. Hernandez, A.C.; Dominguez, P.A.; Cruz, O.A.; Ivanov, R.; Carballo, C.A.; Zepeda, B.R. Laser in agriculture. *Int. Agrophys.* **2010**, *24*, 407–422.
5. Nadimi, M.; Sun, D.W.; Paliwal, J. Recent applications of novel laser techniques for enhancing agricultural production. *Laser Phys.* **2021**, *31*, 053001. [CrossRef]
6. Abu-Elsaoud, A.M.; Tuleukhanov, S.T. Can He-Ne laser induce changes in oxidative stress and antioxidant activities of wheat cultivars from Kazakhstan and Egypt. *Sci. Int.* **2013**, *1*, 39–50. [CrossRef]
7. Spampinato, C.; Valastro, S.; Calogero, G.; Smecca, E.; Mannino, G.; Arena, V.; Balestrini, R.; Sillo, F.; Ciná, L.; La Magna, A.; et al. Improved radicchio seedling growth under CsPbI3 perovskite rooftop in a laboratory-scale greenhouse for Agrivoltaics application. *Nat. Commun.* **2025**, *16*, 2190. [CrossRef]
8. Liscum, E.; Hodgson, D.W.; Campbell, T.J. Blue light signaling through the cryptochromes and phototropins. So that's what the blues is all about. *Plant Physiol.* **2003**, *133*, 1429–1436. [CrossRef] [PubMed]
9. Christie, J.M. Phototropin blue-light receptors. *Annu. Rev. Plant Biol.* **2007**, *58*, 21–45. [CrossRef]
10. Ren, M.; Liu, S.; Tang, C.; Mao, G.; Gai, P.; Guo, X.; Zheng, H.; Tang, Q. Photomorphogenesis and photosynthetic traits changes in rice seedlings responding to red and blue light. *Int. J. Mol. Sci.* **2023**, *24*, 11333. [CrossRef] [PubMed]
11. Ren, M.; Liu, S.; Mao, G.; Tang, C.; Gai, P.; Guo, X.; Zheng, H.; Wang, W.; Tang, Q. Simultaneous application of red and blue light regulate carbon and nitrogen metabolism, induces antioxidant defense system and promote growth in rice seedlings under low light stress. *Int. J. Mol. Sci.* **2023**, *24*, 10706. [CrossRef]
12. Rintamäki, E.; Salo, R.; Lehtonen, E.; Aro, E.M. Regulation of D1-protein degradation during photoinhibition of photosystem II in vivo: Phosphorylation of the D1 protein in various plant groups. *Planta* **1995**, *195*, 379–386. [CrossRef]
13. Wang, F.; Sun, H.; Rong, L.; Li, Z.; An, T.; Hu, W.; Ye, Z. Genotypic-dependent alternation in D1 protein turnover and PSII repair cycle in psf mutant rice (*Oryza sativa* L.), as well as its relation to light-induced leaf senescence. *Plant Growth Regul.* **2021**, *95*, 121–136. [CrossRef]
14. Edelman, M.; Mattoo, A.K. D1-protein dynamics in photosystem II: The lingering enigma. *Photosynth. Res.* **2008**, *98*, 609–620. [CrossRef] [PubMed]
15. Sassi, M.; Ruberti, I.; Vernoux, T.; Xu, J. Shedding light on auxin movement: Light-regulation of polar auxin transport in the photocontrol of plant development. *Plant Signal. Behav.* **2013**, *8*, e23355. [CrossRef]
16. Zažímalová, E.; Křeček, P.; Skůpa, P.; Hoyerová, K.; Petrášek, J. Polar transport of the plant hormone auxin–the role of PIN-FORMED (PIN) proteins. *Cell. Mol. Life Sci.* **2007**, *64*, 1621–1637. [CrossRef]
17. Wang, Z.; Luo, H.; Liu, B.; Song, S.; Zhang, X.; Song, Y.; Liu, B. Response of Morphological Plasticity of Quercus variabilis Seedlings to Different Light Quality. *Forests* **2024**, *15*, 2153. [CrossRef]
18. Farrokhzad, Y.; Babaei, A.; Yadollahi, A.; Kashkooli, A.B.; Mokhtassi-Bidgoli, A.; Hesami, S. In vitro photomorphogenesis, plant growth regulators, melatonin content, and DNA methylation under various wavelengths of light in *Phalaenopsis amabilis*. *Plant Cell Tissue Organ Cult. (PCTOC)* **2022**, *149*, 535–548. [CrossRef]
19. Li, D.; Nanseki, T.; Chomei, Y.; Kuang, J. A review of smart agriculture and production practices in Japanese large-scale rice farming. *J. Sci. Food Agric.* **2023**, *103*, 1609–1620. [CrossRef]
20. Lin, Q.; Ouyang, Q.; Huang, S. The application of big data technology in the study of rice variety adaptability: Current status, challenges, and prospects. *Resour. Data J.* **2025**, *4*, 126–140.
21. Ji, H.; Xiao, R.; Lyu, X.; Chen, J.; Zhang, X.; Wang, Z.; Deng, Z.; Wang, Y.; Wang, H.; Li, R.; et al. Differential light-dependent regulation of soybean nodulation by papilionoid-specific HY5 homologs. *Curr. Biol.* **2022**, *32*, 783–795. [CrossRef]
22. Xu, P.; Wang, E. Diversity and regulation of symbiotic nitrogen fixation in plants. *Curr. Biol.* **2023**, *33*, R543–R559. [CrossRef] [PubMed]

23. Gai, S.; Su, L.; Tang, C.; Xia, M.; Zhou, Z. The antagonistic effects of red and blue light radiation on leaf and stem development of pepper (*Capsicum annuum* L.) seedlings. *Plant Sci.* **2025**, *351*, 112338. [CrossRef] [PubMed]
24. Li, L.; Wonder, J.; Helming, T.; van Asselt, G.; Pantazopoulou, C.K.; van de Kaa, Y.; Kohlen, W.; Pierik, R.; Kajala, K. Brassinosteroid and gibberellin signaling are required for Tomato internode elongation in response to low red: Far-red light. *bioRxiv* **2024**. [CrossRef]
25. Xu, Y.; You, C.; Xu, C.; Zhang, C.; Hu, X.; Li, X.; Ma, H.; Gong, J.; Sun, X. Red and blue light promote tomato fruit coloration through modulation of hormone homeostasis and pigment accumulation. *Postharvest Biol. Technol.* **2024**, *207*, 112588. [CrossRef]
26. Li, Y.; Liu, C.; Shi, Q.; Yang, F.; Wei, M. Mixed red and blue light promotes ripening and improves quality of tomato fruit by influencing melatonin content. *Environ. Exp. Bot.* **2021**, *185*, 104407. [CrossRef]
27. Ferreyra, M.L.F.; Serra, P.; Casati, P. Recent advances on the roles of flavonoids as plant protective molecules after UV and high light exposure. *Physiol. Plant.* **2021**, *173*, 736–749. [CrossRef]
28. Zhang, Q.; Yang, W.; Liu, J.; Liu, H.; Lv, Z.; Zhang, C.; Chen, D.; Jiao, Z. Postharvest UV-C irradiation increased the flavonoids and anthocyanins accumulation, phenylpropanoid pathway gene expression, and antioxidant activity in sweet cherries (Prunus avium L.). *Postharvest Biol. Technol.* **2021**, *175*, 111490. [CrossRef]
29. Liang, Y.; Dong, Y.; Yang, Q.; Urano, D.; Wang, Z. Interactive effects of light quality and nitrate supply on growth and metabolic processes in two lettuce cultivars (*Lactuca sativa* L.). *Environ. Exp. Bot.* **2023**, *213*, 105443. [CrossRef]
30. Trivellini, A.; Toscano, S.; Romano, D.; Ferrante, A. The role of blue and red light in the orchestration of secondary metabolites, nutrient transport and plant quality. *Plants* **2023**, *12*, 2026. [CrossRef]
31. Fan, X.-x.; Bian, Z.-h.; Song, B.; Xu, H. Transcriptome analysis reveals the differential regulatory effects of red and blue light on nitrate metabolism in pakchoi (*Brassica campestris* L.). *J. Integr. Agric.* **2022**, *21*, 1015–1027. [CrossRef]
32. Hooks, T.; Masabni, J.; Sun, L.; Niu, G. Effect of pre-harvest supplemental UV-A/Blue and Red/Blue LED lighting on lettuce growth and nutritional quality. *Horticulturae* **2021**, *7*, 80. [CrossRef]
33. Swathy, P.S.; Kiran, K.R.; Joshi, M.B.; Mahato, K.K.; Muthusamy, A. He–Ne laser accelerates seed germination by modulating growth hormones and reprogramming metabolism in brinjal. *Sci. Rep.* **2021**, *11*, 7948. [CrossRef]
34. Shi, L.X.; Schröder, W.P. The low molecular mass subunits of the photosynthetic supracomplex, photosystem II. *Biochim. Biophys. Acta (BBA)-Bioenerg.* **2004**, *1608*, 75–96. [CrossRef]
35. Boyer, P.D. The ATP synthase—A splendid molecular machine. *Annu. Rev. Biochem.* **1997**, *66*, 717–749. [CrossRef] [PubMed]
36. Barber, J. Photosystem II: The engine of life. *Q. Rev. Biophys.* **2003**, *36*, 71–89. [CrossRef] [PubMed]
37. Hanke, G.U.Y.; Mulo, P. Plant type ferredoxins and ferredoxin-dependent metabolism. *Plant Cell Environ.* **2013**, *36*, 1071–1084. [CrossRef] [PubMed]
38. Wan, X.; Wang, Y.; Liang, X.; Yu, H.; Zhou, L.; Qi, X.; Yang, X.; Zhang, X.; Liu, Y.; Song, Y.; et al. Applications and Research Progress of Laser Technology in Agricultural Breeding. *J. Jilin Agric. Univ.* **2025**, *47*, 567–580. [CrossRef]
39. Okla, M.K.; Abdel-Mawgoud, M.; Alamri, S.A.; Abbas, Z.K.; Al-Qahtani, W.H.; Al-Qahtani, S.M.; Al-Harbi, N.A.; Hassan, A.H.A.; Selim, S.; Alruhaili, M.H.; et al. Developmental stages-specific response of Anise plants to laser-induced growth, nutrients accumulation, and essential oil metabolism. *Plants* **2021**, *10*, 2591. [CrossRef]
40. Zrig, A.; Najar, B.; Magdy Korany, S.; Hassan, A.H.; Alsherif, E.A.; Ali Shah, A.; Fahad, S.; Selim, S.; AbdElgawad, H. The interaction effect of laser irradiation and 6-Benzylaminopurine improves the chemical composition and biological activities of Linseed (*Linum usitatissimum*) sprouts. *Biology* **2022**, *11*, 1398. [CrossRef]
41. Zheng, J.; Wu, H.; Zhao, M.; Yang, Z.; Zhou, Z.; Guo, Y.; Lin, Y.; Chen, H. OsMYB3 is a R2R3-MYB gene responsible for anthocyanin biosynthesis in black rice. *Mol. Breed.* **2021**, *41*, 51. [CrossRef] [PubMed]
42. Zhang, X.; Zhang, L.; Dong, F.; Gao, J.; Galbraith, D.W.; Song, C.P. Hydrogen peroxide is involved in abscisic acid-induced stomatal closure in *Vicia faba*. *Plant Physiol.* **2001**, *126*, 1438–1448. [CrossRef] [PubMed]
43. Griffith, O.W. Determination of glutathione and glutathione disulfide using glutathione reductase and 2-vinylpyridine. *Anal Biochem.* **1980**, *106*, 207–212. [CrossRef]
44. Velikova, V.; Yordanov, I.; Edreva, A. Oxidative stress and some antioxidant systems in acid rain-treated bean plants: Protective role of exogenous polyamines. *Plant Sci.* **2000**, *151*, 59–66. [CrossRef]
45. Beauchamp, C.; Fridovich, I. Superoxide dismutase: Improved assays and an assay applicable to acrylamide gels. *Anal. Biochem.* **1971**, *44*, 276–287. [CrossRef]
46. Chance, B.; Maehly, A.C. [136] Assay of catalases and peroxidases. *Methods Enzymol.* **1955**, *2*, 764–775.
47. Aebi, H. [13] Catalase in vitro. In *Methods in Enzymology*; Academic Press: Cambridge, MA, USA, 1984; Volume 105, pp. 121–126.

48. Ramalho, A.S.; Beck, S.; Farinha, C.M.; Clarke, L.A.; Heda, G.D.; Steiner, B.; Sanz, J.; Gallati, S.; Amaral, M.D.; Harris, A.; et al. Methods for RNA extraction, cDNA preparation and analysis of CFTR transcripts. *J. Cyst. Fibros.* **2004**, *3*, 11–15. [CrossRef]
49. Krishnan, K.; Yigit, E.; Karaca, M.; Rodriguez, D.; Langhorst, B.; Shtatland, T.; Munafo, D.; Liu, P.; Apone, L.; Panchapakesa, V.; et al. Low-input transcript profiling with enhanced sensitivity using a highly efficient, low-bias and strand-specific RNA-Seq library preparation method. *Cancer Res.* **2017**, *77* (Suppl. S13), 5406. [CrossRef]

Disclaimer/Publisher's Note: The statements, opinions and data contained in all publications are solely those of the individual author(s) and contributor(s) and not of MDPI and/or the editor(s). MDPI and/or the editor(s) disclaim responsibility for any injury to people or property resulting from any ideas, methods, instructions or products referred to in the content.

plants

MDPI

Article

Chromatin-Associated Pea Apyrase psNTP9 Function as a DNA-Binding Regulatory Protein in Yeast and Arabidopsis

Huan Wang [1], Robert D. Slocum [2,*], Xingbo Cai [1], Greg Clark [1] and Stanley J. Roux [1]

[1] Department of Molecular Biosciences, The University of Texas at Austin, Austin, TX 78712, USA; huanwang2020@utexas.edu (H.W.); caixingbo2018@utexas.edu (X.C.); gbclark@utexas.edu (G.C.); sroux@austin.utexas.edu (S.J.R.)
[2] Department of Biological Sciences, Goucher College, Towson, MD 21204, USA
* Correspondence: robert.slocum@goucher.edu

Abstract

As reported in earlier work, when a pea apyrase, psNTP9 (PS), and a modified version of it, psNTP9-DM (DM), are expressed in *Saccharomyces cerevisiae*, they localize to nuclei, binding to largely non-overlapping promoter regions of chromatin. PS- and DM-expressing yeast also exhibit different expression profiles for potentially regulated target genes, consistent with observed phenotypes. In the present study, we use ChIP-seq assays to show that PS and DM also associate with largely different promoter regions of Arabidopsis genes, with similar non-overlapping expression profiles for potential target genes. Functional studies, using electrophoretic mobility shift assays (EMSA), verified PS-specific binding to yeast or plant promoter binding sites. DM binding to both heterologous dsDNA and to PS-specific binding site sequences was minimal. AlphaFold3 modeling of PS protein binding to a yeast *PHM6* promoter sequence identified potential DNA-binding residues and a potential binding site motif (5′-(G/T)GG(G/T)A-3′) that is also present in two Arabidopsis promoter binding sites. These novel findings extend the previously known functions of PS and other plant apyrases in the Golgi or extracellular matrix, and support their potential function as DNA-binding proteins that can regulate gene expression in both yeast and Arabidopsis.

Keywords: NTPDase; ChIP-seq; DNA-binding; Arabidopsis; apyrase; psNTP9-DM; *PHM6*

1. Introduction

Apyrases (NTPDases; EC 3.6.1.5) hydrolyze NTP and NDP, removing their terminal phosphates. In animals, an important function of apyrases is the hydrolysis of extracellular ATP (eATP), thus modulating a wide range of physiological processes [1]. In plants, regulation of [eATP] by "ecto-apyrase" activities is also important in diverse growth and developmental processes [2–4]. In Arabidopsis, *AtAPY1* expression promotes auxin transport [5], enhances pollen tube growth [6], and regulates stomatal aperture [7] and abiotic stress responses [3]. Another important function of plant apyrases is maintaining the NDP/NMP balance in the Golgi, which is essential for efficient protein glycosylation [8], and apyrase activities in secretory vesicles may help regulate [eATP] in the extracellular matrix [4].

Plant apyrases have also been reported in nuclei [9,10], although their function in this organelle is largely unexplored. In etiolated seedlings, psNTP9 ("PS"), the pea ortholog of *AtAPY1*, was isolated from nuclei [9]. Ectopic expression of *psNTP9* resulted in an enhanced root system architecture, a drought-tolerance phenotype, and increased seed

yields in both Arabidopsis and soybean [11,12]. Constitutive expression of *psNTP9* also increased phosphate contents of yeast, Arabidopsis seedlings, and "hairy root" cultures of corn, soybean, and canola [13,14]. Given the potential importance of these phenotypes for the development of drought-tolerant crops with improved P utilization efficiency, we have been further investigating the mechanisms by which PS regulates plant growth, with a focus on its nuclear functions.

Both PS and AtAPY1 are regulated by calmodulin (CaM) [15,16], and one of two potential CaM-binding sites on PS (PCBS2) was functionally characterized [15]. We introduced two mutations into the second potential CaM-binding site (PCBS1) in PS in an attempt to engineer enhanced CaM-binding to the enzyme, which is designated as the "double mutation" ("DM") version of PS [14]. The PCBS1 sequence overlaps a predicted nuclear localization signal [17], suggesting that CaM binding to that site might regulate targeting of PS to the nucleus. Introduction of these mutations into PCBS1 might also influence nuclear targeting directly, absent CaM binding, or could alter the NTPDase activities of PS. Thus, the DM variant offered a tool to further investigate PS functions.

In a recent study, we generated transgenic lines ectopically expressing *PS* or *DM* in both yeast and Arabidopsis [14]. Purified DM from yeast did not exhibit increased CaM binding or significantly different NTPDase activities, compared with PS. Although PS and DM were both co-purified with nuclei and known chromatin-associated proteins, the amount of DM protein was lower than that of PS. Overexpression of either PS or DM produced significantly different gene expression profiles in both yeast and Arabidopsis, which helped explain the phenotypic effects of PS and DM on growth and phosphate uptake in both organisms. It also raised the question of whether PS and DM proteins have different chromatin binding sites. In yeast, ChIP-seq assays confirmed PS- and DM-specific binding in the promoters of many differentially expressed genes (DEG), suggesting that PS and DM might be functioning in transcriptional regulation. Enriched motifs for known transcription factors (TF) in these binding sites, and sets of potentially regulated target genes, were largely non-overlapping [14].

What remained unresolved was whether PS and DM also had distinct binding sites in Arabidopsis chromatin, and whether they differed in their ability to bind to specific promoter sequences in both yeast and Arabidopsis, either directly or indirectly, through interactions with other DNA-binding proteins. A favored approach to resolving the latter question is the electrophoretic mobility shift assay (EMSA). In this report, we used ChIP-seq assays to identify PS and DM binding sites in the promoters of Arabidopsis genes. Using EMSA, we functionally validated PS binding to promoter sequences for a yeast gene and two Arabidopsis genes that were differentially expressed in response to ectopic expression of *PS*. We further modeled potential DNA-binding sites using AlphaFold3 [18] to characterize possible interactions with enriched TF motifs in these sequences. The results support a potential role for PS and DM in transcriptional regulation of yeast and Arabidopsis genes and provide important new insights into apyrase functions.

2. Results

2.1. Targeting of PS to Plant Nuclei

Hsieh et al. [17] cloned the nuclear-localized pea NTPase (psNTP9) and reported that residues 209–232, which overlap with PCBD1, were a potential bipartite nuclear localization signal (NLS_BP), as is shown in Figure 1. Although this sequence does not fit the consensus Prosite motif PS50079 of (R/K)-(R/K)-(X_{10})-($\geq$3 of 5 = R/K residues) for NLS_BP, Kosugi et al. [19] reported that spacer sequence lengths between 10 and 16 residues did not significantly change function in plant NLS_BP. Kosugi et al. [19] also noted that basic and hydrophobic residues are rare at the center of plant NLS-BP spacer sequences;

thus, the P216R mutation introduced in the PCBD1-DM sequence and located in the center of the spacer sequence (green residues, Figure 1) may interfere with nuclear targeting. The approximately 2-fold lower amount of DM versus PS protein in purified Arabidopsis nuclei supports this possibility [14].

```
NLS_BP              209-KKTAKNAPKVADGDDPYIKKVVLK-232
PCBD1(PS)       205-YAVSKKTAKNAPKVA-219
PCBD1(DM)       205-YAVLKKTAKNARKVA-219
```

Figure 1. The bipartite nuclear localization signal (NLS_BP) overlaps with the putative calmodulin-binding domain 1 (PCBD1) in PS and DM proteins. The native PCBD1 sequence contains the S208L and P216R mutations in the DM protein (bold, underlined; [14]). The P216R mutation is located within the spacer region (green) of NLS_BP.

2.2. PS and DM Have Different Binding Affinities for Heterologous dsDNA

Purified preparations of yeast-expressed PS and DM were tested for their binding to a heterologous double-stranded DNA (dsDNA)-cellulose column and to a column of cellulose alone. PS and DM proteins were considered bound if they did not elute in the first wash (0.05 M NaCl). As judged by immunoblot analysis, at least 20% of the loaded PS bound to the dsDNA-cellulose (Figure 2). A small portion of the bound PS was eluted by 0.3 M NaCl, and significantly more of it was eluted by 0.6 M NaCl. Less than 2% of the loaded DM was bound to the dsDNA-cellulose. All of the bound DM was eluted by 0.6 M NaCl. This indicated that DM had a lower binding affinity to dsDNA cellulose. Neither PS nor DM protein bound to cellulose alone. Ovalbumin was used as a negative control and, as judged by Coomassie blue staining, more than 95% of the ovalbumin loaded onto the dsDNA column was either unbound or eluted in the low-salt (0.05 M NaCl) wash (Figure 2).

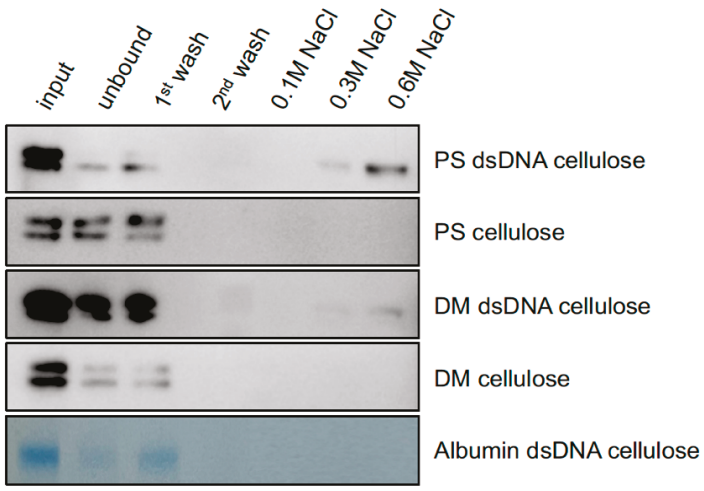

Figure 2. SDS-PAGE immunoblot analysis of the differential binding of PS and DM (4.8 µg loadings) to a dsDNA-cellulose column, and of their non-binding to a cellulose column as the negative control. PS and DM proteins were purified from yeast. Ovalbumin served as a negative protein control.

2.3. Identification of PS and DM Binding Sites in the Promoters of Arabidopsis Genes and Integration with Gene Expression Data

To investigate the genome-wide DNA-binding profiles of PS and DM proteins in *Arabidopsis thaliana*, we performed chromatin immunoprecipitation followed by high-throughput sequencing (ChIP-seq) using 7-day-old transgenic seedlings overexpressing 4Myc-tagged PS or DM proteins. High-confidence peaks were identified within 1–1500 bp upstream of transcription start sites (TSS) and filtered for genes that were differentially

expressed (DE) in corresponding RNA-seq datasets for PS or DM seedlings grown under identical conditions.

Among all identified binding sites, 16,667 were PS-specific, 23,207 sites were DM-specific, and 28,889 represented PS and DM sites that overlapped to varying degrees. Of the total 39,874 PS- or DM-specific binding sites, 13,560 sites (34%) were located in promoters of 12,392 potentially regulated target genes (Table S1). Venn analysis of their potential target genes (Figure S1) showed that only 1625 (13.1%) of these genes exhibited both PS and DM sites in their promoters, while the vast majority of genes contained either PS- or DM-binding sites.

Integration of ChIP-seq binding site and RNA-seq transcriptome datasets showed that approximately 4% of genes with PS- or DM-binding sites in their promoters were differentially expressed (DE) in PS- or DM-overexpressing seedlings, with a smaller number of binding sites being correlated with specific gene expression. For example, out of 213 genes with PS-binding sites in their promoters, only 140 (65.7%) were specifically expressed in PS seedlings, while 53 genes were DE only in DM seedlings, and 20 were DE in both PS and DM seedlings (Table S1). Similarly, only 67 out of 274 genes (24.4%%) with DM-specific binding sites in promoters were DE only in the DM seedlings, with the rest being DE in the PS seedlings or both PS and DM seedlings (Table S1).

2.4. Identification of Enriched Transcription Factor Binding Site Motifs in PS and DM Binding Sites of Arabidopsis Genes

We further characterized PS- and DM-binding sites using motif enrichment analysis performed using the MEME Suite v5.5.7 SEA tool against an Arabidopsis TF motif database. Among all high-confidence binding sites, 17 motifs in 10 different TF families were significantly enriched in PS-specific binding regions; 7 motifs in two TF families were enriched in DM-specific sites (Table 1). Dof TF motifs with an AAAG core sequence were found in 227 PS- and 34 DM-binding sites, making it the most abundant motif (Table 1). Motifs for the bZIP (ABI5) and MYB-related (MYBS1, SRM1) TF (Table 1), which regulate many genes involved in ABA synthesis and signaling [20,21], were statistically the most highly enriched motifs. Their over-representation only in DM-binding sites [14] suggests a potential role for DM in regulating ABA responses (Table S2).

Enriched motifs in PS binding sites are mostly for TF that regulate diverse developmental processes (Table 1). For example, LOB and JKD function in the specification of tissue and organ boundaries [22,23]. The enriched AATAATT motif for homeobox TF is found in 104 PS-binding sites in promoters of 41 unique genes. The promoter of TF HFR1, which regulates genes involved in phytochrome responses [24], has a perfectly conserved ATHB1/HAT5 motif, suggesting the possibility that PS binding might be involved in light-regulated development. GLABRA2 regulates epidermal cell identity [25] and ATHB53 regulates auxin/cytokinin signaling important for root development [26]. Interestingly, PS-binding sites in the promoters of 13 different genes were also enriched for SHN3 motifs. The SHN1-SHN3 TF clade activates genes involved in wax synthesis and cuticle formation in Arabidopsis [27]. A SHN3 motif is also found in the promoter of PER50, a secreted class III peroxidase that functions in H_2O_2 metabolism and lignification of the cell wall [28], processes which impact growth in Arabidopsis seedlings and are regulated, in part, by apyrase expression levels [29].

A list of PS-specific binding sites, enriched motifs, and expression profiles and annotation for potentially regulated target genes that were differentially expressed only in PS seedlings is provided in Table S3.

Table 1. Frequency of statistically enriched TF motifs in PS- or DM-specific binding sites within promoters of Arabidopsis genes. Motif enrichment analyses were carried out using the MEME 5.7.5 suite SEA tool with the DAP-seq database of 872 Arabidopsis transcription factor binding motifs (https://meme-suite.org/meme/tools/sea, accessed 12 November 2025).

Binding Site Specificity	TF Family (DAP Database)	TF Motif	TF Motif Consensus Sequence	Binding Sites with Motif	Percent Total Sites with a TF Motif	*p*-Value (FDR-Corrected)
PS	ABI3VP1	VRN1	VWKTTTTTTTTTTTTTTKB	35	15.56	2.67×10^{-4}
PS	AP2EREBP	SHN3	WCCDCCGCCRCCDCCGCCGCC	11	4.89	1.12×10^{-2}
PS	LOBAS2	LOB	WCCGCCGCCDYCKCCGCCGCH	22	9.78	4.06×10^{-3}
PS	C2H2	JKD, IDD10	WWWWTTTTTGTCKTTTTSTD	15	6.67	9.60×10^{-3}
PS	Homeobox	ATHB53	HCAATAATTGD	37	16.44	1.11×10^{-2}
PS		ATHB20, GL2	HYAATAATTRA	37	16.44	1.11×10^{-2}
PS		ATHB1, HAT5	HYAATAATTRW	30	13.33	1.13×10^{-2}
PS	BBRBPC	BPC1	CTCTYTCTCTCTCTC	66	29.33	7.38×10^{-3}
PS	C2H2	TF3A	CYTCCTCCTCCTCCTCCTC	26	11.56	5.66×10^{-3}
PS	ND	FRS9	CTCTCTCTCTCTCTCTCTCTC	24	10.67	3.50×10^{-3}
PS	WRKY	WRKY27	ANCGTTGACTTTT	26	11.56	1.47×10^{-3}
PS		WRKY7	DNCGTTGACTTTTT	32	14.22	3.30×10^{-3}
DM	bZIP	ABI5	DDTGRWSACGTGGCA	10	9.35	5.99×10^{-3}
DM	MYB related	MYBS1	HWWAWYCTTATCYWH	13	12.15	1.09×10^{-2}
DM		MYBS1	DWWDWRGATAAGRTT	10	9.35	5.99×10^{-3}
DM		SRM1	DWWDWRGATAAGR	10	9.35	5.99×10^{-3}
DM		SRM1	YCTTATCYWHW	11	10.28	5.01×10^{-4}
PS	C2C2dof	DOF1.1	TTTTYACTTTTTYTTTTTTTTTTTTTW	59	26.22	7.71×10^{-5}
PS		DOF1.5, COG1	RWAAAAADDAAAAAGTRAAAA	60	26.67	9.20×10^{-3}
PS		DOF1.7, Adof1	AAAAAVAAAAAGTARAAAAWR	22	9.78	1.86×10^{-3}
PS		DOF5.1	HWTTWACTTTTTBDHTTWW	30	13.33	1.13×10^{-2}
PS		DOF5.6, HCA2	RAAAAAADVAAAAAGKWAAWA	40	17.78	1.60×10^{-3}
DM		DOF3.2	KTWACTTTTTNNYTTTTTT	17	15.89	3.72×10^{-3}
DM		DOF5.8	TTTWTTTACTTTTTBYTTTTT	17	15.89	3.72×10^{-3}

2.5. Functional Characterization of PS and DM Binding Site Motifs in Yeast and Arabidopsis Genes Using EMSA

We adopted the following scheme for selecting PS binding sites for functional studies. We considered only high-confidence binding sites in promoters of genes that were DE only in PS-overexpressing yeast or Arabidopsis seedlings. We then performed sequence enrichment analyses to identify potential TF motifs in those binding sites. Since individual promoters often exhibit multiple binding sites, each of which may contain multiple TF motifs, we selected the binding site with the highest-scoring motif sequence (highest similarity to the motif consensus sequence) for any given DE gene. Further selection criteria included binding site lengths >200 bp and TF motif locations approximately centered within the binding site sequence, which is normally observed for ChIP-seq peaks [30]. A final consideration was given to possible roles for potential PS-regulated target genes in PS-specific phenotypes observed in yeast and Arabidopsis seedlings that overexpress *PS*. This approach led to the selection of a binding site in the yeast *PHM6* gene, identified in a previous study [14]. We also selected two additional sites in Arabidopsis *WRKY42* and *PER50* promoters identified in the present study for *in vitro* DNA-binding studies based on EMSA [31]. PS-specific induction of these genes in RNA-seq assays was validated by qRT-PCR (Table S4).

2.5.1. A PS Binding Site in the PHM6 Promoter Contains an E-Box Motif

Mapping of potential PS and DM binding sites in yeast shows that there is a PS binding site, but not a DM binding site, in the promoter region of *PHM6* (Figure S2). This binding site contains the CACGTG motif (E-box) for the yeast Pho4p transcription factor, which is a bHLH TF involved in regulating genes involved in phosphate metabolism in yeast (Austin and Mayer 2020; Yip et al. 2023) [32,33]. PHM6 (phosphate metabolism protein 6) is involved in phosphate transport and was recently suggested to function in concert with Pi transporters of the plasma membrane to increase Pi uptake in yeast under phosphate surplus conditions (Kulakovskaya et al. 2023) [34]. *PHM6* expression is induced in PS yeast but is not differentially expressed in DM yeast. This suggests that *PHM6* expression could be regulated by PS binding but not by DM binding to the promoter.

In order to validate yeast ChIP-seq data, we investigated whether PS could bind to a PS-specific binding site sequence in the *PHM6* promoter using a biotin-labeled PS binding site oligonucleotide EMSA. The assay identified two distinct bands with decreased mobilities in the PS sample (Figure 3, lane 2). Using twice as much PS protein (Figure 3, lane 3) produced a stronger binding signal and a weaker biotin-labeled *PHM6* signal. The addition of unlabeled *PHM6* competitor oligo decreased the amount of labeled oligo bound to PS (Figure 3, lane 4), supporting binding specificity. Mutated *PHM6* (no E-box motif), used as a negative control, did not produce these band shifts (Figure 3, lanes 5 and 6), and "pYES2 protein", which was purified from the pYES2 empty vector strain by the same method used to purify PS and DM, did not produce the PS-dependent band shift (Figure 3, lane 7). The purified DM protein also did not exhibit significant binding to the *PHM6* oligo (Figure 3, lane 8). Since the purity of PS and DM proteins used in these and other EMSA was only ~1%, the two PS-specific bands (Figure 3, lanes 2 and 3) may represent DNA binding by PS complexed with other proteins. Other low-mobility bands present at the top of each lane may represent DNA-binding by contaminating yeast proteins, such as those seen in the pYES2 control sample.

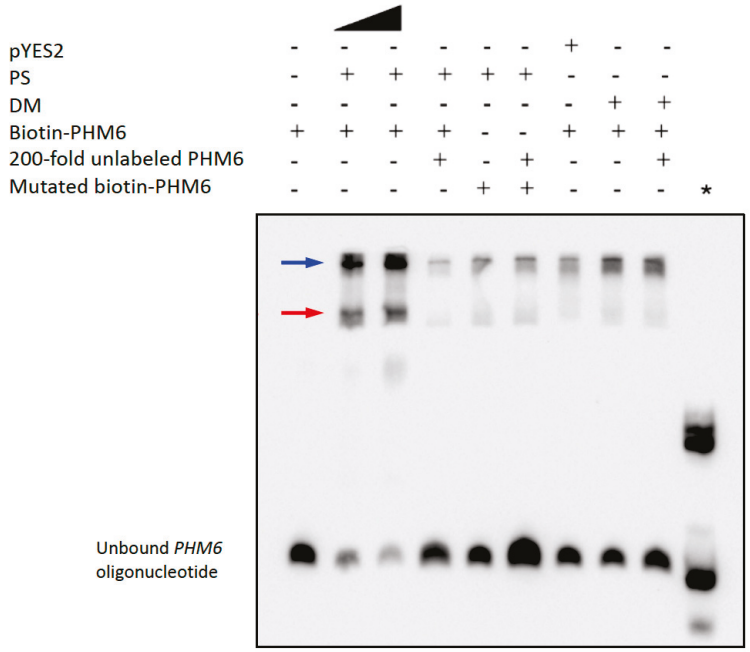

Figure 3. PS binds specifically to the yeast *PHM6* promoter. Sample constituents are indicated by (+). A total of 10 nmol of biotin-labeled probe was used in each lane, and a 200-fold excess amount of unlabeled *PHM6* duplex was used as the competitor. All assay tubes were incubated at room temperature for 20 min to allow for binding to occur. Protein extracted from the pYES2-expressing yeast was used as a negative control. Mutated *PHM6* oligo was also added to the reaction samples as a negative control. Samples were separated on a 6% polyacrylamide native gel. The black triangle represents a doubling of the amount of PS protein. The positive control (*) is Biotin-EBNA Control DNA with EBNA extract provided with the kit and used to validate the assay conditions. The red and blue arrows indicate reduced *PHM6* oligo mobilities resulting from different PS-specific binding interactions. Some low-mobility bands near the top of the gel represent non-specific *PHM6* binding by proteins in the pYES2 control, which are also present in the PS and DM samples. Their binding is not reduced by the excess competitor. The results shown in this figure are representative of two independent assays.

2.5.2. PS Binds to Arabidopsis WRKY42 and PER50 Promoter Sequences with Enriched TF Motifs

To test whether PS binds *WRKY42* and *PER50* promoter sequences, we conducted EMSA using biotin-labeled PS binding-site sequences centered around enriched TF motifs. As shown in Figure 4, the PS sample produced clear, concentration-dependent band shifts with the *WRKY42* oligo containing a DOF1.5 motif (Figure S3), whereas DM did not. The addition of excess unlabeled *WRKY42* decreased the amount of labeled oligo bound by PS, demonstrating binding specificity, and no shift was observed when using a mutated *WRKY42* probe. Similarly, PS, but not DM, caused a distinct shift in the *PER50* probe containing a SHN3 motif (Figure 5 and Figure S4). Again, binding was competitively inhibited by the excess unlabeled probe and was abolished with a mutated *PER50* sequence. Additional band shifts likely resulted from the interactions with other DNA-binding proteins in the samples, as previously noted for the *PHM6* assays.

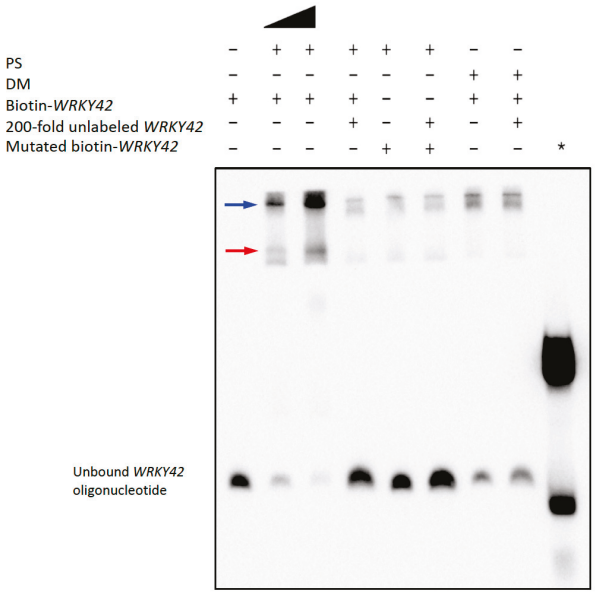

Figure 4. PS binds to the Arabidopsis *WRKY42* promoter. PS-dependent Arabidopsis *WRKY42* binding site shift was detected by EMSA. EMSA using biotin-labeled *WRKY42* DNA probes showed a PS concentration-dependent shift similar to yeast *PHM6* and Arabidopsis *PER50*, with no significant shift seen for DM. The black triangle represents a doubling of the amount of PS protein. The binding specificity was validated by competition with the excess unlabeled *WRKY42* probe and loss of binding with the mutated probe. The positive control (*) was Biotin-EBNA Control DNA with EBNA extract, which was used to validate the assay conditions. The red and blue arrows indicate reduced *WRKY42* oligo mobilities resulting from different PS-specific binding events. Some low-mobility bands near the top of the gel represent non-specific *WRKY42* binding, which is not decreased by the excess competitor. The results shown in this figure are representative of two independent assays.

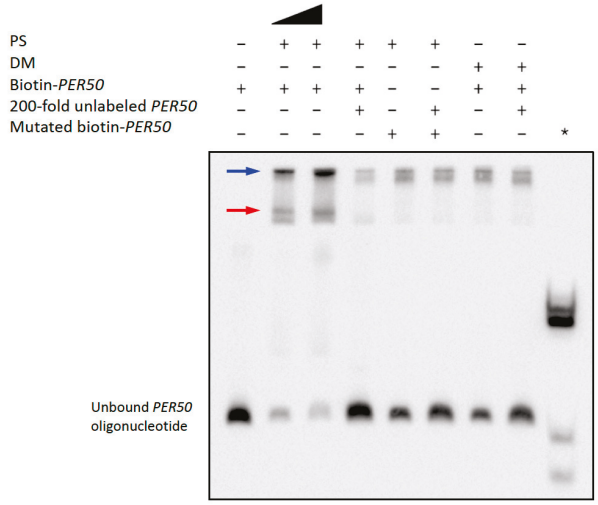

Figure 5. PS binds specifically to the Arabidopsis *PER50* promoter. The PS-dependent Arabidopsis *PER50* binding site shift was detected by EMSA. EMSA using biotin-labeled *PER50* DNA probes showed a PS concentration-dependent shift similar to yeast *PHM6* and Arabidopsis *WRKY42*, with no significant shift seen for DM. The black triangle represents a doubling of the amount of PS protein. The binding specificity was validated by competition with the excess unlabeled *PER50* probe and the loss of binding with the mutated probe. The positive control (*) was Biotin-EBNA Control DNA with EBNA extract, which was used to validate the assay conditions. The red and blue arrows indicate reduced *PER50* oligo mobilities resulting from different PS-specific binding events. Some low-mobility bands near the top of the gel represent non-specific *PER50* binding, which is not decreased by excess competitor. The results shown in this figure are representative of two independent assays.

2.6. Co-Immunoprecipitation Analyses of PS- and DM-Interacting Proteins in Yeast and Arabidopsis

We performed co-IP assays and mass-spec identification of Myc-tagged PS- and DM-interacting proteins from crude yeast extracts prepared using a protocol similar to that used for the partial purification of PS and DM proteins. Parallel co-IP experiments were run with Arabidopsis seedling extracts. Annotated chromatin proteins or TF that co-IP with PS or DM proteins are listed in Table S5. In both yeast and Arabidopsis, two nucleolin-like peptidyl-prolyl *cis*-trans isomerases and a third nucleolin NUCL1 co-IP with both PS and DM. Nucleolins bind a variety of proteins and RNAs and are involved in ribosome biogenesis. It is unclear whether the interacting yeast DNA repair protein MSC1 binds DNA directly. Interestingly, out of 87 plant and 38 yeast interacting partners in co-IP samples, only a single transcription factor, Scarecrow-like protein 30 (SCL30), was identified in seedling samples. SCL30 is in the GRAS TF family, which interacts with a wide variety of *cis*-elements in genes that regulate diverse growth and stress responses [35].

2.7. Structural Basis for Differences in DNA-Binding by PS and DM Proteins

We used AlphaFold3 [18] to model potential PS and DM binding to both test and mutant *PHM6* oligonucleotide sequences used in EMSA (Figure S6). Binding site interaction maps and supporting structure models are presented in Figure 6. These models support potential direct binding of PS to a '-TGGGA-3′ motif adjacent to (or overlapping with; see Figure 6 legend) the enriched CACGTG Pho4p motif in this promoter sequence (Figure 6A). PCBD1 residues K209, K210, and N214 facilitated sequence-specific interactions with major groove nucleobases. PS binding to the mutated oligo involved interactions between PCBD1 residues S208 and K210 and a 5′-TG-3′ sequence at the 3′-end of the *PHM6* oligo, stabilized by additional backbone interactions (Figure 6B). The altered PCBD1 structure seen in the DM protein (S208L, P216R mutations) resulted in its alignment with the minor groove and loss of nucleobase binding. DM residues K186 and K189 interacted with major groove nucleobases 5′-GGA-3′ adjacent to the CACGTG motif (Figure 6C). Compared with PS, DM protein also exhibited fewer stabilizing interactions with the DNA sugar-phosphate backbone, consistent with reduced *PHM6* oligo binding by the DM sample in the EMSA. *PHM6* binding by PS complexed with a single Ca^{2+}CaM molecule, which interacts with the N-terminal sequence and PCBD2 site, was also modeled (Figure 6D), although its binding was not investigated by EMSA. CaM binding to PS, like the DM mutations, aligned PCBD1 residue K210 with the minor groove, where it interacted with G34 within the CACGTG motif and its complementary nucleobase C33. Residue K186 interacted with C22 in the major groove, and PS/CaM binding was stabilized by additional major and minor groove backbone contacts. Additional modeling of PS binding to *WRKY42* and *PER50* sequences predicted "5-TGGTA-3′ and 5′-GGGGA-3′ recognition sequences, respectively, suggesting a 5′-(G/T)GG(G/T)A-3′ consensus sequence. A logo representation of their frequencies is shown in Figure S6.

(**A**)

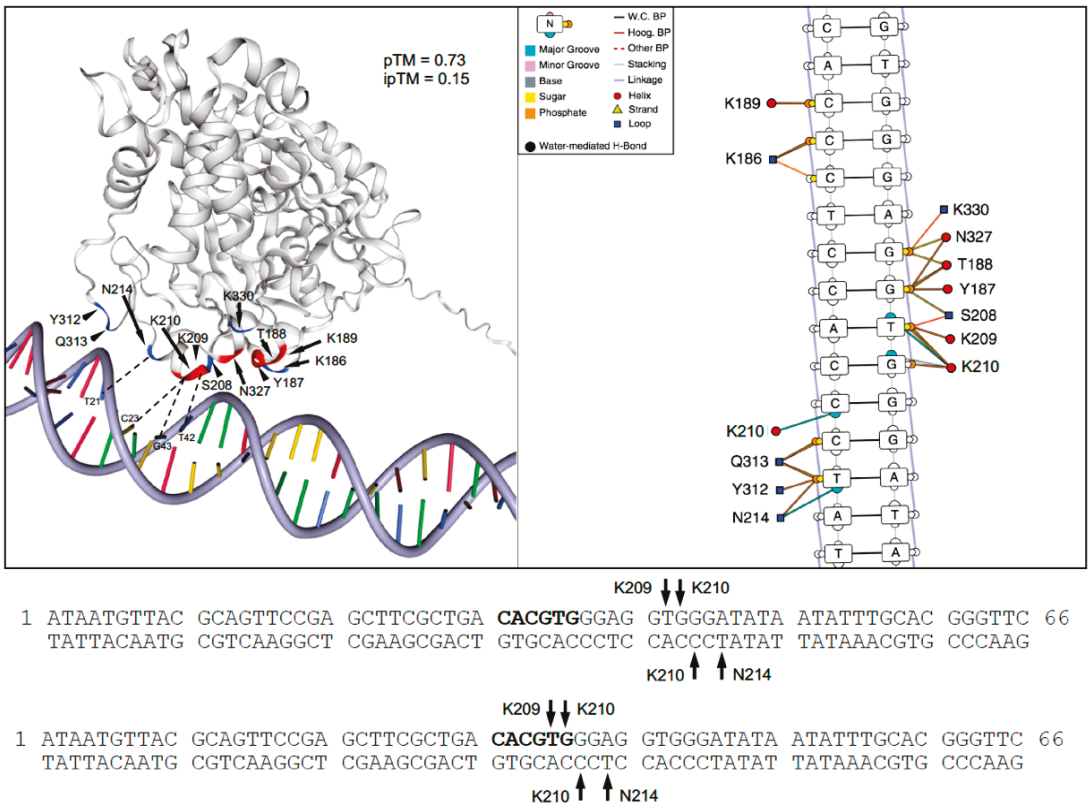

(**B**)

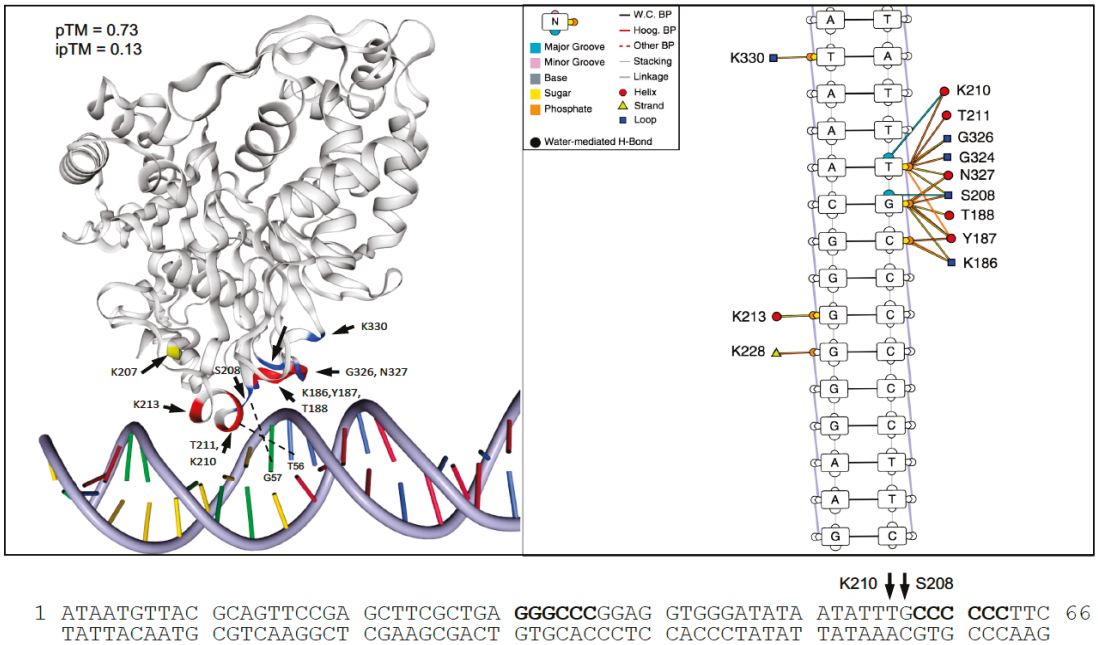

Figure 6. *Cont.*

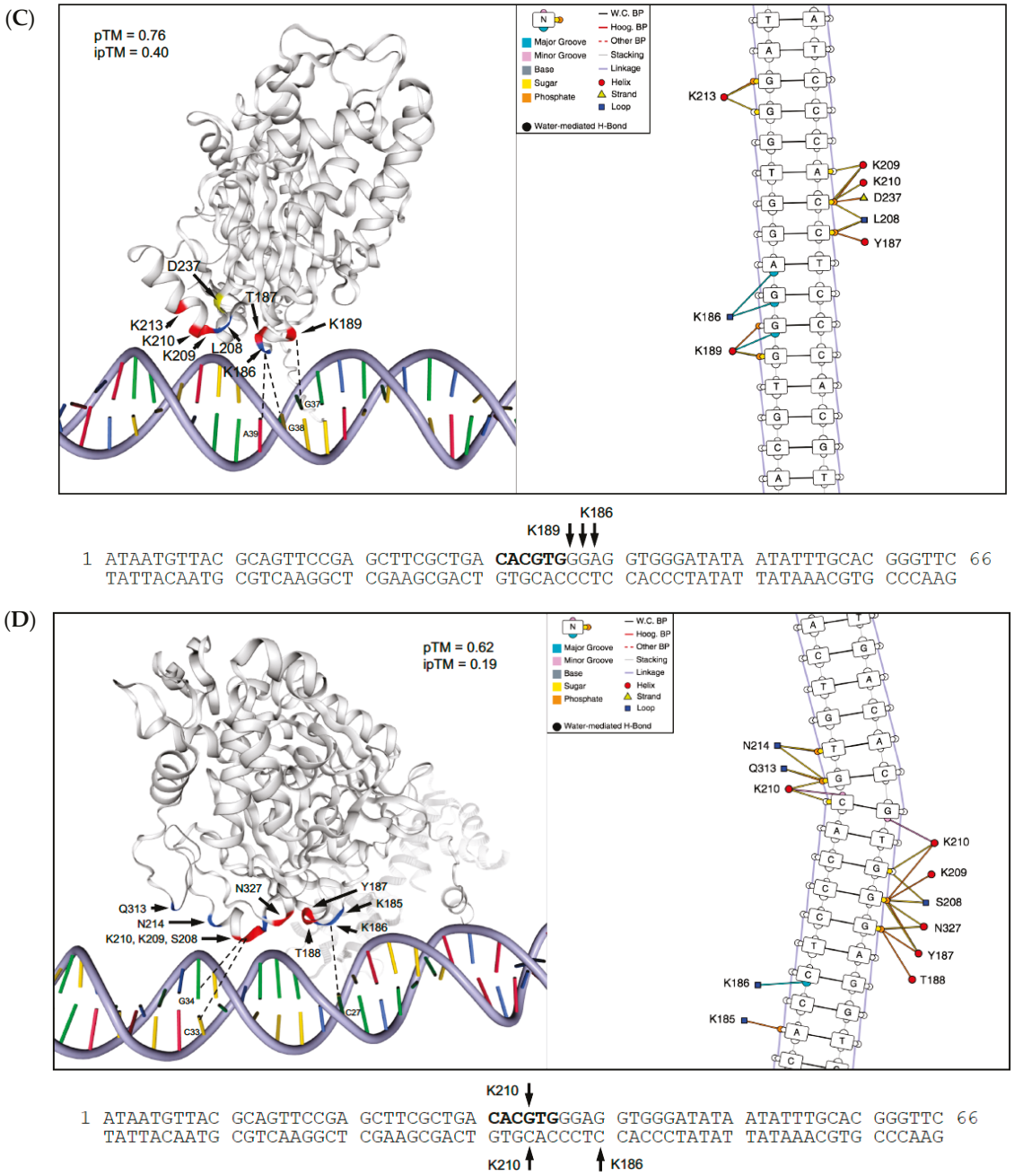

Figure 6. Modeling of mature PS and DM protein binding to *PHM6* oligonucleotide sequences using AlphaFold3 (AF3; [18]). Structures were then visualized, and binding site interaction maps were produced using DNAproDB (https://dnaprodb.usc.edu). For reference, sequence-specific binding is shown on the *PHM6* oligo sequence below the structure and interaction map. PS binding to the PHM6 test oligo is shown in (**A**). AF3 did not predict PS binding to an identical 5′-TGGGA-3′ sequence that overlaps with the CACGTG motif, as shown in the second oligo sequence map. Predicted PS binding to the mutated *PHM6* occurs near the 3′-end of the oligo (**B**). The S208L and P216R mutations in PCBD1 enhance its amphipathic α-helix character and alter DM binding to *PHM6*, decreasing interactions with nucleobases and the sugar-phosphate backbone adjacent to the CACGTG motif (**C**). In the presence of Ca^{2+}, Arabidopsis Calmodulin 1 associates with the N-terminal sequence and PCBD2 α-helix of the PS protein. As in the DM model, the PCBD1 helix aligns with the minor groove, where the interaction with nucleobases C33 and G34 within the CACGTG motif was stabilized by backbone interactions in the major groove (**D**). The overall predicted TM (pTM) and interface-predicted TM (ipTM) confidence values for each model are indicated. pTM values between 0.62 and 0.76 are >0.5 cutoff typical for high-confidence protein structure predictions. ipTM values ranging from 0.13 to 0.40 are all <0.6 cutoff for high-confidence interface predictions.

3. Discussion

Apyrases are located in different subcellular compartments, where they potentially regulate different cellular processes [4]. The pea apyrase PS has been localized in both the ECM [10,13] and in nuclei [9,10]. Its functions in the ECM likely include regulation of [eATP] and downstream purinergic signaling networks, as has been shown for other plant ecto-apyrases [3]. ECM-localized PS activities have also been shown to facilitate Pi mobilization from eATP [13]. However, its functions in the nucleus are poorly understood.

Ectopic expression of PS results in distinct changes in gene expression in Arabidopsis and soybean [12,14], which help to explain the common phenotypes seen in PS plants. These include an expanded root system architecture, enhanced growth and seed yields, increased phosphate uptake, and drought tolerance [11–14]. The purpose of this study was to explore potential functions of the nuclear-localized PS in transcriptional regulation of yeast and Arabidopsis genes.

A previous study confirmed that a bipartite nuclear localization signal (NLS_BP) in PS protein was required for targeting to plant nuclei [14]. In yeast, the enhanced growth phenotype of a PS-overexpression line was not seen in a line expressing a mutant PS protein in which the NLS_BP sequence was deleted. However, the deleted NLS_BP sequence occurs in the "hinge" region of the enzyme and includes potential DNA-binding residues that we identified in the current study. A deletion in this region would likely impair PS function as a TF even if nuclear targeting was not disrupted. Interestingly, the introduction of the two point mutations into the PCBD1-DM sequence reduced the amount of DM protein in Arabidopsis nuclei, relative to PS [14]. However, lower-affinity binding of DM to dsDNA, rather than reduced nuclear targeting, might also explain reduced DM contents in this organelle, with increased loss of DM occurring during purification of chromatin fractions from nuclei. In yeast co-IP experiments, nuclear localization sequence-binding protein NSR1 was an interacting partner with both PS and DM proteins. NSR1 specifically binds the NLS of histone H2B [36], and its binding to the NLS of these proteins may facilitate their transport into the nucleus. Approximately equal amounts of PS and DM protein were found in chromatin fractions from purified yeast nuclei [14], suggesting that the altered NLS-BP spacer sequence does not significantly affect nuclear import of DM protein in yeast.

In the nucleus, PS could interact with chromatin proteins to influence gene expression in a variety of ways. Its NTPDase activities might locally alter [ATP] and ATP-dependent processes in the nucleus, such as DNA replication, transcription, and RNA processing. Nuclear PS activities or interactions with other chromatin proteins might be regulated by Ca^{2+}/CaM binding, as has recently been reported for Calmodulin binding transcription factors (CAMTAs; [37]). CaM, co-purified with PS and other chromatin proteins from nuclei in a yeast PS overexpression line [14], and Ca^{2+}/CaM increased the activity of PS purified from pea nuclei by 3-fold [9]. In the present study, modeling of a Ca^{2+}/CaM-PS complex with the *PHM6* oligonucleotide showed altered binding site interactions around the Pho4p motif. This might be one way that CaM binding could modulate PS interactions with target sequences. PS protein–protein interactions might also be involved in epigenetic modifications or recruitment of transcription factors to their promoter binding sites, as is suggested by the TF SCL-30 in our co-immunoprecipitation analyses.

We used ChIP-seq to identify PS- and DM-binding sites in promoters of Arabidopsis genes, then integrated these data with gene expression data to identify potentially regulated target genes, as had been performed for yeast genes in a previous study [14]. Further functional studies of PS- and DM-binding to yeast or plant promoters included identification of over-represented motifs for known yeast or plant TF in binding site sequences, and characterization of PS- or DM-binding to selected binding site sequences with enriched motifs using EMSA.

The promoter of yeast gene *PHM6* exhibited a PS binding site with a CACGTG motif for the Pho4p TF that regulates phosphate starvation-responsive genes in the *PHO* regulon [33]. Although *PHM6* is induced in response to P limitation, it appears to function in Pi accumulation only under phosphate surplus conditions [34]. Indeed, PS yeast did not accumulate more Pi than a control line at low [Pi], but exhibited approximately 2-fold higher Pi contents than the control after a short incubation in a medium with higher [Pi] [14]. *PHM6* was one of a dozen genes that were induced by P limitation in the PS line and whose promoters exhibited PS-specific binding (no DM-binding sites), suggesting that PS binding might help regulate P homeostasis in this organism. Functional assays with the *PHM6* promoter supported a PS-specific binding to this sequence, with no significant DM binding. Partial binding to the CACGTG motif was supported by the observed lack of PS binding to an oligo containing a mutated Pho4p site. Structure modeling predicted overlapping PS and DM binding sites involving the Pho4p motif, with off-site binding in the mutated oligo. The reduced number of DM interactions with DNA was consistent with lower DNA-binding affinities for this protein, relative to PS. Pho4p was not detected as a PS or DM binding partner in yeast co-IP assays, so indirect binding of PS or DM complexes with this yeast transcription factor does not explain their interactions with its binding site, although complexes with other proteins in the partially purified PS/DM samples could account for the observed binding data.

An enriched DOF1.5 motif 5′-AAAG-3′ is located in a PS-binding site in the promoter for *WRKY42*, which was induced in PS seedlings. EMSA supported PS-specific binding to this sequence, since some band shifts occurred only with PS-containing samples and were not seen if the DOF1.5 motif was mutated. However, structure modeling predicted binding to a ‘5-TGGTA-3′ sequence adjacent to but not overlapping with the DOF1.5 motif. Under conditions of Pi sufficiency in which the seedlings were grown, WRKY42 binds to the promoter of major Pi transporter *PHT1;1* (At5g43350), increasing its expression [38]. Under Pi sufficiency, PHT1;1 plays the major role in Pi uptake into the root, since other PHT1 transporters are repressed [39]. The potential role of PS in regulating *WRKY42* expression, with downstream effects on expression of known WRKY42 targets like *PHT1;1* and *PHO1* [38], was of particular interest to us because a Pi accumulation phenotype has been reported for PS seedlings growing under Pi sufficiency [13,14]. As in yeast, Pi accumulation does not occur in PS seedlings grown under Pi limitation [14], where *WRKY42* is repressed and the WRKY42 protein is degraded [38], further supporting a possible role for this TF in the Pi accumulation phenotype. However, neither *PHT1;1* nor *PHO1* was DE in PS seedlings [14]. Their regulation by WRKY42 was previously studied in overexpression lines exhibiting 50 to 150-fold higher *WRKY42* expression than WT seedlings [38]. The much lower induction level for *WRKY42* in PS seedlings may be below the response threshold for differential expression of these targets. It is noteworthy that of 74 genes with functionally characterized WRKY42 binding sites (PlantRegMap; https://plantregmap.gao-lab.org/cis-map.php; accessed 12 November 2025), only a single target gene, Scarecrow-like 3 (AT1G08695), was DE in PS seedlings (Table S1).

We further demonstrated PS-specific binding to a *PER50* promoter sequence containing SHN3 consensus 5′-GCC-3′ box elements. Binding to an oligo with a mutated SHN3 sequence, which overlapped the 5′-GGGGA-3′ binding site predicted by structure modeling, was abolished. Two important functions for plant peroxidases like PER50 are the regulation of H_2O_2 metabolism in response to oxidative stress and also the utilization of H_2O_2 as a substrate to cross-link proteins and induce lignin formation in the cell wall [28]. The latter processes decrease wall extensibility and growth [29]. Lim et al. [30] showed that suppression of *AtAPY1/2* in the R2-4A line increased H_2O_2 production, and cell wall lignification also increased, in parallel with the induction of five class III peroxidases

and growth inhibition in Arabidopsis seedlings. In contrast, *AtAPY2* overexpression led to the decreased expression of these peroxidases and increased growth in Arabidopsis seedlings [39]. The PS-specific induction of *PER50* was at the statistical cutoff for differential gene expression (FC $\geq$ 1.5), and its contribution to the enhanced growth phenotype of PS seedlings is unclear. It was not DE in the R2-4A line [30]. It is interesting to note, however, that nine other *PER* genes were DE in PS seedlings but not in DM seedlings ([14], Table S6). Two of these peroxidase genes (*PER15*, *PER53*) were strongly induced in the R2-4A line [30] but were repressed in PS seedlings, which is consistent with the proposed model for apyrase-regulated peroxidase expression and growth regulation [4].

PS-specific binding to the enriched SHN3 motif is also interesting in that ectopic expression of PS in soybean induced a large number of genes involved in wax and cuticle synthesis [12]. This resulted in a reduced cuticle permeability that contributed to a drought-tolerance phenotype of these plants, which were not experiencing water limitation. SHN3 belongs to a TF clade whose members activate genes involved in wax synthesis and cuticle formation in Arabidopsis [27]. None of the SHN1-3 TF were DE in PS soybean; thus, PS binding to SHN3 elements may have enhanced cuticle development, allowing the plant to better adapt to actual drought stress. This may help to explain the significantly increased seed yields in field studies with PS soybean [12]. In PS Arabidopsis seedlings, *SHN2* was induced 1.8-fold, and two downstream targets, cutin synthase (*CUS2*) and very-long chain fatty acyl CoA reductase 3 (*CER4*), were induced 1.6- and 1.5-fold, respectively ([14]; RNA-seq dataset). Interestingly, a nearly identical expression profile for *SHN2*, *CUS2*, and *CER4* was also seen in an *AtAPY1* overexpression line in the Ws background (unpublished data), suggesting that induction of wax synthesis and cuticle formation genes may be a common response to overexpression of an "apyrase 1-type" enzyme.

We used AlphaFold3 to model PS and DM binding to both test and mutant sequences of *PHM6*, mapping specific binding site interactions. These modeling studies (1) identified specific PS/DM residues that may be involved in DNA-binding, with the PCBD1 helix playing an important role in interactions with major groove nucleobases; (2) supported sequence-specific binding for PS to a conserved 5′-(G/T)GG(G/T)A-3′ motif in three different binding site sequences, which overlapped or was adjacent to enriched TF motifs in each binding site; (3) elucidated the potential structural basis for observed differences in PS and DM binding to DNA in EMSA, and (4) showed that CaM binding to PS alters binding site interactions around the Pho4p motif in the *PHM6* oligo. Although this tool is trained using static molecular structures in the Protein Data Bank and cannot simulate buffer conditions used for EMSA, it is capable of highly accurate prediction of protein-DNA complexes. Future modeling using molecular dynamics simulations incorporating the EMSA binding conditions will be helpful in refining binding site predictions.

In both yeast [14] and Arabidopsis, there is relatively little overlap between PS- and DM-binding sites, the over-represented TF motifs, or the expression profiles for potentially regulated target genes, suggesting that PS and DM may regulate different transcriptional networks in each organism. More definitive evidence, such as transcriptional activation assays of putative target genes, using wild-type and mutated-motif promoter fragments and highly purified PS and DM proteins, will be needed to understand the potential role of PS in transcriptional regulation.

Future experiments should include functional verification of DM-specific binding site sequences, such as the MYB-related 5′-ATAAG-3′ sequence in the MYBS1 and SRM1 promoters. They should also examine conserved core sequence elements shared by PS- and DM-binding site overlaps. For example, it is interesting that the 5′-AAG-3′ element found in both the PS-specific DOF1.5 and DM-specific MYB-related TF motifs in Arabidopsis promoters is also contained within the yeast Azf1p motif 5′- AAAAGAAA-3′,

which was the most enriched motif in both PS- and DM-specific binding sites in yeast promoters [14]. Enriched TF motifs within PS binding sites exhibit considerable sequence diversity. If these motifs are involved in PS binding, as is suggested by the EMSA data, such binding likely occurs with low sequence specificity, perhaps in complexes with other DNA-binding proteins, such as those identified in co-IP assays. However, the predicted 5′-(G/T)GG(G/T)A-3′ consensus motif derived from modeling studies with the three unrelated promoter sequences used in EMSA suggests a degree of sequence specificity in PS binding. This consensus motif is found within 7% of DOF motifs and 17% of SHN3 motifs within PS binding sites in Table S3. Thus, for a significant number of these genes, PS may function as a DNA-binding regulatory protein, possibly activating or repressing expression of DOF- or SHN3-regulated genes.

4. Conclusions

In the present study, we have shown, for the first time, that a plant apyrase may function as a DNA-binding regulatory protein, extending its known enzymatic functions in the Golgi or the extracellular matrix. The nuclear localization of ectopically expressed PS, functional characterization of PS binding to both yeast and Arabidopsis promoter sequences identified in ChIP-seq assays, and structure modeling of these interactions support this novel function. Mutations in a potential calmodulin-binding site PCBD1 of PS, producing the DM protein, altered binding site interactions *in vivo* (ChIP-seq) and *in vitro* (EMSA), with the latter being supported by structure modeling. Importantly, this altered binding was correlated with differences in genome-wide gene expression profiles and related phenotypic characteristics, such as drought tolerance and increased phosphate acquisition in yeast and plants [11,12,14]. Further studies with other plant apyrases will be needed to confirm their potential roles in transcriptional regulation.

5. Materials and Methods

5.1. Plant Materials and Growth Conditions

Arabidopsis thaliana Columbia-0 (Col-0) ecotype was used as the wild-type control. Transgenic lines overexpressing the PS and DM proteins were generated previously by introducing constructs encoding either PS or a DM variant, which contained two amino acid substitutions within a potential calmodulin binding site and an overlapping nuclear localization signal [14]. Homozygous T3 lines were selected for kanamycin resistance, and transgene expression was confirmed by RT-PCR and Western blot analyses. All seedlings were grown for 7 days on half-strength Murashige and Skoog (1/2x MS) agar plates supplemented with 1% sucrose under) under a full-spectrum light intensity of 150 mmol m^{-2} s^{-1} at 22 °C.

5.2. Assay for Differential Binding of PS and DM to dsDNA-Cellulose

All operations were carried out at 4 °C. Partially purified PS or DM protein fractions (4.8 μg protein in 20 mM Hepes, pH 7.5) were applied to a dsDNA-cellulose column equilibrated with at least 10 bed volumes of Wash Buffer (20 mM Hepes, pH 7.5, 1 mM EDTA, 1mM Pefabloc protease inhibitor). Purified PS/DM was diluted to 160 ng/μL with 20 mM Hepes (pH 7.5) immediately before being loaded onto the column. After application of PS or DM, the column was washed with 3 bed volumes of Wash Buffer, followed by Wash Buffer containing increasing NaCl concentrations (0.05 M, 0.1 M, 0.3 M, and 0.6 M). As negative controls, PS and DM samples were run on cellulose-only control columns, and ovalbumin (6 μg) was run on a dsDNA-cellulose column. Eluted protein fractions were further concentrated and then analyzed by SDS-PAGE immunoblot assays using the highly specific monoclonal antibody 8B6. Ovalbumin was detected by Coomassie Blue staining.

5.3. ChIP-Seq Analyses

5.3.1. Construction and Verification of 4Myc-Tagged PS and DM Overexpression Lines

PS- and *DM*-coding sequences were amplified using relevant primers (Table S7) and cloned into pENTR vectors, respectively. Then, pENTR-PS and pENTR-DM vectors were recombined into the pGWB17 plant expression vector (NovoPro #V005425) behind a 35S promoter and in-frame with an N-terminal 4-Myc tag using LR Clonase II. Recombinant vectors were verified to have no coding errors by sequencing, and then were transformed into the Col-0 background. T1 transformants were identified using c-Myc antibody (9B11, Cell signaling Cat# 2276S) to confirm PS expression. T2 and T3 homozygous transformants were selected in the presence of hygromycin antibiotic screening.

5.3.2. Chromatin Immunoprecipitation (ChIP) and Sequencing Library Preparation

Seven-day-old seedlings were harvested, crosslinked with 1% formaldehyde under vacuum for 10 min, and quenched with 0.125 M glycine. Nuclei were isolated from the seedlings, as previously described [14], and chromatin was fragmented to an average size of 200–500 bp by sonication. Immunoprecipitation of 4Myc-tagged PS and DM proteins was performed using EZview Red Anti-c-Myc Affinity Gel (Cat# E6654, Sigma-Aldrich, St. Louis, MO, USA) for one hour in the dark at 4 °C. Input and ChIP DNA were purified, as was reported for yeast [14], and used for library construction with a NEBNext Ultra II DNA Library Prep Kit, following the manufacturer's protocol.

5.3.3. ChIP-Seq Data Processing, Peak Calling, and Functional Annotation

DNA samples were sequenced by the Genome Sequencing and Analysis Facility (GSAF) at the University of Texas at Austin (Illumina NovaSeq SP, PE150 reads). ChIP-seq data were deposited in the NCBI Sequence Read Archive (accession #PRJNA1268411). fastpXpress, a custom batch fastp script implemented in a Google Colab notebook (https://github.com/rdslocum/fastpXpress; accessed on 12 November 2025), was used to remove adapters and quality trim the initial sequence reads. ChIP-seq analyses were carried out using the CLC Genomics Workbench 10.0.1 platform (Qiagen, Hilden, Germany). An average of 33.7 million reads from two independent experiments were combined and uniquely mapped to the TAIR10 reference genome with an average 38.8x genome coverage. Putative PS- and DM-binding sites were identified ("peak calling") using input controls and overlap analyses, comparing peak profiles in WT versus *PS* and *DM* overexpression lines. Quality control metrics for these assays are summarized in Table S8. Peaks were annotated using expanded Araport11 annotation based upon the AtRTD3 reference transcriptome [40]. High-confidence binding sites (peak shape scores ≥ 2.0 and $p \leq 0.05$) located 1–1500 bp upstream from the TSS of genes on both sense (+) and antisense ($-$) strands were identified. Further overlap analyses identified unique PS- and DM-specific binding sites, and a subset of overlapping PS- and DM-binding sites. Gene Ontology (GO) BioProcess enrichment analysis for potential target genes was performed using the PANTHER 19.0 database (https://www.pantherdb.org/).

5.3.4. PS and DM Binding Site Motif Enrichment Analyses

Identification of conserved *cis*-regulatory elements, via motif enrichment analysis, was conducted using the MEME Suite v5.5.7 SEA tool (https://meme-suite.org/meme/tools/sea; accessed on 12 November 2025) with the DAP-seq database of 872 Arabidopsis transcription factor-binding motifs [41]. Significantly enriched motifs ($\geq$2-fold enrichment, $p \leq 0.01$) were identified in PS- or DM-specific binding site sequences within promoters of genes that were also differentially expressed only in PS- or DM-overexpressing Arabidopsis seedlings, respectively.

5.4. Functional Characterization of PS and DM Binding Sites Using Electrophoretic Mobility Shift Assays

High confidence PS-binding sites located within the promoters of genes that were differentially expressed only in PS yeast, or in PS seedlings, were identified from ChIP-seq analyses. Binding sites exhibiting enriched motifs with high sequence similarities to known TF binding sites that were also located approximately in the center of the binding site were filtered from the larger dataset. The potential functional significance of those binding events was further characterized *in vitro* using electrophoretic mobility shift assays (EMSA). The Pho4p motif CACGTG in the yeast *PHM6* promoter, the Dof1.5 motif AAAAGAAA in the Arabidopsis *WRKY42* promoter, and the SHN3 consensus GCC box motif in the Arabidopsis *PER50* promoter were selected for EMSA validation.

5.4.1. Oligonucleotide Probe Preparation

Double-stranded DNA probes, comprising approximately 30 bp upstream and 30 bp downstream of the central motif, were used in EMSA. Single-stranded forward and reverse complement oligonucleotides were synthesized by Integrated DNA Technologies (IDT, Coralville, IA, USA). Biotin labeling was performed at the 3′ end of each strand using the Biotin 3′- End DNA Labeling Kit (Thermo Scientific #89818) following the manufacturer's protocol. For annealing, equimolar amounts of labeled forward and reverse strands were mixed, denatured at 90 °C for 1 min, and slowly cooled to room temperature, followed by incubation at the melting temperature for 30 min. Unlabeled competitor probes were prepared in parallel using the same annealing steps. For each candidate binding site, a corresponding mutated oligonucleotide probe was synthesized by altering the core motif sequence. The mutated regions were designed to disrupt potential binding without introducing matches to other known TF motifs in the dataset. Motif scanning analysis confirmed that the mutated elements did not overlap with any enriched motifs identified in PS binding sites.

5.4.2. EMSA Procedure

EMSA reactions were performed using the LightShift® Chemiluminescent EMSA Kit (Thermo Scientific #20148), following the manufacturer's protocol. Recombinant PS and DM proteins were purified as described in the protein expression and purification section. Binding reactions were assembled in 20 µL volumes containing 10 nmol biotin-labeled probe, 200 ng (4.2 pmol) recombinant PS or DM protein, and binding buffer (10 mM Tris, pH 7.5, 50 mM KCl, 1 mM DTT, 1 µg/µL poly dI·dC). For competition assays, a 200-fold molar excess (2 µmol) of unlabeled competitor probe was included. Reactions were incubated at room temperature for 30 min and resolved on 6% native polyacrylamide gels in 0.5x TBE buffer at 100 V. DNA-protein complexes were transferred to a nylon membrane, cross-linked, and detected using the chemiluminescent detection reagents provided in the kit. Positive control reactions were performed using Biotin-EBNA Control DNA and EBNA extract supplied with the kit.

5.5. Purification of PS and DM Proteins

The purified PS and DM were partially purified from extracts of PS- or DM-overexpressing strains [14]. Yeast cells (~2 g wet weight) were homogenized with a Kinematica polytron homogenizer in 10 mL of homogenization buffer (50 mM Tris-Cl pH 7.4, 150 mM NaCl, 0.2% NP-40, 10% Glycerol, 1 mM PMSF protease inhibitor) then centrifuged at 13,000× g for 10 min at 4 °C. After filtering the supernatant through a 0.45 µm filter, proteins in the supernatant were enriched by ammonium sulfate precipitation (20%, then 80% w/v). The pellet was washed and dissolved in resuspension buffer (60 mM Hepes pH 7.5, 3 mM $MgCl_2$, 1 mM Pefabloc, and 10 mM 2-mercaptoethanol), then

the solution was dialyzed against 10 mM Tris-HCl and 20 mM NaCl at pH 8.0 buffer for 4 h. The sample was then concentrated using an Amicon concentrator. The final protein concentration was confirmed by using the Bradford method. PS and DM purity was ~1% in these protein preparations, which contained approximately equal amounts of PS and DM protein, as estimated by SDS-PAGE immunoblot analyses using the highly specific monoclonal antibody 8B6 and ≥95% purity PS protein as the standard for densitometric analysis (Figure S7). The antibody and purified PS protein were commercially prepared by GenScript (Piscataway, NJ, USA).

5.6. Co-IP for Yeast and Arabidopsis

5.6.1. Yeast Protein Preparation

Yeast NS219 transformed with pYES2 vector alone (empty vector (EV) control), pYES2-psNTP9, or pYES2-psNTP9-DM were initially cultured in 4 mL liquid yeast nitrogen base (uracil dropoff) with glucose, pH 5.2. The culture was grown at 30 °C for 48 h on a 250 rpm shaker. After 48 h, the cultures were inoculated (starting OD_{660} = 0.03) into 100 mL of induction medium containing 2% galactose and grown to a final OD_{600} = 0.6–0.8. Cells were harvested by centrifugation at 3000× *g* for 10 min at 4 °C. The cell pellet was dissolved in YeastBusterTM Reagent and THP Solution with 25 U Benzonase® Nuclease and 500 µL protease inhibitors and incubated for 20 min at room temperature. Insoluble cell debris was removed by centrifugation at 16,000× *g* for 20 min at 4 °C, and the supernatant was used in the following immunoprecipitation step.

5.6.2. Arabidopsis Protein Preparation

Seven-day-old Arabidopsis seedlings (~5 g) of ecotype Columbia (CS907), or PS-4Myc, or DM-4Myc transgenic lines, were collected and ground in liquid nitrogen. Total protein was solubilized in extraction buffer (50 mM Tris, pH 7.5, 150 mM NaCl, 1 mM EDTA, 0.1% Tween-20, 0.25 mM DTT, 1× protease inhibitor cocktail, 1 mM PMSF). The extracts were centrifuged at 20,000× *g* for 15 min, and the supernatant was used in the immunoprecipitation step.

5.6.3. Co-Immunoprecipitation

Yeast or Arabidopsis seedling extracts were incubated with EZview Red Anti-c-Myc Affinity Gel (Cat# E6654, Sigma-Aldrich) for one hour in the dark at 4 °C. Resin was washed with 1 mL of TBS-T three times for 10 min each. Myc-tagged proteins were eluted with 50 µL 0.2 M Glycine pH 2.6, then the eluate was immediately neutralized with 120 µL pH 9.4 Tris-HCl. SDS-PAGE immunoblot analyses with Anti-Myc antibody were used to detect immunoprecipitated Myc-tagged PS or DM proteins.

5.6.4. Mass Spectrometry Analysis

Co-IP preparations were submitted for mass spectrometry analysis at the Biological Mass Spectrometry Facility, UT Austin Center for Biomedical Research Support (RRID:SCR_021728). Prior to LC-MS analysis, proteins were reduced, alkylated, and digested with trypsin, and the resulting peptides were either manually or robotically desalted using Millipore U-C18 ZipTip pipette tips following the manufacturer's protocol. Data were acquired using an Orbitrap Fusion Tribrid mass spectrometer equipped with an ultra-high-pressure Ultimate 3000 RSLC nanosystem (Thermo Scientific, Waltham, MA, USA). Raw data files were analyzed using MaxQuant version 2.0.3.0 [42]. The LFQ protein quantification strategy [43], match between runs, and a 1% false discovery rate at both the peptide spectrum match and the protein level were employed.

5.6.5. Identification of Potential PS and DM Co-IPs

We considered co-IPs in the control extracts of yeast (pYES2 empty vector) or Arabidopsis seedlings (no ectopic expression of PS or DM) to be "false-positives". If the same co-IPs occurred in PS or DM assays, we did not consider them further. We filtered the list of potential co-IPs (87 Arabidopsis and 51 yeast proteins) using annotated lists of yeast and Arabidopsis TF (SGD, https://www.yeastgenome.org/; AtTFDB, https://agris-knowledgebase.org/AtTFDB; both URLs accessed on 12 November 2025) and chromatin proteins, downloaded from the Uniprot database (https://www.uniprot.org/; accessed on 12 November 2025), to produce a realistic set of co-IPs that may facilitate DNA binding in complexes with PS or DM in EMSA (Table S5).

5.7. Gene Expression Analyses

Gene expression analyses were performed using 7-day-old Arabidopsis seedlings that overexpress PS (PS2 line) or DM (DM4 line). Total RNA concentration and purity were measured using Thermo Scientific NanoDrop 1000 spectrophotometer. Approximately 1 μg of total RNA treated with Amplification Grade DNase I was reverse transcribed using a High-Capacity cDNA Reverse Transcription kit (Applied Biosystems/Thermo Fisher, Waltham, MA, USA).

qRT-PCR was performed using the Life Technologies/AB Biosystems Quant 7 Real-Time PCR System. Power SYBR Green PCR Master Mix (Life Technologies/AB Biosystems, Waltham, MA, USA) was used for RT-qPCR reactions. The qRT-PCR conditions used were hold stage: 50 °C, 2 min, and 95 °C, 10 min; PCR stage: 40 cycles of 95 °C, 15 s, and 60 °C, 1 min. Melting curves generated from machine dissociation conditions were used to identify primer dimers and multiple targets. The primer sequences used are listed in Table S7**.** For each biological replicate, three technical triplicates with ±0.5 CT were used for qRT-PCR analysis. The relative gene expression was calculated by the $2^{-\Delta\Delta CT}$ method [44]. *Actin1* was used as the reference gene in the Arabidopsis qRT-PCR. Statistical significance between treatments was calculated by Student's *t* test, using ΔCT for three biological replicates.

Transcriptome-wide gene expression analyses (RNA-seq) and qRT-PCR validation of expression for selected genes were previously reported [14]. RNA-seq data were deposited in the NCBI Sequence Read Archive (accession #PRJNA449074).

5.8. Structural Studies of PS and DM

AlphaFold3 was accessed via its server (https://alphafoldserver.com/; accessed on 12 November 2025). Sequences used in modeling studies: mature PS (NP_001414507.1; Q22-V455, N-terminal 21 residues deleted), DM protein (mature PS with S208L and P216R mutations), Arabidopsis Calmodulin 1 (NP_198594.1), sense and anti-sense oligonucleotides for *PHM6*, *WRKY42*, and *PER50* binding sites (Table S7). Residue numbering for the full-length precursor PS or DM proteins was used. The CaM1 binding model included Ca^{2+}. All models included K+ and Cl-, since the EMSA binding buffer contained 50 mM KCl.

Supplementary Materials: The following supporting information can be downloaded at: https://www.mdpi.com/article/10.3390/plants14223514/s1. Figure S1: Venn diagram showing overlap between sets of potentially regulated Arabidopsis genes with PS- or DM-specific binding sites in their promoters.; Figure S2: PS-specific binding site in the yeast *PHM6* gene promoter and test and mutated oligo sequences used in functional testing of the binding site with EMSA.; Figure S3: PS-specific binding site in the Arabidopsis *WRKY42* gene promoter and test and mutated oligo sequences used in functional testing of the binding site with EMSA; Figure S4: PS-specific binding site in the Arabidopsis *PER50* gene promoter and test and mutated oligo sequences used in functional testing of the binding site with EMSA; Figure S5: Predicted PS binding sites in yeast (*PHM6*) and Arabidopsis (*WRKY42*, *PER50*)

promoter sequences used in EMSA; Figure S6: AlphaFold3-predicted interactions of mature PS or DM proteins with the yeast *PHM6* promoter binding site.; Figure S7: Purification of PS and DM proteins for use in EMSA.; Table S1: PS- and DM-specific binding sites in promoters of potential target genes and expression patterns for those genes in PS- and DM-overexpressing Arabidopsis seedlings; Table S2: Differentially expressed genes enriched specifically in an Arabidopsis DM-overexpression line are involved in abscisic acid (ABA) signaling or responses to ABA (BioProcess categories GO:0009737; GO:0009269).; Table S3: PS-specific binding sites and enriched transcription factor motifs in promoters of genes that are differentially expressed only in PS Arabidopsis seedlings (NOTE: This is a separate Excel file.).; Table S4: qRT-PCR validation of *WRKY42* and *PER50* expression in RNA-seq datasets.; Table S5: Chromatin proteins or transcription factors that interact with 4Myc-tagged Arabidopsis PS or DM proteins, or 13Myc-tagged yeast PS or DM proteins, in co-IP assays.; Table S6: Expression profiles for peroxidase genes regulated in response to ectopic *PS* or *DM* expression, or suppression of *AtAPY1/2* in Arabidopsis seedlings.; Table S7: PCR primers and oligos used in this study.; Table S8: Quality control metrics for the Arabidopsis ChIP-seq assay.

Author Contributions: Conceptualization, R.D.S., G.C. and S.J.R.; Data curation, R.D.S.; Formal analysis, R.D.S., H.W. and G.C.; Funding acquisition, G.C. and S.J.R.; Methodology, H.W. and X.C.; Project administration, G.C. and S.J.R.; Software, R.D.S.; Validation, H.W. and X.C.; Visualization, R.D.S. and H.W.; Writing—original draft, H.W., R.D.S. and S.J.R.; Writing—review and editing, H.W., R.D.S., G.C. and S.J.R. All authors have read and agreed to the published version of the manuscript.

Funding: This work was supported by a grant from the Texas Crop Science to S.J.R. and G.C. (Award Number: UTA13-000682).

Data Availability Statement: The Arabidopsis ChIP-seq and RNA-seq sequence reads files are available in the NCBI Sequence Reads Archive (accession #PRJNA1268411 and #PRJNA449074, respectively). The custom sequence reads preprocessing script fastpXpress is available at (https://github.com/rdslocum/fastpXpress; accessed on 12 November 2025).

Acknowledgments: We thank the Genomic and Sequencing Facility at the University of Texas for support services.

Conflicts of Interest: S.J.R. and G.C. are consultants to Texas Crop Science, which funded the research presented here. No other authors have conflicts of interest to declare.

Abbreviations

The following abbreviations are used in this manuscript:

NTPDase	nucleoside triphosphate diphosphohydrolase
eATP	extracellular ATP
CaM	calmodulin
PS	pea apyrase psNTP9
DM	"double mutation" version of PS
DEG	differentially expressed genes
TF	transcription factor
EMSA	electrophoretic mobility shift assay
NLS_BP	bipartite nuclear localization signal
PCBD1	potential calmodulin-binding domain 1

References

1. Knowles, A.F. The GDA1_CD39 Superfamily: NTPDases with Diverse Functions. *Purinergic Signal.* **2011**, *7*, 21–45. [CrossRef]
2. Clark, G.B.; Morgan, R.O.; Fernandez, M.P.; Salmi, M.L.; Roux, S.J. Breakthroughs Spotlighting Roles for Extracellular Nucleotides and Apyrases in Stress Responses ands Growth and Development. *Plant Sci.* **2014**, *225*, 107–116. [CrossRef]
3. Clark, G.; Brown, K.A.; Tripathy, M.K.; Roux, S.J. Recent Advances Clarifying the Structure and Function of Plant Apyrases (Nucleoside Triphosphate Diphosphohydrolases). *Int. J. Mol. Sci.* **2021**, *22*, 3283. [CrossRef]

4. Clark, G.; Tripathy, M.K.; Roux, S.J. Growth Regulation by Apyrases: Insights from Altering Their Expression Level in Different Organisms. *Plant Physiol.* **2024**, *194*, 1323–1335. [CrossRef] [PubMed]
5. Liu, X.; Wu, J.; Clark, G.; Lundy, S.; Lim, M.; Arnold, D.; Chan, J.; Tang, W.; Muday, G.K.; Gardner, G.; et al. Role for Apyrases in Polar Auxin Transport in Arabidopsis. *Plant Physiol.* **2012**, *160*, 1985–1995. [CrossRef] [PubMed]
6. Wu, J.; Steinebrunner, I.; Sun, Y.; Butterfield, T.; Torres, J.; Arnold, D.; Gonzalez, A.; Jacob, F.; Reichler, S.; Roux, S.J. Apyrases (Nucleoside Triphosphate-Diphosphohydrolases) Play a Key Role in Growth Control in Arabidopsis. *Plant Physiol.* **2007**, *144*, 961–975. [CrossRef] [PubMed]
7. Clark, G.; Darwin, C.; Mehta, V.; Jackobs, F.; Perry, T.; Hougaard, K.; Roux, S. Effects of Chemical Inhibitors and Apyrase Enzyme Further Document a Role for Apyrases and Extracellular ATP in the Opening and Closing of Stomates in *Arabidopsis*. *Plant Signal. Behav.* **2013**, *8*, e26093. [CrossRef]
8. Chiu, T.-Y.; Lao, J.; Manalansan, B.; Loqué, D.; Roux, S.J.; Heazlewood, J.L. Biochemical Characterization of Arabidopsis APYRASE Family Reveals Their Roles in Regulating Endomembrane NDP/NMP Homoeostasis. *Biochem. J.* **2015**, *472*, 43–54. [CrossRef]
9. Chen, Y.-R.; Datta, N.; Roux, S.J. Purification and Partial Characterization of a Calmodulin-Stimulated Nucleoside Triphosphatase from Pea Nuclei. *J. Biol. Chem.* **1987**, *262*, 10689–10694. [CrossRef]
10. Shibata, K.; Abe, S.; Yoneda, M.; Davies, E. Sub-Cellular Distribution and Isotypes of a 49-KDa Apyrase from *Pisum sativum*. *Plant Physiol. Biochem.* **2002**, *40*, 407–415. [CrossRef]
11. Veerappa, R.; Slocum, R.D.; Siegenthaler, A.; Wang, J.; Clark, G.; Roux, S.J. Ectopic Expression of a Pea Apyrase Enhances Root System Architecture and Drought Survival in Arabidopsis and Soybean. *Plant. Cell Environ.* **2019**, *42*, 337–353. [CrossRef] [PubMed]
12. Sabharwal, T.; Lu, Z.; Slocum, R.D.; Kang, S.; Wang, H.; Jiang, H.-W.; Veerappa, R.; Romanovicz, D.; Nam, J.C.; Birk, S.; et al. Constitutive Expression of a Pea Apyrase, PsNTP9, Increases Seed Yield in Field-Grown Soybean. *Sci. Reports* **2022**, *12*, 10870. [CrossRef] [PubMed]
13. Thomas, C.; Sun, Y.; Naus, K.; Lloyd, A.; Roux, S. Apyrase Functions in Plant Phosphate Nutrition and Mobilizes Phosphate from Extracellular ATP. *Plant Physiol.* **1999**, *119*, 543–552. [CrossRef] [PubMed]
14. Tripathy, M.K.; Wang, H.; Slocum, R.D.; Jiang, H.-W.; Nam, J.-C.; Sabharwal, T.; Veerappa, R.; Brown, K.A.; Cai, X.; Allen Faull, P.; et al. Modified Pea Apyrase Has Altered Nuclear Functions and Enhances the Growth of Yeast and Arabidopsis. *Front. Plant Sci.* **2025**, *16*, 1584871. [CrossRef]
15. Hsieh, H.L.; Song, C.J.; Roux, S.J. Regulation of a Recombinant Pea Nuclear Apyrase by Calmodulin and Casein Kinase II. *Biochim. Biophys. Acta-Gene Struct. Expr.* **2000**, *1494*, 248–255. [CrossRef]
16. Massalski, C.; Bloch, J.; Zebisch, M.; Steinebrunner, I. The Biochemical Properties of the Arabidopsis Ecto-Nucleoside Triphosphate Diphosphohydrolase AtAPY1 Contradict a Direct Role in Purinergic Signaling. *PLoS ONE* **2015**, *10*, e0115832. [CrossRef]
17. Hsieh, H.-L.; Tong, C.-G.; Thomas, C.; Roux, S.J. Light-Modulated Abundance of an mRNA Encoding a Calmodulin-Regulated, Chromatin-Associated NTPase in Pea. *Plant Mol. Biol.* **1996**, *30*, 135–147. [CrossRef]
18. Abramson, J.; Adler, J.; Dunger, J.; Evans, R.; Green, T.; Pritzel, A.; Ronneberger, O.; Willmore, L.; Ballard, A.J.; Bambrick, J.; et al. Accurate Structure Prediction of Biomolecular Interactions with AlphaFold 3. *Nature* **2024**, *630*, 493–500. [CrossRef]
19. Kosugi, S.; Hasebe, M.; Matsumura, N.; Takashima, H.; Miyamoto-Sato, E.; Tomita, M.; Yanagawa, H. Six Classes of Nuclear Localization Signals Specific to Different Binding Grooves of Importinα. *J. Biol. Chem.* **2009**, *284*, 478–485. [CrossRef]
20. Lopez-Molina, L.; Mongrand, S.; McLachlin, D.T.; Chait, B.T.; Chua, N.H. ABI5 Acts Downstream of ABI3 to Execute an ABA-Dependent Growth Arrest during Germination. *Plant J.* **2002**, *32*, 317–328. [CrossRef]
21. Wang, T.; Tohge, T.; Ivakov, A.; Mueller-Roeber, B.; Fernie, A.R.; Mutwil, M.; Schippers, J.H.M.; Persson, S. Salt-Related MYB1 Coordinates Abscisic Acid Biosynthesis and Signaling during Salt Stress in Arabidopsis. *Plant Physiol.* **2015**, *169*, 1027–1041. [CrossRef]
22. Shuai, B.; Reynaga-Peña, C.G.; Springer, P.S. The Lateral Organ Boundaries Gene Defines a Novel, Plant-Specific Gene Family. *Plant Physiol.* **2002**, *129*, 747–761. [CrossRef]
23. Hassan, H.; Scheres, B.; Blilou, I. JACKDAW Controls Epidermal Patterning in the Arabidopsis Root Meristem through a Non-Cell-Autonomous Mechanism. *Development* **2010**, *137*, 1523–1529. [CrossRef]
24. Shi, H.; Zhong, S.; Mo, X.; Liu, N.; Nezames, C.D.; Deng, X.W. HFR1 Sequesters PIF1 to Govern the Transcriptional Network Underlying Light-Initiated Seed Germination in Arabidopsis. *Plant Cell* **2013**, *25*, 3770–3784. [CrossRef] [PubMed]
25. Wang, S.; Barron, C.; Schiefelbein, J.; Chen, J.G. Distinct Relationships between GLABRA2 and Single-Repeat R3 MYB Transcription Factors in the Regulation of Trichome and Root Hair Patterning in Arabidopsis. *New Phytol.* **2010**, *185*, 387–400. [CrossRef] [PubMed]
26. Son, O.; Cho, H.Y.; Kim, M.R.; Lee, H.; Lee, M.S.; Song, E.; Park, J.H.; Nam, K.H.; Chun, J.Y.; Kim, H.J.; et al. Induction of a Homeodomain–Leucine Zipper Gene by Auxin Is Inhibited by Cytokinin in Arabidopsis Roots. *Biochem. Biophys. Res. Commun.* **2004**, *326*, 203–209. [CrossRef] [PubMed]

27. Aharoni, A.; Dixit, S.; Jetter, R.; Thoenes, E.; Van Arkel, G.; Pereira, A. The SHINE Clade of AP2 Domain Transcription Factors Activates Wax Biosynthesis, Alters Cuticle Properties, and Confers Drought Tolerance When Overexpressed in Arabidopsis. *Plant Cell* **2004**, *16*, 2463–2480. [CrossRef]
28. Passardi, F.; Penel, C.; Dunand, C. Performing the Paradoxical: How Plant Peroxidases Modify the Cell Wall. *Trends Plant Sci.* **2004**, *9*, 534–540. [CrossRef]
29. Lim, M.H.; Wu, J.; Yao, J.; Gallardo, I.F.; Dugger, J.W.; Webb, L.J.; Huang, J.; Salmi, M.L.; Song, J.; Clark, G.; et al. Apyrase Suppression Raises Extracellular ATP Levels and Induces Gene Expression and Cell Wall Changes Characteristic of Stress Responses. *Plant Physiol.* **2014**, *164*, 2054–2067. [CrossRef]
30. Bailey, T.L.; MacHanick, P. Inferring Direct DNA Binding from ChIP-Seq. *Nucleic Acids Res.* **2012**, *40*, e128. [CrossRef]
31. Hellman, L.M.; Fried, M.G. Electrophoretic Mobility Shift Assay (EMSA) for Detecting Protein–Nucleic Acid Interactions. *Nat. Protoc.* **2007**, *2*, 1849–1861. [CrossRef]
32. Austin, S.; Mayer, A. Phosphate Homeostasis—A Vital Metabolic Equilibrium Maintained Through the INPHORS Signaling Pathway. *Front. Microbiol.* **2020**, *11*, 539723. [CrossRef] [PubMed]
33. Yip, H.M.; Cheng, S.; Olson, E.J.; Crone, M.; Maerkl, S.J. Perfect Adaptation Achieved by Transport Limitations Governs the Inorganic Phosphate Response in *S. cerevisiae*. *Proc. Natl. Acad. Sci. USA* **2023**, *120*, e2212151120. [CrossRef]
34. Kulakovskaya, E.; Zvonarev, A.; Kulakovskaya, T. PHM6 and PHM7 Genes Are Essential for Phosphate Surplus in the Cells of *Saccharomyces cerevisiae*. *Arch. Microbiol.* **2023**, *205*, 47. [CrossRef]
35. Jaiswal, V.; Kakkar, M.; Kumari, P.; Zinta, G.; Gahlaut, V.; Kumar, S. Multifaceted Roles of GRAS Transcription Factors in Growth and Stress Responses in Plants. *iScience* **2022**, *25*, 105026. [CrossRef]
36. Lee, W.C.; Xue, Z.; Mélèse, T. The NSR1 Gene Encodes a Protein That Specifically Binds Nuclear Localization Sequences and Has Two RNA Recognition Motifs. *J. Cell Biol.* **1991**, *113*, 1–12. [CrossRef]
37. Liu, Y.; Qiao, Y.; Liao, W. Calmodulin-Binding Transcription Factors: Roles in Plant Response to Abiotic Stresses. *Plants* **2025**, *14*, 532. [CrossRef]
38. Su, T.; Xu, Q.; Zhang, F.C.; Chen, Y.; Li, L.Q.; Wu, W.H.; Chen, Y.F. WRKY42 Modulates Phosphate Homeostasis through Regulating Phosphate Translocation and Acquisition in Arabidopsis. *Plant Physiol.* **2015**, *167*, 1579–1591. [CrossRef]
39. Shin, H.; Shin, H.S.; Dewbre, G.R.; Harrison, M.J. Phosphate Transport in Arabidopsis: Pht1;1 and Pht1;4 Play a Major Role in Phosphate Acquisition from Both Low- and High-Phosphate Environments. *Plant J.* **2004**, *39*, 629–642. [CrossRef]
40. Zhang, R.; Kuo, R.; Coulter, M.; Calixto, C.P.G.; Entizne, J.C.; Guo, W.; Marquez, Y.; Milne, L.; Riegler, S.; Matsui, A.; et al. A High-Resolution Single-Molecule Sequencing-Based Arabidopsis Transcriptome Using Novel Methods of Iso-Seq Analysis. *Genome Biol.* **2022**, *23*, 149. [CrossRef]
41. O'Malley, R.C.; Huang, S.S.C.; Song, L.; Lewsey, M.G.; Bartlett, A.; Nery, J.R.; Galli, M.; Gallavotti, A.; Ecker, J.R. Cistrome and Epicistrome Features Shape the Regulatory DNA Landscape. *Cell* **2016**, *165*, 1280–1292. [CrossRef]
42. Cox, J.; Mann, M. MaxQuant Enables High Peptide Identification Rates, Individualized p.p.b.-Range Mass Accuracies and Proteome-Wide Protein Quantification. *Nat. Biotechnol.* **2008**, *26*, 1367–1372. [CrossRef] [PubMed]
43. Cox, J.; Hein, M.Y.; Luber, C.A.; Paron, I.; Nagaraj, N.; Mann, M. Accurate Proteome-Wide Label-Free Quantification by Delayed Normalization and Maximal Peptide Ratio Extraction, Termed MaxLFQ. *Mol. Cell. Proteom.* **2014**, *13*, 2513–2526. [CrossRef] [PubMed]
44. Livak, K.J.; Schmittgen, T.D. Analysis of Relative Gene Expression Data Using Real-Time Quantitative PCR and the $2^{-\Delta\Delta CT}$ Method. *Methods* **2001**, *25*, 402–408. [CrossRef]

Disclaimer/Publisher's Note: The statements, opinions and data contained in all publications are solely those of the individual author(s) and contributor(s) and not of MDPI and/or the editor(s). MDPI and/or the editor(s) disclaim responsibility for any injury to people or property resulting from any ideas, methods, instructions or products referred to in the content.

plants

MDPI

Article

Rolling Leaf 2 Controls Leaf Rolling by Regulating Adaxial-Side Bulliform Cell Number and Size in Rice

Yu-Jia Leng [1,2,3,†], Shi-Yu Qiang [1,†], Wen-Yu Zhou [1,†], Shuai Lu [1], Tao Tao [1], Hao-Cheng Zhang [1], Wen-Xiang Cui [1], Ya-Fan Zheng [1], Hong-Bo Liu [1], Qing-Qing Yang [1], Ming-Qiu Zhang [1], Zhi-Di Yang [1], Fu-Xiang Xu [1], Hai-Dong Huan [1], Xu Wei [1], Xiu-Ling Cai [1,2,3], Su-Kui Jin [3,4,*] and Ji-Ping Gao [1,2,3,*]

[1] Jiangsu Key Laboratory of Crop Genomics and Molecular Breeding, Zhongshan Biological Breeding Laboratory, Key Laboratory of Plant Functional Genomics of the Ministry of Educations, Agricultural College of Yangzhou University, Yangzhou 225009, China; yujialeng@yzu.edu.cn (Y.-J.L.)
[2] Jiangsu Co-Innovation Center for Modern Industrial Technology of Grain Crops, Jiangsu Key Laboratory of Crop Genetics and Physiology, Yangzhou University, Yangzhou 225009, China
[3] Yangzhou Modern Seed Innovation Institute, Gaoyou 225600, China
[4] Joint International Research Laboratory of Agriculture and Agri-Product Safety, the Ministry of Education of China, Yangzhou University, Yangzhou 225009, China
* Correspondence: skjin@yzu.edu.cn (S.-K.J.); jpgao@yzu.edu.cn (J.-P.G.)
† These authors contributed equally to this work.

Abstract

Leaves represent an important organ in plant photosynthesis, and moderately rolled leaves would be beneficial in establishing an ideal plant architecture and thereby increasing rice yields. In this study, a stable inherited rolled leaf mutant was obtained via ethyl methanesulfonate (EMS) mutagenesis from *japonica* variety WYJ27, which was named *rll2* (*rolling leaf 2*). *rll2* showed a leaf-rolling phenotype at the seedling stage, which increased with growth. Compared with the wild type, the leaves at all levels of *rll2* were significantly shorter and narrower, and the leaf-rolling index gradually decreased from the highest leaf to the third-highest leaf. Semi-thin sections showed that the bulliform cells of *rll2* were significantly larger than those of the wild type, and the number of cells was significantly higher than that of the wild type. Genetic analysis showed that *rll2* is controlled by a pair of recessive nuclear genes. Map-based cloning revealed that *RLL2* encodes a conserved and plant-specific calpain-like cysteine proteinase. *RLL2* was mainly expressed in young roots, shoots, spikelets, and panicles. Transcriptome sequencing showed that a total of 104 genes were differentially expressed in the wild type and *rll2*. Moreover, several transcription factor genes were significantly altered in the *rll2* mutant. Taken together, our findings indicate that *RLL2* plays an important role in leaf rolling by regulating bulliform cells, which may be useful in breeding rice with an ideal plant architecture.

Keywords: rice; rolling leaf; bulliform cells; genetic analysis; map-based cloning; *RLL2*

1. Introduction

Leaves represent the main site of photosynthesis in plants and provide energy for plant growth. As an important part of plant architecture, leaf morphology is closely related to rice yields [1]. Moderate leaf rolling not only contributes to improving light acceptance, delaying leaf senescence, and accelerating the accumulation of dry matter but also helps to improve root system activity and strengthen lodging resistance [2,3]. Therefore, the study of leaf rolling has high practical value in high-yield rice breeding.

Leaf development is a complex process comprising cell division and expansion, axis determination, and tissue differentiation and specification [4]. In rice, leaf development involves three stages: the initiation of leaf primordia, polarity establishment and maintenance, and leaf flattening and intercalary growth [5,6]. The leaf primordium originates from the peripheral zone of the apical shoot meristem (SAM) [7], develops along the adaxial–abaxial, medial–lateral, and apical–basal polarity axes, and finally forms mature leaves [8,9]. This developmental process is regulated by complex regulatory networks involving numerous functional genes, transcription factors, phytohormones, and microRNAs [1,3]. To date, many genes controlling leaf rolling have been identified in rice, such as *SHALLOT-LIKE1/ROLLED LEAF 9* (*SLL1/RL9*) [10,11], *SHALLOT-LIKE1* (*SLL2*) [12], *SEMI-ROLLED LEAF 1* (*SRL1*) [13,14], *SEMI-ROLLED LEAF 1* (*SRL2*) [2], *ABAXIALLY CURLED LEAF 1* (*ACL1*) [15], *ABAXIALLY CURLED LEAF 2* (*ACL2*) [15], *NARROW AND ROLLED LEAF 1* (*NRL1*) [16], *NARROW LEAF 7* (*NAL7*) [17], *Rolling-leaf14* (*RL14*) [18], *ADAXIALIZED LEAF 1* (*ADL1*) [19], *ARGONAUTE 1b* (*AGO1b*) [20], *Rolled and Erect Leaf 1* (*REL1*) [21], *lateral organ boundaries domain* (*LBD*) gene *LBD3-7* [22], zinc finger homeodomain class homeobox gene *OsZHD1* [23], class IV homeodomain gene *CFL1* [24], class III HD-Zip gene *OsHOX32* [25], *RICE OUTERMOST CELLSPECIFIC GENE* (*Roc*) family gene *Roc5* [26], and *Roc8* [27]. Most of these genes regulate leaf rolling by changing the morphology of leaf bulliform cells, sclerenchyma cells, cells in vascular bundles, cuticle, epidermal cells, and mesophyll cells.

Bulliform cells, also called hygroscopic cells or motor cells, are among the most important cell structures and are found on the adaxial epidermis of the leaf. A change in osmotic pressure in bulliform cells can cause leaf rolling. Advances in research have suggested that leaf rolling is primarily caused by bulliform cell changes in rice [21]. For example, *SLL1* encodes a SHAQKYF-class MYB family transcription factor. The *sll1* mutant shows a leaf-rolling phenotype due to the formation of bulliform cells on the abaxial epidermis [10]. *SRL1* encodes a putative glycosylphosphatidylinositol-anchored protein, which causes adaxial rolling in leaves by inhibiting the formation of bulliform cells [13]. *REL1* encodes a high-degree conservation and unknown-function protein in monocot plants. The *rel1* mutant shows a leaf rolling due to an increase in the size and number of bulliform cells [21]. Although many genes relating to leaf rolling have been identified, the molecular mechanisms behind leaf rolling in rice are not yet fully understood. In the present study, we identified and characterized a rolled-leaf mutant, named *rolling leaf 2* (*rll2*), from a *japonica* variety Wuyunjing27 (WYJ27) EMS mutant library. Using a map-based cloning method, we cloned the *RLL2* gene and found that it encodes a conserved and plant-specific calpain-like cysteine proteinase, allelic to the *ADL1* gene. The loss of *RLL2* function leads to an increase in the number and size of bulliform cells on the adaxial side of the leaf, resulting in abaxially rolled leaves. This study enhances our understanding of the role of *RLL2/ADL1* in leaf rolling.

2. Materials and Methods

2.1. Plant Materials

The rice *rll2* mutant was obtained from ethyl methanesulfonate-treated (EMS) *japonica* cultivar Wuyunjing27 (WYJ27). An F_2 segregation population was obtained by crossing *rll2* with an *indica* cultivar IR36. WYJ27, IR36, *rll2*, and F_2 segregation populations were germinated and sown on Yangzhou University's experimental farms in Lingshui (110°00′ E, 18°31′ N) and Yangzhou (119′ 42 E, 32°39′ N) during the rice-growing season. After 30 days, the seedlings were transplanted into a field at a density of 18 cm × 18 cm. About 150 kg N ha^{-1} (as urea), 130 kg K_2O ha^{-1}, and 60 kg P_2O_5 ha^{-1} were added to

each field. Field management, including irrigation and pest control, followed normal agricultural practices.

2.2. Measurement of Leaf-Rolling Index and Agronomic Traits

The leaf-rolling index (LRI) was calculated using the following formula: LRI = (Lw − Ln)/Lw × 100% [28]. Lw was defined as the largest leaf width in the fully expanded leaves; Ln was defined as the natural distance of the leaf margins. The plant height (PH), tiller number (TN), primary branch number (PBN), secondary branch number (SBN), and grain number per panicle (GNPP) were measured at 25 days after heading. The plant height was measured from the base to the tip of the tallest panicle. The panicle at the highest point on the plant was selected to investigate the grain number. Except for two marginal plants on each side, twenty independent plants were randomly selected to score the phenotypic data. The rice grains were harvested at 35 days after flowering, dried in the sun, and then transferred to a room-temperature environment. Once the physical and chemical properties were stable, the grain shape traits, including grain length (GL), grain width (GW), and thousand-grain weight (TGW), were determined using the WSeen SC-G automatic seed testing system and thousand-grain weight analysis system (Hangzhou WSeen Detection Technology Co., Ltd., Hangzhou, China). About 150–200 grains were evaluated. Grain thickness (GT) was measured using a digital vernier caliper. A total of ten grains were used to measure GT.

2.3. Histology and Microscopic Observation

Hand-cut sections of WT and *rll2* leaves (about 35 days after sowing) were observed on a slide with an OLYMPUS SZX16 stereomicroscope (Olympus Corporation, Tokyo, Japan). To observe leaf anatomy in detail, young leaves were fixed in a formalin–acetic acid–alcohol (FAA) solution (50% ethanol, 5% formaldehyde, 5% glacial acetic acid = 18:1:1 *v*:*v*:*v*) at 4 °C overnight. After dehydration in serial concentrations of ethanol (50%, 70%, 90%, 100%, 100%), they were infiltrated and embedded in Technovit 7100 resin (Heraeus Kulzer, Hanau, Germany). Sectioning (3 μm) was conducted with the Leica RM2265 (Leica, Wetzlar, Germany). Slices were spread on a platform at 42 °C and stained using toluidine blue at room temperature for 15 min. Observations and photography were carried out using the Leica DM2500 LED light microscope (Leica, Wetzlar, Germany).

2.4. Genetic Analysis and Map-Based Cloning of RLL2

An F_2 mapping population was derived from a cross between *rll2* and IR36. A total of 859 individuals with the mutant phenotype were used for fine mapping. The *rll2* loucs was first mapped to an interval between markers M1 and M2 on chromosome 2. Further, it was narrowed to a 225 kb region between maker M6 and M7. The molecular markers were developed with Primer Premier 5 software (Premier Biosoft International, Palo Alto, CA, USA) based on sequence differences between the *japonica* variety Nipponbare and the *indica* variety 93-11. The molecular markers used in this study are listed in Table S1. Gene prediction and sequence analysis were performed using the Rice Genome Annotation Project (http://rice.uga.edu/index.shtml (accessed on 3 September 2023)) databases. For the identification of the candidate gene, the corresponding DNA fragments were amplified from WYJ27 and *rll2* using Kod FX (TOYOBO, Osaka, Japan) and sequencing using Applied Biosystems 3730xl DNA Analyzers (Applied Biosystems, Carlsbad, CA, USA). The primers for sequencing in this study are listed in Table S2.

2.5. Phylogenetic Analysis

The amino acid sequences of the RLL2 homological proteins were retrieved by searching the NCBI BLAST database (https://blast.ncbi.nlm.nih.gov/Blast.cgi (accessed on 10 June 2024)) using the total amino acid sequences of RLL2. Phylogenetic trees were con-

structed with the aligned protein sequences using MEGA 12 software based on the neighbor-joining statistical method with the following parameters: Poisson model, uniform rate, pairwise deletion, and bootstrap (1000 replicates) [29].

2.6. RNA Extraction and qRT-PCR

The total RNA of various tissues in WYJ27 and *rll2* was extracted using the RNAprep Pure Plant kit (TIANGEN, Beijing, China), and reverse transcription into cDNA was conducted with the PrimeScript™ RT reagent kit with gDNA Eraser (TaKaRa, Shiga, Japan) according to the manufacturer's instructions. The cDNA was used for real-time RT-PCR using the TB Green® Premix EX Taq™ kit (TaKaRa, Shiga, Japan) and gene-specific primers (Table S3) with a CFX Connect™ Real-Time System (Bio-Rad Laboratories, Hercules, CA, USA). The rice *ACTIN* gene was used as an internal standard to normalize the expression level of *RLL2* and other tested genes. The relative expression levels were calculated based on the comparative Ct method using the $2^{-\Delta\Delta Ct}$ formula [30].

2.7. RNA-Seq Analysis

Twenty days after sowing, the flat leaves of wild-type WYJ27 and the rolled leaves of the mutant *rll2* were selected for transcriptome sequencing, and each sample was pooled for total RNA isolation with three biological replicates. Total RNA was extracted using the RNAprep Pure Plant kit (TIANGEN, Beijing, China) according to the manufacturer's protocol. Transcriptome sequencing was performed by Biomarker Technologies Corporation using the Illumina HiSeq2500 system (Illumina, San Diego, CA, USA). Transcriptome assembly was performed according to the protocol described previously [31]. In brief, the raw RNA-Seq data were processed using in-house Perl scripts to trim adapters and low-quality sequences and then assembled using Trinity based on left.fq and right.fq [32]. Differential expression analysis was performed using the DESeq R package (version 1.40.0). The fold change (FC) ≥ 2 and false discovery rate (FDR) < 0.01 were used as the screening criteria. Gene function was annotated based on the KEGG (Kyoto Encyclopedia of Genes and Genomes) and GO (Gene Ontology) databases. GO and KEGG pathway enrichment analysis was performed using BMKCloud (www.biocloud.net).

2.8. Statistical Analysis

Data are presented as the mean $\pm$ standard deviations of multiple biological replicates ($n \geq 3$). Significant differences were assessed using Student's t test. $p < 0.05$ and $p < 0.01$ were defined as significant and highly significant, respectively.

3. Results

3.1. Phenotypic Characterization of the rll2 Mutant

The *rll2* mutant was identified by screening an ethyl methanesulfonate (EMS) mutant library for the 'Wuyunjing 27' (WYJ27) background and had abaxially rolled leaves throughout the entire growth period (Figure 1A–C). The leaf-rolling index (LRI) of *rll2* at the heading stage from the highest (flag leaf) to the third-highest leaf was 60.9%, 51.9%, and 26.9%, respectively, whereas wild-type WYJ27 leaves were nearly flat (Figure 1H). *rll2* also displayed short and narrow leaves; the length and width of the highest, second-highest, third-highest, and fourth-highest leaves in *rll2* were 80.1%, 87.1%, 93.6%, and 74.8% and 94.0%, 94.5%, 89.2%, and 89.0% of those for the wild type, respectively (Figure 1F,G). Furthermore, the yield traits including plant height, internode length, tillering number, primary branch number, secondary branch number, grain number per panicle, grain length, grain width, and thousand-grain weight in *rll2* were significantly lower than those of

the wild type (Figure 1D,E; Table 1). Taken together, these results indicate that *RLL2* has pleiotropic effects in rice growth and development.

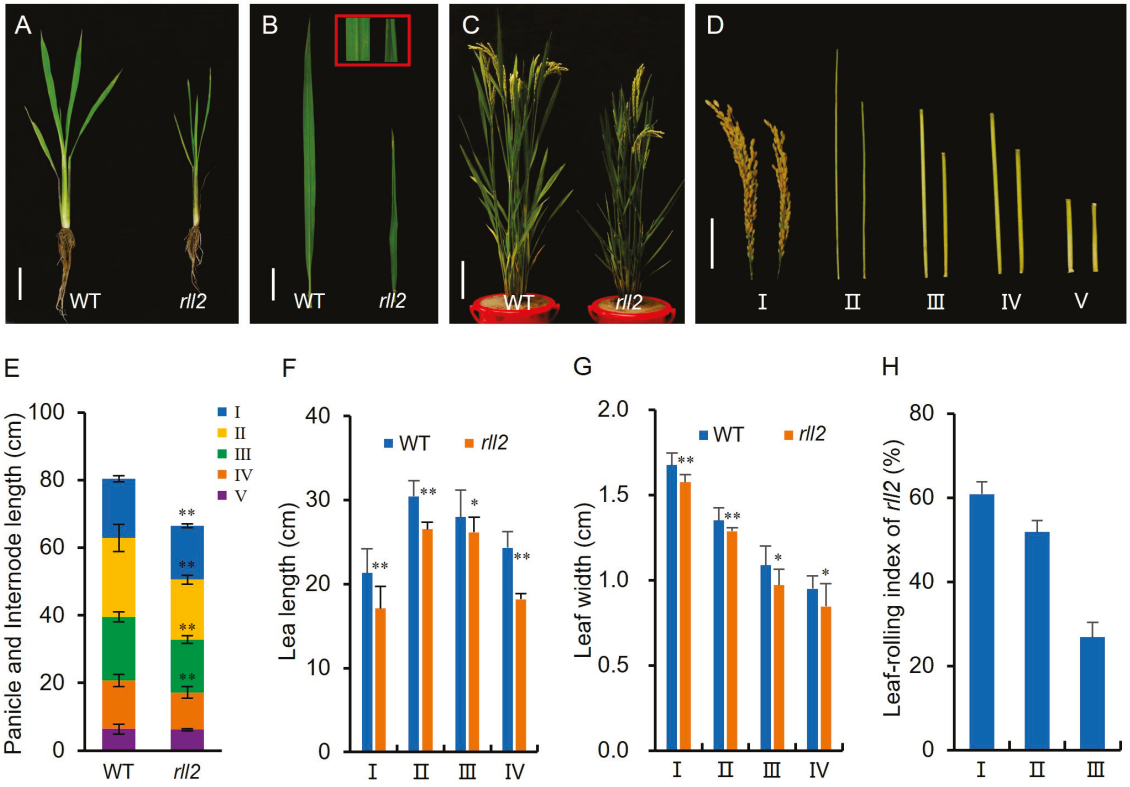

Figure 1. Comparison of wild-type and *rll2* phenotypes. (**A**) Phenotype of the wild type (WYJ27, left) and *rll2* mutant (right) at 35 days after sowing. Scale bar = 5 cm. (**B**) Difference in leaf phenotype between the wild type (left) and *rll2* (right) mutant 35 days after sowing. Scale bar = 2 cm. (**C**) Phenotype of the wild type (WYJ27, left) and *rll2* mutant (right) 10 days after heading. Scale bar = 5 cm. (**D**) Phenotype of panicles and internodes between the wild type (WYJ27, left) and *rll2* mutant (right) at the mature stage. Scale bar = 5 cm. I: panicle, II: highest internodes, III: second-highest internodes, IV: third-highest internodes, V: fourth-highest internodes. (**E**) Statistical analysis of panicle and internode length between the wild type and the *rll2* mutant at the mature stage. F and G. Statistical analysis of leaf length (**F**) and leaf width (**G**) 10 days after heading. (**H**) Leaf-rolling index of the *rll2* mutant 10 days after heading. I: Highest leaf, II: second-highest leaf, III: third-highest leaf, IV: fourth-highest leaf. * Significant difference at $p < 0.05$ determined via *t*-test; ** Significant difference at $p < 0.01$ determined via *t*-test.

Table 1. Comparison of major agronomic traits between the wild type and *rll2*.

Traits	Wild Type	*rll2*
Plant height (cm)	80.4 ± 5.56	66.5 ± 1.02 **
Tillering number	9.6 ± 1.19	9.0 ± 0.76 **
Primary branch number	11.8 ± 1.16	8.6 ± 0.92 **
Secondary branch number	33.0 ± 2.00	24.6 ± 4.93 **
Grain number per panicle	182.0 ± 12.76	135.8 ± 23.36 **
Grain length (mm)	7.6 ± 0.37	7.4 ± 0.28 **
Grain width (mm)	3.5 ± 0.30	3.4 ± 0.30 **
Grain thickness (mm)	2.4 ± 0.03	2.4 ± 0.02
Thousand-grain weight (g)	28.6 ± 0.46	26.1 ± 0.36 **

** Significant difference at $p < 0.01$ determined via *t*-test.

3.2. Bulliform Cell Number and Size Are Increased in *rll2*

To investigate the cause of abaxial leaf rolling in *rll2*, we analyzed cross-sections of leaves f at 35 days after sowing (Figure 2A–D). In contrast to the wild type, more bulliform cells occurred between two vascular bundle ridges in the adaxially leaf. The bulliform cell number for *rll2* was 7.0 ± 0.8 cells, which was significantly higher than that of the wild type (4.3 ± 0.5) (Figure 2E). Furthermore, the bulliform cell area of *rll2* was also significantly higher than that of the wild type (Figure 2F). Those results suggest that the abaxial leaf rolling in *rll2* may be caused by an increase in bulliform cell number and size on the adaxial surface of leaves.

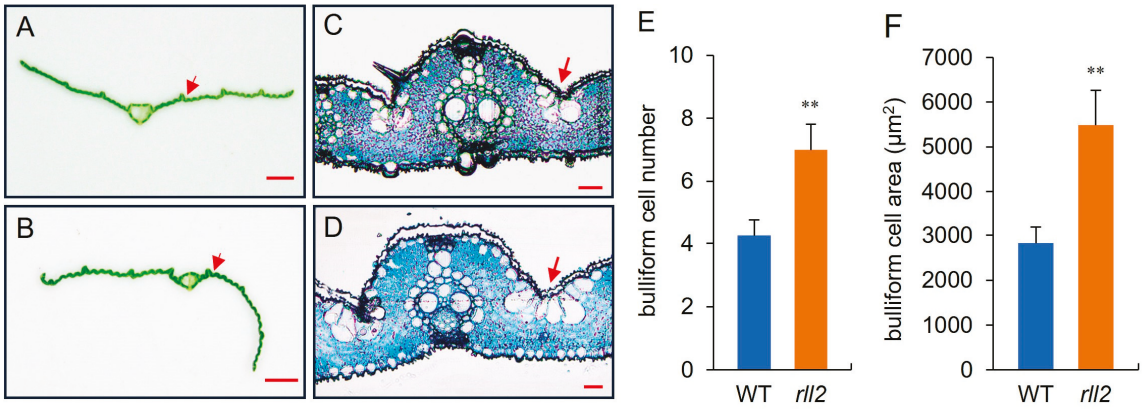

Figure 2. *rll2* shows an increase in bulliform cell number and size. (**A**,**B**). Cross-section of wild-type (**A**) and *rll2* (**B**) leaves 35 days after sowing. WYJ27, scale bar = 2 mm. (**C**,**D**). Semi-thin section of wild-type (**C**) and *rll2* (**D**) leaves 35 days after sowing. WYJ27, scale bar = 100 μm. The red arrow indicates bulliform cells. (**E**,**F**). The numbers (**E**) and areas (**F**) of bulliform cells in WYJ27 and *rll2*. Data are shown as means ± standard deviation. ** Significant difference at $p < 0.01$ determined via *t*-test.

3.3. Map-Based Cloning of *RLL2*

To isolate *RLL2* via map-based cloning, we crossed the *rll2* mutant with an *indica* cultivar, IR36. All the F_1 hybrids exhibited a WT morphological phenotype. In the F_2 segregating populations, the WT morphological phenotype and rolled-leaf phenotype showed a typical segregation ratio of 3:1 (Table 2). This result indicates that *rll2* is controlled by a single recessive nuclear gene. The *RLL2* locus was preliminarily mapped to the chromosome 2 between markers M1 and M2 (Figure 3A). By using a large population of 859 homozygous mutant individuals, *RLL2* was narrowed down to a 225 kb genomic region between markers M6 and M7 on BAC clone AP004161 (Figure 3A). According to the annotations of the rice genome database (Rice Genome Annotation Project, https://rice.uga.edu/), this region comprises twenty putative genes with annotated functions. A known gene controlling leaf rolling, *ADL1* (*LOC_Os02g47970*), was identified in these ORFs. The *adl1* mutant showed abaxially rolled leaves due to an increase in the size and number of bulliform cells. The *rll2* mutant displayed a similar phenotype with *adl1*. DNA sequencing analysis of this ORF revealed the presence of a single nucleotide substitution (C→T) on the 27th exon of *LOC_Os02g47970* in *rll2* compared to the wild type, which resulted in an Arg-to-Cys substitution (Figure 3B,C). Moreover, the expression level of *LOC_Os02g47970* in *rll2* was significantly decreased (Figure 3D). We therefore inferred that *ADL1* was the gene controlling the *rll2* mutant phenotype.

Table 2. Genetic analysis of *rll2*.

Cross Combination	F_1		F_2		$\chi 2$ (3:1)
	Wild-Type Phenotype	*rll2* Phenotype	Wild-Type Phenotype	*rll2* Phenotype	
rll2/IR36	36	0	483	169	0.2945
IR36/*rll2*	28	0	363	109	0.9153

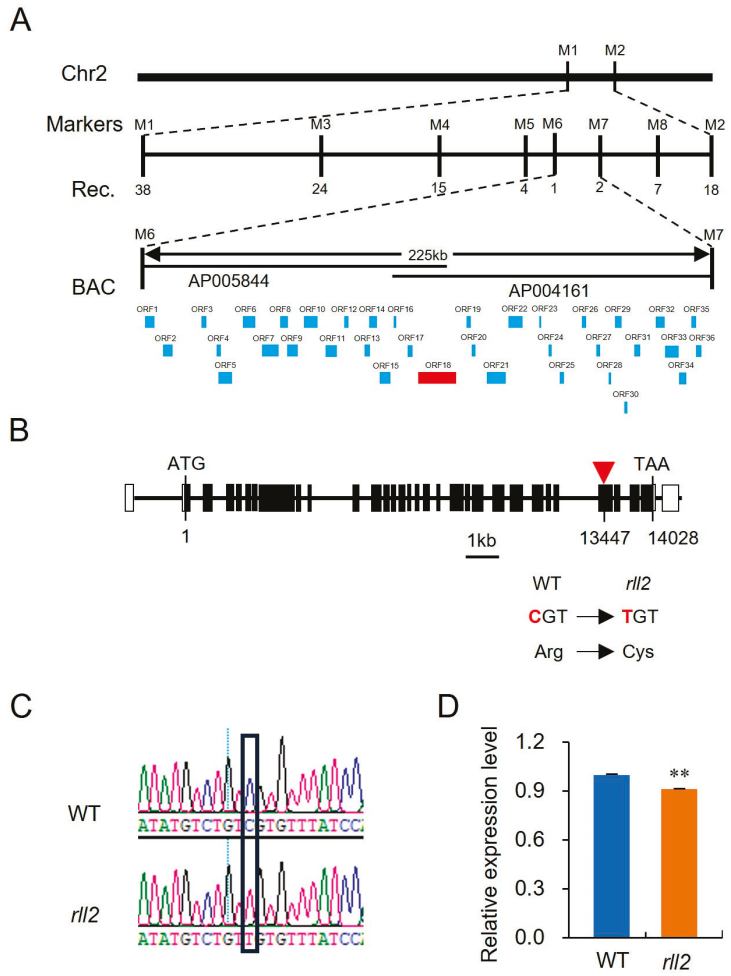

Figure 3. Map-based cloning of *RLL2*. (**A**) Fine mapping of *RLL2*. The *RLL2* locus was mapped to a 225 kb region on chromosome 2. (**B**) Schematic diagram of *RLL2*. Black rectangles represent exons. White rectangles represent 5′ and 3′-UTR. The red inverted triangle represents the mutant site. (**C**) Sequencing analysis of ORF18 between WYJ27 and *rll2*. (**D**) The expression levels of LOC_Os02g47970 in WYJ27 and the *rll2* mutant. Each sample comprised three independent experiments. ** $p < 0.01$.

3.4. RLL2 Encodes a Conserved and Plant-Specific Protein

Sequence analysis indicated that *RLL2* cDNA is 6489 bp in length and encodes a protein of 2162 amino acid residues, including 22 transmembrane regions, 1 CysPc domain, and 1 calpain_III domain (Figure 4A). We performed a BLASTP search against the NCBI non-redundant protein database, revealing 31 proteins from other plant species with significant homology (≥70% identity at the amino acid level) to RLL2, which suggests that RLL2 is a plant-specific protein and shares conserved biochemical functions. To elucidate the evolutionary relationships among RLL2 proteins, a phylogenetic tree was constructed using the neighbor-joining method in MEGA 12 [29]. The 32 proteins were classified into three clades (Figure 4B). Clade A belongs to Gramineae and shows high identity (>90%) with the RLL2 protein. The identity of clade B and clade C with the RLL2 protein was lower than

that of clade A, which ranged from 76.26% to 81.16%. This result indicates that the RLL2 protein is very conserved in evolution.

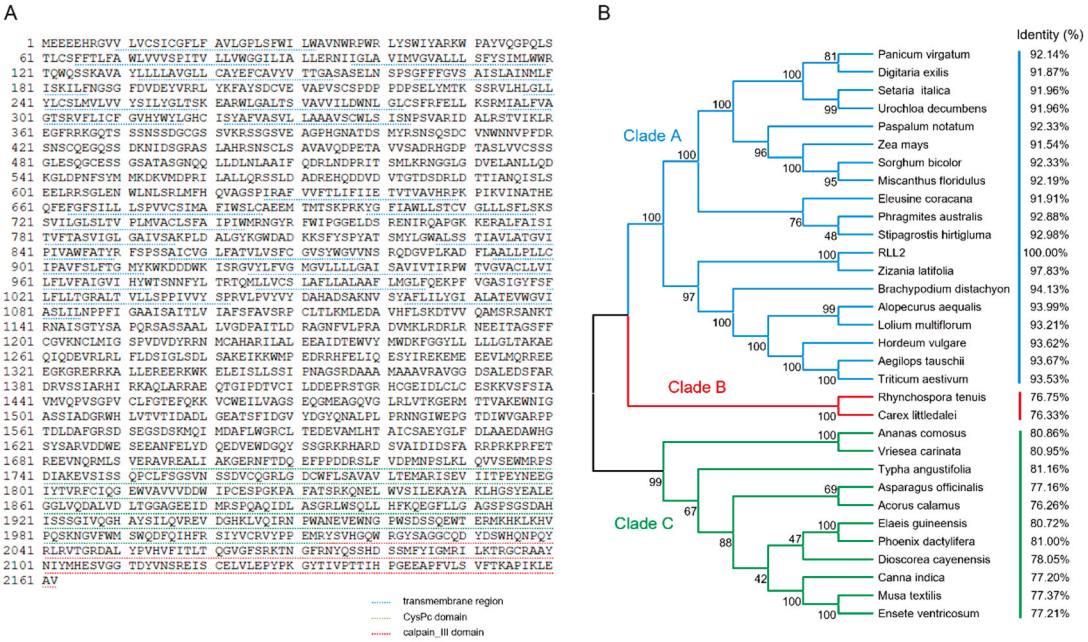

Figure 4. Amino acid sequence and phylogenetic analysis of RLL2. (**A**) Amino acid sequence of RLL2. The blue dotted line, red dotted line, and green dotted line represent the transmembrane region, CysPc domain, and calpain_III domain, respectively. (**B**) Phylogenetic relationships among RLL2-like proteins.

3.5. Expression Patterns of RLL2

To determine the expression patterns of *RLL2* in rice, quantitative real-time RT-PCR (qRT-PCR) was used to detect the expression levels of *RLL2* in WYJ27 issues, such as young roots, shoots, stems, leaves, leaf sheaths, spikelets, and panicles. The results showed that *RLL2* was expressed in all tissues, with high expression in young roots, shoots, spikelet and panicles and low expression in stems and leaf sheaths (Figure 5).

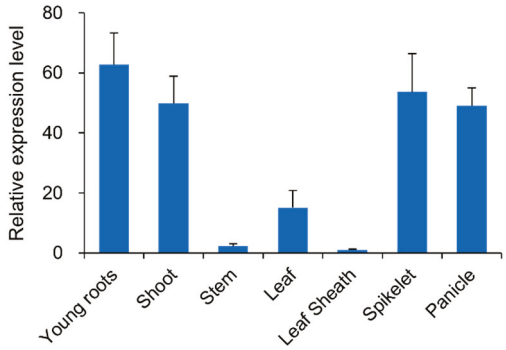

Figure 5. Expression pattern of *RLL2*. Each sample comprised three independent experiments.

3.6. GO and KEGG Analyses of Rolling Leaf Regulation via RLL2

To further unravel the function of *RLL2* in rice, leaves from wild-type and *rll2* plants at 20 d were used for transcriptome analysis. A total of 104 differentially expressed genes (DEGs) were found; 42 genes were up-regulated and 62 were down-regulated in *rll2* plants (Figure 6A,B; Table S5). Among these genes, 12 transcription factor genes were found, 10 of which have been reported. We measured the expression levels of these genes using qRT-PCR, and the results showed that the expression levels of three genes

(*OsbHLH056*, *OsDREB1B*, and *OsWRKY71*) were significantly increased and those of seven genes (*OsDREB1A*, *OsAP2-39*, *PCF2*, *OsERF74*, *OsNAC5*, *OsNAC19*, and *LOC_Os05g50340*) were significantly reduced in *rll2* leaves (Figure S1; Table S5).

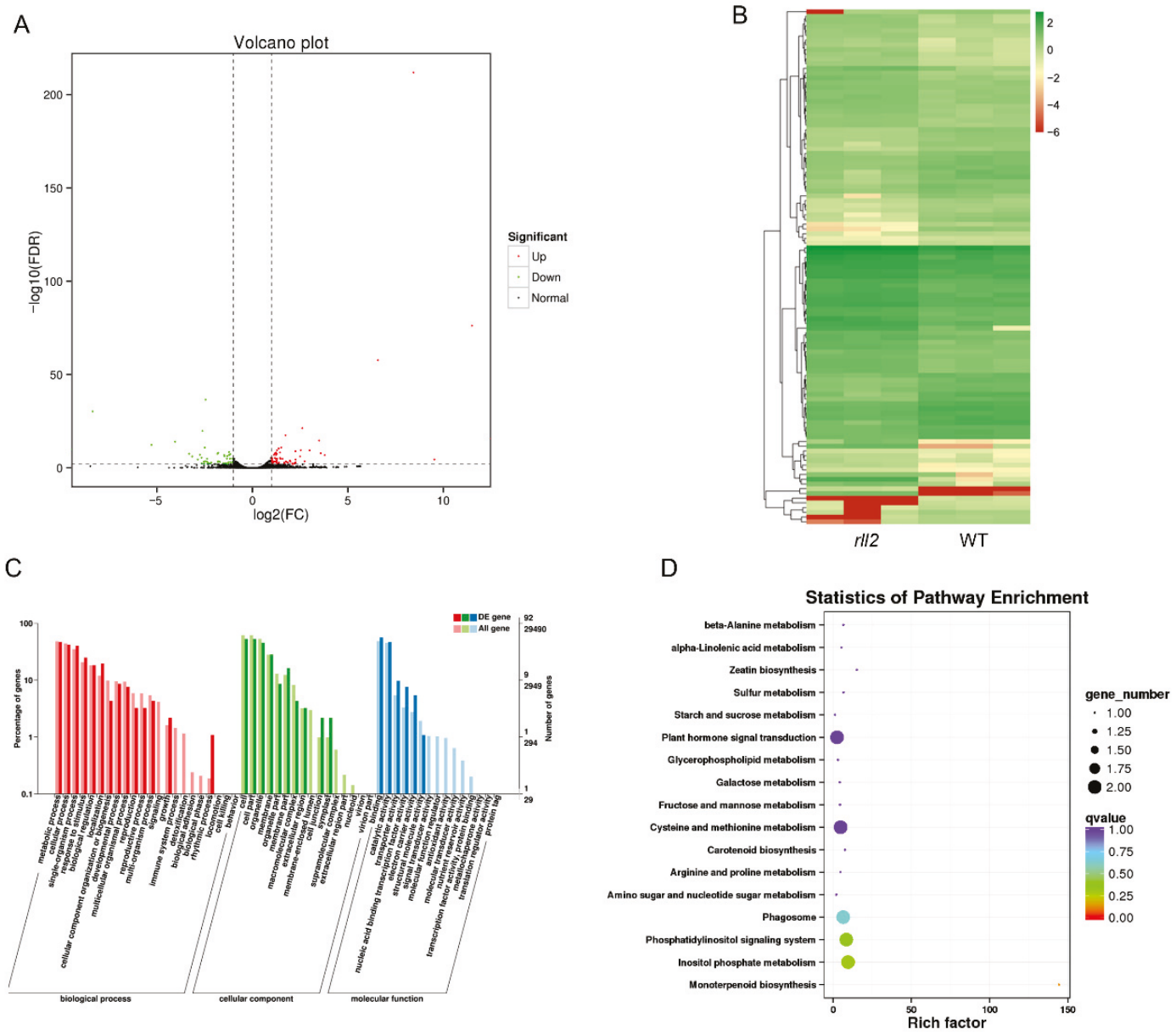

Figure 6. Transcriptome analysis of the wild type and *rll2*. (**A**) Volcano map of differentially expressed genes between the wild type and *rll2*. (**B**) Cluster diagram of differentially expressed genes between the wild type and *rll2*. (**C**) GO enrichment analysis for the wild type and *rll2*. (**D**) KEGG pathway enrichment analysis for the wild type and *rll2*.

The GO enrichment analysis of DEGs is shown in Figure 6C and Table S6. In the cellular component analysis, DEGs were found to mainly be involved in the cell, cell part, organelle, membrane, and membrane part. In the molecular function analysis, DEGs were found to mainly be involved in binding, catalytic activity, transporter activity, and nucleic acid binding transcription factor activity. In the biological process analysis, DEGs were found to mainly be involved in the metabolic process, cellular process, single-organism process, response to stimulus, localization, and biological regulation. KEGG pathway enrichment analysis showed that the DEGs were mainly concentrated in plant hormone

signal transduction, cysteine and methionine metabolism, phagosome, inositol phosphate metabolism, and the phosphatidylinositol signaling system (Figure 6D).

3.7. RLL2 Affects the Expression Levels of Leaf Development-Related Genes

Leaf development is regulated by several genes, such as *YABBY* genes [33–36]. We measured the expression levels of *YABBY* genes in young leaves via qRT-PCR. Compared with the wild type, *YABBY2* and *YABBY6* were significantly up-regulated in *rll2*, while *YABBY1*, *YABBY3*, *YABBY4*, and *YABBY5* were significantly down-regulated in *rll2* (Figure 7). This result suggests that *rll2* phenotypes may be related to altered transcriptional activity of *YABBY* genes.

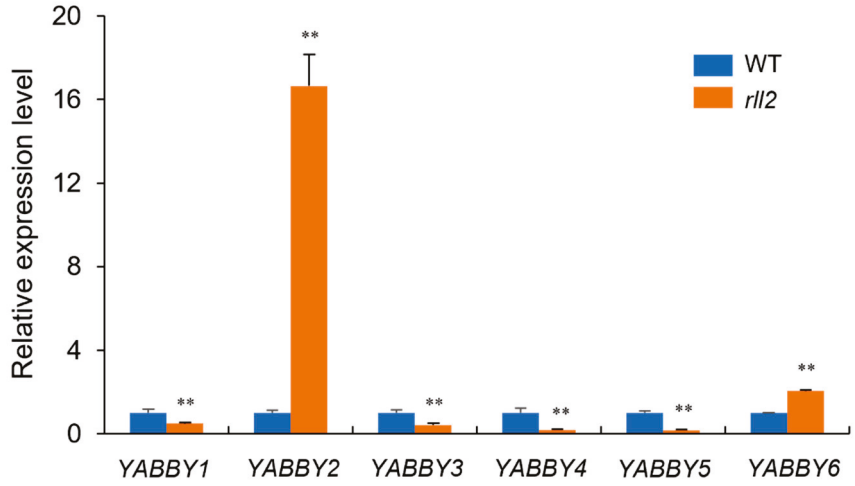

Figure 7. Expression levels of *YABBY* genes in the wild type and *rll2*. Each sample comprised three independent experiments. ** Significant difference at $p < 0.01$ determined via *t*-test.

4. Discussion

4.1. RLL2 Plays an Important Role in Regulating the Size and Number of Leaf Bulliform Cells in Rice

Bulliform cells (motor cells), which are distributed on the upper epidermis of leaves, are the most important cell structures in leaves [27]. Bulliform cells are strongly linked to leaf-rolling phenotypes in rice [37]. Many studies have shown that alternations to bulliform cells arranged on the adaxial surface of the leaf lead to adaxial or abaxial rolling in mature leaves [21]. To date, over 10 genes controlling bulliform cell development have been reported in rice; *ACL1* [15], *ACL2* [15], *NRL1* [16], *NAL7* [17], and *RL14* [18] positively regulate the development of bulliform cells, while *SRL1* [13,14], *ADL1* [19], *OsLBD3-7* [22], *OsZHD1* [23], and *Roc5* [26] negatively regulate the development of bulliform cells. In this study, we identified *RLL2* as a key regulator of leaf rolling. Compared to the wild type, *rll2* showed a higher number and size of bulliform cells, leading to abaxial leaf rolling (Figure 2). Our results strongly suggest that *RLL2* plays a negative role in the formation of bulliform cells on the adaxial leaf surface.

4.2. RLL2 Is a New Allelic Variant of ADL1

Leaves are the main photosynthetic organs in plants. Moderate leaf rolling is considered to be an important part of the ideal rice phenotype, the development of which is of great significance in improving photosynthetic efficiency and grain yields [2,10,38]. However, the molecular mechanisms underlying leaf rolling remain unclear. In this study, we identified the *rll2* mutant from an EMS-mutagenized *japonica* variety, WYJ27 (Figure 1). Using a map-based cloning method, gene sequencing, and qRT-PCR, we found that the

candidate gene is *ADL1*/*LOC_Os02g47970*, which encodes calpain-like cysteine proteinase (Figures 3 and 4). Hibara et al. (2009) reported seven *ADL1* allelic mutants (*adl1-1*, *adl1-2*, *adl1-3*, *adl1-s1*, *adl1-s2*, *adl1-g1*, and *adl1-g2*), which produced a base mutation in exon 30, 26, 4, 26, 19, 27, and 20, respectively, resulting in changes in the amino acids encoded [19]. In our study, we identified an *RLL2* mutation on the 27th exon, with a C to T change (Figure 3B,C), indicating that *RLL2* is a new allelic mutant of *ADL1* [19]. The *rll2* mutant showed a rolling leaf phenotype similar to that of the *adl1* mutant, but there were some phenotypic differences among the *rll2*/*adl1* mutant alleles; for example, the *adl1* mutant showed bulliform cells on the abaxial side of leaves, while the mutant *rll2* did not. *adl1-1*, *adl1-2*, and *adl1-3* showed defects in leaf polarity and leaf primordium insertion in the SAM. *adl1-s1* and *adl1-s2* produced shootless embryos. The embryos of *adl1-g1* and *adl1-g2* stopped growing at the globular stage, and the endosperm lacked a ventral aleurone layer [19]. This indicates that different mutant *RLL2*/*ADL1* alleles have different effects on rice development. In addition, KEGG pathway enrichment analysis showed that cysteine and methionine metabolism genes differed between the wild type and *rll2* (Figure 6D). These changes may impact the function of calpain-like cysteine proteinase in *rll2*. Further investigation is needed to fully understand the role of *RLL2* in rice.

4.3. Transcription Factor Genes Participate in the Development of Leaves in RLL2

Transcription factors (TFs) are a group of DNA-binding proteins that regulate gene expression and are involved in a diverse range of biological processes in plants [39]. In rice, several transcription factors have been reported as being involved in the regulation of leaf rolling; For example, *SLL1* encodes an SHAQKYF-class MYB transcription factor belonging to the KANADI family. It regulates leaf rolling in rice by regulating the development of cells on the abaxial side of the leaf [10]. *Roc8* is a member of the plant-specific homeodomain leucine zipper IV (HD-Zip IV) gene family, encoding a class of homeobox transcription factors. The overexpression of *Roc8* causes leaf rolling on the adaxial side, and its knockout causes leaf rolling on the abaxial side [27]. *OsMYB103L* encodes an R2R3-MYB transcription factor. The overexpression of *OsMYB103L* leads to a rolled-leaf phenotype. Further analysis shows that *OsMYB103L* regulates cellulose synthesis by targeting *CESA* genes, thereby affecting leaf rolling [40]. In our study, the expression levels of 10 transcription factor genes changed in 104 DEGs, indicating that transcription factors play an important role in leaf rolling (Figure S1; Table S5).

YABBY genes are plant-specific transcription factors that play an important role in the regulation of a diverse range of developmental processes, such as the establishment of adaxial–abaxial polarity, laminal expansion, and floral organ development [36,41,42]. Many *YABBY* genes have been studied in monocotyledon plants, and several *YABBY* genes have been cloned in rice. *OsYABBY1* shows homology with *AtYAB2* and *AtYAB5*, is expressed in sclerenchyma, and participates in the development of the stamen, carpel, and meristem [43]. *YAB3* is closely related to maize *ZmYAB14* and *Arabidopsis FILAMENTOUS FLOWER* (*FIL*), which is mainly related to the development of leaves [33]. *OsYABBY4* is involved in the development of the vascular structure [44]. *OsYABBY5* (*TOB1*) plays a vital role in promoting lateral organ development and maintaining meristem organization in the rice spikelet [36]. *DROOPING LEAF* (*DL*), a rice orthologue of CRC, is mainly related to carpel specification and midvein development in rice [45]. In our study, the expression level of *YABBY* genes in the *rll2* mutant was altered. *YABBY2* and *YABBY6* were significantly up-regulated in *rll2*, while *YABBY1*, *YABBY3*, *YABBY4*, and *YABBY5* were significantly down-regulated. In particular, the expression of *YABBY2* was significantly up-regulated (16-fold) in *rll2* (Figure 7). This suggests that the *rll2* phenotype may be related to altered transcriptional activity in *YABBY* genes.

Rice leaf morphology is an important component in achieving the ideal plant architecture and significantly impacts rice yields [1]. Using mutagenesis techniques to identify mutants with moderately rolled leaves is beneficial in breeding crops with the desired architecture [2]. Although our study shows that *RLL2* plays an important role in regulating leaf rolling, more research is needed on, for example, the effect of *RLL2* gene mutation on calpain-like cysteine proteinase activity, how transcription factors genes affect the development of bulliform cells by regulating *RLL2*, and whether certain *RLL2* alleles are preponderant in the improvement of rice leaf morphology. These questions require further study.

5. Conclusions

The *rolling leaf 2* (*rll2*) mutant was obtained through the ethyl methanesulfonate (EMS) mutagenesis of the *japonica* variety WYJ27. The *rll2* mutant displayed abaxially rolled leaves throughout the entire growth period. We demonstrated that *rll2* is a new allele of *ADL1*, which encodes a CysPc domain and calpain_III domain protein. We suggest that the increase in the number and size of bulliform cells is causative of leaf rolling in the *rll2* mutant. Moreover, qRT-PCR showed that the expression of some transcription factor genes changed significantly in *rll2*. Our study provides a novel allelic mutant to explore the function of *RLL2*. At the same time, it provides useful information for furthering the improvement of rice architecture.

Supplementary Materials: The following supporting information can be downloaded at: https://www.mdpi.com/article/10.3390/plants14213373/s1, Figure S1. Expression levels of twelve transcription factor genes in wild type and *rll2*; Table S1. The primers used for gene mapping; Table S2. The primer used for *RLL2* gene sequencing; Table S3. The primer used for qRT-PCR; Table S4. The candidate gene for *RLL2* between marker M6 and M7; Table S5. Differentially expressed gene in wild type and *rll2*; Table S6. GO enrichment analysis of differentially expressed genes in *rll2*. References [46–81] are cited in the Supplementary Materials.

Author Contributions: Y.-J.L., and J.-P.G. proposed the concept; Y.-J.L., S.-Y.Q., W.-Y.Z., S.L., T.T., H.-C.Z., W.-X.C., Y.-F.Z., H.-B.L., Q.-Q.Y., M.-Q.Z., Z.-D.Y., F.-X.X., H.-D.H., X.W., S.-K.J., and X.-L.C. collected the phenotypic data and performed the field experiments, data collection, and analysis; Y.-J.L. drafted the manuscript; Y.-J.L. and J.-P.G. revised and finalized the manuscript. All authors have read and agreed to the published version of the manuscript.

Funding: This work was supported by grants from Jiangsu Province Government (BE2022336), the Natural Science Foundation of the Jiangsu Higher Education Institutions of China (22KJA210003), the open funds of the Jiangsu Key Laboratory of Crop Genomics and Molecular Breeding (PL202403), and the Priority Academic Program Development of Jiangsu Higher Education Institutions.

Data Availability Statement: The original contributions presented in this study are included in the article/Supplementary Material. Further inquiries can be directed to the corresponding authors.

Conflicts of Interest: The authors declare no conflicts of interest.

References

1. Gong, X.; Chen, J.; Chen, Y.; He, Y.; Jiang, D. Advancements in Rice Leaf Development Research. *Plants* **2024**, *13*, 904. [CrossRef] [PubMed]
2. Liu, X.; Li, M.; Liu, K.; Tang, D.; Sun, M.; Li, Y.; Shen, Y.; Du, G.; Cheng, Z. *Semi-Rolled Leaf2* modulates rice leaf rolling by regulating abaxial side cell differentiation. *J. Exp. Bot.* **2016**, *67*, 2139–2150. [CrossRef] [PubMed]
3. Wang, J.; Xu, J.; Wang, L.; Zhou, M.; Nian, J.; Chen, M.; Lu, X.; Liu, X.; Wang, Z.; Cen, J.; et al. SEMI-ROLLED LEAF 10 stabilizes catalase isozyme B to regulate leaf morphology and thermotolerance in rice (*Oryza sativa* L.). *Plant Biotechnol. J.* **2023**, *21*, 819–838. [CrossRef]

4. Moulia, B. Leaves as shell structures: Double curvature, auto stresses, and minimal mechanical energy constraints on leaf rolling in grasses. *J. Plant Growth Regul.* **2000**, *19*, 19–30. [CrossRef]
5. Wang, H.; Kong, F.; Zhou, C. From genes to networks: The genetic control of leaf development. *J. Integr. Plant Biol.* **2021**, *63*, 1181–1196. [CrossRef]
6. Du, F.; Guan, C.; Jiao, Y. Molecular mechanisms of leaf morphogenesis. *Mol. Plant* **2018**, *11*, 1117–1134. [CrossRef]
7. Shen, W.; Sun, J.; Xiao, Z.; Feng, P.; Zhang, T.; He, G.; Sang, X. Narrow and stripe leaf 2 regulates leaf width by modulating cell cycle progression in rice. *Rice* **2023**, *16*, 20–31. [CrossRef]
8. Hasson, A.; Blein, T.; Laufs, P. Leaving the meristem behind: The genetic and molecular control of leaf patterning and morphogenesis. *Comptes Rendus Biol.* **2010**, *333*, 350–360. [CrossRef]
9. Moon, J.; Hake, S. How a leaf gets its shape. *Curr. Opin. Plant Biol.* **2011**, *14*, 24–30. [CrossRef]
10. Zhang, G.H.; Xu, Q.; Zhu, X.D.; Qian, Q.; Xue, H.W. SHALLOT-LIKE1 is a KANADI transcription factor that modulates rice leaf rolling by regulating leaf abaxial cell development. *Plant Cell* **2009**, *21*, 719–735. [CrossRef]
11. Yan, S.; Yan, C.J.; Zeng, X.H.; Yang, Y.C.; Fang, Y.W.; Tian, C.Y.; Sun, Y.W.; Cheng, Z.K.; Gu, M.H. *ROLLED LEAF 9*, encoding a GARP protein, regulates the leaf abaxial cell fate in rice. *Plant Mol. Biol.* **2008**, *68*, 239–250. [CrossRef]
12. Zhang, J.J.; Wu, S.Y.; Jiang, L.; Wang, J.L.; Zhang, X.; Guo, X.P.; Wu, C.Y.; Wan, J.M. A detailed analysis of the leaf rolling mutant *sll2* reveals complex nature in regulation of bulliform cell development in rice (*Oryza sativa* L.). *Plant Biol.* **2015**, *17*, 437–448. [CrossRef]
13. Xiang, J.J.; Zhang, G.H.; Qian, Q.; Xue, H.W. *Semi-rolled leaf 1* encodes a putative glycosylphosphatidylinositol-anchored protein and modulates rice leaf rolling by regulating the formation of bulliform cells. *Plant Physiol.* **2012**, *159*, 1488–1500. [CrossRef]
14. Li, W.Q.; Zhang, M.J.; Gan, P.F.; Qiao, L.; Yang, S.Q.; Miao, H.; Wang, G.F.; Zhang, M.M.; Liu, W.T.; Li, H.F.; et al. CLD1/SRL1 modulates leaf rolling by affecting cell wall formation, epidermis integrity and water homeostasis in rice. *Plant J.* **2017**, *92*, 904–923. [CrossRef]
15. Li, L.; Shi, Z.Y.; Li, L.; Shen, G.Z.; Wang, X.Q.; An, L.S.; Zhang, J.L. Overexpression of *ACL1* (*abaxially curled leaf 1*) increased bulliform cells and induced abaxial curling of leaf blades in rice. *Mol. Plant* **2010**, *3*, 807–817. [CrossRef]
16. Hu, J.; Zhu, L.; Zeng, D.; Gao, Z.; Guo, L.; Fang, Y.; Zhang, G.; Dong, G.; Yan, M.; Liu, J.; et al. Identification and characterization of *NARROW AND ROLLED LEAF 1*, a novel gene regulating leaf morphology and plant architecture in rice. *Plant Mol. Biol.* **2010**, *73*, 283–292. [CrossRef] [PubMed]
17. Fujino, K.; Matsuda, Y.; Ozawa, K.; Nishimura, T.; Koshiba, T.; Fraaije, M.W.; Sekiguchi, H. *NARROW LEAF 7* controls leaf shape mediated by auxin in rice. *Mol. Genet. Genomics* **2008**, *279*, 499–507. [CrossRef] [PubMed]
18. Fang, L.K.; Zhao, F.M.; Cong, Y.F.; Sang, X.; Du, Q.; Wang, D.; Li, Y.; Ling, Y.; Yang, Z.; He, G. Rolling-leaf14 is a 2OG-Fe (II) oxygenase family protein that modulates rice leaf rolling by affecting secondary cell wall formation in leaves. *Plant Biotechnol. J.* **2012**, *10*, 524–532. [CrossRef] [PubMed]
19. Hibara, K.; Obara, M.; Hayashida, E.; Abe, M.; Ishimaru, T.; Satoh, H.; Itoh, J.I.; Nagato, Y. The *ADAXIALIZED LEAF 1* gene functions in leaf and embryonic pattern formation in rice. *Dev. Biol.* **2009**, *334*, 345–354. [CrossRef]
20. Li, Y.; Yang, Y.; Liu, Y.; Li, D.; Zhao, Y.; Li, Z.; Liu, Y.; Jiang, D.; Li, J.; Zhou, H. Overexpression of *OsAGO1b* induces adaxially rolled leaves by affecting leaf abaxial sclerenchymatous cell development in rice. *Rice* **2019**, *12*, 60. [CrossRef]
21. Chen, Q.; Xie, Q.; Gao, J.; Wang, W.; Sun, B.; Liu, B.; Zhu, H.; Peng, H.; Zhao, H.; Liu, C.; et al. Characterization of *Rolled and Erect Leaf 1* in regulating leave morphology in rice. *J. Exp. Bot.* **2015**, *66*, 6047–6058. [CrossRef]
22. Li, C.; Zou, X.; Zhang, C.; Shao, Q.; Liu, J.; Liu, B.; Li, H.; Zhao, T. *OsLBD3-7* overexpression induced adaxially rolled leaves in rice. *PLoS ONE* **2016**, *11*, e0156413. [CrossRef]
23. Xu, Y.; Wang, Y.; Long, Q.; Huang, J.; Wang, Y.; Zhou, K.; Zheng, M.; Sun, J.; Chen, H.; Chen, S.; et al. Overexpression of *OsZHD1*, a zinc finger homeodomain class homeobox transcription factor, induce abaxially curled and drooping leaf in rice. *Planta* **2014**, *239*, 803–816. [CrossRef]
24. Wu, R.H.; Li, S.B.; He, S.; Waßmann, F.; Yu, C.; Qin, G.; Schreiber, L.; Qu, L.J.; Gu, H. CFL1, a WW domain protein, regulates cuticle development by modulating the function of HDG1, a class IV homeodomain transcription factor, in rice and *Arabidopsis*. *Plant Cell* **2011**, *23*, 3392–3411. [CrossRef]
25. Li, Y.Y.; Shen, A.; Xiong, W.; Sun, Q.L.; Luo, Q.; Song, T.; Li, Z.L.; Luan, W.J. Overexpression of OsHox32 results in pleiotropic effects on plant type architecture and leaf development in rice. *Rice* **2016**, *9*, 46. [CrossRef] [PubMed]
26. Zou, L.P.; Sun, X.H.; Zhang, Z.G.; Liu, P.; Wu, J.X.; Tian, C.J.; Qiu, J.L.; Lu, T.G. Leaf rolling controlled by the homeodomain leucine zipper Class IV gene *Roc5* in rice. *Plant Physiol.* **2011**, *156*, 1589–1602. [CrossRef] [PubMed]
27. Sun, J.; Cui, X.; Teng, S.; Zhao, K.; Wang, Y.; Chen, Z.; Sun, X.; Wu, J.; Ai, P.; Quick, W.P.; et al. HD-ZIP IV gene *Roc8* regulates the size of bulliform cells and lignin content in rice. *Plant Biotechnol. J.* **2020**, *18*, 2559–2572. [CrossRef] [PubMed]
28. Yang, X.; Wang, J.; Mao, X.; Li, C.; Li, L.; Xue, Y.; He, L.; Jing, R. A locus controlling leaf rolling degree in wheat under drought stress identified by bulked segregant analysis. *Plants* **2022**, *11*, 2076. [CrossRef]

29. Kumar, S.; Stecher, G.; Suleski, M.; Sanderford, M.; Sharma, S.; Tamura, K. MEGA12: Molecular evolutionary genetics analysis version 12 for adaptive and green computing. *Mol. Biol. Evol.* **2024**, *41*, msae263. [CrossRef]
30. Livak, K.J.; Schmittgen, T.D. Analysis of relative gene expression data using real time quantitative PCR and the $2^{-\Delta\Delta CT}$ method. *Methods* **2001**, *25*, 402–408. [CrossRef]
31. Yu, L.; Chen, X.; Wang, Z.; Wang, S.; Wang, Y.; Zhu, Q.; Li, S.; Xiang, C. Arabidopsis *Enhanced Drought Tolerance1/HOMEODOMAIN GLABROUS11* confers drought tolerance in transgenic rice without yield penalty. *Plant Physiol.* **2013**, *162*, 1378–1391. [CrossRef]
32. Grabherr, M.G.; Haas, B.J.; Yassour, M.; Levin, J.Z.; Thompson, D.A.; Amit, I.; Adiconis, X.; Fan, L.; Raychowdhury, R.; Zeng, Q. Trinity: Reconstructing a full-length transcriptome without a genome from RNA-Seq data. *Nat. Biotechnol.* **2011**, *29*, 644–652. [CrossRef]
33. Dai, M.Q.; Hu, Y.F.; Zhao, Y.; Liu, H.F.; Zhou, D.X. A WUSCHEL-LIKE HOMEOBOX gene represses a YABBY gene expression required for rice leaf development. *Plant Physiol.* **2007**, *144*, 380–390. [CrossRef]
34. Stahle, M.I.; Kuehlich, J.; Staron, L.; von Arnim, A.G.; Golz, J.F. YABBYs and the transcriptional corepressors LEUNIG and LEUNIG_HOMOLOG maintain leaf polarity and meristem activity in *Arabidopsis*. *Plant Cell* **2009**, *21*, 3105–3118. [CrossRef] [PubMed]
35. Sarojam, R.; Sappl, P.G.; Goldshmidt, A.; Efroni, I.; Floyd, S.K.; Eshed, Y.; Bowman, J.L. Differentiating Arabidopsis shoots from leaves by combined YABBY activities. *Plant Cell* **2010**, *22*, 2113–2130. [CrossRef]
36. Tanaka, W.; Toriba, T.; Ohmori, Y.; Yoshida, A.; Kawai, A.; Mayama-Tsuchida, T.; Ichikawa, H.; Mitsuda, N.; Ohme-Takagi, M.; Hirano, H.Y. The YABBY gene *TONGARI-BOUSHI1* is involved in lateral organ development and maintenance of meristem organization in the rice spikelet. *Plant Cell* **2012**, *24*, 80–95. [CrossRef] [PubMed]
37. Xu, P.; Ali, A.; Han, B.; Wu, X. Current advances in molecular basis and mechanisms regulating leaf morphology in rice. *Front. Plant Sci.* **2018**, *9*, 1528. [CrossRef]
38. Yuan, L. Super-high yield hybrid rice breeding. *Hybrid. Rice* **1997**, *12*, 1–6.
39. Inukai, S.; Kock, K.H.; Bulyk, M.L. Transcription factor–DNA binding: Beyond binding site motifs. *Curr. Opin. Genet. Dev.* **2017**, *27*, 110–119. [CrossRef]
40. Yang, C.; Li, D.; Liu, X.; Ji, C.; Hao, L.; Zhao, X.; Li, X.; Chen, C.; Cheng, Z.; Zhu, L. OsMYB103L, an R2R3-MYB transcription factor, influences leaf rolling and mechanical strength in rice (*Oryza sativa* L.). *BMC Plant Biol.* **2014**, *14*, 158. [CrossRef]
41. Eckardt, N.A. *YABBY* genes and the development and origin of seed plant leaves. *Plant Cell* **2010**, *22*, 2103. [CrossRef]
42. Ha, C.M.; Jun, J.H.; Fletcher, J.C. Control of Arabidopsis leaf morphogenesis through regulation of the *YABBY* and *KNOX* families of transcription factors. *Genetics* **2010**, *186*, 197–206. [CrossRef]
43. Toriba, T.; Harada, K.; Takamura, A.; Nakamura, H.; Ichikawa, H.; Suzaki, T.; Hirano, H.Y. Molecular characterization the *YABBY* gene family in *Oryza sativa* and expression analysis of *OsYABBY1*. *Mol. Genet. Genomics* **2007**, *277*, 457–468. [CrossRef] [PubMed]
44. Liu, H.L.; Xu, Y.Y.; Xu, Z.H.; Chong, K. A rice YABBY gene, *OsYABBY4*, preferentially expresses in developing vascular tissue. *Dev. Genes. Evol.* **2007**, *217*, 629–637. [CrossRef] [PubMed]
45. Yamaguchi, T.; Nagasawa, N.; Kawasaki, S.; Matsuoka, M.; Nagato, Y.; Hirano, H.Y. The YABBY gene *DROOPING LEAF* regulates carpel specification and midrib development in *Oryza sativa*. *Plant Cell* **2004**, *16*, 500–509. [CrossRef] [PubMed]
46. Ogo, Y.; Itai, R.N.; Nakanishi, H.; Inoue, H.; Kobayashi, T.; Suzuki, M.; Takahashi, M.; Mori, S.; Nishizawa, N.K. Isolation and characterization of IRO2, a novel iron-regulated bHLH transcription factor in graminaceous plants. *J. Exp. Bot.* **2006**, *57*, 2867–2878. [CrossRef]
47. Wang, S.; Li, L.; Ying, Y.; Wang, J.; Shao, J.F.; Yamaji, N.; Whelan, J.; Ma, J.F.; Shou, H. A transcription factor OsbHLH156 regulates Strategy II iron acquisition through localising IRO2 to the nucleus in rice. *New Phytol.* **2020**, *225*, 1247–1260. [CrossRef]
48. Mao, X.; Zhang, J.; Liu, W.; Yan, S.; Liu, Q.; Fu, H.; Zhao, J.; Huang, W.; Dong, J.; Zhang, S.; et al. The MKKK62-MKK3-MAPK7/14 module negatively regulates seed dormancy in rice. *Rice* **2019**, *12*, 2. [CrossRef]
49. Haga, K.; Iino, M. Phytochrome-mediated transcriptional up-regulation of *ALLENE OXIDE SYNTHASE* in rice seedlings. *Plant Cell Physiol.* **2004**, *45*, 119–128. [CrossRef]
50. Pramanik, M.H.R.; Imai, R. Functional identification of a trehalose 6-phosphate phosphatase gene that is involved in transient induction of trehalose biosynthesis during chilling stress in rice. *Plant Mol. Biol.* **2005**, *58*, 751–762. [CrossRef]
51. Xiao, Y.; Zhang, H.; Li, Z.; Huang, T.; Akihiro, T.; Xu, J.; Xu, H.; Lin, F. An amino acid transporter-like protein (OsATL15) facilitates the systematic distribution of thiamethoxam in rice for controlling the brown planthopper. *Plant Biotechnol. J.* **2022**, *20*, 1888–1901. [CrossRef]
52. Liu, Z.; Mei, E.; Tian, X.; He, M.; Tang, J.; Xu, M.; Liu, J.; Song, L.; Li, X.; Wang, Z.; et al. OsMKKK70 regulates grain size and leaf angle in rice through the OsMKK4-OsMAPK6-OsWRKY53 signaling pathway. *J. Integr. Plant Biol.* **2021**, *63*, 2043–2057. [CrossRef]
53. Yang, S.H.; Choi, D. Characterization of genes encoding ABA 8′-hydroxylase in ethylene-induced stem growth of deepwater rice (*Oryza sativa* L.). *Biochem. Biophys. Res. Commun.* **2006**, *350*, 685–690. [CrossRef]

54. Yaish, M.W.; El-kereamy, A.; Zhu, T.; Beatty, P.H.; Good, A.G.; Bi, Y.M.; Rothstein, S.J. The APETALA-2-Like transcription factor OsAP2-39 controls key interactions between abscisic acid and gibberellin in Rice. *PLoS Genet.* **2010**, *6*, e1001098. [CrossRef]
55. Kosugi, S.; Ohashi, Y. PCF1 and PCF2 specifically bind to *cis* elements in the rice proliferating cell nuclear antigen gene. *Plant Cell* **1997**, *9*, 1607–1619.
56. Dubouzet, J.G.; Sakuma, Y.; Ito, Y.; Kasuga, M.; Dubouzet, E.G.; Miura, S.; Seki, M.; Shinozaki, K.; Yamaguchi-Shinozaki, K. *OsDREB* genes in rice, *Oryza sativa* L., encode transcription activators that function in drought-, high-salt- and cold-responsive gene expression. *Plant J.* **2003**, *33*, 751–763. [CrossRef]
57. Jia, M.; Meng, X.; Song, X.; Zhang, D.; Kou, L.; Zhang, J.; Jing, Y.; Liu, G.; Liu, H.; Huang, X.; et al. Chilling-induced phosphorylation of IPA1 by OsSAPK6 activates chilling tolerance responses in rice. *Cell Discov.* **2022**, *8*, 71. [CrossRef]
58. Feng, X.; Zhang, L.; Wei, X.; Zhou, Y.; Dai, Y.; Zhu, Z. OsJAZ13 negatively regulates jasmonate signaling and activates hypersensitive cell death response in rice. *Int. J. Mol. Sci.* **2020**, *21*, 4379. [CrossRef]
59. Xia, C.; Liang, G.; Chong, K.; Xu, Y. The COG1-OsSERL2 complex senses cold to trigger signaling network for chilling tolerance in *japonica* rice. *Nat. Commun.* **2023**, *14*, 3104. [CrossRef]
60. Xie, Z.; Zhang, Z.L.; Zou, X.; Huang, J.; Ruas, P.; Thompson, D.; Shen, Q.J. Annotations and functional analyses of the rice *WRKY* gene superfamily reveal positive and negative regulators of abscisic acid signaling in aleurone cells. *Plant Physiol.* **2005**, *137*, 176–189. [CrossRef]
61. Liu, X.; Bai, X.; Wang, X.; Chu, C. OsWRKY71, a rice transcription factor, is involved in rice defense response. *J. Plant Physiol.* **2007**, *164*, 969–979. [CrossRef]
62. Takahashi, R.; Ishimaru, Y.; Nakanishi, H.; Nishizawa, N.K. Role of the iron transporter OsNRAMP1 in cadmium uptake and accumulation in rice. *Plant Signal. Behav.* **2011**, *6*, 1813–1816. [CrossRef]
63. Lin, R.; Zhao, W.; Meng, X.; Wang, M.; Peng, Y. Rice gene *OsNAC19* encodes a novel NAC-domain transcription factor and responds to infection by *Magnaporthe grisea*. *Plant Sci.* **2007**, *172*, 120–130. [CrossRef]
64. Kobayashi, T.; Nagano, A.J.; Nishizawa, N.K. Iron deficiency-inducible peptide-coding genes *OsIMA1* and *OsIMA2* positively regulate a major pathway of iron uptake and translocation in rice. *J. Exp. Bot.* **2021**, *72*, 2196–2211. [CrossRef]
65. Fu, J.; Pei, W.; He, L.; Ma, B.; Tang, C.; Zhu, L.; Wang, L.; Zhong, Y.; Chen, G.; Wang, Q.; et al. ZmEREB92 plays a negative role in seed germination by regulating ethylene signaling and starch mobilization in maize. *PLoS Genet.* **2023**, *19*, e1011052. [CrossRef]
66. Sperotto, R.A.; Ricachenevsky, F.K.; Duarte, G.L.; Boff, T.; Lopes, K.L.; Sperb, E.R.; Grusak, M.A.; Fett, J.P. Identification of up-regulated genes in flag leaves during rice grain filling and characterization of OsNAC5, a new ABA-dependent transcription factor. *Planta* **2009**, *230*, 985–1002. [CrossRef]
67. Hakata, M.; Kuroda, M.; Ohsumi, A.; Hirose, T.; Nakamura, H.; Muramatsu, M.; Ichikawa, H.; Yamakawa, H. Overexpression of a rice TIFY gene increases grain size through enhanced accumulation of carbohydrates in the stem. *Biosci. Biotechnol. Biochem.* **2012**, *76*, 2129–2134. [CrossRef]
68. Gutha, L.R.; Reddy, A.R. Rice *DREB1B* promoter shows distinct stress-specific responses, and the overexpression of cDNA in tobacco confers improved abiotic and biotic stress tolerance. *Plant Mol. Biol.* **2008**, *68*, 533–555. [CrossRef]
69. Wang, T.; Ma, Y.Q.; Huang, X.X.; Mu, T.J.; Li, Y.J.; Li, X.K.; Liu, X.; Hou, B.K. Overexpression of *OsUGT3* enhances drought and salt tolerance through modulating ABA synthesis and scavenging ROS in rice. *Environ. Exp. Bot.* **2021**, *192*, 104653. [CrossRef]
70. Sharma, E.; Bhatnagar, A.; Bhaskar, A.; Majee, S.M.; Kieffer, M.; Kepinski, S.; Khurana, P.; Khurana, J.P. Stress-induced F-Box protein-coding gene *OsFBX257* modulates drought stress adaptations and ABA responses in rice. *Plant Cell Environ.* **2023**, *46*, 1207–1231. [CrossRef]
71. Philippe, R.; Courtois, B.; McNally, K.L.; Mournet, P.; El-Malki, R.; Paslier, M.C.L.; Fabre, D.; Billot, C.; Brunel, D.; Glaszmann, J.C.; et al. Structure, allelic diversity and selection of Asr genes, candidate for drought tolerance, in *Oryza sativa* L. and wild relatives. *Theor. Appl. Genet.* **2010**, *121*, 769–787. [CrossRef]
72. Wang, R.; Jing, W.; Xiao, L.; Jin, Y.; Shen, L.; Zhang, W. The rice high-affinity potassium transporter1;1 is involved in salt tolerance and regulated by an MYB-Type transcription factor. *Plant Physiol.* **2015**, *168*, 1076–1090. [CrossRef]
73. Hwang, H.; Yoon, J.; Kim, H.Y.; Min, M.K.; Kim, J.A.; Choi, E.H.; Lan, W.Z.; Bae, Y.M.; Luan, S.; Cho, H.; et al. Unique features of two potassium channels, OsKAT2 and OsKAT3, expressed in rice guard cells. *PLoS ONE* **2013**, *8*, e72541. [CrossRef]
74. Lee, D.K.; Redillas, M.C.F.R.; Jung, H.; Choi, S.; Kim, Y.S.; Kim, J.K. A nitrogen molecular sensing system, comprised of the *ALLANTOINASE* and *UREIDE PERMEASE 1* genes, can be used to monitor N status in rice. *Front. Plant Sci.* **2018**, *9*, 444. [CrossRef]
75. Liu, H.; Guo, Z.; Gu, F.; Ke, S.; Sun, D.; Dong, S.; Liu, W.; Huang, M.; Xiao, W.; Yang, G.; et al. 4-coumarate-CoA ligase-like gene *OsAAE3* negatively mediates the rice blast resistance, floret development and lignin biosynthesis. *Front. Plant Sci.* **2016**, *7*, 2041. [CrossRef]
76. Lv, Y.; Shao, G.; Jiao, G.; Sheng, Z.; Xie, L.; Hu, S.; Tang, S.; Wei, X.; Hu, P. Targeted mutagenesis of *POLYAMINE OXIDASE 5* that negatively regulates mesocotyl elongation enables the generation of direct-seeding rice with improved grain yield. *Mol. Plant* **2021**, *14*, 344–351. [CrossRef]

77. Carlessi, M.; Mariotti, L.; Giaume, F.; Fornara, F.; Perata, P.; Gonzali, S. Targeted knockout of the gene *OsHOL1* removes methyl iodide emissions from rice plants. *Sci. Rep.* **2021**, *11*, 17010. [CrossRef]
78. Iwamoto, M.; Baba-Kasal, A.; Kiyota, S.; Hara, N.; Takano, M. *ACO1*, a gene for aminocyclopropane-1-carboxylate oxidase: Effects on internode elongation at the heading stage in rice. *Plant Cell Environ.* **2010**, *33*, 805–815. [CrossRef]
79. Kim, J.Y.; Chung, Y.S.; Ok, S.H.; Lee, S.G.; Chung, W.I.; Kim, I.Y.; Shin, J.S. Characterization of the full-length sequences of phospholipase A2 induced during flower development. *Biochim Biophys Acta.* **1999**, *1489*, 389–392. [CrossRef]
80. Zan, X.; Zhou, Z.; Wan, J.; Chen, H.; Zhu, J.; Xu, H.; Zhang, J.; Li, X.; Gao, X.; Chen, R.; et al. Overexpression of *OsHAD3*, a member of HAD superfamily, decreases drought tolerance of rice. *Rice* **2023**, *16*, 31. [CrossRef]
81. Fan, X.; Wu, J.; Chen, T.; Tie, W.; Chen, H.; Zhou, F.; Lin, Y. Loss-of-function mutation of rice SLAC7 decreases chloroplast stability and induces a photoprotection mechanism in rice. *J. Integr. Plant Biol.* **2015**, *57*, 1063–1077. [CrossRef]

Disclaimer/Publisher's Note: The statements, opinions and data contained in all publications are solely those of the individual author(s) and contributor(s) and not of MDPI and/or the editor(s). MDPI and/or the editor(s) disclaim responsibility for any injury to people or property resulting from any ideas, methods, instructions or products referred to in the content.

plants

MDPI

Article

Genome-Wide Linkage Mapping of Root System Architecture-Related Traits Under Drought Stress in Common Wheat (*Triticum aestivum* L.)

Yirong Jin [1], Guiju Chen [2], Xiaodong Qiu [3], Fuyan Wang [1], Hui Jin [4], Liang Zhang [1], Cheng Liu [5], Jianjun Liu [5], Wenjing Li [6,*] and Peng Liu [1,*]

[1] Dezhou Academy of Agricultural Sciences, Dezhou 253015, China; jyr2014@163.com (Y.J.)
[2] Wheat Research Institute, Jining Academy of Agricultural Sciences, Jining 272000, China
[3] Department of Science and Technology of Shandong Province, Jinan 250101, China
[4] Institute of Forage and Grassland Sciences, Heilongjiang Academy of Agricultural Sciences, Harbin 150086, China
[5] Crop Research Institute, Shandong Academy of Agricultural Sciences, Jinan 250100, China
[6] College of Life Science, Langfang Normal University, Langfang 065000, China
* Correspondence: liwenjing@lfnu.edu.cn (W.L.); liup9@163.com (P.L.); Tel./Fax: +86-82108889 (P.L.)

Abstract

Drought severely threatens wheat production. Under drought conditions, root system architecture (DRSA)-related traits in common wheat significantly affect wheat production. In China, Zhoumai16 is a high-yield winter wheat variety in the Huang-Huai wheat region. It is suitable for high-fertilizer and high-water cultivation and has moderate drought tolerance. DK171 is a newly developed high-yield and stress-tolerant variety, with higher drought tolerance. Thus, identifying genetic loci associated with DRSA-related traits from DK171 and developing available molecular markers are of great importance for enhancing wheat stress tolerance breeding. In this study, DRSA-related traits, including the total root dry weight (DDRW), total root length (DTRL), total root area (DTRA), and the number of root tips (DNRT) under drought stress, were assessed using the hydroponic system in Zhoumai16/DK171 recombinant inbred lines (RIL) population. A total of five quantitative trait loci (QTL) for DRSA-related traits were identified, e.g., *QDDRW.daas-1BL*, *QDTRS.daas-4AL*, *QDNRT.daas-4DS*, *QDTRL.daas-3AL*, and *QDDRW.daas-5D*, and explained 6.1% to 18.9% of the phenotypic variances, respectively. Among these, *QDTRS.daas-4AL* and *QDTRL.daas-3AL* were consistent with previous reports, whereas the *QDDRW.daas-1BL*, *QDNRT.daas-4DS*, and *QDDRW.daas-5D* are novel. The favorable alleles of *QDTRS.daas-4AL* and *QDNRT.daas-4DS* were inherited from Zhoumai16, whereas the favorable alleles for *QDDRW.daas-1BL*, *QDTRL.daas-3AL*, and *QDDRW.daas-5D* were contributed by DK171. Furthermore, five kompetitive allele-specific PCR (KASP) markers, *Kasp_1BL_DTRS* (*QDDRW.daas-1BL*), *Kasp_3AL_DTRS* (*QDTRL.daas-3AL*), *Kasp_4A_DTRS* (*QDTRA.daas-4A*), *Kasp_5D_DDRW* (*QDDRW.daas-5D*), and *Kasp_4D_DNRT* (*QDNRT.daas-4D*), were developed and validated in a diverse panel with 108 wheat varieties mainly from China. Additionally, eight candidate genes related to plant hormone regulation, ABC transporters, and calcium-dependent lipid-binding domain proteins were identified. This study offers new loci, candidate genes, and available KASP markers for wheat drought tolerance breeding and facilitating progress in developing drought-tolerant wheat cultivars.

Keywords: bread wheat; drought tolerance; marker-assisted selection; root system architecture (RSA)

1. Introduction

Common wheat is one of the most crucial staple crops for human consumption and serves as the primary food crop in arid and semi-arid regions worldwide. Drought is the most significant abiotic stress affecting wheat production, severely constraining its sustainable cultivation [1]. Agricultural water inputs are required, resulting in considerable waste of labor and water resources. Therefore, breeding drought-tolerant and water-efficient varieties is the most effective, economical, and environmentally safe approach to reduce the losses caused by drought [2–4].

Wheat root system morphology and physiological regulation determine its drought tolerance. Drought tolerance of wheat seedlings is crucial for plant development and production. Root length, surface area, and number of root tips are key root system architecture under drought conditions (DRSA) traits [5–8]. These characteristics determine the root spatial distribution and primary composition, significantly affecting water and nutrient uptake. Maximum root length forms the basis for water uptake, while the root tip number, root diameter, root length, and root density are closely related to root dry weight, volume, and surface area. Together, these traits determine the plant anchoring strength in the soil profile and its capacity to absorb soil solutions [9,10]. However, the evaluation of these traits is limited by environmental conditions and measurement methods, making it time-consuming and labor-intensive [7,9,10]. Therefore, identifying stable and effective loci for wheat drought tolerance, developing molecular markers for breeding, and elucidating the genetic mechanisms of DRSA-related traits will accelerate the efficient improvement of drought tolerance.

Recently, advancements in high-throughput genotyping technologies, such as re-sequencing and SNP chips [11], effective analysis tools, such as linkage mapping [12–16], and association mapping [17,18] have become common methods for identifying loci of complex traits [6,8,12–14]. Over the past two decades, over 50 loci associated with DRSA-related traits have been reported and mainly distributed on chromosomes 1A, 2B, 3A, 3B, 5B, and 6D [6,8,19–21]. Although some genetic loci related to root traits in wheat seedlings under drought stress have been reported, many of these loci are linked to SSR markers, which are not efficient for practical use. Additionally, some loci are influenced by complex genetic backgrounds or are linked to non-desirable agronomic traits, making them unsuitable for breeding applications. Therefore, discovering new genetic loci and developing molecular markers that are applicable in breeding holds significant importance for optimizing wheat root systems and achieving high and stable yields. Zhoumai16 (Zhou8425B/Zhou 9) is a high-yield, disease-resistant wheat variety with a significant cultivation area in the Huang-Huai wheat region of China. It is suitable for high-fertilizer and high-water cultivation and has moderate drought tolerance. DK171 (Liangxing66/Shixin828) is a newly developed high-yield and stress-tolerant variety in recent years, with strong drought resistance inherited by Shixin828. In this study, five loci for seedling-stage DRSA-related traits were identified in the Zhoumai16/DK171 recombinant inbred line (RIL) population using the wheat 90K SNP array. The main goal of this study is to uncover the genetic basis of DRSA traits and develop breeding-friendly kompetitive allele-specific PCR (KASP) markers to enhance wheat DRSA-related trait improvement.

2. Results

2.1. Phenotypic Evaluation

Zhoumai16 is a high-yielding variety suitable for high-fertility, water-rich regions, while DK171 is a wheat variety that combines high yield with water conservation. For Zhoumai16, the means of total root length (DTRL), total root surface (DTRS), number of root tips (DNRT), and dry root weight (DDRW) were 35.9 cm, 8.0 cm^2, 123.6, and 0.0312 g,

respectively. For DK171, these values were 47.2 cm, 8.9 cm^2, 168.9, and 0.0339 g. The DTRL, DTRS, DNRT, and DDRW of DK171 were significantly higher than Zhoumai16 ($p < 0.05$). All four DRSA-related traits exhibited continuous and significantly wide variation across the 262 RILs (Table A1 and Figures 1 and A1). The means of DTRL, DTRS, DNRT, and DDRW were 40.2 cm (range: 24.1–63.8 cm), 7.8 cm^2 (range: 5.4–10.7 cm^2), 106.9 (range: 24.7–213.7), and 0.0282 g (range: 0.0162–0.0413 g). The standard deviation and coefficient of variation for DTRL, DTRS, DNRT, and DDRW were 6.58 cm (16.4%), 1.06 cm^2 (13.6%), 35.7 (33.4%), and 0.0041 g (14.5%). Significant correlation was observed between DDRW, DTRL, DTRA, and DNRT, with a correlation coefficient of 0.603 ($p < 0.05$) between DTRL and DTRS ($R^2 = 0.56$), DTRL and DNRT ($R^2 = 0.31$), DTRL and DRW ($R^2 = 0.32$), DTRS and DNRT ($R^2 = 0.33$), and DNRT and DRW ($R^2 = 0.30$) ($p < 0.05$).

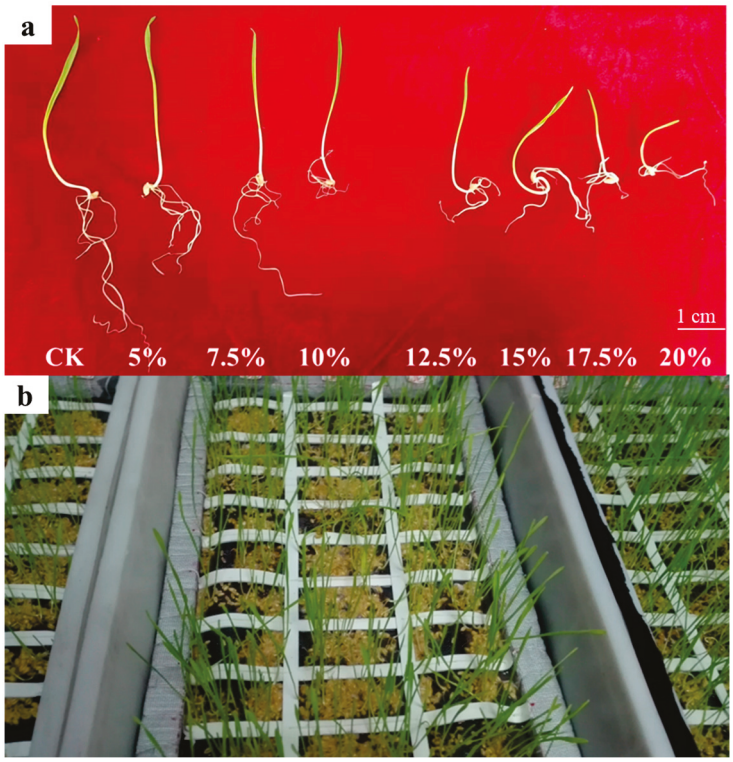

Figure 1. The DRSA-related traits in the Zhoumai16/DK171 RIL population. (**a**) Root growth of wheat seedlings under different concentrations. Root development status under different concentrations of PEG6000, with 12.5% ultimately selected as the drought condition for root phenotypic characterization (5-day). PEG-6000 was used to simulate drought stress. At concentrations of 5–10%, there was no significant reduction in germination potential or germination rate, while concentrations of 12.5–20% significantly inhibited germination. Based on the comparative analysis of relative germination rates and germination potentials at different concentrations, a concentration of 12.5% was selected for the assessment of seedling-related phenotypes. (**b**) Bulk phenotyping of wheat seedling root traits. Bulk evaluation of root phenotypes under 12.5% PEG6000 conditions (8-day growth status).

2.2. QTL Identification

This genetic map includes all 21 chromosomes, with red representing QTL and black lines representing backbone SNP markers.

Two QTL for DDRW were identified on chromosomes 1BL and 5DL, referred to as *QDDRW.daas-1BL* (*wsnp_Ex_rep_c67299_65845319-Excalibur_rep_c107035_354*) and *QDDRW.daas-5D* (*BobWhite_c5176_1164-RAC875_rep_c78046_324*), respectively. These QTLs explained 18.9% (additive effect: −0.002 g) and 7.5% (additive effect: −0.0007 g) of the total phenotypic variances (PVEs) (Table 1; Figure 1). *QDTRS.daas-4AL* for DTRS was identified on 4AL chromosome (613.6–615.2 Mb, *IAAV7132-wsnp_JD_c38619_27992279*) and explained

9.6% of the PVEs with additive effect −0.275 cm^2. *QDNRT.daas-4DS* for DNRT was identified on chromosome 4DS (1.2–3.6 Mb, *RAC875_rep_c76650_164-Kukri_c15720_884*) and explained 8.1% of the PVEs with additive effect -7.6. *QDTRL.daas-3AL* for DNRT was identified on chromosome 3AL (650.4–659.4 Mb, *Kukri_rep_c69970_717-Kukri_rep_c103783_1380*) and explained 6.1% (additive effect: −1.272 g) of the PVEs. The favorable allele of *QDTRL.daas-3AL*, *QDDRW.daas-1BL* and *QDDRW.daas-5D* were contributed by DK171, whereas the favorable allele of *QDTRS.daas-4AL* and *QDNRT.daas-4DS* were contributed by Zhoumai16 (Table 1; Figure 2).

Table 1. QTL for DRSA-related traits in Zhoumai16/DK171 RIL population.

QTL	Chromosome	Genetic Interval	Physical Position (Mb)	LOD	R^2	Add
QDDRW.daas-1BL	1B	*wsnp_Ex_rep_c67299_65845319~ Excalibur_rep_c107035_354*	586.3–609.0	11.1	18.9	−0.002
QDTRL.daas-3AL	3A	*Kukri_rep_c69970_717~Kukri_rep_c103783_1380*	650.4–659.4	3.0	6.1	−1.27
QDTRS.daas-4AL	4A	*IAAV7132~wsnp_JD_c38619_27992279*	613.6–615.2	3.5	9.6	0.28
QDNRT.daas-4DS	4D	*RAC875_rep_c76650_164~Kukri_c15720_884*	1.2–3.6	3.2	8.1	7.61
QDDRW.daas-5D	5D	*BobWhite_c5176_1164~RAC875_rep_c78046_324*	378.9–393.5	3.1	7.5	−0.001

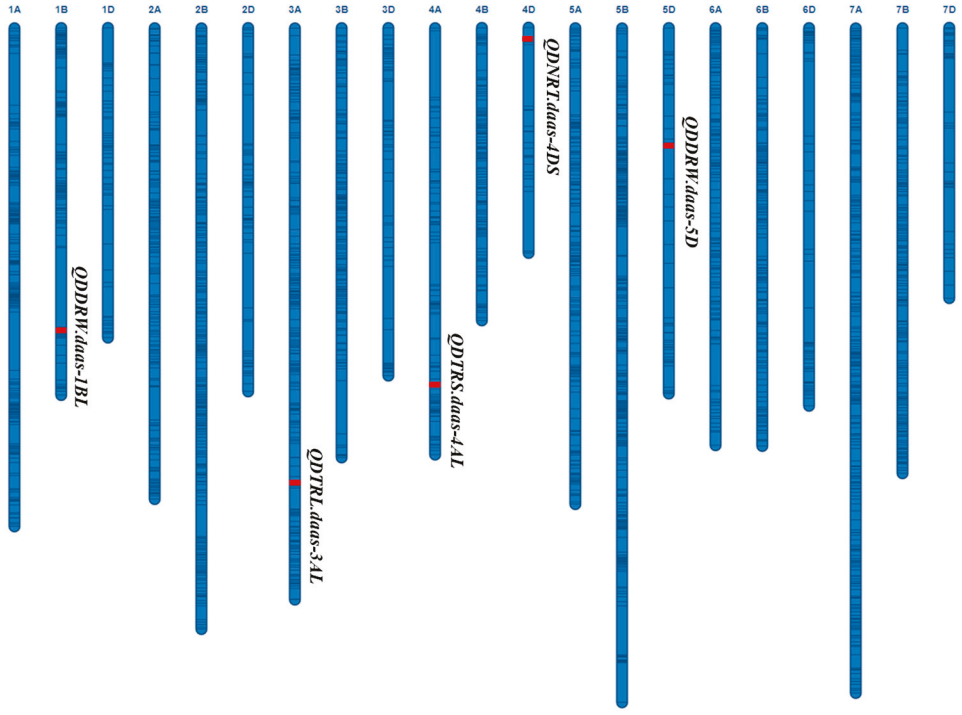

Figure 2. QTL for the DRSA-related traits in the Zhoumai16/DK171 RIL population.

2.3. Candidate Genes Identification

Eight candidate genes were identified and involved in the biological metabolism, including the plant hormones, ABC transporter and calcium-dependent lipid-binding domain protein. Two candidate genes for *QDDRW.daas-1BL* were identified, e.g., *TraesCS1B01G356600* and *TraesCS1B01G373900*, encoded the auxin-responsive protein and the ABC transporter family protein, respectively. Both *TraesCS3A01G406200* and *TraesCS3A01G416300* were candidate genes for *QDTRL.daas-3AL* and encoded the gibberellin 20 oxidase and the auxin transport protein, respectively. For *QDTRS.daas-4AL*, *TraesCS4A01G326400* were selected as the candidate gene and encoded the ethylene-responsive transcription factor. *TraesCS4D01G001900* (*QDNRT.daas-4DS*) encoded the

calcium-dependent lipid-binding domain protein. *TraesCS4D01G002400* of *QDDRW.daas-5D* encoded the ethylene-responsive transcription factor. *TraesCS5D01G285900* identified at the genetic interval of *QDDRW.daas-5D* and encoded the auxin-induced in root cultures protein (Tables 2 and A2, Figure 3). The expressions of the seven candidate genes in Zhoumai16 and DK171 were detected using the qRT-PCR. Of these, *TraesCS1B01G356600*, *TraesCS4D01G002400*, and *TraesCS5D01G285900* showed no significant differences between the parents, whereas *TraesCS4D01G002400* and *TraesCS5D01G285900* showed more than 2.3–3.5 folds higher expression in Zhoumai16 compared to DK171; *TraesCS3A01G416300*, *TraesCS4A01G326400*, and *TraesCS4D01G001900* showed more than 3.1–4.3 folds higher expression in DK171 compared to Zhoumai16 (Figure 4).

Table 2. The candidate genes for DRSA-related traits identified in the Zhoumai16/DK171 RIL population.

QTL	Candidate Gene	Chromosome	Start (bp)	Annotation
QDDRW.daas-1BL	*TraesCS1B01G356600*	1B	585539303	Auxin-responsive protein
QDDRW.daas-1BL	*TraesCS1B01G373900*	1B	604319205	ABC transporter A family protein
QDTRL.daas-3AL	*TraesCS3A01G406200*	3A	650429434	Gibberellin 20 oxidase 2
QDTRL.daas-3AL	*TraesCS3A01G416300*	3A	658983005	Auxin transport protein (BIG)
QDTRS.daas-4AL	*TraesCS4A01G326400*	4A	613543523	Ethylene-responsive transcription factor
QDNRT.daas-4DS	*TraesCS4D01G001900*	4D	1239483	Calcium-dependent lipid-binding domain protein
QDNRT.daas-4DS	*TraesCS4D01G002400*	4D	1288444	Ethylene-responsive transcription factor
QDDRW.daas-5D	*TraesCS5D01G285900*	5D	386209788	Auxin-induced in root cultures protein 12

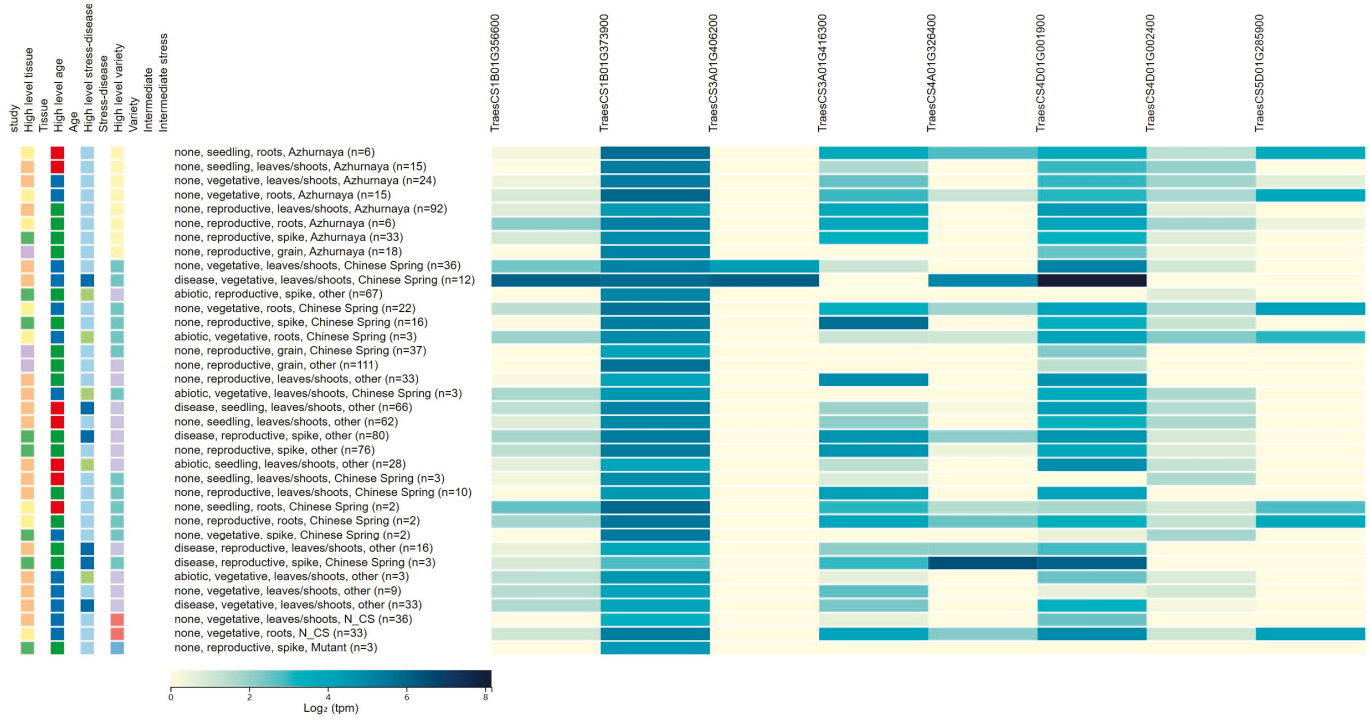

Figure 3. The expression patterns for the eight candidate genes associated with DRSA-related traits. The left side of the figure represents the expression patterns of candidate genes in different tissues and at various developmental stages. The data originates from wheat expression data. The specific transcriptome data can be downloaded from this website (http://wheat-expression.com/, accessed on 24 June 2025).

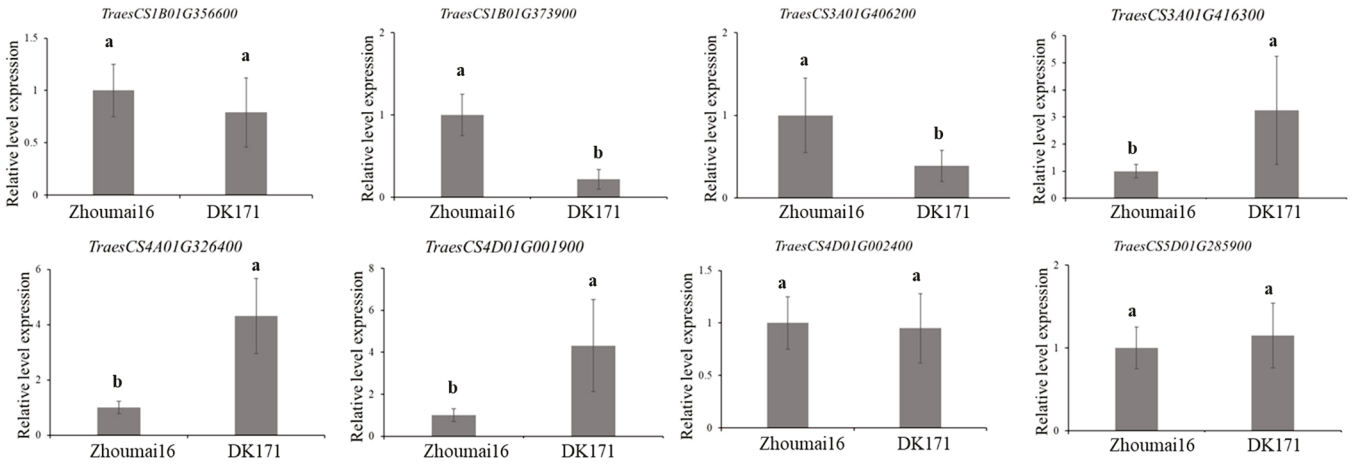

Figure 4. The qRT-PCR results for the candidate genes identified in this study. Transcriptional analysis was conducted in the RIL population of Zhoumai16 and DK171, where different letters indicate significant differences at the $p < 0.05$ level.

2.4. QTL Validation

All five QTLs were employed in the development of KASP markers. A total of 5 KASP markers, *Kasp-1BL-DDRW* (*QDDRW.daas-1BL*, *wsnp_Ex_rep_c67299_65845319*, 586.3 Mb) and *Kasp-3AL-DTRL* (*QDTRL.daas-3AL*, *Kukri_rep_c69970_717*, 650.4 Mb), *Kasp_DTRS_4A* (*QDTRL.daas-4A*, *wsnp_Ex_c7280_12498193*, 725.6 Mb), *Kasp_DDRW_5D* (*QDDRW.daas-5D*, *IACX2960*, 347.5 Mb) and *Kasp_DNRT_4D* (*QDNRT.daas-4D*, *Kukri_rep_c68594_530*, 12.7 Mb), were successfully developed. To validate the efficacy of the 5 KASP markers, a diverse panel of 108 cultivars was employed. For *Kasp-1BL-DDRW*, the allele (AA) account for 60.2% (mean DDRW: 0.0262 g) exhibited lower DDRW compared to the allele (GG), which account for 38.9% with mean DDRW 0.0230 g ($p < 0.05$). For *Kasp-3AL-DTRL*, the allele (AA) account for 66.7% (mean DTRL: 63.52 cm) exhibited higher DTRL compared to the allele (GG), which account for 32.4% with mean DTRL of 56.60 cm^2 ($p < 0.05$). For *Kasp_DTRS_4A*, the allele (AA) account for 38.9% (mean DTRL: 5.968 cm^2) exhibited lower DTRS compared to the allele (GG), which account for 55.6% with mean DTRS 6.993 cm^2 ($p < 0.05$). For *Kasp_DDRW_5D*, the favorable allele (CC 10.2%, a mean DRW of 0.0297 g) showed higher DDRW than unfavorable allele (TT, 88.9%, mean DDRW of 0.0244 g) at $p = 0.05$ level. For *Kasp_DNRT_4D*, the favorable allele (CC 65.7%, mean DNRT of 97.8) showed higher DNRT than the unfavorable allele (TT, 30.6%, mean DNRT of 83.0) ($p = 0.05$) (Tables 3, 4 and A3).

Table 3. Effects of *Kasp_4AL_DTRS*, *Kasp_4DS_DNRT*, and *Kasp_5D_DDRW* on DRSA-related traits in the natural population.

Marker Name	QTL	Genotype [a]	Number of Lines	Phenotype	*p*-Value
Kasp_1BL_DDRW	*QDDRW.daas-1BL*	*AA*	74	6.80 (DTRS)	0.023 *
		GG	33	5.85 (DTRS)	
Kasp_3AL_DTRL	*QDTRL.daas-3AL*	*AA*	72	63.52 (DTRL)	0.010 *
		GG	35	56.60 (DTRL)	
Kasp_4AL_DTRS	*QDTRS.daas-4AL*	*GG*	60	6.99 (DTRS)	0.021 *
		AA	42	5.97 (DTRS)	
Kasp_4DS_DNRT	*QDNRT.daas-4DS*	*TT*	33	83.0 (DNRT)	0.009 *
		CC	71	97.7 (DNRT)	
Kasp_5D_DDRW	*QDDRW.daas-5D*	*CC*	11	0.0297 (DDRW)	0.039 *
		TT	96	0.0245 (DDRW)	

[a] The italic is the favorable allele. * Significant at $p < 0.05$.

Table 4. The primers of the KASP markers identified in this study.

Kasp Name	Primer	Sequence
Kasp-1BL-DDRW	FAM	GAAGGTGACCAAGTTCATGCTTTGAGGCGACCACCCTGA
	HEX	GAAGGTCGGAGTCAACGGATTTTGAGGCGACCACCCTGG
	COMMON	GCAGCCGTTATTCAACTTCTAA
Kasp-3AL-DTRL	FAM	GAAGGTGACCAAGTTCATGCTCCTTCTGGATTGATGGTTCTCA
	HEX	GAAGGTCGGAGTCAACGGATTCCTTCTGGATTGATGGTTCTCG
	COMMON	TCTGCCTCGAAGTCTTCATTT
Kasp_4AL_DTRS	FAM	GAAGGTGACCAAGTTCATGCTCATTGCCAAATGTTTGCTGTATT
	HEX	GAAGGTCGGAGTCAACGGATTCATTGCCAAATGTTTGCTGTATC
	COMMON	CATTATCAGATGATACCACGTCG
Kasp_4DS_DNRT	FAM	GAAGGTGACCAAGTTCATGCTTGAACTCGGCTGATACCAGA
	HEX	GAAGGTCGGAGTCAACGGATTGAACTCGGCTGATACCAGG
	COMMON	GGTGATGGCGAACCTAGAAAC
Kasp_5D_DDRW	FAM	GAAGGTGACCAAGTTCATGCTCATTGCCAAATGTTTGCTGTATT
	HEX	GAAGGTCGGAGTCAACGGATTCATTGCCAAATGTTTGCTGTATC
	COMMON	CATTATCAGATGATACCACGTCG

The underlined nucleotides are the FAM and HEX primers.

To assess the accuracy of markers in detecting root phenotypes in natural populations, we selected the median value as the threshold for each trait. Phenotype values below the median were categorized as non-superior phenotypes, while those above were classified as superior phenotypes. We calculated the consistency rate between genotypes and phenotypes to provide a reference for the detection and evaluation of wheat root systems under drought conditions. The accuracy rates of *Kasp_1BL_DTRS*, *Kasp_3AL_DTRS*, *Kasp_DTRS_4A*, *Kasp_DDRW_5D*, and *Kasp_DNRT_4D* in detecting superior and non-superior phenotypes for DTRS, DDRW, and DNRT were 66.0% and 75.5%; 90.6% and 92.5%; 60.4% and 73.6%; 58.5% and 79.2%; 52.8% and 66.0%, respectively.

3. Discussion

Roots are the main parts of plants that take up water and nutrients. They also provide support and stability. Wheat has a fibrous root system. As it grows after germination, it develops adventitious roots. These roots are vital for anchoring the plant and absorbing water and nutrients [2,13]. They form the genetic foundation for desirable traits like drought tolerance, salt tolerance, and resistance to falling over (lodging). However, studying the root system of mature plants is difficult. Soil conditions and farming practices easily affect it. Traditional methods for taking root samples are often destructive and complicated, making it hard to measure root traits efficiently [5,14]. Research shows that the root systems of young seedlings are different. They are strongly inherited and less affected by the environment. These young roots can indicate the shape and spread of the mature root system and are closely linked to the plant's ability to handle stress. A good root structure is the basis for having enough root volume and surface area to function well.

To adapt to diverse environments, wheat varieties have accumulated numerous genetic variations. Genetic enhancement of crop roots has seldom been analyzed [14,15]. The identification of QTL provides an effective strategy to develop molecular markers and identify candidate genes [16]. A thorough understanding of the genetic foundation of drought root system architecture traits would aid in optimizing root systems under conditions of nutrient deficiency [2,3,5–8,12–14]. Several QTLs associated with root system architecture-related traits have been uncovered in wheat [17,18]. Root system architecture is a highly adaptable trait across various environments [22]; QTLs governing root system architecture under drought conditions are crucial for enhancing drought toler-

ance. Over 10 loci influencing the number of root tips under drought stress have been mapped on chromosomes 4A, 4B, 4D, 5B, 1D, 6D, and 7D [23]. The locus on chromosome 4D (360.3–396.8 Mb) is different from the loci identified in this study (*QDNRT.daas-4DS* 1.2–3.6 Mb). Thus, *QDNRT.daas-4DS* is a new loci. Over 10 loci for root surface area under drought stress were identified on chromosomes 1D, 2A, 2B, 2D, 3B, 4A, 5B, 5D, 7A, and 7D in common wheat [23]. Of these, the locus on 4A (565.6–598.2 Mb) is nearly adjacent to the *QDTRS.daas-4AL* (613.6–615.2 Mb).

In total, 12 loci for total root length under drought stress were identified on chromosomes 1A, 1D, 2A, 2D, 3A, 3B, 3D, 4B, 5B, 5D, 7A, and 7D [23–25]. In this study, we have identified a locus for total root length under drought stress, *QDTRL.daas-3AL* (650.4–659.4 Mb), which is near the loci on 3AL (632.8–646.3 Mb). Until now, eight loci for DDRW were identified on chromosomes 1B, 2A, 2D, 4A, 4B, 5A, 7A, and 7D [1,26–29]. We identified two loci for DDRW, *QDDRW.daas-1BL* (586.3–609.0 Mb) and *QDDRW.daas-5D* (378.9–393.5 Mb), which differ from the loci located on chromosome 1B (120.2–159.6 Mb) and 5D (489.6–540.3 Mb) mentioned above. Thus, both *QDDRW.daas-1BL* and *QDDRW.daas-5D* are novel.

The genes associated with plant height and vernalization may also have significant effects on root system architecture-related traits [30]. Over the past 80 years, several genetic loci associated with plant height and vernalization have been identified in common wheat, and a number of functional genes have been cloned on chromosome 1B (*Rht2/Rht10* at 19.18 Mb), 4D (*SVP3-4D/BM1-4D* at 469.46 Mb, *Vrn2-4D/ZCCT1-4D* at 509.43 Mb), and 5D (*TaDEP1-5D* at 329.11 Mb, *Rht23* at 524.96 Mb, and *Vrn1-5D* at 470.00 Mb) [31], and 6A (Rht24, 411.93–414.88 Mb) [32]. Based on physical positions, the loci *QDTRS.daas-4AL* (613.6–615.2 Mb) and *QDNRT.daas-4DS* (1.2–3.6 Mb), *QDTRL.daas-3AL* (650.4–659.4 Mb), *QDDRW.daas-1BL* (586.3–609.0 Mb), and *QDDRW.daas-5D* (378.9–393.5 Mb) are different from the reported plant height and vernalization genes.

Notably, compared with previous results and meta-analyses, *QDDRW.daas-1BL*, *QDNRT.daas-4DS*, and *QDDRW.daas-5D* were novel. We have presented the linkage mapping results for agronomic traits in the Zhoumai16/DK171 RIL population [15] and pinpointed several genomic regions linked to both drought root system architecture-related traits and agronomic traits. Specifically, *QDDRW.daas-1BL* (586.3–609.0 Mb) overlaps with a QTL cluster (556–654 Mb) influencing kernel number per spike (KNS), PH, and flag leaf width (FLW), and *QDDRW.daas-5D* (378.9–393.5 Mb) co-locates with a QTL cluster (277.0–491.2 Mb) related to KNS, FLW, TKW, and heading date [15]. These findings suggest that the loci associated with drought response and survival mechanisms may also serve as targets for enhancing yield potential and stability.

The limitation raised regarding the absence of control experiments in this study, which currently prevents definitive verification of whether the identified QTLs are specific to drought conditions. Although these QTLs demonstrated significant effects under drought stress, their potential functionality under non-stress conditions remains unexamined. Unfortunately, insufficient seed availability precluded the inclusion of control treatments in the present experiment. To address this gap, subsequent phenotyping of root-related traits will be conducted under optimal growing conditions. The acquired data will support two analytical approaches: direct QTL mapping under control conditions to compare with drought-induced QTLs, and mapping based on trait ratios between stress and control conditions. These analyses will help distinguish QTLs unique to drought response from those constitutive to plant growth—a distinction critical for breeding applications. While the current study provides directly relevant insights for drought tolerance breeding and genetic dissection under water-limited environments, further validation under controlled

conditions will significantly enhance the biological interpretation and practical utility of these loci.

A total of eight candidate genes were identified, primarily implicated in the biological metabolism of plant hormones and calcium-dependent lipid-binding domain proteins. Among these, *TraesCS4D01G001900* (*QDNRT.daas-4DS*) encodes a CDPK-related kinase, playing a crucial role in diverse signaling pathways for root growth and development [33,34], such as root hair growth and cell length [35]. Additionally, *TraesCS1B01G373900*, associated with *QDDRW.daas-1BL*, encodes an ABC transporter family protein essential for primary root growth and shoot development. Root development is governed by various plant hormones [36]. *TraesCS4A01G326400* (*QDTRS.daas-4AL*) and *TraesCS4D01G002400* (*QDNRT.daas-4DS*) encode ethylene-responsive transcription factors [37]. Ethylene plays diverse roles in growth, development, signal transduction, and cell differentiation, including root growth [8,9], and influences drought root system architecture-related traits like root hair and cluster root formation [25]. *TraesCS1B01G356600* (*QDDRW.daas-1BL*), *TraesCS4D01G002400* (*QDNRT.daas-4DS*), and *TraesCS5D01G285900* (*QDDRW.daas-5D*) encode the auxin-responsive proteins, auxin transport protein, and auxin-induced protein 12 in root cultures. Auxin, a core regulator, integrates with other plant hormones to regulate root development. The biosynthesis, transport, and signaling pathways of auxin, particularly indole-3-acetic acid, are crucial for plant root development [20]. *TraesCS3A01G406200* (*QDTRL.daas-3AL*) encodes the gibberellin 20 oxidase 2 (GA20ox), a key enzyme in gibberellin synthesis [36,37], which regulate various stages of plant growth and development, promoting seed germination, plant growth, flowering induction, and other biological functions.

In this study, the candidate genes were preliminarily screened through bioinformatic annotation and expression profiling analyses. These candidate genes currently serve only as reference targets as their biological functions remain to be experimentally validated. To systematically characterize these candidate genes, the following research pipeline were applied: (1) construction of a secondary mapping population coupled with KASP marker development for high-resolution genetic mapping; (2) comprehensive identification of target genes through integrated transcriptomic and genomic variation analyses; (3) functional validation employing both gene editing (e.g., CRISPR/Cas9) and transgenic complementation approaches. It should be emphasized that the KASP markers utilized in this study were specifically designed as genetic linkage markers rather than functional markers.

Traditional wheat breeding primarily focuses on yield and disease-related traits, with root system architecture closely linked to yield traits. Although traditional breeding has improved root system characteristics, the selection process remains lengthy and less efficient due to the challenges in field measurement of drought root system architecture-related traits [19]. Moreover, seedling root development is crucial for early wheat growth. KASP markers have been widely adopted for detecting genetic variations in wheat, enabling high-throughput genotyping. By utilizing genotype data from wheat SNP arrays for QTL mapping and genome-wide association studies, linked SNPs can be converted into KASP markers, which can then be directly applied in marker-assisted selection breeding programs. This approach facilitates the efficient identification and selection of desirable traits in wheat breeding efforts [19]. KASP markers are extensively applied in the improvement of yield, disease resistance, and quality traits in wheat. In this study, we successfully developed based on tightly linked SNP markers. The accuracy rates of *Kasp_1BL_DTRS*, *Kasp_3AL_DTRS*, *Kasp_DTRS_4A*, *Kasp_DDRW_5D*, and *Kasp_DNRT_4D* in detecting superior and non-superior phenotypes for DTRS, DDRW, and DNRT were 66.0% and 75.5%; 90.6% and 92.5%; 60.4% and 73.6%; 58.5% and 79.2%; 52.8% and 66.0%, respectively. Thus, these KASP markers could be used as valuable tools in MAS breeding programs. Addi-

tionally, accessions carrying more favorable alleles and exhibiting superior DRSA traits along with desirable agronomic characteristics, such as Jinmai 61, Liangxing 99, Yumai 35, Yumai 47, Liangxing 66, Bainong 64, Lumai 8, Yanzhan 4110, Zhengmai 366, Jimai 22, and Aikang 58, are recommended as parental lines for the improvement of drought root system architecture traits.

4. Materials and Methods

4.1. Plant Materials and Phenotypic Traits

Zhoumai16 is a high-yield winter wheat variety in the Huang-Huai wheat region. It is suitable for high-fertilizer and high-water cultivation and has moderate drought tolerance. DK171 is a newly developed high-yield and stress-tolerant winter wheat variety, with higher drought tolerance. This study utilized a Zhoumai16/DK171 $F_{2:6}$~ RIL population to conduct hydroponic experiments under greenhouse drought stress conditions, measuring DRSA-related traits with three replicates.

The standard Hoagland nutrient solution includes: Macronutrients (mg/L): Calcium Nitrate ($Ca(NO_3)_2{\cdot}4H_2O$) at 945 mg/L, Potassium Nitrate (KNO_3) at 607 mg/L, Ammonium Dihydrogen Phosphate ($NH_4H_2PO_4$) at 115 mg/L, Magnesium Sulfate ($MgSO_4{\cdot}7H_2O$) at 493 mg/L. Micronutrients (mg/L): EDTA-Iron (Fe-EDTA) at 20 mg/L, Boric Acid (H_3BO_3) at 2.86 mg/L (or Borax), Manganese Sulfate ($MnSO_4{\cdot}H_2O$) at 2.13 mg/L, Zinc Sulfate ($ZnSO_4{\cdot}7H_2O$) at 0.22 mg/L, Copper Sulfate ($CuSO_4{\cdot}5H_2O$) at 0.08 mg/L, and Ammonium Molybdate ($(NH_4)_6Mo_7O_{24}{\cdot}4H_2O$) at 0.02 mg/L. The solution pH should be adjusted to 5.5–6.5 using acid/base before use. Prepare 1× full-strength Hoagland solution in advance and adjust its pH to 5.8–6.0. Weigh 5.0 g, 7.5 g, 10.0 g, 12.5 g, 15.0 g, 17.5 g, and 20.0 g of PEG 6000 into seven clean beakers. Add about 60 mL of the pre-warmed (50–60 °C) 1× Hoagland solution to each beaker and stir gently on a magnetic stirrer until the PEG 6000 is completely dissolved. Transfer each solution to its corresponding 100 mL volumetric flask, bring the volume to the mark with additional 1× Hoagland solution, and mix thoroughly by inverting the flasks.

The root dry weights of Zhoumai16 plants subjected to 5%, 7.5%, 10%, 12.5%, 15%, 17.5%, and 20% PEG6000 were 0.0128 g, 0.0122 g, 0.0098 g, 0.0090 g, 0.0065 g, 0.0060 g, 0.0052 g, and 0.0026 g, respectively. A 12.5% concentration of PEG 6000 was added to the culture medium to simulate drought conditions. The methodology is as follows: 20 wheat seeds from each line were randomly selected and surface-sterilized with 10% H_2O_2 for 20 min, then placed in Petri dishes containing moist filter paper. When the coleoptile length reached approximately 2 cm, the seedlings were transferred to plastic trays (53 × 27 cm) with Hoagland nutrient solution supplemented with 12.5% PEG 6000 to induce osmotic stress.

These trays were then placed in a constant temperature culture room maintained at 25 °C, with 16 h light and 8 h darkness. After three weeks of growth in the greenhouse, seedling DRSA-related traits, including DDRW, DTRL, DTRA, and DNRT, were measured using the WinRHIZO software V1.0 (https://www.quantitative-plant.org/software/winrhizo, accessed on 24 June 2025) (Regent, Vancouver, BC, Canada). The specific method was as follows: thoroughly washed wheat roots were neatly arranged in a scanning tray, and scanned images were obtained using an Expression 11000XL scanner (Seiko Epson Corporation, Nagano Prefecture, Japan). The scanned images were analyzed using WinRHIZO software. Five plants were measured for each line, with three biological replicates.

This study used 108 varieties to validate the effects of KASP markers. The phenotypic values of DDRW, DTRL, DTRA, and DNRT for this validation population were also uniformly identified using the aforementioned method.

4.2. Genome Wide Linkage Mapping

The Zhoumai16/DK171 RIL population was genotyped using the wheat 90K SNP chip (CapitalBio Corporation, Beijing, China). The quality control followed: SNPs were set at missing data exceeding 20% or minor allele frequency (MAF) below 0.5. Filtered SNPs were classified into bin markers by IciMapping v4.2 [17]. Subsequently, the regression mapping algorithm in JoinMap v4.0 was used to calculate linkage distances for the obtained BIN markers and construct a higher-density linkage map. The successfully constructed linkage map has been previously reported by Wen et al. [18] and Li et al. [15]. Based on the constructed high-density SNP genetic map and the obtained root DRSA-related traits under drought, genome-wide linkage mapping was conducted by the inclusive composite interval mapping (ICIM-add) using IciMapping v4.1 [17]. The logarithm of odds (LOD) threshold for significant QTLs was determined to be 2.60 based on 1000 permutations. The physical positions were determined by IWGSC v1.0.

4.3. Identification of Candidate Genes for Drought-Related Traits

To identify the candidate genes associated with drought-related trait QTLs detected in the Zhoumai16/DK171 RIL population, high-confidence annotation genes within the LD block region surrounding each QTL peak SNP were extracted from the wheat IWGSC v1.0 [21]. Combining annotation, high-confidence genes with relevant annotated functions and differences in the coding regions between the two parents were screened as candidate genes. To investigate the expression patterns and identify candidate genes with notable transcription levels in seedlings or root tissues, we utilized the publicly accessible *Triticum aestivum* gene expression database [12] (http://wheat-expression.com/, accessed on 24 June 2025). After phenotyping, roots were sampled, and RNA was extracted from the root samples using the TRIzol method. cDNA was synthesized using the HiScript II cDNA Synthesis Kit. Primers for qRT-PCR were designed with Primer Premier 5.0. The reaction mixture consisted of 20 μL, including 2 μL of cDNA, 10 μL of ChamQ Universal SYBR qPCR Master Mix, and 0.4 μL of each primer. *TaActin*1 was used as an internal control to normalize the expression levels of different samples. The gene expression levels were analyzed using the $2^{-\Delta\Delta CT}$ method. All assays were performed with two biological replicates and three technical replicates.

4.4. KASP Marker Development and Validation

For all loci, flanking SNPs were converted to KASP markers [19], designed using PolyMarker (http://www.polymarker.info/, accessed on 24 June 2025). The 384-well plates were analyzed on a PHERAstarplus SNP, and genotyping was conducted by KlusterCaller (LGC) (https://www.lgcstandards.com/, accessed on 24 June 2025) (London, UK). All developed KASP markers required genetic effect validation using 108 varieties mainly from the Yellow and Huai Wheat Region [20]. These 108 materials primarily include the main popularized varieties, key backbone parents, and representative lines from the Yellow and Huai River Valleys Wheat Zone.

5. Conclusions

In conclusion, this study highlights the critical role of drought-related root system architecture in enhancing wheat resilience to drought. By analyzing the Zhoumai16/DK171 RIL population, five QTLs associated with DRSA-related traits were identified, including novel loci *QDDRW.daas-1BL*, *QDNRT.daas-4DS*, and *QDDRW.daas-5D*. These QTLs explained 6.1% to 18.9% of the phenotypic variances, with favorable alleles contributed by both Zhoumai16 and DK171. Additionally, five KASP markers were developed and validated, providing valuable tools for MAS breeding. The identification of eight candidate

genes further enriches the genetic resources for wheat drought tolerance. This research advances our understanding of the genetic basis of drought resistance and offers practical tools for breeding drought-tolerant wheat cultivars.

Author Contributions: Y.J. carried out the experimental and wrote the paper. G.C., X.Q., F.W., and H.J. participated in field trials. L.Z., C.L., J.L., and W.L. contributed to data analysis. P.L. designed the experiment and assisted in writing the paper. All authors have read and agreed to the published version of the manuscript.

Funding: This study was financially supported by the Shandong Province Wheat Industry Technology System (SDAIT-01-23); Shandong Agricultural Seeds Engineering Project (2023LZGC009, 2021LZGC013); Shandong Province Key R&D Plan (2022LZG002-4); Taishan Scholarship (tspd20221108); Jinan 20 New Universities Project (202228067).

Institutional Review Board Statement: We declare that these experiments complied with the ethical standards in China.

Data Availability Statement: All datasets generated for this study are included in the article; further inquiries can be directed to the first author.

Conflicts of Interest: The authors declare that they have no competing interests.

Appendix A

Table A1. The drought root system architecture-related traits in Zhoumai16/DK171 RIL population.

Accessions	Total Root Length-Drought (mm)	Total Root Surface-Drought (cm^2)	Total Root Volume-Drought (mm^3)	Dry Root Weight-Drought (g)
LINE1	26.5	5.8	201.0	0.0203
LINE2	25.8	6.0	24.7	0.0169
LINE3	24.1	5.4	35.7	0.0181
LINE4	27.6	6.5	48.3	0.0277
LINE5	35.0	7.6	45.3	0.0276
LINE6	42.5	8.6	73.3	0.0254
LINE7	35.5	8.7	94.3	0.0295
LINE8	38.1	6.1	81.0	0.0271
LINE9	35.5	6.9	105.7	0.0213
LINE10	50.0	10.3	79.3	0.0268
LINE11	26.8	5.7	108.0	0.0235
LINE12	24.6	6.5	57.3	0.0176
LINE13	35.9	8.1	48.7	0.0267
LINE14	37.9	6.4	63.0	0.0209
LINE15	60.6	8.5	70.7	0.0244
LINE16	40.5	9.2	136.7	0.0237
LINE17	42.5	6.7	99.0	0.0279
LINE18	36.2	7.2	137.3	0.0248
LINE19	31.9	6.2	86.0	0.0246
LINE20	NN	NN	NN	NN
LINE21	49.1	8.1	79.3	0.0232
LINE22	42.8	7.9	119.7	0.0284
LINE23	41.8	7.4	104.7	0.0305
LINE24	40.8	6.1	147.0	0.0233
LINE25	44.1	7.8	99.7	0.0286
LINE26	40.6	8.1	84.7	0.0237
LINE27	45.3	8.3	90.0	0.0226

Table A1. *Cont.*

Accessions	Total Root Length-Drought (mm)	Total Root Surface-Drought (cm^2)	Total Root Volume-Drought (mm^3)	Dry Root Weight-Drought (g)
LINE28	43.6	10.7	85.7	0.0271
LINE29	39.4	8.4	103.3	0.0278
LINE30	46.7	8.9	140.0	0.0255
LINE31	NN	NN	NN	NN
LINE32	41.9	8.3	128.3	0.0273
LINE33	35.2	7.6	198.7	0.0310
LINE34	34.5	7.0	96.7	0.0315
LINE35	41.6	8.2	116.7	0.0231
LINE36	38.0	7.2	156.7	0.0206
LINE37	37.4	6.9	84.0	0.0342
LINE38	40.5	10.4	99.0	0.0235
LINE39	35.9	6.0	129.3	0.0298
LINE40	39.3	8.2	82.3	0.0346
LINE41	35.0	8.6	87.0	0.0272
LINE42	40.7	8.3	91.0	0.0259
LINE43	37.0	7.4	163.0	0.0246
LINE44	47.5	9.0	105.0	0.0285
LINE45		6.8	103.7	0.0297
LINE46	40.4	7.7	124.7	0.0292
LINE47	47.3	7.9	101.7	0.0313
LINE48	35.9	9.9	134.3	0.0331
LINE49	35.0	6.0	88.0	0.0238
LINE50	48.5	9.8	114.0	0.0284
LINE51	36.1	8.4	117.0	0.0273
LINE52	52.8	7.6	79.0	0.0296
LINE53	36.2	7.8	114.0	0.0304
LINE54	56.6	10.3	72.0	0.0298
LINE55	42.5	8.1	176.3	0.0285
LINE56	41.9	8.2	128.0	0.0261
LINE57	35.7	7.1	113.3	0.0275
LINE58	36.9	6.9	96.0	0.0303
LINE59	48.0	7.5	126.0	0.0332
LINE60	32.2	7.8	116.3	0.0278
LINE61	47.5	8.6	77.3	0.0266
LINE62	40.3	8.1	129.0	0.0245
LINE63	37.1	7.1	99.0	0.0267
LINE64	44.5	7.5	95.7	0.0299
LINE65	47.8	6.9	139.0	0.0310
LINE66	40.1	7.0	117.7	0.0364
LINE67	41.2	9.2	122.3	0.0295
LINE68	42.8	7.7	141.0	0.0288
LINE69	39.7	6.2	151.7	0.0304
LINE70	NN	NN	NN	NN
LINE71	37.1	9.2	114.7	0.0278
LINE72	41.9	7.8	109.0	0.0315
LINE73	38.6	7.3	112.7	0.0289
LINE74	47.3	9.0	95.0	0.0370
LINE75	42.1	10.6	122.0	0.0221
LINE76	37.1	6.8	144.3	0.0374
LINE77	NN	NN	NN	NN
LINE78	39.0	7.8	89.7	0.0274

Table A1. *Cont.*

Accessions	Total Root Length-Drought (mm)	Total Root Surface-Drought (cm^2)	Total Root Volume-Drought (mm^3)	Dry Root Weight-Drought (g)
LINE79	39.6	6.9	109.7	0.0301
LINE80	43.8	8.5	135.0	0.0255
LINE81	43.1	8.4	102.7	0.0276
LINE82	45.0	7.1	100.0	0.0283
LINE83	40.3	7.8	123.3	0.0256
LINE84	30.8	6.8	82.0	0.0317
LINE85	34.2	7.8	62.3	0.0278
LINE86	NN	NN	NN	NN
LINE87	41.1	6.2	93.0	0.0282
LINE88	37.3	9.5	136.3	0.0236
LINE89	50.6	9.1	143.3	0.0286
LINE90	29.8	6.4	98.3	0.0271
LINE91	30.4	8.7	96.7	0.0274
LINE92	45.5	9.3	100.7	0.0308
LINE93	38.1	7.0	114.0	0.0342
LINE94	44.4	7.9	141.7	0.0282
LINE95	46.9	8.7	139.0	0.0363
LINE96	38.1	7.4	153.3	0.0301
LINE97	27.7	6.8	99.7	0.0247
LINE98	32.8	6.4	53.3	0.0245
LINE99	34.9	8.2	156.3	0.0309
LINE100	46.1	8.0	99.7	0.0298
LINE101	42.4	7.4	117.3	0.0323
LINE102	48.4	8.1	68.3	0.0345
LINE103	50.4	9.2	117.0	0.0272
LINE104	47.3	8.6	121.3	0.0431
LINE105	40.3	7.7	164.7	0.0297
LINE106	45.8	6.0	80.0	0.0305
LINE107	35.7	7.0	145.0	0.0329
LINE108	50.4	8.1	87.7	0.0296
LINE109	43.2	8.2	136.3	0.0287
LINE110	NN	NN	NN	0.0286
LINE111	41.0	6.4	71.7	0.0307
LINE112	NN	NN	NN	0.0274
LINE113	NN	NN	NN	0.0284
LINE114	NN	NN	NN	0.0413
LINE115	NN	NN	NN	0.0302
LINE116	54.5	10.3	97.0	0.0320
LINE117	44.6	7.7	109.7	0.0328
LINE118	NN	NN	NN	0.0256
LINE119	NN	NN	NN	0.0312
LINE120	41.3	7.0	104.3	0.0272
LINE121	38.3	6.0	91.0	0.0278
LINE122	50.3	7.6	77.7	0.0325
LINE123	45.1	8.3	165.3	0.0317
LINE124	44.7	8.2	77.0	0.0306
LINE125	37.8	7.2	101.7	0.0328
LINE126	38.2	6.2	117.0	0.0227
LINE127	30.7	5.7	164.7	0.0206
LINE128	43.8	7.9	55.0	0.0288
LINE129	57.4	7.7	102.7	0.0327

Table A1. *Cont.*

Accessions	Total Root Length-Drought (mm)	Total Root Surface-Drought (cm^2)	Total Root Volume-Drought (mm^3)	Dry Root Weight-Drought (g)
LINE130	49.5	7.8	147.7	0.0345
LINE131	44.4	7.6	125.3	0.0354
LINE132	38.6	7.3	145.3	0.0292
LINE133	45.8	8.6	97.7	0.0278
LINE134	44.3	9.0	67.3	0.0286
LINE135	36.1	6.7	117.0	0.0296
LINE136	34.8	7.3	126.3	0.0322
LINE137	42.3	8.2	143.3	0.0294
LINE138	27.3	6.3	151.3	0.0264
LINE139	36.2	7.5	68.0	0.0308
LINE140	42.1	7.9	137.0	0.0299
LINE141	NN	NN	NN	NN
LINE142	50.2	8.3	204.0	0.0304
LINE143	28.0	6.7	98.7	0.0162
LINE144	36.1	7.1	66.3	0.0284
LINE145	32.9	6.4	70.0	0.0258
LINE146	38.6	9.3	83.3	0.0221
LINE147	45.2	8.6	88.7	0.0280
LINE148	44.6	8.9	196.7	0.0278
LINE149	40.5	8.2	187.3	0.0326
LINE150	46.6	9.4	126.7	0.0308
LINE151	45.4	7.7	150.7	0.0287
LINE152	41.3	8.8	115.3	0.0255
LINE153	37.4	6.8	113.3	0.0251
LINE154	41.0	7.4	89.3	0.0330
LINE155	39.5	6.2	108.0	0.0243
LINE156	56.6	7.9	127.3	0.0207
LINE157	30.6	7.0	142.0	0.0236
LINE158	41.0	9.0	48.0	0.0318
LINE159	49.9	9.9	165.3	0.0323
LINE160	46.7	7.4	213.7	0.0372
LINE161	46.6	8.7	87.7	0.0268
LINE162	33.0	7.0	115.0	0.0293
LINE163	39.9	8.5	86.0	0.0242
LINE164	37.1	7.1	67.7	0.0267
LINE165	43.7	8.6	60.3	0.0350
LINE166	44.4	8.6	119.3	0.0293
LINE167	63.8	9.2	145.0	0.0306
LINE168	41.0	7.6	136.0	0.0279
LINE169	39.0	9.0	122.7	0.0287
LINE170	35.7	7.7	180.0	0.0241
LINE171	52.4	9.0	59.7	0.0230
LINE172	49.4	10.1	172.7	0.0343
LINE173	41.9	7.2	142.3	0.0279
LINE174	44.7	9.2	101.7	0.0271
LINE175	36.8	8.6	121.0	0.0268
LINE176	49.0	8.6	81.0	0.0346
LINE177	48.7	8.8	131.3	0.0304
LINE178	45.5	9.1	202.0	0.0301
LINE179	44.1	8.2	85.7	0.0301
LINE180	32.6	6.7	86.7	0.0253

Table A1. *Cont.*

Accessions	Total Root Length-Drought (mm)	Total Root Surface-Drought (cm^2)	Total Root Volume-Drought (mm^3)	Dry Root Weight-Drought (g)
LINE181	33.7	7.8	53.0	0.0259
LINE182	33.8	6.4	72.0	0.0230
LINE183	50.8	9.7	94.0	0.0212
LINE184	40.6	7.6	71.3	0.0324
LINE185	40.5	8.9	107.0	0.0257
LINE186	41.9	8.2	109.3	0.0277
LINE187	45.8	9.3	96.3	0.0314
LINE188	34.6	7.0	138.0	0.0316
LINE189	35.0	8.0	114.0	0.0317
LINE190	32.0	7.3	120.0	0.0203
LINE191	35.3	7.1	51.3	0.0314
LINE192	41.6	7.2	116.7	0.0311
LINE193	43.9	7.7	58.0	0.0369
LINE194	44.7	8.5	124.0	0.0280
LINE195	42.2	9.3	117.3	0.0323
LINE196	39.1	7.3	189.3	0.0292
LINE197	NN	NN	NN	NN
LINE198	43.5	7.9	85.7	0.0321
LINE199	29.3	7.1	130.0	0.0195
LINE200	51.9	8.3	77.3	0.0233
LINE201	39.5	8.5	65.7	0.0246
LINE202	40.1	7.1	44.7	0.0212
LINE203	40.3	8.2	87.7	0.0284
LINE204	38.6	8.3	96.7	0.0217
LINE205	39.2	8.5	65.0	0.0263
LINE206	39.2	8.2	82.7	0.0229
LINE207	49.0	7.9	72.7	0.0232
LINE208	35.8	7.4	102.0	0.0221
LINE209	NN	NN	NN	NN
LINE210	39.1	7.3	56.7	0.0234
LINE211	44.0	7.9	68.3	0.0306
LINE212	NN	NN	NN	NN
LINE213	34.0	7.8	133.7	0.0309
LINE214	51.4	7.2	87.0	0.0331
LINE215	46.3	9.4	97.7	0.0306
LINE216	46.8	7.8	61.7	0.0338
LINE217	40.2	9.2	107.0	0.0297
LINE218	40.5	8.2	76.3	0.0265
LINE219	36.5	9.1	73.7	0.0258
LINE220	41.4	7.4	67.0	0.0327
LINE221	47.1	9.4	86.0	0.0304
LINE222	38.9	9.6	126.0	0.0276
LINE223	38.5	6.7	103.0	0.0285
LINE224	39.2	7.3	67.3	0.0306
LINE225	35.0	7.1	80.3	0.0281
LINE226	37.4	7.8	82.7	0.0276
LINE227	30.5	7.0	84.7	0.0182
LINE228	33.5	7.2	27.7	0.0280
LINE229	43.4	7.1	81.7	0.0302
LINE230	35.5	7.7	74.7	0.0294

Table A1. *Cont.*

Accessions	Total Root Length-Drought (mm)	Total Root Surface-Drought (cm^2)	Total Root Volume-Drought (mm^3)	Dry Root Weight-Drought (g)
LINE231	NN	0.0	NN	NN
LINE232	42.3	9.1	114.7	0.0268
LINE233	39.7	9.2	102.0	0.0287
LINE234	NN	NN	NN	NN
LINE235	33.2	7.8	95.7	0.0335
LINE236	33.6	7.1	79.3	0.0251
LINE237	41.8	7.3	68.3	0.0303
LINE238	42.4	8.1	95.0	0.0284
LINE239	47.0	8.5	173.7	0.0278
LINE240	38.1	8.1	79.3	0.0322
LINE241	33.2	6.0	80.0	0.0304
LINE242	27.6	6.0	113.3	0.0344
LINE243	33.0	6.1	105.3	0.0262
LINE244	36.8	8.3	157.0	0.0285
LINE245	40.2	7.3	102.0	0.0418
LINE246	32.2	7.4	213.7	0.0227
LINE247	33.1	6.1	112.7	0.0311
LINE248	29.7	8.2	85.3	0.0264
LINE249	26.2	5.6	85.7	0.0235
LINE250	37.7	7.8	57.0	0.0247
LINE251	41.7	6.8	77.0	0.0312
LINE252	28.7	6.9	159.0	0.0230
LINE253	35.1	7.5	79.7	0.0315
LINE254	38.5	7.1	150.0	0.0302
LINE255	28.6	7.2	126.7	0.0294
LINE256	38.9	7.5	108.7	0.0273
LINE257	37.0	7.0	155.0	0.0250
LINE258	41.8	9.0	88.3	0.0348
LINE259	44.1	8.0	118.7	0.0262
LINE260	44.1	9.5	87.3	0.0281
LINE261	34.6	7.0	165.7	0.0234
LINE262	39.7	6.4	78.7	0.0380

Table A2. The qRT-PCR primers for the candidate genes.

Candidate Gene (IWGSC1.0)	Candidate Gene (IWGSC2.1)	Forward Primers (5′-3′)	Reverse Primers (5′-3′)
TraesCS1B01G356600	*TraesCS1B03G0973300*	AGGCTTTCTTGAAGCCCAGA	GACCAGCATCCTGTCTCCTT
TraesCS1B01G373900	*TraesCS1B03G1018500*	GCCCTCAAGGTGAAAGGTCT	CTTCCAGAGCTGCAAGTCG
TraesCS3A01G406200	*TraesCS3A03G0950800*	CATGCGGTGCAACTACTACC	GTGTCGCCGATGTTGATGAC
TraesCS3A01G416300	*TraesCS3A03G0969200*	CATGAGCCTCAACGAGAAGC	CTCTCATGCTGGTACGACGA
TraesCS4A01G326400	*TraesCS4A03G0812600*	AGCAGAACCACCACCTACC	CTGGTGTCGAACGGAAGAAC
TraesCS4D01G001900	*TraesCS4D03G0002800*	AGGAATTTGAGGCTGAAGCG	GGGACGTTGGAGTCGTAGTA
TraesCS4D01G002400	*TraesCS4D03G0003700*	GACACTGGAGTGGAACTGGA	CTAACAGCGGTCATCAAGGC
TraesCS5D01G285900	*TraesCS5D03G0654200*	CTGAGTCTGGTAGCGTGGAG	CCGTCGTTGCCCACGCCGTC

Table A3. The DRSA-related traits in the 108 wheat varieties and the genotype data for the developed KASP markers.

Name	*Kasp_1BL_DDRW*	DDRW (g)	*Kasp_5D_DDRW*	*Kasp_3AL_DTRL*	DDRT (mm)	*Kasp_4DS_DNRT*	DNRT	*Kasp_4AL_DTRS*	DTRS (cm^2)
Aikang 58	GG	0.0304	CC	AA	74.0	CC	100.2	GG	7.7
Bainong 3217	AA	0.0316	TT	AA	54.1	CC	18.6	AA	3.1
Bainong 64	AA	0.0358	TT	AA	88.3	TT	115.2	GG	9.2
Bima 4	GG	0.0198	TT	GG	48.9	TT	11.7	GG	2.4
Gaoyou 503	AA	0.0291	TT	AA	58.6	CC	57.6	GG	5.2
Gaocheng 8901	AA	0.0316	TT	AA	90.5	CC	123.5	GG	10.4
Huapei 5	GG	0.0235	TT	AA	61.5	CC	22.7	GG	3.6
Huaimai 18	AA	0.0251	TT	GG	64.5	TC	69.5	GG	5.9
Huaimai 20	GG	0.0287	TT	AA	80.2	CC	48.8	AA	6.1
Huaimai 21	GG	0.0345	CC	GG	64.0	TT	16.7	AA	3.2
Jimai 19	GG	0.0313	CC	GG	86.1	CC	170.8	AA	11.4
Jimai 20	AA	0.0324	TT	GG	62.9	CC	69.8	GG	6
Jimai 21	GG	0.0222	TT	AA	46.8	CC	10.8	AA	2.2
Jimai 22	GG	0.0307	CC	GG	59.6	CC	103.9	AA	6.3
Jinan 13	AA	0.0299	TT	AA	77.9	TT	23	AA	4.1
Jinan 17	GG	0.0233	TT	AA	36.8	CC	14.4	AA	2.1
Jining 16	AA	0.0196	TT	AA	44.8	CC	10.3	AA	2.1
Jishi 02-1	AA	0.0259	TT	GG	36.0	CC	8	GG	1.7
Jinmai 61	AA	0.0384	TT	AA	66.5	CC	44.9	GG	4.8
Lankao 24	GG	0.0279	TT	GG	61.6	TT	30.9	AA	4.2
Lankao 2	GG	0.0252	TT	AA	69.5	TT	162.5	AA	9.4
Lankao 906	AA	0.0326	TT	AA	54.9	TT	58.3	AA	5.3
Liangxing 66	AA	0.0361	CC	AA	92.7	CC	234	AA	12.8
Liangxing 99	GG	0.0364	CC	GG	61.1	CC	18.6	GG	3.3
Linhan 2	AA	0.0247	TT	AA	79.5	TT	49.6	GG	5.8
Linkang 12	AA	0.0265	TT	AA	63.9	TT	62	AA	5.6
Linmai 2	GG	0.0184	TT	GG	58.6	CC	55.8	GG	5
Linmai 4	AA	0.0245	TT	AA	45.1	CC	47.8	AA	4
Lumai 15	AA	0.0271	TT	GG	57.9	CC	23.7	GG	3.6
Lumai 21	GG	0.0203	TT	AA	54.3	CC	79.4	GG	5.8
Lumai 23	AA	0.0283	TT	AA	76.1	CC	70.1	AA	6.8
Lumai 5	GG	0.0118	CC	GG	60.7	TT	23.9	AG	3.6
Lumai 6	AA	0.024	TT	AA	63.1	CC	61.7	AA	5.6
Lumai 7	AA	0.0297	TT	AA	70.3	CC	68	GG	6.6
Lumai 8	AA	0.0357	TT	GG	62.0	CC	24.8	GG	3.9
Lumai 9	GG	0.0184	TT	AA	81.6	CC	150.8	GG	10.9
Luyuan 502	AA	0.0243	TT	AA	51.8	CC	129.4	GG	7.1
Luohan 2	AA	0.023	TT	GG	61.9	TT	79	AA	6.8
Luomai 21	GG	0.0271	TT	AA	66.7	CC	122.5	GG	8.9
Neixiang 188	AA	0.028	TT	GG	58.1	TT	85	GG	5.9
Neixiang 5	AA	0.019	TT	AA	63.2	CC	77.8	AA	6.8
Shannong 20	AA	0.0232	TT	GG	63.7	TT	166.8	GG	9.5
Shan 150	AA	0.028	TT	AA	67.1	TT	72.2	GG	6.8
Shan 229	AA	0.0294	TT	AA	89.5	CC	140	GG	10.5
Shan 253	AA	0.0202	TT	AA	69.5	CC	295.4	GG	12.2
Shan 354	AA	0.022	TT	GG	55.0	CC	66.9	AA	5.9
Shan 512	AA	0.0226	TT	AA	47.3	CC	71	AA	5
Shan 715	GG	0.0316	CC	GG	72.0	CC	80	AA	7
Shanmai 94	AA	0.0158	TT	AA	59.7	TT	224.4	AA	11.3
Shannong 78-59	AA	0.0279	TT	GG	45.2	TT	64.4	AA	5
Shanyou 225	AA	0.0219	TT	GG	68.0	TT	90.7	AA	7.1
DK171	GG	0.0214	TT	AA	62.3	CC	54.5	GG	5.4
Shijiazhuang 15	AA	0.0252	TT	AA	65.4	CC	31.4	AA	4.3
Shixin 733	GG	0.0199	TT	GG	63.0	TT	60.5	AA	5.9
Shiyou 17	AA	0.0246	TT	AA	68.2	CC	83.2	GG	7.1
Sunong 6	AA	0.0237	TT	AA	69.8	CC	199.5	GG	11.6
Taishan 5	GG	0.0288	TT	AA	64.5	TT	177.3	GG	8.8
Wanmai 19	AA	0.0183	TT	AA	62.5	CC	228.1	GG	11.3
Wanmai 29	AA	0.026	TT	AA	47.6	CC	235.6	GG	8.4
Wanmai 38	AA	0.0208	TT	AA	77.1	CC	190.9	GG	11.8
Wanmai 50	AA	0.017	TT	AA	70.0	CC	293.3	GG	13.8
Wanmai 52	GG	0.0212	TT	AA	58.6	CC	99	GG	7.1
Wanmai 53	AA	0.0213	TT	AA	71.6	CC	140.1	GG	9.5
Wennong 14	AA	0.0211	TT	AA	47.8	CC	156.2	AA	7.7
Wennong 5	AA	0.025	TT	AA	71.3	CC	159.4	GG	10.2
Wunong 148	AA	0.023	TT	AA	50.1	TT	23.7	AA	3.2
Xinnong 291	AA	0.0372	TT	AA	71.3	TT	39	GG	5
Xiaoyan 22	AA	0.0224	TT	GG	63.6	CC	128.8	AA	8.1
Xiaoyan 54	GG	0.023	TT	AA	60.2	CC	102.1	AA	5.6
Xiaoyan 6	AA	0.0287	TT	AA	46.3	CC	119.9	AA	8.6
Xiaoyan 81	AA	0.026	TT	AA	75.6	CC	91.2	AA	6.9
Xinmai 19	AA	0.0231	TT	AA	68.7	CC	108	GG	9
Xinmai 9	GG	0.0268	CC	GG	81.0	TT	12.7	AG	2.8
Yannong 18	AA	0.0223	TT	AA	61.3	TT	68.1	GG	6
Yannong 19	GG	0.0244	TT	AA	64.9	CC	99.2	GG	6
Yanzhan 4110	GG	0.0356	CC	GG	52.6	TC	54.6	GG	5.8
Yumai 18	AA	0.0268	TT	AA	67.6	CC	155.8	AA	8.6
Yumai 21	AA	0.0293	TT	AA	58.9	CC	42.7	AA	5.3
Yumai 2	AA	0.0224	TT	AA	75.3	CC	62.4	AA	5.5
Yumai 34	AA	0.0254	TT	AA	60.6	TT	168.9	GG	9.2
Yumai 35	AA	0.0363	TT	AA	61.2	TT	44.9	GG	5.4
Yumai 47	GG	0.0363	CC	GG	68.8	CC	76.1	AG	5.6
Yumai 49	AA	0.0194	TT	AA	48.2	TT	169.7	GG	7.1
Yumai 50	AA	0.0151	TT	AA	49.3	CC	9.7	AA	1.9
Yumai 63	AA	0.02	TT	GG	37.9	CC	97.3	AA	7.2

Table A3. *Cont.*

Name	*Kasp_1BL_DDRW*	DDRW (g)	*Kasp_5D_DDRW*	*Kasp_3AL_DTRL*	DDRT (mm)	*Kasp_4DS_DNRT*	DNRT	*Kasp_4AL_DTRS*	DTRS (cm^2)
Yumai 7	AA	0.0218	TT	AA	59.1	CC	80.5	GG	6.2
Zheng 9023	AA	0.0227	TT	AA	53.5	CC	58.9	AA	4.5
Zhengmai 366	GG	0.0318	TT	GG	41.8	CC	74.1	GG	5.6
Zhengyin 1	AA	0.0237	TT	AA	56.8	TT	181.6	GG	8.6
Zhengzhou 3	AA	0.0302	TT	AA	63.4	TC	140.2	AA	9.4
Zhongmai 871	AA	0.0235	TT	GG	77.7	CC	306.2	GG	10.8
Zhongmai 875	AA	0.0266	TT	AA	52.3	CC	93.6	GG	7
Zhongmai 895	GG	0.026	TT	GG	61.3	CC	148.6	GG	9.2
Zhongyu 5	AA	0.0259	TT	AA	65.3	TT	94.4	GG	7.1
Zhou 8425B	AA	0.0262	TT	AA	58.1	TT	68.7	GG	6
Zhoumai16	GG	0.0182	TT	AA	57.9	CC	58	GG	5.5
Zhoumai 18	AA	0.0236	TT	AA	59.1	CC	13.3	GG	2.6
Zhoumai 19	AA	0.0252	TT	GG	52.4	CC	40.5	GG	3.9
Zhoumai 22	AA	0.0197	TT	GG	47.5	TT	60.9	GG	4.7
Zhoumai 23	GG	0.0181	TT	GG	46.7	CC	88.5	GG	5.3
Zhoumai 25	AA	0.0155	TT	GG	47.8	TT	74.1	GG	4.5
Zhoumai 26	GG	0.0166	CC	GG	40.6	CC	133.9	GG	8.4
Zhoumai 28	AA	0.0195	TT	AA	56.7	CC	94.6	GG	5.6
Zhoumai 30	GG	0.015	TT	GG	46.2	TT	107.8	AA	5.5
Zhoumai 31	AA	0.0162	TT	GG	44.4	CC	36.8	GG	3.8
Zhoumai 32	GG	0.0178	TT	AA	48.1	CC	127	AA	9
Zimai 12	AA	0.0263	TT	AA	73.7	TT	50	AA	5.6
Zixuan 2	AA	0.0224	TT	AA	67.8	CC	141.5	GG	7.9

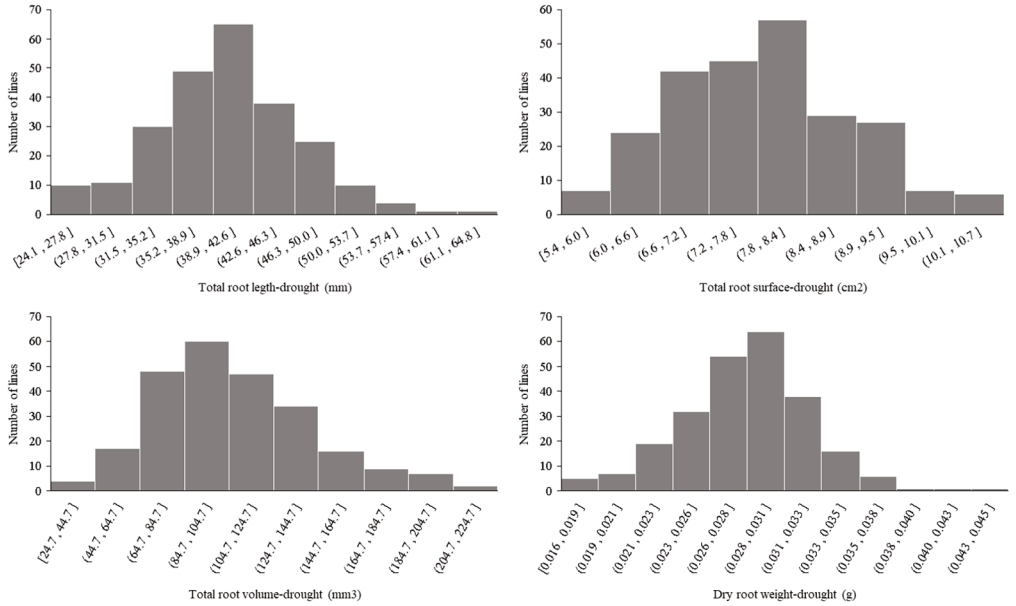

Figure A1. Frequency distribution of the DRSA-related traits in the Zhoumai16/DK171 RIL population.

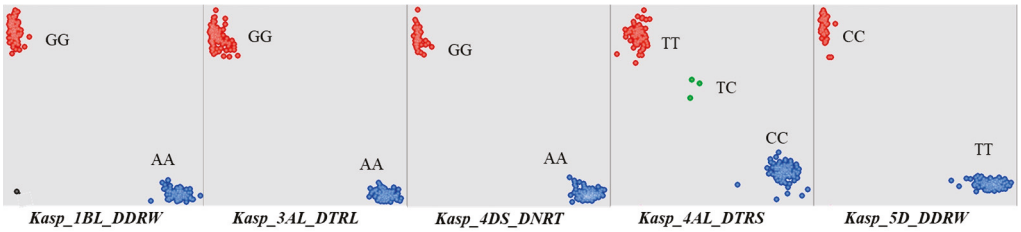

Figure A2. The genotype of the KASP markers.

References

1. Kadam, N.N.; Tamilselvan, A.; Lawas, L.M.; Quinones, C.; Bahuguna, R.N.; Thomson, M.J.; Dingkuhn, M.; Muthurajan, R.; Struik, P.C.; Yin, X.; et al. Genetic control of plasticity in root morphology and anatomy of rice in response to water deficit. *Plant Physiol.* **2017**, *174*, 2302–2315. [CrossRef]
2. Ayalew, H.; Liu, H.; Börner, A.; Kobiljski, B.; Liu, C.J.; Yan, G.J. Genome-wide association mapping of major root length QTLs under PEG-induced water stress in wheat. *Front. Plant Sci.* **2018**, *9*, 1759. [CrossRef]
3. Mohammadi, R. Breeding for increased drought tolerance in wheat: A review. *Crop Pasture Sci.* **2018**, *69*, 223–241. [CrossRef]

4. Bapela, T.; Shimelis, H.; Tsilo, T.J.; Mathew, I. Genetic improvement of wheat for drought tolerance: Progress, challenges and opportunities. *Plants* **2022**, *11*, 1331. [CrossRef] [PubMed]
5. Beyer, S.; Daba, S.; Tyagi, P.; Bockelman, H.; Brown-Guedira, G.; IWGSC; Mohammadi, M. Loci and candidate genes controlling root traits in wheat seedlings—A wheat root GWAS. *Funct. Integr. Genom.* **2019**, *19*, 91–107. [CrossRef]
6. Mathew, I.; Shimelis, H.; Shayanowako, A.I.T.; Laing, M.; Chaplot, V. Genome-wide association study of drought tolerance and biomass allocation in wheat. *PLoS ONE* **2019**, *14*, e0225383. [CrossRef]
7. Sabar, M.; Shabir, G.; Shah, S.M.; Aslam, K.; Naveed, S.A.; Arif, M. Identification and mapping of QTLs associated with drought tolerance traits in rice by a cross between Super Basmati and IR55419-04. *Breed. Sci.* **2019**, *69*, 169–178. [CrossRef] [PubMed]
8. Chen, H.X.; Wei, J.T.; Tian, R.; Zeng, Z.Y.; Tang, H.P.; Liu, Y.L.; Xu, Q.; Deng, M.; Jiang, Q.T.; Chen, G.Y.; et al. A major quantitative trait locus for wheat total root length associated with precipitation distribution. *Front. Plant Sci.* **2022**, *13*, 995183. [CrossRef] [PubMed]
9. Yang, M.J.; Wang, C.R.; Hassan, M.A.; Wu, Y.Y.; Xia, X.C.; Shi, S.B.; Xiao, Y.G.; He, Z.H. QTL mapping of seedling biomass and root traits under different nitrogen conditions in bread wheat (*Triticum aestivum* L.). *J. Integr. Agric.* **2021**, *20*, 1180–1192. [CrossRef]
10. Wang, X.; Wang, H.; Liu, S.; Zhang, B.; Zhang, J.; Li, Z.; Wang, Y.; Xie, C.; Huang, L.; Cao, T.; et al. Genetic mapping of quantitative trait loci for yield and yield components in an advanced backcross population derived from a cultivated × wild soybean cross. *Theor. Appl. Genet.* **2014**, *127*, 581–589.
11. Soriano, J.M.; Alvaro, F. Discovering consensus genomic regions in wheat for root-related traits by QTL meta-analysis. *Sci. Rep.* **2019**, *9*, 10537. [CrossRef]
12. Meng, L.; Li, H.; Zhang, L.; Wang, J. QTL IciMapping: Integrated software for genetic linkage map construction and quantitative trait locus mapping in biparental populations. *Crop J.* **2015**, *3*, 269–283. [CrossRef]
13. Wen, W.; He, Z.H.; Gao, F.M.; Liu, J.D.; Jin, H.; Zhai, S.N.; Qu, Y.Y.; Xia, X.C. A high-density consensus map of common wheat integrating four mapping populations scanned by the 90K SNP array. *Front. Plant Sci.* **2017**, *8*, 1389. [CrossRef]
14. Rasheed, A.; Hao, Y.; Xia, X.; Khan, A.; Xu, Y.; Varshney, R.K.; He, Z. Crop breeding chips and genotyping platforms: Progress, challenges, and perspectives. *Mol. Plant* **2017**, *10*, 1047–1064. [CrossRef]
15. Liu, R.X.; Wu, F.K.; Xin, Y.; Yu, L.; Wang, Z.Q.; Liu, S.H.; Deng, M.; Ma, J.; Wei, Y.M.; Zhang, Y.L.; et al. Quantitative trait loci analysis for root traits in synthetic hexaploid wheat under drought stress conditions. *J. Integr. Agric.* **2020**, *19*, 1947–1960. [CrossRef]
16. International Wheat Genome Sequencing Consortium (IWGSC). The Wheat Genome Reference Sequence. Available online: https://www.wheatgenome.org/projects/reference-genome-project/refseq-v1.0/ (accessed on 1 January 2023).
17. Wheat Expression Database. Available online: www.wheat-expression.com (accessed on 1 January 2023).
18. Collard, B.C.Y.; Jahufer, M.Z.Z.; Brouwer, J.B.; Pang, E.C.K. An introduction to markers, quantitative trait loci (QTL) mapping and marker-assisted selection for crop improvement: The basic concepts. *Euphytica* **2005**, *142*, 169–196. [CrossRef]
19. Nehe, A.S.; Foulkes, M.J.; Ozturk, I.; Rasheed, A.; York, L.; Kefauver, S.C.; Ozdemir, F.; Morgounov, A. Root and canopy traits and adaptability genes explain drought tolerance responses in winter wheat. *PLoS ONE* **2021**, *16*, e0242472. [CrossRef] [PubMed]
20. Jin, Y.R.; Wang, Y.M.; Liu, J.D.; Wang, F.Y.; Qiu, X.D.; Liu, P. Genome-wide linkage mapping of root system architecture-related traits in common wheat (*Triticum aestivum* L.). *Front. Plant Sci.* **2023**, *14*, 1274392. [CrossRef] [PubMed]
21. Li, Q.X.; Wang, W.Q.; Wang, W.L.; Zhang, G.Q.; Liu, Y.; Wang, Y.; Wang, W. Wheat F-box protein gene *TaFBA1* is involved in plant tolerance to heat stress. *Front. Plant Sci.* **2018**, *9*, 521. [CrossRef] [PubMed]
22. Ye, H.; Roorkiwal, M.; Valliyodan, B.; Zhou, L.J.; Chen, P.Y.; Varshney, R.K.; Nguyen, H.T. Genetic diversity of root system architecture in response to drought stress in grain legumes. *J. Exp. Bot.* **2018**, *69*, 3267–3277. [CrossRef]
23. Ibrahim, S.E.; Schubert, A.; Pillen, K.; Léon, J. QTL analysis of drought tolerance for seedling root morphological traits in an advanced backcross population of spring wheat. *Theor. Appl. Genet.* **2012**, *124*, 533–545.
24. Liu, W.X.; Wang, J.R.; Wang, C.Y.; Ma, G.; Wei, Q.R.; Lu, H.F.; Xie, Y.X.; Ma, D.Y.; Kang, G.Z. Root growth, water and nitrogen use efficiencies in winter wheat under different irrigation and nitrogen regimes in North China Plain. *Front. Plant Sci.* **2018**, *9*, 1798. [CrossRef] [PubMed]
25. Li, C.N.; Li, L.; Reynolds, M.P.; Wang, J.Y.; Chang, X.P.; Mao, X.G.; Jing, R.L. Recognizing the hidden half in wheat: Root system attributes associated with drought tolerance. *J. Exp. Bot.* **2021**, *72*, 5117–5133. [CrossRef]
26. Alahmad, S.; El Hassouni, K.; Bassi, F.M.; Dinglasan, E.; Youssef, C.; Quarry, G.; Aksoy, A.; Mazzucotelli, E.; Juhász, A.; Able, J.A.; et al. A major root architecture QTL responding to water limitation in durum wheat. *Front. Plant Sci.* **2019**, *10*, 436. [CrossRef]
27. Rufo, R.; Salvi, S.; Royo, C.; Soriano, J.M. Exploring the genetic architecture of root-related traits in Mediterranean bread wheat landraces by genome-wide association analysis. *Agronomy* **2020**, *10*, 613. [CrossRef]
28. Xu, P.; Zhao, P.X.; Cai, X.T.; Mao, J.L.; Miao, Z.Q.; Xiang, C.B. Integration of jasmonic acid and ethylene into auxin signaling in root development. *Front. Plant Sci.* **2020**, *11*, 271. [CrossRef]
29. Tian, X.L.; Xia, X.C.; Xu, D.G.; Liu, Y.Q.; Xie, L.; Hassan, M.A.; Song, J.; Li, F.J.; Wang, D.S.; Zhang, Y.; et al. *Rht24b*, an ancient variation of *TaGA2ox-A9*, reduces plant height without yield penalty in wheat. *New Phytol.* **2022**, *233*, 738–750. [CrossRef]

30. Li, A.L.; Zhu, Y.F.; Tan, X.M.; Wang, X.; Wei, B.; Guo, H.Z.; Zhang, Z.L.; Chen, X.B.; Zhao, G.Y.; Kong, X.Y.; et al. Evolutionary and functional study of the *CDPK* gene family in wheat (*Triticum aestivum* L.). *Plant Mol. Biol.* **2008**, *66*, 429–443. [CrossRef]
31. Sun, T.; Wang, Y.; Wang, M.; Li, T.T.; Zhou, Y.; Wang, X.T.; Wei, S.Y.; He, G.Y.; Yang, G.X. Identification and comprehensive analyses of the *CBL* and *CIPK* gene families in wheat (*Triticum aestivum* L.). *BMC Plant Biol.* **2015**, *15*, 269. [CrossRef] [PubMed]
32. Ivashuta, S.I.; Petrick, J.S.; Heisel, S.E.; Zhang, Y.J.; Guo, L.; Reynolds, T.L.; Rice, J.F.; Allen, E.; Roberts, J.K. Endogenous small RNAs in grain: Semi-quantification and sequence homology to human and animal genes. *Food Chem. Toxicol.* **2009**, *47*, 353–360. [CrossRef] [PubMed]
33. Petricka, J.J.; Winter, C.M.; Benfey, P.N. Control of *Arabidopsis* root development. *Annu. Rev. Plant Biol.* **2012**, *63*, 563–590. [CrossRef] [PubMed]
34. Miao, Z.Q.; Zhao, P.X.; Mao, J.L.; Yu, L.H.; Yuan, Y.; Tang, H.; Liu, Z.B.; Xiang, C.B. *HOMEOBOX PROTEIN52* mediates the crosstalk between ethylene and auxin signaling during primary root elongation by modulating auxin transport-related gene expression. *Plant Cell* **2018**, *30*, 2761–2778. [CrossRef] [PubMed]
35. Divte, P.; Yadav, P.; Jain, P.K.; Paul, S.; Singh, B. Ethylene regulation of root growth and phytosiderophore biosynthesis determines iron deficiency tolerance in wheat (*Triticum* spp.). *Environ. Exp. Bot.* **2019**, *162*, 1–13. [CrossRef]
36. Hu, Z.R.; Wang, R.; Zheng, M.; Liu, X.B.; Meng, F.; Wu, H.L.; Yao, Y.Y.; Xin, M.M.; Peng, H.R.; Ni, Z.F.; et al. *TaWRKY51* promotes lateral root formation through negative regulation of ethylene biosynthesis in wheat (*Triticum aestivum* L.). *Plant J.* **2018**, *96*, 372–388. [CrossRef]
37. Zhao, Y.D. Essential roles of local auxin biosynthesis in plant development and in adaptation to environmental changes. *Annu. Rev. Plant Biol.* **2018**, *69*, 417–435. [CrossRef]

Disclaimer/Publisher's Note: The statements, opinions and data contained in all publications are solely those of the individual author(s) and contributor(s) and not of MDPI and/or the editor(s). MDPI and/or the editor(s) disclaim responsibility for any injury to people or property resulting from any ideas, methods, instructions or products referred to in the content.

plants

MDPI

Article

Identification and Expression Characteristics of the Cryptochrome Gene Family in *Chimonobambusa sichuanensis*

Yining Kong [1,†], Changlai Liu [1,†], Tianshuai Li [1], Ji Fang [2] and Guohua Liu [1,*]

[1] National Key Laboratory for the Development and Utilization of Forest Food Resources, Co-Innovation Centre for Sustainable Forestry in Southern China, Bamboo Research Institute, Nanjing Forestry University, Nanjing 210037, China; kongyining2001@126.com (Y.K.); lcl2012@njfu.edu.cn (C.L.); lts123@njfu.edu.cn (T.L.)
[2] Jiangsu Vocational College of Agriculture and Forestry, Nanjing 210037, China; jifang625@126.com
* Correspondence: ghliu@njfu.edu.cn
† These authors contributed equally to this work.

Abstract: Cryptochrome is an important class of blue-light receptors involved in various physiological activities such as photomorphogenesis and abiotic stress regulation in plants. In order to investigate the molecular mechanism of blue-light-induced color change in *Chimonobambusa sichuanensis*, we screened and cloned the gene encoding the blue-light receptor Cryptochrome. In order to investigate the molecular mechanism of blue-light-induced color change in *Chimonobambusa sichuanensis*, we screened and cloned the gene encoding the blue-light receptor Cryptochrome in *Ch.sichuanensis*, and analyzed the expression characteristics of the Cryptochrome gene in *Ch.sichuanensis* under different light intensities, light quality, and temperatures by qRT-PCR. Through homologous cloning, a total of four *CsCRY* genes were obtained in the *Ch.sichuanensis* genome, namely, *CsCRY1a*, *CsCRY1b*, *CsCRY2*, and *CsCRY3*. Structural domain analyses of the encoded proteins of the four genes revealed that all CsCRYs proteins had the typical photoreceptor structural domain, PRK (protein kinase C-related kinase). Phylogenetic tree analyses revealed that the four genes *CsCRY1a*, *CsCRY1b*, *CsCRY2*, and *CsCRY3* could be categorized into three subfamilies, with *CsCRY1a* and *CsCRY1b* clustered in subfamily I, *CsCRY2* classified in subfamily II, and *CsCRY3* belonging to subfamily III. All CsCRYs proteins lacked signal peptides and the instability index was higher than 40, among which the isoelectric points of *CsCRY1a*, *CsCRY1b*, and *CsCRY2* were around five. qRT-PCR analysis revealed that the expression of all four *CsCRYs* genes was up-regulated at 75 μmol·m^{-2}·s^{-1} blue-light illumination for 4 h. In addition, under treatments of different light quality, the expression of *CsCRY2* genes was significantly higher under blue light than under red light and a mixture of red light and blue light with a light intensity of 1:1; the expression of *CsCRY1a* and *CsCSY1b* was significantly higher in the mixed light of red and blue light than in the single light treatment, while under different temperature gradients, *CsCRYs* genes were highly expressed under low-temperature stress at −5 °C and 0 °C. This study provides a basis for further research on blue-light-induced color change in *Ch.sichuanensis* and expands the scope of Cryptochrome gene research.

Keywords: *CRY* gene family; *Ch.sichuanensis*; blue-light stress; low-temperature stress

1. Introduction

Bambusoideae is the largest of the 12 subfamilies in Poaceae, which currently has 127 genera and over 1680 species worldwide, including both herbaceous and woody bamboos. Among these, the genus *Chimonobambusa*, belonging to the Arundinarieae tribe and

Shlbataeinae subtribe within Bambusoideae, represents an important bamboo species. It has applications in food, pharmaceuticals, timber, chemical raw materials, and landscaping, and is primarily distributed in high-altitude regions of China, Laos, Vietnam, Myanmar, and India, exhibiting strong cold tolerance [1]. The *Chimonobambusa* genera produce shoots in autumn and overwinter as shoots or young plants; their culms turn purple before winter. In our previous research on *Chimonobambusa*, specifically *Chimonobambusa sichuanensis* (commonly known as "Yueyue Bamboo"), we discovered that the color change of culms before overwintering is associated with blue light and influenced by temperature, where blue light is a necessary condition for color change, while the depth and presence of coloration are modulated by temperature. A transcriptomic analysis of *Chimonobambusa sichuanensis* culms before and after blue-light-induced color changes revealed that the blue-light receptor gene *CRY* was significantly induced by blue light [2].

Cryptochromes (CRYs) are blue-light photoreceptor proteins that play pivotal roles in regulating diverse biological processes across multiple species, including plants, animals, and microorganisms. Initially identified in Arabidopsis thaliana, CRYs are evolutionarily conserved and functionally versatile, mediating light-dependent responses such as photomorphogenesis, circadian rhythm regulation, DNA repair, and stress adaptation [3]. Cryptochromes are characterized by two primary structural domains. One is the N-terminal domain, known as the photolyase homology region (PHR), which shares high homology with photolyases, enzymes that repair UV-induced DNA damage. This domain binds flavin adenine dinucleotide (FAD) as a chromophore, enabling blue-light absorption. Key residues forming the FAD-binding cavity (e.g., TGYP and LLDAD motifs) are highly conserved, as observed in *Sorghum bicolor* SbCRY1a/1b and *Arabidopsis* AtCRY1. The C-terminal domain (C-terminal extension, CTE) is variable across species and critical for signal transduction. In plants, the CTE contains conserved motifs (e.g., DAS domain) that mediate interactions with downstream signaling partners like COP1 (Constitutive Photomorphogenic 1) and SPA (Suppressor of Phytochrome A). For instance, *Arabidopsis* CRY1 recruits the SWR1 complex via interactions with SWC6 and ARP6 to regulate H2A.Z histone deposition, thereby modulating light-responsive gene expression [4]. Previous studies have found that plants contain three main classes of Cryptochrome proteins: CRY1, CRY2, and CRY3 [5]. It is generally believed that CRY1 plays a dominant role in blue-light-induced photomorphogenesis, whereas CRY2 mainly regulates photoperiodicity to affect flowering time, and CRY3 plays an important role in the regulation of photoperiods and biological clocks. There is an overlap in the functions of the two proteins, CRY1 and CRY2, in regulating flowering. Although CRY1, CRY2, and CRY3 are the same blue-light receptor, their structural domains are very different and they have different light-responsive functions [6,7]. CRY1 and CRY2 both have a DNA photolyase domain and FAD binding domain, which mainly contain an N-terminal photorepair enzyme homology region (PHR) and C-terminal regulatory region. But not every CRY member of all species has a complete structure. For example, studies have shown that the DASH cryptochrome, also known as CRY3, lacks a C-terminal regulatory region [8]. At the same time, studies have found that corn, wheat, Arabidopsis and rice CRY1 proteins all contain a PHR domain and CCE domain, but their CRY2 proteins only have one PHR domain.

Studies have confirmed that *CRY* is involved in the response of plants to light stress. Different *CRYs* may mediate different blue-light responses through different modes of action. In Arabidopsis thaliana, *CRY1* mediates the blue-light-dependent inhibition of hypocotyl elongation, and *CRY1* can promote blue-light-induced anthocyanin accumulation. The function of *CRY2* in the early photomorphogenesis of Arabidopsis thaliana seedlings was mainly under low and medium light intensity, and the *CRY2* mutant showed an obvious hypocotyl phenotype under low-intensity blue light (<10 $\mu mol \cdot m^{-2} \cdot s^{-1}$), but

did not change significantly under high-intensity blue-light stress. In addition, blue light and *CRY1* and *CRY2* were found to jointly regulate the transcription of SIG5, a transcription factor in the chloroplast signaling pathway in response to light stress in Arabidopsis [9]. Found in ferns, *CRY3* is a photoreceptor that mediates the blue-light inhibition of spore germination and plays a role in promoting the growth of plants under conditions of weak light stress.

At the same time, CRY is involved in the response of plants to temperature stress. Previous studies have found that CRY interacts with PIF4 and PIF5 in a blue-light-dependent manner. CRY1 and PIF4 interact to repress the transcription of PIF4, which in turn represses the expression of auxin-related genes such as YUC8, IAA19, IAA29, and heat-induced hypocotyl elongation by inhibiting cell elongation. CRY1 and CRY2, as well as PIF4 and PIF5, can regulate the expression of downstream genes responding to cold stress by binding to the same promoter regions of downstream genes [10]. Key genes in the CRY2 signaling pathway, such as HY5 and COP1, are involved in the regulation of cold-stress signaling. It was also found, in Arabidopsis thaliana, that CRY2 plays a role in the regulation of flowering dependent on environmental temperature, and the late-flowering phenotype of CRY2 mutants is more obvious at 16 °C than at 23 °C; that is, CRY2 mutations may lead to plants that are more sensitive to changes in environmental temperature. The temperature-responsive phenotype of the CRY2 mutant was significantly inhibited by a mutant that lost temperature sensitivity, TFL-1. But so far, there are few studies on the relationship between CRY and temperature stress. In order to explore the relationship between low-temperature stress and temperature stress in more detail, research is urgently needed. In this study, the *CsCRYs* gene family in Sichuan Province was identified and analyzed, which provided a theoretical reference for the subsequent gene cloning and functional analysis of the *CsCRYs* gene family in Sichuan Province. Although previous researchers have studied *CRY* genes in a variety of plants, there is still a lot of room for development in genetic studies of numerous bamboo species.

2. Materials and Methods

2.1. Chimonobambusa sichuanensis CsCRYs Gene Selected Based on Phyllostachys Edulis CRY Sequences

Use the protein sequence and DNA sequence of the cryptochrome gene of *Phyllostachys edulis* to search the sequence database of *Chimonobambusa sichuanensis* constructed by our laboratory [11], including the protein sequences and cDNA sequences contained in the gene database and the transcriptome database. The software used is the blast software package in TBtools v2.154, with the parameters of E-value < 1×10^{-5}, percentage identity > 90%, and query cover > 90%, and at the same time, sequence homology analysis was performed using SnapGene v6.0.2 for multiple sequence alignment, followed by redundancy removal via BLASTN against the NCBI nr database (https://www.ncbi.nlm.nih.gov/cdd/) (accessed on 20 September 2023) (E-value set to 0.001, other parameters set to default). Four non-redundant gene sequences were retained according to their closest orthologs in the UniProtKB and Swiss-Prot databases. The portion of the *Ch.sichuanensis* Cryptochrome gene family protein sequences with high sequence similarity was presented as a visualization plot using the program ESPript 3 (https://espript.ibcp.fr/ESPript/ESPript/index.php) (accessed on 3 February 2024). The sequence similarities depiction parameter was set to PAM250, the Global score was set to 0.2 and the Diff. score was set to 0.5.

2.2. Structural Domain Analysis of CsCRYs

The conserved motifs of *Ch.sichuanensis CRY* protein sequences were identified using the online analysis tool MEME v5.5.8 (http://meme-suite.org/) (accessed on 25 September

2023). Parameters were set to a maximum of 10 motifs, motif lengths were set to 20–50 amino acid residues, and site distributions were set to either zero or one occurrence per sequence (contributing motif sites). At the same time, the protein sequences of 55 *CRYS* genes from other 11 species were analyzed by motif analysis, and the differences between the CsCRY protein motif of *Ch.sichuanensis* and CsCRY protein motif of other species were aligned. Using NCBI batch CD search (https://www.ncbi.nlm.nih.gov/Structure/bwrpsb/bwrpsb.cgi) (accessed on 20 September 2023), the conserved domain of the gene was obtained. The results of CDD were input by TBtools software, and the conserved domains of the *Ch.Sichuanensis CsCRYs* family were visualized. Other plant types included the following: *Arabidopsis thaliana* (ID: 826470, 839529, and 832554), *O. sativa* (LOC9270575, LOC4336008, LOC4329738, LOC9270575, and LOC4341749), *Triticum aestivum* (LOC119322215, LOC123157423, LOC123164714, LOC119317171, and LOC123149308), *Zea mays* (LOC100502533, LOC100194126, LOC133921908, and LOC100384475), *Glycine max* (LOC100797839, LOC114409283, LOC100815428, LOC100786551, LOC100783312, and LOC100233234), *Hordeum vulgare* (LOC123413527, LOC123406235, and LOC114377802), *Sorghum bicolor* (LOC110435145, LOC110436666, LOC8069379, and LOC8078292), *Populus trichocarpa* (LOC7495156, LOC7486597, LOC18100781, and LOC18102473), *Gossypium hirsutum* (LOC107957756, LOC121217897, LOC107940541, LOC107936243, LOC107905111, LOC107900827, LOC107902007, LOC107961766, and LOC107929100), *Physcomitrella patens* (LOC112284608, LOC112273862, and LOC112284678), and *Phyllostachys edulis*. The gene numbers of the alignment sequences listed above are in parentheses. A phylogenetic analysis was conducted of the *CsCRYs* gene family in *Ch.sichuanensis.*

The sequences of the plants were obtained from the TAIR10 database (http://www.Arabidopsis.org/) (accessed on 20 September 2023), Ensembe Plant database (http://plants.ensembl.org/index.html) (accessed on 20 September 2023), and PFAM database (http://pfam, sanger.ac.uk) (accessed on 20 September 2023). Mega X software v11 was used to perform multiple alignment analysis of *Arabidopsis thaliana AtCRY*, *O. sativa OsCRY*, *Sorghum bicolor SbCRY*, *Triticum aestivum TaCRY*, *Hordeum vulgare HvCRY*, *Populus trichocarpa PtCRY*, *Zea* mays *ZmCRY*, *Glycine max GmCRY*, *Gossypium hirsutum GhCRY*, *Physcomitrium sphaericum PsCRY*, *Phyllostachys edulis PheCRY*, and the conserved domain sequences of *CRY* in *Ch.sichuanensis*. Bootstrap was set to 1000 and the online software Evolview (https://www.evolgenius.info/) (accessed on 21 September 2023) was used to depict the evolutionary tree. The parameters were set to Neighbor-Join and a Bootstrap of 1000.

2.3. Chimonobambusa sichuanensis CsCRYs Gene Family Proteins

Subcellular localization prediction was performed using the Plant-mPLoc online tool (http://www.csbio.sjtu.edu.cn/bioinf/plant-multi/) (accessed on 2 March 2024) and the WoLF PSORT: Protein Subcellular Localization Prediction (https://wolfpsort.hgc.jp/) (accessed on 2 March 2024).

The secondary structure of CsCRYs proteins was predicted by the online tool SOPMA (https://npsa.lyon.inserm.fr/cgi-bin/npsa_automat.pl?page=/NPSA/npsa_sopma.html) (accessed on 28 April 2024). In addition, the tertiary structure of CsCRYs proteins was modeled and displayed by the Swiss-Model interactive tool (https://swissmodel.expasy.org/) (accessed on 2 March 2024). BUSCA (https://busca.biocomp.unibo.it/) (accessed on 2 March 2024) and ExPASy ProtParam (https://web.expasy.org/protparam/) (accessed on 2 March 2024) online software were used to predict physicochemical protein properties such as the molecular weight, theoretical isoelectric point, number of amino acids, and instability coefficient.

2.4. CsCRYs Gene Expression Pattern in Chimonobambusa sichuanensis Under Different Environmental Conditions

Firstly, light quality was set as the environmental variable, and *Ch.sichuanensis* hydroponic seedlings were cultivated in the greenhouse of Nanjing Forestry University Bamboo Research Institute, cultured at a constant temperature of 20 °C. Hydroponics seedlings were treated with three kinds of light without interruption: single blue light and red light with a light intensity of 100 μmol·m^{-2}·s^{-1}, and mixed light with a total light intensity of 100 μmol·m^{-2}·s^{-1}. The mixed light was composed of red light and blue light with a light intensity ratio of 1:1.

Next, light intensity was set as the environmental variable, and the bamboo seedlings were irradiated uninterruptedly using blue light with total light intensities of 50, 75, and 100 μmol·m^{-2}·s^{-1}. Finally, temperature was set as the environmental variable, and bamboo seedlings were irradiated using constant natural light with a light intensity of 100 μmol·m^{-2}·s^{-1}, and treated with different temperature gradients: −5 °C, 0 °C, 5 °C, 10 °C, and 20 °C. Three pots of bamboo seedlings with similar growth were set as the replicate control, and leaves were collected every 4 h. The sampling times were 0 h, 4 h, 8 h, 12 h, 16 h, 20 h, and 24 h. First, the RNA extraction kit from Vazyme Biotech company (Nanjing, China), the VeZol-Pure Total RNA Isolation Kit, was used and sample RNA was extracted. Secondly, the cDNA: HiScript IV 1st Strand cDNA Synthesis Kit (+gDNA wiper) and reverse transcription reagent were obtained from Vazyme Biotech company. Finally, a quantitative reagent from Hunan Accurate Biology company, the SYBR greenpro Taq HS plant qRT-PCR kit, was used to quantitatively detect the expression of cryptochrome *CsCRYs* in the leaves of *Ch.sichuanensis* in the different environments by qRT-PCR. The quantitative primers and PCR amplification procedures are shown in Table 1, and the spectra of processing conditions are shown in Figure S2 in the Supplementary Materials.

Table 1. Physical and chemical properties and subcellular localization of CsCRYs protein in *Chimonobambusa sichuanensis*.

Indicators	*CsCRY1a*	*CsCRY1b*	*CsCRY2*	*CsCRY3*
Nucleotide length	2139	2094	1476	1833
Protein length	712	697	491	610
Isoelectric point	5.44	5.46	5.08	9.30
Aliphatic index	78.64	80.04	85.58	79.46
Instability index	54.36	51.53	51.19	41.41
Hydrophilic coefficient	−0.433	−0.413	−0.317	−0.356
Relative molecular mass	80.10	79.08	54.15	68.63
α-helix ratio (%)	36.8	39.2	34.6	37.1
Beta-sheet	4.4	4.2	8.4	6.1
Proportion of extended chain (%)	10.7	8.8	10.6	12.5
Subcellular localization	Cytoplasm	Cytoplasm	Nucleus	Chloroplast

3. Results and Analysis

3.1. Sequence Domain of CsCRYs Protein in Chimonobambusa sichuanensis

Using the *Phyllostachys edulis CRY* genes as reference genes, four *CRY* gene sequences of *Ch.sichuanensis* were obtained through homology comparison. The four *CRY* sequences were aligned with the NR database to confirm their identity as *CRYs* genes. Based on the homology alignment results, the four sequences were named *CsCRY1a*, *CsCRY1b*, *CsCRY2*, and *CsCRY3*. Among them, *CsCRY1a* is 2139 bp in length and encodes 712 proteins; *CsCRY1b* is 2094 bp in length and encodes 697 proteins; *CsCRY2* is 1476 bp in length and encodes 491 amino acids; and *CsCRY3* is 1833 bp in length and encodes 610 amino acids (Figure 1A).

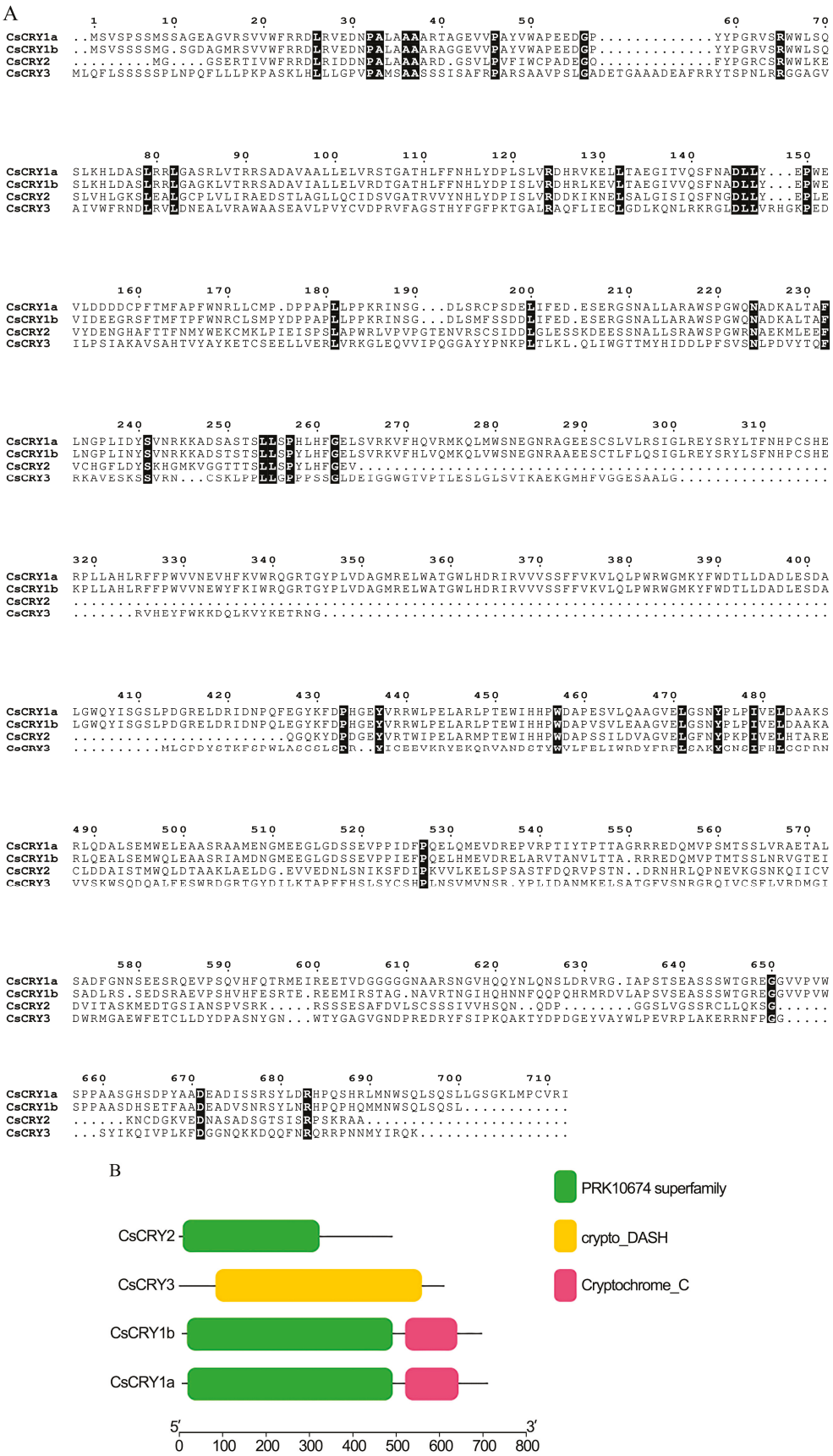

Figure 1. Sequence alignment and analysis of *Ch.sichuanensis CsCRYs* gene family proteins. Note: (**A**) Protein sequence alignment of the *Ch.sichuanensis CsCRYs* gene family; (**B**) analysis of conserved domains of the *Ch.sichuanensis CsCRYs* gene family.

Using MEGA v11 software, the sequence alignment of the four CRYs proteins was performed to construct their evolutionary relationships. *CsCRY1a* and *CsCRY1b* showed the highest similarity at 34.21% similarity, while *CsCRY2* and *CsCRY3* had a similarity of 21.48%. The four CsCRYs protein sequences share only 72 common amino acids. The structural domain analysis of the four CsCRYs proteins using ESPript 3 revealed that CsCRY1b and CsCRY1a have identical domains, both possessing the PRK10674 superfamily and Cryptochrome C domains (Figure 1B), as well as the photolyase homology region (PHR) domain and the C-terminal extension domain. CsCRY2 only contains the PRK10674 superfamily domain, while CsCRY3 only has the crypto_DASH domain, showing significant differences.

3.2. Structural Characterization of Chimonobambusa sichuanensis CsCRYs Gene Family

In order to explore the structural characteristics of CsCRYs, four genetic structures were visually analyzed using MEME and TBtools, and the results are shown in Figure 2A. Motif analysis showed that Motifs 1, 4, 6, and 7 were present in the four CsCRY proteins CsCRY1a, CsCRY1b, CsCRY2, and CsCRY3, and Motifs 1, 8, and 9 together constituted the homologous domain of the CsCRY1 subfamily, as shown by the conserved domain analysis (Figure 2C). The conserved motifs of CsCRY1a and CsCRY1b are the same so that they can be integrated into the same subfamily. The presence or absence of Motif 9 is the criterion for the identification of the CsCRY1 subfamily. The CsCRY2 subfamily differs from the other subfamilies in that Motif 3 is missing. Similarly, the CsCRY3 subfamily did not contain Motifs 2, 5, 8, and 10 compared to the other subfamilies (Figure 2A). Motifs 1, 2, 4, 5, 6, 8, and 10 constitute the PRK10674 conserved domain, which is common to photoreceptors, and Motif 9 constitutes the Cryptochrome_C conserved domain, which is unique to the *CsCRYs* family. Conserved motif analysis revealed that Motif 2, Motif 4, and Motif 6 are highly conserved among all family members, indicating that these motifs play a fundamental and important role in CRY protein function (Figure 2B). The motif differences between subclasses are as follows: CsCRY1 has Motif 3 and Motif 7 compared to CsCRY2, and CsCRY3 was identified as Cryptochrome_DASH due to the lack of Motif 2 and Motif 10, whereas CsCRY1 and CsCRY2 are from different subclasses but contain Motif 5, and there is slight difference between different subclasses.

To further explore the similarities and differences between the *CsCRYs* gene family and other species, the conserved motifs of the *CRY* gene family in the four *CsCRYs* genes and several species were compared and analyzed (Figure 2A). A total of 59 gene sequences, distinguished by 10 conserved motifs (Motif 1–Motif 10), were examined using the online software MEME for the *CRY* gene families in the four *CsCRYs* genes and other species. The results showed that each *CRY* gene contains 1 to 10 motifs. An analysis of this result in conjunction with Figure 2A,C shows that *CsCRY1a* and *CsCRY1b* have the same motif and both consist of two structural domains; Motifs 3, 5, 6, 9, and 10 form the PRK10674-Superfamily structural domain, which is related to signaling; and the rest, Motifs 1, 2, 7, and 8, form the Cryptochrome-C structural domain, which is related to photosynthetic signaling and interaction with downstream signals, and is similar to other species such as wheat, sorghum, and maize, which also consist of these two structural domains in their CRY1 sequences and have the same motif composition, which can be regarded as a strong evidence for the identification of *CRY1*. Interestingly, *Phyllostachys edulis PheCRY1a*, which is very close to *Ch.sichuanensis*, lacks Motifs 3, 5, and 10, which suggests that there are differences in their sequence compositions despite having the same structural domains, and *CsCRY2* is similar to *CRY2* genes of other species in that it possesses a PRK10674-Superfamily structural domain, which is not of the same length in different species. *CsCRY2* consists of Motifs 2, 3, 5, 7, 9, and 10, with Motif 8 missing compared to wheat, sorghum,

and maize, and this fragment is not found in *Phyllostachys* edulis (Figure 2A). *CRY3* is more consistent in all species and consists of the Crypto-DASH structural domain, which is a marker for identifying CRY3 and consists of Motifs 1, 2, 4, 5, and 6, which is present in both *CsCRY3* and *AtCRY3* and *ZmCRY3*.

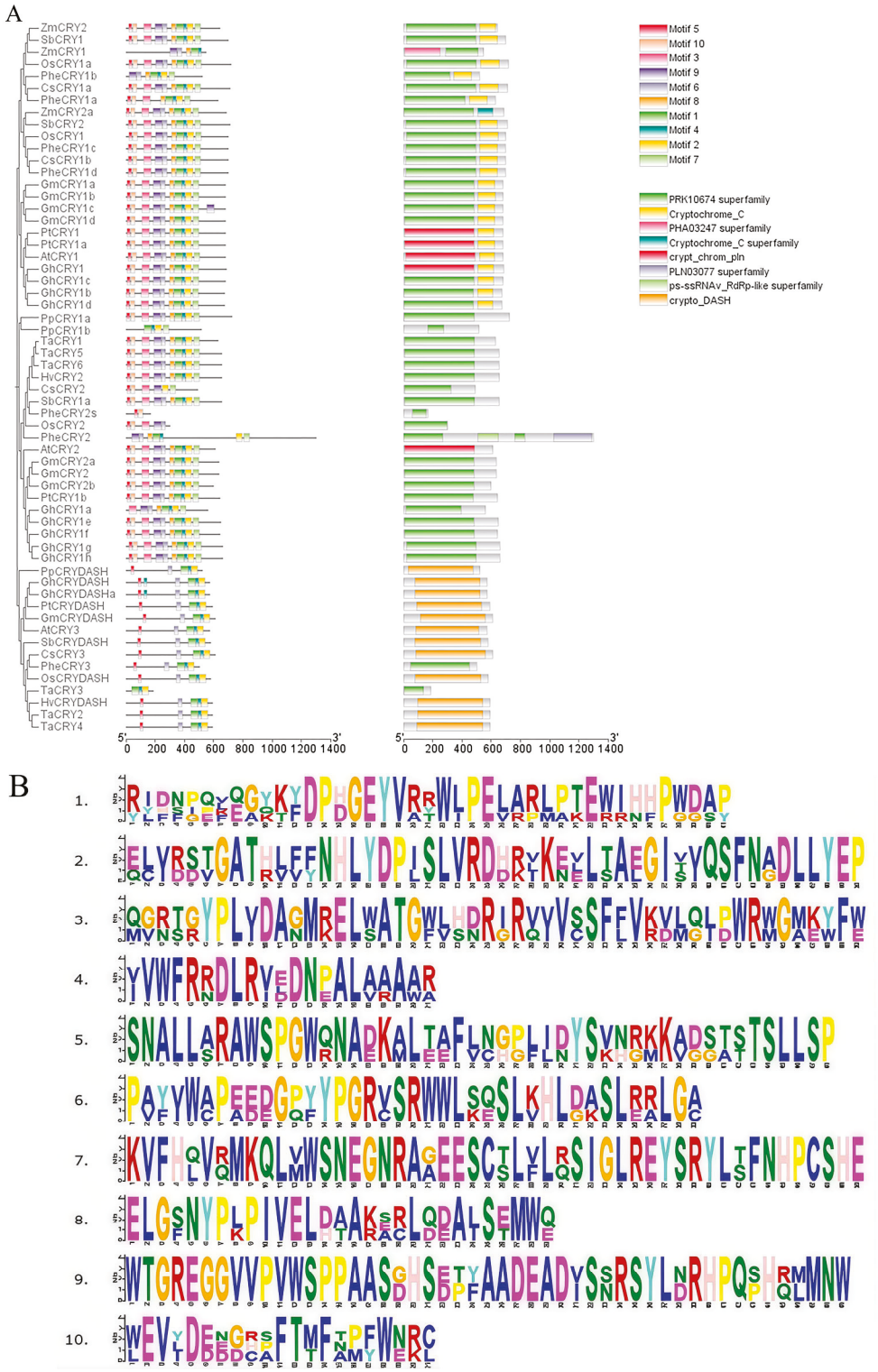

Figure 2. *Cont.*



Figure 2. Evolutionary tree and motif comparison of *CRYs* gene families in multiple species. Note: Plant species include Chimonobambusa sichuanensis (Cs), Arabidopsis thaliana (At), O. sativa (Os), Triticum aestivum (Ta), Zea mays (Zm), Glycine max (Gm), Hordeum vulgare (Hv), Sorghum bicolor (Sb), Populus trichocarpa (Pt), Gossypium hirsutum (Gh), Physcomitrella patens (Pp), and Phyllostachys edulis (Phe). (**A**) Evolutionary tree and conserved structural domain analysis of *CRY* gene families in multiple species; (**B**) *Chimonobambusa sichuanensis CsCRYs* gene family motifs; and (**C**) *CRY* gene family motifs in multiple species.

3.3. Genetic Relationship of Chimonobambusa sichuanensis CsCRYs Gene

In order to explore the genetic relationship between *CsCRYs* genes of *Chimonobambusa sichuanensis* and other species, four CsCRYs protein sequences of *Chimonobambusa sichuanensis* were aligned with 55 CRYs protein sequences of 10 other species, and the results were as shown in the phylogenetic tree in Figure 2A; all *CRYs* genes were divided into three subfamilies. The *CsCRYs* gene of *Chimonobambusa sichuanensis* was distributed in all three subtribes (subtribes I-III). Among them, there are two members in subfamily I (*CsCRY1a*, *CsCRY1b*), one member in subfamily II (*CsCRY2*), and one member in subfamily III (*CsCRY3*). The members belonging to the same subclade have the same protein structure, and the branches (*CsCRY1a~3*) are consistent with the results of the conserved motif analysis. The evolutionary relationship can be seen in that *CsCRY1a* and *CsCRY1b* are clustered into a subfamily with *PheCRY1a* and *PheCRY1b* of *Phyllostachys edulis*, and *CsCRY1a* and *PheCRY1a* are clustered into a branch in the evolutionary tree before polymerizing with *CsCRY1b*, which proves that in this subfamily, *CsCRY1a* is more closely related to *PheCRY1a* (Figure 2A). *CsCRY1a*, *CsCRY1b*, *PheCRY1a*, and *PheCRY1b* all have the PRK10674-Superfamily as well as Cryptochrome-C structural domains, which are shared by members of this subfamily in the evolutionary tree, which is a common feature of subfamily I. *CsCRY1a*, *CsCRY1b*, and *PheCRY1a* are all related to *PheCRY1a*. Similarly, *CsCRY2* is located in subfamily II and is closer to *PheCRY2s*, which proves that in this subfamily, *CsCRY2* is more closely related to *PheCRY2s* (Figure 2A). Both *CsCRY2* and *PheCRY2* have the PRK10674-Superfamily structural domain, which is shared by members of subfamily II in the evolutionary tree. *CsCRY3*, in turn, constitutes a small branch with *PheCRY3*, which proves that *CsCRY3* is more closely related to *Phyllostachys edulis PheCRY3* in subfamily

III (Figure 2A). Both *CsCRY3* and *PheCRY3* have the Crypto-DASH structural domain, which is shared by members of this subfamily in the evolutionary tree, and is a common characteristic of subfamily III as well as a criterion for its identification. All four *CsCRYs* family sequences of *Ch.sichuanensis* showed very close affinity with the *PheCRYs* family sequences of *Phyllostachys edulis* and were highly similar in classification, which proved the correctness of the screening. The branching of the phylogenetic tree can effectively reflect the evolutionary relationship of *CRY* genes in each species.

Among them, some motifs are common to all members, such as Motif 5 (except *TaCRY3*, *PpCRY1b*, and *ZmCRY1*), and *CRY* gene family members of most species contain Motif 1, Motif 2, Motif 3, Motif 4, Motif 5, and Motif 10. The results indicate that they are *CRY* gene family members and Motifs 3, 5, 6, 9, and 10 constitute the PRK10674 conserved domain, Motifs 1, 2, 4, 7, and 8 constitute the Cryptochrome_C conserved domain, and Motifs 1, 2, 4, and 6 constitute the Cryptochrome_DASH domain (Figure 2A,B). The above results indicate that there are both similarities and differences in the functions of *CRY* genes among different subfamilies.

A total of four members of the *Ch.sichuanensis CsCRYs* gene family were accurately identified through the mining of *Ch.sichuanensis* transcriptome data, and this number was determined from seven *Phyllostachys edulis* sequences screened by previous authors, among which *PheCRY3* and *PheCRY4* were demonstrated to have repetitive sites and could be spliced into a single sequence in the present study. This is consistent with the classification of *CRY* families in other plant species such as *Arabidopsis*, rice, companion mineral Sedum, alfalfa, and soybean (Figure 2C). All four screened sequences of *Ch.sichuanensis* corresponded to *Phyllostachys edulis* sequences, which can be classified into three subfamilies (subfamilies I-III) based on their structural features. Compared with the classification results of other species, which are similar to that of *Arabidopsis*, the *Arabidopsis* cryptochrome gene family consists of members of three subfamilies: *AtCRY1*, *AtCRY2*, and *AtCRY3*. Among them, *CRY3* belongs to the CRY-DASH branch, and evolutionarily, *CRY3* is an intermediate between Cryptochrome and photolyase. In contrast, although the *PheCRY* gene family of *Phyllostachys edulis* is divided into three subfamilies, the number in each subfamily is not equally distributed, which is different from *Arabidopsis* and *Ch.sichuanensis*. By analyzing other species classifications, all of these results showed differences, implying that there are structural and functional differences in *CRY* proteins from different plant species.

3.4. Physicochemical Properties and Secondary Structures of Four CsCRYs Family Proteins from Chimonobambusa sichuanensis

The protein lengths of *Chimonobusa sichuanensis* CsCRYs ranged from 491 to 712 bp, and most *Ch.sichuanensis CsCRYs* genes and protein lengths had little variation, except for CsCRY2, which had the smallest protein length. In order to understand the relative molecular mass and isoelectric point of CsCRYs proteins, the physical and chemical properties of CsCRYs were analyzed by ProtParam software on the Expasy website, and the relative molecular mass of the four proteins was 54. The relative molecular mass of the CsCRY2 protein was the smallest, and the relative molecular mass of CsCRY1a was the largest. From the isoelectric point analysis of the four proteins, it can be seen that the isoelectric point of the CsCRY3 protein is greater than 7, which indicates a basic protein, and the isoelectric point of the other three CsCRYs proteins is about 5, which indicates an acidic protein. The instability coefficients of the four CsCRYs ranged from 41.41 to 54.36, all of which were greater than 40, indicating that they were unstable proteins. The average hydrophilicity coefficient of the CsCRYs protein was -0.433~-0.317, which was less than 0, so it was a hydrophilic protein. Protein location analysis showed that CsCRY1a and CsCRY1b were distributed in the cytoplasm, while CsCRY2 was located in the nucleus and CsCRY3 was located in the chloroplast (Table 1). Using Signal p6.0

(https://services.healthtech.dtu.dk/services/SignalP-6.0/) (accessed on 10 April 2024) and the TMHMM website (https://services.healthtech.dtu.dk/services/TMHMM-2.0/) (accessed on 10 April 2024) showed that the signal peptide ratio Sec/SPI of the four proteins was 0, and the signal peptide index was less than 0.5. The results showed that there was no signal peptide in the CsCRYs protein of *Ch.sichuanensis*. It can be seen from the comprehensive analysis of the results in Figure S1 in the Supplementary Materials that the CsCRYs protein of the *Ch.sichuanensis* has no signal peptide and no transmembrane domain, which is consistent with the above subcellular prediction results.

In order to further analyze the molecular structure of the four proteins, the three-dimensional structure of the four CsCRYs proteins was analyzed through the database PSIPRED (http://bioinf.cs.ucl.ac.uk/psipred/) (accessed on 10 April 2024). The results showed that a random coil was the most dominant secondary structure (Figure 3, Table 2) in the four CsCRYs proteins, and the proportion of α-helix was between 34.62% and 39.17%, and the proportion of β-sheet was between 4.16% and 8.35%. The evaluation of the 3D model predictions showed low values for both Ramachandran Outliers and Clash Score, indicating a high reliability of the model predictions (Table 2).

Table 2. Analysis data for CsCRYs protein three-dimensional prediction diagram and prediction results of the transmembrane structure of the signal peptide.

Indicators	*CsCRY1a*	*CsCRY1b*	*CsCRY2*	*CsCRY3*
Clash score	0.46	1.00	0.51	0.93
Ramachandran outliers	1.00%	1.87%	1.60%	3.62%
Rotamer outliers	1.34%	1.17%	5.05%	2.32%
Cis non-proline	0.77%	0.77%	1.27%	0.18%
Sec/SPI	0	0	0	0
C-score	0.121	0.111	0.115	0.145
S-score	0.149	0.163	0.171	0.388
Y-score	0.124	0.121	0.114	0.153
Mean-S	0.126	0.129	0.117	0.156
Mean-D	0.125	0.125	0.116	0.155
The probability that the N-terminus is on the cytoplasmic side	0.00037	0.00020	0.00370	0.00044
Number of transmembrane amino acids	0.00053	0.00076	0.01276	0.00499
Number of amino acids outside the membrane	712	697	491	610

3.5. Expression Pattern of Cryptochrome CsCRYs Gene in Chimonobambusa sichuanensis Under Different Environmental Condition

In order to analyze the functional differences of four *CsCRYs* genes in *Chimonobambusa sichuanensis*, the hydroponic seedlings of *Chimonobambusa sichuanensis* were used as experimental materials, and the gene expression levels were analyzed by setting different light intensities and treatments. The gene expression of the four *CsCRYs* genes had certain differences after being treated by different light intensities, among which *CsCRY1a*, *CsCRY1b*, and *CsCRY2* genes responded rapidly in a short period of time (2–6 h), and the gene expression of the three genes increased significantly after being treated by blue light for 2–6 h. The gene expression response (12–24 h) decreased (Figure 4A–C), while the expression pattern of *CsCRY3* gene expression showed a down–up–down trend (Figure 4D), showing special expression characteristics. The expression of *CsCRY1a*, *CsCRY1b*, and *CsCRY2* genes was the highest under 75 $\mu mol \cdot m^{-2} \cdot s^{-1}$ blue light in the rapid response stage (2–6 h) of light treatment. However, the 50 $\mu mol \cdot m^{-2} \cdot s^{-1}$ treatment group showed higher gene expression during the 12–24 h period of the blue-light treatment of these three genes. It is speculated that *CsCRY1a*, *CsCRY1b*, and *CsCRY2* are continuously adapted to low-intensity blue light. The expression of the *CsCRY3* gene in the 100 $\mu mol \cdot m^{-2} \cdot s^{-1}$ light treatment group was significantly higher than that in other groups at most time points ($p < 0.01$), and may be involved in the regulation of the long-term stress of high light intensity, and may be related to environmental adaptability. It can be seen from Figure 4 that *CsCRY1a*, *CsCRY1b*, and

CsCRY2 mediate short-term blue-light stress, and *CsCRY3* plays a unique role in sustained high light stress. Quantitative primers and internal reference genes are shown in Table S1 in Supplementary Materials, and the spectra of treatment conditions are shown in the Figure S2 in Supplementary Materials.

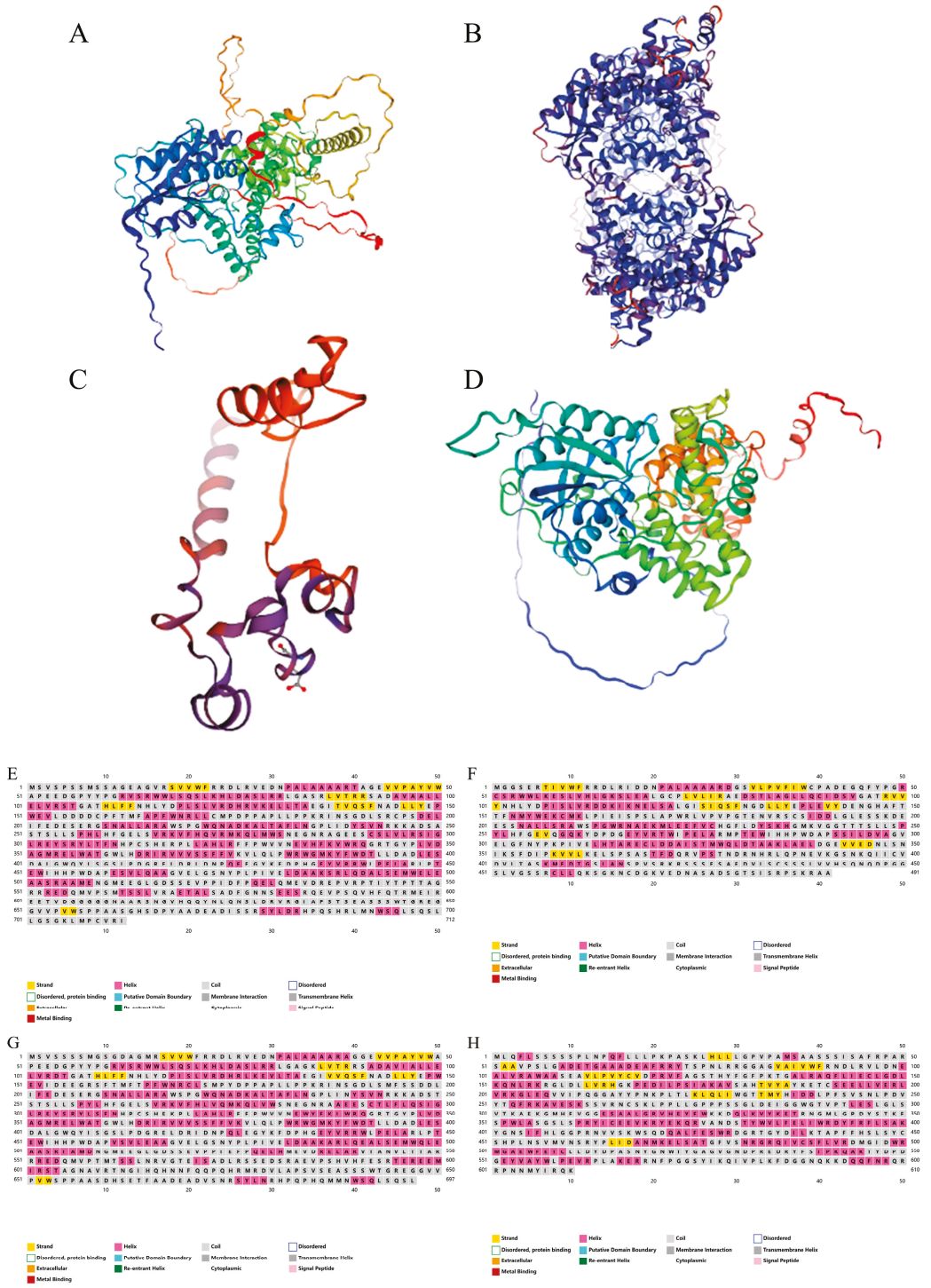

Figure 3. Protein structure prediction of CsCRYs family members in *Chimonobambusa sichuanensis*. Note: (**A**) Predicted secondary structure of CsCRY1a protein; (**B**) predicted secondary structure of CsCRY1b protein; (**C**): predicted secondary structure of CsCRY2 protein diagram; (**D**) CsCRY3 protein secondary structure prediction diagram; (**E**) predicted 3D structure of CsCRY1a protein, which is based on the construction of a corn CRY1 gene model with a matching similarity degree of 88.97%, gene number LOC100384475; (**F**) predicted 3D structure of CsCRY1b protein, which is based on the

construction of a corn CRY1 gene model with a matching similarity of 82.01%, gene number LOC100384475; (**G**) predicted 3D structure of CsCRY2 protein, based on a maize OsCRY2 gene model construct with a matching similarity of 80.37%, number J013042O16; and (**H**) predicted 3D structure of CsCRY3 protein, which is based on the construction of the OsCRY3-DASH gene model of Japonicoideae with a matching similarity of 88.79%, number Q651U1.

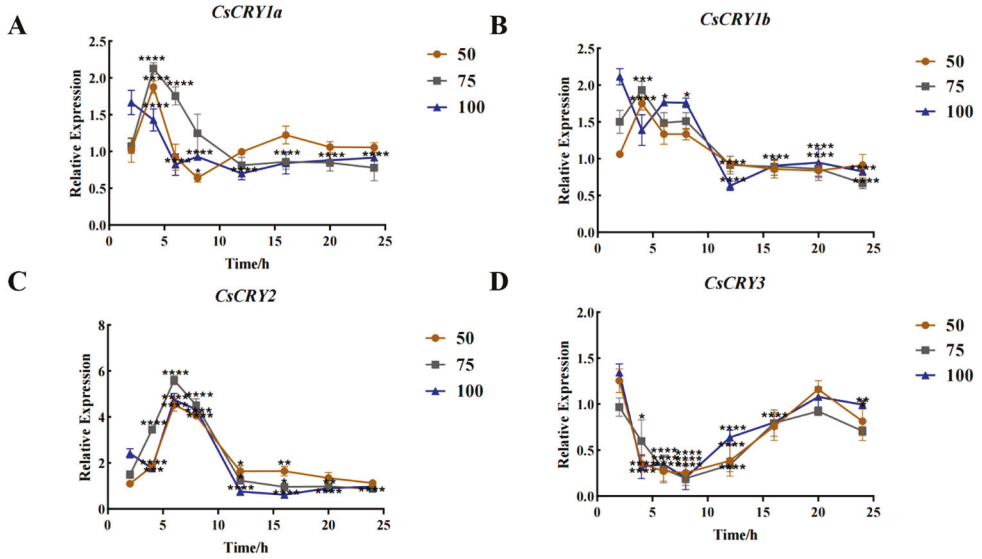

Figure 4. Gene expression of *Chimonobambusa sichuanensis CsCRYs* family members under different blue-light treatments. Note: (**A**) CsCRY1a gene expression; (**B**) CsCRY1b gene expression; (**C**) CsCRY2 gene expression; and (**D**) CsCRY3 gene expression. Data were normalized by qRT-PCR to the expression level of each gene at 3 h. Values are expressed as mean ± SD. Statistically significant differences were analyzed using two-way ANOVA (* $p < 0.05$, ** $p < 0.01$, *** $p < 0.001$, and **** $p < 0.0001$).

In order to understand the response of the four genes to different light qualities, bamboo seedlings were treated with different light qualities, and the gene expression of *CsCRYs* was shown in Figure 5. The gene expression levels of both *CsCRY1a* and *CsCRY1b* were the highest under red and blue mixed light (Figure 5A,B). The response of *CsCRY2* to blue light was higher than that to red light and red–blue mixed light, and the expression of *CsCRY3* was relatively high in the early stage of blue-light treatment (2–10 H), but the response of *CsCRY3* to different color light was not significant after 10 H of different quality light treatment.

In order to explore the relationship between the *CsCRYs* gene and temperature in *Ch.sichuanensis*, bamboo seedlings were treated at different temperatures (−5 °C to −20 °C). The results showed that with the decrease in treatment temperature, the expression of *CsCRY2* increased significantly, reaching the peak at −5 °C (Figure 6), which was consistent with the data from the transcriptome study on *Ch.sichuanensis* culms in winter in our laboratory, and confirmed that it was involved in the regulation of cold resistance. The expression of other members *CsCRY1a*, *CsCRY1b,* and *CsCRY3* did not change significantly, and the expression of the three genes increased slightly with the decrease in temperature, indicating that there was functional differentiation among the *CsCRYs* gene families. The results showed that *CsCRY2* had both blue-light sensing and low-temperature response functions in *CsCRYs*, and it was inferred that *CsCRY2* was the key molecule for bamboo to adapt to a winter environment.

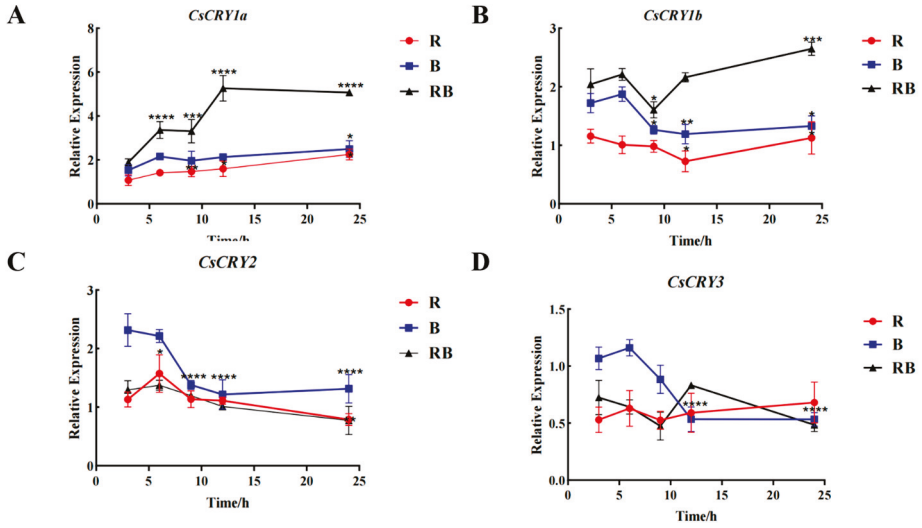

Figure 5. Gene expression of *Chimonobambusa sichuanensis CsCRYs* family members under different light quality treatments. Note: (**A**) *CsCRY1a* gene expression; (**B**) *CsCRY1b* gene expression; (**C**) *CsCRY2* gene expression; and (**D**) *CsCRY3* gene expression. Data were normalized by qRT-PCR to the expression level of each gene at 3 h. Values are expressed as mean ± SD. Statistically significant differences were analyzed using two-way ANOVA (* $p < 0.05$, ** $p < 0.01$, *** $p < 0.001$, and **** $p < 0.0001$).

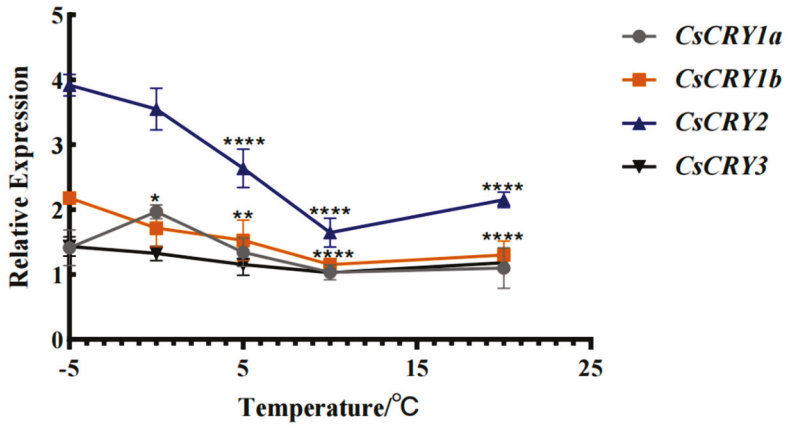

Figure 6. Gene expression of *Chimonobambusa sichuanensis CsCRYs* family members under different temperature treatments. Note: Data were normalized by qRT-PCR to the expression level of each gene at −5 °C. Values are expressed as mean ± SD. Statistically significant differences were analyzed using two-way ANOVA (* $p < 0.05$, ** $p < 0.01$, and **** $p < 0.0001$).

4. Discussion

4.1. Structural Domain Differences Drive the Functional Differentiation of CsCRYs in Chimonobambusa sichuanensis

First, this study speculated that the conserved domain is related to the short-term stress response: by analyzing the composition of the conserved motif of CsCRYs, it was found that CsCRY1a, CsCRY1b, and CsCRY2 all contain the PRK10674-Superfamily domain (Figure 2), which is highly conserved (Section 2.3) and may explain the consistency in the expression trend of the three genes in the short-term response (2–6 h) to low-to-medium-intensity blue light (50–75 μmol·m^{-2}·s^{-1}) (Figure 4A–C). After this conserved domain binds to FAD and FMN, it can participate in the signal transduction process and regulate the expression of downstream genes and cell activities. The difference is that in the sequences of Phyllostachys pubescens screened by predecessors, no similar PheCRY3 protein has this domain. Moreover, through domain analysis, it was found that PheCRY3 and PheCRY4,

as determined in previous publications, have high repeatability, and may have the same sequence. The above results are consistent with the mechanism of early blue-light signal transduction mediated by *AtCRY1* and *AtCRY2* in *Arabidopsis thaliana* [12], suggesting that members of this subfamily may participate in stress response through photoreceptor-COP1 interaction in *Ch.sichuanensis*.

Secondly, the Crypto-DASH domain is involved in long-term stress regulation: the unique Crypto-DASH domain of CsCRY3 (Figure 2) may regulate its functional specificity by binding to FAD/MTHF. As shown in Figure 4D, CsCRY3 exhibits a high expression pattern under 100 $\mu mol \cdot m^{-2} \cdot s^{-1}$ blue light, which is presumed to be involved in long-term high light stress adaptation [13]. This phenomenon is similar to the mechanism by which AtCRY3 disrupts DNA repair in *Arabidopsis* [14], suggesting that members of the Crypto-Dash subfamily may respond to persistent environmental stress through conformational stability regulation. The structural analysis of the above four CsCRYs proteins once again confirms that the structure of the gene is closely related to its function, and the domain differences drive the functional differentiation of CsCRYs in *Ch.sichuanensis*. These results reflect the unity and variability of its structure [15,16].

In addition, the CsCRY2 protein domain of *Ch.sichuanensis* determines that it has both light and temperature responses. Previous studies in *Arabidopsis* thaliana have found that *AtCRY2* not only participates in the process of photomorphological construction, but also participates in the regulation of cold resistance under low-temperature stress [17], while *AtCRY1* and *AtCRY3* do not have this function [18,19]. In this study, in the process of exploring *CsCRY2* of *Ch.sichuanensis*, it was found that it also has dual functions of responding to temperature and light (Figure 6). By comparing the changing trend of *CsCRY2* gene expression under different light treatments, it is believed that *CsCRY2* gene may be involved in resisting blue-light stress. Short-term response. In addition, *CsCRY2* was found to have a low-temperature response mechanism through low-temperature stress treatment of *Ch.sichuanensis*. Because the domain of this gene is different from other *CsCRYs* genes (Section 2.1 of this study), it is speculated that this gene is a key member of the *CsCRYs* family in response to light, and it is speculated that CsCRY2, as a blue-light low-temperature cross-signaling node, may regulate downstream stress genes by activating the COP1/HY5 pathway.

From the results of -5 °C treatment, it can be seen that the expression level of CsCRY2 reached its peak here (Figure 6), indicating that it participates in the regulation of cold resistance. Previous studies have shown that Arabidopsis AtCRY2 can integrate light signaling and low-temperature response by activating the COP1/HY5 pathway. The results of this study further support the evolutionary conservation of CsCRY2 as a blue-light low-temperature crossover node.

4.2. Subcellular Localization of CsCRys in Chimonobambusa sichuanensis

The results of the subcellular localization of CsCRY1a and CsCRY1b in *Ch.sichuanensis* showed that CsCRY1a and CsCRY1b were located in the cytoplasm, and AtCRY1 in *Arabidopsis thaliana* was a nucleus–cytoplasm transport protein, which could act in both the nucleus and cytoplasm. As a species closely related to *Ch.sichuanensis* in the evolutionary tree, OsCRY1 in rice was also found to play a role in the cytoplasm in previous studies [20]. The subcellular localization of CsCRY2 was found in the nucleus, and AtCRY2 is also a nuclear localization protein in *Arabidopsis*. Both AtCRY3 and CsCRY3 are distributed in chloroplasts, suggesting that they play a role in regulating organelle transcription [21–23]. Localization among different species is conservative, which supports the reliability of prediction in this study. In view of the similarity between homologous genes, the similarity rate between CsCRY1a and OsCRY1 (LOC102709715) DNA was 87.98%; the similarity

rate between CsCRY1b and OsCRY1 (LOC4336008) DNA was 89.45%; the similarity rate between CsCRY1b and OsCRY1 (LOC102709715) DNA was 89.45%; the similarity between CsCRY2 and OsCRY2 (AB103094.1) was 87.66%; and the similarity rate between CsCRY3 and OsCRY3 (LOC4341749) was 86.16%. Combined with the prediction results of this study, we believe that the cell localization data in rice and *Arabidopsis* can provide indirect support for the localization of CsCRYs, which supports the accuracy of the prediction results. In order to confirm the accuracy of the prediction and build a foundation for subsequent related experiments, it is still necessary to verify the subcellular localization of CsCRYs (see Section 3.5 for the prediction results) and interacting proteins in tobacco through GFP tags in the future, and to construct gene knockout lines to verify the function. The analysis of CsCRYs protein structure by Signalp6.0 software showed that there was no signal peptide structure in the CsCRYs protein of *Ch.sichuanensis*, and its functional domain was mainly responsible for protein binding, which provided help for light signal transmission. This characteristic endows the CsCRYs protein with excellent structural stability and functional diversity. This precise regulation mechanism not only ensures the ion balance between the internal and external environment of the cell, but also is the key to the function of plant photosynthesis.

Ch.sichuanensis has multiple ecological advantages such as being evergreen, having cold tolerance, and other characteristics, including special characteristics related to shooting and morphological changes. In this study, based on the previous study demonstrating the blue-light-induced discoloration of *Ch.sichuanensis* bamboo culm, four *CsCRYs* genes were successfully obtained, and their properties and expression under different environmental stresses were further discussed [24].

Supplementary Materials: The following supporting information can be downloaded at: https://www.mdpi.com/article/10.3390/plants14111637/s1, Figure S1: Predicted transmembrane structure of CsCRYs proteins in *Chimonobambusa sichuanensis*.; Figure S2: Spectra of different light intensity treatment conditions; Table S1: Quantitative primers for the *CsCRYs* in *Chimonobambusa sichuanensis*.

Author Contributions: Conceptualization, Y.K. and C.L.; resources, G.L. and J.F.; writing—original draft preparation, Y.K.; writing—review and editing Y.K. and C.L.; Software, T.L.; project administration, G.L.; funding acquisition, G.L. All authors have read and agreed to the published version of the manuscript.

Funding: This research was supported by the National Key Research and Development Program: "14th Five-Year" National Key Research and Development Program, High-efficiency Cultivation Technology of Bamboo Shoot Forest with Southwest Characteristics; Project Number: 2023YFD220120302.

Data Availability Statement: The data presented in this study are available on request from the corresponding author. The data will not be disclosed as we have further research to do in our lab.

Conflicts of Interest: The authors declare no conflicts of interest.

References

1. Zhang, Y.T.; Xia, N.H.; Lin, S.Y.; Ding, Y.L. Spatial distribution characteristics and influencing factors of *Chimonobambusa* in China. *J. Nanjing For. Univ. (Nat. Sci. Ed.)* **2025**, *49*, 107–114.
2. Liu, C.L.; Xiong, X.; Li, T.S.; Duan, Y.H.; Yang, F.; Liu, G.H. The discoloration mechanism of *Ch.sichuanensis* clumunder colored film covering based on transcriptome analysis. *Plant Physiol. J.* **2025**, *61*, 83–96.
3. Batschauer, A. New insights into the regulation of *Arabidopsis* cryptochrome 1. *New Phytol.* **2022**, *234*, 1109–1111. [CrossRef] [PubMed]
4. Miao, L.X.; Xu, F.; Zhao, J.C.; Jiang, L.; Yang, G.Q.; Zhang, S.L.; Xu, P.; Wei, X.X.; Cao, X.L.; Liu, Y.; et al. Arabidopsis cryptochrome 1 controls photomorphogenesis through regulation of H2A.Z deposition. *Plant Cell* **2021**, *33*, 1961–1979. [CrossRef] [PubMed]
5. Li, Q.H.; Yang, H.Q. Cryptochrome signaling in plants. *Photochem. Photobiol.* **2007**, *83*, 94–101. [CrossRef]

6. Emery, P.; So, W.V.; Kaneko, M.; Hall, J.C.; Rosbash, M. CRY, a Drosophila clock and light-regulated cryptochrome, is a major contributor to circadian rhythm resetting and photosensitivity. *Cell* **1998**, *95*, 669–679. [CrossRef]
7. Lin, C.; Yang, H.; Guo, H.; Mockler, T.; Chen, J.; Cashmore, A.R. Enhancement of blue-light sensitivity of *Arabidopsis* seedlings by a blue light receptor cryptochrome 2. *Proc. Natl. Acad. Sci. USA* **1998**, *95*, 2686–2690. [CrossRef] [PubMed]
8. Pokorny, R.; Klar, T.; Hennecke, U.; Carell, T.; Batschauer, A.; Essen, L.O. Recognition and repair of UV lesions in loop structures of duplex DNA by DASH-type cryptochrome. *Proc. Natl. Acad. Sci. USA* **2008**, *105*, 21023–21027. [CrossRef]
9. Belbin, F.E.; Noordally, Z.B.; Wetherill, S.J.; Atkins, K.A.; Franklin, K.A.; Dodd, A.N. Integration of light and circadian signals that regulate chloroplast transcription by a nuclear-encoded sigma factor. *New Phytol.* **2017**, *213*, 727–738. [CrossRef]
10. Ma, D.; Li, X.; Guo, Y.; Chu, J.; Fang, S.; Yan, C.; Noel, J.P.; Liu, H. Cryptochrome 1 interacts with PIF4 to regulate high temperature-mediated hypocotyl elongation in response to blue light. *Proc. Natl. Acad. Sci. USA* **2016**, *113*, 224–229. [CrossRef]
11. Chen, Z.Y. Functional Study of PhemiR156-PheSPLand PheCRY in Moso Bamboo. Master's Thesis, Fujian Agriculture and Forestry University, Fuzhou, China, 2022.
12. Liu, H.T.; Yu, X.H.; Li, K.W.; Klejnot, J.; Yang, H.Y.; Lisiero, D.; Lin, C.T. Photoexcited CRY2 Interacts with CIB1 to Regulate Transcription and Floral Initiation in Arabidopsis. *Science* **2008**, *322*, 1535–1539. [CrossRef] [PubMed]
13. Rredhi, A.; Petersen, J.; Schubert, M.; Westermann, M.; Wagner, V.; Li, W.; Oldemeyer, S.; Kottke, T.; Mittag, M. DASH cryptochrome 1, a UV-A receptor, balances the photosynthetic machinery of Chlamydomonas reinhardtii. *New Phytol.* **2021**, *232*, 610–624. [CrossRef] [PubMed]
14. Kavakli, I.H.; Ozturk, N.; Gul, S. DNA repair by photolyases. *Adv. Protein Chem. Struct. Biol.* **2019**, *115*, 1–19. [PubMed]
15. Banas, A.K.; Leja, K.; Zglobicki, P.; Jedynak, P.; Kowalska, E.; Strzalka, W.; Grzyb, J.; Mysliwa-Kurdziel, B. De-etiolation is Almost Color Blind: The Study of Photosynthesis Awakening under Blue and Red Light. *Plant Cell Physiol.* **2024**, *65*, 1993–2017. [CrossRef]
16. Zuo, Z.C.; Liu, H.T.; Liu, B.; Liu, X.M.; Lin, C.T. Blue Light-Dependent Interaction of CRY2 with SPA1 Regulates COP1 activity and Floral Initiation in *Arabidopsis*. *Curr. Biol.* **2011**, *21*, 841–847. [CrossRef]
17. Li, Y.P.; Shi, Y.T.; Li, M.Z.; Fu, D.Y.; Wu, S.F.; Li, J.G.; Gong, Z.Z.; Liu, H.T.; Yang, S.H. The CRY2-COP1-HY5-BBX7/8 module regulates blue light-dependent cold acclimation in Arabidopsis. *Plant Cell* **2021**, *33*, 3555–3573. [CrossRef]
18. Matsumoto, N.; Hirano, T.; Iwasaki, T.; Yamamoto, N. Functional analysis and intracellular localization of rice cryptochromes. *Plant Physiol.* **2003**, *133*, 1494–1503. [CrossRef]
19. Liu, B.B.; Yang, Z.H.; Gomez, A.; Liu, B.; Lin, C.T.; Oka, Y. Signaling mechanisms of plant cryptochromes in *Arabidopsis thaliana*. *J. Plant Res.* **2016**, *129*, 137–148. [CrossRef] [PubMed]
20. Hirose, F.; Inagaki, N.; Hanada, A.; Yamaguchi, S.; Kamiya, Y.; Miyao, A.; Hirochika, H.; Takano, M. Cryptochrome and Phytochrome Cooperatively but Independently Reduce Active Gibberellin Content in Rice Seedlings under Light Irradiation. *Plant Cell Physiol.* **2012**, *53*, 1570–1582. [CrossRef]
21. He, G.H.; Liu, J.; Dong, H.X.; Sun, J.Q. The Blue-Light Receptor CRY1 Interacts with BZR1 and BIN2 to Modulate the Phosphorylation and Nuclear Function of BZR1 in Repressing BR Signaling in Arabidopsis. *Mol. Plant* **2019**, *12*, 689–703. [CrossRef]
22. Jiang, B.C.; Zhong, Z.H.; Gu, L.F.; Zhang, X.Y.; Wei, J.B.; Ye, C.; Lin, G.F.; Qu, G.P.; Xiang, X.; Wen, C.J.; et al. Light-induced LLPS of the CRY2/SPA1/FIO1 complex regulating mRNA methylation and chlorophyll homeostasis in Arabidopsis. *Nat. Plants* **2023**, *9*, 2042–2058. [CrossRef] [PubMed]
23. Pfeifer, A.; Mathes, T.; Lu, Y.H.; Hegemann, P.; Kottke, T. Blue Light Induces Global and Localized Conformational Changes in the Kinase Domain of Full-Length Phototropin. *Biochemistry* **2010**, *49*, 1024–1032. [CrossRef] [PubMed]
24. Shao, X.Y.; Xiong, X.; Yang, F.; Zhao, Y.F.; Liu, C.L.; Liu, G.H. Full-length transcriptome sequencing analysis of *Chimonobambusa sichuanensis* after discoloration of bamboo culm. *Jiangsu J. Agric. Sci.* **2024**, *40*, 538–551.

Disclaimer/Publisher's Note: The statements, opinions and data contained in all publications are solely those of the individual author(s) and contributor(s) and not of MDPI and/or the editor(s). MDPI and/or the editor(s) disclaim responsibility for any injury to people or property resulting from any ideas, methods, instructions or products referred to in the content.

plants

MDPI

Article

QTL-Seq and Fine-Mapping Analyses Identify QTL and Candidate Genes Controlling Snake-like Pod Surface Trait in Vegetable Cowpea Yardlong Bean

Khwanruedee Thepphomwong [1], Makawan Srichan [2], Artitaya Deeroum [1], Kularb Laosatit [1] and Prakit Somta [1,*]

[1] Department of Agronomy, Faculty of Agriculture at Kamphaeng Saen, Kasetsart University, Kamphaeng Saen Campus, Nakhon Pathom 73140, Thailand; khwanruedee.th@ku.th (K.T.); artitaya.de@ku.th (A.D.); fagrkal@ku.ac.th (K.L.)

[2] Tropical Vegetable Research Center, Department of Horticulture, Faculty of Agriculture at Kamphaeng Saen, Kasetsart University, Kamphaeng Saen Campus, Nakhon Pathom 73140, Thailand; makawan.sr@ku.th

* Correspondence: agrpks@ku.ac.th

Abstract: Yardlong bean is a vegetable type of cowpea grown for fresh and immature pods. "Thua Ngu" is a specialty yardlong bean cultivar with its unique snake-like pod surface and highly crispy pods that may be useful for the breeding of a new cultivar(s). The objectives of this study were to determine the mode of inheritance of the snake-like pod trait and locate the genome region controlling this trait in Thua Ngu. Microscopic observation revealed that the shape, size, and organization of cells of immature and mature pods of Thua Ngu were clearly different from those of "Raya" (normal yardlong bean). Fiber analysis showed that lignin content in immature and mature pods of Thua Ngu was 2.05- and 3.45-fold higher than that in Raya. Segregation analysis using F_2 and $F_{2:3}$ populations of the cross Thua Ngu × Raya demonstrated that a single gene controls the snake-like pod trait. QTL-seq analysis using the F_2 population revealed a major locus, *qSlp4.1*, for the snake-like pod trait. Fine-mapping using F_2 and $F_{2:3}$ populations delimited *qSlp4.1* to a 152.88 Kbp region containing nine genes. Genes with functions involved in cell morphology and/or lignin formation, including *Vigun04g163400*, *Vigun04g163600*, and *Vigun04g163700*, were identified as candidate genes for the snake-like pod trait.

Keywords: yardlong bean; pod surface; lignin; QTL; QTL-seq

1. Introduction

Yardlong bean (*Vigna unguiculata* ssp. *unguiculata* cv.gr. *sesquipedalis*), also known as asparagus bean and string bean, is a vegetable type of cowpea (*Vigna unguiculata* (L.) Walp.), a self-pollinated plant with diploid genome ($2n = 2\times = 22$) [1]. It is mainly grown and consumed in Southeast Asia and China for young and tender pods. The pods of yardlong bean are usually 30–60 cm in length, albeit the pods of some cultivars are 70–90 cm in length [1,2]. The pods can be harvested several times, starting about 40–50 days after planting. The pods are consumed in both fresh and cooked forms and are prepared into varieties of dishes, such as salad, soup, and stir fired [3]. It is an economic crop of several countries in Southeast Asia and China, albeit there are no official statistics on the cultivation area and production of this crop. In some countries, such as Thailand, Myanmar, Cambodia, Philippines, and Indonesia, yardlong bean is produced commercially year-round. Pod traits related to eating and cooking qualities and appearance, including pod length, thickness, color, tenderness, firmness, crispiness, surface smoothness, and sweetness, are important for the marketing/commercialization of yardlong bean [3].

Yardlong bean is believed to be selected and evolved from the grain cowpea (*Vigna unguiculata* ssp. *unguiculata* cv.gr. *unguiculata*), possibly in South or Southeast Asia [4]. Due to strong selection in pod characteristics, yardlong bean is clearly genetically different from grain cowpea, and genomic regions associated with traits showing differential selection between yardlong bean and grain cowpea have been identified [5]. Landrace cultivars of crops are important sources of genes for the genetic improvement of new commercial/modern cultivars [6]. Thailand lies in a center of diversity of yardlong bean. "Thua Ngu", which is translated as "snake bean", is a local yardlong bean cultivar in southern Thailand and is known by local people in the region for its unique snake-like pod appearance and crispiness. Compared with the pods of normal yardlong bean cultivars, the pod surface of Thua Ngu is rougher, thicker, and much more snake-like. In addition, the pods of Thua Ngu are obviously twisted, while those of normal yardlong bean are relatively straight. The pods of Thua Ngu are popularly prepared into stir-fired dishes. Nonetheless, at present, there has been no report on the genetic basis of the pod trait in Thua Ngu.

Plant breeders always focus on pod-related traits in yardlong bean breeding programs. Nonetheless, there is limited knowledge on genetics and genomics on these traits. Quantitative trait loci (QTLs) controlling pod length, pod tenderness, total soluble solid content, and fiber content have been identified in the yardlong bean [3,7,8]. QTLs controlling pod tenderness, pod length, and fiber content appeared to be the same or closely linked [3,7]. In this study, we aimed to determine the mode of inheritance of the snake-like pod trait and locate the genome region controlling this trait in Thua Ngu. A major quantitative trait locus (QTL) controlling the snake-like pod trait was identified, and candidate genes for the trait were discovered.

2. Results

2.1. Differences in Pod Appearance and Morphology Between Thua Ngu and Raya

The appearance and morphology of Thua Ngu were compared with Raya. Raya is a normal type and commercial cultivar of yardlong bean. Thua Ngu and Raya expressed contrasting pod appearances. The immature pod surface (marketable pod stage; 8 days after flower blooming) of Thua Ngu was clearly rougher than that of Raya (Figure 1). The observation of the immature pods using a field-emission scanning electron microscope (FE-SEM) revealed that Thua Ngu possessed a large and rough wave-like surface, while Raya possessed a small and fine wave-like surface (Figure 2).

The examination of pods in the immature (8 days after flower blooming) and mature stages by cross-section microscopy revealed that in both stages, cells in the pods of Thua Ngu were better organized than those of Raya (Figure 3). In Thua Ngu, the cells appeared to be packed, while in Raya, the cells appeared to be loose. In addition, the shape and size of the cells in the pods of Thua Ngu were different from those of the pods of Raya. In Thua Ngu, the majority of the cells were round or oval in shape, while in Raya, most of the cells were oblong. The differences in cell shape and size were clearly evident in the immature pods.



Figure 1. Characteristics of immature pods of Thua Ngu, Raya, and their F_1 hybrid. Inset shows the whole pods of Thua Ngu (**left**), Raya (**right**), and their F_1 hybrid (**middle**).

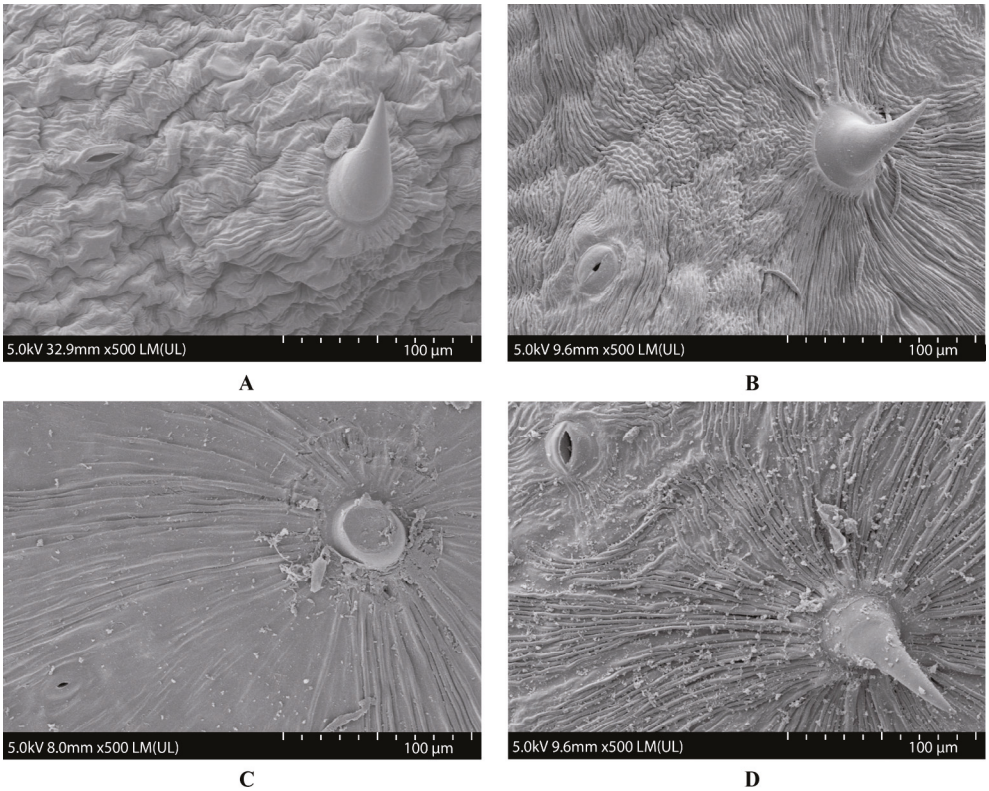

Figure 2. Pod surface structure of immature and mature pods of Thua Ngu and Raya revealed by field-emission scanning electron microscope. Immature pods of Thua Ngu and Raya are shown in (**A**) and (**B**), respectively, while mature pods are shown in (**C**) and (**D**), respectively.

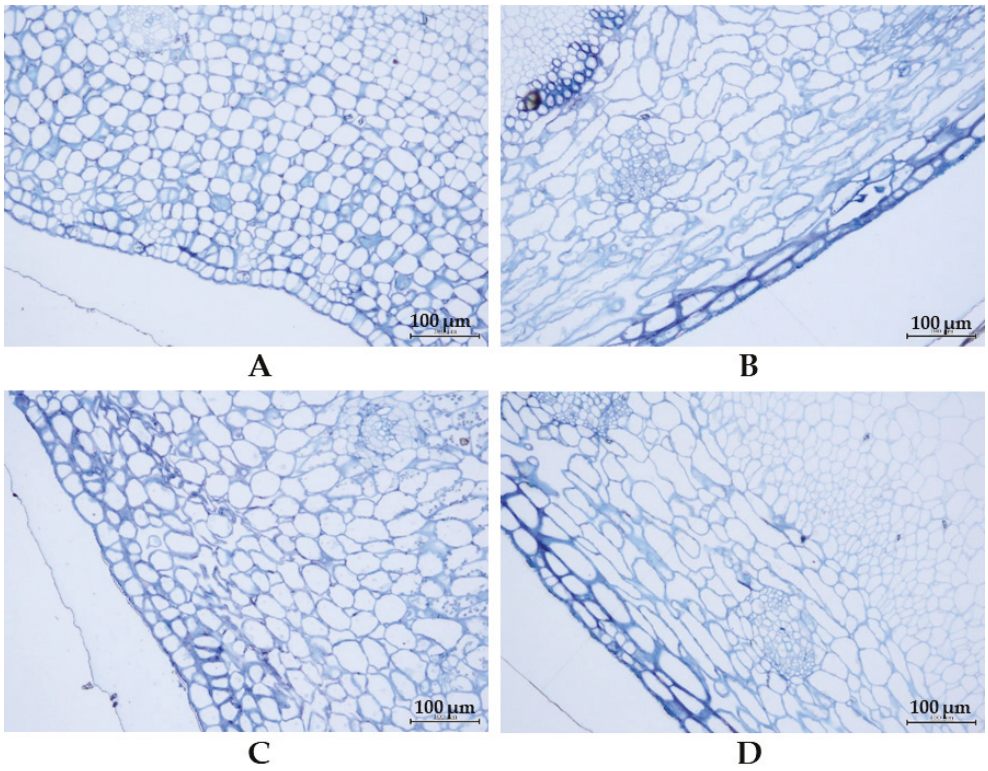

Figure 3. Cell shape, size, and density of immature and mature pods of Thua Ngu and Raya revealed by cross-section microscopy. Immature pods of Thua Ngu and Raya are shown in (**A**) and (**B**), respectively, while mature pods are shown in (**C**) and (**D**), respectively.

2.2. Differences in Pod Chemical Contents Between Thua Ngu and Raya

Immature and mature pods of Thua Ngu and Raya were analyzed for fiber contents, including cellulose, hemicellulose, and lignin. The results of fiber analysis are summarized in Table 1. In the immature pod stage, Thua Ngu possessed significantly lower cellulose and lignin contents but higher hemicellulose content than Raya. In the mature pod stage, Thua Ngu possessed statistically lower cellulose, hemicellulose, and lignin contents than Raya. However, among these three fibers, the most striking difference between Thua Ngu and Raya was lignin; Thua Ngu had 2.05- and 3.45-fold higher pod lignin content than Raya.

Table 1. Ranges and means of percentage of pod fiber contents in Thua Ngu and Raya.

Type of Fiber	Stage of Pod	Thua Ngu		Raya		*t*-Test	*p*-Value
		Range	Mean ± SD	Range	Mean ± SD		
Cellulose	Immature	9.28–10.88	9.84 ± 0.70	10.17–11.36	10.70 ± 0.53	−2.39	0.0378
	Mature	12.73–21.32	16.61 ± 3.48	18.22–22.53	20.68 ± 1.86	−2.52	0.0304
Hemicellulose	Immature	4.58–5.77	4.94 ± 0.44	3.41–4.67	4.33 ± 0.47	2.35	0.0406
	Mature	7.41–12.73	10.05 ± 1.90	8.90–12.29	11.12 ± 1.49	−1.08	0.3035
Lignin	Immature	0.07–0.64	0.34 ± 0.24	0.35–0.95	0.70 ± 0.25	−2.50	0.0316
	Mature	0.76–1.43	1.10 ± 0.26	2.94–4.44	3.81 ± 0.53	−11.25	0.0005

Data are from six plants/replicates.

2.3. Mendelian Inheritance of Snake-like Pod in F_2 Population

The inheritance of the snake-like (Ngu-type) pod trait in Thua Ngu was determined in F_2 and $F_{2:3}$ populations of the cross Thua Ngu × Raya. Chi-square (χ^2) analysis in the F_2 population showed that the segregation did not fit the 1 (snake-like pod): 2 (semi-snake-like pod): 1 (normal pod) ratio at the probability level of 0.05, but it fitted the 1:2:1 ratio at the

probability level of 0.01 (Table 2). However, χ^2 analysis in the $F_{2:3}$ population demonstrated that the segregation fitted the 1:2:1 ratio at both probability levels, 0.05 and 0.01 (Table 2). These results suggested that the snake-like pod trait in Thua Ngu is controlled by a single gene, designated as *Snake-like pod* (*Slp*).

Table 2. Chi-square (χ^2) analysis results of the snake-like pod trait in the F_2 and $F_{2:3}$ populations of the cross Thua Ngu × Raya.

Population	No. of Plants	No. Observed Plants [1]	No. Expected Plants [1]	χ^2 Value	*p*-Value
F_2	227	56:129:42	1:2:1	5.96	0.05
$F_{2:3}$	260	59:134:67	1:2:1	0.74	0.69

[1] Snake-like pod: semi-snake-like (F_1-like) pod: normal pod.

2.4. QTL-Seq Identified a Major Locus Controlling Snake-like Pod Surface Trait

QTL-seq was carried out to identify the genome region controlling the snake-like pod trait. Four DNA sequencing libraries were prepared: two from the parents (Thua Ngu and Raya) and two from bulked DNA (snake-like pod (SLPD) bulk and normal pod (NPD) bulk). These DNA libraries were whole-genome re-sequenced by using the Illumina NovaSeq 6000 Sequencing System (Illumina, San Diego, CA, USA). Results from the resequencing are summarized in Table 3. The sequencing yielded 157,417,310 reads for Thua Ngu, 141,492,570 reads for Raya, 206,626,290 reads for SLPD-bulk, and 169,252,490 reads for NPD-bulk, which were equivalent to 23.6, 21.2, 21.0, and 25.4 Gb, corresponding to sequencing depths of 30.49, 35.64, 40.47, and 32.92, respectively. The sequence alignment against the cowpea reference genome (Vigna unguiculata 2.1) revealed that the genome coverage rates of these sequence data were 97.39%, 92.08%, 97.18%, and 97.20%, respectively. Read mapping identified a total of 3,545,281 SNPs and 709,233 InDels, with 1,403,307 and 256,049 filtered as high-quality SNPs and InDels, respectively.

Table 3. Statistics of Illumina short-read sequencing for Ngu, Raya, bulked DNA of F_2 plants with snake-like pods (SLPD-bulk), and bulked DNA of F_2 plants with normal pods (NPD-bulk).

Sample	Total Reads	Raw Data (Gb)	Clean Reads	Mapping Rate (%)	Genome Coverage (%)	Average Depth
Ngu	157,417,310	23.6	146,209,198	84.5	97.39	30.49
Raya	141,492,570	21.2	130,397,263	84.3	92.08	35.64
SLPD	206,626,290	21.0	191,749,197	89.4	97.18	40.47
NPD	169,252,490	25.4	156,981,684	89.4	97.20	32.92

QTL-seq analysis using Δ(SNP-index) identified a single QTL for the snake-like pod surface trait (Figure 4 and Table 4). The QTL located on chromosome 4 at the position ranging from 36,200,001 to 42,731,077 with the Δ(SNP-index) value of 0.3253. However, QTL-seq analysis based on the G′-value revealed five QTLs for the snake-like pod surface trait, one each on chromosomes 4, 7, and 11, and two on chromosome 8 (Figure 4 and Table 4). Thus, the QTL-seq analysis by Δ(SNP-index) and G′-statistic pinpointed a single QTL for the snake-like pod surface trait on chromosome 4, designated as *qSpl4.1*.

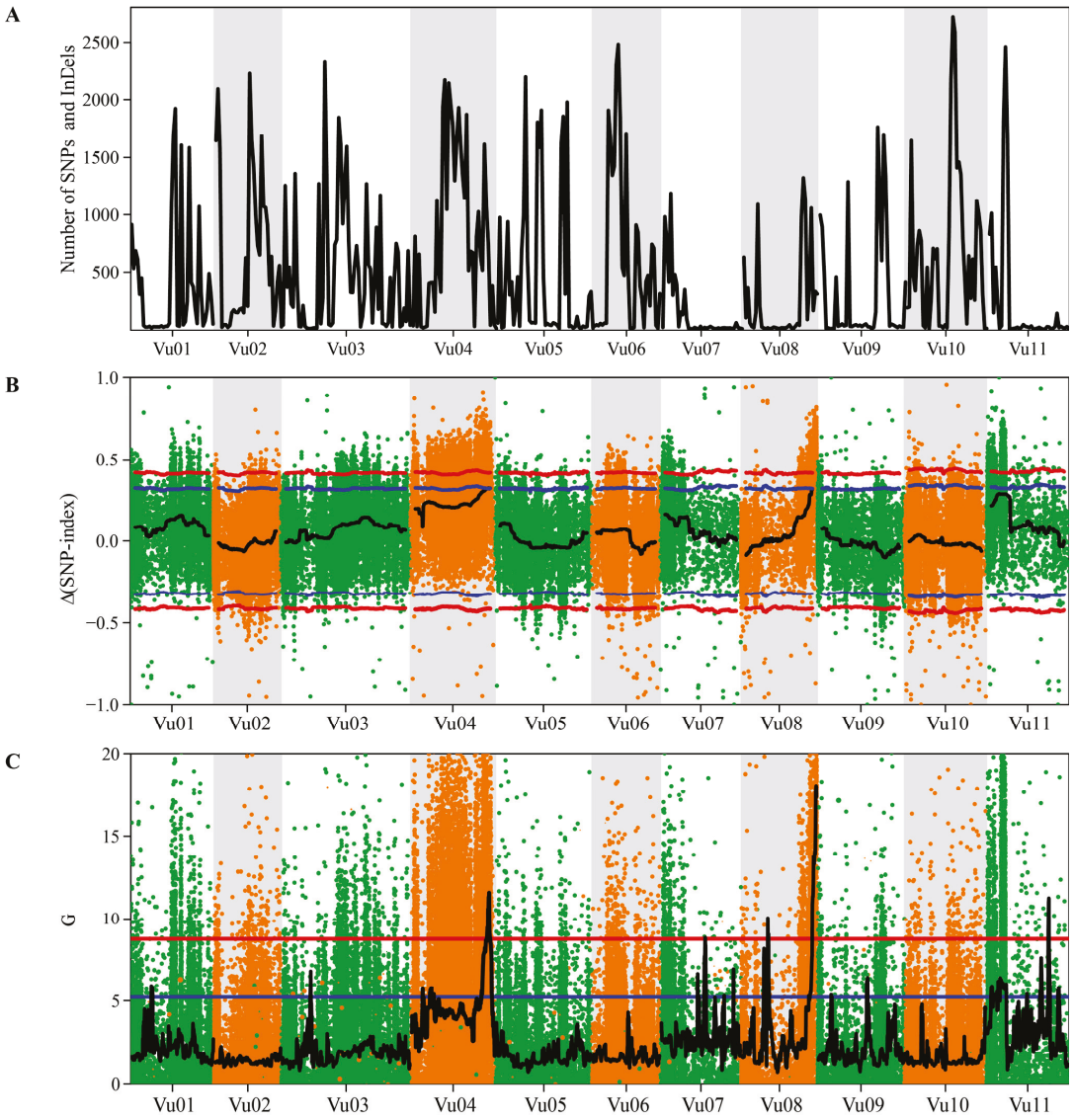

Figure 4. Quantitative trait loci for snake-like pod in yardlong bean identified by QTL-seq. Plots were produced with a 1 Mb sliding window: distribution of single-nucleotide polymorphisms (SNPs) in each window along the mungbean chromosomes (**A**); Δ(SNP-index) with two-sided confidence intervals—95% (red) and 99% (blue) (**B**); and G′-value with two-sided confidence intervals—95% (red) and 99% (blue) (**C**).

Table 4. QTLs controlling snake-like pod trait in yardlong bean detected by QTL-seq analysis based on Δ(SNP-index) and G′-statistic methods.

Method	Chromosome	Position (bp)	Length (bp)	No. of SNPs and InDels	Peak of Δ(SNP-Index)	Maximum of G-Stat
Δ(SNP-index)	4	36,200,001–42,731,077	6,531,076	3577	0.3253	-
G′-statistic	4	38,000,001–40,500,000	2,499,999	1083	-	11.5729
	7	22,100,001–23,100,000	999,999	22	-	8.7993
	8	12,800,001–14,200,000	1,399,999	17	-	10.0492
		35,300,001–38,363,498	3,063,497	757	-	18.0799
	11	30,700,001–32,000,000	1,299,999	19	-	11.244

2.5. Fine-Mapping of qSlp4.1

The *qSlp4.1* locus identified by QTL-seq was further investigated by QTL fine-mapping. One hundred and seventy-three new SSR markers were developed from a 400 kb region, 37,999,905 bp to 39,997,744 bp, on chromosome 4 of the cowpea reference genome covering

qSlp4.1 (Supplementary Table S1). Marker screening between Thua Ngu and Raya revealed 77 polymorphic markers (Supplementary Table S1), of which 19 markers were selected and used to analyze the F_2 and $F_{2:3}$ populations.

The linkage map constructed for the F_2 population was 78.2 cM in total length (Supplementary Figure S1). QTL analysis by the ICIM method revealed that *qSlp4.1* located between the markers VuSLPSSR185 and VuSLPSSR191. *qSlp4-1* explained 31.40% of the pod surface score variation in this population with additive and dominant effects of 0.45 and −0.28, respectively (Table 5 and Figure 5A).

Table 5. Locations and effects of *qSlp4.1* controlling the snake-like pod surface trait detected by the ICIM method in the F_2 and $F_{2:3}$ populations of the cross Thua Ngu × Raya.

Population	Location (cM)	Marker Interval	LOD Score	Percentage of Variance Explained by QTL	Additive Effect	Dominant Effect
F_2	9.0	VuSLPSSR185–VuSLPSSR191	18.19	31.40	0.45	−0.28
$F_{2:3}$	77.00	VuSLPSSR182–VuSLPSSR185	11.63	19.24	0.42	−0.06

The *qSlp4.1* locus identified by fine-mapping in the F_2 population was confirmed by using $F_{2:3}$ population. The linkage map constructed for the $F_{2:3}$ population was 126.0 cM in total length (Supplementary Figure S2). ICIM localized *qSlp4.1* to the region between the markers VuSLPSSR182 and VuSLPSSR185. *qSlp4.1* accounted for 19.24% of the pod surface score variation in this population. It showed an additive effect of 0.42 and a dominant effect of −0.06 (Table 5 and Figure 5B).

2.6. Candidate Genes

Based on the results of QTL mapping in the F_2 and $F_{2:3}$ populations, the *qSlp4.1* locus located in the interval region of the markers VuSLPSSR182 and VuSLPSSR191. BLASTN search against the cowpea reference genome revealed that these markers located at the positions 38,728,679 and 38,881,561, respectively. So, the two markers were 152.88 Kbp apart. Based on the cowpea reference genome, there existed nine genes in the 152.88 kbp region (Table 6). Among these, genes are predicted to encode six different proteins, including sugar kinase, MADS-box protein, gibberellin A44 oxidase, carboxylesterase 9-related protein, pentatricopeptide repeat (PPR), and hypothetical protein. Four of the genes encode carboxylesterase 9-related protein.

Table 6. Cowpea genes locating within the interval of markers VuSLPSSR182 and VuSLPSSR191 containing *qSlp4.1*.

Gene	Location on Cowpea Chromosome 4	Encoded Protein	Homologous Gene in *Arabidopsis thaliana*
Vigun04g163400	38729477..38732599	Sugar kinase	*AT5G51830* (*FRK1*, *FRUCTOKINASE 1*, *FRK7*, and *FRUCTOKINASE 7*)
Vigun04g163600	38737147..38745823	MADS-box protein	*AT2G45650* (*AGL6* and *AGAMOUS-LIKE 6*)
Vigun04g163700	38794766..38796717	Gibberellin A44 oxidase	*AT4G25420* (*GA20OX1*)
Vigun04g163800	38805392..38806670	Carboxylesterase 9-related protein	*AT5G62180* (*CXE20* and *CARBOXYLESTERASE 20*)
Vigun04g163900	38812815..38814262	Carboxylesterase 9-related protein	*AT5G62180* (*CXE20* and *CARBOXYLESTERASE 20*)
Vigun04g164000	38820160..38821585	Carboxylesterase 9-related protein	*AT5G62180* (*CXE20* and *CARBOXYLESTERASE 20*)

Table 6. *Cont.*

Gene	Location on Cowpea Chromosome 4	Encoded Protein	Homologous Gene in *Arabidopsis thaliana*
Vigun04g164100	38826706..38830585	Pentatricopeptide repeat	*AT1G80880* (*TETRATRICOPEPTIDE REPEAT (TPR)-LIKE SUPERFAMILY PROTEIN*)
Vigun04g164200	38830603..38832039	Carboxylesterase 9-related protein	*AT5G62180* (*CXE20* and *CARBOXYLESTERASE 20*)
Vigun04g164300	38848168..38852702	Hypothetical protein	*AT5G51800*

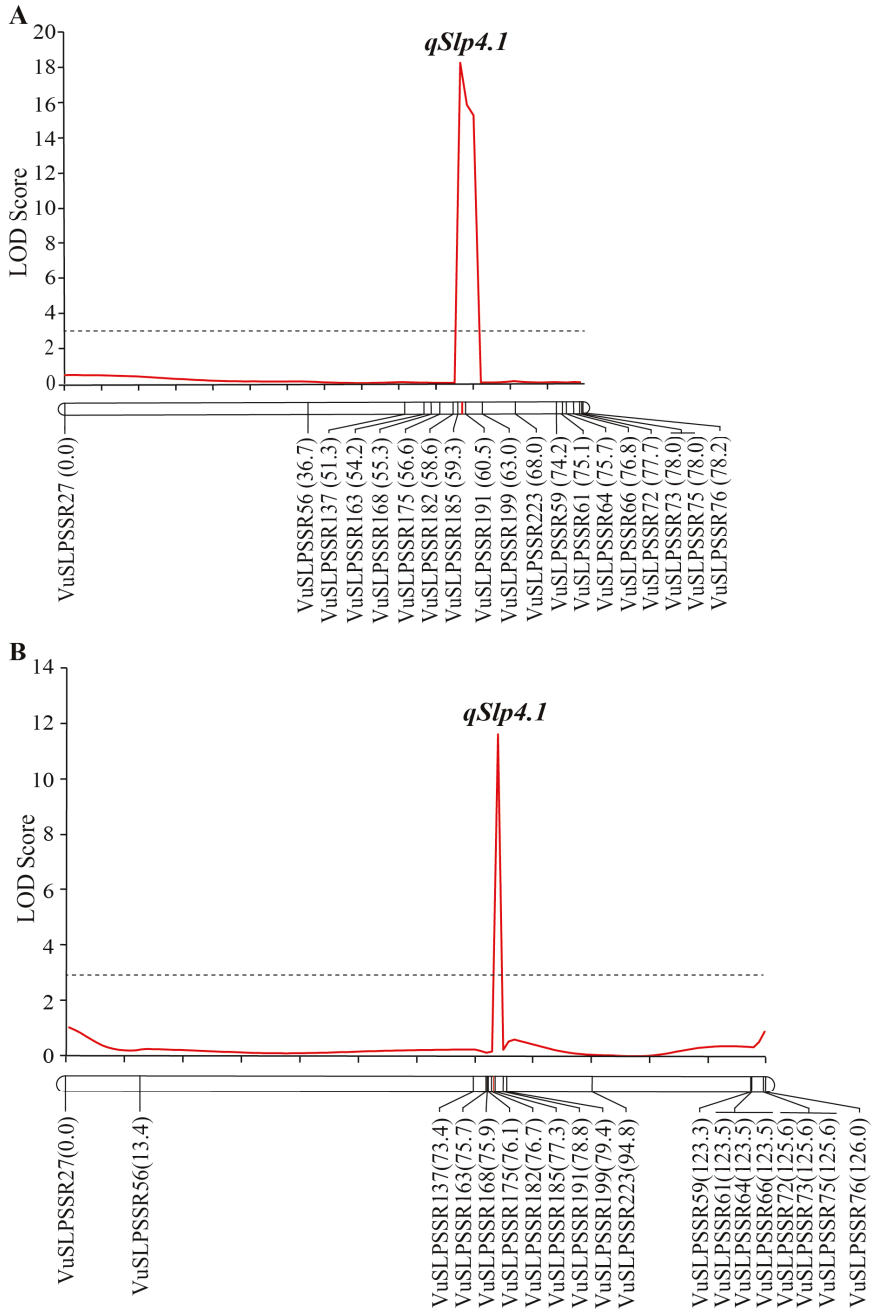

Figure 5. *qSlp4.1* in F_2 (**A**) and $F_{2:3}$ (**B**) populations of the cross Thua Ngu × Raya detected by inclusive composite interval mapping method. Dotted line represents LOD threshold for QTL.

3. Discussion

Local germplasm possessing a specialty/unique trait(s) is a useful genetic resource for the breeding of a new cultivar(s) with high market value and demand [6]. Since yardlong bean is used for its long, crisp, and tender pods in both fresh and processed forms, traits related to appearance, texture, taste, flavor, and nutritive value are important characters for consumer preference and price [3,9]. In this study, we investigated the pod surface, cell wall, and fibers of specialty yardlong bean, Thua Ngu, which possesses a unique immature pod appearance in comparison with the normal yardlong bean, Raya (Figure 1). It appeared that the size, density, and organization of cells and the lignin content in immature pods were clearly different between Thua Ngu and Raya (Figures 2 and 3 and Table 1). Differences in these cell morphologies/properties and lignin content may contribute to snake-like pod appearance and pod crispiness in Thua Ngu. The lignin content in the pods of Thua Ngu was 2.05- and 3.45-fold higher than that in Raya, depending on the pod developmental stage. Lignin is a complex polymer deposited directly in the cell wall of specialized cells. It plays a key role in the appearance and function of vascular pods. It affects plant development by strengthening plant organs and tissue robustness by increasing reinforcement in cell walls [10,11]. It can significantly modify cell morphology, including area, length, width, roundness, circularity, and solidity [12]. Thus, high lignin content may cause high cell density, well-organized/packed cells, and round/oval cell shape in the pods of Thua Ngu.

Segregation analysis suggested that that a single gene controls the snake-like pod phenotype in Thua Ngu (Table 2), and QTL-seq analysis also identified a single QTL, *qSlp4.1*, on cowpea chromosome 4 controlling the snake-like pod phenotype (Figure 4). These results strongly indicate that a single locus controls the snake-like pod phenotype in Thua Ngu. Fine-mapping and bioinformatics analyses revealed nine genes encoding six different annotated proteins as candidate genes for the snake-like pod phenotype (Figure 5 and Tables 5 and 6). However, based on the function of those genes/proteins, the *Vigun04g163400*, *Vigun04g163600*, and *Vigun04g163700* genes encoding sugar kinase, MADS-box protein, and gibberellin A44 oxidase, respectively, are considered candidate genes for the snake-like pod surface trait in Thua Ngu.

Vigun04g163600 is predicted to encode a sugar kinase protein that is homolog to the FRUCTOKINASE 1 (FRK1)/FRUCTOKINASE 7 (FRK1) of *Arabidopsis thaliana* L. FRK1 is an enzyme responsible for phosphorylating fructose, converting it into fructose-1-phosphate, a key step in fructose metabolism [13]. Nonetheless, a study in tomato (*Solanum lycopersicum* L.) by gene overexpression and antisense gene suppression illustrated that FRK1 plays an important role in vascular tissue development and that the suppression of this gene results in decreased lignification, leading to distorted xylem vessels and phloem fibers [14]. The study also showed that FRK1 has an effect on cell size and cell wall characteristics in phloem fibers, which are crucial to tissue and plant strength and support [14].

Vigun04g163600 is predicted to encode a MADS-box protein that is homolog to the AGAMOUS-LIKE6 (AGL6) of *A. thaliana*. MADS-box proteins are transcription factors and play pivotal roles in growth, development, and environmental adaptation, especially flowering time, in plants [15,16]. Nonetheless, a study in *A. thaliana* showed that the *AGAMOUS-LIKE15* (*AGL15*) gene plays a role in lignin biosynthesis through the regulation of the expression of the *PRX17* gene, a peroxidase involved in age-dependent lignified tissue formation, including changes in cell wall properties [17], while a study in chickpea (*Cicer arietinum* L.) demonstrated an association between the *AGAMOUS-like X2* (*CaAGLX2*) gene and pod wall development [18]. In addition, studies showed that ALG6 is a regulator of floral organ identity and spikelet meristem development in wheat [19] and regulates floral organ and meristem identity in rice [20]. Moreover, a recent study in *Phalaenopsis* orchid by virus-induced gene silencing showed that the *ALG6* gene is involved in lignin forma-

tion possibly through the regulation of the expression of *VND1/MYB46/MYB63/MYB85* genes [21], which are important regulators of cell wall biosynthesis.

Vigun04g163700 is predicted to encode gibberellin-A44 oxidase (gibberellin-44 dioxygenase), a key oxidase enzyme in gibberellin biosynthesis that catalyzes the conversion of gibberellin-44 (GA44) into gibberellin-19 (GA19) [22]. GA19 is a precursor to gibberellin-1 (GA1), a bioeffector gibberellin crucial to various growth and developmental processes [23]. Gibberellin (GA) affects plant phenotypes in several aspects through cell growth regulation [24]. For an example, GA-deficient sunflower showed a reduction in leaf area, a thicker lamina, smaller abaxial pavement cells, a stomatal density enhancement, and a guard cell length reduction [25]. However, additional studies including fine-mapping, gene sequencing, and gene expression analysis should be conducted to identify the causal gene controlling the snake-like pod surface trait in Thua Ngu.

4. Materials and Methods

4.1. Characterization of Pod Morphology

The pod surface and pod wall structure of Ngu and Raya were investigated by using a microscope as per Paopun et al. [26] and Chai et al. [27], respectively. Raya is a commercial and standard type of yardlong bean with normal pod appearance from Thailand. In brief, for the pod surface, fresh and dry pods of each accession were cut into $1 \times 1 \times 1$ mm sections by using a Leica SM2010R Sliding Microtome (Leica Microsystems, Wetzlar, Germany). After that, the samples were treated with 2.5% glutaraldehyde, washed with 0.1 phosphate buffer, and fixed with osmium tetroxide (OsO4). Subsequently, the fixed samples were immersed in liquid nitrogen and dried in a K750X Peltier-Cooled EM Freeze Dryer (Quorum Technologies, East Sussex, UK) for 36 h. After that, the dried samples were coated with gold particles by using an IB-2 ion coater (EIKO Corporation, Tokyo, Japan) and then examined by an SU8020 field-emission scanning electron microscope (FE-SEM) (Hitachi, Tokyo, Japan).

In case of the pod wall structure, cross-sections were obtained. In brief, pods were soaked in sterile water and fixed with 2.5% glutaraldehyde and 4% paraformaldehyde in PBS buffer. After that, the pods were washed with PBS and postfixed in 1% osmium tetroxide, dehydrated in a series of ethanol dilutions, embedded in LR White resin, and polymerized. Cross-sections were cut in the middle of the pod by using a Leica EM UC7 (Leica Microsystems, Wetzlar, Germany).

4.2. Determination of Pod Fiber Content

Young and mature pods of pods of Ngu and Raya were analyzed for fiber contents including cellulose, hemicellulose, and lignin, as per the procedures described by Suanum et al. [7] with six plants/replicates. Briefly, young and mature pods harvested from each plant of each cultivar were dried and ground into powder and then sieved through a 1 μm sieve. After that, the powder samples were analyzed for neutral detergent fiber, acid detergent fiber, and acid detergent lignin by using an ANKOM-200 Fiber Analyzer (ANKOM Technology, Macedon, NY, USA). Subsequently, the ANKOM bags containing the residual of the ADF procedure were placed in an ANKOM II Daisy incubator and submerged in 72% H_2SO_4. The samples were altered in the incubator, washed by using hot water and acetone, dried, and weighed. Subsequently, the sample bag containing the remaining residual fiber was burnt, and the resultant ash was weighed. Pods of each plant were analyzed twice for fiber contents. The amounts of neutral detergent fiber, acid detergent fiber, acid detergent lignin, and ash were used to calculate cellulose, hemicellulose, and lignin contents.

4.3. Population Mapping, Phenotyping of Pod Surface, and DNA Extraction

Two segregating populations, F_2 and $F_{2:3}$ generations, generated from the crossing of Thua Ngu (female parent) and "Raya" (male parent), were used in this study. Raya is a commercial yardlong bean cultivar with normal pod appearance. The F_2 population comprised 227 individuals which were grown together with their parents in an experimental field of Kasetsart University, Kamphaeng Saen Campus, Nakhon Pathom, Thailand, from May to August 2021. Eight days after flowering, pods of each plant were harvested for pod surface visual assessment. F_2 plants having snake-like (Thua Ngu-like) pods, semi-snake-like (F_1 hybrid-like) pods, and normal (Raya-like) pods (Figure 1) were given scores of 3, 2, and 1, respectively.

The $F_{2:3}$ population comprised 260 individuals. It was derived from the self-pollination of two F_2 plants showing heterozygosity at the SSR markers VuSLPSSR185 and VuSLPSSR191 flanking the *qPds* QTL detected in the F_2 population. The $F_{2:3}$ population and its parents were grown from March to June 2023 in the same field used to grow the F_2 population. The evaluation and scoring of the pod surface in the $F_{2:3}$ population were the same as those described for the F_2 population.

Total genomic DNA was extracted from young leaves of F_2, $F_{2:3}$, and parental plants by using the CTAB method [28].

4.4. QTL Analysis for Pod Surface Trait by Bulked Segregant Analysis Coupled to Whole-Genome Sequencing (QTL-Seq)

QTL-seq analysis [29] was carried out by using the F_2 population to identify the QTL controlling pod surface appearance. Two DNA groups of the F_2 plants expressing contrasting pod surface appearance—normal pod (NPD-bulk) vs. snake-like pod (NGU-bulk)—were constructed. Each group/bulk contained pooled DNA from 25 plants. The DNA of the two bulks and their parents were whole-genome-sequenced by next-generation sequencing. Paired-end sequencing libraries with insert sizes of ~ 350 bp were constructed by using an Illumina TruSeq Library Prep Kit (Illumina, San Diego, CA, USA). The concentration of the libraries was determined by a Qubit® 2.0 fluorometer (Thermo Fisher Scientific, Waltham, MA, USA). The insert size was assessed by using an Agilent® 2100 Bioanalyzer (Agilent Technologies, Santa Clara, CA, USA). Libraries with appropriate insert size and an effective concentration of more than 2 nM were sequenced by using the Illumina NovaSeq 6000 System (Illumina, San Diego, CA, USA). Subsequently, raw paired-end reads were trimmed and quality-controlled by using Trimmomatic [30]. High-quality sequencing reads were aligned against the reference genome of cowpea variety "IT97K-499-35" [31], version 2.1 (Vigna unguiculata v1.2; www.phytozome.net; accessed 15 March 2024), by using the Burrows-Wheeler Alignment tool [32]. Sequence Alignment/Map format files were imported into SAMtools [33]; then, SNPs and short insertion/deletion (InDel) (1–10 bp) were detected by using Genome Analysis Toolkit 4.1.2.0 [34].

QTL-seq analysis was performed by using the R package QTLseqr [35]. SNPs detected with minimum total read depth = 10, maximum total read depth = 500, minimum read depth = 10, and minimum genotype quality (minGQ) = 99 were used in QTL-seq analysis. Δ(SNP-index) [29] and G′-value [36] were calculated by using a sliding window size of 1 Mb, a 95–to-99% confidence interval, and a q-value threshold of 0.01 with 10,000 iterations, while the filter method "ΔSNP" was calculated by using a threshold of 0.01 in the G′ analysis.

4.5. Development of New DNA Markers and Fine-Mapping of QTL Controlling Pod Surface Trait

Once the QTL controlling the pod surface trait was identified by QTL-seq, the QTL was further investigated by QTL fine-mapping. A genome region of 400 Kb of the reference

cowpea genome cultivar IT97K-499-35 [31] covering the location of *qPds* (200 Kb of sequence on the left and right sides of the maximum G′-value position) was searched for simple sequence repeats (SSRs) by using SSRIT software [37]. After that, primers for SSRs were designed by using Primer3 software [38] and screened for polymorphisms between Thua Ngu and Raya by polymerase chain reaction (PCR) and gel electrophoresis, as described by Yundaeng et al. [39]. In brief, PCR was carried out in a total volume of 10 μL containing 5 ng of DNA template, 1 × *Taq* buffer, 2 mM $MgCl_2$, 0.2 mM dNTPs, 1 U *Taq* DNA polymerase, and 2.5 μM each of forward and reverse primers. Amplification was performed at 94 °C for 3 min followed by 35 cycles at 94 °C for 30 s, 55 °C for 30 s, 72 °C for 30 s, and 72 °C for 10 min. PCR products were electrophoresed on 5% polyacrylamide gel and visualized by silver staining. Nineteen markers showing clear and polymorphic DNA bands were used to analyze the F_2 and $F_{2:3}$ populations for QTL mapping.

For each population, a linkage map was constructed by using QTL IciMapping 4.2 [40]. Markers were grouped by using a logarithm of odds (LOD) value of 5.0 and then ordered by using the REcombination Counting and ORDering method [41]. Distances between markers were calculated by using Kosambi's mapping function [42]. The QTL for CLS resistance was located onto the linkage map by using the inclusive composite interval mapping method (ICIM) [43] by QTL IciMapping 4.2. ICIM was performed at every 0.1 cM with a PIN value of 0.001. An LOD score threshold of 3.0 was used to determine the QTL.

4.6. Identification and Sequencing of Candidate Genes

The nucleotide sequences of the SSR markers VuSLPSSR185 and VuSLPSSR191 covering *qSlp4.1* were subjected to BLASTN search against the cowpea genome cultivar IT97K-499-35 [Vigna unguiculata v1.2; accessed 15 June 2024] to determine the physical genome region of *qSlp4.1*. Genes locating within the *qSlp4.1* region were considered candidate genes for the snake-like pod surface trait.

4.7. Statistical Analysis

Significant differences in cellulose, hemicellulose, and lignin contents in pods between Thua Ngu and Raya were determined by the *t*-test by using R program 2.14.0 [44]. In the F_2 and $F_{2:3}$ populations, the numbers of plants exhibiting snake-like pods (pod score = 3), semi-snake-like pods (pod score = 2), and normal pods (pod score = 1) were subjected to segregation analysis by the chi-square test (χ^2) by using R program 2.14.0 [44].

Supplementary Materials: The following supporting information can be downloaded at: https://www.mdpi.com/article/10.3390/plants14101447/s1, Figure S1: Genetic linkage map constructed for F_2 population of the cross Thua Ngu × Raya. Genetic distance of the markers on the map are shown in unit of centimorgan.; Figure S2; Genetic linkage map constructed for $F_{2:3}$ population of the cross Thua Ngu × Raya. Genetic distance of the markers on the map are shown in unit of centimorgan.; Table S1: Primers used in this study.

Author Contributions: Conceptualization, P.S. and K.L.; methodology, P.S., K.T. and K.L.; validation, P.S.; formal analysis, K.T. and M.S.; investigation, K.T., A.D., P.S. and K.L.; data curation, P.S.; writing—original draft preparation, K.T. and P.S.; writing—review and editing, P.S. and K.L.; visualization, K.T.; supervision, P.S.; project administration, K.L.; funding acquisition, P.S. and K.L. All authors have read and agreed to the published version of the manuscript.

Funding: This research study was funded by the NSRF via the Program Management Unit for Human Resources and Institutional Development, Research, and Innovation, grant number B16F640185. The APC was funded by the Kasetsart University Research and Development Institute.

Data Availability Statement: The whole-genome resequencing data generated for Thua Ngu and Raya in this study are available from the National Center for Biotechnology Information (NCBI: https://www.ncbi.nlm.nih.gov) under BioProject numbers PRJNA1244560 and PRJNA1246342, respectively.

Acknowledgments: This research study was supported in part by the Graduate Program Scholarship from The Graduate School, Kasetsart University.

Conflicts of Interest: The authors declare no conflicts of interest. The funders had no role in the design of the study; in the collection, analyses, or interpretation of data; in the writing of the manuscript; or in the decision to publish the results.

Abbreviations

The following abbreviations are used in this manuscript:

QTL	Quantitative trait locus
ICIM	Inclusive composite interval mapping
FE-SEM	Field-emission scanning electron microscope
SSR	Simple sequence repeat
BLASTN	Basic local alignment search tool for nucleotide sequences

References

1. Singh, B.B. Cowpea [*Vigna unguiculata* (L.) Walp.]. In *Genetic Resources Chromosome Engineering and Crop Improvement*, 2nd ed.; Singh, R.J., Jauhar, P.P., Eds.; Taylor & Francis, LLC: Abingdon, UK, 2005; pp. 117–161.
2. Verdcourt, B. Studies in the Leguminosae–Papilionoideae for the 'Flora of Tropical East Africa': IV. *Kew Bull.* **1970**, *24*, 507–569. [CrossRef]
3. Kongjaimun, A.; Somta, P.; Tomooka, N.; Kaga, A.; Vaughan, D.A.; Srinives, P. QTL mapping of pod tenderness and total soluble solid in yardlong bean [*Vigna unguiculata* (L.) Walp. subsp. *unguiculata* cv.-gr. *sesquipedalis*]. *Euphytica* **2013**, *189*, 217–223. [CrossRef]
4. Steele, W.M.; Mehra, K.L. Structure, evolution, and adaptation to farming systems and environments in Vigna. In *Advances in Legume Sciences*, 2nd ed.; Summerfield, R.J., Bunting, A.H., Eds.; Royal Botanic Gardens: Kew, UK, 1980; pp. 393–404.
5. Wu, X.; Hu, Z.; Zhang, Y.; Li, M.; Liao, N.; Dong, J.; Wang, B.; Wu, J.; Wu, X.; Wang, Y.; et al. Differential selection of yield and quality traits has shaped genomic signatures of cowpea domestication and improvement. *Nat. Genet.* **2024**, *56*, 992–1005. [CrossRef] [PubMed]
6. Lazaridi, E.; Kapazoglou, A.; Gerakari, M.; Kleftogianni, K.; Passa, K.; Sarri, E.; Papasotiropoulos, V.; Tani, E.; Bebeli, P.J. Crop landraces and indigenous varieties: A valuable source of genes for plant breeding. *Plants* **2024**, *13*, 758. [CrossRef] [PubMed]
7. Suanum, W.; Somta, P.; Kongjaimun, A.; Yimram, T.; Kaga, A.; Tomooka, N.; Takahashi, Y.; Srinives, P. Co-localization of QTLs for pod fiber content and pod shattering in F_2 and backcross populations between yardlong bean and wild cowpea. *Mol. Breed.* **2016**, *36*, 80. [CrossRef]
8. Watcharatpong, P.; Kaga, A.; Chen, X.; Somta, P. Narrowing down a major QTL region conferring pod fiber contents in yardlong bean (*Vigna unguiculata*), a vegetable cowpea. *Genes* **2020**, *11*, 363. [CrossRef]
9. Kader, A.A. Maturity, ripening, and quality relationships of fruit-vegetable. *Acta Hort.* **1996**, *434*, 249–256. [CrossRef]
10. Ozparpucu, M.; Ruggeberg, M.; Gierlinger, N.; Cesarino, I.; Vanholme, R.; Boerjan, W.; Burgert, I. Unravelling the impact of lignin on cell wall mechanics: A comprehensive study on young poplar trees downregulated for CINNAMYL ALCOHOL DEHYDROGENASE (CAD). *Plant J.* **2017**, *91*, 480–490. [CrossRef]
11. Ozparpucu, M.; Gierlinger, N.; Cesarino, I.; Burgert, I.; Boerjan, W.; Ruggeberg, M. Significant influence of lignin on axial elastic modulus of poplar wood at low microfibril angles under wet conditions. *J. Exp. Bot.* **2019**, *70*, 4039–4047. [CrossRef]
12. Selig, M.; Walz, K.; Lauer, J.; Rolauffs, C.; Hart, M.L. Therapeutic modulation of cell morphology and phenotype of diseased human cells towards a healthier cell state using lignin. *Polymers* **2023**, *15*, 3041. [CrossRef]
13. Stein, O.; Granot, D. Plant fructokinases: Evolutionary, developmental, and metabolic aspects in sink tissues. *Front. Plant Sci.* **2018**, *9*, 339. [CrossRef] [PubMed]
14. Stein, O.; Secchi, F.; German, M.A.; Damari-Weissler, H.; Aloni, R.; Holbrook, N.M.; Zwieniecky, M.A.; Granot, D. The tomato cytosolic fructokinase FRK1 is important for phloem fiber development. *Biol. Plant.* **2018**, *62*, 353–361. [CrossRef]
15. Schilling, S.; Pan, S.; Kennedy, A.; Melzer, R. MADS-box genes and crop domestication: The jack of all traits. *J. Exp. Bot.* **2018**, *69*, 71447–71469. [CrossRef] [PubMed]

16. Zhang, Z.; Zou, W.; Lin, P.; Wang, Z.; Chen, Y.; Yang, X.; Zhao, W.; Zhang, Y.; Wang, D.; Que, Y.; et al. Evolution and function of MADS-box transcription factors in plants. *Int. J. Mol. Sci.* **2024**, *25*, 13278. [CrossRef]
17. Cosio, C.; Ranocha, P.; Francoz, E.; Burlat, V.; Zheng, Y.; Perry, S.E.; Ripoll, J.J.; Yanofsky, M.; Dunand, C. The class III peroxidase PRX17 is a direct target of the MADS-box transcription factor AGAMOUS-LIKE15 (AGL15) and participates in lignified tissue formation. *New Phytol.* **2017**, *213*, 250–263. [CrossRef]
18. Vasantrao, J.M.; Baruah, I.K.; Panda, D.; Bhattacharjee, M.; Acharjee, S.; Sarmah, B.K. Transcript profiling of chickpea pod wall revealed the expression of floral homeotic gene AGAMOUS-like X2 (CaAGLX2). *Mol. Biol. Rep.* **2019**, *46*, 5713–5722. [CrossRef]
19. Kong, X.; Wang, F.; Geng, S.; Guan, J.; Tao, S.; Jia, M.; Sun, G.; Wang, Z.; Wang, K.; Ye, X.; et al. The wheat AGL6-like MADS-box gene is a master regulator for floral organ identity and a target for spikelet meristem development manipulation. *Plant Biotechnol. J.* **2022**, *20*, 75–88. [CrossRef]
20. Li, H.; Liang, W.; Jia, R.; Yin, C.; Zong, J.; Kong, H.; Zhang, D. The AGL6-like gene OsMADS6 regulates floral organ and meristem identities in rice. *Cell Res.* **2010**, *20*, 299–313. [CrossRef]
21. Hsu, H.F.; Chen, W.H.; Shen, Y.H.; Hsu, W.H.; Mao, W.T.; Yang, C.H. Multifunctional evolution of B and AGL6 MADS box genes in orchids. *Nat. Commun.* **2021**, *12*, 902. [CrossRef]
22. Schomburg, D.; Schomburg, I. Gibberellin-44 dioxygenase. In *Class 1 Oxidoreductases XI. Springer Handbook of Enzymes*; Springer: Berlin/Heidelberg, Germany, 2006; Volume 26. [CrossRef]
23. Zanewich, K.P.; Rood, S.B. Gibberellins and heterosis in crops and trees: An integrative review and preliminary study with brassica. *Plants* **2020**, *9*, 139. [CrossRef]
24. Castro-Camba, R.; Sánchez, C.; Vidal, N.; Vielba, J.M. Plant development and crop yield: The role of gibberellins. *Plants* **2022**, *11*, 2650. [CrossRef] [PubMed]
25. Gallego-Giraldo, L.; García-Martínez, J.L.; Moritz, T.; López-Díaz, I. Flowering in tobacco needs gibberellins but is not promoted by the levels of active GA1 and GA4 in the apical shoot. *Plant Cell Physiol.* **2007**, *48*, 615–625. [CrossRef]
26. Paopun, Y.; Thanomchat, P. Freeze drying versus chemical fixation technique for scanning electron microscope of succulent and aquatic plant leaves. *Microsc. Microanal. Res.* **2017**, *1*, 28–32. [CrossRef]
27. Chai, M.; Zhou, C.; Molina, I.; Fu, C.; Nakashima, J.; Li, G.; Zhang, W.; Park, J.; Tang, Y.; Jiang, Q.; et al. A class II KNOX gene, *KNOX4*, controls seed physical dormancy. *Proc. Natl. Acad. Sci. USA* **2016**, *113*, 6997–7002. [CrossRef] [PubMed]
28. Lodhi, M.A.; Ye, G.N.; Weeden, N.F.; Reisch, B.I. A simple and efficient method for DNA extraction from grapevine cultivars and *Vitis* species. *Plant Mol. Biol. Rep.* **1994**, *12*, 6–13. [CrossRef]
29. Takagi, H.; Abe, A.; Yoshida, K.; Kosugi, S.; Natsume, S.; Mitsuoka, C.; Uemura, A.; Utsushi, H.; Tamiru, M.; Takuno, S.; et al. QTL-seq: Rapid mapping of quantitative trait loci in rice by whole genome resequencing of DNA from two bulked populations. *Plant J.* **2013**, *74*, 174–183. [CrossRef]
30. Bolger, A.M.; Lohse, M.; Usadel, B. Trimmomatic: A flexible trimmer for Illumina sequence data. *Bioinformatics* **2014**, *30*, 2114–2120. [CrossRef]
31. Lonardi, S.; Muñoz-Amatriaín, M.; Liang, Q.; Shu, S.; Wanamaker, S.I.; Lo, S.; Tanskanen, J.; Schulman, A.H.; Zhu, T.; Luo, M.C.; et al. The genome of cowpea (*Vigna unguiculata* [L.] Walp.). *Plant J.* **2019**, *98*, 767–782. [CrossRef]
32. Li, H.; Durbin, R. Fast and accurate short read alignment with Burrows-Wheeler transform. *Bioinformatics* **2009**, *25*, 1754–1760. [CrossRef]
33. Li, H.; Handsaker, B.; Wysoker, A.; Fennell, T.; Ruan, J.; Homer, N.; Marth, G.; Abecasis, G.; Durbin, R. The sequence alignment/map format and SAMtools. *Bioinformatics* **2009**, *25*, 2078–2079. [CrossRef]
34. McKenna, A.; Hanna, M.; Banks, E.; Sivachenko, A.; Cibulskis, K.; Kernytsky, A.; Garimella, K.; Altshuler, D.; Gabriel, S.; Daly, M. The genome analysis toolkit: A MapReduce framework for analyzing next-generation DNA sequencing data. *Genome Res.* **2010**, *20*, 1297–1303. [CrossRef] [PubMed]
35. Mansfeld, B.N.; Grumet, R. QTLseqr: An R package for bulk segregant analysis with next-generation sequencing. *Plant Genome* **2018**, *11*, 180006. [CrossRef] [PubMed]
36. Magwene, P.M.; Willis, J.H.; Kelly, J.K. The statistics of bulk segregant analysis using next generation sequencing. *PLoS Comput. Biol.* **2011**, *7*, e1002255. [CrossRef]
37. Temnykh, S.; DeClerck, G.; Lukashova, A.; Lipovich, L.; Cartinhour, S.; McCouch, S. Computational and experimental analysis of microsatellites in rice (*Oryza sativa* L.): Frequency, length variation, transposon associations, and genetic marker potential. *Genome Res.* **2001**, *11*, 1441–1452. [CrossRef]
38. Untergasser, A.; Cutcutache, I.; Koressaar, T.; Ye, J.; Faircloth, B.C.; Remm, M.; Rozen, S.G. Primer3–new capabilities and interfaces. *Nucleic Acids Res.* **2012**, *40*, e115. [CrossRef] [PubMed]
39. Yundaeng, C.; Somta, P.; Chen, J.; Yuan, X.; Chankaew, S.; Chen, X. Fine mapping of QTL conferring Cercospora leaf spot disease resistance in mungbean revealed TAF5 as candidate gene for the resistance. *Theor. Appl. Genet.* **2021**, *134*, 701–714. [CrossRef]
40. Meng, L.; Li, H.; Zhang, L.; Wang, J. QTL IciMapping: Integrated software for genetic linkage map construction and quantitative trait locus mapping in biparental populations. *Crop J.* **2015**, *3*, 269–283. [CrossRef]

41. Van Os, H.; Stam, P.; Visser, R.G.; Van Eck, H.J. RECORD: A novel method for ordering loci on a genetic linkage map. *Theor. Appl. Genet.* **2005**, *112*, 30–40. [CrossRef]
42. Kosambi, D.D. The estimation of map distances from recombination values. *Ann. Eugen.* **1943**, *12*, 172–175. [CrossRef]
43. Li, H.; Ye, G.; Wang, J. A modified algorithm for the improvement of composite interval mapping. *Genetics* **2007**, *175*, 361–374. [CrossRef]
44. R Core Team. *R: A Language and Environment for Statistical Computing, version 4.2.0*; R Foundation for Statistical Computing: Vienna, Austria, 2022.

Disclaimer/Publisher's Note: The statements, opinions and data contained in all publications are solely those of the individual author(s) and contributor(s) and not of MDPI and/or the editor(s). MDPI and/or the editor(s) disclaim responsibility for any injury to people or property resulting from any ideas, methods, instructions or products referred to in the content.

plants

MDPI

Review

Protein Post-Translational Modifications in Plant Abiotic Stress Responses

Gengmi Li [1,†], Baohua Feng [2,†], Qian-Hao Zhu [3], Kaifeng Jiang [1,*] and Tao Zhang [1,*]

[1] Key Laboratory of Southwest Rice Biology and Genetic Breeding, Ministry of Agriculture/Luzhou Branch of National Rice Improvement Center, Rice and Sorghum Research Institute, Sichuan Academy of Agricultural Sciences, Deyang 618000, China; wilfred123@163.com
[2] State Key Laboratory of Rice Biology and Breeding, China National Center for Rice Improvement, China National Rice Research Institute, Hangzhou 310006, China; fengbaohua@caas.cn
[3] Commonwealth Scientific and Industrial Research Organization, Agriculture and Food, GPO Box 1700, Canberra, ACT 2601, Australia; qianhao.zhu@csiro.au
* Correspondence: jiangkf67@126.com (K.J.); yszht@163.com (T.Z.)
† These authors contributed equally to this work.

Abstract

Protein post-translational modifications (PTMs), as an important biological process of plants responding to environmental stimuli, can regulate the chemical decoration and properties of translated proteins by altering amino acid side chains or protein terminal structures, thereby affecting the synthesis, assembly, localization, function, and degradation of proteins. Notably, PTMs regulate protein function without changing protein expression levels. Two dozen types of PTMs have been identified. This review summarizes the molecular mechanisms of major types of PTMs, including phosphorylation, ubiquitination, SUMOylation, glycosylation, methylation, and acetylation, with a focus on their regulatory roles in plant responses to abiotic stresses. Under heat stress, phosphorylation activates transcription factors such as HSFA1 (heat shock transcription factor 1), while SUMOylation regulates the activity of HSFA1/HSFA2 in the heat stress signaling pathway. Upon cold stress, phosphorylation, ubiquitination, and S-acylation collectively regulate the expression of cold tolerance-related genes. The drought stress response relies on SnRK2s (Sucrose 321 non-Fermenting 1-related protein kinase 2s) -mediated phosphorylation, regulation of ARF7 (auxin response factor 7) by SUMOylation, and ubiquitination. In salt stress, the coupling of phosphorylation of SOS (salt overly sensitive) pathway-related proteins, ubiquitination, and phospholipid metabolism maintains ion homeostasis. Additionally, PTMs play a key role in ABA-mediated abiotic stress responses by regulating core components of signal transduction, such as PYR (pyrabactin resistance)/PYL (PYR1-LIKE)/RCAR (regulatory components of ABA receptor) receptors, PP2Cs (protein phosphatases type 2C), and SnRK2s. On the basis of the synthesis of the regulatory mechanisms of PTMs, we discuss how PTMs can be manipulated to breed abiotic stress resilient crops and the issues to be addressed to achieve the goal, such as crosstalk between PTMs, technical challenges in investigating PTMs and identifying PTM substrates.

Keywords: phosphorylation; ubiquitination; SUMOylation; PTMs; abiotic stress response

1. Introduction

Plants are constantly exposed to a variety of unsuitable environments, limiting their growth and development, particularly under the reality of global warming. Protein post-translational modification (PTM) is the process of chemically modifying proteins after they

are translated. Many types of PTMs have been documented. The Plant PTM Viewer 2.0 (https://www.psb.ugent.be/webtools/ptm-viewer/ptm_info.php (accessed on 11 November 2025)) lists 24 types of PTMs covering 437,404 PTM sites of 143,688 proteins. Some of these PTMs occur at specific amino acid residue(s), some at the C- or N-terminus of proteins. These modifications impact stability and localization of proteins, and assembly of protein complexes, thereby regulating functions of proteins without altering their expression level [1]. PTMs play a pivotal role in plants' responses to environmental stimuli, occurring critically and rapidly in response to changing environmental conditions, so having the potential to be harnessed for improving plants' capacity to combat the effects of adverse environments.

This review summarizes the research progress of PTMs in plants. Given the scope (both the diverse types of PTMs and the number of plant species) of the studies on plant PTMs, our focus here was on the main types of PTMs, including phosphorylation, ubiquitination, SUMOylation, glycosylation, methylation, and acetylation investigated in model monocotyledonous (rice) and dicotyledonous (*Arabidopsis*) species, and their functions in abiotic stress response. On the basis of synthesizing the main findings, we propose strategies by which PTMs could be employed in breeding climate-smart and abiotic stress resilient crops.

2. Main Types of Post-Translational Modifications

2.1. Phosphorylation

Protein phosphorylation is catalyzed by protein kinases and has the most diverse target proteins (Table 1). Protein kinases mediate the reaction by transferring the γ-phosphate group—the terminal, high-energy phosphate moiety—from nucleotide triphosphates (typically adenosine triphosphate (ATP), and occasionally guanosine triphosphate (GTP)) to specific amino acid residues of target proteins [2]. It was first identified by Levene and Alsberg in egg yolk protein [3]. In *Arabidopsis thaliana*, around 41% of the expressed proteins are phosphorylated by protein kinases and the phosphorylation sites are mainly serine (Ser), threonine (Thr), and tyrosine (Tyr) residues and rarely on N-terminal under different conditions [4,5]. Recently, the combination of TurboID-based proximity labeling (TbPL) with mass spectrometry (hereafter referred to as TbPL-MS) and the multiplexed assay for kinase specificity (MAKS) has significantly accelerated research advancements in the field of protein phosphorylation [6–8], leading to the identification of more than 43,000 phosphorylation sites in *Arabidopsis* [5]. Phosphorylation changes the features of proteins involved in mitogen-activated protein kinases (MAPKs), calcium-dependent protein kinases (CDPKs/CPKs), calcineurin-interacting protein kinases (CIPKs), and so on. All of them play pivotal roles in the abiotic stress response [9,10].

2.2. Ubiquitination

Ubiquitin is a small-molecule protein that is widely present in eukaryotes and highly conserved. It contains 76 amino acids with a molecular weight of approximately 8.5 kD. The ubiquitination process is catalyzed by a cascade of three enzymes, namely ubiquitin-activating enzyme E1, ubiquitin-conjugating enzyme E2, and ubiquitin-ligase enzyme E3 [11]. The ubiquitination process is reversible: deubiquitinating enzymes (DUBs) can hydrolyze the ubiquitin chains on target proteins, recycle ubiquitin molecules, and thus maintain the homeostasis of the ubiquitin pool [12]. Ubiquitin-activating enzyme E1 utilizes energy provided by ATP to activate ubiquitin (Ub) molecules, forming a Ub-E1 complex. Through transesterification, the Ub-E1 complex transfers Ub molecules to ubiquitin-conjugating enzyme E2, resulting in the formation of an Ub-E2 complex. Finally, under the action of ubiquitin-ligase enzyme E3, Ub molecules are covalently linked to

https://doi.org/10.3390/plants15010052

the lysine (Lys) residues of the target protein(Figure 1A) [13,14]. Ubiquitination modification participates in a variety of biological processes by influencing protein stability, protein subcellular localization, and protein–protein interactions, to regulate cell cycle, circadian rhythm, hormone signal transduction, growth and development, as well as responses to abiotic and biotic stresses [15]. The rice genome contains 6 genes encoding E1 ubiquitin-activating enzymes, 48 genes encoding E2 ubiquitin-conjugating enzymes or E2-like proteins, more than 1500 genes encoding E3 ubiquitin-ligases, and 95 genes encoding deubiquitinating enzymes (DUBs); these enzymes target key components involved in numerous biological processes in rice, such as plant growth and responses to abiotic and biotic stresses [16,17].

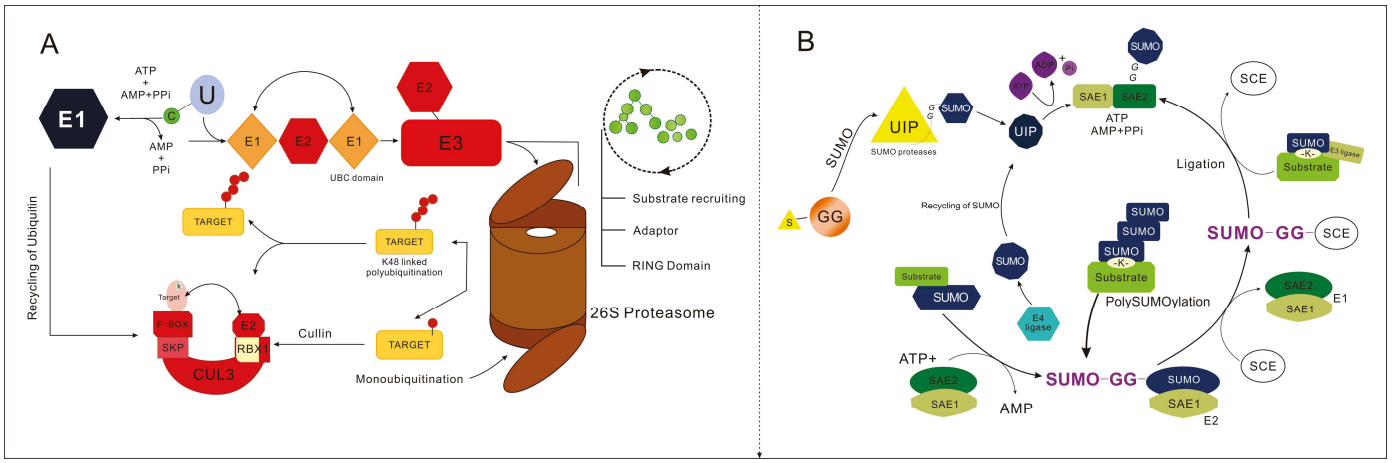

Figure 1. Ubiquitination and SUMOylation in plants. (**A**) Ubiquitination regulation pathway; (**B**) SUMOylation regulation pathway.

2.3. SUMOylation

A Small Ubiquitin-like Modifier (SUMO) molecule consists of approximately 100 amino acids. It shares only 12–16% sequence similarity with ubiquitin, yet the two proteins form highly similar three-dimensional structures after folding. Like ubiquitination modification, SUMOylation is also an ATP-dependent cascade enzymatic reaction: under the combined action of specific E1 activating enzymes, E2 conjugating enzymes, and E3 ligases, mature SUMO molecules covalently bind to the Lys residues of target proteins via isopeptide bonds (Figure 1B) [18]. SUMOylation often regulates protein stability, activity, structure, localization, and protein–protein interactions by competing with ubiquitination modification sites, and is also involved in various biological processes such as transcriptional regulation, cell cycle regulation, and environmental response [19,20].

2.4. Glycosylation

The glycosylation modification of proteins mainly occurs in the Golgi apparatus and the endoplasmic reticulum. Under the action of various glycosyltransferases, sugar chains bind to amino acid residues on polypeptide chains and form glycosidic bonds [21]. The newly generated glycosylated proteins undergo further transport, splicing, and modification, and finally exert their functions at specific sites. There are four main types: N-glycosylation, O-glycosylation, C-mannosylation, and glycosylphosphatidylinositol (GPI)-mediated glycosylation, among which the first two are the most prominent types [22–24]. N-glycosylation modification refers to the covalent attachment of N-glycans to asparagine residues in the consensus sequence Asn-X-Ser/Thr/Cys (where X represents any amino acid except proline) of polypeptide chains via N-glycosidic bonds [25,26]. In contrast, O-glycosylation modification occurs through the formation of O-glycosidic bonds between

the hydroxyl termini of serine or threonine residues in the protein peptide chain and glycosyl groups [27].

2.5. Methylations

Under the catalysis of different protein methyltransferases, methyl groups can be transferred from the methyl donor S-adenosylmethionine (SAM) to the side chains of amino acids such as arginine and lysine. Most protein methylation processes are dynamic and reversible, with the dynamic balance co-regulated by methyltransferases and demethylases [28]. Protein methylation exhibits amino acid preference, predominantly occurring on arginine and lysine residues. Among these, arginine methylation is catalyzed by protein arginine methyltransferases (PRMTs) [29]. To date, nine PRMTs have been identified [30]. They catalyze arginine monomethylation, symmetric dimethylarginine (SDMA), or asymmetric dimethylarginine (ADMA) [31]. In contrast to arginine methylation, lysine can undergo monomethylation, dimethylation, and trimethylation [32]. Lysine methylation is catalyzed by protein lysine methyltransferases (PKMTs) and demethylated by lysine demethylases (KDMs).

2.6. Acetylation

Lysine acetyltransferases catalyze the transfer of acetyl groups to the ε-amino side chains of lysine residues, forming protein acetylation modifications, which can be reversed by lysine deacetylases. In plant mitochondria, some lysine acetylation events can also occur through non-enzymatic reactions [33]. Lysine acetylation includes both histone and non-histone acetylation. Histone lysine acetylation mainly occurs at the N-terminus of core histones and is a key post-translational modification that influences chromatin structure. Lysine acetylation facilitates the dissociation of histones from DNA octamers and induces nucleosome relaxation, thereby enabling specific binding of various transcription factors to DNA binding sites and regulating gene expression levels [34]. Numerous studies have demonstrated that reversible and rapid changes in histone acetylation play crucial regulatory roles in plant growth and development, as well as abiotic/biotic stress responses [34–36]. Non-histone acetylation is relatively conserved evolutionarily from bacteria to mammals. Non-histone acetylation regulates various biological processes by modulating enzyme activity [37,38], protein–protein interactions, and protein stability [39,40]. Most molecular functions of plant non-histone acetylated proteins are associated with catalytic activity and binding, and their roles in plant seed germination and reproductive growth have been extensively investigated [41–43].

2.7. S-Nitrosylation

As an important signaling molecule, nitric oxide (NO) is extensively involved in regulating various physiological and biological processes across diverse organisms. S-nitrosylation is a NO-dependent and reversible redox-based post-translational modification (PTM), in which the NO group is covalently attached to the free sulfhydryl group of a specific cysteine residue in the target protein, thereby forming S-nitrosothiol (SNO) [44]. S-nitrosylation is widely present in various organisms and regulates multiple biological processes in plants, such as growth, immune response, stress response, chlorophyll metabolism, and photosynthesis [45,46]. It has become the primary mechanism for transmitting the biological activity of NO in abiotic stress responses [47]. Its regulatory functions are primarily manifested in five aspects: Firstly, S-nitrosylation can affect protein stability by altering protein half-life to modulate protein abundance; secondly, this modification can directly regulate the biochemical activities of proteins, including enzyme activity and catalytic efficiency; thirdly, S-nitrosylation can induce conformational changes in proteins, thereby altering their functional states; fourth, it can regulate the subcellular localization

https://doi.org/10.3390/plants15010052

of proteins, influencing their spatial distribution within cells; finally, S-nitrosylation can modulate protein–protein interactions, which in turn affects signal transduction pathways and molecular networks [48–50].

2.8. Other PTMs

Lysine crotonylation is an evolutionarily conserved acylation modification. It mainly occurs on lysine residues of histones, and is primarily distributed on histones in the promoter regions or potential enhancer regions of active genes. This modification is widely involved in regulating the initiation, activation, and expression of genes, thereby affecting the physiological processes of plants [51]. In rice seedlings, 1265 lysine crotonylation sites have been identified on 690 proteins. Among these, 51% of the lysine-crotonylated proteins are located in chloroplasts, and the degree of lysine crotonylation modification is positively correlated with the gene expression levels [52].

Table 1. Representative major types of PTMs and their functions in plants.

Types of PTM	Modified Amino Acid Residue	Number of Proteins with Modifications	Main Functions	Ref.
Phosphorylation	S, T, Y, D, N-term	82,207	Plant growth and development, response to abiotic/biotic stresses, substance metabolism, energy balance, intracellular homeostasis, and signal network integration	[53]
Ubiquitination	K, N-term	8315	Timing and homeostasis of plant growth and development, response to abiotic/biotic stresses, substance metabolism, energy balance, intracellular homeostasis, and signal network integration	[54]
SUMOylation	K	139	Response to abiotic/biotic stresses, timing and homeostasis of plant growth and development, maintain genome stability, substance metabolism, energy balance, intracellular homeostasis, and signal network integration	[55]
N-glycosylation	N, P, R	3258	Protein folding, plant growth and development, response to biotic stresses, substance metabolism, energy balance, intracellular homeostasis, and signal network integration	[56]
Methylation	R, K, C	1299	Epigenetic regulation	[57]
Acetylation	K, N-terminus	23,042	Epigenetic regulation	[34]
S-nitrosylation	C	5924	Response to abiotic/biotic stresses, plant growth and development	
Crotonylation	K	15,404	Photosynthesis, various substance metabolisms, and protein synthesis and quality control	[58]
2-Hydroxyisobuturylation	K	34,884	Gene transcription, balance of substance metabolism, and response to biotic stresses	[59]
S-sulfenylation	C	3871	Cellular redox homeostasis	[60]
Reversible Cysteine Oxidation	C	3826	Cellular redox homeostasis	[61]
Succinylation	K	2450	Substance metabolism, energy balance, cellular homeostasis, and epigenetic regulation	[59]
S-Acylation	C, N-term	1524	Plant growth and development	[60]
Carbonylation	R, K, P, T, Y	188	Clearance of damaged proteins, and maintenance of cellular homeostasis	[62]
S-cyanylation	C	132	Cyanide metabolism and toxicity detoxification	[60]

3. Post-Translational Modifications in Plant Abiotic Stress

3.1. Heat Stress

Typically, a temperature that is 5~10 °C higher than the optimal growth temperature for plants is sufficient to induce the heat stress response. Some studies suggest that the perception site for high temperatures is the plasma membrane [63]. The Cyclic Nucleotide-Gated Ca^{2+} Channels (CNGCs) and ANNEXIN1 (ANN1) in the plasma membrane respond to the increase in membrane fluidity caused by high temperatures, promoting the entry of apoplastic Ca^{2+} into the cytoplasm. Under high-temperature conditions, the content of cytoplasmic cAMP increases and can activate CNGCs. Researchers believe that enzymes with adenylate cyclase activity are also among the membrane-associated temperature receptors. Ca^{2+} signals are transduced by calmodulin (CaM) and calcium-dependent protein kinases (CDPKs). During this process, Ca^{2+} initiates a specific signal transduction cascade that can activate kinases by binding to CaM associated with CNGCs. The activated kinases then phosphorylate and activate HSFA1, leading to the dissociation of HSP70/HSP90 that interacts with HSFA1 (Figure 2B). This sequence of events ultimately activates the signal transduction pathway in plants in response to heat stress [64–66].

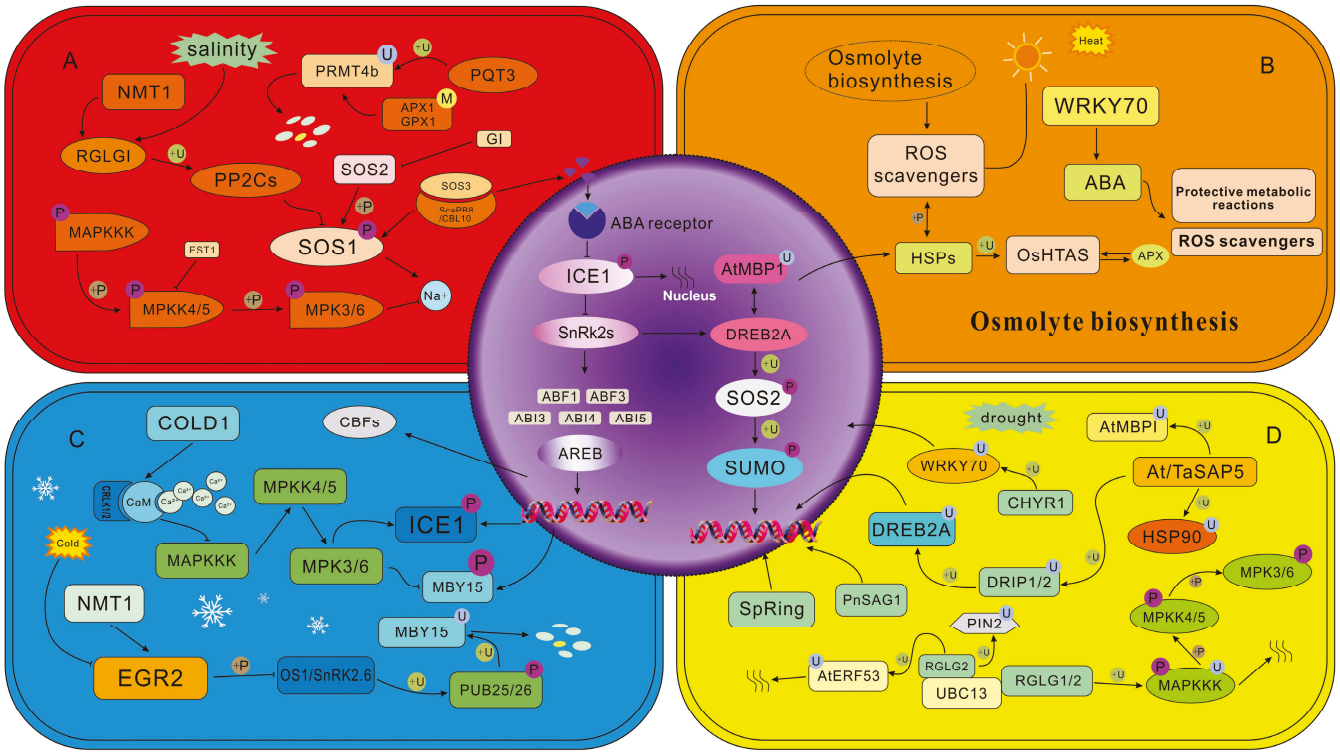

Figure 2. Post-translational modifications in plant abiotic stress. (**A**) Salt stress. (**B**) Heat stress. (**C**) Cold Stress. (**D**) Drought Stress.

The transcriptional regulatory network under heat stress requires the involvement of multiple transcriptional regulators. Heat shock transcription factor (HSF) is a key regulator of heat shock response transcription; the binding activity of yeast HSF to target sites differs by more than 200-fold between 15~39 °C. Although HSF in all states can bind to DNA, its activity is affected by its phosphorylation status [67]. In plants, HSFA1 (heat shock transcription factor 1), HSFA2, and HSFA3 are all important transcription factors involved in response to heat stress [68–70]. When plants are subjected to heat shock stress, they rapidly adjust the expression patterns of related genes to adapt to the elevated ambient temperature. Among these regulators, HSFA1s act as core transcription factors in the plant

https://doi.org/10.3390/plants15010052

heat shock response, helping to regulate the expression of numerous downstream heat shock-responsive genes [71].

The activity of HSFA1 is tightly regulated at the protein level, primarily through PTMs and protein–protein interactions. In *Arabidopsis thaliana*, protein kinases that interact with HSFA1 include CDC2a (cyclin-dependent kinase 2a), CBK3 (CaM-binding protein kinase 3), and PP7 (Calmodulin-binding Protein Phosphatase 7). These kinases can regulate the heat shock response process by phosphorylating or dephosphorylating HSFA1 [72–74]. HSFA1 may also undergo SUMOylation during the heat shock response, and this modification inhibits the activity of HSFA1 [75]. Additionally, under normal temperature conditions, HSFA1 can form a protein complex with HSP70, thereby inhibiting HSFA1 activity. When cells are subjected to heat shock stress, the concentration of misfolded proteins in the cell increases. These denatured proteins competitively bind to HSP70 with HSFA1, thereby releasing HSFA1 and activating the expression of downstream heat shock-responsive genes [76,77].

SUMOylation participates in plant acquired thermotolerance by regulating HSFA2. Specifically, SUMO1 can bind to the lysine at position 315 of HSFA2, thereby inhibiting its transcriptional activity. In plants overexpressing *SUMO1*, the expression of downstream HSPs is significantly reduced after heat treatment [78]. In contrast, SUMO1 can also specifically modify the lysine at position 298 of HSFA1, which promotes the latter's transcriptional activity [79]. DREB2A (dehydration-responsive element binding protein 2A) is also a core transcription factor involved in the response to high-temperature stress. Under normal conditions, DREB2A is unstable and degraded via the 26S proteasome pathway. However, under high-temperature conditions, SIZ1-mediated SUMOylation of DREB2A inhibits the interaction between DREB2A and the proteasomal degradation system, thereby enhancing the stability of DREB2A protein [80]. DREB2A is known to upregulate *HSFA3* expression, implying that DREB2C might also be implicated in the regulatory network of HSFA3 [81].

The activity regulation of HSFA1 is a typical case of crosstalk between phosphorylation and SUMOylation. Phosphorylation by kinases such as CDC2a activates HSFA1, while SUMOylation at the K298 residue further enhances its transcriptional activity; in contrast, SUMOylation of HSFA2 at the K315 residue represses its function. This residue-specific crosstalk pattern suggests that SUMOylation acts as an elaborate molecular switch governing the HSF family. However, dynamic tracking data are currently lacking to clarify whether phosphorylation affects the residue selectivity of SUMOylation and the temporal regulatory relationship between these two modifications (i.e., whether phosphorylation precedes SUMOylation). In addition, the crosstalk synergistic effects among different HSF members (e.g., whether phosphorylation of HSFA1 facilitates SUMOylation of HSFA2) have not been thoroughly investigated; most existing studies focus on individual members, lacking an integrated analysis of the global modification network of the family proteins.

3.2. Cold Stress

Under cold stress, the first rapid response factors are these key cold sensors, including COLD1/RGA1, Ca^{2+} channels, and plasma membrane-localized receptor-like kinases (RLKs) [82]. Among them, COLD1/RGA1 and Ca^{2+} channels have been the subject of extensive research. *COLD1* encodes a G-protein regulator, which is localized to the plasma membrane and endoplasmic reticulum. It is the first cold sensor identified in rice. When plants are exposed to cold stress, COLD1 interacts with the G-protein α subunit RGA1 to activate Ca^{2+} channels, thereby promoting Ca^{2+} influx and triggering the signal pathway for low-temperature response [83]. After perceiving low temperatures, plants rapidly respond to cold stress through the MAPK cascade signal transmission and the ICE1-CBF-COR module [84]. CNGCs, Glutamate Receptor-Like Channels (GLRs), and Mid1-Complementing Activity 1/2 (MCA1/MCA2) channels with complementary activities

https://doi.org/10.3390/plants15010052

are the main Ca^{2+} channel proteins involved in cold signal perception [85]. CNGCs are a class of non-selective cation channels localized to the plasma membrane. They activate the cAMP or cGMP cyclase activity by binding to G-protein-coupled receptors, leading to the release of cAMP or cGMP and the opening of Ca^{2+} channels [86]. In rice, the cyclic nucleotide-gated channels OsCNGC14, OsCNGC16, and OsCNGC9 all positively regulate the process of rice resistance to cold stress. After mutation of the OsCNGC14 and OsCNGC16 genes, cold-induced Ca^{2+} influx decreases, and the plants become sensitive to cold stress [87]. The opening and closing of the Ca^{2+} channel controlled by OsCNGC9 is regulated by the phosphorylation of the OsSAPK8 kinase. Under cold stress conditions, OsCNGC9 is phosphorylated, the Ca^{2+} channel opens, and the cold tolerance of rice plants is enhanced [88]. MCA1 and MCA2 are two calcium-permeable mechanosensitive channel proteins in *Arabidopsis thaliana*. They convert extracellular mechanical signals (including stretch, pressure, gravity, and osmotic pressure) into intracellular Ca^{2+} fluxes to transmit cold signals [89].

Plant kinase cascade reactions are crucial processes in the plant's cold stress response, linking cold signals to cellular responses through MAPK cascade reactions [90]. After MAPKK (Mitogen-Activated Protein Kinase Kinase) and two calmodulin-regulated receptor-like kinases, CRLK1 (Calmodulin-Regulated Receptor-Like Kinase 1) and CRLK2, receive cold signals, they transmit the signals via the MEKK1-MEK2-MPK4 kinase pathway. Furthermore, the MEKK1-MEK2-MPK4 pathway inhibits the phosphorylation of ICE1 (Inducer of CBF Expression 1) by MPK3/6 through antagonizing the MKK4/5-MPK3/6 reaction, thereby enhancing the plant's ability to resist cold stress [91]. In addition, under cold stress, CRPK1 (Cold-Responsive Protein Kinase 1) can phosphorylate 14-3-3 proteins. The phosphorylated 14-3-3 proteins, acting as shuttle proteins, translocate from the cytoplasm to the nucleus, where they bind to the nucleus-localized CBF1/3 (C-repeat Binding Factor 1/3) and promote their degradation, thus negatively regulating the plant's cold tolerance process [92].

ICE1 is the primary regulator of CBFs (C-Repeat Binding Factors) and a member of the bHLH (basic Helix–Loop–Helix) transcription factor family. It positively regulates plant cold tolerance through the ICE1-CBF-COR pathway. ICE1 can bind to the promoter region of CBF genes to regulate CBF expression, and CBFs, acting as transcription factors, activate the expression of *COR* (Cold-Responsive) genes—key genes involved in the plant's defense against cold stress. In *Arabidopsis thaliana*, MPK3/MPK6 (Mitogen-Activated Protein Kinase 3/6) phosphorylates ICE1, leading to a decrease in ICE1 stability and thereby negatively regulating plant cold tolerance [84]. In contrast, phosphorylation of ICE1 by OsMPK3 increases ICE1 stability, enhancing the plant cold stress tolerance in rice [93]. These results indicate that the core molecular modules for cold signal perception and transmission exhibit functional divergence across different plant species. *Arabidopsis* OST1 (Open Stomata 1), also known as SnRK2.6 (Sucrose Non-Fermenting 1-Related Protein Kinase 2.6), is a key regulator in cold signal transduction. Under cold stress, OST1 can bind to and phosphorylate ICE1, preventing ICE1 from being degraded by the 26S proteasome. This process enhances the transcriptional activity of CBFs and improves plant cold tolerance [94,95]. *HOS1* (High Expression of Osmotically Responsive Gene 1) encodes an E3 ubiquitin ligase. It negatively regulates plant cold tolerance by ubiquitinating ICE1. The protein kinase BIN2 (Brassinosteroid-Insensitive 2) further modulates the plant's cold response: it phosphorylates ICE1, which in turn promotes the ubiquitination and degradation of ICE1 by HOS1 (Figure 2C) [96,97]. In *Arabidopsis thaliana*, phosphorylation by MPK3/ MPK 6 promotes the ubiquitin-dependent degradation of ICE1, whereas in rice, phosphorylation by OsMPK3 enhances ICE1 stability. This species-specific divergence

https://doi.org/10.3390/plants15010052

implies evolutionary differentiation in the crosstalk mechanism. However, interspecies comparative analysis of ICE1 phosphorylation residues has not been performed to date.

Trehalose is a stable non-reducing disaccharide. It acts as a glucose storage and transport molecule, an energy source, and a key stress-responsive compound that exerts a protective function under stress conditions. In rice, significantly increasing the expression levels of two key enzymes in the trehalose synthesis pathway—*OsTPS1* (Trehalose-6-Phosphate Synthase 1) and *OsTPP1* (Trehalose-6-Phosphate Phosphatase 1)—can notably raise trehalose content, thereby enhancing the cold tolerance of rice plants [98]. Cold-induced OsPP2C27 (Protein Phosphatase 2C 27) is able to directly dephosphorylate phosphorylated OsMAPK3 and OsbHLH002. This process negatively regulates the OsMAPK3-OsbHLH002-OsTPP1 signaling pathway, preventing the continuous activation of positive regulatory pathways in response to cold stress and maintaining the normal growth of rice plants under low-temperature conditions [99]. Recent studies have revealed that under non-stress conditions, the S-acyltransferase MtPAT9 can interact with MtNAC80 and mediate its S-acylation modification, which in turn facilitates the membrane localization of MtNAC80. Under cold stress conditions, the thioesterase MtAPT1—responsible for deacetylation—oligomerizes into an enzymatically active tetramer. This active MtAPT1 tetramer catalyzes the de-S-acylation of MtNAC80, enabling MtNAC80 to translocate into the nucleus [100]. Once in the nucleus, MtNAC80 directly activates the expression of the *MtGSTU1* gene. This activation promotes the scavenging of malondialdehyde (MDA) and hydrogen peroxide (H_2O_2), thereby enabling the plant to resist cold stress [101]. In Chinese cabbage, NO accumulated under cold stress induces the S-nitrosylation of monodehydroascorbate reductase (MDHAR), which significantly enhances the role of brassinosteroid (BR) in the cold tolerance of Chinese cabbage [102].

3.3. Drought Stress

When the water potential of the rhizosphere decreases to a certain level, it triggers osmotic stress. This prevents plants from absorbing water from the soil, leading to the massive accumulation of abscisic acid (ABA). The ABA receptors, including pyrabactin resistance (PYR), PYR1-LIKE (PYL), and regulatory components of ABA receptor (RCAR), bind to ABA and interact with class A protein phosphatases (PP2Cs, protein phosphatase 2Cs). This interaction activates class III SNF1-related protein kinase 2 (SnRK2s, sucrose non-fermenting 1-related protein kinase 2s) [103–105]. As a type of serine/threonine protein kinase, SnRK2s are widely present in plants. In terms of drought resistance in *Arabidopsis thaliana*, SnRK2.6 (also known as OST1, open stomata 1) regulates the expression of numerous drought-related genes, the activity of ion channels, and metabolic pathways, serving as a hub for plant droughtstress responses. Its activation state directly affects the plant's ability to cope with drought stress. ABA-activated SnRK2s precisely regulate the ion concentration inside and outside cells through the phosphorylation modification of plasma membrane ion channel proteins [106,107]. This regulation helps maintain cell turgor, controls the opening and closing of stomata, reduces water loss, and optimizes water use efficiency [108,109]. Under the condition of massive ABA accumulation, OST1 directly phosphorylates transcription factors such as ABA-responsive element binding factors (ABF) and ABA-responsive element binding proteins (AREB). This phosphorylation promotes the transcription of a series of drought-resistant genes, which are involved in physiological processes such as maintaining cellular osmotic balance, scavenging reactive oxygen species, and repairing damaged cell membranes, thereby comprehensively enhancing the plant's viability in arid environments [110–112]. Rapidly accelerated fibrosarcoma (RAF)-like kinases play a key role in ABA/drought and osmotic stress signaling pathways by activating the activity of SnRK2s. Under mild drought stress, RAF kinases of the B2 subgroup are activated. They

https://doi.org/10.3390/plants15010052

initiate the activation process of SnRK2s through phosphorylation modification. Under more severe drought conditions, dehydration stress-activated RAFs of the B3 subgroup can further enhance the activity of SnRK2s. This indicates that RAF protein kinases of the B2 and B3 subgroups activate ABA-dependent SnRK2s (SnRK2.2/2.3/2.6). In contrast, RAF kinases of the B4 subgroup (RAF16/18/20/24/35/40/42) activate class I SnRK2s (ABA-independent SnRK2s) in an ABA-independent manner. Class I SnRK2s, through directly interacting with, phosphorylate varicose (VCS), a scaffold protein of the mRNA decapping complex. The class I SnRK2s-VCS signaling module plays an important role in regulating the expression of drought-responsive genes as well as root structure and development. After sensing osmotic stress signals, RAF kinases promote the enhancement of SnRK2s activity through phosphorylation. This process can not only proceed independently in the absence of ABA but also synergize with the ABA signaling pathway to jointly regulate the plant's drought stress response [113–119]. This dual regulatory mechanism enables plants to cope more flexibly with drought stress with different intensities and durations, thereby improving their viability and adaptability. In addition, studies have found that RAF22 enhances the phosphatase activity of ABI1 through phosphorylation. Conversely, ABI1 can enhance the kinase activity of RAF22 through dephosphorylation, forming a positive feedback loop. Under drought stress conditions, ABA-activated OST1 inhibits the activity of RAF22 through phosphorylation, thereby regulating the balance between plant growth and stress response under drought conditions. The study reveals the dynamic regulatory mechanism among RAF22, ABI1, and OST1 [120]. In terms of transcriptional regulatory modifications, AREB1, AREB2, and ABF3 in ABA-responsive elements (ABRE) are phosphorylated and activated under drought stress, thereby regulating the expression of various drought-responsive genes [112]. In tomatoes, Calcium-dependent protein kinases (CPKs) can perceive and transduce drought signals. By phosphorylating and activating tonoplast sugar transporter 2 (TST2), CPKs promote the accumulation of soluble sugars in cells, thereby enhancing the drought tolerance of tomatoes [121]. OsbZIP23, a member of the ABA signaling pathway, cooperates with histone modification (histone H3K4 trimethylation, H3K4me3) to regulate the expression of drought-responsive genes, thereby positively regulating the drought resistance of rice [122]. Under drought stress, OsWRKY55 can interact with and be activated by four mitogen-activated protein kinases (MAPKs), namely OsMPK7, OsMPK9, OsMPK20-1, and OsMPK20-4, thereby enhancing the drought tolerance of rice at the seedling stage [123]. Drought-activated SnRK2 directly phosphorylates SPCH, a key transcription factor for stomatal development. SnRK2-mediated phosphorylation leads to the degradation of the SPCH protein, thereby inhibiting stomatal development to reduce water loss and improve drought resistance [124]. The transcription factor auxin response factor 7 (ARF7) can induce the asymmetric expression of lateral organ boundaries-domain 16 (LBD16) in lateral root cells, guiding roots to grow toward water. SUMOylation negatively regulates the DNA-binding activity of ARF7. Dry conditions promote the SUMOylation of ARF7, while humid conditions inhibit it, initiating transcriptional regulation and promoting lateral root formation [125]. In rice, deep rooting 1 (DRO1) is negatively regulated by auxin. It participates in the elongation of root tip cells and promotes the downward bending of roots in response to gravity. High expression of *DRO1* directs root growth deeper into the soil, allowing the plant to absorb water from deeper soil layers [126]. Under drought stress, the rice E3 ubiquitin ligase soil-surface rooting 1 (SOR1) can ubiquitinate and degrade indole acetic acid 26 (OsIAA26). Located downstream of the AFB2-auxin-OsIAA9 signaling module, this degradation reduces auxin concentration, increases *DRO1* expression, and enhances drought tolerance [127]. In the latest research on sweet potato, the IbNIEL-IbNAC087 module was found to regulate jasmonic acid (JA)-dependent salt and drought stress responses, in which the RING-type E3 ubiqui-

tin ligase IbNIEL can ubiquitinate and degrades the NAC transcription factor IbNAC087 by ubiquitination, so to reduce JA content and thereby negatively regulating the drought and salt tolerance of sweet potato [128]. In apple, The leucine zipper transcription factor MdHDZ27 can promote the expression of dehydration-responsive genes *MdRD29A* (dehydration 29A) and MdRD29B, while MdBT2, a protein containing BTB-BACK-TAZ domains, can ubiquitinate and degrade MdHDZ27 [129]. Also in apple, the bHLH transcription factor MdbHLH160 can directly upregulate the expression of the dehydration-responsive element-binding factor (DREB) family gene *MdDREB2A-like*, to enhance drought tolerance, whereas MdBT2 can ubiquitinate and degrade MdbHLH160 to negatively regulate drought tolerance (Figure 2D) [130].

3.4. Salt Stress

In the plant response to salt–alkali stress, the SOS (Salt Overly Sensitive) signaling pathway is widely regarded as the core module for maintaining ion homeostasis. This pathway mainly consists of four key components: SOS1, SOS2, SOS3, and SCaBP8 (also known as CBL10) [131]. Among them: *SOS1* encodes a plasma membrane-localized Na^+/H^+ antiporter, whose function is to effectively extrude excess Na^+ from the cytoplasm to the extracellular space; SOS2, as a key serine/threonine protein kinase, plays a central role in the signal amplification process; SOS3 and SCaBP8, as calcium sensors belonging to the CBL (calcineurin B-like proteins) family, can sensitively detect changes in cytoplasmic Ca^{2+} concentration induced by salt stress. The classical activation mode of the SOS signal can be summarized as follows: salt stress causes a transient increase in cytoplasmic Ca^{2+}; after sensing this change, SOS3 and SCaBP8 bind to SOS2 to form a kinase complex, which relieves the autoinhibitory state of SOS2 and activates its kinase activity; subsequently, the activated SOS2 complex phosphorylates the cytoplasmic tail of SOS1. This process significantly enhances the Na^+/H^+ exchange activity of SOS1, thereby accelerating the extrusion of Na^+ and ensuring the homeostatic balance of cytoplasmic ions (Figure 2A) [131].

Although the classical Ca^{2+}-dependent SOS activation mechanism has been widely accepted, recent studies have revealed that under calcium-deficient conditions, SCaBP1 (CBL2) can directly bind to the FISL motif of PKS24 (a member of the SOS2 family) through its C-terminal tail, thereby activating the kinase activity of PKS24. Notably, the phosphorylation of PKS24 at the Thr-211 and Thr-212 sites is crucial for this process [132]. This finding challenges the traditional view that SOS signal activation strictly depends on changes in cytoplasmic Ca^{2+}, indicating that plants possess the ability to flexibly activate salt tolerance mechanisms under various ionic environment conditions. Under salt stress, phosphatidylinositol (PI) is converted into phosphatidylinositol 4-phosphate (PI4P). The latter indirectly enhances SOS1 activity by relieving the inhibitory effect on plasma membrane H^+-ATPase. Meanwhile, phosphatidic acid (PA) can directly bind to SOS2, thereby promoting the localization of SOS2 on the plasma membrane and its stable activation. These studies reveal the tight coupling between phospholipid metabolism and the SOS pathway, highlighting the key regulatory role of dynamic changes in the phospholipid environment in salt stress signal transduction [133].Phosphorylation of SCaBP family members is a conserved regulatory mechanism. PKS24-mediated phosphorylation of SCaBP1 at the Ser-216 site enhances the binding affinity between SCaBP1 and PKS24 and stabilizes the formation of the signal complex [134]. Under non-stress conditions, 14-3-3 proteins can bind to SOS2, thereby inhibiting its kinase activity and effectively blocking the downstream activation process of SOS1 [135]. When salt stress occurs, the binding between 14-3 and 3 proteins and SOS2 decreases, allowing the activation cascade to be initiated. Two protein phosphatases, namely PP2C.D6 and PP2C.D7, have been further identified. Under normal conditions, these two phosphatases inhibit the activity of SOS1 through dephosphorylation [136]. How-

https://doi.org/10.3390/plants15010052

ever, under salt stress conditions, SCaBP8 can inhibit the activity of these two phosphatases, relieving their negative effect on SOS1 and enhancing the ability of Na^+ efflux.

In the plasma membrane Na^+/H^+ antiport system, the phosphorylation regulatory mechanism of SOS1 cytoplasmic tail determines the antiport activity under salt stress, and this process is activated and regulated by the SOS2-SOS3 complex [137]. Structural biology studies have resolved the cytoplasmic domain (CPD) of SOS1 at high resolution, revealing that it contains three important structural regions: the inhibitory functional domain (IFD) with an inhibitory role, the cyclic nucleotide binding domain-like (CNBD-like) domain with an activating role, and the autoinhibitory domain (AI) with an autoinhibitory function. Among these regions, the IFD cooperates with the AI domain to maintain SOS1 in a low-activity state. After salt stress triggers the phosphorylation by SOS2, the AI domain is released, which promotes the conformational change in SOS1 and increases the Na^+/H^+ exchange rate [138]. In the regulation of phospholipid metabolism and plasma membrane H^+-ATPase, phosphatidic acid (PA) acts as a salt stress signaling molecule that can directly bind to SOS2, promoting the activation of SOS2 and its recruitment to the plasma membrane region. In this process, PA not only functions as a signaling mediator but also can bind to and activate MAPK6. The activated MAPK6 is capable of phosphorylating SOS1, thereby promoting Na^+ efflux and enhancing the salt tolerance of plants [133,139].

In terms of ubiquitination, three genes encoding E2 (AtUBC7, AtUBC13, and AtUBC14) have been shown to respond to high-salt stress and may play a role in the degradation process of misfolded proteins in the endoplasmic reticulum [140].

Overexpression of the RING-type E3 gene *IbATL38* from sweet potato (*Ipomoea batatas*) in *Arabidopsis thaliana* enhances the latter's salt tolerance. It upregulates the expression of stress-responsive genes in anABA-signaling-dependent manner and reduces the accumulation of reactive oxygen species (ROS) [141]. In *Arabidopsis thaliana*, the RING-type E3 genes *AtATL31* and *AtATL6* negatively regulate plant salt tolerance, but this regulation is independent of the ABA signaling pathway [142]. In rice (*Oryza sativa*), the RING-type E3 gene *OsSIRP4* is highly expressed under salt stress. In transgenic rice overexpressing *OsSIRP4*, the activity of enzymes related to ROS scavenging is decreased, the accumulation of proline and soluble sugars is significantly reduced, and the expression of genes related to K^+/Na^+ homeostasis is downregulated. Additionally, OsSIRP4 can interact with the peroxisome biogenesis factor OsPEX11, thereby negatively regulating the salt stress response [143]. Under salt stress, the HMG box-containing transcription factor MdHMGB15 in apple enhances the expression of *MdXERICO*, encoding a RING-type E3 ubiquitin ligase, thereby mediating the ubiquitination and degradation of MdNRP and improving salt tolerance [144]. In soybean, an E3 ubiquitin ligase, GmCHYR16, negatively regulates salt tolerance by mediating the ubiquitination and degradation of GmERF71, an AP2/ERF transcription factor [145]. A study on *Arabidopsis thaliana* has shown that the ubiquitin-conjugating enzyme UBC34 can ubiquitinate proton-pumping pyrophosphatase (AVP1), a key stress-responsive factor, thereby reducing its activity and negatively regulating plant salt tolerance [146].

In recent years, S-nitrosylation has been uncovered as a key regulatory mechanism in plant salt tolerance. In tomato, salt stress induces the accumulation of NO in roots. High concentrations of NO lead to the S-nitrosylation of γ-aminobutyric acid transaminase 1 (SlGABA-TP1) at cysteine residues 316/258/316 (Cys316/258/316), which reduces its enzymatic activity and increases γ-aminobutyric acid (GABA) content. Through interaction with SlALMT14, GABA decreases the efflux of malic acid from roots, thereby affecting the plant's saline–alkali tolerance [147]. NO stimulates the transcription of caffeic acid O-methyltransferase (COMT) and the biosynthesis of melatonin, which scavenges excess NO at the proteomic level and alleviates nitrosative damage. Under saline–alkali stress, plasma membrane-localized H^+-ATPase 2 (HA2) undergoes S-nitrosylation at cysteine-206

(Cys206), impairing its interaction with 14-3-3 protein 1 (TFT1). This S-nitrosylation of HA2 leads to reduced enzyme activity and decreased H^+ efflux, thereby compromising the plant's saline–alkali tolerance. Conversely, melatonin produced by COMT mitigates the S-nitrosylation of HA2, restoring its function and the saline–alkali tolerance of tomato plants [148]. Also in tomato, drought and salt stresses induce the production of NO, which activates the expression of genes encoding Δ1-pyrroline-5-carboxylate synthetase (SlP5CS) and Δ1-pyrroline-5-carboxylate reductase (SlP5CR), thereby promoting proline accumulation to cope with stresses. The S-nitrosylation of SlP5CR enables tomato plants to better adapt to changes in NAD(P)H levels under stress conditions, enhancing SlP5CR activity and proline biosynthesis during stress exposure [149]. NO-mediated S-nitrosylation of BRI1-associated kinase 1 (BAK1) enhances its interaction with BRASSINOSTEROID INSENSITIVE 1 (BRI1), promoting the activation of the brassinosteroid (BR) signaling pathway and thereby improving the salt tolerance of tomato plants [150].

In terms of thePTM-mediated regulation of NAC transcription factors, tomato can mediate the ubiquitination and degradation of SlNAC35, a member of the NAC transcription factor family, via the E3 ubiquitin ligase SlMIEL1. This process enhances the transcription of *allene oxide cyclase* (*AOC*) gene, leading to jasmonic acid (JA) accumulation and thereby improving salt tolerance [151]. In apple, the NAC transcription factor MdNAC104 can be ubiquitinated and degraded via the 26S proteasome pathway, which increases the γ-aminobutyric acid (GABA) content in plant roots and thereby enhances salt tolerance [152]. In soybean, cells can directly perceive and transduce reactive oxygen species (ROS) signals through hydrogen peroxide (H_2O_2)-mediated post-translational modifications (PTMs) of cysteine residues in proteins. The cysteine residues of NAC WITH TRANS-MEMBRANE MOTIF1-LIKE 1 (GmNTL1) are oxidatively modified by H_2O_2, facilitating its release from the endoplasmic reticulum (ER) membrane and translocation to the nucleus. By binding to and activating the promoter of the *respiratory burst oxidase homolog B* (*GmRbohB*) gene, GmNTL1 initiates the amplification of downstream ROS production, forming a positive feedback loop that precisely regulates its own activity. Salt stress-induced oxidation of GmNTL1, via H_2O_2-mediated post-translational oxidative modification, promotes its nuclear localization and transcriptional activity, thereby enhancing the salt tolerance of soybean [153].

3.5. PTMs in ABA Signaling Transduction

As one of the classic plant hormones, ABA is not only involved in plant growth and development processes, such as seed dormancy and germination, root system development, leaf senescence, and floral transition, but also plays a crucial role in plant stress responses [154,155]. Moreover, PTMs of proteins exert a significant function in the ABA signal transduction pathway. In the absence of ABA or stress signals, the key component of energy metabolism, the TOR (Target of Rapamycin) kinase complex, phosphorylates PYL1/4, thereby blocking the ABA signal. When plants are subjected to stress, SnRK2s are activated and phosphorylate Raptor B, the regulatory subunit of TOR. This leads to the inhibition of TOR kinase activity, preventing it from activating energy regulation, which in turn inhibits plant growth and promotes plant survival under stress conditions. These results indicate that the TOR kinase complex and the ABA signal exert antagonistic effects to regulate plant growth and survival under stress [156,157]. *Arabidopsis* casein kinases AELs (Arabidopsis EL1-like proteins, AEL1-AEL4) phosphorylate Ser136 of PYL1 and Ser109 of PYR1. The deletion of AELs reduces the ubiquitination of PYL1/PYR1, resulting in slower degradation of PYR/PYLs. This suggests that there exists a phosphorylation-mediated ubiquitination degradation pathway for PYL1/PYR1. Interestingly, phosphorylation at different sites of the receptor may exert opposite effects [158]. CARK1 (cytosolic ABA

receptor kinase 1) phosphorylates the threonine residues at positions 77/78 (T77/T78) of PYL8/PYR1, which enhances the stability of PYL8/PYR1 and strengthens its inhibitory effect on PP2Cs, thereby promoting ABA signal transduction [159]. Phosphorylation of PYL1 at Ser136 by AEL kinases promotes its ubiquitination and degradation, whereas phosphorylation of PYL8 at T77/T78 by CARK1 enhances its stability. Such contradictions may stem from the functional specificity of phosphorylation residues—Ser136 is located in the ABA-binding domain of PYL1, and its phosphorylation may impair ABA-binding capacity and recruit E3 ubiquitin ligases; in contrast, T77/T78 reside in the dimerization domain of PYL8, and their phosphorylation may strengthen the interaction between PYL8 and PP2Cs, thereby inhibiting its degradation. However, systematic identification of phosphorylation residues across different members of the PYL family is currently lacking (Figure 3). Moreover, whether phosphorylation of PYLs by different kinases exhibits a competitive relationship, and whether ABA modulates the crosstalk balance by affecting kinase activity, remain insufficiently investigated. In addition, whether phosphorylation modification of PYL receptors displays species-specific divergence, and whether their regulatory patterns in crops are consistent with those in Arabidopsis thaliana, still require more empirical data to support.

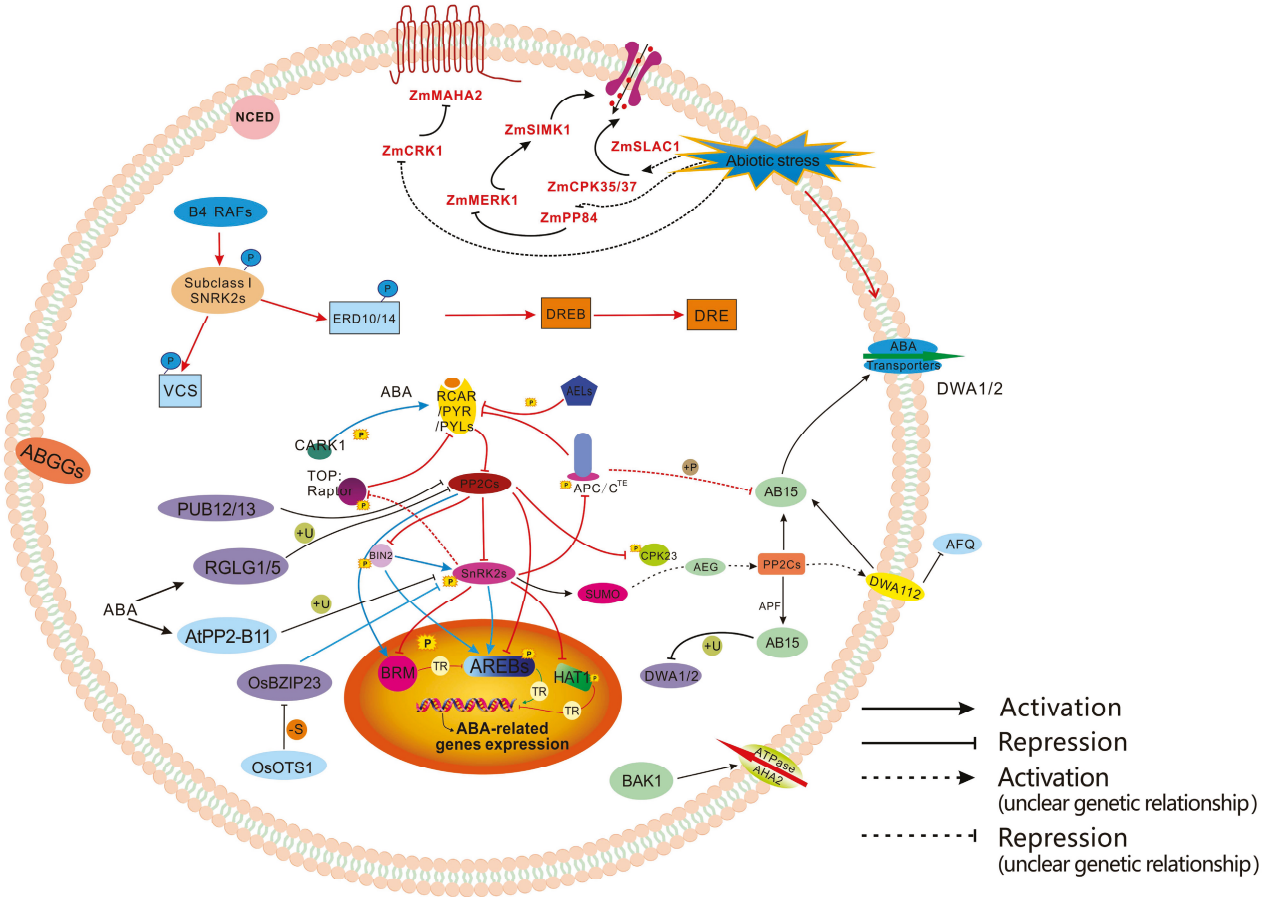

Figure 3. PTMs in ABA signaling transduction.

When plants perceive the ABA signal, the inhibition of SnRK2s is relieved. SnRK2s recover partial activity through intramolecular interactions between their kinase catalytic domain and regulatory domain, and then autophosphorylate multiple amino acid residues in the activation loop to restore full kinase activity, thereby phosphorylating downstream substrates [160].In addition to autophosphorylation of SnRK2s, multiple kinases such as BIN2 (brassinosteroid insensitive 2), BAK1 (BRI1-associated receptor kinase 1), HT1 (high

leaf temperature 1), and casein kinase CK2 (casein kinase 2) can also phosphorylate SnRK2s. BIN2 belongs to the GSK3 (glycogen synthase kinase 3) kinase family and regulates a variety of signaling processes, including inhibiting BR signal transduction, suppressing auxin signal transduction, and modulating stomatal movement [161–164]. It is one of the key components in the BR signaling pathway [164]. In the ABA signaling pathway, BIN2 phosphorylates and activates SnRK2.2/2.3, and at the same time, it also phosphorylates and activates ABI5 [165]. Latest studies have shown that ABI1/2 (ABA-insensitive 1/2), two key PP2Cs in the ABA pathway, inhibit BIN2 kinase activity by dephosphorylating BIN2. These results indicate that BIN2 is a key factor integrating the two major hormone signaling pathways of BR and ABA [166].BAK1, another kinase in the BR signaling pathway, also phosphorylates SnRK2.6/OST1 (open stomata 1) and antagonizes ABI1 in regulating the phosphorylation of OST1 and stomatal movement [161]. CK2 is a highly conserved protein kinase that forms heterodimers or tetramers composed of catalytic subunits and regulatory subunits [167]. ZmCK2 from maize phosphorylates amino acid residues in the C-terminal domain of ZmOST1, promoting the binding of ZmOST1 to PP2Cs, thereby inhibiting the activity of OST1 and ABA signal transduction [162]. HT1 is a negative regulator of CO_2-induced stomatal closure; it inhibits the kinase activity of OST1 through phosphorylation, thereby suppressing stomatal closure [163]. Furthermore, kinases such as MPKs and phosphatases such as PP2A and PP1 all affect the phosphorylation level and kinase activity of SnRK2s, but whether they directly regulate the phosphorylation of SnRK2s requires further verification (Figure 3) [168]. The traditional view holds that the activation of SnRK2s relies on autophosphorylation following the relief of PP2C-mediated inhibition, whereas recent studies have revealed that kinases such as BIN2, BAK1 and BIK1 can directly phosphorylate SnRK2s and activate their activity [169]. The hierarchical relationship and synergistic mechanism between these two activation modes remain unclear—does the relief of PP2C inhibition provide a prerequisite for kinase-mediated phosphorylation in the ABA signaling pathway? Or do these two pathways function independently and target distinct SnRK2 members? In addition, SnRK2s harbor multiple phosphorylation sites; whether different kinases modify distinct sites and elicit divergent activity effects has not been elucidated. The core of this controversy lies in the insufficient understanding of the hierarchical regulatory network underlying SnRK2 activation. Future research should employ in vitro reconstitution assays and residue-specific phosphorylation antibodies to clarify the sequential order and functional contribution of different phosphorylation events.

AREBs/ABFs belong to the basic leucine zipper (bZIP) family of transcription factors, such as ABI5, ABF1-ABF4, OsbZIP23, and OsbZIP46 [111]. They activate or repress the expression of their target genes by binding to the ABA response element (ABRE). AREBs/ABFs are phosphorylated by SnRK2s and directly dephosphorylated by ABI1/2 [170]. Most transcription factors have their transcriptional activity activated after being phosphorylated by SnRK2s. For instance, in rice, OsbZIP23 is phosphorylated by SAPK2 (a homolog of SnRK2s in rice that participates in ABA signal transduction), which activates its transcriptional activity. This activation then promotes the expression of *OsNCED4* and the synthesis of ABA [171]. Recent studies have shown that after ABFs are phosphorylated by SnRK2s, they promote the expression of *ABI1/2*. Subsequently, the protein levels of ABI1/2 increase, enhancing the dephosphorylation of ABFs and thereby repressing the transcriptional activity of ABFs [172]. This forms a feedback pathway that precisely regulates the ABA signal and mediates the desensitization response to ABA. Some transcription factors, however, have their transcriptional activity inhibited after phosphorylation by SnRK2s. Under normal conditions, for example, unphosphorylated HAT1 (homeodomain-leucine zipper protein 1) binds to the promoter of *NCED3*, repressing the expression of *NCED3* and the synthesis of ABA. Under drought conditions, HAT1 is

https://doi.org/10.3390/plants15010052

phosphorylated by SnRK2s, which inhibits its transcriptional repressor activity. This leads to an increase in ABA content in plants, enabling them to respond to drought stress [173].In addition to SnRK2s and PP2Cs, a variety of other kinases or phosphatases are also involved in regulating the phosphorylation modification of AREBs/ABFs. In pepper, CaSnRK2.4 can activate the NAC transcription factor CaNAC035 through phosphorylation to upregulate two key ABA biosynthesis genes (CaAAO3 and CaNCED3), thereby enhancing cold stress tolerance [174].

During the process of ABA promoted stomatal closure, SnRK2s phosphorylate and activate SLAC1, thereby facilitating anion (A^-) efflux; ABI1 directly dephosphorylates SLAC1, inhibiting stomatal closure. Meanwhile, SnRK2s phosphorylate and inhibit the activity of KAT1, preventing potassium ion (K^+) influx [175]. SnRK2s also phosphorylate the bHLH-type transcription factor AKS1 (ABA-responsive kinase substrate 1), inducing AKS1 to depolymerize into a monomeric form. This depolymerization causes AKS1 to lose the ability to bind to its target gene *KAT1*, thereby inhibiting the expression of *KAT1* [176]. Beyond this pathway, ABI1 also inhibits the phosphorylation of SLAC1 by CPK23 (calcium-dependent protein kinase 23) through dephosphorylating CPK23, forming a SnRK2s-independent pathway that regulates stomatal movement; CPK6 also phosphorylates SLAC1, partially substituting for the function of OST1 [177]. The kinase GHR1 (guard cell hydrogen peroxide-resistant 1) phosphorylates and activates SLAC1, participating in ABA-regulated stomatal closure. This process is inhibited by ABI2 but not by ABI1 [178]. Additionally, during CO_2-induced stomatal closure, HT1 not only inhibits OST1 but also suppresses GHR1 and SLAC1 through phosphorylation. In maize, ZmCPK35 and ZmCPK37 can phosphorylate ZmSLAC1 to regulate guard cell channel activity [179]. CALCIUM-DEPENDENT PROTEIN KINASE RELATED KINASE 1 (ZmCRK1) interacts with the plasma membrane proton ATPase ZmMHA2, and inhibits its proton pump activity by phosphorylating the Ser-901 site of ZmMHA2, leading to impaired ABA-induced H^+ efflux and negatively regulating drought tolerance [180]. In contrast, CO_2 can promote the phosphorylation of MPK4/MPK12, which in turn inhibits the kinase activity of HT1 [181]. SnRK2s also phosphorylate other functional proteins, enabling plants to exhibit a variety of physiological changes after perceiving the ABA signal (Figure 3).

ABA receptors PYR1/PYL/RCAR, which are specific recognition receptors, along with their downstream PP2Cs and SnRK2s, are all core components of the ABA signaling pathway and subjected to PTMs. Specifically, the RING-type E3 ubiquitin ligase RSL1 (ring finger of seed longevity 1) can directly interact with PYR1 and PYL4 to mediate their ubiquitination and degradation, thereby reducing plant sensitivity to ABA [182]. The ubiquitin E2-like protein VPS23A (vacuolar protein sorting 23A) can recognize the ABA receptor complex RSL1-PYL4 and its K63-linked ubiquitin chain, promoting the complex to enter the vesicular transport pathway and thus affecting its subcellular localization and stability [183]. In *Arabidopsis thaliana*, four E3 ubiquitin ligases—SINAT1 (seven in absentia of *Arabidopsis thaliana* 1), SINAT2, SINAT3, and SINAT4—can regulate the ubiquitination and proteasomal degradation of VPS23A and FREE1, thereby reducing the stability of these two proteins and positively regulating the ABA signaling pathway [184]. Meanwhile, the RING-type E3 ubiquitin ligase XBAT35 (E3 ligase XB3 ortholog 5 in *Arabidopsis thaliana*) can also catalyze the ubiquitination of VPS23A, which is subsequently degraded by the proteasome, further exerting a positive regulatory effect on the ABA signaling pathway [185]. Two deubiquitinating enzymes involved in deubiquitination—UBP12 (ubiquitin-specific protease 12) and UBP13—enhance the stability of VPS23A by catalyzing its deubiquitination [186]. This increased stability of VPS23A in turn promotes the degradation of ABA receptors, thereby negatively regulating the ABA signaling pathway. Additionally, UBP12 and UBP13 can catalyze the deubiquitination of XBAT35, leading to the stabilization of XBAT35 pro-

https://doi.org/10.3390/plants15010052

tein. Notably, XBAT35 competes with VPS23A for binding to UBP12 and UBP13, which enables the fine-tuning of VPS23A ubiquitination and degradation [187]. The E2 ubiquitin-conjugating enzyme UBC26 can directly bind to PYL4 and regulate the ubiquitination and degradation of PYL4, thereby negatively regulating the ABA signaling pathway. Importantly, this regulatory process requires the joint participation of the RING-type E3 ubiquitin ligases RFA1 (RING finger ABA-related 1) and RFA4 [188].

Ubiquitination of the protein phosphatase family (PP2C) is involved in the signal transduction pathway of ABA. U-box-type E3 ligases (PUBs, plant U-box E3 ligases) are involved in the ubiquitination and degradation of ABI1 [189]. RGLG1 (RING domain ligase 1) and RGLG5 from the RING-type E3 ubiquitin ligase family participate in the ubiquitination of three PP2C proteins, namely AHG3, ABI2, and HAB2 [190]. Additionally, the BPM (BTB/POZ and MATH domain proteins) subunits (BPM3 and BPM5) of the E3 ubiquitin ligase CRL3s (Cullin3-RING-based E3 ligases) can also interact with PP2C protein phosphatases such as ABI1, ABI2, and HAB1 to regulate their ubiquitination [191].

SnRK2, a key kinase in the ABA signaling pathway, is also regulated by ubiquitination. AtPP2-B11 is an F-box protein in the SCF (SKP1/Cullin/F-box) E3 ubiquitin ligase complex; it can ubiquitinate SnRK2.3 and promote its degradation by the 26S proteasome [192]. HOS15 (high osmotic stress 15), a substrate receptor protein in the CUL4-DDB1 E3 ubiquitin ligase complex, can facilitate the ubiquitination of SnRK2.6/OST1, which is then degraded by the 26S proteasome [193].

The stability of SnRK2.6/OST1 is also regulated by the de-SUMOylation mediated by the SUMO protease ESD4 and its interacting protein NUA (nuclear pore anchor), thereby negatively regulating the ABA signaling pathway [194,195]. Therefore, we hypothesize that the reason why SUMOylation enhances protein stability is most likely by competing with ubiquitin for binding to the lysine residues of proteins.

Transcriptional regulators in the ABA signaling pathway are also involved in the regulation of ubiquitination. Studies have shown that the transcription factor ABI3 (abscisic acid-insensitive 3) with a B3 domain can bind to the E3 ubiquitin ligase AIP2 (ABI3-interacting protein 2) and the U-box-type E3 ubiquitin ligase PUB9 (plant U-box 9), and is subsequently degraded by the proteasome, thereby negatively regulating the ABA signaling pathway [196–198]. The lysine at position 344 in the C3 domain of the bZIP transcription factor ABI5 (abscisic acid-insensitive 5) is ubiquitinated by the RING-type E3 ubiquitin ligase KEG; this ubiquitination leads to ABI5 degradation by the proteasome, which negatively regulates the ABA signaling pathway [199,200]. Additionally, the RING-type E3 ubiquitin ligase SDIR1can ubiquitinate SDIRIP1 (SDIR1-interacting protein 1), resulting in SDIRIP1 degradation by the 26S proteasome. This process further upregulates the transcriptional level of the *ABI5* gene, thereby positively regulating the ABA signaling pathway [201,202]. The lysine at position 391 of ABI5 can also be SUMOylated under the catalysis of the SUMO ligase SIZ1. This SUMO modification protects ABI5 from proteasomal degradation, thus negatively regulating the ABA signaling pathway [203]. MYB30 is a negative regulator of the ABA signaling pathway. The lysines at positions 165 and 283 of MYB30 can be ubiquitinated and degraded by the RING-type E3 ubiquitin ligase RHA2b (RING-H2 finger protein A2b); MYB30 can also be ubiquitinated by the E3 ligase MIEL1 (MYB30-interacting E3 ligase 1) [204,205]. Moreover, SIZ1 can catalyze the SUMOylation of the lysine at position 283 of MYB30. Similar to its modification of ABI5, this SUMOylation also enhances the stability of MYB30 [206].

4. PTM Crosstalk

In cells, crosstalk occurs between any two or more different PTMs through two molecular modes: (1) Different modifications coordinately regulate the molecular function

of the same substrate protein. In this mode, one type PTM affects other PTM(s) at the same amino acid site(s) or adjacent amino acids; (2) Multiple enzymes with "writer" or "eraser" functions sequentially use each other as substrates to alter enzyme activity by adding or removing modifications, and to form positive regulatory or feedback regulatory loops to exert their functions [207–209].

4.1. Crosstalk Between Phosphorylation and Ubiquitination

For some proteins, after being modified by phosphorylation, they become the targets of ubiquitination to induce the degradation of substrate proteins through cis-regulation, a process termed "phosphodegron (a phosphorylated motif that mediates ubiquitination-dependent degradation)" [210]. This process usually involves a specific phospho-motif on the substrate protein serving as an anchoring site for the ubiquitin ligase. When the motif is phosphorylated, it induces the binding of the ubiquitin ligase to the substrate and initiates the ubiquitination-mediated degradation process. For example, when *Arabidopsis thaliana* is subjected to high-concentration metal ion stress, its iron-regulated transporter 1 (IRT1) is regulated by activating the phosphodegron mechanism [211]. After IRT1 is modified by phosphorylation, it provides a binding region for the E3 ubiquitin ligase IRT1-degradation factor 1 (IDF1). IDF1 ubiquitinates two lysine sites of IRT1, thereby inducing the endocytosis and degradation of IRT1. Under high-carbon and low-nitrogen nutrient stress, at least one amino acid residue of ATL31 in *Arabidopsis thaliana* is phosphorylated by CIPK [212]. After 14-3-3 protein binds to the E3 ligase ATL31, it induces the sequential phosphorylation of 4 amino acid sites at the C-terminus of ATL31 [213]. Moreover, the interaction between these two proteins is crucial for the ubiquitination of ATL31 and the degradation of 14-3-3 protein induced by ATL31 [214]. This indicates that the phosphorylation of E3 ubiquitin ligase can activate its interaction with substrates.

Most extracellular signals are transmitted into the cell through membrane-localized receptor kinases. Generally, once receptor kinases are activated by ligands, they undergo phosphorylation and ubiquitination modifications, which in turn induce the intracellular translocation, turnover, or degradation of receptor kinases and facilitate signal transmission. Studies have shown that the signaling pathways of the flagellin-sensitive 2 (FLS2) receptor and the brassinosteroid insensitive 1 (BRI1) receptor are both regulated by the "phosphorylation–ubiquitination modification" crosstalk mode [215,216]. When these two receptor kinases sense their respective ligands (flagellin and BR, respectively), FLS2 and BRI1 form complexes with BAK1 kinase, respectively, undergo endocytosis into the cell, and jointly activate downstream pathways. Importantly, both flagellin and BR signals phosphorylate the conserved amino acid residues of the E3 ubiquitin ligases PUB12/13, thereby activating the interaction between PUB12/13 and their respective receptors (FLS2 and BRI1) and ultimately leading to their degradation. Although the mechanisms by which FLS2 and BRI1 recruit ubiquitin ligases are different, phosphorylation of FLS2 and BRI1 plays a decisive role in the PUB12/13-mediated degradation pathway [215,216]. In the ABA signaling pathway, when the protein kinase SnRK2.3 is activated and phosphorylates the substrate protein PP2-B11, it induces the proteasomal degradation of PP2-B11 through a ubiquitination-dependent pathway, thereby regulating the ABA signaling pathway and abiotic stress response [31].

4.2. Crosstalk Between Phosphorylation and SUMOylation

The first reported protein with the "phosphorylation–SUMOylation " crosstalk regulatory mode is CESTA, a core transcription factor in the brassinosteroid signaling pathway [217]. Studies have found that treating plants with BR leads to the SUMO1 and SUMO1-like ubiquitin modification of lysine 72 (K72) in CESTA, which in turn induces the

nuclear translocation of CESTA and activates its transcriptional activity. However, CPK can attenuate this ubiquitin-like modification process and nuclear translocation effect by phosphorylating CESTA [217]. There are a few reports on this type of crosstalk in plant immunity, but no such protein with a role in abiotic stress response has been reported.

4.3. Crosstalk Between Ubiquitination and SUMOylation

Ubiquitination and ubiquitin-like can either antagonize or synergistically regulate each other [218]. Although both modifications involve the E1-E2-E3 signaling pathway, their molecular regulatory modes are different. Furthermore, ubiquitination and SUMOylation compete for the same lysine site. Early studies found that under salt stress, SUMOylation of lysine 65 (K65) in the DELLA protein repressor of GA (RGA) promotes the expression of this RGA [219]. When this site is mutated to arginine, the expression level of RGA remains unchanged. Further studies have shown that the lysine site K65 of RGA is co-regulated by two modifications, namely SUMOylation and ubiquitination, and SUMOylation can protect RGA from gibberellin-mediated degradation via the ubiquitination pathway. Another study found that SUMOylation and ubiquitination compete for 4 lysine sites (Lys50, Lys276, Lys281, and Lys291) of the protein kinase RACK1B, and the SUMOylation of these 4 lysine sites enhances the sensitivity of RACK1B to ABA-mediated ubiquitination and degradation [220].

4.4. Crosstalk Between Phosphorylation, Ubiquitination, and SUMOylation

The synergistic regulatory mode of three PTMs (phosphorylation, ubiquitination, and SUMOylation) was first reported in animal cells. These three modifications synergistically regulate the genotoxic stress response mechanism and induce processes such as the nuclear localization of the kinase subunit of the NEMO protein [221]. A similar regulatory mechanism also exists in plants. SnRK1 kinase can form a complex with SnRK2 and PP2C, participating in the ABA-dependent environmental response pathway [222]. The activation of SnRK1 depends on the threonine phosphorylation in the T-loop region. The phosphorylation of this site induces the E3 ubiquitin-like ligase SIZ1 to act on multiple subunits of SnRK1 through the ubiquitin-like modification process, leading to the degradation of SnRK1 [223]. This study indicates that SnRK1 exerts its function through SUMOylation induced by the phosphorylation process and the subsequent degradation pathway, and weakens the further transmission of adverse signals to downstream components through a negative feedback regulation mode.

5. Conclusions and Perspectives

PTMs of proteins can regulate protein structure, dynamics, and biological functions. They serve as an important regulatory mechanism for plants to rapidly respond to environmental stimuli during their life activities. Given that PTMs can quickly and accurately activate, perceive, integrate, and transmit extracellular signals to downstream pathways, genes encoding proteins subjected to PTMs are ideal targets of genetic engineering for breeding stress-resilient crops.

Regulating gene expression in plants can be effectively achieved using tools such as CRISPR-mediated gene editing and RNA interference (RNAi) [224]. For protein-coding genes, their function can be modulated at multiple levels: DNA, mRNA, and protein. CRISPR-mediated gene editing technologies are powerful tools for modifying crop DNA [225], altering protein sequences, and modifying epigenetic marks [226,227], thereby influencing gene expression level, protein abundance, translation efficiency, and protein activity. For the genes subject to PTMs, at the transcription level, their expression level can be altered by targeting the cis-regulatory elements of promoters; at the post-

https://doi.org/10.3390/plants15010052

transcriptional level, their RNA level can be modulated by RNAi or miRNA mimics; at the post-translational level, the abundance and/or function of the protein can be manipulated by targeting the PTM sites [228]. Together, these approaches enable quantitative and qualitative control of protein synthesis.

Beyond protein synthesis, plants also regulate protein homeostasis at multiple levels (including trafficking, localization, and degradation) through PTMs. Protein condensation mediated by phase separation and phase transition is a key process in protein homeostasis regulation [229–232], and this process plays important roles in plant development and responses to environmental stresses [233,234]. The homeostasis of all proteins, including condensation-prone proteins, is primarily regulated by protein degradation mechanisms, mainly the ubiquitin–proteasome system (UPS) and the autophagy system [235,236]. The UPS mediates the transfer of ubiquitin to substrates through the coordinated action of E1 activating enzymes, E2 conjugating enzymes, and E3 ligases, which typically leads to substrate polyubiquitination and subsequent degradation by the proteasome [226,231,232]. In contrast, the autophagy system is responsible for degrading not only proteins but also organelles to maintain cellular homeostasis [237]. A recent study developed the Targeted Condensation-prone-protein Degradation (TCD) strategy using the E3 ubiquitin ligase E3TCD1. The X-E3TCD1 fusion protein acts as a genetically engineered degrader that can selectively target endogenous proteins with condensation propensity [238]. Proteolysis-targeting chimeras (PROTACs) are defined as heterobifunctional constructs comprising two distinct ligands: one that specifically engages a protein of interest (POI) and another capable of recruiting an E3 ubiquitin ligase. Through chemical induction of proximity between the POI and the recruited E3 ligase, the POI undergoes ubiquitination, followed by its selective degradation via the ubiquitin–proteasome system (UPS) [239]. The development of PROTACs for crop improvement via E3 ubiquitin ligases remains in its nascent stage. Notably, the homologous substrate recognition subunits of E3 ubiquitin ligases serve as promising candidates for integration into PROTAC design frameworks. By mediating the ubiquitination of diverse protein substrates, these subunits modulate a broad spectrum of cellular processes in plants, thereby establishing themselves as valuable resources for advancing PROTAC technologies. Under stress conditions, the abundance and composition of E3 ubiquitin ligases exhibit distinct variations across different plant organs and crop cultivars. Omics-based approaches—including transcriptomics and proteomics—are indispensable for characterizing the expression profiles of E3 ubiquitin ligases under specific contexts. Such investigations would lay the foundation for customizing PROTAC systems to suit targeted scenarios, such as different crop cultivars or specific plant organs. Nevertheless, future development efforts must adequately address the inherent diversity of E3 ubiquitin ligases while further elucidating the functional mechanisms and structural features of plant-specific E3 ubiquitin ligases [240].

Despite targeting E3 ubiquitin ligases, key regulators of environmental signal responses, as the key molecular targets and technical scaffolds, will significantly advance the understanding and manipulation of abiotic stress responses in crops. In future research, it is essential to integrate multi-omics technologies to identify more PTM targets associated with strong stress tolerance and high yield. Meanwhile, combining TCD/PROTACs with CRISPR-mediated gene editing to precisely modify proteins involved in PTMs holds high promise for crop improvements, but the development of artificial degradation systems based on the two technologies still faces numerous challenges in terms of crop genetic improvement.

Author Contributions: G.L. and T.Z. conceptualized and designed the review. G.L. and B.F. wrote the original draft. T.Z., K.J. and Q.-H.Z. edited and finalized the manuscript. T.Z. and K.J. funding acquisition. All authors have read and agreed to the published version of the manuscript.

Funding: This work was supported by Natural Science Foundation of Sichuan Province (25NSFSC0332), Sichuan Rice Innovation Team (SCCXTD-2024-SD-6), Key Science and Technology Project of Sichuan Province (2022ZDZX0012-02), Sichuan Key Project of Rice Breeding (2021YFYZ0016), Independent Innovation of Sichuan Province (2022CCZX066), the 1+9 Open Competition Project of Sichuan Academy of Agricultural Sciences (1+9KJGG002, 1+9KJGG001), Original Innovation Program of SAAS (YSCX2035-010), and Key Projects of Rice and Sorghum Research Institute (2020SZDYF008, 2020SZDYF001, 2020SZDYF003).

Data Availability Statement: No new data were generated in association with this article.

Conflicts of Interest: The authors declare no conflicts of interest.

References

1. Millar, A.H.; Heazlewood, J.L.; Giglione, C.; Holdsworth, M.J.; Bachmair, A.; Schulze, W.X. The Scope, Functions, and Dynamics of Posttranslational Protein Modifications. *Annu. Rev. Plant Biol.* **2019**, *70*, 119–151. [CrossRef]
2. Zhang, Z.; Dong, Y.; Wang, X.; Gao, Y.; Xian, X.; Li, J.; Wang, Y. Protein post-translational modifications (PTM(S)) unlocking resilience to abiotic stress in horticultural crops: A review. *Int. J. Biol. Macromol.* **2025**, *306*, 141772. [CrossRef]
3. Levene, P.A.; Alsberg, C.L. The Cleavage Products of Vitellin. *J. Biol. Chem.* **1906**, *2*, 127–133. [CrossRef]
4. Li, P.; Liu, J. Protein Phosphorylation in Plant Cell Signaling. *Methods Mol. Biol.* **2021**, *2358*, 45–71. [CrossRef]
5. Mergner, J.; Frejno, M.; List, M.; Papacek, M.; Chen, X.; Chaudhary, A.; Samaras, P.; Richter, S.; Shikata, H.; Messerer, M.; et al. Mass-spectrometry-based draft of the Arabidopsis proteome. *Nature* **2020**, *579*, 409–414. [CrossRef] [PubMed]
6. Clark, N.M.; Nolan, T.M.; Wang, P.; Song, G.; Montes, C.; Valentine, C.T.; Guo, H.; Sozzani, R.; Yin, Y.; Walley, J.W. Integrated omics networks reveal the temporal signaling events of brassinosteroid response in Arabidopsis. *Nat. Commun.* **2021**, *12*, 5858. [CrossRef]
7. Kim, T.W.; Park, C.H.; Hsu, C.C.; Kim, Y.W.; Ko, Y.W.; Zhang, Z.; Zhu, J.Y.; Hsiao, Y.C.; Branon, T.; Kaasik, K.; et al. Mapping the signaling network of BIN2 kinase using TurboID-mediated biotin labeling and phosphoproteomics. *Plant Cell* **2023**, *35*, 975–993. [CrossRef] [PubMed]
8. Montes, C.; Wang, P.; Liao, C.Y.; Nolan, T.M.; Song, G.; Clark, N.M.; Elmore, J.M.; Guo, H.; Bassham, D.C.; Yin, Y.; et al. Integration of multi-omics data reveals interplay between brassinosteroid and Target of Rapamycin Complex signaling in Arabidopsis. *New Phytol.* **2022**, *236*, 893–910. [CrossRef]
9. Meng, X.; Zhang, S. MAPK cascades in plant disease resistance signaling. *Annu. Rev. Phytopathol.* **2013**, *51*, 245–266. [CrossRef]
10. Zhang, M.; Su, J.; Zhang, Y.; Xu, J.; Zhang, S. Conveying endogenous and exogenous signals: MAPK cascades in plant growth and defense. *Curr. Opin. Plant Biol.* **2018**, *45*, 1–10. [CrossRef]
11. Wilkinson, K.D. Ubiquitination and deubiquitination: Targeting of proteins for degradation by the proteasome. *Semin. Cell Dev. Biol.* **2000**, *11*, 141–148. [CrossRef] [PubMed]
12. Isono, E.; Nagel, M.K. Deubiquitylating enzymes and their emerging role in plant biology. *Front. Plant Sci.* **2014**, *5*, 56. [CrossRef]
13. Chen, Z.J.; Sun, L.J. Nonproteolytic functions of ubiquitin in cell signaling. *Mol. Cell* **2009**, *33*, 275–286. [CrossRef]
14. Komander, D.; Rape, M. The ubiquitin code. *Annu. Rev. Biochem.* **2012**, *81*, 203–229. [CrossRef]
15. Meusser, B.; Hirsch, C.; Jarosch, E.; Sommer, T. ERAD: The long road to destruction. *Nat. Cell Biol.* **2005**, *7*, 766–772. [CrossRef]
16. E, Z.; Zhang, Y.; Li, T.; Wang, L.; Zhao, H. Characterization of the Ubiquitin-Conjugating Enzyme Gene Family in Rice and Evaluation of Expression Profiles under Abiotic Stresses and Hormone Treatments. *PLoS ONE* **2015**, *10*, e0122621. [CrossRef]
17. Wang, R.; You, X.; Zhang, C.; Fang, H.; Wang, M.; Zhang, F.; Kang, H.; Xu, X.; Liu, Z.; Wang, J.; et al. An ORFeome of rice E3 ubiquitin ligases for global analysis of the ubiquitination interactome. *Genome Biol.* **2022**, *23*, 154. [CrossRef]
18. Kurepa, J.; Walker, J.M.; Smalle, J.; Gosink, M.M.; Davis, S.J.; Durham, T.L.; Sung, D.Y.; Vierstra, R.D. The small ubiquitin-like modifier (SUMO) protein modification system in Arabidopsis. Accumulation of SUMO1 and -2 conjugates is increased by stress. *J. Biol. Chem.* **2003**, *278*, 6862–6872. [CrossRef]
19. Park, H.C.; Choi, W.; Park, H.J.; Cheong, M.S.; Koo, Y.D.; Shin, G.; Chung, W.S.; Kim, W.Y.; Kim, M.G.; Bressan, R.A.; et al. Identification and molecular properties of SUMO-binding proteins in Arabidopsis. *Mol. Cells* **2011**, *32*, 143–151. [CrossRef] [PubMed]
20. Seo, J.; Lee, K.J. Post-translational modifications and their biological functions: Proteomic analysis and systematic approaches. *J. Biochem. Mol. Biol.* **2004**, *37*, 35–44. [CrossRef]

21. Yang, X.; Qian, K. Protein O-GlcNAcylation: Emerging mechanisms and functions. *Nat. Rev. Mol. Cell Biol.* **2017**, *18*, 452–465. [CrossRef] [PubMed]
22. Breitling, J.; Aebi, M. N-linked protein glycosylation in the endoplasmic reticulum. *Cold Spring Harb. Perspect. Biol.* **2013**, *5*, a013359. [CrossRef] [PubMed]
23. Fujita, M.; Kinoshita, T. GPI-anchor remodeling: Potential functions of GPI-anchors in intracellular trafficking and membrane dynamics. *Biochim. Biophys. Acta (BBA)-Mol. Cell Biol. Lipids* **2012**, *1821*, 1050–1058. [CrossRef]
24. Liu, C.; Talbot, N.J.; Chen, X.L. Protein glycosylation during infection by plant pathogenic fungi. *New Phytol.* **2021**, *230*, 1329–1335. [CrossRef] [PubMed]
25. Vanier, G.; Lucas, P.L.; Loutelier-Bourhis, C.; Vanier, J.; Plasson, C.; Walet-Balieu, M.L.; Tchi-Song, P.C.; Remy-Jouet, I.; Richard, V.; Bernard, S.; et al. Heterologous expression of the N-acetylglucosaminyltransferase I dictates a reinvestigation of the N-glycosylation pathway in Chlamydomonas reinhardtii. *Sci. Rep.* **2017**, *7*, 10156. [CrossRef]
26. Zhang, S.; Li, W.; Lu, H.; Liu, Y. Quantification of N-glycosylation site occupancy status based on labeling/label-free strategies with LC-MS/MS. *Talanta* **2017**, *170*, 509–513. [CrossRef]
27. Moon, S.P.; Javed, A.; Hard, E.R.; Pratt, M.R. Methods for Studying Site-Specific O-GlcNAc Modifications: Successes, Limitations, and Important Future Goals. *JACS Au* **2022**, *2*, 74–83. [CrossRef]
28. Murn, J.; Shi, Y. The winding path of protein methylation research: Milestones and new frontiers. *Nat. Rev. Mol. Cell Biol.* **2017**, *18*, 517–527. [CrossRef]
29. Yang, Y.; Bedford, M.T. Protein arginine methyltransferases and cancer. *Nat. Rev. Cancer* **2013**, *13*, 37–50. [CrossRef]
30. Hwang, J.W.; Cho, Y.; Bae, G.U.; Kim, S.N.; Kim, Y.K. Protein arginine methyltransferases: Promising targets for cancer therapy. *Exp. Mol. Med.* **2021**, *53*, 788–808. [CrossRef]
31. Tewary, S.K.; Zheng, Y.G.; Ho, M.C. Protein arginine methyltransferases: Insights into the enzyme structure and mechanism at the atomic level. *Cell. Mol. Life Sci.* **2019**, *76*, 2917–2932. [CrossRef]
32. Zhang, X.; Wen, H.; Shi, X. Lysine methylation: Beyond histones. *Acta Biochim. Biophys. Sin.* **2012**, *44*, 14–27. [CrossRef]
33. König, A.C.; Hartl, M.; Boersema, P.J.; Mann, M.; Finkemeier, I. The mitochondrial lysine acetylome of Arabidopsis. *Mitochondrion* **2014**, *19 Pt B*, 252–260. [CrossRef]
34. Liu, X.; Yang, S.; Yu, C.W.; Chen, C.Y.; Wu, K. Histone Acetylation and Plant Development. *Enzymes* **2016**, *40*, 173–199. [CrossRef] [PubMed]
35. Kim, J.M.; To, T.K.; Ishida, J.; Morosawa, T.; Kawashima, M.; Matsui, A.; Toyoda, T.; Kimura, H.; Shinozaki, K.; Seki, M. Alterations of lysine modifications on the histone H3 N-tail under drought stress conditions in Arabidopsis thaliana. *Plant Cell Physiol.* **2008**, *49*, 1580–1588. [CrossRef] [PubMed]
36. Chen, Z.J.; Tian, L. Roles of dynamic and reversible histone acetylation in plant development and polyploidy. *Biochim. Biophys. Acta (BBA)-Gene Struct. Expr.* **2007**, *1769*, 295–307. [CrossRef] [PubMed]
37. Nambi, S.; Gupta, K.; Bhattacharyya, M.; Ramakrishnan, P.; Ravikumar, V.; Siddiqui, N.; Thomas, A.T.; Visweswariah, S.S. Cyclic AMP-dependent protein lysine acylation in mycobacteria regulates fatty acid and propionate metabolism. *J. Biol. Chem.* **2013**, *288*, 14114–14124. [CrossRef]
38. Wang, Q.; Zhang, Y.; Yang, C.; Xiong, H.; Lin, Y.; Yao, J.; Li, H.; Xie, L.; Zhao, W.; Yao, Y.; et al. Acetylation of metabolic enzymes coordinates carbon source utilization and metabolic flux. *Science* **2010**, *327*, 1004–1007. [CrossRef]
39. Liang, W.; Malhotra, A.; Deutscher, M.P. Acetylation regulates the stability of a bacterial protein: Growth stage-dependent modification of RNase R. *Mol. Cell* **2011**, *44*, 160–166. [CrossRef]
40. Scroggins, B.T.; Robzyk, K.; Wang, D.; Marcu, M.G.; Tsutsumi, S.; Beebe, K.; Cotter, R.J.; Felts, S.; Toft, D.; Karnitz, L.; et al. An acetylation site in the middle domain of Hsp90 regulates chaperone function. *Mol. Cell* **2007**, *25*, 151–159. [CrossRef]
41. Zhou, H.; Finkemeier, I.; Guan, W.; Tossounian, M.A.; Wei, B.; Young, D.; Huang, J.; Messens, J.; Yang, X.; Zhu, J.; et al. Oxidative stress-triggered interactions between the succinyl- and acetyl-proteomes of rice leaves. *Plant Cell Environ.* **2018**, *41*, 1139–1153. [CrossRef]
42. Meng, X.; Lv, Y.; Mujahid, H.; Edelmann, M.J.; Zhao, H.; Peng, X.; Peng, Z. Proteome-wide lysine acetylation identification in developing rice (*Oryza sativa*) seeds and protein co-modification by acetylation, succinylation, ubiquitination, and phosphorylation. *Biochim. Biophys. Acta (BBA)-Proteins Proteom.* **2018**, *1866*, 451–463. [CrossRef]
43. Jiang, J.; Gai, Z.; Wang, Y.; Fan, K.; Sun, L.; Wang, H.; Ding, Z. Comprehensive proteome analyses of lysine acetylation in tea leaves by sensing nitrogen nutrition. *BMC Genom.* **2018**, *19*, 840. [CrossRef]
44. Feng, J.; Chen, L.; Zuo, J. Protein S-Nitrosylation in plants: Current progresses and challenges. *J. Integr. Plant Biol.* **2019**, *61*, 1206–1223. [CrossRef] [PubMed]
45. Wei, L.; Zhao, J.; Zhong, Y.; Wu, X.; Wei, S.; Liu, Y. The roles of protein S-nitrosylation in regulating the growth and development of plants: A review. *Int. J. Biol. Macromol.* **2025**, *307*, 142204. [CrossRef] [PubMed]
46. Liu, Y.; Liu, Z.; Wu, X.; Fang, H.; Huang, D.; Pan, X.; Liao, W. Role of protein S-nitrosylation in plant growth and development. *Plant Cell Rep.* **2024**, *43*, 204. [CrossRef]

47. Rodríguez-Ruiz, M.; Mioto, P.T.; Palma, J.M.; Corpas, F.J. Detection of Protein S-nitrosothiols (SNOs) in Plant Samples on Diaminofluorescein (DAF) Gels. *Bio-Protocol* **2017**, *7*, e2559. [CrossRef]
48. Lamotte, O.; Bertoldo, J.B.; Besson-Bard, A.; Rosnoblet, C.; Aimé, S.; Hichami, S.; Terenzi, H.; Wendehenne, D. Protein S-nitrosylation: Specificity and identification strategies in plants. *Front. Chem.* **2014**, *2*, 114. [CrossRef]
49. Astier, J.; Rasul, S.; Koen, E.; Manzoor, H.; Besson-Bard, A.; Lamotte, O.; Jeandroz, S.; Durner, J.; Lindermayr, C.; Wendehenne, D. S-nitrosylation: An emerging post-translational protein modification in plants. *Plant Sci.* **2011**, *181*, 527–533. [CrossRef] [PubMed]
50. Hess, D.T.; Matsumoto, A.; Kim, S.O.; Marshall, H.E.; Stamler, J.S. Protein S-nitrosylation: Purview and parameters. *Nat. Rev. Mol. Cell Biol.* **2005**, *6*, 150–166. [CrossRef]
51. Tan, M.; Luo, H.; Lee, S.; Jin, F.; Yang, J.S.; Montellier, E.; Buchou, T.; Cheng, Z.; Rousseaux, S.; Rajagopal, N.; et al. Identification of 67 histone marks and histone lysine crotonylation as a new type of histone modification. *Cell* **2011**, *146*, 1016–1028. [CrossRef]
52. Liu, S.; Xue, C.; Fang, Y.; Chen, G.; Peng, X.; Zhou, Y.; Chen, C.; Liu, G.; Gu, M.; Wang, K.; et al. Global Involvement of Lysine Crotonylation in Protein Modification and Transcription Regulation in Rice. *Mol. Cell. Proteom.* **2018**, *17*, 1922–1936. [CrossRef]
53. Zhang, W.J.; Zhou, Y.; Zhang, Y.; Su, Y.H.; Xu, T. Protein phosphorylation: A molecular switch in plant signaling. *Cell Rep.* **2023**, *42*, 112729. [CrossRef] [PubMed]
54. Akhter, D.; Zhang, Y.; Hu, J.; Pan, R. Protein ubiquitination in plant peroxisomes. *J. Integr. Plant Biol.* **2023**, *65*, 371–380. [CrossRef]
55. Han, D.; Lai, J.; Yang, C. SUMOylation: A critical transcription modulator in plant cells. *Plant Sci.* **2021**, *310*, 110987. [CrossRef] [PubMed]
56. Jiang, H.; Du, Y.; Fu, M.; Jiao, W. N-Glycosylation-The Behind-the-Scenes 'Manipulative Hand' of Plant Pathogen Invasiveness. *Mol. Plant Pathol.* **2025**, *26*, e70123. [CrossRef]
57. Shi, Z.; Li, Z.; Zhang, G. The mechanism of histone lysine methylation of plant involved in gene expression and regulation. *Yi Chuan* **2014**, *36*, 208–219.
58. Contreras-de la Rosa, P.A.; Aragón-Rodríguez, C.; Ceja-López, J.A.; García-Arteaga, K.F.; De-la-Peña, C. Lysine crotonylation: A challenging new player in the epigenetic regulation of plants. *J. Proteom.* **2022**, *255*, 104488. [CrossRef]
59. Zhang, N.; Wang, S.; Tian, H.; Li, S.; Liu, L.; Li, J.; Chen, D.; Zhao, S.; Yan, X.; Niaz, M.; et al. Functions of lysine 2-hydroxyisobutyrylation and future perspectives on plants. *Proteomics* **2023**, *23*, e2300045. [CrossRef] [PubMed]
60. Corpas, F.J.; González-Gordo, S.; Rodríguez-Ruiz, M.; Muñoz-Vargas, M.A.; Palma, J.M. Thiol-based Oxidative Posttranslational Modifications (OxiPTMs) of Plant Proteins. *Plant Cell Physiol.* **2022**, *63*, 889–900. [CrossRef]
61. Cosse, M.; Rehders, T.; Eirich, J.; Finkemeier, I.; Selinski, J. Cysteine oxidation as a regulatory mechanism of Arabidopsis plastidial NAD-dependent malate dehydrogenase. *Physiol. Plant.* **2024**, *176*, e14340. [CrossRef] [PubMed]
62. Ciacka, K.; Tymiński, M.; Gniazdowska, A.; Krasuska, U. Carbonylation of proteins-an element of plant ageing. *Planta* **2020**, *252*, 12. [CrossRef]
63. Wang, R.; Mei, Y.; Xu, L.; Zhu, X.; Wang, Y.; Guo, J.; Liu, L. Differential proteomic analysis reveals sequential heat stress-responsive regulatory network in radish (*Raphanus sativus* L.) taproot. *Planta* **2018**, *247*, 1109–1122. [CrossRef]
64. Zhou, Y.; Xu, F.; Shao, Y.; He, J. Regulatory Mechanisms of Heat Stress Response and Thermomorphogenesis in Plants. *Plants* **2022**, *11*, 3410. [CrossRef]
65. Huang, L.Z.; Zhou, M.; Ding, Y.F.; Zhu, C. Gene Networks Involved in Plant Heat Stress Response and Tolerance. *Int. J. Mol. Sci.* **2022**, *23*, 11970. [CrossRef] [PubMed]
66. Guihur, A.; Rebeaud, M.E.; Goloubinoff, P. How do plants feel the heat and survive? *Trends Biochem. Sci.* **2022**, *47*, 824–838. [CrossRef]
67. Sorger, P.K.; Pelham, H.R. Yeast heat shock factor is an essential DNA-binding protein that exhibits temperature-dependent phosphorylation. *Cell* **1988**, *54*, 855–864. [CrossRef]
68. Liu, H.C.; Liao, H.T.; Charng, Y.Y. The role of class A1 heat shock factors (HSFA1s) in response to heat and other stresses in Arabidopsis. *Plant Cell Environ.* **2011**, *34*, 738–751. [CrossRef]
69. Schramm, F.; Larkindale, J.; Kiehlmann, E.; Ganguli, A.; Englich, G.; Vierling, E.; von Koskull-Döring, P. A cascade of transcription factor DREB2A and heat stress transcription factor HsfA3 regulates the heat stress response of Arabidopsis. *Plant J.* **2008**, *53*, 264–274. [CrossRef]
70. Charng, Y.Y.; Liu, H.C.; Liu, N.Y.; Chi, W.T.; Wang, C.N.; Chang, S.H.; Wang, T.T. A heat-inducible transcription factor, HsfA2, is required for extension of acquired thermotolerance in Arabidopsis. *Plant Physiol.* **2007**, *143*, 251–262. [CrossRef] [PubMed]
71. Li, B.; Gao, K.; Ren, H.; Tang, W. Molecular mechanisms governing plant responses to high temperatures. *J. Integr. Plant Biol.* **2018**, *60*, 757–779. [CrossRef]
72. Kurop, M.K.; Huyen, C.M.; Kelly, J.H.; Blagg, B.S.J. The heat shock response and small molecule regulators. *Eur. J. Med. Chem.* **2021**, *226*, 113846. [CrossRef] [PubMed]
73. Liu, H.T.; Li, G.L.; Chang, H.; Sun, D.Y.; Zhou, R.G.; Li, B. Calmodulin-binding protein phosphatase PP7 is involved in thermotolerance in Arabidopsis. *Plant Cell Environ.* **2007**, *30*, 156–164. [CrossRef]

74. Reindl, A.; Schöffl, F.; Schell, J.; Koncz, C.; Bakó, L. Phosphorylation by a cyclin-dependent kinase modulates DNA binding of the Arabidopsis heat-shock transcription factor HSF1 in vitro. *Plant Physiol.* **1997**, *115*, 93–100. [CrossRef]
75. Zhang, S.; Wang, S.; Lv, J.; Liu, Z.; Wang, Y.; Ma, N.; Meng, Q. SUMO E3 Ligase SlSIZ1 Facilitates Heat Tolerance in Tomato. *Plant Cell Physiol.* **2018**, *59*, 58–71. [CrossRef]
76. Ohama, N.; Kusakabe, K.; Mizoi, J.; Zhao, H.; Kidokoro, S.; Koizumi, S.; Takahashi, F.; Ishida, T.; Yanagisawa, S.; Shinozaki, K.; et al. The Transcriptional Cascade in the Heat Stress Response of Arabidopsis Is Strictly Regulated at the Level of Transcription Factor Expression. *Plant Cell* **2016**, *28*, 181–201. [CrossRef]
77. Hahn, A.; Bublak, D.; Schleiff, E.; Scharf, K.D. Crosstalk between Hsp90 and Hsp70 chaperones and heat stress transcription factors in tomato. *Plant Cell* **2011**, *23*, 741–755. [CrossRef]
78. Cohen-Peer, R.; Schuster, S.; Meiri, D.; Breiman, A.; Avni, A. Sumoylation of Arabidopsis heat shock factor A2 (HsfA2) modifies its activity during acquired thermotholerance. *Plant Mol. Biol.* **2010**, *74*, 33–45. [CrossRef]
79. Hong, Y.; Rogers, R.; Matunis, M.J.; Mayhew, C.N.; Goodson, M.L.; Park-Sarge, O.K.; Sarge, K.D. Regulation of heat shock transcription factor 1 by stress-induced SUMO-1 modification. *J. Biol. Chem.* **2001**, *276*, 40263–40267. [CrossRef] [PubMed]
80. Wang, F.; Liu, Y.; Shi, Y.; Han, D.; Wu, Y.; Ye, W.; Yang, H.; Li, G.; Cui, F.; Wan, S.; et al. SUMOylation Stabilizes the Transcription Factor DREB2A to Improve Plant Thermotolerance. *Plant Physiol.* **2020**, *183*, 41–50. [CrossRef] [PubMed]
81. Chen, H.; Hwang, J.E.; Lim, C.J.; Kim, D.Y.; Lee, S.Y.; Lim, C.O. Arabidopsis DREB2C functions as a transcriptional activator of HsfA3 during the heat stress response. *Biochem. Biophys. Res. Commun.* **2010**, *401*, 238–244. [CrossRef]
82. Guo, X.; Liu, D.; Chong, K. Cold signaling in plants: Insights into mechanisms and regulation. *J. Integr. Plant Biol.* **2018**, *60*, 745–756. [CrossRef]
83. Ma, Y.; Dai, X.; Xu, Y.; Luo, W.; Zheng, X.; Zeng, D.; Pan, Y.; Lin, X.; Liu, H.; Zhang, D.; et al. COLD1 confers chilling tolerance in rice. *Cell* **2015**, *160*, 1209–1221. [CrossRef]
84. Shi, Y.; Ding, Y.; Yang, S. Molecular Regulation of CBF Signaling in Cold Acclimation. *Trends Plant Sci.* **2018**, *23*, 623–637. [CrossRef]
85. Iqbal, Z.; Memon, A.G.; Ahmad, A.; Iqbal, M.S. Calcium Mediated Cold Acclimation in Plants: Underlying Signaling and Molecular Mechanisms. *Front. Plant Sci.* **2022**, *13*, 855559. [CrossRef]
86. Flynn, G.E.; Johnson, J.P., Jr.; Zagotta, W.N. Cyclic nucleotide-gated channels: Shedding light on the opening of a channel pore. *Nat. Rev. Neurosci.* **2001**, *2*, 643–651. [CrossRef]
87. Cui, Y.; Lu, S.; Li, Z.; Cheng, J.; Hu, P.; Zhu, T.; Wang, X.; Jin, M.; Wang, X.; Li, L.; et al. CYCLIC NUCLEOTIDE-GATED ION CHANNELs 14 and 16 Promote Tolerance to Heat and Chilling in Rice. *Plant Physiol.* **2020**, *183*, 1794–1808. [CrossRef] [PubMed]
88. Wang, B.; Li, L.; Peng, D.; Liu, M.; Wei, A.; Li, X. TaFDL2-1A interacts with TabZIP8-7A protein to cope with drought stress via the abscisic acid signaling pathway. *Plant Sci.* **2021**, *311*, 111022. [CrossRef]
89. Hattori, T.; Otomi, Y.; Nakajima, Y.; Soga, K.; Wakabayashi, K.; Iida, H.; Hoson, T. MCA1 and MCA2 Are Involved in the Response to Hypergravity in Arabidopsis Hypocotyls. *Plants* **2020**, *9*, 590. [CrossRef]
90. Saucedo-García, M.; González-Córdova, C.D.; Ponce-Pineda, I.G.; Cano-Ramírez, D.; Romero-Colín, F.M.; Arroyo-Pérez, E.E.; King-Díaz, B.; Zavafer, A.; Gavilanes-Ruíz, M. Effects of MPK3 and MPK6 kinases on the chloroplast architecture and function induced by cold acclimation in Arabidopsis. *Photosynth. Res.* **2021**, *149*, 201–212. [CrossRef]
91. Zhao, C.; Wang, P.; Si, T.; Hsu, C.C.; Wang, L.; Zayed, O.; Yu, Z.; Zhu, Y.; Dong, J.; Tao, W.A.; et al. MAP Kinase Cascades Regulate the Cold Response by Modulating ICE1 Protein Stability. *Dev. Cell* **2017**, *43*, 618–629.e5. [CrossRef]
92. Liu, Z.; Jia, Y.; Ding, Y.; Shi, Y.; Li, Z.; Guo, Y.; Gong, Z.; Yang, S. Plasma Membrane CRPK1-Mediated Phosphorylation of 14-3-3 Proteins Induces Their Nuclear Import to Fine-Tune CBF Signaling during Cold Response. *Mol. Cell* **2017**, *66*, 117–128.e5. [CrossRef]
93. Li, H.; Ding, Y.; Shi, Y.; Zhang, X.; Zhang, S.; Gong, Z.; Yang, S. MPK3- and MPK6-Mediated ICE1 Phosphorylation Negatively Regulates ICE1 Stability and Freezing Tolerance in Arabidopsis. *Dev. Cell* **2017**, *43*, 630–642.e4. [CrossRef]
94. Ding, Y.; Lv, J.; Shi, Y.; Gao, J.; Hua, J.; Song, C.; Gong, Z.; Yang, S. EGR2 phosphatase regulates OST1 kinase activity and freezing tolerance in Arabidopsis. *EMBO J.* **2019**, *38*, e99819. [CrossRef]
95. Lang, Z.; Zhu, J. OST1 phosphorylates ICE1 to enhance plant cold tolerance. *Sci. China Life Sci.* **2015**, *58*, 317–318. [CrossRef] [PubMed]
96. Margalha, L.; Elias, A.; Belda-Palazón, B.; Peixoto, B.; Confraria, A.; Baena-González, E. HOS1 promotes plant tolerance to low-energy stress via the SnRK1 protein kinase. *Plant J.* **2023**, *115*, 627–641. [CrossRef] [PubMed]
97. Ye, K.; Li, H.; Ding, Y.; Shi, Y.; Song, C.; Gong, Z.; Yang, S. BRASSINOSTEROID-INSENSITIVE2 Negatively Regulates the Stability of Transcription Factor ICE1 in Response to Cold Stress in Arabidopsis. *Plant Cell* **2019**, *31*, 2682–2696. [CrossRef]
98. Zhang, Z.; Li, J.; Pan, Y.; Li, J.; Zhou, L.; Shi, H.; Zeng, Y.; Guo, H.; Yang, S.; Zheng, W.; et al. Natural variation in CTB4a enhances rice adaptation to cold habitats. *Nat. Commun.* **2017**, *8*, 14788. [CrossRef] [PubMed]
99. Li, J.; Chen, Y.; Zhang, R.; Wang, R.; Wu, B.; Zhang, H.; Xiao, G. OsWRKY70 Plays Opposite Roles in Blast Resistance and Cold Stress Tolerance in Rice. *Rice* **2024**, *17*, 61. [CrossRef]

100. Ji, T.; Zheng, L.; Wu, J.; Duan, M.; Liu, Q.; Liu, P.; Shen, C.; Liu, J.; Ye, Q.; Wen, J.; et al. The thioesterase APT1 is a bidirectional-adjustment redox sensor. *Nat. Commun.* **2023**, *14*, 2807. [CrossRef]
101. Ye, Q.; Zheng, L.; Liu, P.; Liu, Q.; Ji, T.; Liu, J.; Gao, Y.; Liu, L.; Dong, J.; Wang, T. The S-acylation cycle of transcription factor MtNAC80 influences cold stress responses in Medicago truncatula. *Plant Cell* **2024**, *36*, 2629–2651. [CrossRef] [PubMed]
102. Gao, X.; Ma, J.; Wang, G.; Huang, S.; Wu, X.; Hu, L.; Yu, J. The S-nitrosylation of monodehydroascorbate reductase positively regulated the low temperature tolerance of mini Chinese cabbage. *Int. J. Biol. Macromol.* **2024**, *281*, 136047. [CrossRef]
103. Mukherjee, A.; Dwivedi, S.; Bhagavatula, L.; Datta, S. Integration of light and ABA signaling pathways to combat drought stress in plants. *Plant Cell Rep.* **2023**, *42*, 829–841. [CrossRef] [PubMed]
104. Hsu, P.K.; Dubeaux, G.; Takahashi, Y.; Schroeder, J.I. Signaling mechanisms in abscisic acid-mediated stomatal closure. *Plant J.* **2021**, *105*, 307–321. [CrossRef]
105. Chen, X.; Ding, Y.; Yang, Y.; Song, C.; Wang, B.; Yang, S.; Guo, Y.; Gong, Z. Protein kinases in plant responses to drought, salt, and cold stress. *J. Integr. Plant Biol.* **2021**, *63*, 53–78. [CrossRef]
106. Liu, H.; Song, S.; Zhang, H.; Li, Y.; Niu, L.; Zhang, J.; Wang, W. Signaling Transduction of ABA, ROS, and Ca(2+) in Plant Stomatal Closure in Response to Drought. *Int. J. Mol. Sci.* **2022**, *23*, 14824. [CrossRef]
107. Hasan, M.M.; Liu, X.D.; Waseem, M.; Guang-Qian, Y.; Alabdallah, N.M.; Jahan, M.S.; Fang, X.W. ABA activated SnRK2 kinases: An emerging role in plant growth and physiology. *Plant Signal. Behav.* **2022**, *17*, 2071024. [CrossRef] [PubMed]
108. Brandt, B.; Brodsky, D.E.; Xue, S.; Negi, J.; Iba, K.; Kangasjärvi, J.; Ghassemian, M.; Stephan, A.B.; Hu, H.; Schroeder, J.I. Reconstitution of abscisic acid activation of SLAC1 anion channel by CPK6 and OST1 kinases and branched ABI1 PP2C phosphatase action. *Proc. Natl. Acad. Sci. USA* **2012**, *109*, 10593–10598. [CrossRef]
109. Sato, A.; Sato, Y.; Fukao, Y.; Fujiwara, M.; Umezawa, T.; Shinozaki, K.; Hibi, T.; Taniguchi, M.; Miyake, H.; Goto, D.B.; et al. Threonine at position 306 of the KAT1 potassium channel is essential for channel activity and is a target site for ABA-activated SnRK2/OST1/SnRK2.6 protein kinase. *Biochem. J.* **2009**, *424*, 439–448. [CrossRef]
110. Yoshida, T.; Fujita, Y.; Maruyama, K.; Mogami, J.; Todaka, D.; Shinozaki, K.; Yamaguchi-Shinozaki, K. Four Arabidopsis AREB/ABF transcription factors function predominantly in gene expression downstream of SnRK2 kinases in abscisic acid signalling in response to osmotic stress. *Plant Cell Environ.* **2015**, *38*, 35–49. [CrossRef]
111. Fujita, Y.; Yoshida, T.; Yamaguchi-Shinozaki, K. Pivotal role of the AREB/ABF-SnRK2 pathway in ABRE-mediated transcription in response to osmotic stress in plants. *Physiol. Plant.* **2013**, *147*, 15–27. [CrossRef]
112. Fujita, Y.; Fujita, M.; Shinozaki, K.; Yamaguchi-Shinozaki, K. ABA-mediated transcriptional regulation in response to osmotic stress in plants. *J. Plant Res.* **2011**, *124*, 509–525. [CrossRef]
113. Soma, F.; Takahashi, F.; Kidokoro, S.; Kameoka, H.; Suzuki, T.; Uga, Y.; Shinozaki, K.; Yamaguchi-Shinozaki, K. Constitutively active B2 Raf-like kinases are required for drought-responsive gene expression upstream of ABA-activated SnRK2 kinases. *Proc. Natl. Acad. Sci. USA* **2023**, *120*, e2221863120. [CrossRef]
114. Pizzio, G.A.; Rodriguez, P.L. Dual regulation of SnRK2 signaling by Raf-like MAPKKKs. *Mol. Plant* **2022**, *15*, 1260–1262. [CrossRef]
115. Lin, Z.; Li, Y.; Wang, Y.; Liu, X.; Ma, L.; Zhang, Z.; Mu, C.; Zhang, Y.; Peng, L.; Xie, S.; et al. Initiation and amplification of SnRK2 activation in abscisic acid signaling. *Nat. Commun.* **2021**, *12*, 2456. [CrossRef]
116. Islam, M.; Inoue, T.; Hiraide, M.; Khatun, N.; Jahan, A.; Kuwata, K.; Katagiri, S.; Umezawa, T.; Yotsui, I.; Sakata, Y.; et al. Activation of SnRK2 by Raf-like kinase ARK represents a primary mechanism of ABA and abiotic stress responses. *Plant Physiol.* **2021**, *185*, 533–546. [CrossRef]
117. Lin, Z.; Li, Y.; Zhang, Z.; Liu, X.; Hsu, C.C.; Du, Y.; Sang, T.; Zhu, C.; Wang, Y.; Satheesh, V.; et al. A RAF-SnRK2 kinase cascade mediates early osmotic stress signaling in higher plants. *Nat. Commun.* **2020**, *11*, 613. [CrossRef]
118. Katsuta, S.; Masuda, G.; Bak, H.; Shinozawa, A.; Kamiyama, Y.; Umezawa, T.; Takezawa, D.; Yotsui, I.; Taji, T.; Sakata, Y. Arabidopsis Raf-like kinases act as positive regulators of subclass III SnRK2 in osmostress signaling. *Plant J.* **2020**, *103*, 634–644. [CrossRef]
119. Fàbregas, N.; Yoshida, T.; Fernie, A.R. Role of Raf-like kinases in SnRK2 activation and osmotic stress response in plants. *Nat. Commun.* **2020**, *11*, 6184. [CrossRef]
120. Sun, Z.; Feng, Z.; Ding, Y.; Qi, Y.; Jiang, S.; Li, Z.; Wang, Y.; Qi, J.; Song, C.; Yang, S.; et al. RAF22, ABI1 and OST1 form a dynamic interactive network that optimizes plant growth and responses to drought stress in Arabidopsis. *Mol. Plant* **2022**, *15*, 1192–1210. [CrossRef]
121. Zhu, C.; Jing, B.; Lin, T.; Li, X.; Zhang, M.; Zhou, Y.; Yu, J.; Hu, Z. Phosphorylation of sugar transporter TST2 by protein kinase CPK27 enhances drought tolerance in tomato. *Plant Physiol.* **2024**, *195*, 1005–1024. [CrossRef]
122. Zong, W.; Yang, J.; Fu, J.; Xiong, L. Synergistic regulation of drought-responsive genes by transcription factor OsbZIP23 and histone modification in rice. *J. Integr. Plant Biol.* **2020**, *62*, 723–729. [CrossRef]
123. Huang, K.; Wu, T.; Ma, Z.; Li, Z.; Chen, H.; Zhang, M.; Bian, M.; Bai, H.; Jiang, W.; Du, X. Rice Transcription Factor OsWRKY55 Is Involved in the Drought Response and Regulation of Plant Growth. *Int. J. Mol. Sci.* **2021**, *22*, 4337. [CrossRef]

124. Yang, X.; Gavya, S.L.; Zhou, Z.; Urano, D.; Lau, O.S. Abscisic acid regulates stomatal production by imprinting a SnRK2 kinase-mediated phosphocode on the master regulator SPEECHLESS. *Sci. Adv.* **2022**, *8*, eadd2063. [CrossRef]
125. Orosa-Puente, B.; Leftley, N.; von Wangenheim, D.; Banda, J.; Srivastava, A.K.; Hill, K.; Truskina, J.; Bhosale, R.; Morris, E.; Srivastava, M.; et al. Root branching toward water involves posttranslational modification of transcription factor ARF7. *Science* **2018**, *362*, 1407–1410. [CrossRef]
126. Uga, Y.; Sugimoto, K.; Ogawa, S.; Rane, J.; Ishitani, M.; Hara, N.; Kitomi, Y.; Inukai, Y.; Ono, K.; Kanno, N.; et al. Control of root system architecture by DEEPER ROOTING 1 increases rice yield under drought conditions. *Nat. Genet.* **2013**, *45*, 1097–1102. [CrossRef]
127. Chen, H.; Ma, B.; Zhou, Y.; He, S.J.; Tang, S.Y.; Lu, X.; Xie, Q.; Chen, S.Y.; Zhang, J.S. E3 ubiquitin ligase SOR1 regulates ethylene response in rice root by modulating stability of Aux/IAA protein. *Proc. Natl. Acad. Sci. USA* **2018**, *115*, 4513–4518. [CrossRef]
128. Li, X.; Wang, Z.; Sun, S.; Dai, Z.; Zhang, J.; Wang, W.; Peng, K.; Geng, W.; Xia, S.; Liu, Q.; et al. IbNIEL-mediated degradation of IbNAC087 regulates jasmonic acid-dependent salt and drought tolerance in sweet potato. *J. Integr. Plant Biol.* **2024**, *66*, 176–195. [CrossRef]
129. Zhang, Q.Y.; Ma, C.N.; Gu, K.D.; Wang, J.H.; Yu, J.Q.; Liu, B.; Wang, Y.; He, J.X.; Hu, D.G.; Sun, Q. The BTB-BACK-TAZ domain protein MdBT2 reduces drought resistance by weakening the positive regulatory effect of MdHDZ27 on apple drought tolerance via ubiquitination. *Plant J.* **2024**, *119*, 283–299. [CrossRef]
130. Mao, K.; Yang, J.; Sun, Y.; Guo, X.; Qiu, L.; Mei, Q.; Li, N.; Ma, F. MdbHLH160 is stabilized via reduced MdBT2-mediated degradation to promote MdSOD1 and MdDREB2A-like expression for apple drought tolerance. *Plant Physiol.* **2024**, *194*, 1181–1203. [CrossRef]
131. Zhou, H.; Shi, H.; Yang, Y.; Feng, X.; Chen, X.; Xiao, F.; Lin, H.; Guo, Y. Insights into plant salt stress signaling and tolerance. *J. Genet. Genom.* **2024**, *51*, 16–34. [CrossRef]
132. Lin, H.; Du, W.; Yang, Y.; Schumaker, K.S.; Guo, Y. A calcium-independent activation of the Arabidopsis SOS2-like protein kinase24 by its interacting SOS3-like calcium binding protein1. *Plant Physiol.* **2014**, *164*, 2197–2206. [CrossRef]
133. Li, J.; Shen, L.; Han, X.; He, G.; Fan, W.; Li, Y.; Yang, S.; Zhang, Z.; Yang, Y.; Jin, W.; et al. Phosphatidic acid-regulated SOS2 controls sodium and potassium homeostasis in Arabidopsis under salt stress. *EMBO J.* **2023**, *42*, e112401. [CrossRef]
134. Du, W.; Lin, H.; Chen, S.; Wu, Y.; Zhang, J.; Fuglsang, A.T.; Palmgren, M.G.; Wu, W.; Guo, Y. Phosphorylation of SOS3-like calcium-binding proteins by their interacting SOS2-like protein kinases is a common regulatory mechanism in Arabidopsis. *Plant Physiol.* **2011**, *156*, 2235–2243. [CrossRef]
135. Zhou, H.; Lin, H.; Chen, S.; Becker, K.; Yang, Y.; Zhao, J.; Kudla, J.; Schumaker, K.S.; Guo, Y. Inhibition of the Arabidopsis salt overly sensitive pathway by 14-3-3 proteins. *Plant Cell* **2014**, *26*, 1166–1182. [CrossRef]
136. Fu, H.; Yu, X.; Jiang, Y.; Wang, Y.; Yang, Y.; Chen, S.; Chen, Q.; Guo, Y. SALT OVERLY SENSITIVE 1 is inhibited by clade D Protein phosphatase 2C D6 and D7 in Arabidopsis thaliana. *Plant Cell* **2023**, *35*, 279–297. [CrossRef]
137. Guo, Y.; Halfter, U.; Ishitani, M.; Zhu, J.K. Molecular characterization of functional domains in the protein kinase SOS2 that is required for plant salt tolerance. *Plant Cell* **2001**, *13*, 1383–1400. [CrossRef]
138. Zhang, Y.; Zhou, J.; Ni, X.; Wang, Q.; Jia, Y.; Xu, X.; Wu, H.; Fu, P.; Wen, H.; Guo, Y.; et al. Structural basis for the activity regulation of Salt Overly Sensitive 1 in Arabidopsis salt tolerance. *Nat. Plants* **2023**, *9*, 1915–1923. [CrossRef]
139. Yu, L.; Nie, J.; Cao, C.; Jin, Y.; Yan, M.; Wang, F.; Liu, J.; Xiao, Y.; Liang, Y.; Zhang, W. Phosphatidic acid mediates salt stress response by regulation of MPK6 in Arabidopsis thaliana. *New Phytol.* **2010**, *188*, 762–773. [CrossRef]
140. Feng, H.; Wang, S.; Dong, D.; Zhou, R.; Wang, H. Arabidopsis Ubiquitin-Conjugating Enzymes UBC7, UBC13, and UBC14 Are Required in Plant Responses to Multiple Stress Conditions. *Plants* **2020**, *9*, 723. [CrossRef]
141. Du, B.; Nie, N.; Sun, S.; Hu, Y.; Bai, Y.; He, S.; Zhao, N.; Liu, Q.; Zhai, H. A novel sweetpotato RING-H2 type E3 ubiquitin ligase gene IbATL38 enhances salt tolerance in transgenic Arabidopsis. *Plant Sci.* **2021**, *304*, 110802. [CrossRef]
142. Du, M.; Lu, D.; Liu, X. The Arabidopsis ubiquitin ligases ATL31 and ATL6 regulate plant response to salt stress in an ABA-independent manner. *Biochem. Biophys. Res. Commun.* **2023**, *685*, 149156. [CrossRef]
143. Kim, J.H.; Jang, C.S. E3 ligase, the *Oryza sativa* salt-induced RING finger protein 4 (OsSIRP4), negatively regulates salt stress responses via degradation of the OsPEX11-1 protein. *Plant Mol. Biol.* **2021**, *105*, 231–245. [CrossRef]
144. Liu, R.X.; Li, S.S.; Yue, Q.Y.; Li, H.L.; Lu, J.; Li, W.C.; Wang, Y.N.; Liu, J.X.; Guo, X.L.; Wu, X.; et al. MdHMGB15-MdXERICO-MdNRP module mediates salt tolerance of apple by regulating the expression of salt stress-related genes. *J. Adv. Res.* **2025**, *79*, 61–74. [CrossRef]
145. Wu, T.; Wang, Y.; Jin, J.; Zhao, B.; Wu, S.; Jia, B.; Sun, X.; Zhang, D.; Sun, M. Soybean RING-type E3 ligase GmCHYR16 ubiquitinates the GmERF71 transcription factor for degradation to negatively regulate bicarbonate stress tolerance. *New Phytol.* **2025**, *246*, 1128–1146. [CrossRef] [PubMed]
146. Xu, Q.; Zhang, X.; Zhao, R.; Li, S.; Liesche, J. UBIQUITIN-CONJUGATING ENZYME34 mediates pyrophosphatase AVP1 turnover and regulates abiotic stress responses in Arabidopsis. *Plant Physiol.* **2025**, *197*, kiaf015. [CrossRef]

147. Liu, M.; Cao, B.; Wei, J.W.; Gong, B. Redesigning a S-nitrosylated pyruvate-dependent GABA transaminase 1 to generate high-malate and saline-alkali-tolerant tomato. *New Phytol.* **2024**, *242*, 2148–2162. [CrossRef]
148. Wei, J.W.; Liu, M.; Zhao, D.; Du, P.; Yan, L.; Liu, D.; Shi, Q.; Yang, C.; Qin, G.; Gong, B. Melatonin confers saline-alkali tolerance in tomato by alleviating nitrosative damage and S-nitrosylation of H+-ATPase 2. *Plant Cell* **2025**, *37*, koaf035. [CrossRef] [PubMed]
149. Liu, W.; Wei, J.W.; Shan, Q.; Liu, M.; Xu, J.; Gong, B. Genetic engineering of drought- and salt-tolerant tomato via Δ1-pyrroline-5-carboxylate reductase S-nitrosylation. *Plant Physiol.* **2024**, *195*, 1038–1052. [CrossRef] [PubMed]
150. Wei, L.; Hou, X.; Feng, L.; Liu, Y.; Kong, Y.; Cui, A.; Qiao, Y.; Hu, D.; Wang, C.; Liu, H.; et al. SERK3A and SERK3B could be S-nitrosylated and enhance the salt resistance in tomato seedlings. *Int. J. Biol. Macromol.* **2024**, *273*, 133084. [CrossRef]
151. Meng, X.; Kang, Z.; Zhang, Y.; Li, Q.; Hu, S.; Zhu, C.; Li, T.; Li, G.; Hu, X. The RING-finger E3 ubiquitin ligase SlMIEL1 interacts with SlNAC35 to regulate JA biosynthesis and mediate saline-alkali stress responses in tomato. *Plant J.* **2025**, *124*, e70598. [CrossRef]
152. Li, Y.; Tian, X.; Liu, T.; Shi, Y.; Li, Y.; Wang, H.; Cui, Y.; Lu, S.; Gong, X.; Mao, K.; et al. MdSINA2-MdNAC104 Module Regulates Apple Alkaline Resistance by Affecting γ-Aminobutyric Acid Synthesis and Transport. *Adv. Sci.* **2024**, *11*, e2400930. [CrossRef]
153. Zhang, W.; Zhi, W.; Qiao, H.; Huang, J.; Li, S.; Lu, Q.; Wang, N.; Li, Q.; Zhou, Q.; Sun, J.; et al. H2O2-dependent oxidation of the transcription factor GmNTL1 promotes salt tolerance in soybean. *Plant Cell* **2023**, *36*, 112–135. [CrossRef]
154. Vishwakarma, K.; Upadhyay, N.; Kumar, N.; Yadav, G.; Singh, J.; Mishra, R.K.; Kumar, V.; Verma, R.; Upadhyay, R.G.; Pandey, M.; et al. Abscisic Acid Signaling and Abiotic Stress Tolerance in Plants: A Review on Current Knowledge and Future Prospects. *Front. Plant Sci.* **2017**, *8*, 161. [CrossRef]
155. Dong, T.; Park, Y.; Hwang, I. Abscisic acid: Biosynthesis, inactivation, homoeostasis and signalling. *Essays Biochem.* **2015**, *58*, 29–48. [CrossRef] [PubMed]
156. Wang, P.; Zhao, Y.; Li, Z.; Hsu, C.C.; Liu, X.; Fu, L.; Hou, Y.J.; Du, Y.; Xie, S.; Zhang, C.; et al. Reciprocal Regulation of the TOR Kinase and ABA Receptor Balances Plant Growth and Stress Response. *Mol. Cell* **2018**, *69*, 100–112.e6. [CrossRef] [PubMed]
157. Rosenberger, C.L.; Chen, J. To Grow or Not to Grow: TOR and SnRK2 Coordinate Growth and Stress Response in Arabidopsis. *Mol. Cell* **2018**, *69*, 3–4. [CrossRef] [PubMed]
158. Chen, H.H.; Qu, L.; Xu, Z.H.; Zhu, J.K.; Xue, H.W. EL1-like Casein Kinases Suppress ABA Signaling and Responses by Phosphorylating and Destabilizing the ABA Receptors PYR/PYLs in Arabidopsis. *Mol. Plant* **2018**, *11*, 706–719. [CrossRef]
159. Zhang, L.; Li, X.; Li, D.; Sun, Y.; Li, Y.; Luo, Q.; Liu, Z.; Wang, J.; Li, X.; Zhang, H.; et al. CARK1 mediates ABA signaling by phosphorylation of ABA receptors. *Cell Discov.* **2018**, *4*, 30. [CrossRef]
160. Ng, L.M.; Soon, F.F.; Zhou, X.E.; West, G.M.; Kovach, A.; Suino-Powell, K.M.; Chalmers, M.J.; Li, J.; Yong, E.L.; Zhu, J.K.; et al. Structural basis for basal activity and autoactivation of abscisic acid (ABA) signaling SnRK2 kinases. *Proc. Natl. Acad. Sci. USA* **2011**, *108*, 21259–21264. [CrossRef]
161. Shang, Y.; Dai, C.; Lee, M.M.; Kwak, J.M.; Nam, K.H. BRI1-Associated Receptor Kinase 1 Regulates Guard Cell ABA Signaling Mediated by Open Stomata 1 in Arabidopsis. *Mol. Plant* **2016**, *9*, 447–460. [CrossRef] [PubMed]
162. Vilela, B.; Nájar, E.; Lumbreras, V.; Leung, J.; Pagès, M. Casein Kinase 2 Negatively Regulates Abscisic Acid-Activated SnRK2s in the Core Abscisic Acid-Signaling Module. *Mol. Plant* **2015**, *8*, 709–721. [CrossRef] [PubMed]
163. Tian, W.; Hou, C.; Ren, Z.; Pan, Y.; Jia, J.; Zhang, H.; Bai, F.; Zhang, P.; Zhu, H.; He, Y.; et al. A molecular pathway for CO_2 response in Arabidopsis guard cells. *Nat. Commun.* **2015**, *6*, 6057. [CrossRef]
164. Cai, Z.; Liu, J.; Wang, H.; Yang, C.; Chen, Y.; Li, Y.; Pan, S.; Dong, R.; Tang, G.; Barajas-Lopez Jde, D.; et al. GSK3-like kinases positively modulate abscisic acid signaling through phosphorylating subgroup III SnRK2s in Arabidopsis. *Proc. Natl. Acad. Sci. USA* **2014**, *111*, 9651–9656. [CrossRef]
165. Hu, R.; Zhu, Y.; Shen, G.; Zhang, H. TAP46 plays a positive role in the ABSCISIC ACID INSENSITIVE5-regulated gene expression in Arabidopsis. *Plant Physiol.* **2014**, *164*, 721–734. [CrossRef]
166. Wang, H.; Tang, J.; Liu, J.; Hu, J.; Liu, J.; Chen, Y.; Cai, Z.; Wang, X. Abscisic Acid Signaling Inhibits Brassinosteroid Signaling through Dampening the Dephosphorylation of BIN2 by ABI1 and ABI2. *Mol. Plant* **2018**, *11*, 315–325. [CrossRef]
167. Mulekar, J.J.; Huq, E. Expanding roles of protein kinase CK2 in regulating plant growth and development. *J. Exp. Bot.* **2014**, *65*, 2883–2893. [CrossRef]
168. Hou, Y.J.; Zhu, Y.; Wang, P.; Zhao, Y.; Xie, S.; Batelli, G.; Wang, B.; Duan, C.G.; Wang, X.; Xing, L.; et al. Type One Protein Phosphatase 1 and Its Regulatory Protein Inhibitor 2 Negatively Regulate ABA Signaling. *PLoS Genet.* **2016**, *12*, e1005835. [CrossRef] [PubMed]
169. Li, G.J.; Chen, K.; Sun, S.; Zhao, Y. Osmotic signaling releases PP2C-mediated inhibition of Arabidopsis SnRK2s via the receptor-like cytoplasmic kinase BIK1. *EMBO J.* **2024**, *43*, 6076–6103. [CrossRef]
170. Bhatnagar, N.; Min, M.K.; Choi, E.H.; Kim, N.; Moon, S.J.; Yoon, I.; Kwon, T.; Jung, K.H.; Kim, B.G. The protein phosphatase 2C clade A protein OsPP2C51 positively regulates seed germination by directly inactivating OsbZIP10. *Plant Mol. Biol.* **2017**, *93*, 389–401. [CrossRef]

171. Zong, W.; Tang, N.; Yang, J.; Peng, L.; Ma, S.; Xu, Y.; Li, G.; Xiong, L. Feedback Regulation of ABA Signaling and Biosynthesis by a bZIP Transcription Factor Targets Drought-Resistance-Related Genes. *Plant Physiol.* **2016**, *171*, 2810–2825. [CrossRef] [PubMed]
172. Wang, X.; Guo, C.; Peng, J.; Li, C.; Wan, F.; Zhang, S.; Zhou, Y.; Yan, Y.; Qi, L.; Sun, K.; et al. ABRE-BINDING FACTORS play a role in the feedback regulation of ABA signaling by mediating rapid ABA induction of ABA co-receptor genes. *New Phytol.* **2019**, *221*, 341–355. [CrossRef]
173. Tan, W.; Zhang, D.; Zhou, H.; Zheng, T.; Yin, Y.; Lin, H. Transcription factor HAT1 is a substrate of SnRK2.3 kinase and negatively regulates ABA synthesis and signaling in Arabidopsis responding to drought. *PLoS Genet.* **2018**, *14*, e1007336. [CrossRef]
174. Zhang, H.; Pei, Y.; Zhu, F.; He, Q.; Zhou, Y.; Ma, B.; Chen, X.; Guo, J.; Khan, A.; Jahangir, M.; et al. CaSnRK2.4-mediated phosphorylation of CaNAC035 regulates abscisic acid synthesis in pepper (*Capsicum annuum* L.) responding to cold stress. *Plant J.* **2024**, *117*, 1377–1391. [CrossRef]
175. Geiger, D.; Scherzer, S.; Mumm, P.; Stange, A.; Marten, I.; Bauer, H.; Ache, P.; Matschi, S.; Liese, A.; Al-Rasheid, K.A.; et al. Activity of guard cell anion channel SLAC1 is controlled by drought-stress signaling kinase-phosphatase pair. *Proc. Natl. Acad. Sci. USA* **2009**, *106*, 21425–21430. [CrossRef]
176. Takahashi, Y.; Ebisu, Y.; Shimazaki, K.I. Reconstitution of Abscisic Acid Signaling from the Receptor to DNA via bHLH Transcription Factors. *Plant Physiol.* **2017**, *174*, 815–822. [CrossRef]
177. Geiger, D.; Scherzer, S.; Mumm, P.; Marten, I.; Ache, P.; Matschi, S.; Liese, A.; Wellmann, C.; Al-Rasheid, K.A.; Grill, E.; et al. Guard cell anion channel SLAC1 is regulated by CDPK protein kinases with distinct Ca^{2+} affinities. *Proc. Natl. Acad. Sci. USA* **2010**, *107*, 8023–8028. [CrossRef]
178. Hua, D.; Wang, C.; He, J.; Liao, H.; Duan, Y.; Zhu, Z.; Guo, Y.; Chen, Z.; Gong, Z. A plasma membrane receptor kinase, GHR1, mediates abscisic acid- and hydrogen peroxide-regulated stomatal movement in Arabidopsis. *Plant Cell* **2012**, *24*, 2546–2561. [CrossRef]
179. Li, X.D.; Gao, Y.Q.; Wu, W.H.; Chen, L.M.; Wang, Y. Two calcium-dependent protein kinases enhance maize drought tolerance by activating anion channel ZmSLAC1 in guard cells. *Plant Biotechnol. J.* **2022**, *20*, 143–157. [CrossRef]
180. Liu, J.; Li, X.D.; Jia, D.; Qi, L.; Jing, R.; Hao, J.; Wang, Z.; Cheng, J.; Chen, L.M. ZmCRK1 negatively regulates maize's response to drought stress by phosphorylating plasma membrane H(+)-ATPase ZmMHA2. *New Phytol.* **2024**, *244*, 1362–1376. [CrossRef]
181. Hõrak, H.; Sierla, M.; Tõldsepp, K.; Wang, C.; Wang, Y.S.; Nuhkat, M.; Valk, E.; Pechter, P.; Merilo, E.; Salojärvi, J.; et al. A Dominant Mutation in the HT1 Kinase Uncovers Roles of MAP Kinases and GHR1 in CO2-Induced Stomatal Closure. *Plant Cell* **2016**, *28*, 2493–2509. [CrossRef]
182. Bueso, E.; Rodriguez, L.; Lorenzo-Orts, L.; Gonzalez-Guzman, M.; Sayas, E.; Muñoz-Bertomeu, J.; Ibañez, C.; Serrano, R.; Rodriguez, P.L. The single-subunit RING-type E3 ubiquitin ligase RSL1 targets PYL4 and PYR1 ABA receptors in plasma membrane to modulate abscisic acid signaling. *Plant J.* **2014**, *80*, 1057–1071. [CrossRef] [PubMed]
183. Yu, F.; Lou, L.; Tian, M.; Li, Q.; Ding, Y.; Cao, X.; Wu, Y.; Belda-Palazon, B.; Rodriguez, P.L.; Yang, S.; et al. ESCRT-I Component VPS23A Affects ABA Signaling by Recognizing ABA Receptors for Endosomal Degradation. *Mol. Plant* **2016**, *9*, 1570–1582. [CrossRef]
184. Xia, F.N.; Zeng, B.; Liu, H.S.; Qi, H.; Xie, L.J.; Yu, L.J.; Chen, Q.F.; Li, J.F.; Chen, Y.Q.; Jiang, L.; et al. SINAT E3 Ubiquitin Ligases Mediate FREE1 and VPS23A Degradation to Modulate Abscisic Acid Signaling. *Plant Cell* **2020**, *32*, 3290–3310. [CrossRef]
185. Yu, F.; Cao, X.; Liu, G.; Wang, Q.; Xia, R.; Zhang, X.; Xie, Q. ESCRT-I Component VPS23A Is Targeted by E3 Ubiquitin Ligase XBAT35 for Proteasome-Mediated Degradation in Modulating ABA Signaling. *Mol. Plant* **2020**, *13*, 1556–1569. [CrossRef]
186. Liu, G.; Liang, J.; Lou, L.; Tian, M.; Zhang, X.; Liu, L.; Zhao, Q.; Xia, R.; Wu, Y.; Xie, Q.; et al. The deubiquitinases UBP12 and UBP13 integrate with the E3 ubiquitin ligase XBAT35.2 to modulate VPS23A stability in ABA signaling. *Sci. Adv.* **2022**, *8*, eabl5765. [CrossRef]
187. Li, Q.; Serio, R.J.; Schofield, A.; Liu, H.; Rasmussen, S.R.; Hofius, D.; Stone, S.L. Arabidopsis RING-type E3 ubiquitin ligase XBAT35.2 promotes proteasome-dependent degradation of ACD11 to attenuate abiotic stress tolerance. *Plant J.* **2020**, *104*, 1712–1723. [CrossRef] [PubMed]
188. Fernandez, M.A.; Belda-Palazon, B.; Julian, J.; Coego, A.; Lozano-Juste, J.; Iñigo, S.; Rodriguez, L.; Bueso, E.; Goossens, A.; Rodriguez, P.L. RBR-Type E3 Ligases and the Ubiquitin-Conjugating Enzyme UBC26 Regulate Abscisic Acid Receptor Levels and Signaling. *Plant Physiol.* **2020**, *182*, 1723–1742. [CrossRef]
189. Kong, L.; Cheng, J.; Zhu, Y.; Ding, Y.; Meng, J.; Chen, Z.; Xie, Q.; Guo, Y.; Li, J.; Yang, S.; et al. Degradation of the ABA co-receptor ABI1 by PUB12/13 U-box E3 ligases. *Nat. Commun.* **2015**, *6*, 8630. [CrossRef] [PubMed]
190. Wu, Q.; Zhang, X.; Peirats-Llobet, M.; Belda-Palazon, B.; Wang, X.; Cui, S.; Yu, X.; Rodriguez, P.L.; An, C. Ubiquitin Ligases RGLG1 and RGLG5 Regulate Abscisic Acid Signaling by Controlling the Turnover of Phosphatase PP2CA. *Plant Cell* **2016**, *28*, 2178–2196. [CrossRef]
191. Julian, J.; Coego, A.; Lozano-Juste, J.; Lechner, E.; Wu, Q.; Zhang, X.; Merilo, E.; Belda-Palazon, B.; Park, S.Y.; Cutler, S.R.; et al. The MATH-BTB BPM3 and BPM5 subunits of Cullin3-RING E3 ubiquitin ligases target PP2CA and other clade A PP2Cs for degradation. *Proc. Natl. Acad. Sci. USA* **2019**, *116*, 15725–15734. [CrossRef]

192. Cheng, C.; Wang, Z.; Ren, Z.; Zhi, L.; Yao, B.; Su, C.; Liu, L.; Li, X. SCFAtPP2-B11 modulates ABA signaling by facilitating SnRK2.3 degradation in Arabidopsis thaliana. *PLoS Genet.* **2017**, *13*, e1006947. [CrossRef]
193. Ali, A.; Kim, J.K.; Jan, M.; Khan, H.A.; Khan, I.U.; Shen, M.; Park, J.; Lim, C.J.; Hussain, S.; Baek, D.; et al. Rheostatic Control of ABA Signaling through HOS15-Mediated OST1 Degradation. *Mol. Plant* **2019**, *12*, 1447–1462. [CrossRef]
194. Cui, X.; Lv, M.; Cao, Y.; Li, Z.; Liu, Y.; Ren, Z.; Zhang, H. NUA and ESD4 negatively regulate ABA signaling during seed germination. *Stress Biol.* **2022**, *2*, 38. [CrossRef]
195. Chang, Y.N.; Wang, Z.; Ren, Z.; Wang, C.H.; Wang, P.; Zhu, J.K.; Li, X.; Duan, C.G. NUCLEAR PORE ANCHOR and EARLY IN SHORT DAYS 4 negatively regulate abscisic acid signaling by inhibiting Snf1-related protein kinase2 activity and stability in Arabidopsis. *J. Integr. Plant Biol.* **2022**, *64*, 2060–2074. [CrossRef]
196. Samuel, M.A.; Mudgil, Y.; Salt, J.N.; Delmas, F.; Ramachandran, S.; Chilelli, A.; Goring, D.R. Interactions between the S-domain receptor kinases and AtPUB-ARM E3 ubiquitin ligases suggest a conserved signaling pathway in Arabidopsis. *Plant Physiol.* **2008**, *147*, 2084–2095. [CrossRef]
197. Zhang, X.; Garreton, V.; Chua, N.H. The AIP2 E3 ligase acts as a novel negative regulator of ABA signaling by promoting ABI3 degradation. *Genes Dev.* **2005**, *19*, 1532–1543. [CrossRef]
198. Kurup, S.; Jones, H.D.; Holdsworth, M.J. Interactions of the developmental regulator ABI3 with proteins identified from developing Arabidopsis seeds. *Plant J.* **2000**, *21*, 143–155. [CrossRef]
199. Liu, H.; Stone, S.L. Cytoplasmic degradation of the Arabidopsis transcription factor abscisic acid insensitive 5 is mediated by the RING-type E3 ligase KEEP ON GOING. *J. Biol. Chem.* **2013**, *288*, 20267–20279. [CrossRef]
200. Stone, S.L.; Williams, L.A.; Farmer, L.M.; Vierstra, R.D.; Callis, J. KEEP ON GOING, a RING E3 ligase essential for Arabidopsis growth and development, is involved in abscisic acid signaling. *Plant Cell* **2006**, *18*, 3415–3428. [CrossRef]
201. Zhang, H.; Cui, F.; Wu, Y.; Lou, L.; Liu, L.; Tian, M.; Ning, Y.; Shu, K.; Tang, S.; Xie, Q. The RING finger ubiquitin E3 ligase SDIR1 targets SDIR1-INTERACTING PROTEIN1 for degradation to modulate the salt stress response and ABA signaling in Arabidopsis. *Plant Cell* **2015**, *27*, 214–227. [CrossRef]
202. Zhang, Y.; Yang, C.; Li, Y.; Zheng, N.; Chen, H.; Zhao, Q.; Gao, T.; Guo, H.; Xie, Q. SDIR1 is a RING finger E3 ligase that positively regulates stress-responsive abscisic acid signaling in Arabidopsis. *Plant Cell* **2007**, *19*, 1912–1929. [CrossRef]
203. Miura, K.; Lee, J.; Jin, J.B.; Yoo, C.Y.; Miura, T.; Hasegawa, P.M. Sumoylation of ABI5 by the Arabidopsis SUMO E3 ligase SIZ1 negatively regulates abscisic acid signaling. *Proc. Natl. Acad. Sci. USA* **2009**, *106*, 5418–5423. [CrossRef]
204. Zheng, Y.; Chen, Z.; Ma, L.; Liao, C. The Ubiquitin E3 Ligase RHA2b Promotes Degradation of MYB30 in Abscisic Acid Signaling. *Plant Physiol.* **2018**, *178*, 428–440. [CrossRef]
205. Lee, H.G.; Seo, P.J. The Arabidopsis MIEL1 E3 ligase negatively regulates ABA signalling by promoting protein turnover of MYB96. *Nat. Commun.* **2016**, *7*, 12525. [CrossRef]
206. Zheng, Y.; Schumaker, K.S.; Guo, Y. Sumoylation of transcription factor MYB30 by the small ubiquitin-like modifier E3 ligase SIZ1 mediates abscisic acid response in Arabidopsis thaliana. *Proc. Natl. Acad. Sci. USA* **2012**, *109*, 12822–12827. [CrossRef]
207. Barbour, H.; Nkwe, N.S.; Estavoyer, B.; Messmer, C.; Gushul-Leclaire, M.; Villot, R.; Uriarte, M.; Boulay, K.; Hlayhel, S.; Farhat, B.; et al. An inventory of crosstalk between ubiquitination and other post-translational modifications in orchestrating cellular processes. *iScience* **2023**, *26*, 106276. [CrossRef]
208. Zhang, Y.; Zeng, L. Crosstalk between Ubiquitination and Other Post-translational Protein Modifications in Plant Immunity. *Plant Commun.* **2020**, *1*, 100041. [CrossRef]
209. Chen, Y.; Hoehenwarter, W. Changes in the Phosphoproteome and Metabolome Link Early Signaling Events to Rearrangement of Photosynthesis and Central Metabolism in Salinity and Oxidative Stress Response in Arabidopsis. *Plant Physiol.* **2015**, *169*, 3021–3033. [CrossRef]
210. Filipčík, P.; Curry, J.R.; Mace, P.D. When Worlds Collide-Mechanisms at the Interface between Phosphorylation and Ubiquitination. *J. Mol. Biol.* **2017**, *429*, 1097–1113. [CrossRef]
211. Dubeaux, G.; Neveu, J.; Zelazny, E.; Vert, G. Metal Sensing by the IRT1 Transporter-Receptor Orchestrates Its Own Degradation and Plant Metal Nutrition. *Mol. Cell* **2018**, *69*, 953–964.e5. [CrossRef]
212. Yasuda, S.; Aoyama, S.; Hasegawa, Y.; Sato, T.; Yamaguchi, J. Arabidopsis CBL-Interacting Protein Kinases Regulate Carbon/Nitrogen-Nutrient Response by Phosphorylating Ubiquitin Ligase ATL31. *Mol. Plant* **2017**, *10*, 605–618. [CrossRef] [PubMed]
213. Yasuda, S.; Sato, T.; Maekawa, S.; Aoyama, S.; Fukao, Y.; Yamaguchi, J. Phosphorylation of Arabidopsis ubiquitin ligase ATL31 is critical for plant carbon/nitrogen nutrient balance response and controls the stability of 14-3-3 proteins. *J. Biol. Chem.* **2014**, *289*, 15179–15193. [CrossRef] [PubMed]
214. Sato, T.; Maekawa, S.; Yasuda, S.; Domeki, Y.; Sueyoshi, K.; Fujiwara, M.; Fukao, Y.; Goto, D.B.; Yamaguchi, J. Identification of 14-3-3 proteins as a target of ATL31 ubiquitin ligase, a regulator of the C/N response in Arabidopsis. *Plant J.* **2011**, *68*, 137–146. [CrossRef]

215. Zhou, J.; Liu, D.; Wang, P.; Ma, X.; Lin, W.; Chen, S.; Mishev, K.; Lu, D.; Kumar, R.; Vanhoutte, I.; et al. Regulation of Arabidopsis brassinosteroid receptor BRI1 endocytosis and degradation by plant U-box PUB12/PUB13-mediated ubiquitination. *Proc. Natl. Acad. Sci. USA* **2018**, *115*, E1906–E1915. [CrossRef]
216. Lu, D.; Lin, W.; Gao, X.; Wu, S.; Cheng, C.; Avila, J.; Heese, A.; Devarenne, T.P.; He, P.; Shan, L. Direct ubiquitination of pattern recognition receptor FLS2 attenuates plant innate immunity. *Science* **2011**, *332*, 1439–1442. [CrossRef]
217. Shahpasandzadeh, H.; Popova, B.; Kleinknecht, A.; Fraser, P.E.; Outeiro, T.F.; Braus, G.H. Interplay between sumoylation and phosphorylation for protection against α-synuclein inclusions. *J. Biol. Chem.* **2014**, *289*, 31224–31240. [CrossRef]
218. Geoffroy, M.C.; Hay, R.T. An additional role for SUMO in ubiquitin-mediated proteolysis. *Nat. Rev. Mol. Cell Biol.* **2009**, *10*, 564–568. [CrossRef]
219. Conti, L.; Nelis, S.; Zhang, C.; Woodcock, A.; Swarup, R.; Galbiati, M.; Tonelli, C.; Napier, R.; Hedden, P.; Bennett, M.; et al. Small Ubiquitin-like Modifier protein SUMO enables plants to control growth independently of the phytohormone gibberellin. *Dev. Cell* **2014**, *28*, 102–110. [CrossRef]
220. Guo, R.; Sun, W. Sumoylation stabilizes RACK1B and enhance its interaction with RAP2.6 in the abscisic acid response. *Sci. Rep.* **2017**, *7*, 44090. [CrossRef]
221. Huang, T.T.; Wuerzberger-Davis, S.M.; Wu, Z.H.; Miyamoto, S. Sequential modification of NEMO/IKKgamma by SUMO-1 and ubiquitin mediates NF-kappaB activation by genotoxic stress. *Cell* **2003**, *115*, 565–576. [CrossRef]
222. Belda-Palazón, B.; Adamo, M.; Valerio, C.; Ferreira, L.J.; Confraria, A.; Reis-Barata, D.; Rodrigues, A.; Meyer, C.; Rodriguez, P.L.; Baena-González, E. A dual function of SnRK2 kinases in the regulation of SnRK1 and plant growth. *Nat. Plants* **2020**, *6*, 1345–1353. [CrossRef]
223. Crozet, P.; Margalha, L.; Butowt, R.; Fernandes, N.; Elias, C.A.; Orosa, B.; Tomanov, K.; Teige, M.; Bachmair, A.; Sadanandom, A.; et al. SUMOylation represses SnRK1 signaling in Arabidopsis. *Plant J.* **2016**, *85*, 120–133. [CrossRef]
224. Bailey-Serres, J.; Parker, J.E.; Ainsworth, E.A.; Oldroyd, G.E.D.; Schroeder, J.I. Genetic strategies for improving crop yields. *Nature* **2019**, *575*, 109–118. [CrossRef]
225. Liu, G.; Lin, Q.; Jin, S.; Gao, C. The CRISPR-Cas toolbox and gene editing technologies. *Mol. Cell* **2022**, *82*, 333–347. [CrossRef]
226. Mou, R.; Niu, R.; Yang, R.; Xu, G. Engineering crop performance with upstream open reading frames. *Trends Plant Sci.* **2025**, *30*, 311–323. [CrossRef]
227. Cardi, T.; Murovec, J.; Bakhsh, A.; Boniecka, J.; Bruegmann, T.; Bull, S.E.; Eeckhaut, T.; Fladung, M.; Galovic, V.; Linkiewicz, A.; et al. CRISPR/Cas-mediated plant genome editing: Outstanding challenges a decade after implementation. *Trends Plant Sci.* **2023**, *28*, 1144–1165. [CrossRef]
228. Kamthan, A.; Chaudhuri, A.; Kamthan, M.; Datta, A. Small RNAs in plants: Recent development and application for crop improvement. *Front. Plant Sci.* **2015**, *6*, 208. [CrossRef]
229. Fang, X.; Li, P. SnapShot: Condensates in plant biology. *Cell* **2024**, *187*, 2894–2894.e1. [CrossRef]
230. Solis-Miranda, J.; Chodasiewicz, M.; Skirycz, A.; Fernie, A.R.; Moschou, P.N.; Bozhkov, P.V.; Gutierrez-Beltran, E. Stress-related biomolecular condensates in plants. *Plant Cell* **2023**, *35*, 3187–3204. [CrossRef]
231. Maruri-Lopez, I.; Chodasiewicz, M. Involvement of small molecules and metabolites in regulation of biomolecular condensate properties. *Curr. Opin. Plant Biol.* **2023**, *74*, 102385. [CrossRef] [PubMed]
232. Hatzianestis, I.H.; Mountourakis, F.; Stavridou, S.; Moschou, P.N. Plant condensates: No longer membrane-less? *Trends Plant Sci.* **2023**, *28*, 1101–1112. [CrossRef]
233. Wu, X.; Su, T.; Zhang, S.; Zhang, Y.; Wong, C.E.; Ma, J.; Shao, Y.; Hua, C.; Shen, L.; Yu, H. N(6)-methyladenosine-mediated feedback regulation of abscisic acid perception via phase-separated ECT8 condensates in Arabidopsis. *Nat. Plants* **2024**, *10*, 469–482. [CrossRef]
234. Zhou, Y.; Niu, R.; Tang, Z.; Mou, R.; Wang, Z.; Zhu, S.; Yang, H.; Ding, P.; Xu, G. Plant HEM1 specifies a condensation domain to control immune gene translation. *Nat. Plants* **2023**, *9*, 289–301. [CrossRef]
235. Tang, Z.; Shi, S.; Niu, R.; Zhou, Y.; Wang, Z.; Fu, R.; Mou, R.; Chen, S.; Ding, P.; Xu, G. Alleviating protein-condensation-associated damage at the endoplasmic reticulum enhances plant disease tolerance. *Cell Host Microbe* **2024**, *32*, 1552–1565.e8. [CrossRef]
236. Eckardt, N.A.; Avin-Wittenberg, T.; Bassham, D.C.; Chen, P.; Chen, Q.; Fang, J.; Genschik, P.; Ghifari, A.S.; Guercio, A.M.; Gibbs, D.J.; et al. The lowdown on breakdown: Open questions in plant proteolysis. *Plant Cell* **2024**, *36*, 2931–2975. [CrossRef]
237. Klionsky, D.J.; Abdel-Aziz, A.K.; Abdelfatah, S.; Abdellatif, M.; Abdoli, A.; Abel, S.; Abeliovich, H.; Abildgaard, M.H.; Abudu, Y.P.; Acevedo-Arozena, A.; et al. Guidelines for the use and interpretation of assays for monitoring autophagy (4th edition). *Autophagy* **2021**, *17*, 1–382. [CrossRef]
238. Luo, M.; Zhu, S.; Dang, H.; Wen, Q.; Niu, R.; Long, J.; Wang, Z.; Tong, Y.; Ning, Y.; Yuan, M.; et al. Genetically-encoded targeted protein degradation technology to remove endogenous condensation-prone proteins and improve crop performance. *Nat. Commun.* **2025**, *16*, 1159. [CrossRef] [PubMed]

239. Li, K.; Crews, C.M. PROTACs: Past, present and future. *Chem. Soc. Rev.* **2022**, *51*, 5214–5236. [CrossRef] [PubMed]
240. Su, Y.; Ngea, G.L.N.; Wang, K.; Lu, Y.; Godana, E.A.; Ackah, M.; Yang, Q.; Zhang, H. Deciphering the mechanism of E3 ubiquitin ligases in plant responses to abiotic and biotic stresses and perspectives on PROTACs for crop resistance. *Plant Biotechnol. J.* **2024**, *22*, 2811–2843. [CrossRef]

Disclaimer/Publisher's Note: The statements, opinions and data contained in all publications are solely those of the individual author(s) and contributor(s) and not of MDPI and/or the editor(s). MDPI and/or the editor(s) disclaim responsibility for any injury to people or property resulting from any ideas, methods, instructions or products referred to in the content.

plants

MDPI

Review

Research Progress on Rice-Blast-Resistance-Related Genes

Biaobiao Cheng [1], Beibei Lv [1], Qiangbing Xuan [1], Yunfang Li [1], Jing Li [1], Weihong Liang [1,2,*] and Junjie Wang [1,2,*]

[1] College of Life Science, Henan Normal University, Xinxiang 453007, China; cbb521970@outlook.com
[2] The Observation and Research Field Station of Taihang Mountain Forest Ecosystems of Henan Province, Xinxiang 453007, China
* Correspondence: liangwh@htu.edu.cn (W.L.); 2019093@htu.edu.cn (J.W.); Tel.: +86-373-3326340 (J.W.)

Abstract

As a staple food crop, *Oryza sativa* L. is not only the basis of global food and nutrition security but also an important cornerstone of national economic development and social stability. However, the growth of rice is often accompanied by the threat of rice blast, which can lead to the death of seedlings or plants before heading. In the later stages of growth, a severe leaf blast infection will reduce the leaf area at the filling stage, thereby reducing the grain yield. The study of rice blast resistance genes and susceptibility genes is a key strategy for controlling the occurrence of rice blast and ensuring sustainable rice production. This paper reviews the impact of rice blast on the global economy and food security in recent years, describes the immune mechanism of rice blast resistance, and introduces the latest progress in related research. At the same time, the main genes of rice blast resistance and the resistance-related genes, as well as the susceptibility genes identified or cloned in recent years, are summarized. This paper also discusses the application of conventional breeding, molecular-marker-assisted breeding, gene editing, and other technologies in rice blast resistance breeding. The problem of accurately finding avirulence genes for *R* genes in current disease-resistant breeding is discussed and explored, aiming to improve rice blast resistance, agronomic traits, and yield in a sustainable way.

Keywords: rice; rice blast; resistance gene; susceptibility genes; breeding

1. Introduction

Oryza sativa L. cultivation worldwide accounts for about 140 million to 157 million hectares, accounting for 90% of the total planting area, as about 50% of the population (mainly in Asia and Africa) relies on it as a staple food, meaning that rice plays an important role in food security [1]. According to the Food and Agriculture Organization (FAO) [2], global food production needs to increase by about 60% by 2050 to meet the needs of the rapidly growing population. However, rice blast is a common disease in the rice-planting process, which reduces global rice production by about 30% every year, and the yield loss can be as high as 50%, posing a serious threat to food security [3]. *R* genes are important components of rice's immune system, specifically recognizing pathogens and activating immune responses (including triggering pattern immunity, triggering immunity, or atypical immune pathways) that confer resistance to rice blast [4]. In this paper, the immune mechanism of rice against rice blast is systematically reviewed, and the resistance-related genes and susceptibility genes, including the main genes, protein kinases, and transcription factors involved in rice's resistance to rice blast, are summarized. At the same time, the application of conventional breeding, molecular marker-assisted breeding, gene editing,

genomics-assisted breeding, rapid breeding, and artificial intelligence combined with these new genomics and biotechnology methods in rice blast resistance breeding is discussed.

2. Molecular Mechanisms of Rice Immunity and Rice Blast Invasion

The survival of rice depends on its innate immune system, which consists of two layers: pathogen-associated molecular pattern (PAMP)-triggered immunity (PTI), and effect-triggered immunity (ETI). PTI is triggered by cell-surface-localized pattern-recognition receptors (PRRs), while ETI is activated by pathogen effector proteins through intracellular localized receptors called nucleotide-binding domain leucine-rich repeats (NLRs) [5]. Once the rice is infected with pathogenic bacteria, the two immunizations of PTI and ETI will be gradually activated to resist the systematic invasion of rice blast. Therefore, in-depth study of plant resistance mechanisms is the key to effective prevention of rice blast.

2.1. Infection Mechanism of Rice Blast Fungus

Magnaporthe oryzae is internationally recognized as the most harmful fungal pathogen with respect to rice; it belongs to the Ascomycota, and it has two types: asexual and sexual, belonging to Botrytis and Ascomycota, respectively [6]. The asexual rice blast fungus mainly uses conidia and hyphae as the source of infection; it has the characteristics of strong infection ability and rapid spread, which can greatly reduce the yield of rice. In severe cases, it is accompanied by no harvest of rice throughout the year [7]. The disease can be divided into four types—seedling blast, leaf blast, panicle blast, and joint blast—according to the different occurrence periods and the different parts damaged by the disease [8].

The conidia of rice blast fungus are transmitted through various media, form dome-shaped appendages after they are born on the surface of rice, and secrete mucus to firmly adhere to the leaf surface in order to invade plant tissues. The attachment continuously absorbs water from the leaf dew and accumulates osmotic fluid. As repolarization progresses, the top of the attachment will produce puncture nails, which will destroy the host cell wall with the help of mechanical force [9]. Subsequently, the penetration hyphae differentiate into bulbous invasive hyphae at the host plasma membrane and secrete effector proteins, which are virulence factors that can suppress the host cell's immune mechanisms [10]. Rice blast fungus invades adjacent cells through plasmodesmata, interferes with the host's nutrient absorption, and leads to cell death—which, in turn, damages the tissue to form lesions. These lesions can produce conidia again and spread through the medium to initiate the next round of infection (Figure 1) [11].

2.2. Mechanisms of Action of PTI and ETI

With the evolution of pathogen populations, rice has gradually formed a variety of defense mechanisms in the host–pathogen co-evolution process. Two kinds of immune systems have been deeply studied and clarified [12]. One is the PTI induced by pathogenic molecules. PRRs on the surface of plant cells can recognize pathogen-associated molecular patterns (PAMPs) secreted by pathogens and trigger non-specific immune responses [13], including the production of reactive oxygen species (ROS) and lignin, as well as the regulation of mitogen-activated protein kinase (MAPK) cascades and defense genes, laying the foundation for the initiation of ETI while inhibiting the virulence of pathogens [14]. The second is the ETI induced by pathogenic bacteria effector proteins. In order to break through PTI, pathogenic bacteria have evolved effectors that can inhibit it, and plants have accordingly evolved *R* genes against effectors, triggering a highly specific immune response called ETI [15]. Rice blast infects rice through its own effectors. The rice *R* gene encodes a resistance protein (R-protein) that specifically recognizes the effector encoded by the rice

blast avirulence gene (AVR) and induces signal transduction (such as MAPK cascades or Ca^{+} bursts) to trigger the defense response of ETI, and the effector becomes a 'non-toxic factor' (Avr protein), resulting in infection failure [16,17]. With the continuous evolution of pathogenic bacteria, the newly generated effectors are often unable to be recognized by the existing *R* genes. In order to cope with this challenge, rice will correspondingly evolve new *R* genes to identify these new effectors and trigger the second or even multiple effector-triggered immunity (ETI) responses, eventually forming a highly dynamic and complex plant immune network (Figure 2) [18].

So far, at least 146 rice blast *R* genes have been identified, and the NLR protein accounts for 86.4% of the total *R* genes in the cloned *R* gene pool, including *Pik* and its alleles *Pik-m*, *Pik-p*, *Piks*, *Pikh*, *Pike*, *Pi1*, *Pikg*, and *Pik-W25* in the *Pik* locus, *Pii* in the *Pi5* and *Pi5* loci, and *Pia* and *Pi-CO39* in the *Pia* locus [19]. Zhai et al. found that rice deubiquitinase *PICI1* is a key hub for plant immunity (PTI and ETI), which activates immunity by deubiquitinating and stabilizing methionine synthase and promoting the methionine–ethylene biosynthesis pathway. Plant immune receptor nucleotide-binding site (NBS)–leucine-rich repeat (LRR) proteins (such as *PigmR*) maintain the activity of methionine–ethylene immune cascade by protecting *PICI1* from the degradation of rice blast effector proteins [20].

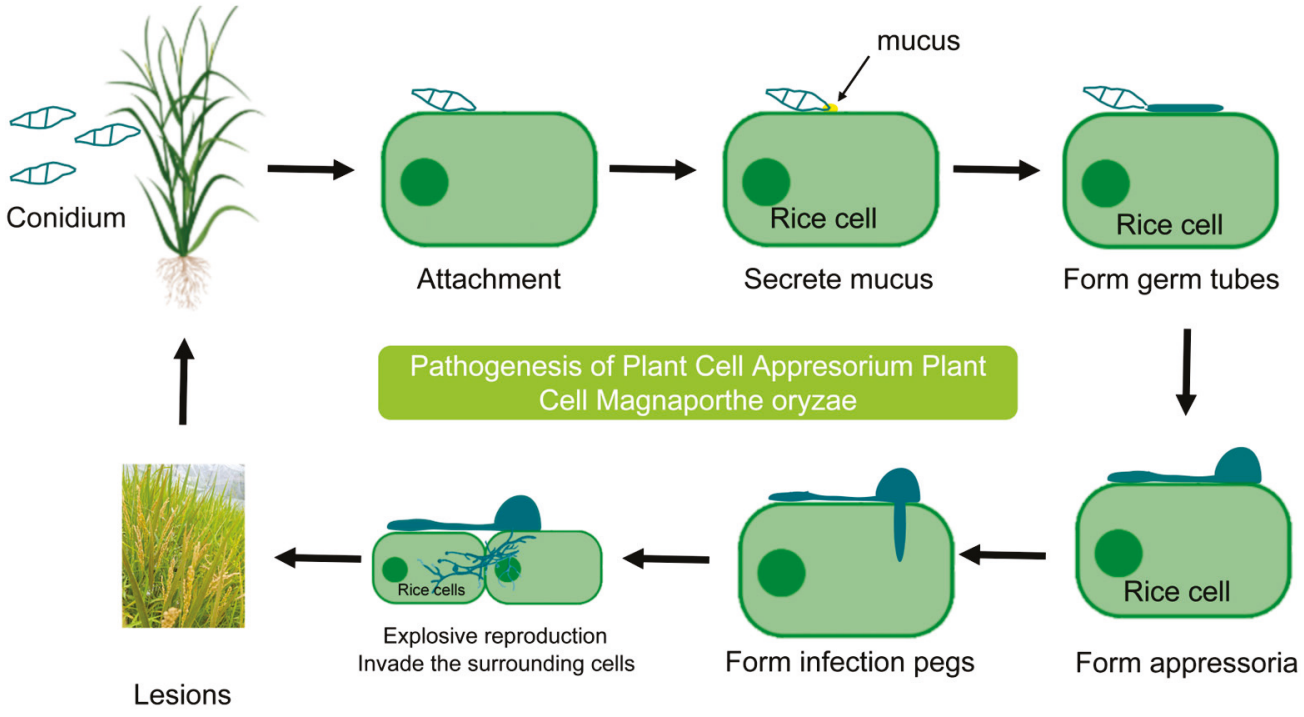

Figure 1. Mechanism of rice blast infection: This figure shows the process of rice blast infection. Conidia adhere to rice leaves through the medium and secrete mucus to form penetrating hyphae, which gradually evolve into spherical infectious hyphae and secrete effector proteins. Conidia invade adjacent cells through plasmodesmata, thereby damaging tissues and forming lesions. The lesions produce conidia again to initiate a new round of infection.

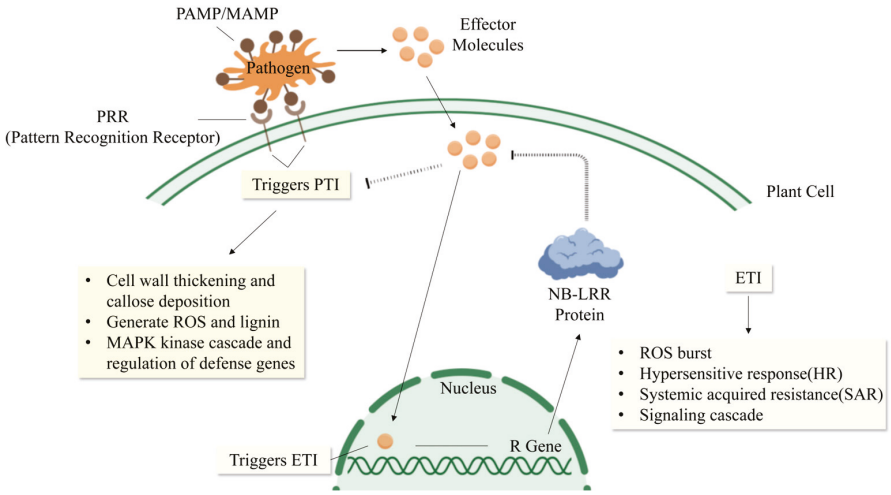

Figure 2. The reaction mechanism of PTI and ETI in rice's innate immune system during rice blast infection [21]: PAMPs secreted by pathogenic bacteria are recognized by PRRs and trigger non-specific immune responses, resulting in a series of physiological responses, such as cell wall thickening and callose deposition, ROS and lignin production, MAPK cascade, and defense gene regulation, triggering the PTI defense response. The effector factors secreted by pathogenic bacteria specifically bind to the *R* gene and induce signal transduction, such as ROS burst, hypersensitive response (HR), systemic acquired resistance (SAR), and signal cascade, triggering the ETI defense response, and making effector proteins non-toxic.

3. Research Progress on Rice Blast Resistance Genes

In recent years, with the development of map-based cloning and genome-wide association analysis techniques, a large number of rice blast resistance genes and their related quantitative trait loci (QTLs) have been successfully excavated and identified. To date, more than 500 rice blast resistance QTLs have been identified, and more than 146 *R* genes have been identified, of which 38 have been molecularly characterized [19,22]. According to the mechanism of rice blast resistance, rice blast resistance-related genes can be divided into major resistance *R* genes, protein kinases, ubiquitin ligases, transcription factors, hormones, miRNA, and secondary metabolic enzymes.

3.1. Mechanism of Rice Blast Resistance Controlled by Major Resistance Genes (R Genes)

By molecular cloning of *R* genes and resistance QTLs, 38 major *R* genes distributed on 10 chromosomes (excluding chromosomes 5 and 7) were identified (Table A1) [23–26]. Based on the structural characteristics of the cloned primitive cell *R* gene and the predicted protein encoded by the resistance QTL, the encoded R proteins can be divided into the following types: The first is the nucleotide-binding site–leucine-rich repeat protein (NBS-LRR), for example, *pi9* is the first cloned major disease resistance gene and broad-spectrum disease resistance gene [27,28]. Zhou et al. identified 13 novel *Pi9* alleles with insertions or deletions from 361 blast-resistant rice varieties; among them, *Pi9-Type3*, *Type4*, *Type5*, *Type6*, *Type9*, *Type10*, and *Type11* can confer broad-spectrum resistance to rice blast [29]. Yu et al. identified a rice blast resistance gene *Pb2* encoding NLR protein by genome-wide association mapping [25]. *Piks* is a new NBS-LRR-*type R gene* cloned from the pick site [26]. The second type is receptor-like kinases (RLKs), such as *pid2* and *pi68*, which encode transmembrane receptor protein kinases with a serine/threonine kinase (STK) domain and have gene-to-gene resistance to rice blast race ZB15 [30,31]. *Pi65* is an LRR-RLK-type gene cloned from the resistant japonica rice variety Gang Yu 129; it is located on chromosome 11 near the telomere side of the *pik* locus [24]. The third class is the repeat-rich protein armadillo (ARM). *Ptr* is an atypical broad-spectrum disease resistance gene cloned in the resistant material Katy,

and it is an allele of *pi-ta2*; its resistance allele *ptr-BHA* is effective against a variety of rice blast fungus races, such as the virulent races *IB-33* and *IE-1* [32,33]. The fourth category is proline-rich proteins. The first cloned *R* gene *pi21* encodes a proline-rich protein, which contains a putative heavy-metal-binding domain and several protein–protein interaction motifs. The deletion of the proline-rich motif in the dominant allele *Pi21* confers resistance to it, indicating that there is a unique mechanism of loss of function in partial resistance of plants [34]. Meanwhile, bsr-d1 encodes a *C_2H_2-type* transcription factor. Inhibition of *bsr-d1* expression can reduce the degradation of H_2O_2 and increase the accumulation of H_2O_2 in cells to enhance rice blast resistance [35].

Most of the cloned resistance genes were clustered on chromosomes 1, 6, 9, and 11 (Figure 3), and most of them were obtained by map-based cloning of the known *R* gene alleles, while the resistance genes on other chromosomes usually existed in the form of independent genes [26,36–38]. In the *pi5*, *pik*, and *pia* gene clusters, all of the resistance genes are controlled by double-gene multi-alleles. One gene is responsible for pathogen recognition, which, in turn, activates the other gene to perform a disease resistance function [26,36–38]. Among the cloned resistance genes, the resistance gene loci determined by the LRR allele are mainly *pish*, *pi9*, *pid3*, *pi36*, and *pi-ta*. Some rice blast resistance genes, such as *pi2*, *pi5*, *pi9*, *pi54*, *pigm*, *pizt*, *pi50*, *pi56*, *pi64*, *pi68*, and *ptr*, showed broad-spectrum resistance to physiological races from various rice regions in the world, but most of these genes were only resistant to leaf blast. Only a limited number of *R* genes, such as *pb1*, *pi25*, *pi64*, and *pi68*, could effectively control panicle blast, among which *pi25*, *pi64*, and *pi68* were resistant to both leaf blast and panicle blast [29,31,39].

3.2. Resistance Mechanism of Rice Blast Controlled by Protein Kinases

As the first barrier against a variety of pathogens, the cell membrane has evolved a class of transmembrane receptors that can specifically recognize microbial-related molecules such as bacterial flagellin and fungal chitin [40]. A series of downstream immune responses are activated by receptor recognition, which is commonly referred to as PTI [13]. PTI plays a defensive role through a variety of immune pathways, including calcium influx, MAPK cascade reaction, RLK signal transduction, ROS burst, plant hormone signaling pathways, transcription reprogramming, cell wall enhancement, and synthesis and secretion of antibacterial compounds. Among them, protein kinases such as RLKs, receptor-like cytoplasmic kinases (RLCKs), MAPKs, and calcium-dependent protein kinases (CDPKs) play a central role in mediating rice blast resistance [41].

RLKs transmit signaling molecules to cellular mechanisms and initiate signaling pathways. Genome-wide association analysis showed that there were 125 wall-associated kinase (WAK/WAKL) family members in the rice genome, of which 67 encoded WAK-type receptor kinases (WAK-RLKs), some of which were confirmed to be involved in rice blast resistance [42]. For example (Figure 4), *OsWAK1* can phosphorylate itself and the transcription regulator *OsRFP1*, and its expression can be induced by infection, mechanical damage, salicylic acid (SA), and methyl jasmonate (MeJA) treatment. The overexpression of *OsWAK1* significantly increased the resistance of rice to rice blast [43]. In addition, the early transcriptional regulation of *OsWAK91* and *OsWAK92* genes was induced by chitin under the regulation of the CEBiP receptor. *OsWAK91* is involved in the production of H_2O_2 and promotes the expression of rice blast resistance genes [44]. Overexpression of *OsWAK5* increased lignin content, enhanced rice blast resistance, and reduced the lesion area and pathogen load, and the defense-related gene oschitinase3 was significantly upregulated in overexpression lines [45]. For example, *OsWAK112d* negatively regulates rice's resistance to rice blast infection and is a negative regulator of disease resistance [44]. *Pi21* encodes a protein rich in proline and cysteine [34], and *ptr* encodes a protein containing an armadillo

repeat sequence, which is required for broad-spectrum blast resistance [33]. However, these two proteins have not been characterized in terms of their biochemical function. The *DR* genes/alleles that have been identified as having broad-spectrum resistance to rice blast include *bsr-k1* (broad-spectrum resistance-*Kitaake 1*), *bsr-d1* (broad-spectrum resistance-*Digu 1*), and *IPA1*. *Bsr-k1* encodes an RNA-binding protein that regulates RNA turnover of phenylalanine ammonia lyase (PAL) family genes [34]. *IPA1* encodes a squamous promoter-binding protein-like (SPL) transcription factor (TF), which activates defense-related *WRKY45* during rice blast fungus infection [46]. *OsBDR1* encodes a receptor-like kinase that phosphorylates the mitogen-activated protein kinase MPK3 to form a molecular module that negatively regulates the biosynthesis of jasmonic acid resistance hormones and terpene phytoalexins, thereby negatively regulating rice blast resistance [47].

U-box E3 ligase *SPL11* negatively regulates plant programmed cell death (PCD) and immunity. SPL11 cell death inhibitor *SDS2* encodes an S-domain receptor-like kinase. *SDS2* interacts with U-box E3 ligase *SPL11* and phosphorylates *SPL11*. *SDS2* mutation leads to reduced immune response and enhanced susceptibility to rice blast in rice. In addition, *SDS2* interacts with two receptor-like cytoplasmic kinases *OsRLCK118/176*, stimulating the production of reactive oxygen species by phosphorylating NADPH oxidase *OsRbohB*, thereby positively regulating immune responses and increasing resistance to rice blast. Therefore, the plasma membrane retention protein complex composed of *SDS2*, *SPL11*, and *OsRLCK118/176* controls the PCD and rice blast immune responses in rice [48].

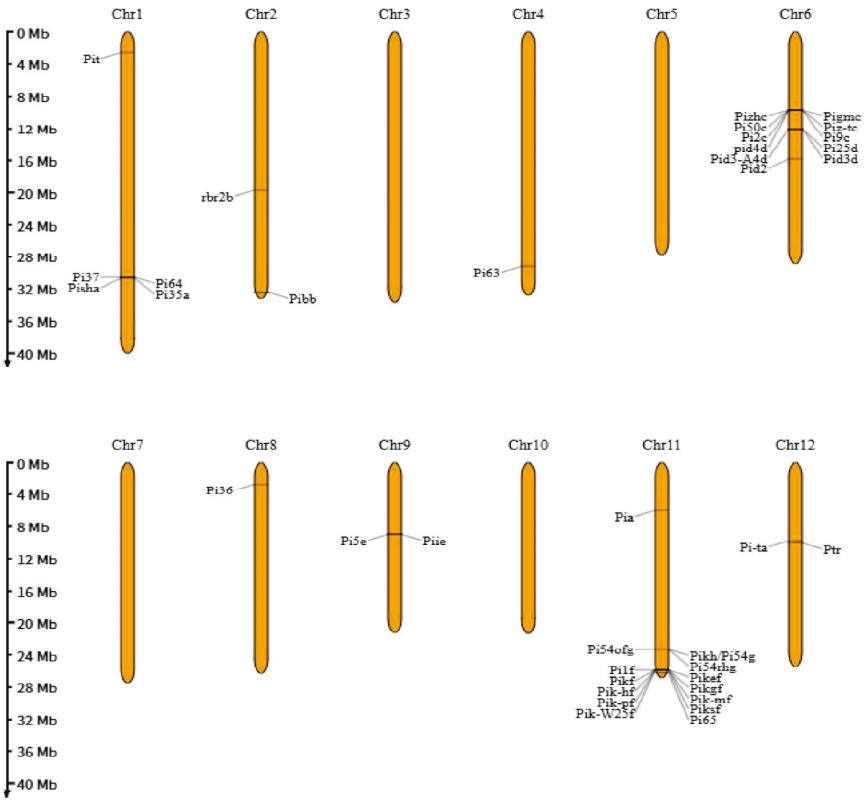

Figure 3. Distribution of the cloned R gene in chromosomes.

CDPK is an important hub of plant calcium signal transduction and plays a crucial regulatory role in the immune response of rice. Studies [49] have shown that *OsCPK4* is involved in the signal cascade after pathogen recognition and exerts a defensive effect by inhibiting fungal penetration. When *OsCPK4* is constitutively activated, the defense signal can respond more quickly and strongly, significantly improving rice blast resistance.

Another protein kinase, *OsCPK10* can not only autophosphorylate but also phosphorylate casein in a calcium-dependent manner, which may regulate disease resistance by activating SA and jasmonic acid (JA) dependent defense genes [50]. CDPKs regulate the downstream elements of the Ca signaling pathway. Studies on the overexpression and knockout of the rice CDPK gene *OsCPK12* showed that *OsCPK12* showed higher susceptibility to rice blast by reducing the accumulation of ROS and enhancing the sensitivity to abscisic acid (ABA) [51]. Li et al.'s study revealed the molecular mechanisms of two calmodulin kinases (*OsCPK18* and *OsCPK4*) in the IV subfamily of rice in regulating the balance of rice growth and disease resistance [52]. Studies [53] have shown that the calcium-dependent protein kinase *OsCPK18* is both a kinase and a substrate of the mitogen-activated protein kinase *OsMPK5*, and that the two can be phosphorylated. Transcriptome analysis showed that the *CPK18-MPK5* signaling pathway inhibited the expression of growth- and disease-resistance-related genes and negatively regulated rice blast resistance. Using Clustered Regularly Interspaced Short Palindromic Repeats (CRISPR/Cas9) to edit the phosphorylation sites of this process, rice lines with both high yield and disease resistance can be obtained [52]. The CRISPR/Cas9 system, as a powerful, efficient, and versatile genome-editing tool, has demonstrated great potential in breeding crops with enhanced disease resistance. By precisely targeting key susceptibility (S) genes or negative regulators, it enables the development of transgene-free, disease-resistant varieties, thereby helping to circumvent the regulatory challenges associated with genetically modified crops [54]. The Ca^{2+} sensor protein encoded by the rice susceptibility factor rod1 is endowed with rice blast resistance by the natural variant of rod1 caused by single-nucleotide deletion [55]. The expression level of the peroxidase-related gene *Os10g39170* plays a key role in rice blast resistance. Studies have shown that the expression of this gene can negatively regulate the level of H_2O_2 in rice, thereby weakening the resistance of rice to rice blast [35].

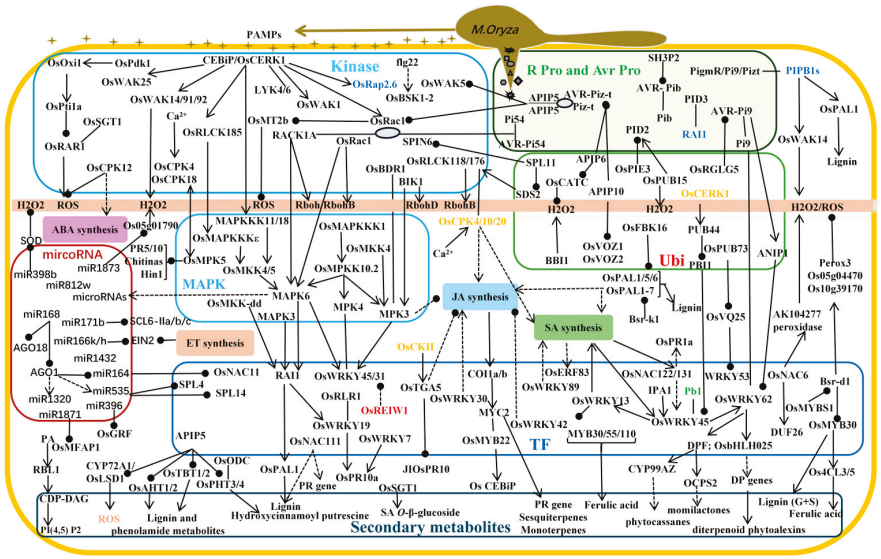

Figure 4. Mechanism of rice blast resistance mediated by disease-related genes: rice blast resistance working model mediated by protein kinase; ubiquitin ligase *APIP5*- and *APIP10*-mediated rice blast resistance working model; transcription factor *OsMYB30*-mediated rice blast resistance working model; rice blast resistance working model mediated by small RNAs miR1871 and miR369; plant hormone-mediated rice blast resistance working model. Note: triangular arrows represent promotion; the circular arrow represents inhibition; the straight line represents the interaction; the dotted line representation mechanism is not clear; the hollow circle represents several genes that can interact with one another.

MAPKs are a class of intracellular serine/threonine protein kinases that are highly conserved in eukaryotic cells. Rice MAPK cascades play a crucial role in regulating rice's resistance to rice blast. *OsMAPKKKε* is an early kinase in MAPK cascade, which interacts with and phosphorylates *OsMKK4*. *OsRLCK1* enhances the phosphorylation of *OsMAPKKKε* by phosphorylating and activating *OsRLCK185* (Figure 4) [56]. The expression of the *SMG1*-encoded kinase *OsMKK4* leads to the shift in metabolic flux from glycolysis to the biosynthesis of secondary metabolites, and it depends on *OsMPK6* to induce cell death, diterpene phytoalexin and lignin synthesis, etc., to enhance rice blast resistance, but it does not cause extracellular ROS production [57].

Some other types of kinases also play an important role in the process of rice blast resistance. For example, casein kinase II *OsCk2α2* can interact with the negative regulator of rice blast resistance *OsTGA5*, reduce the transcriptional inhibition of *OsTGA5*, and enhance the resistance to rice blast [58]. The interaction or antagonism between *RAR1* and *SGT1* plays an important role in the immune system of plants [57].

3.3. Partial Resistance Mechanism of Rice Blast Controlled by Ubiquitin Ligases

The ubiquitin–proteasome system (UPS) determines the stability of intracellular proteins and plays an important role in the PTI and ETI immune responses against rice blast [59]. *APIP6*, *APIP10*, *OsRGLG5*, and *OsBBI1* of the RING family belong to E3 ubiquitin ligase (Figure 4). *APIP6* promotes flg22-induced ROS accumulation by targeting the rice blast fungus effector *Avr-piz t* and rice's own *OsCatC*. In vitro, *APIP6* ubiquitinates *Avrpiz-t* in the form of a homodimer, and *Avrpiz-t* feedback can inhibit the enzyme activity of *APIP6* [60,61]. *APIP10* can negatively regulate the basic resistance to rice blast fungus and positively regulate the ETI response mediated by the NLR protein *piz-t* by ubiquitinating the transcription factors *OsVOZ1* and *OsVOZ2* [62]. *OsRGLG5* degrades the effector *Avrpi9* via ubiquitination during rice blast fungus infection. *Avrpi9* can also initiate feedback to reduce the stability of the *OsRGLG5* protein [63]. By promoting the deposition of H_2O_2 and phenolic compounds in the cell wall, OsBBI1 significantly thickens the cell wall, thereby conferring broad-spectrum resistance to rice blast [64].

The UPS plays an important role in regulating plants' PTI and ETI immune responses by maintaining the stability of immune-related proteins in the regulation of rice blast resistance. Through the identification of rice blast-sensitive genes, it was found that the F-box E3 ligase *OsFBK16* was the core interaction protein of the phenylalanine ammonia lyase family *OsPAL1~7*, revealing the molecular mechanism of *OsFBK16* negatively regulating rice blast resistance by degrading *OsPALS* [65]. The E3 ubiquitin ligase *OsPIE3* negatively regulates rice blast resistance mediated by the receptor-like kinase *pid2*. *OsPIE* promotes the recruitment of *pid2* from the plasma membrane to the nucleus by changing the subcellular localization of *pid2*, and it relies on the ubiquitin–protease system to achieve the degradation of *pid2*. Compared with the wild type, the resistance of the *OsPIE3* deletion mutant to the rice blast fungus race *ZB15* is enhanced, while the resistance of the *OsPIE3* overexpression line is significantly weakened [66].

3.4. Mechanism of Rice Blast Resistance Controlled by Transcription Factors

TF, also known as trans-acting factor, is activated by intracellular signal transduction when rice is infected with rice blast fungus, and then it regulates the expression of a series of stress-response genes, thereby mediating the resistance to rice blast [42]. At present, it has been reported that there are three main types of transcription factors related to rice blast resistance: WRKY transcription factors, MYB transcription factors, and NAC transcription factors (Figure 4).

WRKY transcription factors can directly or indirectly participate in two or more stress responses and have important biological functions. The transcription factor *OsWRKY31* is regulated by phosphorylation and ubiquitination; it can form a ternary complex with *OsMKK10-2* and *OsMPK3* and interact with them for phosphorylation, which can increase the expression of disease resistance-related genes and the accumulation of SA and JA; it can also be ubiquitinated by the E3 ubiquitin ligase *OsREIW1* to promote its degradation, but the phosphorylation of *OsWRKY31* alleviates its degradation [67].

WRKY45 is a key regulator involved in the immune response to rice blast and bacterial blight in rice. In the absence of pathogen infection, the ubiquitin ligase PUB44 is phosphorylated in an oscerk1-dependent manner, which, in turn, mediates the degradation of *PBI1*. The phosphorylation of *WRKY45* by MAPK and the degradation of *PBI1* completely activate *WRKY45* [68]. *OsWRKY45-1* and *OsWRKY45-2* are two alleles, and their coding products are only 10 amino acids different. Both alleles play a positive regulatory role in rice blast resistance [69]. *OsWRKY45-1* enhances rice's resistance to pathogens by regulating the expression of defense-related genes and promoting the accumulation of SA and JA. *WRKY45-2* can transcriptionally activate *WRKY13*, while *WRKY13* directly inhibits *WRKY42*, which constitutes a sequential transcriptional regulatory cascade. Finally, *WRKY42* negatively regulates the defense response of rice to rice blast fungus by inhibiting genes related to the JA signaling pathway (Figure 4) [68].

Studies have shown that *bsr-d1* can indirectly negatively regulate the expression of *OsMYB30*, and that *OsMYB30* promotes the significant thickening of epidermal sclerenchyma cells by regulating the accumulation of 4-coumaric acid, thereby inhibiting the invasion of rice blast fungus at the early stage of infection [70,71].

The *bZIP* transcription factor *APIP5* is a negative regulator of cell death and rice immunity. It was found that, on the one hand, *APIP5* can form homodimers and interact with the fungal effector *Avrpiz-t* in the cytoplasm to promote the entry of rice blast fungus into the dead-body nutrition stage. The resistance gene *Piz-t* promotes the accumulation of APIP protein by binding to *APIP5*, thereby inhibiting cell necrosis and blocking the transformation of rice blast fungus from the living nutrition stage to the dead nutrition stage. On the other hand, *APIP5*, as a transcription factor, can directly bind to the promoters of cell wall-related kinase *OsWAK5*, cytochrome P450 CYP72A1, putrescine hydroxycinnamoyl transferase *OsPHT4*, agmatine hydroxycinnamoyl transferase genes *OsAHT1/OsAHT2*, tryptamine hydroxycinnamoyl transferase genes *OsTBT1/OsTBT2*, and tyramine hydroxycinnamoyl transferase genes *OsTHT1/OsTHT2*, inhibiting their transcription [45].

NAC transcription factors are among the plant-specific transcription factors. *OsNAC6* is one of them, which is highly similar to the ATAF subfamily; it is induced under abiotic stress and fungal disease infection, and its overexpression can significantly reduce the degree of rice blast infection [72]. Sun et al. identified two homologous genes of rice NAC transcription factors, *OsNAC122* and *OsNAC131*, which can regulate the expression of other defense and signal-related genes and play an important role in rice's disease resistance [73]. The rice transcription inhibitor *MYBS1* binds to the *bsr-d1* promoter and reduces the expression of *bsr-d1*, which inhibits the degradation of hydrogen peroxide, leads to the accumulation of H_2O_2, and confers resistance to rice blast [4]. *ERF922* encodes an Apetala2/ethylene response factor (AP2/ERF) transcription factor and is induced by rice blast. Knockout of *ERF922* can enhance the resistance of rice to rice blast, indicating that this gene plays a negative regulatory role in disease resistance [74].

3.5. Partial Resistance Mechanism of Rice Blast Controlled by microRNA

MicroRNAs (miRNAs) can bind to Argonautes (AGO protein family) to form the RNA-induced silencing complex (RISC), which targets specific mRNAs in a sequence-

complementary manner and inhibits gene expression via transcriptional cleavage or translational inhibition [75]. Studies have shown that miRNA is one of the important mechanisms regulating plants' growth, development, and defense through target gene expression [76,77]. For example, the polycistronic miRNAs of the miR166 family members mir166k and miR166h play the role of positive rice immune regulators by regulating the expression of the ethylene signaling pathway gene EIN2 [78]. Recently, Li et al. found that overexpression of mir171b in rice plants (Ox171b) not only enhanced their rice blast resistance and defense response but also delayed their heading date. The mutants of the target genes *SCL6-IIa*, *SCL6-IIb*, and *SCL6-IIc* of *miR171b* have similar phenotypes to *Ox171b*, indicating that mir171b coordinates yield, growth period, and rice blast resistance by regulating the *SCL6-II* gene (Figure 4) [79].

Mir168 targets AGO1, a key component of the RISC. Overexpression of mir168 in rice significantly inhibited the mimic target of AGO1-miR168 (mim168), weakened the negative regulation of miR168 on AGO1, and thereby enhanced the resistance of rice to rice blast, while promoting the increase in tillers, shortening the growth period, and increasing the yield [80].

Not only have recent studies have found that mir168 targets AGO1, an important component of the RNA-induced silencing complex, but also bioinformatics prediction and gene expression analysis have confirmed that *OsAGO18* is a potential target gene. KEGG enrichment analysis showed that osmir168 was involved in many key biological processes, such as plant hormone signal transduction and plant–pathogen interaction [81]. *OsMFAP1* encodes a microfilament-related protein located near the cell wall and can positively regulate the PTI response. However, mir1871 reduced rice blast resistance by inhibiting the expression of *OsMFAP1*. Inhibition of mir1871 function and overexpression of OsMFAP1 can enhance the PTI response of rice, thereby significantly improving its resistance to rice blast [82]. Mir396 can target the expression of growth regulators and negatively regulate the resistance of rice to rice blast by inhibiting a variety of *OsGRF*, thereby differentially controlling the growth and yield of rice [83].

3.6. Partial Resistance Mechanism of Rice Blast Controlled by Plant Hormones

Plant hormones are signaling molecules that are produced at extremely low concentrations in plants and can trigger physiological effects; they are involved in the regulation of various stages of plants' growth and development. With the deepening of plant biology research, it has been confirmed that plant hormones play an important role in plants' disease resistance and stress resistance [84].

Phospholipids are essential components of biofilm formation and are involved in various biological and physiological processes, including cell development and responses to biotic and abiotic stresses. It has been found that the cytidine diphosphate diacylglycerol synthase RBL1 is a key enzyme in phospholipid biosynthesis; as a cytidine diphosphate glycerol (CDP-DAG) synthase, it plays an important role in the synthesis of phosphatidylinositol and can regulate programmed cell death and immune response (Figure 4) [85]. In addition, phospholipid inositol diphosphate ($PtdInsP_2$) is localized in rice as a disease susceptibility factor, especially in the enrichment of infection-specific structures, such as the biotype-interacting complex (BIC) and extra-invasive hyphal membrane (EIHM) [85]. Zhou et al. found that *bsr-k1* encodes a tetratricopeptide repeat (TPR) protein with RNA-binding activity, which can bind to the mRNAs of multiple members of the immune response-related *OsPAL* family (*OsPAL1-7*), promote the folding and degradation of these mRNAs in rice, and weaken the immune response of rice by reducing the synthesis of lignin. Single-base mutation leads to the loss of function of the *bsr-k1* protein, which greatly reduces its ability to bind to *OsPAL* gene mRNA, thereby

significantly increasing the mRNA expression of *OsPAL* family genes, promoting lignin synthesis, and enhancing the immune response. This variation confers broad-spectrum resistance to rice [34]. Meng et al. [86] identified an activator *OsbHLH6* that activates JA signaling and inhibits SA signaling pathways within 24 h after rice blast infection, thereby reducing rice blast resistance. After 24 h, osnpr1 induced *OsbHLH6* export from the nucleus to the cytosol and inhibited *OsbHLH6*-mediated JA and SA signaling activation, thereby conferring resistance to rice blast. *OsTrxm* plays an important role in the redox regulation of chloroplasts, and RNAi treatment will increase the content of H_2O_2. The interaction between *OsMESL* and *OsTrxm* can synergistically negatively regulate the production of ROS and JA [87].

JA plays an important role in plants' growth, development, senescence, and various stresses. JA participates in and regulates the disease resistance mechanisms of plants in the form of defense signaling molecules. For example, when rice blast fungus infection occurs, overexpression of the transcription factor *WRKY30* activates the expression of the JA synthesis-related genes *LOX* and *AOS2*, the pathogen-related genes *PR3* and *PR10*, and the accumulation of endogenous JA under the stress of pathogenic fungi [88].

At 22 °C, JA synthesis decreased, while at 28 °C, rice blast fungus induced JA synthesis and activated the JA signaling pathway, which improved rice disease resistance [71]. Therefore, the application of MeJA in a warm environment can improve the resistance of rice to rice blast by activating the disease resistance mechanism, which makes it a commonly used drug for the prevention and control of rice blast.

ABA plays an important role in many physiological processes of plants' life cycle. ABA is closely related to the establishment of seed dormancy, seed germination, root development, reproductive growth, abiotic stress response, resistance to pathogen invasion, and induction of stomatal closure [89]. ABA is considered to be a negative regulator of rice blast resistance. Exogenous application of ABA and low temperatures will increase the sensitivity of rice blast-susceptible varieties. So far, the molecular and biochemical mechanisms associated with ABA-mediated susceptibility to rice blast remain unclear [90]. Due to the inhibition of systemic acquired resistance (SAR) mediated by the SA, JA, and ET signaling pathways, excessive production of ABA in plants may adversely affect their disease resistance [91]. For example, the ETI signaling pathway regulator *OsEIL1* in rice can bind to the promoters of the nicotinamide adenine dinucleotide phosphate oxidase gene *OsRboh* and the JA biosynthesis gene *OsOPR4* and activate their expression, thereby promoting ROS accumulation [92].

3.7. Resistance Mechanism of Rice Blast Controlled by Secondary Metabolites

Secondary metabolites play a crucial role in plants' resistance to external invasion; they are not only an important guarantee for plant life activities—such as plant hormones (IAA, GA), photosynthetic pigments (carotenoids), and anthocyanins (volatile substances attract insects to pollinate)—but also a protective barrier for plants against external threats, such as polyphenol tannins, which are toxic to animals or microorganisms but harmless to plants themselves. Secondary metabolites often become important drugs or industrial raw materials. For example, secondary metabolites (flavonoids) regulate oxidative stress. Flavonoids can balance ROS and directly kill pathogens, while avoiding the impact of excess ROS on host cells. Superoxide dismutase (SOD) is involved in the synthesis of lignin and the crosslinking of cell wall components to enhance the structural resistance of plants' physical barriers. SOD, aldehyde oxidase (AOX), catalase (CAT), etc., can remove excessive ROS and maintain intracellular homeostasis [87].

PAL is a key rate-limiting enzyme in phenylpropanoid metabolism; it regulates the rate of phenylalanine entering the phenylpropanoid metabolic pathway and affects the

accumulation of secondary metabolites such as lignin, flavonoids, isoflavones, alkaloids, and benzoate glycosides in plants. The expression of the agmatine hydroxycinnamoyl transferase genes *OsAHT1*/*OsAHT2* and tryptamine hydroxycinnamoyl transferase genes *OsTBT1*/*OsTBT2* was induced by rice blast infection; the contents of phenolic metabolites and lignin in rice were increased, the fungal biomass was decreased, the transcription levels of the defense-related genes *OsChitinase3* and *OsPR10* were increased, and the resistance of rice to rice blast was enhanced [93]. As a damage-associated molecular pattern (DAMP), the receptor *OsCERK1* on rice cell membranes can recognize the endoglucanase secreted by rice blast fungus to degrade the hemicellulose of rice cell walls and activate rice's cellular immune response [94]. Shen et al. used a metabolite-based genome-wide association study (GWAS) to find that the tyramine hydroxycinnamoyl transferase genes *OsTHT1* and *OsTHT2* are involved in the metabolic accumulation of hydroxycinnamic acid, hydroxycinnamaldehyde, hydroxycinnamyl alcohol, flavonoids, and phytoalexin, thereby mediating disease resistance. This is related to the enhancement of phytoalexin and the metabolic reprogramming of the phenylpropanoid pathway. In addition, the expression of the defense signal-related genes *OsPR1a*, *OsPR5*, *OsEDS1*, and *OsCht1* increased with the increase in H_2O_2 content in overexpression lines, while the expression of defense signal-related genes decreased with the increase in H_2O_2 content in double-knockout lines [95].

4. Rice Blast Resistance Breeding

In the 1980s, rice varieties planted in China carried rice blast resistance genes, which could effectively prevent and control rice blast fungus at that time. However, with the emergence of new pathogenic strains (Tables A2 and A3), these genes gradually lost their effectiveness, resulting in a decline in rice's disease resistance. In view of the rapid variation in rice blast fungus, scholars at home and abroad have carried out a lot of research to explore how to effectively use resistance genes to maintain persistent and stable resistance [96]. Researchers have cloned a number of broad-spectrum disease-resistant *R* genes and conducted in-depth research in combination with high-quality varieties [97]. At present, the breeding of resistant varieties can be classified into conventional breeding, molecular-assisted selection breeding, genome-wide selection breeding, and gene-editing breeding.

4.1. Induce Blast Resistance Through Marker-Assisted Selection Breeding

Rice blast resistance breeding mainly adopts cross and backcross methods, including conventional breeding and molecular breeding. Among them, conventional breeding introduces disease resistance genes into varieties through hybridization, such as Huanghuazhan [96], but it has the disadvantages of a long cycle and heavy workload. In recent years, with the development of biotechnology, more and more genes related to rice blast resistance have been cloned. The application of new technologies such as gene editing has brought a breakthrough opportunity for disease resistance breeding. For example, the hybrid rice Tianyou 998 not only has strong resistance to rice blast and bacterial blight but also has excellent rice quality [98]. Kuang Haochi et al. [99] developed an indica restorer line Luhui 37 with high yield and strong resistance through conventional breeding, and they further developed Chuanyouxiang 37. Despite the limitations of conventional and hybrid breeding techniques, they are still the main means of rice blast resistance breeding in China [100].

4.2. Induce Blast Resistance Through Marker-Assisted Selection Breeding

Marker-assisted selection (MAS) technology can transfer one or more target genes to high-quality varieties in a more lasting combination, thus accelerating the integration of rice blast *R* genes in traditional breeding [101]. By identifying and combining multiple resistance

genes, MAS has developed rice lines with broad-spectrum and durable resistance [102]. Transgenic technology introduces known resistance genes into excellent rice varieties through particle bombardment or Agrobacterium-mediated methods to rapidly improve their resistance to rice blast [19].

Jia et al. [101] have made significant progress in identifying the markers of the Rita gene. In order to locate the *Pi66 (t)* gene on chromosome 11, the new PCR markers *WRKY41*, NBS-LRR-970-1, and NBS-LRR-970-2 were developed, and their separation effect with *pi66 (t)* was verified, providing an important tool for related gene screening. The functional marker GM was used to hybridize *R6888* carrying *pigm* and Luoyang 69 carrying *Bph6*/*Bph9*. Combined with molecular genotype screening and agronomic trait phenotypic evaluation, the F pedigree with stable inheritance and excellent traits was screened. Subsequently, the excellent lines were hybridized with thermosensitive genic male sterile (TGMS) lines, the gene pyramiding of *Bph6*, *Bph9*, and *pigm* was successfully achieved, and the restorer lines with high resistance to both rice blast and brown planthopper were developed [103].

In addition, MAS technology is widely used in the management of bacterial blight (BB) in India. Through MAS technology, three BB resistance genes (*Xa21*, *Xa13*, and *Xa5*) were introduced into aromatic short-grain rice (HUR917), and rice varieties with broad-spectrum resistance to BB were successfully cultivated, which further proved the utility of MAS in accelerating trait infiltration [104] (Figure 5).

Ye et al. [105] introduced the rice blast resistance genes *pigm* and *pi-ta*, as well as the aroma gene *Badh2*, into high-quality HR1212 japonica rice via a molecular marker-assisted selection backcross method. The obtained introgression lines not only significantly enhanced the resistance to panicle blast but also improved the yield, while maintaining the excellent taste quality similar to HR1212. The new TPAP functional marker developed by Mao et al. [106] achieved the efficient and accurate detection of these resistance genes and significantly shortened the breeding cycle. Using MAS, three broad-spectrum blast resistance genes (*Pita*, *PibI*, and *Pid2*) were simultaneously introduced into the high-yield japonica rice variety YF47, and an excellent new line (YJ144) was bred. The leaf blast index and the incidence of panicle blast were significantly reduced, and the yield and appearance quality were improved. Wang et al. [107] successfully introduced the broad-spectrum rice blast resistance gene *Pigm* into the excellent thermosensitive genic male sterile line LK638S through molecular marker-assisted selection, which significantly improved its disease resistance, and cultivated an improved line LZ36S with high resistance and excellent agronomic traits and yield potential, along with its derivative hybrid varieties. At the same time, the effectiveness of molecular marker-assisted selection in overcoming the drag of gene linkage and achieving the accurate introduction of target genes was verified, providing an efficient strategy for rice disease resistance breeding. In addition, qi et al. [108] successfully mapped and cloned the new rice blast resistance gene *Pik-W25* by bulked segregant analysis (bsa-seq); its resistance is mediated by *Pik-W25-1* and *Pik-W25-2*, which can recognize *AvrPik-C* and fill the gap in the existing *Pik* allele recognition spectrum. The results of the field experiments showed that the introduction of the *Pik-W25* allele enhanced disease resistance without sacrificing agronomic traits.

These studies emphasize that marker-assisted breeding methods provide new ideas for rice blast resistance breeding in strengthening rice blast management and rice breeding, with the potential to greatly improve resistance to multiple diseases.

4.3. Inducing Rice Blast Resistance by Genomics-Assisted Breeding

Genomics-assisted breeding (GAB) encompasses genome-wide selection breeding and molecular marker-assisted breeding. Genomic selection (GS) breeding is the use of whole-genome sequencing to predict quantitative traits that depend on genotype,

environment, and control by minor genes [109]. Compared with molecular-assisted markers, genome-wide selective breeding has higher efficiency in quantitative traits regulated by multiple genes, and it is not limited by conventional species or hybrids in practical applications. Since the first reference genome of Nippon bare was published in 2005, the Rice Atlas database has been constructed by deep genome resequencing of 6044 modern rice varieties [110,111].

Through genome resequencing of 200 japonica rice varieties in Zhejiang and other places, *piz-t* was identified by GWAS and XPCLR as the main rice blast resistance gene of japonica rice varieties in Central China and had excellent effects on yield and rice quality, leading to the cultivation of varieties *XY99* and *JXY1* with excellent taste, high yield, and broad-spectrum resistance to rice blast [112].

The results showed that 546 rice germplasm resources in Northeast China were analyzed by resequencing, and the genome-wide association analysis of 22 agronomic traits was carried out to construct the molecular model of Northeast China. On this basis, a series of molecular modules—such as the heading date gene Hd1; grain type genes *GW5*, *GS3*, and *GL7*; rice blast resistance genes *pita*, *ptr*, and *pib*; yield trait loci *qSB2*, *qSB8*, and *qSB10*; and lodging resistance gene *SCM2*—were concentrated in the same variety or breeding material, and the rice variety 'Zhongkefa No.5' was successfully bred, achieving the synergistic improvement of high yield, high quality, disease resistance, and lodging, marking breakthrough progress in multi-trait molecular modules [113]. *Pi1*, *pi2*, *piz*, *pi9*, and *pigm* were introduced into the genome of *Kongyu131* by continuous backcrossing and genome-wide selection to produce multi-line varieties with blast resistance [114]. The whole-genome molecular marker-assisted selection technique combined with the conventional backcross breeding method was used to improve the rice blast resistance of Chaoyouqian R900, and an improved R900 line with homozygous resistance genes was obtained. This variety retained its original potential and agronomic traits, and its rice blast resistance was also improved [115].

Feng et al. [116] successfully identified and deeply analyzed the rice blast resistance gene *SBRR1* and its elite allele *SBRR1-R* through a GWAS, revealing its great potential in rice disease resistance breeding. *SBRR1-R* can significantly upregulate gene expression through the specific binding of its promoter to the transcription factor bHLH57, thereby enhancing resistance to rice blast fungus.

Julian R Greenwood et al. [117] successfully identified and verified the novel functional alleles of the rice blast resistance genes *Ptr* and *Pia* via GWAS allele analysis of 3000 rice genomes. The newly identified *Ptrb* allele confers specific resistance to the specific rice blast strains Mo15-23 and Mo15-24. In addition, two new functional alleles of the Pia gene (*RGA4* and *RGA5*) were also identified; they had amino acid changes in the HMA effector-binding domain and could recognize *AVR1-CO39* and *AVR-Pia* effectors, but they did not show a differential resistance response to rice blast isolates.

In the process of molecular breeding, balancing rice yield, disease resistance, and quality is a huge challenge. Using genome-wide selection breeding to improve existing rice varieties rapidly improves their rice blast resistance, yield, and quality, and it can be directly applied to production, providing an important guarantee for food security.

4.4. Induce Blast Resistance Through Gene-Editing Breeding

The rise in gene-editing technology provides a new technical platform for broad-spectrum resistance breeding against rice blast. The CRISPR/Cas9 system, as a rapidly developing gene-editing tool, has shown broad application prospects in the breeding of rice and other crops [97].

The *bsr-d1* gene of Jigeng88 (JG88) was knocked out by CRISPR/Cas9 technology, and the mutant (KO) was obtained. After inoculation with *ZA41*, the level of ROS in the mutant increased significantly, indicating that the *bsr-d1* gene mutation could enhance the resistance to rice blast [118]. In another study, the *SD1* gene was edited by CRISPR/Cas9 and introduced into the variety 'Shuihuai 119' by Agrobacterium-mediated transformation to obtain homozygous mutants. Phenotypic analysis showed that the mutant not only had significantly improved agronomic traits but also had improved resistance to rice blast [119] (Figure 5).

The triple-knockout mutants of the susceptibility genes *pi21*, *bsr-d1*, and *xa5* were constructed by CRISPR/Cas9 technology in the background of japonica rice NPB. Studies have shown that the broad-spectrum resistance of rice to rice blast and bacterial blight after triple-gene mutation is significantly higher than that of single-gene mutation [120].

Against the background of the indica TGMS rice line *Longke638S* (LK638S), the susceptibility genes *pi21*, *bsr-d1*, and *OsERF922* were knocked out by CRISPR/Cas9, and the varieties with enhanced resistance to rice blast and no adverse effects on agronomic traits were successfully cultivated [121] (Figure 5). Some scholars have used CRISPR/Cas9 gene-editing technology to introduce the genes *EPSPS*, *OsLecRK1*, *Bph14*, *Cry1C*, *Xa23*, and *Pi9* into excellent rice varieties to enhance their resistance to rice blast [122].

Xu et al. [123] constructed a co-editing vector pC1300-2 × 35S: Cas9-g^{Pita}-g^{Pi21}-$_{gERF922}$ via CRISPR/Cas9-mediated site-directed editing of the rice blast susceptibility genes *Pita*, *Pi21*, and *ERF922*, obtaining *Pi21* single-mutant homozygous lines and *Pita*, *Pi21*, and *ERF922* triple-mutant homozygous lines with the long-grain japonica restorer line L1014 as the receptor. The results showed that the rice blast resistance of homozygous mutants was improved. Li et al. [124] identified the U-box E3 ubiquitin ligase OsPUB41 as promoting the ubiquitination of OsPALs and further leading to the protein degradation of these key enzymes, which directly inhibited the accumulation of lignin. CRISPR/Cas9 was used to knock out the U-box E3 ubiquitin ligase *OsPUB41* that negatively regulates rice blast resistance, so that *OsPALs* proteins were stabilized and accumulated, thereby enhancing the biosynthesis of lignin and, ultimately, significantly improving the disease resistance of rice. Sha et al. [85] identified the key role of rice's *RBL1* gene in balancing broad-spectrum disease resistance and yield. RBL1 was finely regulated by CRISPR/Cas9 technology, and an excellent allele $RBL1^{\Delta 12}$ was obtained. This gene confers broad-spectrum resistance to rice blast fungus, bacterial blight fungus, and rice false smut fungus, which not only does not lead to a decrease in yield but also shows a significant yield advantage in high-incidence areas. Yu et al. [125] artificially explored the specific function of the *bZIP* transcription factor *OsbZIP76* and constructed *OsbZIP76*-knockout rice lines via CRISPR/Cas9. Compared with the wild type, *OsbZIP76* knockout resulted in a significant increase in the susceptibility of rice to bacterial blight and rice blast. It was revealed that *OsbZIP76* plays an important role in plants' immune activation by positively regulating the expression of defense genes and mediating ABA sensitivity.

Cláudio Bezerra [126] successfully knocked out two specific susceptibility genes in rice using CRISPR/Cas9 gene-editing technology, developing a new rice line with significant resistance to rice blast. Compared with traditional breeding methods, gene-editing technology can introduce resistance traits more accurately and efficiently, and it can overcome the problem of easy loss of resistance in existing resistant varieties.

In summary, CRISPR/Cas9 technology for rice blast resistance breeding shows great potential in the development of new varieties with broad-spectrum disease resistance; it not only provides an important tool for molecular breeding of rice disease resistance but also opens up a new pathway for the enhancement of disease resistance in other crops.

4.5. Assist Rice Blast Resistance Breeding Through AI Technology

Artificial intelligence protein structure prediction tools (such as AlphaFold2, Rosetta Fold, and AlphaFold3) have important potential in the identification and sequencing of disease resistance genes [127]. Advances in genome sequencing and assembly technology have promoted the development of pangenomes, enabling them to be constructed in eukaryotes, fungi, plants, and animals [128]. Compared with a single genome, pangenomes can identify new genes, structural variations, and the presence/absence of variations, and they can track the origin and evolution of gene families related to important agronomic traits such as disease resistance [129].

The interaction between the rice blast *Avr* gene and rice *R* gene was predicted by AlphaFold3. Structural analysis showed that *Avr-pita* could bind to *Pi-ta* through the LRR domain, while *Avr-pik* recognized *OsHIPP19* using the heavy-metal-associated (HMA) domain and interacted with *pi9* through the adjacent LRR domain. Shang et al. [130] systematically analyzed the NBS-LRR genes in the rice pangenome and found that most of the NLR genes exist in their wild ancestor species. Although pangenomics has made great progress, it also faces great challenges in data analysis, computing resources, and experimental verification while revealing genomic diversity [128]. Therefore, these findings enhance the understanding of plant–pathogen interaction mechanisms and contribute greatly to rice blast resistance breeding programs [101].

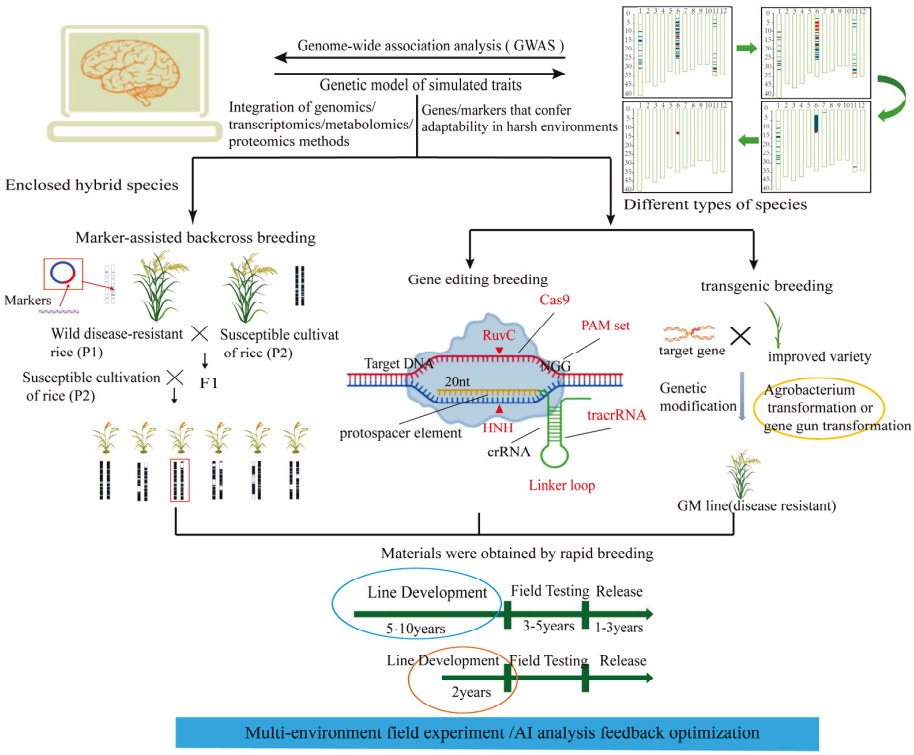

Figure 5. High-quality target genes were selected by rice breeding technology [131,132]. According to the goals and needs, artificial intelligence-assisted breeding and genomics-assisted breeding were used to predict excellent combinations and excellent gene mapping, and then multiple *R* genes were combined by molecular marker-assisted breeding and gene pyramids, and markers were used to quickly screen and locate *R* genes. Then, through gene editing and transgenic breeding, gene modification was carried out to give rice a new shape. Finally, the target new varieties were screened by multi-environment field testing.

5. Conclusions

In recent years, significant progress has been made in rice blast resistance mechanisms and breeding technology. The application of advanced techniques—such as the cloning of broad-spectrum disease resistance genes, the identification of susceptibility genes, and gene editing—has laid a solid foundation for the cultivation of disease-resistant rice varieties. The discovery of disease resistance genes and susceptibility genes not only improves the accuracy of breeding but also deepens the understanding of the immune mechanisms of rice [133]. The cultivation of disease-resistant rice varieties is a rapidly developing field, which benefits from the continuous advancement of genetics and molecular technology. The gene-pair gene model provides a theoretical basis for the interactions between plants and pathogens, and it highlights the direction for the development of breeding strategies to enhance the resistance of rice to major diseases [127]. However, the rapid variation in pathogenic bacteria, the incomplete analysis of some *R* gene resistance mechanisms, and the balance between disease resistance and agronomic traits are still the main challenges.

6. Future Prospects

Although significant progress has been made in the identification and application of *R* genes, the rapid evolution of rice blast fungus has led to the collapse of *R*-gene-mediated resistance. Future research should strengthen multi-trait collaborative genome selection and develop high-resolution, high-throughput functional markers to improve breeding efficiency and resistance persistence. Future research should focus on the systematic analysis of the interaction mechanisms between pathogens and hosts, especially via an in-depth study of the synergistic effects of PTI and ETI. At the same time, atomic-scale insights into the R-*Avr* recognition mechanism in rice and other crops have demonstrated the feasibility of designing synthetic *R* genes with extended pathogen recognition spectra [134]. Since breeding practices are usually centered on simultaneously improving yield and disease resistance, there may already be some crop varieties that have both of these advantages and contain similar genes. However, these varieties and the genes they carry have not been fully studied and elaborated [40]. In terms of opportunities, the integration of cutting-edge technologies such as gene editing, genomics-assisted breeding, rapid breeding, and artificial intelligence will provide unprecedented possibilities for the efficient and accurate breeding of new disease-resistant varieties. Although the CRISPR/Cas9 system still faces challenges such as off-target effects and commercialization barriers, advances in Cas9 protein engineering, optimized gRNA design, and the introduction of novel systems such as Cas13 are gradually addressing these limitations. In the future, by integrating functional genomics, synthetic biology, and systems biology, CRISPR/Cas9 is expected to enable the simultaneous improvement of multiple traits. The future directions of research should focus on the construction of a comprehensive breeding system with broad-spectrum, durable resistance and excellent agronomic traits so as to realize efficient transformation from laboratory results to large-scale promotion, thereby playing a key role in ensuring global rice production safety and food supply.

Author Contributions: Conceptualization, B.C., B.L., Q.X., J.L., Y.L. and J.W.; investigation, B.C.; writing—original draft preparation, B.C.; writing—review, J.W., Q.X. and W.L.; writing—editing, B.C. All authors have read and agreed to the published version of the manuscript.

Funding: This work was funded by the National Natural Science Foundation of China (32201248).

Institutional Review Board Statement: Not applicable.

Informed Consent Statement: Not applicable.

Data Availability Statement: All data are shown in the main manuscript.

Conflicts of Interest: The authors declare no conflicts of interest.

Abbreviations

The following abbreviations are used in this manuscript:

PTI	PAMP-triggered immunity
PAMP	pathogen-associated molecular pattern
ETI	elicit effector-triggered immunity
PRRs	Pattern recognition receptors
NLR	nucleotide-binding domain leucine-rich repeat
PAMP	Pathogen-associated molecular patterns
aROS	reactive oxygen species
MAPK	mitogen-activated protein kinase
AVR	avirulence gene
NBS	nucleotide binding sites
LRR	leucine rich repeat
QTL	quantitative trait locus
NBS-LRR	nucleotide binding site–leucine-rich repeat protein
RLKs	Receptor-like kinase
STK	serine/threonine kinase domain
ARM	Armadillo
RLCK	receptor-like cytoplasmic kinase
CDPKs	Calcium-Dependent Protein Kinases
WAK-RLKs	WAK-type receptor kinases
SA	salicylic acid
MeJA	Methyl Jasmonate
WAK/WAKL	Wall-associated kinases
PAL	Phenylalanine Ammonia-Lyase
SPL	Squamosa promoter-binding protein-like
TF	transcription factors
JA	jasmonic acid
ABA	Abscisic acid
UPS	ubiquitin–proteasome system
miRNAs	MicroRNAs
AGO	Argonaute
RISC	RNA-induced silencing complex
CDP-DAG	cytidine diphosphate glycerol
PtdInsP2	phospholipid inositol diphosphate
BIC	biotype interacting complex
EIHM	Extra-invasive hyphal membrane
TPR	tetratricopeptide repeats
IAA	auxin
GA	gibberellins
SOD	Superoxide Dismutase
AOX	aldehyde oxidase
CAT	Catalase
DAMP	damage-associated molecular patterns
GWAS	Genome-wide association analysis
MAS	Marker-Assisted Selection
GS	Genomic Selection
HR	hypersensitive response
PCD	programmed cell death
CRISPR/Cas9	Clustered Regularly Interspaced Short Palindromic Repeats

Appendix A

Table A1. Summary of the main *R* genes of cloned rice blast in rice.

Gene Name	Coding Protein	Chr	Cloning Method	Donor	Reference
Pit	CNL	1	Map-based cloning	K59	[135]
Pish [a]	NLR	1	Mutagenesis-based cloning	Nipponbarc	[136]
Pi35 [a]	NLR	1	Map-based cloning	Hokkai-188	[137]
Pi37	NLR	1	Map-based cloning	St. No. 1	[138]
Pi64	CNL	1	Map-based cloning	Yangmaogu	[39]
Pib [b]	NLR	2	Map-based cloning	BL1	[28,139]
rbr2 [b]	CNL	2	Map-based cloning	Minghui 63	[140]
Pi63	CNL	4	Map-based cloning	Kahei	[141]
Pid2	B-lectin RLK	6	Map-based cloning	Digu	[30]
Pid3 [d]	NLR	6	Comparative Genomics	MC276	[142]
pid4 [d]	CNL	6	Transcriptome and comparative genomics	Digu	[143]
Pid3-A4 [d]	NLR	6	Allelic mining	A4 (*Oryza rufipogon*)	[144]
Pi25 [d]	NLR	6	Map-based cloning	Gumei2	[145]
Pi9 [c]	CNL	6	Map-based cloning	75-1-127	[27]
Pi2 [c]	CNL	6	Map-based cloning	C101A51	[146]
Piz-t [c]	CNL	6	Map-based cloning	Toride 1	[146]
Pi50 [c]	CNL	6	Map-based cloning	Er-Ba-zhan	[147]
Pigm [c]	CNL	6	Map-based cloning	Gumei 4	[148]
Pizh [c]	CNL	6	Map-based cloning	Zhonghua 11	[149]
Pi36	CNL	8	Map-based cloning	Q61	[150]
Pi5 [e]	CNL	9	Map-based cloning	RIL260	[151]
Pii [e]	CNL	9	Allele mining	Fujisaka5	[36]
Pik [h]/*Pi54* [g]	CNL	11	Map-based cloning	Tetep	[152]
Pi54rh [g]	CNL	11	Allele mining	Oryza rhizomatis	[153]
Pi54of [g]	CNL	11	Allele mining	Oryza officinalis	[154]
Pia	NLR	11	Multifaceted genomics approach	Nipponbare	[155]
Pik [f]	NLR	11	Map-based cloning	Kusabue	[156]
Pike [f]	CNL	11	Map-based cloning	Xiangzao 143	[157]
Piks [f]	CNL	11	Allele mining	IRBLKs-F5	[26]
Pi1 [f]	CNL	11	Map-based cloning	C101LAC	[158]
Pik-p [f]	CNL	11	Map-based cloning	K60	[159]
Pik-m [f]	CNL	11	Map-based cloning	Tsuyuake	[160]
Pik-h [f]	CNL	11	Map-based cloning	K3	[161]
Pikg [f]	CNL	11	Allele mining	accession G9	[162]
Pi65	LRR-RLK	11	Map-based cloning	GangYu65	[24]
Pik-W25 [f]	CNL	11	BSA mapping	WR25	[108]
Pi-ta	NLR	12	Map-based cloning	Katy	[163]
Ptr	ARM repeats	12	Map-based cloning	BHA	[33]

[a−h] These marked genes are allelic to each other.

Table A2. Information on rice blast-resistant varieties.

S. No	Variety	Breeding Techniques	Researcher or Unit
1	Chunjiang 25	Crossbreeding	Wu Mingguo et al. [164]
2	shangyou 63	Crossbreeding	Xiuxia Yang et al. [165]
3	Tiejing 16	MAS	Ma et al. [166]
4	K59	Crossbreeding	Yang Wangxing et al. [167]
5	Nipponbarc	Crossbreeding	Aichi Prefectural Agricultural Experiment Station [168]
6	Hokkai-188	Crossbreeding	Nguyen, Fukuoka et al. [138]
7	St. No. 1	Genome Editing	Hayano-Saito [169]
8	Yangmaogu	Crossbreeding	Jian Ma et al. [39]

Table A2. *Cont.*

S. No	Variety	Breeding Techniques	Researcher or Unit
9	BL1	Backcross	Sedeek, S et al. [170]
10	Minghui 63	Crossbreeding	Wang et al. [171]
11	Kahei	Mas	Miyamoto M., Yano M., Hirasawa H et al. [141]
12	Digu	Crossbreeding	Lihuang Zhu, Xuewei Chen et al. [30]
13	MC276	Gs	Wan, Moroberekan et al. [172]
14	Gumei2	Crossbreeding	Jie Chen [145]
15	Tetep	Mas	Atul Singh [173]
16	Zhonghua 11	Gs	Xue-Feng Yao [174]
17	Q61	Crossbreeding	Xie et al. [150]
18	Fujisaka5	Backcross	Fujimaki Hiroshi et al. [175]
19	Oryza rhizomatis	Crossbreeding	Vaughan et al. [154]
20	Nipponbare	Crossbreeding	Okuyama et al. [155]
21	Kusabue	Crossbreeding	Zhai et al. [156]
22	Xiangzao 143	Gs	Hunan Rice Research Institute [157]
23	K60	Crossbreeding	Yuan et al. [159]
24	YF47	Backcross	Mao et al. [106]

Table A3. Information on races of rice blast strains [176,177].

Source Cultivarsa	Year of Isolation	Races	State	Frequency of Occurrence
Caffey	2014	IC-17	Arkansas	The most common race
CL 151	2013	1B-25	Arkansas	Uncommon race
HR12		MG01	south of indian	The most common race
CL 151	2015	1B-1	Arkansas	The most common race
CL 261	2013	IA-37	Arkansas	Uncommon race
70-15		MG-8	south of indian	The most common race
CL 261	2013	IA-69	Arkansas	Uncommon race
Jupiter	2015	IA-113	Arkansas	Uncommon race
CL 261	2012	1B-17	Arkansas	The most common race
Jupiter	2013	IG-1	Arkansas	Uncommon race
CL 261	2012	1B-49	Arkansas	The most common race
Jupiter	2015	IA-1	Arkansas	Uncommon race
CL 261	2012	IC-9	Arkansas	Uncommon race
CL 261	2013	IE-1	Arkansas	The most common race
		FJ81278	fujian province china	The most common race
CL 262	2013	1B-41	Arkansas	Uncommon race
Colorado	2013	IC-1	Texas	Uncommon race
CL 261	2013	IA-65	Arkansas	Uncommon race
Jupiter	2013	1B-21	Louisiana	Uncommon race
LA 2025	2013	1B-37	Louisiana	Uncommon race
		HN19311	hunan province in china	The most common race

References

1. Qi, Z.; Zhou, X.; Tian, L.; Zhang, H.; Cai, L.; Tang, F. Temporal and spatial variation of microbial communities in stored rice grains from two major depots in China. *Food Res. Int.* **2022**, *152*, 110876. [CrossRef]
2. Le Mouël, C.; Forslund, A. How can we feed the world in 2050? A review of the responses from global scenario studies. *Eur. Rev. Agric. Econ.* **2017**, *44*, 541–591. [CrossRef]
3. Li, J.; Lu, L.; Wang, Q.; Shi, Z.; Li, C.; Guo, Z. Genome Re-Sequencing Reveals the Host-Specific Origin of Genetic Variation in Magnaporthe Species. *Front. Genet.* **2022**, *16*, 1664–8021. [CrossRef]
4. Han, X.; Li, S.; Zeng, Q.; Sun, P.; Wu, D.; Wu, J.; Yu, X.; Lai, Z.; Milne, R.J.; Kang, Z.; et al. Genetic engineering, including genome editing, for enhancing broad-spectrum disease resistance in crops. *Plant Commun.* **2025**, *6*, 101195. [CrossRef] [PubMed]
5. Cui, H.; Tsuda, K.; Parker, J.E. Effector-Triggered Immunity: From Pathogen Perception to Robust Defense. *Annu. Rev. Plant Biol.* **2015**, *66*, 487–511. [CrossRef]
6. Odjo, T.; Diagne, D.; Adreit, H.; Milazzo, J.; Raveloson, H.; Andriantsimialona, D.; Kassankogno, A.I.; Ravel, S.; Gumedzoé, Y.M.D.; Ouedraogo, I.; et al. Structure of African Populations of *Pyricularia oryzae* from Rice. *Phytopathology* **2021**, *111*, 1428–1437. [CrossRef]
7. Wang, L.; Zuo, S.-M.; Zhang, Y.-F.; Chen, Z.-X.; Pan, X.-B.; Huang, S.-W. Genetic Structure of Rice Blast Pathogen *Magnaporthe oryzae* in Sichuan Province. *Chin. J. Rice Sci.* **2015**, *29*, 327–334. [CrossRef]
8. Gupta, L.; Vermani, M.; Kaur Ahluwalia, S.; Vijayaraghavan, P. Molecular virulence determinants of *Magnaporthe oryzae*: Disease pathogenesis and recent interventions for disease management in rice plant. *Mycology* **2021**, *12*, 174–187. [CrossRef]
9. Ryder, L.S.; Dagdas, Y.F.; Kershaw, M.J.; Venkataraman, C.; Madzvamuse, A.; Yan, X.; Cruz-Mireles, N.; Soanes, D.M.; Oses-Ruiz, M.; Styles, V.; et al. A sensor kinase controls turgor-driven plant infection by the rice blast fungus. *Nature* **2019**, *574*, 423–427. [CrossRef] [PubMed]
10. Yan, X.; Tang, B.; Ryder, L.S.; MacLean, D.; Were, V.M.; Eseola, A.B.; Cruz-Mireles, N.; Ma, W.; Foster, A.J.; Osés-Ruiz, M.; et al. The transcriptional landscape of plant infection by the rice blast fungus *Magnaporthe oryzae* reveals distinct families of temporally co-regulated and structurally conserved effectors. *Plant Cell* **2023**, *35*, 1360–1385. [CrossRef] [PubMed]
11. Zhang, Y.; Lubberstedt, T.; Xu, M. The Genetic and Molecular Basis of Plant Resistance to Pathogens. *J. Genet. Genom.* **2013**, *40*, 23–35. [CrossRef]
12. Sun, L.; Zhang, J. Regulatory role of receptor-like cytoplasmic kinases in early immune signaling events in plants. *FEMS Microbiol. Rev.* **2020**, *44*, 845–856. [CrossRef]
13. Shiu, S.-H.; Karlowski, W.M.; Pan, R.; Tzeng, Y.-H.; Mayer, K.F.X.; Li, W.-H. Comparative analysis of the receptor-like kinase family in Arabidopsis and rice. *Plant Cell* **2004**, *16*, 1220–1234. [CrossRef]
14. Zipfel, C. Plant pattern-recognition receptors. *Trends Immunol.* **2014**, *35*, 345–351. [CrossRef] [PubMed]
15. Li, Y.; Roychowdhury, R.; Govta, L.; Jaiwar, S.; Wei, Z.Z.; Shams, I.; Fahima, T. Intracellular Reactive Oxygen Species-Aided Localized Cell Death Contributing to Immune Responses Against Wheat Powdery Mildew Pathogen. *Phytopathology* **2023**, *113*, 884–892. [CrossRef] [PubMed]
16. Agarrwal, R.; Ahire, T.P.; Manjunatha, N.; Pokhare, S.S.; Ojha, R.; Salvi, P. Imperative Role of R-Genes and Associated Molecular Mechanisms in Plant Disease Resistance. In *Biotechnological Advances for Disease Tolerance in Plants*; Springer: Singapore, 2024; pp. 73–97. [CrossRef]
17. Dow, M.; Newman, M.A.; von Roepenack, E. The Induction and Modulation of Plant Defense Responses by Bacterial Lipopolysaccharides. *Annu. Rev. Phytopathol.* **2000**, *38*, 241–261. [CrossRef] [PubMed]
18. Tongyu, Z. Advances in plant immunity and disease resistance breeding. *SPIE* **2023**, *12611*, 1261107. [CrossRef]
19. Huang, X.; Yao, W.; Chen, Q.; Lin, J.; Huang, J.; Zou, Y.; Guo, C.; He, B.; Yuan, X.; Xu, C.; et al. A century of advances in molecular genetics and breeding for sustainable resistance to rice blast disease. *Theor. Appl. Genet.* **2025**, *138*, 174. [CrossRef]
20. Zhai, K.; Liang, D.; Li, H.; Jiao, F.; Yan, B.; Liu, J.; Lei, Z.; Huang, L.; Gong, X.; Wang, X.; et al. NLRs guard metabolism to coordinate pattern- and effector-triggered immunity. *Nature* **2022**, *601*, 245–251. [CrossRef]
21. Danso Ofori, A.; Zheng, T.; Titriku, J.; Appiah, C.; Xiang, X.; Kandhro, A.G.; Ahmed, M.I.; Zheng, A. The Role of Genetic Resistance in Rice Disease Management. *Int. J. Mol. Sci.* **2025**, *26*, 956. [CrossRef]
22. Sahu, P.K.; Sao, R.; Choudhary, D.K.; Thada, A.; Kumar, V.; Mondal, S.; Das, B.K.; Jankuloski, L.; Sharma, D. Advancement in the Breeding, Biotechnological and Genomic Tools towards Development of Durable Genetic Resistance against the Rice Blast Disease. *Plants* **2022**, *11*, 2386. [CrossRef]
23. Lv, Q.H.; Huang, Z.; Xu, X.; Tang, L.; Liu, H.; Wang, C.; Zhou, Z.; Xin, Y.; Xing, J.; Peng, Z.; et al. Allelic variation of the rice blast resistance gene Pid3 in cultivated rice worldwide. *Sci. Rep.* **2017**, *7*, 10362. [CrossRef]
24. Wang, L.; Ma, Z.; Kang, H.; Gu, S.; Mukhina, Z.; Wang, C.; Wang, H.; Bai, Y.; Sui, G.; Zheng, W.; et al. Cloning and functional analysis of the novel rice blast resistance gene Pi65 in japonica rice. *Theor. Appl. Genet.* **2022**, *135*, 173–183. [CrossRef]
25. Yu, Y.; Ma, L.; Wang, X.; Zhao, Z.; Wang, W.; Fan, Y.; Liu, K.; Jiang, T.; Xiong, Z.; Song, Q.; et al. Genome-Wide Association Study Identifies a Rice Panicle Blast Resistance Gene, Pb2, Encoding NLR Protein. *Int. J. Mol. Sci.* **2022**, *23*, 5668. [CrossRef]
26. Xiao, G.; Wang, W.; Liu, M.; Li, Y.; Liu, J.; Franceschetti, M.; Yi, Z.; Zhu, X.; Zhang, Z.; Lu, G.; et al. The Piks allele of the NLR immune receptor Pik breaks the recognition of AvrPik effectors of rice blast fungus. *J. Integr. Plant Biol.* **2023**, *65*, 810–824. [CrossRef]

27. Qu, S.; Liu, G.; Zhou, B.; Bellizzi, M.; Zeng, L.; Dai, L.; Han, B.; Wang, G.L. The broad-spectrum blast resistance gene Pi9 encodes a nucleotide-binding site-leucine-rich repeat protein and is a member of a multigene family in rice. *Genetics* **2006**, *172*, 1901–1914. [CrossRef]
28. Wang, Z.X.; Yano, M.; Yamanouchi, U.; Iwamoto, M.; Monna, L.; Hayasaka, H.; Katayose, Y.; Sasaki, T. The Pib gene for rice blast resistance belongs to the nucleotide binding and leucine-rich repeat class of plant disease resistance genes. *Plant J.* **1999**, *19*, 55–64. [CrossRef]
29. Li, W.; Chern, M.; Yin, J.; Wang, J.; Chen, X. Recent advances in broad-spectrum resistance to the rice blast disease. *Curr. Opin. Plant Biol.* **2019**, *50*, 114–120. [CrossRef]
30. Chen, X.; Shang, J.; Chen, D.; Lei, C.; Zou, Y.; Zhai, W.; Liu, G.; Xu, J.; Ling, Z.; Cao, G.; et al. A B-lectin receptor kinase gene conferring rice blast resistance. *Plant J.* **2006**, *46*, 794–804. [CrossRef] [PubMed]
31. Devi, S.; Singh, K.; Umakanth, B.; Vishalakshi, B.; Rao, K.V.S.; Suneel, B.; Sharma, S.K.; Kadambari, G.K.M.; Prasad, M.S.; Senguttvel, P.; et al. Identification and Characterization of a Large Effect QTL from *Oryza glumaepatula* Revealed Pi68(t) as Putative Candidate Gene for Rice Blast Resistance. *Rice* **2020**, *13*, 17. [CrossRef] [PubMed]
32. Zhao, H.; Liu, Y.; Jia, M.H.; Jia, Y. An Allelic Variant of the Broad-Spectrum Blast Resistance Gene Ptr in Weedy Rice Is Associated with Resistance to the Most Virulent Blast Race IB-33. *Plant Dis.* **2022**, *106*, 1675–1680. [CrossRef]
33. Zhao, H.; Wang, X.; Jia, Y.; Minkenberg, B.; Wheatley, M.; Fan, J.; Jia, M.H.; Famoso, A.; Edwards, J.D.; Wamishe, Y.; et al. The rice blast resistance gene Ptr encodes an atypical protein required for broad-spectrum disease resistance. *Nat. Commun.* **2018**, *9*, 2039. [CrossRef]
34. Zhou, X.; Liao, H.; Chern, M.; Yin, J.; Chen, Y.; Wang, J.; Zhu, X.; Chen, Z.; Yuan, C.; Zhao, W.; et al. Loss of function of a rice TPR-domain RNA-binding protein confers broad-spectrum disease resistance. *Science* **2018**, *115*, 3174–3179. [CrossRef]
35. Li, W.; Zhu, Z.; Chern, M.; Yin, J.; Yang, C.; Ran, L.; Cheng, M.; He, M.; Wang, K.; Wang, J.; et al. A Natural Allele of a Transcription Factor in Rice Confers Broad-Spectrum Blast Resistance. *Cell* **2017**, *170*, 114–126.e15. [CrossRef]
36. Vo, K.T.X.; Lee, S.K.; Halane, M.K.; Song, M.Y.; Hoang, T.V.; Kim, C.Y.; Park, S.Y.; Jeon, J.; Kim, S.T.; Sohn, K.H.; et al. Pi5 and Pii Paired NLRs Are Functionally Exchangeable and Confer Similar Disease Resistance Specificity. *Mol. Cells* **2019**, *42*, 637–645. [CrossRef] [PubMed]
37. Shimizu, M.; Hirabuchi, A.; Sugihara, Y.; Abe, A.; Takeda, T.; Kobayashi, M.; Hiraka, Y.; Kanzaki, E.; Oikawa, K.; Saitoh, H.; et al. A genetically linked pair of NLR immune receptors shows contrasting patterns of evolution. *Proc. Natl. Acad. Sci USA* **2022**, *119*, e2116896119. [CrossRef] [PubMed]
38. Kovi, B.; Sakai, T.; Abe, A.; Kanzaki, E.; Terauchi, R.; Shimizu, M. Isolation of Pikps, an allele of Pik, from the aus rice cultivar Shoni. *Genes Genet. Syst.* **2023**, *97*, 229–235. [CrossRef]
39. Ma, J.; Lei, C.; Xu, X.; Hao, K.; Wang, J.; Cheng, Z.; Ma, X.; Ma, J.; Zhou, K.; Zhang, X.; et al. Pi64, Encoding a Novel CC-NBS-LRR Protein, Confers Resistance to Leaf and Neck Blast in Rice. *Mol. Plant Microbe Interact.* **2015**, *28*, 558–568. [CrossRef]
40. Wang, Y.; Pruitt, R.N.; Nürnberger, T.; Wang, Y. Evasion of plant immunity by microbial pathogens. *Nat. Rev. Microbiol.* **2022**, *20*, 449–464. [CrossRef] [PubMed]
41. Bundó, M.; Coca, M. Calcium-dependent protein kinase OsCPK10 mediates both drought tolerance and blast disease resistance in rice plants. *J. Exp. Bot.* **2017**, *68*, 2963–2975. [CrossRef]
42. Hamdi, J.; Kmeli, N.; Bettaieb, I.; Bouktila, D. Wall-Associated Kinase (WAK) and WAK-like Kinase Gene Family in Sugar Beet: Genome-Wide Characterization and In Silico Expression Analysis in Response to Beet Cyst Nematode (*Heterodera schachtii* Schmidt) Infection. *J. Plant Growth Regul.* **2025**, *44*, 1713–1727. [CrossRef]
43. Li, H.; Zhou, S.Y.; Zhao, W.S.; Su, S.C.; Peng, Y.L. A novel wall-associated receptor-like protein kinase gene, OsWAK1, plays important roles in rice blast disease resistance. *Plant Mol. Biol.* **2009**, *69*, 337–346. [CrossRef] [PubMed]
44. Delteil, A.; Gobbato, E.; Cayrol, B.; Estevan, J.; Michel-Romiti, C.; Dievart, A.; Kroj, T.; Morel, J.B. Several wall-associated kinases participate positively and negatively in basal defense against rice blast fungus. *BMC Plant Biol.* **2016**, *16*, 17. [CrossRef]
45. Zhang, F.; Fang, H.; Wang, M.; He, F.; Tao, H.; Wang, R.; Long, J.; Wang, J.; Wang, G.L.; Ning, Y. APIP5 functions as a transcription factor and an RNA-binding protein to modulate cell death and immunity in rice. *Nucleic Acids Res.* **2022**, *50*, 5064–5079. [CrossRef] [PubMed]
46. Wang, J.; Zhou, L.; Shi, H.; Chern, M.X.; Yu, H.; Yi, H.; He, M.; Yin, J.; Zhu, X.; Li, Y.; et al. A single transcription factor promotes both yield and immunity in rice. *Science* **2018**, *361*, 1026–1028. [CrossRef]
47. Wang, L.; Xu, G.; Li, L.; Ruan, M.; Bennion, A.; Wang, G.-L.; Li, R.; Qu, S. The OsBDR1-MPK3 module negatively regulates blast resistance by suppressing the jasmonate signaling and terpenoid biosynthesis pathway. *Proc. Natl. Acad. Sci. USA* **2023**, *120*, e2211102120. [CrossRef]
48. Fan, J.; Bai, P.; Ning, Y.; Wang, J.; Shi, X.; Xiong, Y.; Zhang, K.; He, F.; Zhang, C.; Wang, R.; et al. The Monocot-Specific Receptor-like Kinase SDS2 Controls Cell Death and Immunity in Rice. *Cell Host Microbe* **2018**, *23*, 498–510.e5. [CrossRef] [PubMed]
49. Bundo, M.; Coca, M. Enhancing blast disease resistance by overexpression of the calcium-dependent protein kinase OsCPK4 in rice. *Plant Biotechnol. J.* **2016**, *14*, 1357–1367. [CrossRef]
50. Wongsa, T.; Chankaew, S.; Monkham, T.; Sanitchon, J. Broad-Spectrum Resistance and Monogenic Inheritance of Bacterial Blight Resistance in an Indigenous Upland Rice Germplasm ULR207. *Agronomy* **2024**, *14*, 898. [CrossRef]
51. Wang, B.; Xue, P.; Zhang, Y.; Zhan, X.; Wu, W.; Yu, P.; Chen, D.; Fu, J.; Hong, Y.; Shen, X.; et al. OsCPK12 phosphorylates OsCATA and OsCATC to regulate H_2O_2 homeostasis and improve oxidative stress tolerance in rice. *Plant Commun.* **2024**, *5*, 100780. [CrossRef]

52. Li, H.; Zhang, Y.; Wu, C.; Bi, J.; Chen, Y.; Jiang, C.; Cui, M.; Chen, Y.; Hou, X.; Yuan, M.; et al. Fine-tuning OsCPK18/OsCPK4 activity via genome editing of phosphorylation motif improves rice yield and immunity. *Plant Biotechnol. J.* **2022**, *20*, 2258–2271. [CrossRef]
53. Chen, M.; Ni, L.; Chen, J.; Sun, M.; Qin, C.; Zhang, G.; Zhang, A.; Jiang, M. Rice calcium/calmodulin-dependent protein kinase directly phosphorylates a mitogen-activated protein kinase kinase to regulate abscisic acid responses. *Plant Cell* **2021**, *33*, 1790–1812. [CrossRef]
54. Ahmad, S.; Wei, X.; Sheng, Z.; Hu, P.; Tang, S. CRISPR/Cas9 for development of disease resistance in plants: Recent progress, limitations and future prospects. *Brief. Funct. Genom.* **2020**, *19*, 26–39. [CrossRef]
55. Gao, C.; Tang, D.; Wang, W. The Role of Ubiquitination in Plant Immunity: Fine-Tuning Immune Signaling and Beyond. *Plant Cell Physiol.* **2022**, *63*, 1405–1413. [CrossRef]
56. Wang, C.; Wang, G.; Zhang, C.; Zhu, P.; Dai, H.; Yu, N.; He, Z.; Xu, L.; Wang, E. OsCERK1-Mediated Chitin Perception and Immune Signaling Requires Receptor-like Cytoplasmic Kinase 185 to Activate an MAPK Cascade in Rice. *Mol. Plant* **2017**, *10*, 619–633. [CrossRef] [PubMed]
57. Liu, S.; Wang, T.; Meng, G.; Liu, J.; Lu, D.; Liu, X.; Zeng, Y. Cytological observation and transcriptome analysis reveal dynamic changes of *Rhizoctonia solani* colonization on leaf sheath and different genes recruited between the resistant and susceptible genotypes in rice. *Front. Plant Sci.* **2022**, *13*, 599–612. [CrossRef]
58. Niu, Y.; Huang, X.; He, Z.; Zhang, Q.; Meng, H.; Shi, H.; Feng, B.; Zhou, Y.; Zhang, J.; Lu, G.; et al. Phosphorylation of OsTGA5 by casein kinase II compromises its suppression of defense-related gene transcription in rice. *Plant Cell* **2022**, *34*, 3425–3442. [CrossRef]
59. Ban, Z.; Estelle, M. CUL3 E3 ligases in plant development and environmental response. *Nat. Plants* **2021**, *7*, 6–16. [CrossRef] [PubMed]
60. Younas, M.U.; Ahmad, I.; Qasim, M.; Ijaz, Z.; Rajput, N.; Parveen Memon, S.; ULZaman, W.; Jiang, X.; Zhang, Y.; Zuo, S. Progress in the Management of Rice Blast Disease: The Role of Avirulence and Resistance Genes through Gene-for-Gene Interactions. *Agronomy* **2024**, *14*, 163. [CrossRef]
61. Zheng, Y.; Zhang, X.; Liu, Y.; Zhu, T.; Wu, X.; Ning, Y.; Liu, J.; Wang, D. Crystal structure of rice APIP6 reveals a new dimerization mode of RING-type E3 ligases that facilities the construction of its working model. *Phytopathol. Res.* **2023**, *5*, 31. [CrossRef]
62. Wang, J.; Wang, R.; Fang, H.; Zhang, C.; Zhang, F.; Hao, Z.; You, X.; Shi, X.; Park, C.H.; Hua, K.; et al. Two VOZ transcription factors link an E3 ligase and an NLR immune receptor to modulate immunity in rice. *Mol. Plant* **2021**, *14*, 253–266. [CrossRef] [PubMed]
63. Liu, Z.; Qiu, J.; Shen, Z.; Wang, C.; Jiang, N.; Shi, H.; Kou, Y. The E3 ubiquitin ligase OsRGLG5 targeted by the *Magnaporthe oryzae* effector AvrPi9 confers basal resistance against rice blast. *Plant Commun.* **2023**, *4*, 100626. [CrossRef]
64. Gou, M.; Balint-Kurti, P.; Xu, M.; Yang, Q. Quantitative disease resistance: Multifaceted players in plant defense. *Cell Res.* **2023**, *65*, 594–610. [CrossRef]
65. Wang, R.; You, X.; Zhang, C.; Fang, H.; Wang, M.; Zhang, F.; Kang, H.; Xu, X.; Liu, Z.; Wang, J.; et al. An ORFeome of rice E3 ubiquitin ligases for global analysis of the ubiquitination interactome. *Genome Biol.* **2022**, *23*, 154. [CrossRef] [PubMed]
66. Wang, K.; Li, S.; Chen, L.; Tian, H.; Chen, C.; Fu, Y.; Du, H.; Hu, Z.; Li, R.; Du, Y.; et al. E3 ubiquitin ligase OsPIE3 destabilises the B-lectin receptor-like kinase PID2 to control blast disease resistance in rice. *New Phytol.* **2023**, *237*, 1826–1842. [CrossRef]
67. Wang, S.; Han, S.; Zhou, X.; Zhao, C.; Guo, L.; Zhang, J.; Liu, F.; Huo, Q.; Zhao, W.; Guo, Z.; et al. Phosphorylation and ubiquitination of OsWRKY31 are integral to OsMKK10-2-mediated defense responses in rice. *Plant Cell* **2023**, *35*, 2391–2412. [CrossRef]
68. Ichimaru, K.; Yamaguchi, K.; Harada, K.; Nishio, Y.; Hori, M.; Ishikawa, K.; Inoue, H.; Shigeta, S.; Inoue, K.; Shimada, K.; et al. Cooperative regulation of PBI1 and MAPKs controls WRKY45 transcription factor in rice immunity. *Nat. Commun.* **2022**, *13*, 2397. [CrossRef] [PubMed]
69. Son, S.; Song, G.; Nam, S.; Lee, J.; Hwang, D.-J.; Suh, E.-J.; Park, S.R. OsWRKY65 enhances immunity against fungal and bacterial pathogens in rice. *Crop J.* **2024**, *12*, 470–481. [CrossRef]
70. Li, W.; Wang, K.; Chern, M.; Liu, Y.; Zhu, Z.; Liu, J.; Zhu, X.; Yin, J.; Ran, L.; Xiong, J.; et al. Sclerenchyma cell thickening through enhanced lignification induced by OsMYB30 prevents fungal penetration of rice leaves. *New Phytol.* **2020**, *226*, 1850–1863. [CrossRef]
71. Qiu, J.; Xie, J.; Chen, Y.; Shen, Z.; Shi, H.; Naqvi, N.I.; Qian, Q.; Liang, Y.; Kou, Y. Warm temperature compromises JA-regulated basal resistance to enhance *Magnaporthe oryzae* infection in rice. *Mol. Plant* **2022**, *15*, 723–739. [CrossRef]
72. Huang, L.; Ökmen, B.; Stolze, S.C.; Kastl, M.; Khan, M.; Hilbig, D.; Nakagami, H.; Djamei, A.; Doehlemann, G. The fungal pathogen Ustilago maydis targets the maize corepressor RELK2 to modulate host transcription for tumorigenesis. *New Phytol.* **2024**, *241*, 1747–1762. [CrossRef] [PubMed]
73. Sun, L.; Zhang, H.; Li, D.; Huang, L.; Hong, Y.; Ding, X.S.; Nelson, R.S.; Zhou, X.; Song, F. Functions of rice NAC transcriptional factors, ONAC122 and ONAC131, in defense responses against *Magnaporthe grisea*. *Plant Mol. Biol.* **2013**, *81*, 41–56. [CrossRef] [PubMed]
74. Bui, H.; Dong, G.; Le, C.; Chu, H.; Duong, D.; Phung, L.; Phung, H.; Nguyen, C.; Nguyen, N.; Nguyen, P.; et al. Designing CRISPR/Cas9 System Targeting OsERF922 Gene of J02 Rice Variety. *Asian J. Plant Sci.* **2023**, *22*, 66–74. [CrossRef]
75. Yang, X.; Zhang, L.; Yang, Y.; Schmid, M.; Wang, Y. miRNA Mediated Regulation and Interaction between Plants and Pathogens. *Int. J. Mol. Sci.* **2021**, *22*, 2913. [CrossRef]
76. Li, Y.; Jeyakumar, J.M.J.; Feng, Q.; Zhao, Z.-X.; Fan, J.; Khaskheli, M.I.; Wang, W.-M. The roles of rice microRNAs in rice-*Magnaporthe oryzae* interaction. *Phytopathol. Res.* **2019**, *1*, 33. [CrossRef]

77. Zhang, L.L.; Huang, Y.Y.; Zheng, Y.P.; Liu, X.X.; Zhou, S.X.; Yang, X.M.; Liu, S.L.; Li, Y.; Li, J.L.; Zhao, S.L.; et al. Osa-miR535 targets SQUAMOSA promoter binding protein-like 4 to regulate blast disease resistance in rice. *Plant J.* **2022**, *110*, 166–178. [CrossRef]
78. Salvador-Guirao, R.; Hsing, Y.I.; San Segundo, B. The Polycistronic miR166k-166h Positively Regulates Rice Immunity via Post-transcriptional Control of EIN2. *Front. Plant Sci.* **2018**, *9*, 337. [CrossRef]
79. Li, Y.; Tong, Y.; He, X.; Zhu, Y.; Li, T.; Lin, X.; Mao, W.; Gishkori, Z.G.N.; Zhao, Z.; Zhang, J.; et al. The rice miR171b–SCL6-IIs module controls blast resistance, grain yield, and flowering. *Crop J.* **2022**, *10*, 117–127. [CrossRef]
80. Wang, H.; Li, Y.; Chern, M.; Zhu, Y.; Zhang, L.L.; Lu, J.H.; Li, X.P.; Dang, W.Q.; Ma, X.C.; Yang, Z.R.; et al. Suppression of rice miR168 improves yield, flowering time and immunity. *Nat. Plants* **2021**, *7*, 129–136. [CrossRef]
81. Zhou, J.; Zhang, R.; Jia, X.; Tang, X.; Guo, Y.; Yang, H.; Zheng, X.; Qian, Q.; Qi, Y.; Zhang, Y. CRISPR-Cas9 mediated OsMIR168a knockout reveals its pleiotropy in rice. *Plant Biotechnol. J.* **2022**, *20*, 310–322. [CrossRef] [PubMed]
82. Li, Y.; Li, T.T.; He, X.R.; Zhu, Y.; Feng, Q.; Yang, X.M.; Zhou, X.H.; Li, G.B.; Ji, Y.P.; Zhao, J.H.; et al. Blocking Osa-miR1871 enhances rice resistance against *Magnaporthe oryzae* and yield. *Plant Biotechnol. J.* **2022**, *20*, 646–659. [CrossRef]
83. Chandran, V.; Wang, H.; Gao, F.; Cao, X.L.; Chen, Y.P.; Li, G.B.; Zhu, Y.; Yang, X.M.; Zhang, L.L.; Zhao, Z.X.; et al. miR396-OsGRFs Module Balances Growth and Rice Blast Disease-Resistance. *Front. Plant Sci.* **2018**, *9*, 1999. [CrossRef] [PubMed]
84. Barna, B.; Fodor, J.; Harrach, B.D.; Pogany, M.; Kiraly, Z. The Janus face of reactive oxygen species in resistance and susceptibility of plants to necrotrophic and biotrophic pathogens. *Plant Physiol. Biochem.* **2012**, *59*, 37–43. [CrossRef]
85. Sha, G.; Sun, P.; Kong, X.; Han, X.; Sun, Q.; Fouillen, L.; Zhao, J.; Li, Y.; Yang, L.; Wang, Y.; et al. Genome editing of a rice CDP-DAG synthase confers multipathogen resistance. *Nature* **2023**, *618*, 1017–1023. [CrossRef]
86. Meng, F.; Yang, C.; Cao, J.; Chen, H.; Pang, J.; Zhao, Q.; Wang, Z.; Qing Fu, Z.; Liu, J. A bHLH transcription activator regulates defense signaling by nucleo-cytosolic trafficking in rice. *J. Integr. Plant Biol.* **2020**, *62*, 1552–1573. [CrossRef]
87. Hu, B.; Zhou, Y.; Zhou, Z.; Sun, B.; Zhou, F.; Yin, C.; Ma, W.; Chen, H.; Lin, Y. Repressed OsMESL expression triggers reactive oxygen species-mediated broad-spectrum disease resistance in rice. *Plant Biotechnol. J.* **2021**, *19*, 1511–1522. [CrossRef] [PubMed]
88. Peng, X.; Hu, Y.; Tang, X.; Zhou, P.; Deng, X.; Wang, H.; Guo, Z. Constitutive expression of rice WRKY30 gene increases the endogenous jasmonic acid accumulation, PR gene expression and resistance to fungal pathogens in rice. *Planta* **2012**, *236*, 1485–1498. [CrossRef]
89. Ying, W.; Liao, L.; Wei, H.; Gao, Y.; Liu, X.; Sun, L. Structural basis for abscisic acid efflux mediated by ABCG25 in Arabidopsis thaliana. *Nat. Plants* **2023**, *9*, 1697–1708. [CrossRef] [PubMed]
90. Jiang, C.J.; Shimono, M.; Sugano, S.; Kojima, M.; Yazawa, K.; Yoshida, R.; Inoue, H.; Hayashi, N.; Sakakibara, H.; Takatsuji, H. Abscisic Acid Interacts Antagonistically with Salicylic Acid Signaling Pathway in Rice–*Magnaporthe grisea* Interaction. *Mol. Plant Microbe Interact.* **2010**, *23*, 791–798. [CrossRef]
91. Tian, H.; Xu, L.; Li, X.; Zhang, Y. Salicylic acid: The roles in plant immunity and crosstalk with other hormones. *J. Integr. Plant Biol.* **2025**, *67*, 773–785. [CrossRef]
92. Yang, Q.; He, Y.; Kabahuma, M.; Chaya, T.; Kelly, A.; Borrego, E.; Bian, Y.; El Kasmi, F.; Yang, L.; Teixeira, P.; et al. A gene encoding maize caffeoyl-CoA O-methyltransferase confers quantitative resistance to multiple pathogens. *Nat. Genet.* **2017**, *49*, 1364–1372. [CrossRef]
93. Fang, H.; Zhang, F.; Zhang, C.; Wang, D.; Shen, S.; He, F.; Tao, H.; Wang, R.; Wang, M.; Wang, D.; et al. Function of hydroxycinnamoyl transferases for the biosynthesis of phenolamides in rice resistance to *Magnaporthe oryzae*. *J. Genet. Genom.* **2022**, *49*, 776–786. [CrossRef]
94. Yang, C.; Liu, R.; Pang, J.; Ren, B.; Zhou, H.; Wang, G.; Wang, E.; Liu, J. Poaceae-specific cell wall-derived oligosaccharides activate plant immunity via OsCERK1 during *Magnaporthe oryzae* infection in rice. *Nat. Commun.* **2021**, *12*, 2178. [CrossRef] [PubMed]
95. Shen, S.; Peng, M.; Fang, H.; Wang, Z.; Zhou, S.; Jing, X.; Zhang, M.; Yang, C.; Guo, H.; Li, Y.; et al. An Oryza-specific hydroxycinnamoyl tyramine gene cluster contributes to enhanced disease resistance. *Sci. Bull.* **2021**, *66*, 2369–2380. [CrossRef]
96. Xu, X.-M.; Liang, K.-J.; Zhang, S.-G.; Shang, W.; Zhang, Y.-Y.; Wei, X.-Y.; Ke, B. Analysis of Indica-Japonica Differentiation in Rice Parents and Derived Lines Using ILP Markers. *Agric. Sci. China* **2009**, *8*, 1409–1418. [CrossRef]
97. He, X.; Liu, X.; Wang, L.; Wang, L.; Lin, F.; Cheng, Y.; Chen, Z.; Liao, Y.; Pan, Q. Identification of the novel recessive gene pi55(t) conferring resistance to *Magnaporthe oryzae*. *Sci. China Life Sci.* **2012**, *55*, 141–149. [CrossRef]
98. Romero, F.M.; Gatica-Arias, A. CRISPR/Cas9: Development and Application in Rice Breeding. *Rice Sci.* **2019**, *26*, 265–281. [CrossRef]
99. Xie, B.; Wang, L.; Li, H.; Huo, H.; Cui, C.; Sun, B.; Ma, Y.; Wang, J.; Yin, G.; Zuo, P. An interface-reinforced rhombohedral Prussian blue analogue in semi-solid state electrolyte for sodium-ion battery. *Energy Storage Mater.* **2021**, *36*, 99–107. [CrossRef]
100. Zhao, C.; Wang, Y.; Li, Z.; Chen, W.; Xu, Q.; He, D.; Xi, D.; Zhang, Q.; Yuan, T.; Qu, Y.; et al. Solid-Diffusion Synthesis of Single-Atom Catalysts Directly from Bulk Metal for Efficient CO2 Reduction. *Joule* **2019**, *3*, 584–594. [CrossRef]
101. Pedrozo, R.; Osakina, A.; Huang, Y.; Nicolli, C.P.; Wang, L.; Jia, Y. Status on Genetic Resistance to Rice Blast Disease in the Post-Genomic Era. *Plants* **2025**, *14*, 807. [CrossRef]
102. Deng, Z.; Qin, P.; Liu, K.; Jiang, N.; Yan, T.; Zhang, X.; Fu, C.; He, G.; Wang, K.; Yang, Y. The Development of Multi-Resistant Rice Restorer Lines and Hybrid Varieties by Pyramiding Resistance Genes against Blast and Brown Planthopper. *Agronomy* **2024**, *14*, 878. [CrossRef]

103. Qin, P.; Jiang, N.; Hu, X.; Zhu, Y.; Deng, Z.; Bai, Z.; Fu, J.; Zhang, X.; Wang, K.; Chen, S.; et al. Breeding a series of new rice restorer lines with blast resistance and low-to-intermediate apparent amylose contents by integrating marker-assisted and phenotypic selection. *J. Phytopathol.* **2021**, *169*, 667–677. [CrossRef]
104. Kumar, M.; Singh, R.P.; Jena, D.; Singh, V.; Rout, D.; Arsode, P.B.; Choudhary, M.; Singh, P.; Chahar, S.; Samantaray, S.; et al. Marker-Assisted Improvement for Durable Bacterial Blight Resistance in Aromatic Rice Cultivar HUR 917 Popular in Eastern Parts of India. *Plants* **2023**, *12*, 1363. [CrossRef]
105. Ye, J.; Wang, K.; Wang, Y.; Zhao, Z.; Yan, Y.; Yang, H.; Zhang, L.; Hu, Z.; Shi, Z.; Sun, D.; et al. Improving panicle blast resistance and fragrance in a high-quality japonica rice variety through breeding. *Front. Plant Sci.* **2024**, *15*, 1507827. [CrossRef]
106. Mao, T.; Zhu, M.; Ahmad, S.; Ye, G.; Sheng, Z.; Hu, S.; Jiao, G.; Xie, L.; Tang, S.; Wei, X.; et al. Superior japonica rice variety YJ144 with improved rice blast resistance, yield, and quality achieved using molecular design and multiple breeding strategies. *Mol. Breed.* **2021**, *41*, 65. [CrossRef]
107. Wang, K.; Fu, C.; Fu, X.; Qin, P.; Hu, X.; Zhang, X.; Deng, Z.; Yan, T.; Jiang, N.; Li, Y.; et al. Enhancing the blast resistance of an elite thermo-sensitive genic male sterile line (TGMS) Longke638S and its derived hybrid varieties by incorporating Pigm gene. *Mol. Breed.* **2025**, *45*, 35. [CrossRef]
108. Qi, Z.; Meng, X.; Xu, M.; Du, Y.; Yu, J.; Song, T.; Pan, X.; Zhang, R.; Cao, H.; Yu, M.; et al. A novel Pik allele confers extended resistance to rice blast. *Plant Cell Environ.* **2024**, *12*, 4800–4814. [CrossRef] [PubMed]
109. Meuwissen, T.H.E.; Hayes, B.J.; Goddard, M.E. Prediction of total genetic value using genome-wide dense marker maps. *Genetics* **2001**, *157*, 1819–1829. [CrossRef]
110. Sasaki, T. The map-based sequence of the rice genome. *Nature* **2005**, *436*, 793–800. [CrossRef]
111. Ma, X.; Wang, H.; Yan, S.; Zhou, C.; Zhou, K.; Zhang, Q.; Li, M.; Yang, Y.; Li, D.; Song, P.; et al. Large-scale genomic and phenomic analyses of modern cultivars empower future rice breeding design. *Mol. Plant* **2025**, *18*, 651–668. [CrossRef] [PubMed]
112. Xiao, N.; Pan, C.; Li, Y.; Wu, Y.; Cai, Y.; Lu, Y.; Wang, R.; Yu, L.; Shi, W.; Kang, H.; et al. Genomic insight into balancing high yield, good quality, and blast resistance of japonica rice. *Genome Biol.* **2021**, *22*, 283. [CrossRef] [PubMed]
113. Chen, Z.; Bu, Q.; Liu, G.; Wang, M.; Wang, H.; Liu, H.; Li, X.; Li, H.; Fang, J.; Liang, Y.; et al. Genomic decoding of breeding history to guide breeding-by-design in rice. *Natl. Sci. Rev.* **2023**, *10*, nwad029. [CrossRef]
114. Yu, S.; Ali, J.; Zhou, S.; Ren, G.; Xie, H.; Xu, J.; Yu, X.; Zhou, F.; Peng, S.; Ma, L.; et al. From Green Super Rice to green agriculture: Reaping the promise of functional genomics research. *Mol. Plant* **2022**, *15*, 9–26. [CrossRef]
115. He, Z.; Xin, Y.; Wang, C.; Yang, H.; Xu, Z.; Cheng, J.; Li, Z.; Ye, C.; Yin, H.; Xie, Z.; et al. Genomics-Assisted improvement of super high-yield hybrid rice variety "super 1000" for resistance to bacterial blight and blast diseases. *Front. Plant Sci.* **2022**, *13*, 881244. [CrossRef]
116. Feng, Z.; Gao, P.; Wang, G.; Kang, H.; Zhao, J.; Xie, W.; Chen, R.; Ju, R.; Wang, X.; Wei, Z.; et al. Natural variation in SBRR1 shows high potential for sheath blight resistance breeding in rice. *Nat. Genet.* **2025**, *57*, 2004–2016. [CrossRef]
117. Greenwood, J.R.; Lacorte-Apostol, V.; Kroj, T.; Padilla, J.; Telebanco-Yanoria, M.J.; Glaus, A.N.; Roulin, A.; Padilla, A.; Zhou, B.; Keller, B.; et al. Genome-wide association analysis uncovers rice blast resistance alleles of Ptr and Pia. *Commun. Biol.* **2024**, *7*, 607. [CrossRef]
118. Zhang, Y.; Lin, X.-F.; Li, L.; Piao, R.-H.; Wu, S.; Song, A.; Gao, M.; Jin, Y.-M. CRISPR/Cas9-mediated knockout of Bsr-d1 enhances the blast resistance of rice in Northeast China. *Plant Cell Rep.* **2024**, *43*, 100. [CrossRef]
119. Li, G.; Gao, Q.; Li, W.; Zhang, W.; Wang, J.; Chen, B.; Wang, D.; Gao, H.; Xu, W.; Chen, H.; et al. Directed Knockout of SD1 Gene Improves Lodging Resistance and Blast Resistance of Rice. *Chin. J. Rice Sci.* **2023**, *37*, 359–367. [CrossRef]
120. Tao, H.; Shi, X.; He, F.; Wang, D.; Xiao, N.; Fang, H.; Wang, R.; Zhang, F.; Wang, M.; Li, A.; et al. Engineering broad-spectrum disease-resistant rice by editing multiple susceptibility genes. *J. Integr. Plant Biol.* **2021**, *63*, 1639–1648. [CrossRef] [PubMed]
121. Zhou, Y.; Xu, S.; Jiang, N.; Zhao, X.; Bai, Z.; Liu, J.; Yao, W.; Tang, Q.; Xiao, G.; Lv, C.; et al. Engineering of rice varieties with enhanced resistances to both blast and bacterial blight diseases via CRISPR/Cas9. *Plant Biotechnol. J.* **2022**, *20*, 876–885. [CrossRef] [PubMed]
122. Li, C.; Zhou, Z.; Xiong, X.; Li, C.; Li, C.; Shen, E.; Wang, J.; Zha, W.; Wu, B.; Chen, H.; et al. Development of a multi-resistance and high-yield rice variety using multigene transformation and gene editing. *Plant Biotechnol. J.* **2024**, *22*, 3118–3120. [CrossRef]
123. Xu, P.; Wang, H.; Tu, R.; Liu, Q.; Wu, W.; Fu, X.; Cao, L.; Shen, X. Orientation Improvement of Blast Resistance in Rice via CRISPR/Cas9 System. *Chin. J. Rice Sci.* **2019**, *33*, 313–322. [CrossRef]
124. Xu, L.; Tang, Y.; Wang, M.; Peng, X.; Shi, H.; Zhang, Z.; Zhang, Y.; Yin, J.; Xiong, Q.; Lu, X.; et al. U-box E3 ubiquitin ligase OsPUB41 represses rice blast resistance by promoting degradation of OsPALs. *New Phytol.* **2025**, *247*, 2312–2327. [CrossRef]
125. Jung, Y.J.; Kim, J.Y.; Cho, Y.G.; Kang, K.K. CRISPR/Cas9-Mediated Knockout of OsbZIP76 Reveals Its Role in ABA-Associated Immune Signaling in Rice. *Int. J. Mol. Sci.* **2025**, *26*, 6374. [CrossRef]
126. Bezerra, C. Science Uses Gene Editing to Develop Blast-Resistant Rice. Available online: https://www.seedtoday.com/article/1030135/science-uses-gene-editing-to-develop-blast-resistant-rice (accessed on 20 August 2025).
127. Yu, T.; Sun, M.K.; Liang, L.K. Receptors in the Induction of the Plant Innate Immunity. *Mol. Plant Microbe Interact.* **2021**, *34*, 587–601. [CrossRef]

128. Golicz, A.A.; Bayer, P.E.; Bhalla, P.L.; Batley, J.; Edwards, D. Pangenomics Comes of Age: From Bacteria to Plant and Animal Applications. *Trends Genet.* **2020**, *36*, 132–145. [CrossRef] [PubMed]
129. Tettelin, H.; Masignani, V.; Cieslewicz, M.J.; Donati, C.; Medini, D.; Ward, N.L.; Angiuoli, S.V.; Crabtree, J.; Jones, A.L.; Durkin, A.S.; et al. Genome analysis of multiple pathogenic isolates of Streptococcus agalactiae: Implications for the microbial "pan-genome". *Proc. Natl. Acad. Sci. USA* **2005**, *102*, 13950–13955. [CrossRef] [PubMed]
130. Shang, L.; Li, X.; He, H.; Yuan, Q.; Song, Y.; Wei, Z.; Lin, H.; Hu, M.; Zhao, F.X.; Zhang, C.; et al. A super pan-genomic landscape of rice. *Cell Res.* **2022**, *32*, 878–896. [CrossRef]
131. Watson, A.; Ghosh, S.; Williams, M.J.; Cuddy, W.S.; Simmonds, J.; Rey, M.D.; Asyraf Md Hatta, M.; Hinchliffe, A.; Steed, A.; Reynolds, D.; et al. Speed breeding is a powerful tool to accelerate crop research and breeding. *Nat. Plants* **2018**, *4*, 23–29. [CrossRef]
132. Jiang, S.; Li, H.; Zhang, L.; Mu, W.; Zhang, Y.; Chen, T.; Wu, J.; Tang, H.; Zheng, S.; Liu, Y.; et al. Generic Diagramming Platform (GDP). A comprehensive database of high-quality biomedical graphics. *Nucleic Acids Res.* **2025**, *53*, 1670–1676. [CrossRef]
133. Feng, Q.; Wang, H.; Yang, X.; Hu, Z.; Zhou, X.; Xiang, L.; Xiong, X.; He, X.; Zhu, Y.; Li, G.; et al. Osa-miR160a confers broad-spectrum resistance to fungal and bacterial pathogens in rice. *New Phytol.* **2022**, *236*, 2216–2232. [CrossRef]
134. Maidment, J.; Shimizu, M.; Bentham, A.; Vera, S.; Franceschetti, M.; Longya, A.; Stevenson, C.; De la Concepcion, J.; Białas, A.; Kamoun, S.; et al. Effector target-guided engineering of an integrated domain expands the disease resistance profile of a rice NLR immune receptor. *Elife* **2023**, *12*, e81123. [CrossRef]
135. Hayashi, K.; Yasuda, N.; Fujita, Y.; Koizumi, S.; Yoshida, H. Identification of the blast resistance gene Pit in rice cultivars using functional markers. *Theor. Appl. Genet.* **2010**, *121*, 1357–1367. [CrossRef] [PubMed]
136. Takahashi, A.; Hayashi, N.; Miyao, A.; Hirochika, H. Unique features of the rice blast resistance Pish locus revealed by large scale retrotransposon-tagging. *BMC Plant Biol.* **2010**, *10*, 175. [CrossRef] [PubMed]
137. Fukuoka, S.; Yamamoto, S.-I.; Mizobuchi, R.; Yamanouchi, U.; Ono, K.; Kitazawa, N.; Yasuda, N.; Fujita, Y.; Thi Thanh Nguyen, T.; Koizumi, S.; et al. Multiple functional polymorphisms in a single disease resistance gene in rice enhance durable resistance to blast. *Sci. Rep.* **2014**, *4*, 4550. [CrossRef]
138. Lin, F.; Chen, S.; Que, Z.; Wang, L.; Liu, X.; Pan, Q. The blast resistance gene Pi37 encodes a nucleotide binding site leucine-rich repeat protein and is a member of a resistance gene cluster on rice chromosome 1. *Genetics* **2007**, *177*, 1871–1880. [CrossRef] [PubMed]
139. Zhang, S.; Wang, L.; Wu, W.; He, L.; Yang, X.; Pan, Q. Function and evolution of *Magnaporthe oryzae* avirulence gene AvrPib responding to the rice blast resistance gene Pib. *Sci Rep* **2015**, *5*, 11642. [CrossRef]
140. Chen, H.; Wang, S.; Xing, Y.; Xu, C.; Hayes, P.M.; Zhang, Q. Comparative analyses of genomic locations and race specificities of loci for quantitative resistance to *Pyricularia grisea* in rice and barley. *Proc. Natl. Acad. Sci. USA* **2003**, *100*, 2544–2549. [CrossRef]
141. Xu, X.; Hayashi, N.; Wang, C.-T.; Fukuoka, S.; Kawasaki, S.; Takatsuji, H.; Jiang, C.-J. Rice blast resistance gene Pikahei-1(t), a member of a resistance gene cluster on chromosome 4, encodes a nucleotide-binding site and leucine-rich repeat protein. *Mol. Breed.* **2014**, *34*, 691–700. [CrossRef]
142. Inukai, T.; Nagashima, S.; Kato, M. Pid3-I1 is a race-specific partial-resistance allele at the Pid3 blast resistance locus in rice. *Theor. Appl. Genet.* **2019**, *132*, 395–404. [CrossRef]
143. Chen, Z.; Zhao, W.; Zhu, X.; Zou, C.; Yin, J.; Chern, M.; Zhou, X.; Ying, H.; Jiang, X.; Li, Y.; et al. Identification and characterization of rice blast resistance gene Pid4 by a combination of transcriptomic profiling and genome analysis. *J. Genet. Genom.* **2018**, *45*, 663–672. [CrossRef]
144. Lv, Q.; Xu, X.; Shang, J.; Jiang, G.; Pang, Z.; Zhou, Z.; Wang, J.; Liu, Y.; Li, T.; Li, X.; et al. Functional analysis of Pid3-A4, an ortholog of rice blast resistance gene Pid3 revealed by allele mining in common wild rice. *Phytopathology* **2013**, *103*, 594–599. [CrossRef]
145. Chen, J.; Shi, Y.; Liu, W.; Chai, R.; Fu, Y.; Zhuang, J.; Wu, J. A Pid3 allele from rice cultivar Gumei2 confers resistance to *Magnaporthe oryzae*. *J. Genet. Genom.* **2011**, *38*, 209–216. [CrossRef]
146. Zhou, B.; Qu, S.; Liu, G.; Dolan, M.; Sakai, H.; Lu, G.; Bellizzi, M.; Wang, G.-L. The eight amino-acid differences within three leucine-rich repeats between Pi2 and Piz-t resistance proteins determine the resistance specificity to *Magnaporthe grisea*. *Mol. Plant Microbe Interact.* **2006**, *19*, 1216–1228. [CrossRef]
147. Su, J.; Wang, W.; Han, J.; Chen, S.; Wang, C.; Zeng, L.; Feng, A.; Yang, J.; Zhou, B.; Zhu, X. Functional divergence of duplicated genes results in a novel blast resistance gene Pi50 at the Pi2/9 locus. *Theor. Appl. Genet.* **2015**, *128*, 2213–2225. [CrossRef] [PubMed]
148. Deng, Y.; Zhai, K.; Xie, Z.; Yang, D.; Zhu, X.; Liu, J.; Wang, X.; Qin, P.; Yang, Y.; Zhang, G.; et al. Epigenetic regulation of antagonistic receptors confers rice blast resistance with yield balance. *Science* **2017**, *355*, 962–965. [CrossRef]
149. Xie, Z.; Yan, B.; Shou, J.; Tang, J.; Wang, X.; Zhai, K.; Liu, J.; Li, Q.; Luo, M.; Deng, Y.; et al. A nucleotide-binding site-leucine-rich repeat receptor pair confers broad-spectrum disease resistance through physical association in rice. *Philos. Trans. R Soc. Lond. B Biol. Sci.* **2019**, *374*, 20180308. [CrossRef]
150. Liu, X.; Lin, F.; Wang, L.; Pan, Q. The in silico map-based cloning of Pi36, a rice coiled-coil nucleotide-binding site leucine-rich repeat gene that confers race-specific resistance to the blast fungus. *Genetics* **2007**, *176*, 2541–2549. [CrossRef] [PubMed]

151. Lee, S.K.; Song, M.Y.; Seo, Y.S.; Kim, H.K.; Ko, S.; Cao, P.J.; Suh, J.P.; Yi, G.; Roh, J.H.; Lee, S.; et al. Rice Pi5-mediated resistance to *Magnaporthe oryzae* requires the presence of two coiled-coil-nucleotide-binding-leucine-rich repeat genes. *Genetics* **2009**, *181*, 1627–1638. [CrossRef] [PubMed]
152. Zhai, C.; Zhang, Y.; Yao, N.; Lin, F.; Liu, Z.; Dong, Z.; Wang, L.; Pan, Q. Function and interaction of the coupled genes responsible for Pik-h encoded rice blast resistance. *PLoS ONE* **2014**, *9*, e98067. [CrossRef]
153. Das, A.; Soubam, D.; Singh, P.K.; Thakur, S.; Singh, N.K.; Sharma, T.R. A novel blast resistance gene, Pi54rh cloned from wild species of rice, *Oryza rhizomatis* confers broad spectrum resistance to *Magnaporthe oryzae*. *Funct. Integr. Genom.* **2012**, *12*, 215–228. [CrossRef]
154. Devanna, N.B.; Vijayan, J.; Sharma, T.R. The blast resistance gene Pi54of cloned from *Oryza officinalis* interacts with Avr-Pi54 through its novel non-LRR domains. *PLoS ONE* **2014**, *9*, e104840. [CrossRef]
155. Okuyama, Y.; Kanzaki, H.; Abe, A.; Yoshida, K.; Tamiru, M.; Saitoh, H.; Fujibe, T.; Matsumura, H.; Shenton, M.; Galam, D.C.; et al. A multifaceted genomics approach allows the isolation of the rice Pia-blast resistance gene consisting of two adjacent NBS-LRR protein genes. *Plant J.* **2011**, *66*, 467–479. [CrossRef]
156. Zhai, C.; Lin, F.; Dong, Z.; He, X.; Yuan, B.; Zeng, X.; Wang, L.; Pan, Q. The isolation and characterization of Pik, a rice blast resistance gene which emerged after rice domestication. *New Phytol.* **2011**, *189*, 321–334. [CrossRef]
157. Chen, J.; Peng, P.; Tian, J.; He, Y.; Zhang, L.; Liu, Z.; Yin, D.; Zhang, Z. Pike, a rice blast resistance allele consisting of two adjacent NBS–LRR genes, was identified as a novel allele at the Pik locus. *Mol. Breed.* **2015**, *35*, 117. [CrossRef]
158. Hua, L.; Wu, J.; Chen, C.; Wu, W.; He, X.; Lin, F.; Wang, L.; Ashikawa, I.; Matsumoto, T.; Wang, L.; et al. The isolation of Pi1, an allele at the Pik locus which confers broad spectrum resistance to rice blast. *Theor. Appl. Genet.* **2012**, *125*, 1047–1055. [CrossRef]
159. Yuan, B.; Zhai, C.; Wang, W.; Zeng, X.; Xu, X.; Hu, H.; Lin, F.; Wang, L.; Pan, Q. The Pik-p resistance to *Magnaporthe oryzae* in rice is mediated by a pair of closely linked CC-NBS-LRR genes. *Theor. Appl. Genet.* **2011**, *122*, 1017–1028. [CrossRef] [PubMed]
160. Ashikawa, I.; Hayashi, N.; Yamane, H.; Kanamori, H.; Wu, J.; Matsumoto, T.; Ono, K.; Yano, M. Two adjacent nucleotide-binding site-leucine-rich repeat class genes are required to confer Pikm-specific rice blast resistance. *Genetics* **2008**, *180*, 2267–2276. [CrossRef] [PubMed]
161. Sharma, T.R.; Madhav, M.S.; Singh, B.K.; Shanker, P.; Jana, T.K.; Dalal, V.; Pandit, A.; Singh, A.; Gaikwad, K.; Upreti, H.C.; et al. High-resolution mapping, cloning and molecular characterization of the Pi-k^h gene of rice, which confers resistance to *Magnaporthe grisea*. *Mol. Genet. Genom.* **2005**, *274*, 569–578. [CrossRef] [PubMed]
162. Meng, F.; He, Y.; Chen, J.; Long, X.; Wang, H.; Zhu, M.; Liu, S.; Cai, Q.; Zhang, Z. Analysis of natural variation of the rice blast resistance gene Pike and identification of a novel allele Pikg. *Mol. Genet. Genom.* **2021**, *296*, 939–952. [CrossRef]
163. Bryan, G.T.; Wu, K.-S.; Farrall, L.; Jia, Y.; Hershey, H.P.; McAdams, S.A.; Faulk, K.N.; Donaldson, G.K.; Tarchini, R.; Valent, B. A single amino acid difference distinguishes resistant and susceptible alleles of the rice blast resistance gene Pi-ta. *Plant Cell* **2000**, *11*, 2033–2046. [CrossRef]
164. Lin, J.; Song, X.; Wu, M.; Ruan, G. Breeding and Utilization of Japonicalinous CMS Line Chunjiang 19A with Wide Compatibility and High Outcrossing Rate. *Agron. For.* **2012**, *13*, 537–540. [CrossRef]
165. Yang, X.; Li, Y.; Ren, B.; Ding, L.; Gao, C.; Shen, Q.; Guo, S. Drought-induced root aerenchyma formation restricts water uptake in rice seedlings supplied with nitrate. *Plant Cell Physiol.* **2012**, *53*, 495–504. [CrossRef]
166. Liu, G.; Zhu, P.; Liu, Y.; Kong, D.; Wang, J.; Luo, L.; Yu, X. Molecular Marker-Assisted Selection of a New Water-Saving and Drought-Resistant Rice (WDR) Restoration Line, Hanhui 8200, for Enhanced Resistance to Rice Blast. *Agronomy* **2024**, *14*, 1504. [CrossRef]
167. Cui, Y.; Li, C.; Zhou, F.; Chen, H.; Zhang, W.; Ma, W.; Lin, Y. Developing of transgenic glyphosate-tolerant Indica restorer line with commercial application potential. *Mol. Breed.* **2020**, *40*, 43. [CrossRef]
168. Hori, K.; Yamamoto, T.; Yano, M. Genetic dissection of agronomically important traits in closely related temperate japonica rice cultivars. *Breed. Sci.* **2017**, *67*, 427–434. [CrossRef] [PubMed]
169. Hayano-Saito, Y.; Hayashi, K. Stvb-i, a Rice Gene Conferring Durable Resistance to Rice stripe virus, Protects Plant Growth From Heat Stress. *Front. Plant Sci.* **2020**, *11*, 519. [CrossRef]
170. Sedeek, S.; Aboyousef, M.; El-Rafaee, I.; Abdallah, A.; Hammoud, S.; El-Malky, M.; El-Namkay, R.; El-Abd, A.; Ammar, M.; Abdelkhalik, A.; et al. Giza 183 Egyptian rice variety: A step to confront climate change challenges. *Egypt. J. Agric. Res.* **2023**, *101*, 519–537. [CrossRef]
171. Wang, Y.; Fu, X.; Gao, G.; He, Y. Improving the Grain Quality of Minghui63, a Restorer Line of Rice with Good Quality through Marker-Assisted Selection. *Mol. Plant Breed.* **2009**, *7*, 661–665. [CrossRef]
172. Wang, G.L.; Mackill, D.J.; Bonman, J.M.; McCouch, S.R.; Champoux, M.C.; Nelson, R.J. RFLP mapping of genes conferring complete and partial resistance to blast in a durably resistant rice cultivar. *Genetics* **1994**, *136*, 1421–1434. [CrossRef] [PubMed]
173. Singh, A.; Singh, V.K.; Singh, S.P.; Pandian, R.T.P.; Ellur, R.K.; Singh, D.; Bhowmick, P.K.; Krishnan, S.G.; Nagarajan, M.; Vinod, K.K.; et al. Molecular breeding for the development of multiple disease resistance in Basmati rice. *AoB Plants* **2012**, *2012*, pls029. [CrossRef]
174. Yao, X.F.; Sun, Z.; Xu, X.; Li, H.; Liu, C.M. Complete Genome Assembly of Japonica Rice Variety Zhonghua 11. *Plant Commun.* **2025**, *25*, 101463. [CrossRef] [PubMed]

175. Hasan, M.M.; Rafii, M.Y.; Ismail, M.R.; Mahmood, M.; Rahim, H.A.; Alam, M.A.; Ashkani, S.; Malek, M.A.; Latif, M.A. Marker-assisted backcrossing: A useful method for rice improvement. *Biotechnology* **2015**, *29*, 237–254. [CrossRef] [PubMed]
176. Wang, X.; Jia, Y.; Wamishe, Y.; Jia, M.H.; Valent, B. Dynamic Changes in the Rice Blast Population in the United States Over Six Decades. *Mol. Plant Microbe Interact.* **2017**, *30*, 803–812. [CrossRef] [PubMed]
177. Chen, C.; Lian, B.; Hu, J.; Zhai, H.; Wang, X.; Venu, R.; Liu, E.; Wang, Z.; Chen, M.; Wang, B.; et al. Genome comparison of two *Magnaporthe oryzae* field isolates reveals genome variations and potential virulence effectors. *BMC Genom.* **2013**, *14*, 887. [CrossRef]

Disclaimer/Publisher's Note: The statements, opinions and data contained in all publications are solely those of the individual author(s) and contributor(s) and not of MDPI and/or the editor(s). MDPI and/or the editor(s) disclaim responsibility for any injury to people or property resulting from any ideas, methods, instructions or products referred to in the content.

plants

MDPI

Brief Report

Expression of the *Nicotiana benthamiana* Retrozyme 1 (NbRZ1) Genomic Locus

Alexander A. Lezzhov, Anastasia K. Atabekova , Denis A. Chergintsev, Andrey G. Solovyev and Sergey Y. Morozov *

A. N. Belozersky Institute of Physico-Chemical Biology, Moscow State University, 119992 Moscow, Russia; lezzhov-genetic@mail.ru (A.A.L.); asya_atabekova@mail.ru (A.K.A.); ledumpalustre86@gmail.com (D.A.C.); solovyev@belozersky.msu.ru (A.G.S.)

* Correspondence: morozov@genebee.msu.ru; Tel.: +7-(495)-939-31-98

Abstract: Retrozymes are a class of non-autonomous plant retrotransposons that have long terminal repeats (LTRs) containing hammerhead ribozymes (HHRs) that facilitate the circularization of the retrozyme RNA. The LTR of *Nicotiana benthamiana* retrozyme 1 (NbRZ1) has been shown to contain a promoter that directs transcription of this retroelement. In this study, we identified the transcription start site of the promoter contained in the LTR of NbRZ1 and mapped the promoter region essential for its transcriptional activity. Using transgenic *Arabidopsis thaliana* plants carrying the GUS gene under the control of the NbRZ1 LTR, the NbRZ1 transcript was demonstrated to potentially encode a protein targeted for proteasomal degradation in the plant cell. Overexpression of this protein in plants using a viral expression vector was found to cause severe necrosis. The data presented suggest a tight regulation of the expression of the NbRZ1-encoded polypeptide in plants and its potential functional importance, although further research is needed to determine whether circular and/or linear retrozyme RNA forms can be translated in plants.

Keywords: retrozymes; retroelements; long terminal repeat; LTR promoter; transcription; ribozymes; circRNA; circRNA translation

1. Introduction

The functions of circular RNAs (circRNAs) in plants and animals have been the subject of intense research in recent years [1,2]. Most of the circRNAs discovered so far are the result of backsplicing, which was previously thought to be the result of misregulation [3]. However, subsequent research has led to a revision of this concept. Current data indicate that circRNAs have important regulatory functions in cells and that the process of their generation is directed and highly regulated [1]. Different mechanisms can exert different functions of circRNAs. It has been shown that circRNAs are able to regulate transcriptional elongation efficiency by forming RNA-DNA hybrids, called R-loops, with corresponding genomic loci, as demonstrated on the model of a circRNA encoded by exon 6 of the *Arabidopsis thaliana SEPALLATA3* gene [4]. In addition, certain circRNAs have been shown to contain microRNA (miRNA) binding sites and thus act as microRNA sponges [5]. miRNA-sponge function has been studied using the model of ciRS-7 (circular RNA sponge for miR-7) [6], which is expressed in the human brain and, due to the presence of multiple miR-7 binding sites, is able to bind the corresponding miR involved in neurogenesis [7]. Furthermore, it has been demonstrated that translation on the circRNA templates can occur in different systems, although the mechanisms and functional significance of the translated products are not yet fully understood [8–11]. Nevertheless, it has been shown that the

protein synthesized on the template of *Drosophila melanogaster* circRNA called CircSfl is associated with increased lifespan longevity [12].

Another recently discovered type of circRNA is formed by the activity of hammerhead ribozymes (HHRs) followed by ligation [13]. This type of circRNA is represented by the transcripts of retrozymes (retrotransposons with hammerhead ribozymes) found in the genomes of some plant and metazoan species [13,14]. These retroelements exhibit a functional duality. On the one hand, they are non-autonomous retrotransposons integrated into the genome, and on the other hand, the transcripts of these retroelements are circRNA. Plant and animal retrozymes have structural differences. In particular, animal retrozymes are non-autonomous, non-LTR retrotransposons with type I HHRs, whereas plant retrozymes contain type III HHRs and are LTR-containing retrotransposons. For mobilization, retrozymes apparently require appropriate autonomous retroelements encoding proteins necessary for reverse transcription (RT) and integration into a new genomic locus. In the case of plant retrozymes, this may be an autonomous Ty3-gypsy family retroelement, whereas in the case of metazoan retrozymes, this role may be played by non-LTR retrotransposons such as LINEs or Penelope-like retroelements [13,14].

Plant retrozyme genomic loci consist of two long direct terminal repeats (LTRs) of approximately 300–400 nt containing type III HHRs and flanking a central region with a primer binding site complementary to the tRNA-Met 3′-terminal sequence and a polypurine tract, both of which are required for DNA synthesis during the mobilization of LTR retrotransposons [13]. It has been demonstrated that retrozymes replicate by a rolling circle mechanism and that both circular and linear replicative intermediates accumulate in different plant organs [13,15]. However, it remains unclear whether this is the result of active transcription of the corresponding genomic locus or the result of RNA-RNA replication since the LTR sequence containing the promoter is highly methylated, making active transcription of this genomic locus unlikely [15]. In addition, retrozyme RNA has been shown to be capable of long-distance transport in plants, making it similar to viroids, which are circular non-coding RNAs capable of rolling-circle replication and systemic transport in plants [16]. Therefore, the circular and linear intermediates of retrozyme RNA detected in plants may be the result of both active RNA-RNA replication and long-distance transport in plants [15,16].

The above data suggest that during their existence in plant genomes, retrozyme circRNAs may have acquired specialized functions that remain to be identified and that activation of retrozyme transcription in response to stress may occur without changing promoter methylation levels, as shown in the case of the LTR-retrotransposon *ONSEN* under heat stress [16,17]. The activation of retroelement transcription in response to stress was demonstrated in a model of several other LTR-containing plant retrotransposons. In particular, the *AtCOPIA4* promoter located in the LTR has been shown to be activated in response to infection, probably due to the presence of binding sites for WRKY transcription factors, which are known to orchestrate transcriptional reprogramming during pathogen-associated molecular pattern-triggered immunity [18]. The 5′ LTRs of two *Phyllostachys edulis* LTR retrotransposons, PHRE1 and PHRE2, contain promoters that are activated during the response to heat stress by interaction with heat-dependent transcription factors [19]. However, in the case of retrozyme promoters, such regulation has yet to be elucidated.

In this study, we identified the transcription start site of the promoter contained in the LTR of *Nicotiana benthamiana* retrozyme 1 (NbRZ1) and mapped the promoter region essential for its transcriptional activity. The NbRZ1 transcript was further shown to potentially encode a protein that is targeted for proteasomal degradation in the plant cell. Using a viral expression vector, it was shown that overexpression of this protein in plants causes severe necrosis.

2. Results

2.1. Mapping of the NbRZ1 Transcription Start Site

The NbRZ1 LTR region (Figure 1A) has been shown to contain a promoter; however, previous attempts to map the NbRZ1 transcription start site failed since, in plant cells, the LTR-directed transcript was efficiently processed by the hammerhead ribozyme (HHR) contained in it, and the 5′-proximal transcript region was cleaved off, preventing identification of the 5′-terminal transcript residue [15]. Therefore, to map the NbRZ1 transcription start site, a point mutation was introduced into the cloned NbRZ1 LTR region to inhibit ribozyme self-cleavage activity. The G to A substitution introduced into the NbRZ1 LTR ribozyme by site-directed mutagenesis (Figure 1B) has been previously shown to completely inhibit the self-cleavage ability of HHRs [20]. The resulting construct was termed LTRmut. The effect of the mutation on NbRZ1 ribozyme activity was analyzed in vitro using a T7 transcript of LTRmut. A transcript of the wild type (wt) LTR was used as a control. After the transcription reaction, RNA samples were analyzed in an agarose gel. Under in vitro transcription conditions, the wt transcript was found to be partially self-cleaved, giving rise to two transcript fragments of the expected size, whereas in the case of the LTRmut transcript, cleavage was significantly inhibited (Figure 1C).

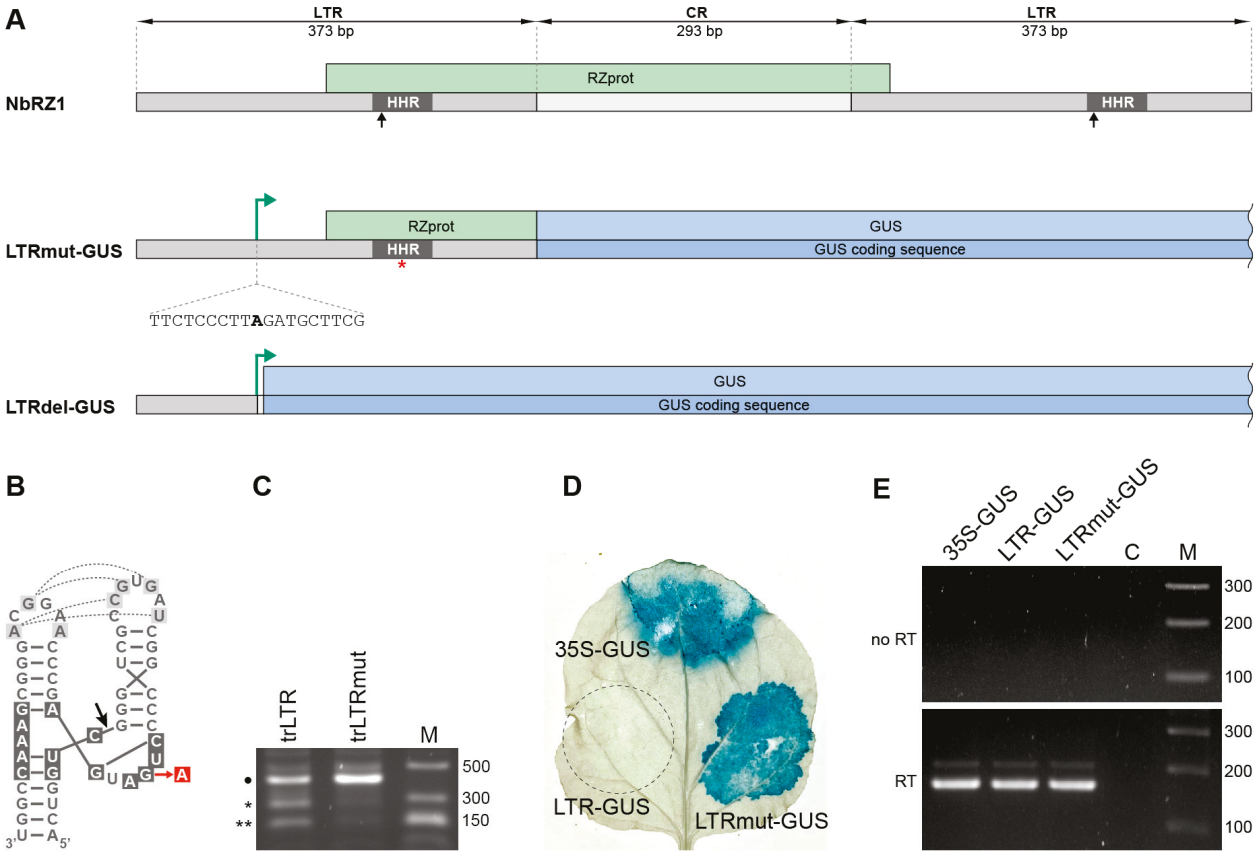

Figure 1. Identification of the transcription start site of the promoter contained in the LTR of NbRZ1. (**A**) Schematic representation of NbRZ1 and reporter constructs LTRmut-GUS and LTRdel-GUS. The positions and lengths of the LTRs and the central region (CR) are indicated. The hammerhead ribozyme (HHR) is shown in dark gray, and the black arrow points to the site of autocatalytic cleavage. The red asterisk indicates a point mutation in HHR that blocks autocatalytic cleavage. The position of the mapped transcription start site is indicated by the green arrow; the inset with the dotted line shows the fragment of the LTR sequence in which the mapped transcription start site at the LTR NbRZ1 promoter is shown in bold. The green box indicates the NbRZ1-encoded

polypeptide RZprot. The GUS coding sequence and the GUS protein are shown in dark and light blue, respectively. (**B**) Structural model of the NbRZ1 hammerhead ribozyme. Residues forming the catalytic center are shown in dark gray boxes. Dotted lines indicate non-canonical interactions in the ribozyme structure. The red arrow indicates a point mutation that results in inhibition of NbRZ1 HHR self-cleavage. The site of autocatalytic cleavage is indicated by the black arrow. (**C**) In vitro analysis of ribozyme processing efficiency. The transcripts of LTRmut (trLTRmut) and LTRwt (trLTR) sequences were used for RNA mobility analysis in agarose gel: M, RNA size markers. The black dot indicates an unprocessed transcript, while the asterisks indicate autocatalytic cleavage products. (**D**) X-Gluc-stained leaf of *N. benthamiana* infiltrated with agrobacterial cultures carrying the LTR-GUS, LTRmut-GUS, and 35S-GUS constructs. (**E**) Total RNA from *N. benthamiana* leaves infiltrated with agrobacterial cultures carrying the LTR-GUS, LTRmut-GUS, and 35S-GUS constructs was analyzed by RT-PCR using GUS-specific primers. No RT, amplification carried out without reverse transcription; C, a control reaction without template; M, DNA size markers.

To map the NbRZ1 transcription start site, the construct LTRmut-GUS was obtained, in which the GUS (*Escherichia coli* β-glucuronidase) coding region was cloned in a binary vector under the transcriptional control of LTRmut (Figure 1A). A similar LTR-GUS construct was obtained using the wt LTR region. Leaves of *N. benthamiana* plants were infiltrated with agrobacterial cultures carrying the LTR-GUS and LTRmut-GUS constructs. As an additional control, agroinfiltration was carried out with a culture carrying the 35S-GUS construct containing the strong constitutive 35S promoter of the *Cauliflower mosaic virus*. At 3 days post infiltration (dpi), the infiltrated leaves were stained for GUS activity with X-gluc, a GUS chromogenic substrate. After staining, a strong blue coloring was clearly visible in leaf areas agroinfiltrated for expression of LTRmut-GUS and 35S-GUS but not in the LTR-GUS-infiltrated area (Figure 1D). Reverse transcription (RT)-PCR analysis confirmed the presence of GUS transcripts in the areas infiltrated for the expression of 35S-GUS, LTR-GUS, and LTRmut-GUS (Figure 1E). These observations show that the LTR-GUS transcript is untranslatable, likely as a result of ribozyme self-cleavage, whereas the LTRmut-GUS transcript can be translated because it lacks the functional ribozyme. Thus, the mutation introduced in the NbRZ1 LTR to give LTRmut efficiently blocks ribozyme-dependent cleavage of the LTR-directed transcript in vivo. In addition, the efficient translation of the LTRmut-GUS-derived mRNA implies that it can have both the 5′-cap structure and the 3′-poly(A) tail, suggesting that the NbRZ1 LTR promoter-driven transcription is carried out by RNA polymerase II.

To determine the NbRZ1 transcription start site, 5′-RACE (rapid amplification of cDNA ends) was performed with GUS-specific primers on total RNA isolated at 3 dpi from *N. benthamiana* leaves agroinfiltrated for LTRmut-GUS expression, and the amplification product was cloned. Sequencing of five independent clones revealed identical sequences; in all clones, the 5′-end of the LTR-specific transcript was mapped to an adenosine residue corresponding to position 116 of the NbRZ1 LTR (Figure 1A).

2.2. Analysis of Retrozyme Expression in Plants

Transgenic *Arabidopsis thaliana* plants were generated using the LTRmut-GUS construct to analyze retrozyme expression in plants further. In transformed plants, for which the presence of the LTRmut-GUS transgene was confirmed by PCR, GUS-specific mRNA was readily detected by RT-PCR with GUS-specific primers (Figure 2A). However, GUS enzymatic activity could not be detected by GUS staining in these plants (Figure 2B).

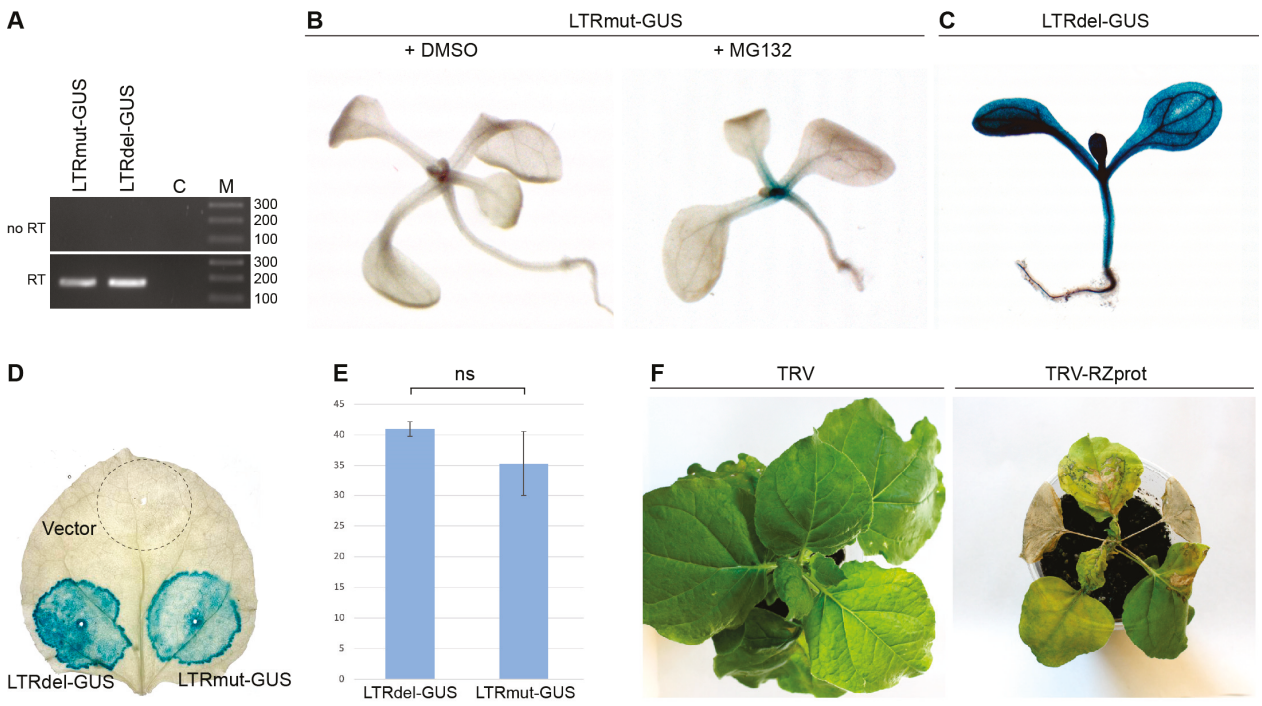

Figure 2. Expression of NbRZ1 in plants. (**A**) Total RNA from *A. thaliana* transgenic lines LTRmut-GUS and LTRdel-GUS analyzed by RT-PCR using GUS-specific primers. No RT; amplification carried out without reverse transcription; C, control reaction without template, M, DNA size markers. (**B**) MG132 proteasome inhibitor treatment and X-Gluc staining of *A. thaliana* LTRmut-GUS transgenic plants. Left, the plant treated with DMSO. Right, plant treated with MG132. (**C**) X-Gluc staining of *A. thaliana* LTRdel-GUS transgenic plant. (**D**) X-Gluc stained leaf of *N. benthamiana* infiltrated with agrobacterial cultures carrying the LTRmut-GUS, LTRdel-GUS, and empty vector constructs. (**E**) Quantitative RT-PCR analysis of GUS RNA levels in *N. benthamiana* leaves infiltrated with agrobacterial cultures carrying the LTR-GUS and LTRmut-GUS constructs. Bars show mean values and standard error; ns indicates no statistically significant difference between LTRmut-GUS and LTRdel-GUS ($p > 0.05$). (**F**) Analysis of the effects of the NbRZ1-encoded polypeptide RZprot on plants using a viral expression vector based on the genome of TRV. *N. benthamiana* plants infiltrated with cultures carrying the TRV and TRV-RZprot are shown.

NbRZ1 contains an open reading frame (ORF) that potentially encodes a 19 kDa polypeptide designated as RZprot (Figure 1A). In the LTRmut-GUS construct, the GUS coding sequence is fused in-frame to a 5′-proximal portion of the RZprot ORF (Figure 1A). Therefore, translation of the LTRmut-GUS transcript could result in a translational fusion of the N-terminal region of RZprot and the GUS protein (Figure 1A). As the LTRmut-GUS transcript, but not a product of its translation, was detected in the transgenic plants, we hypothesized that the RZprot moiety of the RZprot-GUS fusion protein could be targeted for proteasome degradation resulting in degradation of the entire RZprot-GUS protein, as shown for other functional important proteins [21–23]. To verify this hypothesis, seedlings of LTRmut-GUS transgenic plants were treated with MG132, a potent cell-permeable proteasome inhibitor [24]. Further GUS staining of MG132-treated seedlings produced a blue coloring (Figure 2B), confirming, therefore, that the absence of LTRmut-GUS translation product in transgenic plants was caused by its proteasome degradation. As this product was readily detected upon agrobacteria-mediated transient LTRmut-GUS expression (Figure 1D), we suggest that its proteasomal degradation might be rather inefficient and, therefore, manifested only under the conditions of low-level LTRmut-GUS expression in transgenic plants. It should be noted that the GUS gene product is very stable in plants, and staining intensities can increase over time even when expression levels of the gene of

interest are low [25]. This may explain why the LTRmut-GUS and LTRdel-GUS transgenic lines show different levels of staining. In the case of LTRmut-GUS plants, the corresponding translation product was degraded and did not accumulate efficiently in the plants. On the other hand, these data suggest that the RZprot ORF can be expressed in plants, providing a first indication of the retrozyme protein-coding capacity. Further detailed analyses using RZprot-specific antibodies are required to determine whether RZprot is indeed expressed in plants.

To confirm that the proteasomal degradation of the RZprot-GUS fusion protein was directed by the RZprot-specific sequence and to further characterize the NbZR1 LTR promoter, another construct was used to generate transgenic plants. In this construct, termed LTRdel-GUS, the GUS coding sequence was cloned under the control of the NbRZ1 LTR region located upstream of the mapped transcription start site (Figure 1A). In LTRdel-GUS, the RZprot coding region was completely deleted. GUS staining of seedlings of LTRdel-GUS transgenic plants resulted in the appearance of blue coloring (Figure 2C), indicating that the GUS protein lacking the RZprot fragment is not susceptible to proteasomal degradation. On the other hand, these observations show that the 115 bp region of the NbRZ1 LTR located upstream of the transcription start is sufficient for promoter activity. To compare the transcriptional efficiency of the full-length and truncated LTR, *N. benthamiana* leaves were agroinfiltrated for expression of LTRmut-GUS and LTRdel-GUS. GUS staining of infiltrated leaves at 3 dpi revealed similar levels of GUS expression (Figure 2D). Quantitative RT-PCR analysis of GUS RNA levels revealed no statistically significant difference between LTRmut-GUS and LTRdel-GUS ($p > 0.05$). (Figure 2E). These data demonstrate that the major elements of the NbRZ1 promoter are located upstream of the transcription start site.

To analyze the possible effects of the putative NbRZ1-encoded polypeptide RZprot on plants, the RZprot coding sequence was cloned into a viral expression vector based on the genome of *Tobacco rattle virus* (TRV) [26]. As the RZprot ORF contained the ribozyme (Figure 1A) that would mediate self-cleavage of the corresponding RNA in plants, a mutant version of the RZprot ORF was used that carried the point mutation described above for LTRmut; this mutation did not alter the encoded RZprot protein sequence. *N. benthamiana* plants were agroinfiltrated for expression of TRV-RZprot, and the TRV vector was used as a control. Like the TRV vector, TRV-RZprot caused systemic infection of plants; however, the infection symptoms induced by TRV-RZprot were drastically different from those induced by TRV. In control, TRV-infected plants, slight stunting, mild mosaic/yellowing of upper leaves, and occasional necrosis along the leaf veins were observed. In contrast to TRV, TRV-RZprot caused severe necrosis of agroinfiltrated and upper systemically infected leaves (Figure 2F). These observations suggest that high-level expression of RZprotis is detrimental to plants. Therefore, we hypothesize that the expression of RZprot if it occurs under native conditions, can only be at low levels or tightly regulated in a spatial/temporal manner, or both.

3. Discussion

Transposition of retroelements involves transcription of their genomic loci, translation of the resulting mRNA to produce proteins with the required enzymatic activities, reverse transcription leading to the synthesis of double-stranded DNA, and its integration into a new genomic locus [27]. Thus, the key event that initiates the act of transposition is the transcription of a retroelement genomic locus. In LTR-containing retrotransposons, as well as in retroviruses that also contain LTRs, transcription of their genomic loci is controlled by RNA polymerase II promoters located in LTRs [28,29]. In plants, transcriptional activation of such promoters can occur in response to stress, as has been demonstrated for a number of retroelements [17–19]. In this work, we have characterized the promoter contained in

the LTR of the retrozyme NbRZ1, a non-autonomous retrotransposon of *N. benthamiana*. The transcription start site was mapped in the NbZR1 LTR; however, the mechanisms of regulation of the NbZR1 LTR promoter remain undiscovered. It should be noted that regulation of NbZR1 LTR promoter-driven transcription is expected based on the data showing that the NbZR1 LTR is highly methylated [15] likely prevents transcription of this locus, while a substantial amount of retrozyme RNA has been detected in *N. benthamiana* plants [15], indicating that transcription of NbRZ1 and other retrozyme genomic loci may occur under as yet unidentified conditions and is therefore likely to be subject to regulation. As demonstrated in the case of the LTR-retrotransposon *ONSEN*, activation of transcription of LTR-containing retrotransposons can occur without changing promoter methylation levels. Although the exact mechanism of such activation in the case of retrozymes and *ONSEN* has not yet been elucidated, it is conceivable that it could be associated with proteins containing a methyl CpG-binding domain (MBD), which bind chromatin regions with high levels of CG methylation preventing their activation, and that loss of MBD protein function leads to activation of transposable elements without altering the methylation level at the corresponding genomic loci [30,31]. On the other hand, since the circularized retrozyme RNA is capable of autonomous RNA-RNA replication [13,15], it remains to be established whether the retrozyme-specific RNA detected in plants is the result of transcription of genomic loci or autonomous replication. Further experiments are needed to determine whether the retrozyme LTR promoter-directed transcription is activated under specific conditions or at a certain developmental stage.

The retrozyme RNA contains an ORF that may encode a 19 kDa polypeptide called RZprot; expression of this protein has not been demonstrated, and its potential functions have remained unknown. The experiments reported here suggest that RZprot can be translated using the NbRZ1 RNA template. In addition, an N-terminal portion of RZprot fused to GUS was found to induce proteasomal degradation of the fusion protein, suggesting that the accumulation of RZprot in plant cells is tightly controlled. Retrozyme RNA exists in both linear and circular forms in plants [13,15], so it is unclear which of these can serve as a template for RZprot translation. In fact, circRNAs, although apparently lacking the 5′-cap and 3′-poly(A), can still serve as templates for translation that can be initiated in a cap-independent manner due to internal ribosome entry sites (IRES) or translation factors that bind to modified RNA residues [11,32–34]. The possibility of retrozyme circRNA translation is consistent with two available observations. First, the retrozyme circRNA is likely to be rather stable in plant cells since it has been shown, using *Peach latent mosaic viroid* as a model, that the HHR of the same type as in retrozymes most likely adopts an inactive conformation upon circularization, thus preventing its self-cleavage [35,36]. Second, the HHR tertiary structure can serve as an IRES-like element and is distantly topologically related to the structure of the picornavirus IRES [37]. Therefore, the putative translation of retrozyme RNA can be considered as rather possible and requires further experimental evaluation. On the other hand, the translation of RZprot on the template of the linear retrozyme transcript seems less probable since such a transcript can only be translated if it avoids HHR self-cleavage, which is known to be as efficient as 94% at magnesium ion concentrations similar to those in living cells, as has been found for a viroid HHR similar in structure to the retrozyme HHR [38]. It should also be kept in mind that only a product of retrozyme genomic locus transcription can be translated as a linear RNA in a 5′-cap/3′-polyA-dependent manner, as the products of autonomous retrozyme RNA-RNA replication, both linear and circular, apparently lack these terminal structures. Further research is needed to determine whether circular and linear retrozyme forms can be translated in plants.

The data presented in this paper and previously published data on retrozyme biology are consistent with the following model. The activity of the retrozyme LTR promoter and the transcription of retrozyme genomic loci are generally inhibited by DNA methylation and occur only at specific developmental stage(s) or in response to specific stimuli; the synthesized retrozyme RNA can persist in plants due to RNA-RNA replication as well as systemic transport and have as yet unidentified functions [16]. One of these functions may be related to the findings presented here, indicating that the retrozyme RNA has a coding capacity and may be translated to a protein of unknown function. The observations that overexpression of this protein leads to extensive necrosis of plant tissues and that this protein is targeted for proteasomal degradation demonstrate tight regulation of its expression that may indicate its functional importance.

In view of the data presented in this paper, future studies of retrozymes in plants should aim at a more detailed analysis of their transcription and translation.

4. Materials and Methods

4.1. Plant Material

N. benthamiana plants were grown from seed under standard conditions (16 h/8 h light/dark cycles, 24/20 °C day/night temperatures, 50% humidity) in a glasshouse. The 3 to 5-week-old plants were used for agrobacterial-mediated transient protein expression. *A. thaliana* plants were grown from seed after vernalization at 4 °C for 3 days in growth chambers under standard conditions (22/20 °C day/night temperatures, 60–70% relative humidity, and 8 h/16 h light/dark cycles).

4.2. Plant Agroinfiltration

Agrobacterium tumefaciens (strain C58C1 or GV3101) cells were transformed with binary vectors using a freeze–thaw method. Overnight cultures of agrobacteria were grown in the Luria–Bertani (LB) medium at 28 °C with selective antibiotics, 10 mM 2-(*N*-morpholino)ethanesulfonic acid (MES) monohydrate (Sigma-Aldrich, Saint Louis, MO, USA), pH 5.5, and 20 μm acetosyringone (Sigma-Aldrich, Saint Louis, MO, USA). 500 μL of overnight culture was transferred to 5 mL of fresh LB medium at 28 °C with selective antibiotics 10 mM MES, pH 5.5, and 20 μm acetosyringone for 5 h. Cells were pelleted by centrifugation, resuspended in the infiltration medium (10 mM MES, pH 5.5, 10 mM $MgCl_2$ (Sisco Research Laboratories Pvt. Ltd., New Mumbai, India), and 150 mM acetosyringone) and incubated at room temperature for 3–4 h. Prior to infiltration, *A. tumefaciens* suspensions were diluted to a final OD_{600} = 0.3. The agrobacterial cultures were infiltrated onto the abaxial surface of *N. benthamiana* leaves using a needleless syringe.

4.3. Molecular Cloning and Recombinant Constructs

To obtain the pLH-LTRwt:GUS construct, the NbRZ LTR sequence was amplified on the template of the previously published construct NbRZ1 [15] with specific primers (Supplementary Table S1). The resulting amplification product was digested with *Eco*RI-*Nco*I (ThermoFisher Scientific, Waltham, MA, USA) restriction endonucleases and cloned into the pLH* binary vector [39] carrying the GUS coding sequence. For the pLH-LTRmut:GUS construct, the NbRZ LTR sequence was amplified by overlap PCR with appropriate primers (Supplementary Table S1) on the pLH-LTRwt:GUS construct and cloned with *Eco*RI-*Nco*I restriction endonucleases into the pLH* binary vector carrying the GUS coding sequence. The resulting constructs were then used by agroinfiltration for transient expression in N. benthamiana plants.

To generate transgenic *A. thaliana* plants, the pCambia-LTRmut:GUS construct was obtained. For this, the expression cassette from pLH-LTRmut:GUS was subcloned into

pCambia1300 binary vector using *Eco*RI-*Xba*I (ThermoFisher Scientific, Waltham, MA, USA) restriction endonucleases. To obtain the pCambia-LTRdel:GUS construct, the LTR region located upstream of the mapped transcription start site was amplified with specific primers (Supplementary Table S1) on the pLH-LTRmut:GUS template. The resulting amplification product was digested with *Eco*RI-*Nco*I restriction endonucleases and cloned into the pCambia-LTRmut:GUS.

To obtain TRV-RZprot using overlap PCR. In the first step, one PCR product was obtained, using previously described NbRZ1 [15] as a template and RZ-Eco-Nco-P and NbRZ1-LTR-mut-ovl-M (Supplementary Table S1) as primers, and another PCR product was obtained from NbRZ1 using primers TRV-RZ-M and NbRZ1-LTR-mut-ovl-P (Supplementary Table S1). In the second step, two PCR products were fused by amplification with primers RZ-Eco-Nco-P and TRV-RZ-M. The resulting DNA fragment was digested with *Eco*RI-*Sal*I (ThermoFisher Scientific, Waltham, MA, USA) and cloned in a TRV RNA2-based vector [40] digested with *Eco*RI-*Xho*I (ThermoFisher Scientific, Waltham, MA, USA). The recombinant construct for the transient expression of TRV1 was described previously [41]. All obtained constructs were verified with sequencing.

4.4. 5′-RACE

The 5′-RACE analysis was carried out using the Mint RACE kit (Evrogen, Moscow, Russia). This protocol employs the Step-Out RACE procedure, as described in detail earlier [42]. The reverse transcription and subsequent amplification steps were performed according to the manufacturer's instructions, using the primers included in the kit and gene-specific primers (Supplementary Table S1). PCR products were then cloned into the pAL2-T vector (Evrogen, Moscow, Russia) and sequenced.

4.5. GUS Staining

Infiltrated *N. benthamiana* leaves and 2.5-week-old *A. thaliana* seedlings were vacuum-infiltrated and stained overnight at 37 °C in GUS staining buffer (containing 0.05 M sodium phosphate buffer (pH 7.0), 0.2% Triton X-100 (Suzhou Yacoo Science Co., Ltd., Suzhou, Jiangsu, China), 0.5 mM potassium ferrocyanide (LenReactiv, Saint-Petersburg, Russia), 0.5 mM potassium ferricyanide (LenReactiv, Saint-Petersburg, Russia) and 1 mM X-Gluc (Chem-Impex, Wood Dale, IL, USA)). The samples were then incubated for up to 8 h in 95% ethanol and observed.

4.6. Transgenic Lines Generation

The generation of *A. thaliana* transgenic lines was performed using the *A. tumefaciens* strain GV3101 containing the vector pCambia-LTRmut:GUS or pCambia-LTRdel:GUS; the transformation of *A. thaliana* (Col-0) plants was carried out by the floral-dip method [43]. Transformants were screened on 1/2 MS media containing 50 μg/mL hygromycin B (Sisco Research Laboratories Pvt. Ltd., New Delhi, India) and then transferred to soil. Transgenic lines selected from T3 lines were subjected to histochemical staining.

4.7. 26S Proteasome Inhibition

The inhibition of the 26S proteasome in *A. thaliana* seedlings was performed in an MS liquid medium supplemented with 150 μM MG132 (Sigma-Aldrich, Saint Louis, MO, USA) for 12 h. MG132 stock solution (5 mg/mL) was prepared with dimethylsulfoxide (DMSO) (Sigma-Aldrich, Saint Louis, MO, USA). The seedlings were incubated in an MS liquid medium supplemented with DMSO as a control.

4.8. In Vitro Transcription and Ribozyme Processing

RNA used for in vitro ribozyme processing experiments was obtained by in vitro transcription with T7 RNA polymerase (ThermoFisher Scientific, Waltham, MA, USA). The transcripts containing LTRmut and LTRwt sequences were produced by transcription on templates of PCR products containing T7 promoter, which were obtained using the appropriate primers (Supplementary Table S1) using pLH-LTRmut:GUS or pLH-LTRwt:GUS as templates. For analysis of ribozyme processing efficiency, in vitro transcription products were incubated in formamide loading buffer (deionized formamide (Sigma-Aldrich, Saint Louis, MO, USA) 80% (*w*/*v*), EDTA (Sisco Research Laboratories Pvt. Ltd., New Mumbai, India) (pH 8.0) 10 mM, bromophenol blue (LenReactiv, Saint-Petersburg, Russia) 1 mg/mL) at 70 °C for 15 min for RNA denaturation. The samples were then chilled on ice and analyzed in 2% agarose gel.

4.9. Total RNA Extraction, Reverse Transcription and Quantitative PCR

Leaf disks were frozen in liquid nitrogen and ground to fine powder. Total RNA was extracted using ExtractRNA reagent (Evrogen, Moscow, Russia) according to the manufacturer's instructions. To prevent contamination with plant genomic DNA, samples were thoroughly treated with RNase-free DNAseI (ThermoFisher Scientific, Waltham, MA, USA). The total RNA samples (1 μg each) were transcribed into cDNA with oligo(dT) primer using a Revertaid reverse transcriptase (ThermoFisher Scientific, Waltham, MA, USA). Then, 1 μL of three-fold-diluted reverse-transcription product was used for real-time PCR reactions with a qPCRMix M-440 (Synthol, Moscow, Russia) using GUS-specific primers or primers specific for F-box mRNA, which was used as the reference gene (Supplementary Table S1). Reactions were carried out in the CFX Connect Real-Time PCR System (Bio-Rad, Hercules, CA, USA) The C_t value for GUS RNA was normalized to the reference gene mRNA. For the statistical analyses of data, a nonpaired two-tailed Student's *t*-test was applied.

Supplementary Materials: The following supporting information can be downloaded at: https://www.mdpi.com/article/10.3390/plants14081205/s1, Table S1: Primers used in this study.

Author Contributions: Conceptualization, A.A.L. and A.G.S.; investigation, A.A.L., A.K.A. and D.A.C.; writing—original draft preparation, A.A.L., A.G.S. and S.Y.M.; writing—review and editing, all authors; funding acquisition, A.A.L. All authors have read and agreed to the published version of the manuscript.

Funding: This work was supported by the Russian Science Foundation (grant 23-74-01014).

Data Availability Statement: Data are contained within the article and Supplementary Materials.

Conflicts of Interest: The authors declare no conflicts of interest.

References

1. Liu, R.; Ma, Y.; Guo, T.; Li, G. Identification, Biogenesis, Function, and Mechanism of Action of Circular RNAs in Plants. *Plant Commun.* **2023**, *4*, 100430. [CrossRef] [PubMed]
2. Kristensen, L.S.; Andersen, M.S.; Stagsted, L.V.W.; Ebbesen, K.K.; Hansen, T.B.; Kjems, J. The Biogenesis, Biology and Characterization of Circular RNAs. *Nat. Rev. Genet.* **2019**, *20*, 675–691. [CrossRef] [PubMed]
3. Cocquerelle, C.; Mascrez, B.; Hétuin, D.; Bailleul, B. Mis-Splicing Yields Circular RNA Molecules. *FASEB J.* **1993**, *7*, 155–160. [CrossRef]
4. Conn, V.M.; Hugouvieux, V.; Nayak, A.; Conos, S.A.; Capovilla, G.; Cildir, G.; Jourdain, A.; Tergaonkar, V.; Schmid, M.; Zubieta, C.; et al. A CircRNA from SEPALLATA3 Regulates Splicing of Its Cognate mRNA through R-Loop Formation. *Nat. Plants* **2017**, *3*, 17053. [CrossRef] [PubMed]
5. Thomson, D.W.; Dinger, M.E. Endogenous MicroRNA Sponges: Evidence and Controversy. *Nat. Rev. Genet.* **2016**, *17*, 272–283. [CrossRef]

6. Hansen, T.B.; Jensen, T.I.; Clausen, B.H.; Bramsen, J.B.; Finsen, B.; Damgaard, C.K.; Kjems, J. Natural RNA Circles Function as Efficient MicroRNA Sponges. *Nature* **2013**, *495*, 384–388. [CrossRef]
7. Pollock, A.; Bian, S.; Zhang, C.; Chen, Z.; Sun, T. Growth of the Developing Cerebral Cortex Is Controlled by MicroRNA-7 through the P53 Pathway. *Cell Rep.* **2014**, *7*, 1184–1196. [CrossRef]
8. Liao, X.; Li, X.J.; Zheng, G.T.; Chang, F.R.; Fang, L.; Yu, H.; Huang, J.; Zhang, Y.F. Mitochondrion-Encoded Circular RNAs Are Widespread and Translatable in Plants. *Plant Physiol.* **2022**, *189*, 1482–1500. [CrossRef]
9. Chen, R.; Wang, S.K.; Belk, J.A.; Amaya, L.; Li, Z.; Cardenas, A.; Abe, B.T.; Chen, C.K.; Wender, P.A.; Chang, H.Y. Engineering Circular RNA for Enhanced Protein Production. *Nat. Biotechnol.* **2022**, *41*, 262–272. [CrossRef]
10. Yang, Y.; Fan, X.; Mao, M.; Song, X.; Wu, P.; Zhang, Y.; Jin, Y.; Yang, Y.; Chen, L.L.; Wang, Y.; et al. Extensive Translation of Circular RNAs Driven by N6-Methyladenosine. *Cell Res.* **2017**, *27*, 626–641. [CrossRef]
11. Diallo, L.H.; Tatin, F.; David, F.; Godet, A.C.; Zamora, A.; Prats, A.C.; Garmy-Susini, B.; Lacazette, E. How Are CircRNAs Translated by Non-Canonical Initiation Mechanisms? *Biochimie* **2019**, *164*, 45–52. [CrossRef] [PubMed]
12. Weigelt, C.M.; Sehgal, R.; Tain, L.S.; Cheng, J.; Eßer, J.; Pahl, A.; Dieterich, C.; Grönke, S.; Partridge, L. An Insulin-Sensitive Circular RNA That Regulates Lifespan in Drosophila. *Mol. Cell* **2020**, *79*, 268-279.e5. [CrossRef] [PubMed]
13. Cervera, A.; Urbina, D.; de la Peña, M. Retrozymes Are a Unique Family of Non-Autonomous Retrotransposons with Hammerhead Ribozymes That Propagate in Plants through Circular RNAs. *Genome Biol.* **2016**, *17*, 135. [CrossRef] [PubMed]
14. Cervera, A.; De La Peña, M. Small CircRNAs with Self-Cleaving Ribozymes Are Highly Expressed in Diverse Metazoan Transcriptomes. *Nucleic Acids Res.* **2020**, *48*, 5054–5064. [CrossRef]
15. Lezzhov, A.A.; Tolstyko, E.A.; Atabekova, A.K.; Chergintsev, D.A.; Morozov, S.Y.; Solovyev, A.G. In-Plant Persistence and Systemic Transport of Nicotiana Benthamiana Retrozyme RNA. *Int. J. Mol. Sci.* **2022**, *23*, 13890. [CrossRef]
16. Lezzhov, A.A.; Atabekova, A.K.; Chergintsev, D.A.; Lazareva, E.A.; Solovyev, A.G.; Morozov, S.Y. Viroids and Retrozymes: Plant Circular RNAs Capable of Autonomous Replication. *Plants* **2024**, *14*, 61. [CrossRef]
17. Cavrak, V.V.; Lettner, N.; Jamge, S.; Kosarewicz, A.; Bayer, L.M.; Mittelsten Scheid, O. How a Retrotransposon Exploits the Plant's Heat Stress Response for Its Activation. *PLoS Genet.* **2014**, *10*, e1004115. [CrossRef]
18. Zervudacki, J.; Yu, A.; Amesefe, D.; Wang, J.; Drouaud, J.; Navarro, L.; Deleris, A. Transcriptional Control and Exploitation of an Immune-Responsive Family of Plant Retrotransposons. *EMBO J.* **2018**, *37*, e98482. [CrossRef]
19. Papolu, P.K.; Ramakrishnan, M.; Wei, Q.; Vinod, K.K.; Zou, L.H.; Yrjala, K.; Kalendar, R.; Zhou, M. Long Terminal Repeats (LTR) and Transcription Factors Regulate PHRE1 and PHRE2 Activity in Moso Bamboo under Heat Stress. *BMC Plant Biol.* **2021**, *21*, 585. [CrossRef]
20. Ruffner, D.E.; Uhlenbeck, O.C.; Stormo, G.D. Sequence Requirements of the Hammerhead RNA Self-Cleavage Reaction. *Biochemistry* **1990**, *29*, 10695–10702. [CrossRef]
21. Maruri-López, I.; Rodríguez-Kessler, M.; Rodríguez-Hernández, A.A.; Becerra-Flora, A.; Olivares-Grajales, J.E.; Jiménez-Bremont, J.F. A Maize Spermine Synthase 1 PEST Sequence Fused to the GUS Reporter Protein Facilitates Proteolytic Degradation. *Plant Physiol. Biochem.* **2014**, *78*, 80–87. [CrossRef]
22. Gray, W.M.; Kepinski, S.; Rouse, D.; Leyser, O.; Estelle, M. Auxin Regulates SCF(TIR1)-Dependent Degradation of AUX/IAA Proteins. *Nature* **2001**, *414*, 271–276. [CrossRef]
23. Deng, F.; Guo, T.; Lefebvre, M.; Scaglione, S.; Antico, C.J.; Jing, T.; Yang, X.; Shan, W.; Ramonell, K.M. Expression and Regulation of ATL9, an E3 Ubiquitin Ligase Involved in Plant Defense. *PLoS ONE* **2017**, *12*, e0188458. [CrossRef]
24. Lee, D.H.; Goldberg, A.L. Proteasome Inhibitors: Valuable New Tools for Cell Biologists. *Trends Cell Biol.* **1998**, *8*, 397–403. [CrossRef] [PubMed]
25. Mantis, J.; Tague, B.W. Comparing the Utility of β-Glucuronidase and Green Fluorescent Protein for Detection of Weak Promoter Activity in Arabidopsis Thaliana. *Plant Mol. Biol. Report.* **2000**, *18*, 319–330. [CrossRef]
26. Abrahamian, P.; Hammond, R.W.; Hammond, J. Plant Virus-Derived Vectors: Applications in Agricultural and Medical Biotechnology. *Annu. Rev. Virol.* **2020**, *7*, 513–535. [CrossRef] [PubMed]
27. Feschotte, C.; Jiang, N.; Wessler, S.R. Plant Transposable Elements: Where Genetics Meets Genomics. *Nat. Rev. Genet.* **2002**, *3*, 329–341. [CrossRef] [PubMed]
28. Hurst, T.P.; Magiorkinis, G. Epigenetic Control of Human Endogenous Retrovirus Expression: Focus on Regulation of Long-Terminal Repeats (LTRs). *Viruses* **2017**, *9*, 130. [CrossRef]
29. Sabot, F.; Schulman, A.H. Parasitism and the Retrotransposon Life Cycle in Plants: A Hitchhiker's Guide to the Genome. *Heredity* **2006**, *97*, 381–388. [CrossRef]
30. Ichino, L.; Boone, B.A.; Strauskulage, L.; Harris, C.J.; Kaur, G.; Gladstone, M.A.; Tan, M.; Feng, S.; Jami-Alahmadi, Y.; Duttke, S.H.; et al. MBD5 and MBD6 Couple DNA Methylation to Gene Silencing through the J-Domain Protein SILENZIO. *Science* **2021**, *372*, 1434–1439. [CrossRef]

31. Wang, S.; Wang, M.; Ichino, L.; Boone, B.A.; Zhong, Z.; Papareddy, R.K.; Lin, E.K.; Yun, J.; Feng, S.; Jacobsen, S.E. MBD2 Couples DNA Methylation to Transposable Element Silencing during Male Gametogenesis. *Nat. Plants* **2024**, *10*, 13–24. [CrossRef] [PubMed]
32. Fan, X.; Yang, Y.; Chen, C.; Wang, Z. Pervasive Translation of Circular RNAs Driven by Short IRES-like Elements. *Nat. Commun.* **2022**, *13*, 3751. [CrossRef]
33. Meyer, K.D.; Patil, D.P.; Zhou, J.; Zinoviev, A.; Skabkin, M.A.; Elemento, O.; Pestova, T.V.; Qian, S.B.; Jaffrey, S.R. 5′ UTR m(6)A Promotes Cap-Independent Translation. *Cell* **2015**, *163*, 999–1010. [CrossRef] [PubMed]
34. Liu, N.; Zhou, K.I.; Parisien, M.; Dai, Q.; Diatchenko, L.; Pan, T. N6-Methyladenosine Alters RNA Structure to Regulate Binding of a Low-Complexity Protein. *Nucleic Acids Res.* **2017**, *45*, 6051–6063. [CrossRef]
35. Hernández, C.; Flores, R. Plus and Minus RNAs of Peach Latent Mosaic Viroid Self-Cleave in Vitro via Hammerhead Structures. *Proc. Natl. Acad. Sci. USA* **1992**, *89*, 3711–3715. [CrossRef]
36. Flores, R.; Daròs, J.A.; Hernández, C. Avsunviroidae Family: Viroids Containing Hammerhead Ribozymes. *Adv. Virus Res.* **2000**, *55*, 271–323. [CrossRef]
37. López-Galiano, M.J.; Chiba, S.; Forgia, M.; Navarro, B.; Cervera, A.; Babaian, A.; Di Serio, F.; Turina, M.; Peña, M. de la Self-Cleaving Ribozymes Conserved in RNA Viruses Unveil a New Role in Protein Translation. *bioRxiv* **2024**. [CrossRef]
38. Carbonell, A.; De la Peña, M.; Flores, R.; Gago, S. Effects of the Trinucleotide Preceding the Self-Cleavage Site on Eggplant Latent Viroid Hammerheads: Differences in Co- and Post-Transcriptional Self-Cleavage May Explain the Lack of Trinucleotide AUC in Most Natural Hammerheads. *Nucleic Acids Res.* **2006**, *34*, 5613. [CrossRef] [PubMed]
39. Solovyev, A.G.; Minina, E.A.; Makarova, S.S.; Erokhina, T.N.; Makarov, V.V.; Kaplan, I.B.; Kopertekh, L.; Schiemann, J.; Richert-Pöggeler, K.R.; Morozov, S.Y. Subcellular Localization and Self-Interaction of Plant-Specific Nt-4/1 Protein. *Biochimie* **2013**, *95*, 1360–1370. [CrossRef]
40. MacFarlane, S.A.; Popovich, A.H. Efficient Expression of Foreign Proteins in Roots from Tobravirus Vectors. *Virology* **2000**, *267*, 29–35. [CrossRef]
41. Liu, Y.; Schiff, M.; Marathe, R.; Dinesh-Kumar, S.P. Tobacco Rar1, EDS1 and NPR1/NIM1 like Genes Are Required for N-Mediated Resistance to Tobacco Mosaic Virus. *Plant J.* **2002**, *30*, 415–429. [CrossRef] [PubMed]
42. Matz, M.V.; Alieva, N.O.; Chenchik, A.; Lukyanov, S. Amplification of cDNA Ends Using PCR Suppression Effect and Step-out PCR. *Methods Mol. Biol.* **2003**, *221*, 41–49. [CrossRef] [PubMed]
43. Zhang, X.; Henriques, R.; Lin, S.S.; Niu, Q.W.; Chua, N.H. Agrobacterium-Mediated Transformation of Arabidopsis Thaliana Using the Floral Dip Method. *Nat. Protoc.* **2006**, *1*, 641–646. [CrossRef] [PubMed]

Disclaimer/Publisher's Note: The statements, opinions and data contained in all publications are solely those of the individual author(s) and contributor(s) and not of MDPI and/or the editor(s). MDPI and/or the editor(s) disclaim responsibility for any injury to people or property resulting from any ideas, methods, instructions or products referred to in the content.

MDPI AG
Grosspeteranlage 5
4052 Basel
Switzerland
Tel.: +41 61 683 77 34

Plants Editorial Office
E-mail: plants@mdpi.com
www.mdpi.com/journal/plants



Disclaimer/Publisher's Note: The title and front matter of this reprint are at the discretion of the Guest Editors. The publisher is not responsible for their content or any associated concerns. The statements, opinions and data contained in all individual articles are solely those of the individual Editors and contributors and not of MDPI. MDPI disclaims responsibility for any injury to people or property resulting from any ideas, methods, instructions or products referred to in the content.





Academic Open
Access Publishing

mdpi.com

ISBN 978-3-7258-8694-4